

R AND O ADIOLOGY ONCOLOGY

vol.58 no.1
march 2024





Publisher

Association of Radiology and Oncology

Aims and Scope

Radiology and Oncology (ISSN 1318-2099) is a multidisciplinary journal devoted to the publishing original and high-quality scientific papers and review articles, pertinent to oncologic imaging, interventional radiology, nuclear medicine, radiotherapy, clinical and experimental oncology, radiobiology, medical physics, and radiation protection. Papers on more general aspects of interest to the radiologists and oncologists are also published (no case reports).

Editor-in-Chief

Gregor Serša, Institute of Oncology Ljubljana, Department of Experimental Oncology, Ljubljana, Slovenia (Subject Area: Experimental Oncology)

Executive Editor

Viljem Kovač, Institute of Oncology Ljubljana, Outpatient Clinic, Ljubljana, Slovenia (Subject Areas: Clinical Oncology, Radiotherapy)

Deputy Editors

Božidar Casar, Institute of Oncology Ljubljana, Department for Dosimetry and Quality of Radiological Procedures, Ljubljana Slovenia (Subject Area: Medical Physics)

Andrej Čör, Valdoltra Orthopaedic Hospital, Ankaran, Slovenia (Subject Areas: Clinical Oncology, Experimental Oncology)

Maja Čemažar, Institute of Oncology Ljubljana, Department of Experimental Oncology, Ljubljana, Slovenia (Subject Area: Experimental Oncology)

Blaž Grošelj, Institute of Oncology Ljubljana, Department of Radiation Oncology, Ljubljana, Slovenia (Subject Areas: Radiotherapy, Clinical Oncology)

Igor Kocijančič, Medicointerna d.o.o., Ljubljana, Slovenia (Subject Areas: Radiology, Nuclear Medicine)

Miha Oražem, Institute of Oncology Ljubljana, Department of Radiation Oncology, Ljubljana, Slovenia (Subject Areas: Radiotherapy, Clinical Oncology)

Primož Strojanič, Institute of Oncology Ljubljana, Department of Radiation Oncology, Ljubljana, Slovenia (Subject Areas: Radiotherapy, Clinical Oncology)

Katarina Šurlan Popovič, University Medical Center Ljubljana, Institute of Radiology, Ljubljana, Slovenia (Subject Areas: Radiology, Nuclear Medicine)

Editorial Board

Subject Areas: Radiology and Nuclear Medicine

Sotirios Bisdas, University College London, Department of Neuroradiology, London, United Kingdom

Boris Brkljačić, University Hospital "Dubrava", Department of Diagnostic and Interventional Radiology, Zagreb, Croatia

Iztok Caglič, Cambridge University Hospitals, NHS Foundation Trust, Cambridge, United Kingdom

Gordana Ivanac, University Hospital Dubrava, Department of Diagnostic and Interventional Radiology, Zagreb, Croatia

Luka Ležaić, University Medical Centre Ljubljana, Department for Nuclear Medicine, Ljubljana, Slovenia

Maja Mušič Marolt, Institute of Oncology Ljubljana, Department of Radiology, Ljubljana, Slovenia

Igor Serša, Institut Jožef Stefan, Ljubljana, Slovenia

Jernej Vidmar, University Medical Center Ljubljana, Clinical Institute of Radiology, Ljubljana, Slovenia

Žiga Snoj, University Medical Center Ljubljana, Institute of Radiology, Ljubljana, Slovenia

Subject Areas: Clinical Oncology and Radiotherapy

Serena Bonin, University of Trieste, Department of Medical Sciences, Cattinara Hospital, Surgical Pathology Bldg, Molecular Biology Lab, Trieste, Italy

Luca Campana, Manchester University NHS Foundation Trust, Department of Surgery, Manchester, United Kingdom

Christian Dittrich, Kaiser Franz Josef - Spital, Vienna, Austria

Eva Oldenburger, University Hospital Leuven, Department of Radiation Oncology, Leuven, Belgium

Gaber Plavc, Institute of Oncology Ljubljana, Department of Radiation Oncology, Ljubljana, Slovenia

Csaba Polgar, National Institute of Oncology, Budapest, Hungary

Dirk Rades, University of Lubeck, Department of Radiation Oncology, Lubeck, Germany

Ivica Ratoša, Institute of Oncology Ljubljana, Department of Radiation Oncology, Ljubljana, Slovenia

Luis Souhami, McGill University, Montreal, Canada

Borut Štabuc, University Medical Center Ljubljana, Division of Internal Medicine, Department of Gastroenterology, Ljubljana, Slovenia

Subject Area: Experimental Oncology

Jean-Michel Escoffre, University de Tours, Tours, France

Mihaela Jurdana, University of Primorska, Faculty of Health Sciences, Izola, Slovenia

Janko Kos, University of Ljubljana, Faculty of Pharmacy, Ljubljana, Slovenia

Damijan Miklavčič, University of Ljubljana, Faculty of Electrical Engineering, Ljubljana, Slovenia

Gabriele Grassi, Università degli Studi di Trieste, Trieste, Italy

Nina Petrović, Laboratory for Radiobiology and Molecular Genetics, Department of Health and Environment, "VINČA" Institute of Nuclear Sciences-National Institute of the Republic of Serbia, University of Belgrade, Belgrade, Serbia

Kristijan Ramadan, The MRC Weatherall Institute for Molecular Medicine, University of Oxford, United Kingdom

Subject Area: Medical Physics

Robert Jeraj, University of Wisconsin, Carbone Cancer Center, Madison, Wisconsin, USA

Mirjana Josipovic, University of Copenhagen, Faculty of Health, Department of Clinical Medicine, Copenhagen, Denmark

Slaven Jurković, University of Rijeka, Department of Medical Physics and Biophysics, Rijeka, Croatia

Håkan Nyström, Skandionkliniken, Uppsala, Sweden

Ervin B. Podgoršak, McGill University, Medical Physics Unit, Montreal, Canada

Matthew Podgorsak, Roswell Park Cancer Institute, Departments of Biophysics and Radiation Medicine, Buffalo, NY, USA

Editorial office

Radiology and Oncology

Zaloška cesta 2

P. O. Box 2217

SI-1000 Ljubljana

Slovenia

Phone: +386 1 5879 369

Phone/Fax: +386 1 5879 434

E-mail: gsertsa@onko-i.si

Copyright © Radiology and Oncology. All rights reserved.

Reader for English

Vida Kološa

Secretary

Mira Klemencič, Zvezdana Vukmirović, Vijoleta Kaluža, Uroš Kuhar

Design

Monika Fink-Serša, Samo Rován, Ivana Ljubanović

Layout

Matjaž Lužar

Printed by

Tiskarna Ozimek, Slovenia

Published quarterly in 300 copies

Beneficiary name: DRUŠTVO RADIOLOGIJE IN ONKOLOGIJE

Zaloška cesta 2

1000 Ljubljana

Slovenia

Beneficiary bank account number: SI56 02010-0090006751

IBAN: SI56 0201 0009 0006 751

Our bank name: Nova Ljubljanska banka, d.d.,

Ljubljana, Trg republike 2,

1520 Ljubljana; Slovenia

SWIFT: LJBASIX

Subscription fee for institutions EUR 100, individuals EUR 50

The publication of this journal is subsidized by the Slovenian Research Agency.

Indexed and abstracted by:

- Baidu Scholar
- Case
- Chemical Abstracts Service (CAS) - CAPlus
- Chemical Abstracts Service (CAS) - SciFinder
- CNKI Scholar (China National Knowledge Infrastructure)
- CNPIEC - cnpLINKer
- Dimensions
- DOAJ (Directory of Open Access Journals)
- EBSCO (relevant databases)
- EBSCO Discovery Service
- Embase
- Genamics JournalSeek
- Google Scholar
- Japan Science and Technology Agency (JST)
- J-Gate
- Journal Citation Reports/Science Edition
- JournalGuide
- JournalTOCs
- KESLI-NDSL (Korean National Discovery for Science Leaders)
- Medline
- Meta
- Microsoft Academic
- Naviga (Softweco)
- Primo Central (ExLibris)
- ProQuest (relevant databases)
- Publons
- PubMed
- PubMed Central
- PubsHub
- QOAM (Quality Open Access Market)
- ReadCube
- Reaxys
- SCImago (SJR)
- SCOPUS
- Sherpa/RoMEO
- Summon (Serials Solutions/ProQuest)
- TDNet
- Ulrich's Periodicals Directory/ulrichsweb
- WanFang Data
- Web of Science - Current Contents/Clinical Medicine
- Web of Science - Science Citation Index Expanded
- WorldCat (OCLC)

This journal is printed on acid-free paper

On the web: ISSN 1581-3207

<https://content.sciendo.com/raon>

<http://www.radioloncol.com>

contents

review

- 1 **Sarcopenic obesity in cancer**
Mihaela Jurdana, Maja Cemazar
- 9 **The influence of anaesthesia on cancer growth**
Iztok Potocnik, Milena Kerin-Povsic, Jasmina Markovic-Bozic

nuclear medicine

- 15 **Detection performance and prognostic value of initial bone marrow involvement in diffuse large B-cell lymphoma: a single centre ¹⁸F-FDG PET/CT and bone marrow biopsy evaluation study**
Andrej Doma, Katarina Zevnik, Andrej Studen, Veronika Kloboves Prevodnik, Gorana Gasljevic, Barbara Jezersek Novakovic

radiology

- 23 **Looking through the imaging perspective: the importance of imaging necrosis in glioma diagnosis and prognostic prediction – single centre experience**
Hui Ma, Shanmei Zeng, Dingxiang Xie, Wenting Zeng, Yingqian Huang, Liwei Mazu, Nengjin Zhu, Zhiyun Yang, Jianping Chu, Jing Zhao
- 33 **Role of diffusion-weighted imaging in response prediction and evaluation after high dose rate brachytherapy in patients with colorectal liver metastases**
Salma Karim, Ricarda Seidensticker, Max Seidensticker, Jens Ricke, Regina Schinner, Karla Treitl, Johannes Rübenthaler, Maria Ingenerf, Christine Schmid-Tannwald
- 43 **Quantitative assessment of bone marrow infiltration and characterization of tumor burden using dual-layer spectral CT in patients with multiple myeloma**
Xing Xiong, Rong Hong, Xu Fan, Zhengmei Hao, Xiaohui Zhang, Yu Zhang, Chunhong Hu

experimental oncology

- 51 **The equivalence of different types of electric pulses for electrochemotherapy with cisplatin – an *in vitro* study**
Maria Scuderi, Janja Dermol-Cerne, Janez Scancar, Stefan Markovic, Lea Rems, Damijan Miklavcic
- 67 **RAD54B promotes gastric cancer cell migration and angiogenesis via the Wnt/B-catenin pathway**
Jianchao Li, Hui Geng, Xin Li, Shenshan Zou, Xintao Xu

clinical oncology

- 78 **Role of endoscopic ultrasound-guided fine needle aspiration biopsies in diagnosing pancreatic neoplasms in the paediatric population: experience from a tertiary center and review of the literature**
Maja Kebe Radulovic, Jernej Brecelj, Andrej Gruden, Margareta Strojan Flezar
- 87 **Telomere length and *TERT* polymorphisms as biomarkers in asbestos-related diseases**
Ana Mervic, Katja Goricar, Tanja Blagus, Alenka Franko, Katarina Trebusak-Podkrajsek, Metoda Dodic Fikfak, Vita Dolzan, Viljem Kovac
- 99 **The prognostic significance of programmed cell death protein 1 and its ligand on lymphoma cells and tumor-immune cells in diffuse large B-cell lymphoma, not otherwise specified**
Teja Cas Slak, Simona Miceska, Gorana Gasljevic, Lucka Boltezar, Veronika Kloboves-Prevodnik
- 110 **Influence of nutritional status and body composition on postoperative events and outcome in patients treated for primary localized retroperitoneal sarcoma**
Manuel Ramanovic, Marko Novak, Andraz Perhavec, Taja Jordan, Karteek Popuri, Nada Rotovnik Kozjek
- 124 **A retrospective study on improving the accuracy of radiotherapy for patients with breast cancer with lymph node metastasis using Styrofoam**
Jie Li, Lin Yang, Xiaowei Yao, Linlin Xu, Lina Zhao, Fei Bai
- 133 **The influence of cytotoxic drugs on the immunophenotype of blast cells in paediatric B precursor acute lymphoblastic leukaemia**
Tomaz Prelog, Simon Bucek, Andreja Brozic, Jakob Peterlin, Marko Kavcic, Masa Omerzel, Bostjan Markelc, Tanja Jesenko, Veronika Kloboves Prevodnik
- 145 **Multi-institutional study of ‘Sandwich treatment’ for motor area large brain metastases (LBM) with diameter over 3 cm**
Zheng Wang, Haining Chen, Qun Chen, Yucun Zhu, Min Li, Jia Zhou

slovenian abstracts

Sarcopenic obesity in cancer

Mihaela Jurdana¹, Maja Cemazar^{1,2}

¹ Faculty of Health Sciences, University of Primorska, Izola, Slovenia

² Institute of Oncology Ljubljana, Ljubljana, Slovenia

Radiol Oncol 2024; 58(1): 1-8.

Received 2 November 2023

Accepted 4 December 2023

Correspondence to: Mihaela Jurdana, Ph.D., Faculty of Health Sciences, University of Primorska, Polje 42, Izola, Slovenia.

E-mail: mihaela.jurdana@fvz.upr.si

Disclosure: No potential conflicts of interest were disclosed.

This is an open access article distributed under the terms of the CC-BY license (<https://creativecommons.org/licenses/by/4.0/>).

Background. Sarcopenic obesity is a relatively new term. It is a clinical condition characterized by sarcopenia (loss of muscle mass and function) and obesity (increase in fat mass) that mainly affects older adults. As the incidence of sarcopenia and obesity increases worldwide, sarcopenic obesity is becoming a greater problem also in cancer patients. In fact, sarcopenic obesity is associated with poorer treatment outcomes, longer hospital stays, physical disability, and shorter survival in several cancers. Oxidative stress, lipotoxicity, and systemic inflammation, as well as altered expression of skeletal muscle anti-inflammatory myokines in sarcopenic obesity, are also associated with carcinogenesis.

Conclusions. Reported prevalence of sarcopenic obesity in cancer varies because of heterogeneity in definitions and variability in diagnostic criteria used to estimate the prevalence of sarcopenia and obesity. Therefore, the aim of this review is to describe the definitions, prevalence, and diagnostic criteria as well as the mechanisms that cancer has in common with sarcopenic obesity.

Key words: sarcopenia; obesity; cancer; inflammation

Introduction

Sarcopenic obesity is a clinical condition characterised by the coexistence of obesity, excess fat mass (FM) and sarcopenia (decrease in skeletal muscle mass and function).^{1,2} Baumgartner was the first to propose the term sarcopenic obesity, which is considered a unique clinical condition distinct from obesity and sarcopenia alone.¹ The prevalence of sarcopenic obesity is expected to become a public health problem as the prevalence of sarcopenic obesity in adults is rapidly increasing worldwide. The clinical consequences of sarcopenic obesity are considerably more severe than those of sarcopenia or obesity alone. In comparison to both, it can lead to physical disability, morbidity, and even mortality.³ In addition, cancer is another serious global health problem with increasing incidence and mortality worldwide.⁴ Interestingly, sarcopenic obesity is more common in older adult cancer patients and patients with other chronic diseases,

but its prevalence is also increased in younger patients with obesity and chronic diseases such as cancer and is associated with worse treatment outcomes.⁵ Sarcopenic obesity and cancer, as well as other chronic diseases, share some key pathogenetic mechanism such as inflammation, oxidative stress, and insulin resistance, which are considered key factors.⁶⁻⁸ Among these, insulin resistance is considered a central condition in both, cancer and sarcopenic obesity.⁸

Several factors in sarcopenic obesity may lead to progressive loss of muscle mass and altered fat metabolism, which influence each other in a reciprocal pattern. Sarcopenia is known to be a common problem in cancer patients, especially if they are suffering cachexia and is associated with physical disability, surgical complications, increased risk of severe toxicity during cancer treatment, prolonged hospitalisation, and shortened survival.⁶ Sarcopenia can occur at any stage of cancer and in any body mass index (BMI) category and is of-

ten associated with obesity. In addition, obesity, particularly abdominal obesity, can independently lead to loss of muscle mass and function due to the negative effects of oxidative stress, inflammation, and insulin resistance, all of which negatively impact muscle mass.⁷ Recently, there has been an increasing interest in utilizing body composition phenotype as an additional indicator of cancer prognosis. Because the burden of sarcopenia and obesity are concurrent, they can be expected to have a combined impact on health outcomes in several clinical settings, including cancer.⁶

As the prevalence of sarcopenic obesity with poor prognosis is rapidly increasing in cancer patients, in this review we discuss definitions, prevalence, mechanisms and management strategies for sarcopenic obese patients in oncology. This review aims to provide clinician's with additional evidence helping them to make rational decisions that will improve patients' outcome.

Identification of sarcopenic obesity and diagnostic criteria

Sarcopenic obesity has been identified using various definitions and diagnostic criteria. Screening for sarcopenic obesity is based on the simultaneous presence of increased BMI or waist circumference with ethnicity-specific cut-offs and surrogate parameters of sarcopenia (clinical symptoms, validated questionnaires -SARC-F in the elderly). In addition, altered body composition is required to make a definitive diagnosis.^{9,10}

Many studies have investigated the prevalence of sarcopenic obesity in different cohorts of cancer patients, including oropharyngeal¹¹, lung^{12,13}, gastrointestinal^{14,15-24}, liver and pancreatic^{25,26}, urinary²⁷⁻²⁹, breast³⁰, melanoma³¹ and lymphoma.³² On the other hand, the lack of uniform diagnostic criteria for sarcopenic obesity hampers the identification of patients and the assessment of associated outcomes and, consequently, negatively affects the development of prevention and treatment strategies for sarcopenic obesity. The prevalence of sarcopenic obesity in studies that include cancer patients varies from 1-29% in studies of patients in all BMI categories and from 15% to 36% in studies of overweight/obese patients.⁶ The lowest prevalence of sarcopenic obesity is found in early disease stages and the highest in locally advanced or metastatic disease.⁶ Heterogeneity in diagnostic criteria between studies, as well as the metabolic impact of different cancer types,

other patient characteristics such as ethnicity, and concurrent comorbidities, limit interpretation of results. In addition, The European Society for Clinical Nutrition and Metabolism (ESPEN) and the European Association for the Study of Obesity (EASO) confirmed heterogeneity in definition and diagnostic approaches for sarcopenic obesity, due to different definition of obesity and sarcopenia, differences in methodologies to assess body composition and function, as well as in the applied references values for variables used.⁹ Regardless of this variability, most studies report that sarcopenic obesity is an important problem in cancer patients and a negative prognostic factor.

Commonly used technics in oncology setting

Various techniques and body composition parameters with different cut off as well as muscle function parameters have been used to identify sarcopenic obesity. Body composition is traditionally measured using Dual Energy X-ray Absorptiometry (DEXA) or Bioelectrical Impedance Analysis (BIA) but is known to have some limitations.⁹ Currently, computed tomography (CT) and magnetic resonance imaging (MRI) are considered the gold standard methods. Both CT and MRI are not routinely used to assess sarcopenia and obesity due to high costs and radiation concerns for CT.^{33,34} CT should be used when possible (e.g., in patients undergoing a scan for diagnostic reasons in oncology).⁹ In cancer patients, the CT scan provides the highest available precision in determining body composition parameters by measuring the cross-sectional area of total skeletal muscle at the third lumbar vertebra (L3), which correlates strongly with total body skeletal muscle mass.³⁵

The DEXA method, which is considered inexpensive, is the most accurate method for measuring appendicular muscle mass, and exposes the patient to minimal radiation, but is not widely available. The BIA method is an alternative, inexpensive, and readily available method, but results are easily confounded by various factors, especially fluid status.³⁴ All these techniques provide anatomic information about the patient but not functional information, because loss of muscle function is also required to diagnose sarcopenia.³⁶ Therefore, the diagnostic process must include a direct assessment of altered skeletal muscle function parameters along with altered body composition. Thereafter, individuals with a positive di-

TABLE 1. Selected criteria to identify sarcopenic obesity. Altered skeletal muscle function parameters considering muscle strength and physical performance and altered body composition parameters should be present to assess sarcopenic obesity

SCREENING	DIAGNOSIS	STAGES
High BMI and WC (based on ethnic cut-points)	Altered skeletal muscle strength (HGS, chair stand test)	STAGE 1: Without complications
Surrogate markers of sarcopenia: (clinical symptoms or validated questionnaires' e.g. SARC-F)	Altered body composition (increased FM, decrease MM)	STAGE 2: One or more complications attributable to sarcopenic obesity

BMI = body mass index; FM = fat mass; HGS = hand grip strength; MM = muscle mass; SARC-F = strength, assistance in walking, rise from a chair, climb stairs, and falls; WC = waist circumference;

agnosis should be classified into two stages: Stage I, when no clinical complications are present, and Stage II, with clinical complications such as chronic disease (e.g. cancer), dietary events (weight loss, decreased food intake), immobility, falls, and other complaints associated with altered body composition and muscle function.⁹ All procedures are summarized in Table 1.

Biological pathways leading to sarcopenic obesity

The biological pathway leading to sarcopenic obesity includes changes in body composition related to ageing, hormonal changes, the interplay between metabolism and inflammation, environmental factors such as poor nutrition and lack of exercise and chronic diseases.³⁷⁻⁴⁰ This results in a decrease in oxidative capacities, mitochondrial number, atrophy of fast type II muscle fibres and neurodegeneration, decrease in protein synthesis and increase muscle protein degradation.⁴¹

Metabolic disfunctions

Both, skeletal muscle mass and adipose tissue interplay with several cancers at metabolic levels.⁴²⁻⁴⁵ Few studies have investigated the pathway between sarcopenia, obesity and cancer. The mechanisms involved in pathogenesis of metabolic imbalances associated with obesity are in part common with pathway modulating cancer related sarcopenia.⁵ Inflammation promoted by cancer and/or inadequate intake of essential nutrients could contribute to the presence of fatigue and decrease in physical activity and mobility of cancer patients.⁶

Physical inactivity can lead to skeletal muscle loss by reduced protein anabolic pathway and activation of proteolytic pathway.^{5,6} In addition, inadequate food intake can also impair muscle anabolic pathway due to low omega -3 (n-3) fatty

acid intake. Namely, it was demonstrated that low level of n-3 fatty acids is associated with loss of muscle mass and skeletal muscle fat infiltration or myosteatosys.⁴⁶ In addition, atrophy of fast type II muscle fibre and switch to slow type I muscle fibre increase the lipid deposition into the muscle.⁶ Importantly, myosteatosys is associated with metabolic muscle disfunction and muscle function loss and is widespread in cancer associated malnourished patients.^{47,48} A vicious cycle between myocytes and adipocytes is responsible for sarcopenic obesity. Specifically, adipose tissue inflammation and dysfunction leads to overproduction of fatty acids which in combination with low oxidation capacity of skeletal muscle stimulate the formation of intramyocellular lipid (IMCL).⁴⁹ This process blocks the translocation of glucose transporter type 4 (GLUT4) to the surface of the muscle fiber and therefore hampers uptake of glucose by skeletal muscle resulting in a decrease of glucose utilization and increase of fatty acid oxidation in mitochondria, which leads to impaired insulin sensitivity of skeletal muscle, inhibition of mitochondrial respiration, increase in reactive oxygen species formation (ROS), myocyte toxicity, inflammation and finally sarcopenia.^{5,6} Various forms of fat accumulation in skeletal muscle have been associated with insulin resistance, mitochondrial dysfunction and decreased muscle contracting force.⁵⁰ Based on these mechanisms, myosteatosys is a potentially important factor in sarcopenic obesity in the cancer setting, which could contribute to further muscle dysfunction in sarcopenic obese cancer patients and is an independent predictor of reduced survival in cancer patients.^{47,51} Additionally, ectopic fat deposition surrounding muscle accelerate proteolysis in muscle tissue leading to further muscle loss and worsen outcome.⁴⁷

Another consequence of insulin resistance is the reduction in the uptake of amino acids by muscle cells, altering the balance of protein synthesis/degradation in favour of proteolysis. It is proposed

that the amino acids released by muscle proteolysis in sarcopenia contribute to the supply of tumor growth.⁸

Hormonal imbalances

Furthermore, cancer is associated with an alteration in hormones that severely affects skeletal muscle and fat metabolism.⁶ The body composition of cancer patients is associated with insulin, insulin resistance, and the hormone ghrelin, the levels of which are modulated in obese patients and affect skeletal muscle metabolism. In addition, increased levels of stress hormones and a decrease in androgens and estrogens affect the anabolic and catabolic conditions for muscle protein metabolism and lead to alterations in the production and metabolism of anabolic hormones (growth hormone, insulin-like growth factor (IGF-1)) that may result in a sarcopenic obese phenotype.^{52,53} Increasing insulin resistance is associated with an increase in intramyocellular fat mass and loss of muscle function.⁵⁴

Cytokine imbalances

The systemic inflammatory condition in sarcopenic obesity as well as the altered expression of myokines and adipokines are also involved in carcinogenesis. Skeletal muscle and adipose tissue are considered endocrine organs due to release anti-inflammatory myokines and pro-inflammatory cytokines, respectively.⁵⁵ Myokines are proteins released by muscle cells in response to contractions. They play autocrine, paracrine, and endocrine roles in many exercise-induced adaptations (e.g., muscle hypertrophy and cancer protection).^{55,56} The release of pro- and anti-inflammatory cytokines by adipose and muscle tissue has a strong influence on skeletal muscle and adipose tissue metabolism and is involved in various cancer related changes in body composition.⁵ Dysregulation of pro- and anti-inflammatory cytokines is responsible for muscle intracellular adipose tissue. They contribute to the secretion of myostatin a negative regulator of muscle mass secreted by skeletal muscle cells, tumor necrosis factor α (TNF- α), pro-inflammatory interleukin -6 (IL-6), interleukin -1 β (IL-1 β), mononuclear chemoattractant protein-1 (MCP-1), and downregulate the secretion of anti-inflammatory adiponectin, leading to lipotoxicity and insulin resistance.^{8,37,57-59} Inflammatory cytokines directly affect skeletal muscle and accelerate muscle proteins degradation and apoptosis and induces muscle tissue reduction and fat tissue

accumulation.^{5,6,8} Levels of IL -6 and TNF- α are further increased by the hormone leptin, reducing the anabolic pathway of IGF-1 and enhancing lipotoxicity. The cytokine-like hormone leptin is a classic adipokine that is secreted by adipocytes, its blood concentration correlates with triglyceride accumulation in adipocytes.⁶⁰ In addition to this, the impaired secretion of skeletal muscle anti-inflammatory myokines such as interleukin -15 (IL-15), irisin, muscle derived IL-6 accelerate muscle atrophy and disfunction.^{8,56,59,61}

All these cytokines are known to be involved in several cancer induced alteration of body composition.⁶² Altered fat metabolism promotes inflammation, having an important role in cancer and non-cancer muscle wasting⁶³ creating a vicious cycle for sarcopenic obesity, leading to morbidity and mortality.

Sarcopenic obesity and carcinogenesis, therefore, are mediated by mechanisms, such as insulin resistance, adiposity, proteolysis, myosteosis, inflammation, oxidative stress, imbalance of adipokines and myokines (Figure 1).

Therapeutic strategies

Patients with cancer and sarcopenic obesity have several specific adverse clinical outcomes, including higher risk of dose-limiting toxicity, surgical complications, prolonged hospitalisation, physical disability, and shorter survival. This was demonstrated for several cancers.⁶ Chemotherapy has been shown to alter body composition by reducing lean mass, thus favouring the development of sarcopenic obesity.⁶⁴ Low muscle mass and strength is common in any cancer stage and is clearly considered an independent predictor for cancer progression, making it a preferred target in the treatment of sarcopenic obesity. On the other hand, obesity is not univocally associated with worse outcome in cancer patients regardless of the cancer type.⁶⁵ Although obesity is considered an important risk factor for the development of various cancers, the presence of moderate obesity paradoxically appears to be a protective factor that may improve response to treatment and consequently survival in patients but there are conflicting and controversial results.⁶⁶

Several therapeutic strategies, exercise and nutritional exists to counteract sarcopenic obesity. Prado *et al.* have shown that poor nutritional status in cancer is primarily manifested by a severe loss of muscle mass, which can occur at any stage

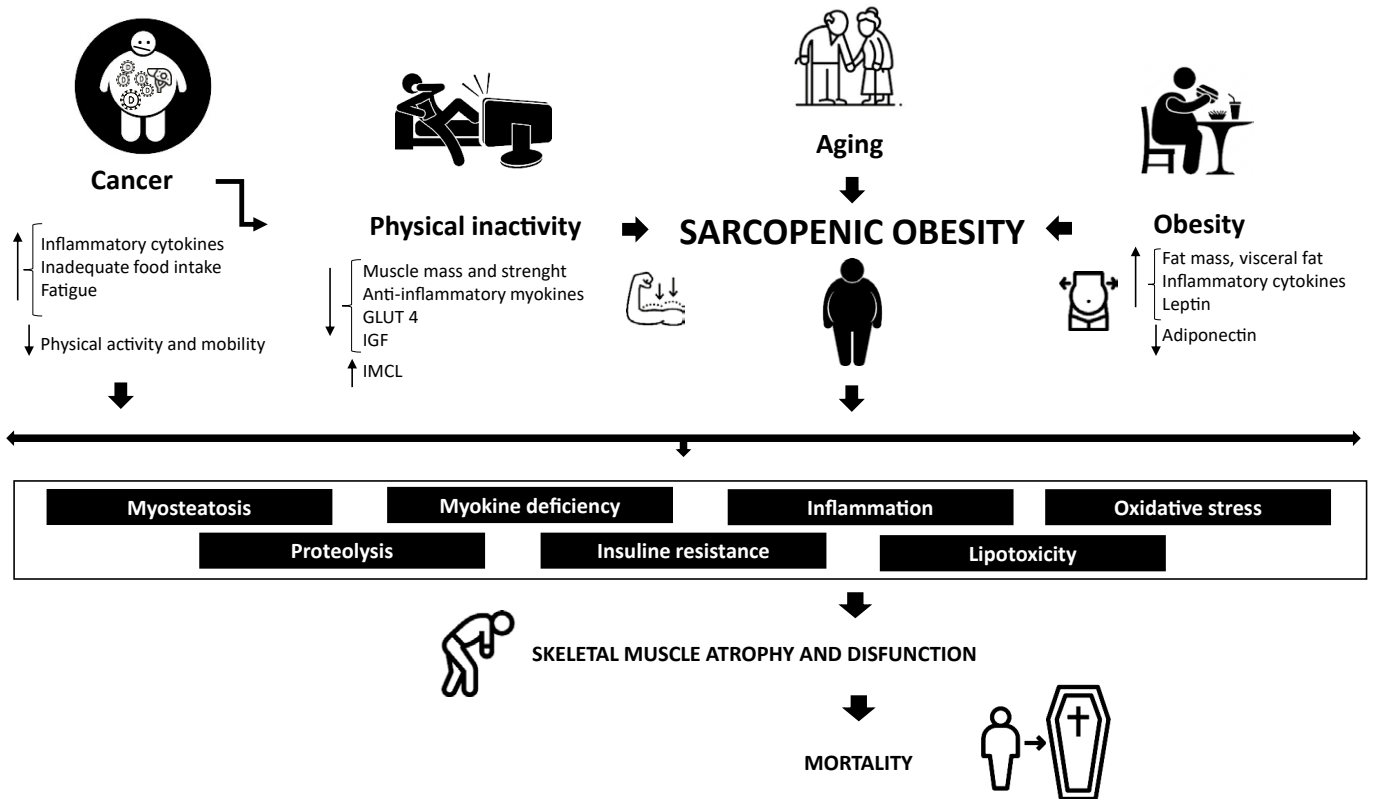


FIGURE 1. Main pathophysiological mechanisms in cancer patients with sarcopenic obesity. Body composition (low skeletal muscle mass and strength, increase in fat mass), inflammation, insulin resistance, myosteatosi s, myokine dysregulation, and oxidative stress in sarcopenic obese cancer patients significantly induce muscle proteolysis, leading to muscle wasting and dysfunction and premature mortality.

(from curative to palliative treatment) and often co-exists with obesity. They have addressed the role of diet in preventing and reversing sarcopenia in cancer patients, which may also apply to sarcopenic obesity.⁶⁷ Nutritional strategies comprise the importance of adequate intake of macro- and micronutrients, including high-quality proteins, branched-chain amino acids (leucine), β -hydroxy- β -methylbutyrate, glutamine, carnitine, creatine, fish oil/eicosapentanoic acid (EPA and DHA), vitamins/minerals (e.g., vitamin D), and multimodal approaches (diet, exercise, and medications) to counteract low muscle mass in cancer.

Moreover, physical activity could be an important and effective treatment strategy to reverse sarcopenia by promoting insulin sensitivity, reducing oxidative stress and inflammation, and stimulating mitochondrial biosynthesis. Both resistance training and aerobic exercise have been shown to improve muscle mass and physical performance.^{68,69} We note that standard treatment recommendations derived from studies in the elderly and certain diseases may not be applicable to cancer patients due to fatigue or pain. However,

many intervention studies of physical activity in cancer indicate some benefit of exercise for muscle strength and endurance.⁷⁰ In addition, cancer obese individuals, who exercise more and are not insulin resistant or hypertensive might then have a lower mortality risk.⁸

Another effective treatment for sarcopenic obesity in older adults and cancer patients is skeletal muscle electrostimulation. It causes contraction of muscle fibres via neuromuscular activation and can induce a change in body composition.⁷¹ Whole-body vibration therapy has been shown to significantly increase muscle strength and function in older adults.⁷² Further clinical studies are needed to verify its efficacy in clinical practise.

Conclusions

The prevalence of sarcopenic obesity is considered a novel factor of great clinical relevance in cancer patients, leading to postoperative complications, worse functional status, and shorter survival possibly mediated by interactions among patho-

physiological mechanisms (inflammation, insulin resistance, dysregulation of myokines and pro-inflammatory cytokines). Specific prevention and treatment strategies are needed to address sarcopenic obesity in cancer patients. One of the major challenges in prevention strategies is to maintain skeletal muscle mass and function and reduce fat mass, because the combination of decreasing skeletal muscle mass and increasing fat mass leads to physical limitations that worsen the prognosis for chronic disease, including cancer. Exercise and proper nutrition are two key components in the prevention and treatment of sarcopenic obesity, but effective interventions should be explored for cancer patients.^{3,4,6,56,73} The key question is how to maintain muscle anabolism in an energy deficit situation to avoid a high percentage of weight loss in the form of lean mass in this muscle loss prone population.

The underestimated prevalence of sarcopenic obesity in cancer are the consequence of the lack of standard methods and definitions used in previous studies. Therefore, further studies need to focus on screening sarcopenic obesity in cancer patients, and additional studies are needed to clarify the pathogenesis of sarcopenic obesity, with emphasis on identifying new markers.

In conclusion, the development of standardised diagnostic criteria is urgently needed. Up to now the identification of sarcopenia by measuring muscle mass and strength as a physical function has been done only in few studies, while in all others muscle mass was used as the only criteria.

ESPEN and EASO have launched an initiative to reach expert consensus on diagnostic procedures that include an assessment of skeletal muscle function followed by an assessment of body composition. Individuals with sarcopenic obesity should be classified into stages 1 and 2 based on clinical complications associated with body composition or muscle dysfunction. The proposed definition should be implemented in routine clinical practice. In addition, validation and prospective follow-up studies and secondary analyses of existing cohorts are proposed and encouraged by ESPEN and EASO.⁹

References

- Baumgartner RN. Body composition in healthy aging. *Ann N Y Acad Sci* 2000; **904**: 437-48. doi: 10.1111/j.1749-6632.2000.tb06498.x
- Barazzoni R, Bischoff SC, Boirie Y, Busetto L, Cederholm T, Dicker D, et al. Sarcopenic obesity: Time to meet the challenge. *Clin Nutr* 2018; **37(6 Pt A)**: 1787-93. doi: 10.1016/j.clnu.2018.04.018
- Gao Q, Mei F, Shang Y, Hu K, Chen F, Zhao L, et al. Global prevalence of sarcopenic obesity in older adults: a systematic review and meta-analysis. *Clin Nutr* 2021; **40**: 4633-41. doi: 10.1016/j.clnu.2021.06.009
- Gao Q, Hu K, Gao J, Shang Y, Mei F, Zhao L, et al. Prevalence and prognostic value of sarcopenic obesity in patients with cancer: a systematic review and meta-analysis. *Nutrition* 2022; **101**: 111704. doi: 10.1016/j.nut.2022.111704
- Gortan Cappellari G, Brasacchio C, Laudisio D, Lubrano C, Pivari F, Barrea L, et al. Sarcopenic obesity: what about in the cancer setting? *Nutrition* 2022; **98**: 111624. doi: 10.1016/j.nut.2022.111624
- Carneiro IP, Mazurak VC, Prado CM. Clinical implications of sarcopenic obesity in cancer. *Curr Oncol Rep* 2016; **18**: 62. doi: 10.1007/s11912-016-0546-5
- Atkins JL, Wannamethee SG. Sarcopenic obesity in ageing: cardiovascular outcomes and mortality. *Br J Nutr* 2020; **124**: 1102-13. doi: 10.1017/S0007114520002172
- Silveira EA, da Silva Filho RR, Spexoto MCB, Haghghatdoost F, Sarrafzadegan N, de Oliveira C. The role of sarcopenic obesity in cancer and cardiovascular disease: a synthesis of the evidence on pathophysiological aspects and clinical implications. *Int J Mol Sci* 2021; **22**: 4339. doi: 10.3390/ijms22094339
- Donini LM, Busetto L, Bischoff SC, Cederholm T, Ballesteros-Pomar MD, Batsis JA, et al. Definition and diagnostic criteria for sarcopenic obesity: ESPEN and EASO consensus statement. *Obes Facts* 2022; **15**: 321-35. doi: 10.1159/000521241
- Batsis JA, Villareal DT. Sarcopenic obesity in older adults: aetiology, epidemiology and treatment strategies. *Nat Rev Endocrinol* 2018; **14**: 513-37. doi: 10.1038/s41574-018-0062-9
- Chargi N, Bril SJ, Swartz JE, Wegner I, Willems SM, de Bree R. Skeletal muscle mass is an imaging biomarker for decreased survival in patients with oropharyngeal squamous cell carcinoma. *Oral Oncol* 2020; **101**: 104519. doi: 10.1016/j.oraloncology.2019.104519
- Kiss N, Beraldo J, Everitt S. Early skeletal muscle loss in non-small cell lung cancer patients receiving chemoradiation and relationship to survival. *Support Care Cancer* 2019; **27**: 2657-64. doi: 10.1007/s00520-018-4563-9
- Recio-Boiles A, Galeas JN, Goldwasser B, Sanchez K, Man LMW, Gentzler RD, et al. Enhancing evaluation of sarcopenia in patients with non-small cell lung cancer (NSCLC) by assessing skeletal muscle index (SMI) at the first lumbar (L1) level on routine chest computed tomography (CT). *Support Care Cancer* 2018; **26**: 2353-59. doi: 10.1007/s00520-018-4051-2
- Lodewick TM, van Nijnatten TJ, van Dam RM, van Mierlo K, Dello SA, Neumann UP, et al. Are sarcopenia, obesity and sarcopenic obesity predictive of outcome in patients with colorectal liver metastases? *HPB (Oxford)* 2015; **17**: 438-46. doi: 10.1111/hpb.12373
- Grotenhuis BA, Shapiro J, van Adrichem S, de Vries M, Koek M, Wijnhoven BP, et al. Sarcopenia/muscle mass is not a prognostic factor for short- and long-term outcome after esophagectomy for cancer. *World J Surg* 2016; **40**: 2698-704. doi: 10.1007/s00268-016-3603-1
- Kim YM, Kim JH, Baik SJ, Chun J, Yoon YH, Park H. Sarcopenia and sarcopenic obesity as novel risk factors for gastric carcinogenesis: a health checkup cohort study. *Front Oncol* 2019; **9**: 1249. doi: 10.3389/fonc.2019.01249
- Lou N, Chi CH, Chen XD, Zhou CJ, Wang SL, Zhuang CL, et al. Sarcopenia in overweight and obese patients is a predictive factor for postoperative complication in gastric cancer: a prospective study. *Eur J Surg Oncol* 2017; **43**: 188-95. doi: 10.1016/j.ejso.2016.09.006
- Nishigori T, Tsunoda S, Okabe H, Tanaka E, Hisamori S, Hosogi H, et al. Impact of sarcopenic obesity on surgical site infection after laparoscopic total gastrectomy. *Ann Surg Oncol* 2016; **23(Suppl 4)**: 524-31. doi: 10.1245/s10434-016-5385-y
- Palmela C, Velho S, Agostinho L, Branco F, Santos M, Santos MP, et al. Body composition as a prognostic factor of neoadjuvant chemotherapy toxicity and outcome in patients with locally advanced gastric cancer. *J Gastric Cancer* 2017; **17**: 74-87. doi: 10.5230/jgc.2017.17.e8
- Sugawara K, Yamashita H, Okumura Y, Yagi K, Yoshimura S, Kawasaki K, et al. Relationships among body composition, muscle strength, and sarcopenia in esophageal squamous cell carcinoma patients. *Support Care Cancer* 2020; **28**: 2797-803. doi: 10.1007/s00520-019-05110-7
- Zhang WT, Lin J, Chen WS, Huang YS, Wu RS, Chen XD, et al. Sarcopenic obesity is associated with severe postoperative complications in gastric cancer patients undergoing gastrectomy: a prospective study. *J Gastrointest Surg* 2018; **22**: 1861-69. doi: 10.1007/s11605-018-3835-5

22. Giani A, Famularo S, Riva L, Tamini N, Ippolito D, Nespoli L, et al. Association between specific presurgical anthropometric indexes and morbidity in patients undergoing rectal cancer resection. *Nutrition*. 2020; **75-76**: 110779. doi: 10.1016/j.nut.2020.110779
23. Han JS, Ryu H, Park U, Kim KW, Shin Y, Kim SO, et al. Association of body composition with long-term survival in non-metastatic rectal cancer patients. *Cancer Res Treat* 2020; **52**: 563-72. doi: 10.4143/crt.2019.249
24. Malietzis G, Currie AC, Athanasiou T, Johns N, Anyamene N, Glynne-Jones R, et al. Influence of body composition profile on outcomes following colorectal cancer surgery. *Br J Surg* 2016; **103**: 572-80. doi: 10.1002/bjs.10075
25. Gruber ES, Jomrich G, Tamandl D, Gnant M, Schindl M, Sahora K. Correction: Sarcopenia and sarcopenic obesity are independent adverse prognostic factors in resectable pancreatic ductal adenocarcinoma. *PLoS One* 2020; **15**: e0244896. doi: 10.1371/journal.pone.0244896. Erratum for: *PLoS One* 2019; **14**: e0215915. doi: 10.1371/journal.pone.0215915
26. Kobayashi A, Kaido T, Hamaguchi Y, Okumura S, Shirai H, Yao S, et al. Impact of sarcopenic obesity on outcomes in patients undergoing hepatectomy for hepatocellular carcinoma. *Ann Surg* 2019; **269**: 924-31. doi: 10.1097/SLA.0000000000002555
27. Kimura Y, Yamada M, Ohji S, Ishiyama D, Nishio N, Otake Y, et al. Presence of sarcopenic obesity and evaluation of the associated muscle quality in Japanese older men with prostate cancer undergoing androgen deprivation therapy. *J Geriatr Oncol* 2019; **10**: 835-8. doi: 10.1016/j.jgo.2019.03.017
28. Kocher NJ, Jafri S, Balabhadra S, Lehman E, Gardner J, Vijay K, et al. Is sarcopenia and sarcopenic obesity associated with clinical and pathological outcomes in patients undergoing radical nephroureterectomy? *Urol Oncol* 2018; **36**: 156. e17-156.e22. doi: 10.1016/j.urolonc.2017.12.004
29. Cushen SJ, Power DG, Murphy KP, McDermott R, Griffin BT, Lim M, et al. Impact of body composition parameters on clinical outcomes in patients with metastatic castrate-resistant prostate cancer treated with docetaxel. *Clin Nutr ESPEN* 2016; **13**: e39-45. doi: 10.1016/j.clnesp.2016.04.001
30. Rier HN, Jager A, Sleijfer S, van Rosmalen J, Kock MCJM, Levin MD. Low muscle attenuation is a prognostic factor for survival in metastatic breast cancer patients treated with first line palliative chemotherapy. *Breast* 2017; **31**: e9-15. doi: 10.1016/j.breast.2016.10.014
31. Heidelberger V, Goldwasser F, Kramkimel N, Jouinot A, Huillard O, Boudou-Rouquette P, et al. Sarcopenic overweight is associated with early acute limiting toxicity of anti-PD1 checkpoint inhibitors in melanoma patients. *Invest New Drugs* 2017; **35**: 436-41. doi: 10.1007/s10637-017-0464-x. Erratum in: *Invest New Drugs* 2017; **35**: 537. doi: 10.1007/s10637-017-0475-7
32. Jabbour J, Manana B, Zahreddine A, Saade C, Charafeddine M, Bazarbachi A, et al. Sarcopenic obesity derived from PET/CT predicts mortality in lymphoma patients undergoing hematopoietic stem cell transplantation. *Curr Res Transl Med* 2019; **67**: 93-9. doi: 10.1016/j.retram.2018.12.001
33. Cruz-Jentoft AJ, Bahat G, Bauer J, Boirie Y, Bruyère O, Cederholm T, et al. Writing group for the European Working Group on Sarcopenia in Older People 2 (EWGSOP2), and the Extended Group for EWGSOP2. Sarcopenia: revised European consensus on definition and diagnosis. *Age Ageing* 2019; **48**: 601. doi: 10.1093/ageing/afz046. Erratum for: *Age Ageing* 2019; **48**: 16-31. doi: 10.1093/ageing/afy169
34. Mei KL, Batsis JA, Mills JB, Holubar SD. Sarcopenia and sarcopenic obesity: do they predict inferior oncologic outcomes after gastrointestinal cancer surgery? *Perioper Med* 2016; **5**: 30. doi: 10.1186/s13741-016-0052-1
35. Prado CM, Heymsfield SB. Lean tissue imaging: a new era for nutritional assessment and intervention. *JPEN J Parenter Enteral Nutr* 2014; **38**: 940-53. doi: 10.1177/0148607114550189. Erratum in: *JPEN J Parenter Enteral Nutr* 2016; **40**: 742. doi: 10.1177/0148607116647919
36. Donini LM, Busetto L, Bauer JM, Bischoff S, Boirie Y, Cederholm T, et al. Critical appraisal of definitions and diagnostic criteria for sarcopenic obesity based on a systematic review. *Clin Nutr* 2020; **39**: 2368-88. doi: 10.1016/j.clnu.2019.11.024
37. Ji T, Li Y, Ma L. Sarcopenic obesity: an emerging public health problem. *Aging Dis* 2022; **13**: 379-88. doi: 10.14336/AD.2021.1006
38. Batsis JA, Villareal DT. Sarcopenic obesity in older adults: aetiology, epidemiology and treatment strategies. *Nat Rev Endocrinol* 2018; **14**: 513-37. doi: 10.1038/s41574-018-0062-9
39. Lynch GM, Murphy CH, Castro EM, Roche HM. Inflammation and metabolism: the role of adiposity in sarcopenic obesity. *Proc Nutr Soc* 2020; **16**: 1-13. doi: 10.1017/S0029665120007119
40. Guo A, Li K, Xiao Q. Sarcopenic obesity: myokines as potential diagnostic biomarkers and therapeutic targets? *Exp Gerontol* 2020; **139**: 111022. doi: 10.1016/j.exger.2020.111022
41. Murton AJ, Marimuthu K, Mallinson JE, Selby AL, Smith K, Rennie MJ, et al. Obesity appears to be associated with altered muscle protein synthetic and breakdown responses to increased nutrient delivery in older men, but not reduced muscle mass or contractile function. *Diabetes* 2015; **64**: 3160-71. doi: 10.2337/db15-0021
42. Abbass T, Dolan RD, Laird BJ, McMillan DC. The relationship between imaging-based body composition analysis and the systemic inflammatory response in patients with cancer: A systematic review. *Cancers* 2019; **11**: 1304. doi: 10.3390/cancers11091304
43. Fouladiun M, Körner U, Bosaeus I, Daneryd P, Hylander A, Lundholm KG. Body composition and time course changes in regional distribution of fat and lean tissue in unselected cancer patients on palliative care – correlations with food intake, metabolism, exercise capacity, and hormones. *Cancer* 2005; **103**: 2189-98. doi: 10.1002/cncr.21013
44. Baracos VE, Martin L, Korc M, Guttridge DC, Fearon KCH. Cancer-associated cachexia. *Nat Rev Dis Primers* 2018; **4**: 17105. doi: 10.1038/nrdp.2017.105
45. Baracos VE, Arribas L. Sarcopenic obesity: hidden muscle wasting and its impact for survival and complications of cancer therapy. *Ann Oncol* 2018; **29**(Suppl 2): ii1-9. doi: 10.1093/annonc/mdx810
46. Murphy RA, Mourtzakis M, Chu QS, Reiman T, Mazurak VC. Skeletal muscle depletion is associated with reduced plasma (n-3) fatty acids in non-small cell lung cancer patients. *J Nutr* 2010; **140**: 1602-6. doi: 10.3945/jn.110.123521
47. Martin L, Gioulbasanis I, Senesse P, Baracos VE. Cancer-associated malnutrition and CT-defined sarcopenia and myosteatosis are endemic in overweight and obese patients. *JPEN J Parenter Enteral Nutr* 2020; **44**: 227-38. doi: 10.1002/jpen.1597
48. Correa-de-Araujo R, Addison O, Miljkovic I, Goodpaster BH, Bergman BC, Clark RV, et al. Myosteatosis in the context of skeletal muscle function deficit: an interdisciplinary workshop at the National Institute on Aging. *Front Physiol* 2020; **11**: 963. doi: 10.3389/fphys.2020.00963
49. Gemmink A, Goodpaster BH, Schrauwen P, Hesselink MKC. Intramyocellular lipid droplets and insulin sensitivity, the human perspective. *Biochim Biophys Acta Mol Cell Biol Lipids* 2017; **1862**(10 Pt B): 1242-9. doi: 10.1016/j.bbalip.2017.07.010
50. Maltais A, Almérás N, Lemieux I, Tremblay A, Bergeron J, Poirier P, et al. Trunk muscle quality assessed by computed tomography: association with adiposity indices and glucose tolerance in men. *Metabolism* 2018; **85**: 205-12. doi: 10.1016/j.metabol.2018.04.003
51. Rollins KE, Tewari N, Ackner A, Awwad A, Madhusudan S, Macdonald IA, et al. The impact of sarcopenia and myosteatosis on outcomes of unresectable pancreatic cancer or distal cholangiocarcinoma. *Clin Nutr* 2016; **35**: 1103-9. doi: 10.1016/j.clnu.2015.08.005
52. Knapp ML, al-Sheibani S, Riches PG, Hanham IW, Phillips RH. Hormonal factors associated with weight loss in patients with advanced breast cancer. *Ann Clin Biochem* 1991; **28** (Pt 5): 480-6. doi: 10.1177/000456329102800510
53. Crown AL, Cottle K, Lightman SL, Falk S, Mohamed-Ali V, Armstrong L, et al. What is the role of the insulin-like growth factor system in the pathophysiology of cancer cachexia, and how is it regulated? *Clin Endocrinol* 2002; **56**: 723-33. doi: 10.1046/j.1365-2265.2002.01540.x
54. Yoshikawa T, Noguchi Y, Doi C, Makino T, Nomura K. Insulin resistance in patients with cancer: relationships with tumor site, tumor stage, body-weight loss, acute-phase response, and energy expenditure. *Nutrition* 2001; **17**: 590-3. doi: 10.1016/s0899-9007(01)00561-5
55. Hoffmann C, Weigert C. Skeletal muscle as an endocrine organ: the role of myokines in exercise adaptations. *Cold Spring Harb Perspect Med* 2017; **7**: a029793. doi: 10.1101/cshperspect.a029793
56. Jurdana M. Physical activity and cancer risk. Actual knowledge and possible biological mechanisms. *Radiol Oncol* 2021; **55**: 7-17. doi: 10.2478/raon-2020-0063
57. Rivas DA, McDonald DJ, Rice NP, Haran PH, Dolnikowski GG, Fielding RA. Diminished anabolic signaling response to insulin induced by intramuscular lipid accumulation is associated with inflammation in aging but not obesity. *Am J Physiol Regul Integr Comp Physiol* 2016; **310**: R561-9. doi: 10.1152/ajpregu.00198.2015

58. Yamauchi T, Kamon J, Minokoshi Y, Ito Y, Waki H, Uchida S, et al. Adiponectin stimulates glucose utilization and fatty-acid oxidation by activating AMP-activated protein kinase. *Nat Med* 2002; **8**: 1288-95. doi: 10.1038/nm788
59. Hong SH, Choi KM. Sarcopenic obesity, insulin resistance, and their implications in cardiovascular and metabolic consequences. *Int J Mol Sci* 2020; **21**: 494. doi: 10.3390/ijms21020494
60. Hamrick MW. Role of the cytokine-like hormone leptin in muscle-bone cross-talk with aging. *J Bone Metab* 2017; **24**: 1-8. doi: 10.11005/jbm.2017.24.1.1
61. Kurdiova T, Balaz M, Vician M, Maderova D, Vlcek M, Valkovic L, et al. Effects of obesity, diabetes and exercise on Fndc5 gene expression and irisin release in human skeletal muscle and adipose tissue: in vivo and in vitro studies. *J Physiol* 2014; **592**: 1091-107. doi: 10.1113/jphysiol.2013.264655
62. Johns N, Greig C, Fearon KC. Is tissue cross-talk important in cancer cachexia? *Crit Rev Oncog* 2012; **17**: 263-76. doi: 10.1615/critrevoncog.v17.i3.40
63. Argilés JM, Busquets S, Stemmler B, López-Soriano FJ. Cancer cachexia: understanding the molecular basis. *Nat Rev Cancer* 2014; **14**: 754-62. doi: 10.1038/nrc3829
64. Prado CM, Baracos VE, McCargar LJ, Reiman T, Mourtzakis M, Tonkin K, et al. Sarcopenia as a determinant of chemotherapy toxicity and time to tumor progression in metastatic breast cancer patients receiving capecitabine treatment. *Clin Cancer Res* 2009; **15**: 2920-6. doi: 10.1158/1078-0432.CCR-08-2242
65. Petrelli F, Cortellini A, Indini A, Tomasello G, Ghidini M, Nigro O, et al. Association of obesity with survival outcomes in patients with cancer: a systematic review and meta-analysis. *JAMA Netw Open* 2021; **4**: e213520 doi: 10.1001/jamanetworkopen.2021.3520
66. Gallo M, Adinolfi V, Barucca V, Prinzi N, Renzelli V, Barrea L, et al. Expected and paradoxical effects of obesity on cancer treatment response. *Rev Endocr Metab Disord* 2021; **22**: 681-702. doi: 10.1007/s11154-020-09597-y
67. Prado CM, Purcell SA, Laviano A. Nutrition interventions to treat low muscle mass in cancer. *J Cachexia Sarcopenia Muscle* 2020; **11**: 366-80. doi: 10.1002/jcsm.12525
68. Argilés JM, Busquets S, López-Soriano FJ, Costelli P, Penna F. Are there any benefits of exercise training in cancer cachexia? *J Cachexia Sarcopenia Muscle* 2012; **3**: 73-6. doi: 10.1007/s13539-012-0067-5
69. Stene GB, Helbostad JL, Balstad TR, Riphagen II, Kaasa S, Oldervoll LM. Effect of physical exercise on muscle mass and strength in cancer patients during treatment--a systematic review. *Crit Rev Oncol Hematol* 2013; **88**: 573-93. doi: 10.1016/j.critrevonc.2013.07.001
70. Galvão DA, Newton RU. Review of exercise intervention studies in cancer patients. *J Clin Oncol* 2005; **23**: 899-909. doi: 10.1200/JCO.2005.06.085
71. Poggiogalle E, Parrinello E, Barazzoni R, Busetto L, Donini LM. Therapeutic strategies for sarcopenic obesity: a systematic review. *Curr Opin Clin Nutr Metab Care* 2021; **24**: 33-41. doi: 10.1097/MCO.0000000000000714
72. Verschuere SM, Bogaerts A, Delecluse C, Claessens AL, Haentjens P, Vanderschueren D, et al. The effects of whole-body vibration training and vitamin D supplementation on muscle strength, muscle mass, and bone density in institutionalized elderly women: a 6-month randomized, controlled trial. *J Bone Miner Res* 2011; **26**: 42-9. doi: 10.1002/jbmr
73. Gyergyek A, Rotovnik Kozjek N, Klen, J. Monitoring the effect of perioperative nutritional care on body composition and functional status in patients with carcinoma of gastrointestinal and hepatobiliary system and pancreas. *Radiol Oncol* 2023; **57**: 371-9. doi: 10.2478/raon-2023-0028

The influence of anaesthesia on cancer growth

Iztok Potocnik^{1,2}, Milena Kerin-Povsic¹, Jasmina Markovic-Bozic^{2,3}

¹ Department of Anaesthesiology and Intensive Care, Institute of Oncology Ljubljana, Ljubljana, Slovenia

² Faculty of Medicine, University of Ljubljana, Ljubljana, Slovenia

³ Department of Anaesthesiology and Surgical Intensive Therapy, University Medical Centre Ljubljana, Ljubljana, Slovenia

Radiol Oncol 2024; 58(1): 9-14.

Received 10 September 2023

Accepted 22 November 2023

Correspondence to: Assit. Prof. Iztok Potočnik, M.D., Ph.D., Department of Anaesthesiology and Intensive Care, Institute of Oncology Ljubljana, Zaloška 2, SI-1000 Ljubljana, Slovenia. E-mail: vpotocnik@onko-i.si

Iztok Potocnik and Jasmina Markovic-Bozic contributed equally to this work.

Disclosure: No potential conflicts of interest were disclosed.

This is an open access article distributed under the terms of the CC-BY license (<https://creativecommons.org/licenses/by/4.0/>).

Background. Oncological patients make up a large proportion of all surgical patients. Through its influence on the patient's inflammatory and immune system, the choice of anaesthetic technique has an indirect impact on the health of the individual patient and on public health. Both the specific and the non-specific immune system have a major influence on the recurrence of carcinomas. The pathophysiological basis for growth and metastasis after surgery is the physiological response to stress. Inflammation is the organism's universal response to stress. Anaesthetics and adjuvants influence perioperative inflammation in different ways and have an indirect effect on tumour growth and metastasis. *In vitro* studies have shown how individual anaesthetics influence the growth and spread of cancer, but clinical studies have not confirmed these results. Nevertheless, it is advisable to use an anaesthetic that has shown lesser effect on the growth of cancer cells *in vitro*.

Conclusions. In this review, we focus on the area of the effects of anaesthesia on tumour growth. The field is still relatively unexplored, there are only few clinical prospective studies and their results are controversial. Based on the review of new research findings we report on recommendations about anaesthetics and anaesthetic techniques that might be preferable for oncological surgical procedures.

Key words: cancer growth; anaesthesia; inflammation

Introduction

Perioperative morbidity and mortality have decreased over time due to the use of modern anaesthesia and surgical techniques. The question arises as to how we can influence long-term morbidity and mortality in cancer patients. Published studies have shown that an appropriate anaesthetic technique (AT) can influence the recurrence and spread of the disease.^{1,2} Oncological patients make up a large proportion of all surgical patients, and their number increases by more than 25% every five years. Two thirds of all cancer patients require at least one operation during treatment. Therefore, the choice of AT has an indirect impact on the health of the individual patient and on public health.^{1,2}

Metastases develop because cancer cells evade the immune system, multiply, and spread to other tissues and organs.³ It has been shown that anaesthesia influences the spread of cancer through the immune system.^{1,2} Both specific and non-specific immune systems have a major influence on metastasis.^{1,2} During the perioperative period, the organism is exposed to many processes that can affect the metastasis. The most important of these are inflammation, anaesthetics, hypothermia and the transfusion of blood products.¹⁻³

Pathophysiology of metastasis

The pathophysiological basis for the growth and metastasis of carcinomas after surgery is the reac-

tion to stress. The universal reaction of the organism to stress is inflammation. The organism reacts to all harmful stimuli with inflammation. During an operation, both the systemic inflammatory reaction and the ischaemia/reperfusion reaction are triggered.⁴ In addition, severe tissue damage occurs, which is also a cause of the stress reaction and inflammation. Inflammatory factors such as interleukins (ILs) and prostaglandins (PGs) are released into the bloodstream as a result of the non-specific inflammatory response. To a certain extent, they have the task of protecting the organism from harmful stimuli, but if the reaction is too strong, additional tissue damage occurs.

When inflammation escalates a vicious circle may be triggered. The most important inflammatory factors that are released and influence the growth of tumour cells are interleukin-6 (IL-6) and prostaglandin E2 (PGE2).⁵ These factors influence the reduced activity of natural killer cells, so that cellular immunity is weakened, and the tumour cells can evade the immune system and multiply. As a result of immunosuppression, certain hormones (catecholamines, PGs and growth factors) are released, which also influence the growth and metastasis of carcinomas. Tumour cells have mechanisms to increase their insensitivity to hypoxia. Due to tissue hypoxia, certain genes are expressed in tumour cells. Hypoxia inducible factor 1-alpha (HIF-1 α) is released, which promotes angiogenesis, proliferation, and metastasis. High HIF-1 α levels are a predictive factor for long-term morbidity and mortality due to postoperative carcinoma growth.⁶

The impact of inflammation on metastasis

Inflammation is a universal physiological defence reaction of the organism that protects the body from harmful factors. It is triggered by the activation of the immune system and causes the elimination of harmful stimuli, prevents the spread of damage and repairs the affected tissue. It involves several reactions: vascular reaction (vasodilatation, exudation), cellular reaction (migration, adhesion, phagocytosis, degranulation) and connective tissue reaction (matrix formation, repair, angiogenesis).^{4,6,7} A distinction is made between non-specific and specific immunity: non-specific immunity is characterised by various cascade reactions and the production of inflammatory factors such as prostaglandins and cytokines. The product of specific immunity are antibodies that are directed pre-

cisely against a specific harmful stimulus such as carcinoma cells. Cellular immunity also includes natural killer cells, which ensure the death of harmful cells (tumour cells, bacteria, blood cells in transfusion derivatives).^{5,6} Both forms of specific immunity function and communicate with each other via signalling molecules. A harmful cell labelled with antibodies is easy prey for the natural killer cells. The inflammatory reaction must be precisely regulated.^{4,6,7} An excessive inflammatory response also damages the body's own tissue and causes postoperative complications. An excessive reaction is referred to as a systemic inflammatory response (SIRS).⁷

An inflammatory reaction is also triggered by tissue damage during the operation.⁸ Inflammation may promote the postoperative growth of any residual tumour and progression of metastasis.^{4,6} Therefore, the least possible invasive surgical technique should be used. There are three harmful perioperative reactions triggered by inflammation.^{8,9} The first harmful reaction is SIRS. The inflammatory event involves the entire organism. Many cytokines are released because their regulatory level is disturbed.⁷⁻¹¹ In severe inflammation, SIRS can lead to organ dysfunction and organ failure. SIRS complications include acute lung injury (ALI), acute renal failure (ARF), shock and multiple organ failure (MOF).^{10,11}

The second harmful reaction is the ischaemia/reperfusion reaction. When ischaemic tissue is reperfused, large amounts of reactive oxygen species (ROS) are released. If they are not neutralised and removed, they can cause tissue damage. The enzyme xanthine oxidase (XOX) plays an important role in this reaction. During ischaemia, it is formed in large quantities by the enzyme xanthine dehydrogenase (XDH) and breaks down purines. XOX remains inactive until sufficient oxygen is available. This happens when the tissue is supplied with blood again.⁷⁻¹¹ In addition, during ischaemia there is a decrease in the regeneration of adenosine triphosphate (ATP) from adenosine diphosphate (ADP). Due to the lack of oxygen, ADP is also reduced to adenosine monophosphate (AMP) in order to generate additional energy.⁷ After reperfusion and replenishment of the tissue with oxygen, XOX is activated, and part of the AMP is degraded to uric acid. During this process, electrons are released and transferred to oxygen to form ROS. If the ROS scavengers are unable to remove these, nearby cells are damaged, and an inflammatory reaction is triggered. It is initially localised, but if severe enough, it leads to SIRS.⁷

The third adverse perioperative reaction is called acute lung injury (ALI) and acute respiratory distress syndrome (ARDS). ARDS leads to cytokine release, damage to the pulmonary vascular endothelium, decreased surfactant production and alveolar surface tension, fluid accumulation and fibrosis. The mortality rate for ARDS is 20-50%.⁷⁻¹¹

The effect of anaesthetics and anaesthetic technique on inflammation and metastasis

The choice of anaesthetic and adjuvants primarily influences perioperative inflammation in various ways and has indirect effects on tumour growth and metastasis.¹²

Rational anaesthesia management has a major influence on the long-term surgical outcome.⁴ Anaesthetics affect the non-specific and specific inflammatory response, the immune cascades and consequently the production of cytokines and the function of inflammatory cells.¹³ For example, propofol increases the number of killer cells but reduces their cytotoxic activity, while sevoflurane increases the number of killer cells but reduces the number and activity of other immune cell types such as CD4 T-helper and CD-8 cytotoxic T-lymphocytes. The overall effect on the immune system and inflammation may depend on many factors, including the specific combination and dose of anaesthetic agents used.¹³

A single agent lowers the level of some cytokines and increases the level of others. Some cytokines are pro-inflammatory (TNF α , IL-1, IL-6, IL-8), while others are anti-inflammatory (IL-10). This further complicates the effect of cytokines. Studies have shown that cytokine levels in the blood increase immediately after induction of anaesthesia and even before surgery.¹⁴ Opioids reduce the inflammatory response because they reduce intracellular cyclic AMP, which is an important factor in stimulating IL-6 synthesis.¹⁵ In addition, neutrophils have opioid receptors on their membrane that inhibit their function.¹⁶

Pain also alters the immune response by increasing the number of activated lymphocytes and decreasing the number of inhibitory T cells and T helper cells. Inflammatory processes are particularly strongly activated in chronic pain.^{17,18}

Studies have shown that intravenous anaesthetics stimulate inflammatory cells to produce cytokines.¹⁹ Intravenous anaesthetics inhibit the polarisation and chemotaxis of neutrophils to a greater extent than volatile anaesthetics (VA).²⁰

Anaesthetics also influence proliferation, lymphocyte count and perioperative immunoglobulin levels in the blood.^{21,22} In addition to the choice of anaesthetic, different regional techniques (epidural, paravertebral anaesthesia) also influence perioperative inflammation depending on the anaesthetics used.^{23,24}

Transfusion of blood derivatives reduces the number of T-cytotoxic leukocytes, TNF production and macrophage chemotaxis.²⁵

Finally, the central nervous system also has an effect on perioperative stress and the immune response, which is the subject of psychoneuroimmunology.^{26,27} Thoughts and emotions also influence the immune system via centres in the brain. The hypothalamus plays a central role because it influences the sympathetic nervous system and the hypothalamic-pituitary-adrenal axis by altering catecholamine levels, corticosteroids, and opioids in the body.²⁷ The concentration of growth hormone and prolactin in the blood also changes.²⁸ All these processes have a significant influence on the function of the immune system. The immune system is inhibited and weakened in a stressful situation.²⁹

There are not many clinical, randomised studies that have investigated the direct influence of AT on tumour growth and metastasis after surgery. The results are often controversial. The studies published in recent years have not shown any advantages of different AT such as regional, general, or combined anaesthesia.³⁰⁻³³

VA modulate the inflammatory response and have a positive anti-inflammatory effect.^{34,35} However, it is not clear whether this also has a negative effect on tumour cells. There are observations that they have a pro-inflammatory effect and therefore accelerate metastasis. The molecular mechanism of this process is not known.³⁶ *In vitro*, they have shown a mild anti-inflammatory and thus protective effect, while increased levels of HIF-1 α have been observed *in vivo*.^{4,7} VA are thought to cause chemoresistance and attenuate the effect of adjuvant chemotherapy.^{1,2} *In vitro*, sevoflurane has been shown to promote inflammation via the nuclear factor kappa B (NF- κ B) pathway.³⁷

Propofol is known to have an anti-inflammatory effect, particularly in the central nervous system, where it prevents perioperative neuroinflammation.^{35,38} Propofol acts in the cell nucleus and influences the formation of NF- κ B. *In vitro* studies have also shown an effect on the transcription of ribonucleic acid (RNA) as well as anti-inflammatory and antioxidant effects. The antitumour effect

of propofol has not yet been confirmed with certainty, but it lowers HIF-1 α levels.¹⁻³ However, in triple-negative breast cancer cell lines, propofol increased the antitumour effect of doxorubicin and paclitaxel.³⁹ However, clinical studies have shown very controversial results.³⁹

According to published studies, ketamine and thiopental have a major impact on inflammation. They influence the function of the immune system by inhibiting NK cells.¹⁻³ Ketamine also increases the level of anti-apoptotic protein.^{2,3}

Anaesthesiologist is faced with the dilemma of whether to anaesthetise a carcinoma patient with total intravenous anaesthesia (TIVA) or with volatile induced and maintained anaesthesia (VIMA). Several studies have confirmed the anti-inflammatory effect of VA. In cardiac surgery, pre- and post-conditioning are used due to the proven anti-inflammatory and tissue-protective effect.⁴⁰ The positive effect of sevoflurane has also been demonstrated in liver surgery, where a strong inflammatory reaction is expected.^{41,42} It is also frequently used in intensive care medicine to sedate patients. It has been shown to have positive effects on the systemic inflammatory response of the organism and works very well in ARDS.⁴³ It is also used in lung surgery. During lung surgery, several reactions are triggered that lead to an excessive inflammatory response. Perioperative unilateral lung ventilation triggers an ischaemia/reperfusion reaction, which can cause additional damage to the lungs already mechanically damaged by the operation. Sevoflurane reduces the concentration of pro-inflammatory factors. Therefore, lung damage is also reduced, and fewer postoperative complications occur.^{9,44} Other studies have shown the pro-inflammatory effect of VA.^{45,46} From this it could be concluded that they cause the progression of cancer, but clinical studies have not confirmed this with certainty.

A recent meta-analysis of TIVA versus VA showed that 7,866 patients with breast, oesophageal or non-small lung cancer had improved recurrence-free survival after VIMA. In addition, studies that included 18,778 patients showed that overall survival was longer after VIMA than after TIVA.⁴⁷ However, there were no differences between the two techniques in terms of the presence of circulating tumour cells in breast cancer patients.⁴⁸ Furthermore, there were no effects on immune cells and cancer-regulating factors between the two AT in colorectal cancer surgery.⁴⁵

The use of regional anaesthesia indirectly reduces the progression of cancer by decreasing the

neuroendocrine response to surgery and reducing the use of opioids and VA.⁴⁹ In addition, recently published and ongoing studies suggest a highly beneficial direct effect of local anaesthetics on carcinoma.⁵⁰⁻⁵² Intraoperative intravenous lidocaine infusion has been associated with reduced intraoperative opioid use and improved overall survival in patients undergoing pancreatic cancer surgery.⁵³

Opioids have been shown to have an unfavourable effect on tumour growth *in vitro*.⁵⁴⁻⁵⁶ Several clinical studies have been published and show a complex relationship that depends on many factors, such as the type of opioid, the amount of opioid administered and adjuvants. The results of the studies are highly controversial but tend to favour a harmful effect of opioids.^{44,55} The different findings on the cancer risk of opioids are a line of research that needs to be pursued as they have major implications for clinical practice given the importance of opioid use in anaesthetic practice and pain management.

The exception is tramadol, which is supposed to protect the body against metastases. It does not inhibit the immune system like other opioids.⁵⁷ Unfortunately, tramadol is rarely used in oncology due to its weak analgesic effect and unpleasant side effects at higher doses.

There are also some studies in the field of anaesthetic adjuvants such as dexmedetomidine and clonidine. *In vitro* results indicated their unfavourable effect on the growth and spread of cancer, but clinical studies have not confirmed it.⁵⁸⁻⁶⁰ Studies have shown that dexmedetomidine has a positive effect on patients anaesthetised with sevoflurane, possibly because it reduces neuroinflammation.⁶¹ However, further studies are needed in this area.

However, there are also some studies on the use of other agents. Nonsteroidal anti-inflammatory drugs have potential anticancer effects.⁶² Beta-blockers affect cancer growth and spread by reducing the sympathetic stress response.⁶³ Dexamethasone reduces inflammation and the immune response by inhibiting NK cells and thus has an unfavourable effect, but low antiemetic doses are not thought to increase cancer growth and spread.⁶⁴ Oxygen causes ROS synthesis and oxidative stress and can induce various degrees of partial to complete transformation from epithelium to mesenchyme in cancer cells. Even if the primary tumours are surgically removed, the effects of hyperoxia on micrometastases and circulating cancer cells may promote cancer progression or recur-

rence. Therefore, it is necessary to use the lowest sufficient concentrations of oxygen.⁶⁵

Conclusions

Recent studies have shown that anaesthesia may play an important role in the growth and spread of cancer. Volatile anaesthetics have proinflammatory effects and can therefore accelerate metastasis. Propofol has an anti-inflammatory and antioxidant effect, causes less neuroinflammation and may have an antitumour effect. Regional anaesthesia plays an important role in reducing the likelihood of metastasis after surgery, as local anaesthetics have a protective effect on cancer recurrence. Opioids, except for tramadol, can accelerate cancer growth and spread and should be avoided or reduced perioperatively. Dexmedetomidine has no effect on the tumour, although it modulates inflammation.

In summary, there are still no clear answers to questions about the carcinogenicity of agents and techniques used during anaesthesia. The field needs further research.

References

- Sherwin A, Wall T, Buggy DJ. Anaesthesia and cancer recurrence. *UpToDate*. [Internet]. Wolters Kluwer. [cited 2023 Sep 4]. Available at: <https://www.uptodate.com/contents/anaesthesia-and-cancer-recurrence>
- Sessler DI, Riedel B. Anaesthesia and cancer recurrence: context for divergent study outcomes. *Anesthesiology* 2019; **130**: 3-5. doi: 10.1097/ALN.0000000000002506
- Lyden D, Ghajar CM, Correia AL, Aguirre-Ghisso JA, Cai S, Rescigno M, et al. Metastasis. *Cancer Cell* 2022; **40**: 787-91. doi: 10.1016/j.ccell.2022.07.010
- Margraf A, Ludwig N, Zarbock A, Rossaint J. Systemic inflammatory response syndrome after surgery: mechanisms and protection. *Anesth Analg* 2020; **131**: 1693-707. doi: 10.1213/ANE.0000000000005175
- Dinarello CA. Historical insights into cytokines. *Eur J Immunol* 2007; **37**(Suppl 1): S34-45. doi: 10.1002/eji.200737772
- Tavare AN, Perry NJ, Benzonana LL, Takata M, Ma D. Cancer recurrence after surgery: direct and indirect effects of anesthetic agents. *Int J Cancer* 2012; **130**: 1237-50. doi: 10.1002/ijc.26448
- Egger G. [Acute inflammation: basics, pathophysiology and clinical manifestations of non-specific immunity]. [German]. Wien, New York: Springer Verlag; 2005.
- Brøchner AC, Toft P. Pathophysiology of the systemic inflammatory response after major accidental trauma. *Scand J Trauma Resusc Emerg Med* 2009; **17**: 43. doi: 10.1186/1757-7241-17-43
- Potočnik I, Novak-Janković V, Šostarić M, Jerin A, Štupnik T, Skitek M, et al. Antiinflammatory effect of sevoflurane in open lung surgery with one-lung ventilation. *Croat Med J* 2014; **55**: 628-37. doi: 10.3325/cmj.2014.55.628
- Evans L, Rhodes A, Alhazzani W, Antonelli M, Coopersmith CM, French C, et al. Surviving sepsis campaign: international guidelines for management of sepsis and septic shock 2021. *Intensive Care Med* 2021; **47**: 1181-247. doi: 10.1007/s00134-021-06506-y
- Vincent JL. Update on surgical sepsis syndrome. *Br J Surg* 2017; **104**: e34-40. doi: 10.1002/bjs.10451
- Stevenson GW, Hall SC, Rudnick S, Seleny FL, Stevenson HC. The effect of anesthetic agents on the human immune response. *Anesthesiology* 1990; **72**: 542-52. doi: 10.1097/0000542-199003000-00024
- Colucci DG, Puig NR, Hernandez-Pand R. Influence of anaesthetic drugs on immune response: from inflammation to immunosuppression. *OA Anaesthetics* 2013; **30**: 21. doi: 10.13172/2052-7853-1-3-1091
- Crozier TA, Müller JE, Quittkat D, Sydow M, Wuttke W, Kettler D. Effect of anaesthesia on the cytokine responses to abdominal surgery. *Br J Anaesth* 1994; **72**: 280-5. doi: 10.1093/bja/72.3.280
- Zhang Y, Lin JX, Vilcek J. Synthesis of interleukin 6 (interferon-beta 2/B cell stimulatory factor 2) in human fibroblasts is triggered by an increase in intracellular cyclic AMP. *J Biol Chem* 1988; **263**: 6177-82. PMID: 2452159
- Lopker A, Abood LG, Hoss W, Lionetti FJ. Stereoselective muscarinic acetylcholine and opiate receptors in human phagocytic leukocytes. *Biochem Pharmacol* 1980; **29**: 1361-5. doi: 10.1016/0006-2952(80)90431-1
- Rossano F, Tufano R, Cipollaro de L'Ero G, Servillo G, Baroni A, Tufano MA. Anesthetic agents induce human mononuclear leucocytes to release cytokines. *Immunopharmacol Immunotoxicol* 1992; **14**: 439-50. doi: 10.3109/08923979209005403
- Malafoglia V, Ilari S, Vitiello L, Tenti M, Balzani E, Muscoli C, et al. The interplay between chronic pain, opioids, and the immune system. *Neuroscientist* 2022; **28**: 613-27. doi: 10.1177/10738584211030493
- Dubowitz JA, Cata JP, De Silva AP, Braat S, Shan D, Yee K, et al. Global Onco-Anaesthesia Research Collaboration Group. Volatile anaesthesia and peri-operative outcomes related to cancer: a feasibility and pilot study for a large, randomised control trial. *Anaesthesia* 2021; **76**: 1198-206. doi: 10.1111/anae.15354
- Galoş EV, Tat TF, Popa R, Efrimescu CI, Finnerty D, Buggy DJ, et al. Neutrophil extracellular trapping and angiogenesis biomarkers after intravenous or inhalation anaesthesia with or without intravenous lidocaine for breast cancer surgery: a prospective, randomised trial. *Br J Anaesth* 2020; **125**: 712-21. doi: 10.1016/j.bja.2020.05.003
- Kurosawa S, Kato M. Anesthetics, immune cells, and immune responses. *J Anesth* 2008; **22**: 263-77. doi: 10.1007/s00540-008-0626-2
- Salo M. Effects of lignocaine and bupivacaine on immunoglobulin synthesis in vitro. *Eur J Anaesth* 1990; **7**: 133-40.
- Novak-Janković V, Paver-Eržen V, Bovill JG, Ihan A, Osredkar J. Effect of epidural and intravenous clonidine on the neuro-endocrine and immune stress response in patients undergoing lung surgery. *Eur J Anaesthesiol* 2000; **17**: 50-6. doi:10.1046/j.1365-2346.2000.00602.x
- Novak-Janković V, Paver-Eržen V, Požlep G. How can we reduce stress response in patients undergoing lung surgery? *Acta Med Croatica* 1997; **51**: 89.
- Cata JP, Wang H, Gottumukkala V, Reuben J, Sessler DI. Inflammatory response, immunosuppression, and cancer recurrence after perioperative blood transfusions. *Br J Anaesth* 2013; **110**: 690-701. doi: 10.1093/bja/aet068
- Dantzer R. Neuroimmune interactions: from the brain to the immune system and vice versa. *Physiol Rev* 2018; **98**: 1477-504. doi: 10.1152/physrev.00039.2016
- Smith SM, Vale WW. The role of the hypothalamic-pituitary-adrenal axis in neuroendocrine responses to stress. *Dialogues Clin Neurosci* 2006; **8**: 383-95. doi: 10.31887/DCNS.2006.8.4/ssmith
- Velkeniers B., Dogusan Z., Naessens F. et al. Prolactin, growth hormone and the immune system in humans. *Cell Mol Life Sci* 1998; **54**: 1102-8. doi: 10.1007/s000180050239
- Dhabhar FS. Enhancing versus suppressive effects of stress on immune function: implications for immunoprotection versus immunopathology. 2008; *Allergy Asthma Clin Immunol* 2008; **4**: 2-11. doi:10.1186/1710-1492-4-1-2
- Sessler DI, Pei L, Huang Y, Fleischmann E, Marhofer P, Kurz A, et al; Breast Cancer Recurrence Collaboration. Recurrence of breast cancer after regional or general anaesthesia: a randomised controlled trial. *Lancet* 2019; **394**: 1807-15. doi: 10.1016/S0140-6736(19)32313-X
- Du YT, Li YW, Zhao BJ, Guo XY, Feng Y, Zuo MZ, Fu C, et al; Peking University Clinical Research Program Study Group. Long-term survival after combined epidural-general anesthesia or general anesthesia alone: follow-up of a randomized trial. *Anesthesiology* 2021; **135**: 233-45. doi: 10.1097/ALN.0000000000003835

32. Xu ZZ, Li HJ, Li MH, Huang SM, Li X, Liu QH, et al. Epidural anesthesia-analgesia and recurrence-free survival after lung cancer surgery: a randomized trial. *Anesthesiology* 2021; **135**: 419-32. doi: 10.1097/ALN.0000000000003873
33. Vahabi S, Eatemadi A. Effects of anesthetic and analgesic techniques on cancer metastasis. *Biomed Pharmacother* 2017; **87**: 1-7. doi: 10.1016/j.biopha.2016.12.073
34. Potočnik I, Hostnik A, Markovič-Božič J. Do inhalational anesthetic agents still hold their place in modern anesthesia practice? *Signa Vitae* 2019; **15**: 14-17. doi: 10.22514/SV152.092019.1
35. Markovic-Bozic J, Karpe B, Potocnik I, Jerin A, Vranic A, Novak-Jankovic V. Effect of propofol and sevoflurane on the inflammatory response of patients undergoing craniotomy. *BMC Anesthesiol* 2016; **16**: 18. doi: 10.1186/s12871-016-0182-5
36. Jiao B, Yang C, Huang NN, Yang N, Jia Wei J, Xu H. Relationship between volatile anesthetics and tumor progression: unveiling the mystery. *Curr Med Sci* 2018; **38**: 962-7. doi: 10.1007/s11596-018-1970-6
37. Zhang L, Zhang J, Yang L, Dong Y, Zhang Y, Xie Z. Isoflurane and sevoflurane increase interleukin-6 levels through the nuclear factor-kappa B pathway in neuroglioma cells. *Br J Anaesth* 2013; **110**(Suppl 1): i82-91. doi: 10.1093/bja/aet115
38. Ulbrich F, Eisert L, Buerkle H, Goebel U, Schallner N. Propofol, but not ketamine or midazolam, exerts neuroprotection after ischemic injury by inhibition of Toll-like receptor 4 and nuclear factor kappa-light-chain-enhancer of activated B-cell signalling. A combined in vitro study and animal study. *Eur J Anaesthesiol* 2016; **33**: 670-80. doi: 10.1097/EJA.0000000000000449
39. Sun C, Liu P, Pei L, Zhao M, Huang Y. Propofol inhibits proliferation and augments the anti-tumor effect of doxorubicin and paclitaxel partly through promoting ferroptosis in triple-negative breast cancer cells. *Front Oncol* 2022; **12**: 837974. doi: 10.3389/fonc.2022.837974
40. El Azab SR, Rosseel PM, De Lange JJ, van Wijk EM, van Strik R, Scheffer GJ. Effect of VIMA with sevoflurane versus TIVA with propofol or midazolam-sufentanil on the cytokine response during CABG surgery. *Eur J Anaesthesiol* 2002; **19**: 276-82. doi: 10.1017/s0265021502000443
41. Minou AF, Dzyadzko AM, Shcherba AE, Rummo OO. The influence of pharmacological preconditioning with sevoflurane on incidence of early allograft dysfunction in liver transplant recipients. *Anesthesiol Res Pract* 2012; **2012**: 930487. doi: 10.1155/2012/930487
42. Jerin A, Pozar-Lukanovic N, Sojar V, Stanisavljevic D, Paver-Erzen V, Osredkar J. Balance of pro- and anti-inflammatory cytokines in liver surgery. *Clin Chem Lab Med* 2003; **41**: 899-903. doi: 10.1515/CCLM.2003.136
43. Jabaudon M, Zhai R, Blondonnet R, Bonda WLM. Inhaled sedation in the intensive care unit. *Anaesth Crit Care Pain Med* 2022; **41**: 101133. doi: 10.1016/j.accpm.2022.101133
44. Song Z, Tan J. Effects of anesthesia and anesthetic techniques on metastasis of lung cancers: a narrative review. *Cancer Manag Res* 2022; **14**: 189-204. doi: 10.2147/CMAR.S343772
45. Oh CS, Park HJ, Piao L, Sohn KM, Koh SE, Hwang DY, et al. Expression profiles of immune cells after propofol or sevoflurane anesthesia for colorectal cancer surgery: a prospective double-blind randomized trial. *Anesthesiology* 2022; **136**: 448-58. doi: 10.1097/ALN.0000000000004119
46. Quan Y, Li S, Wang Y, Liu G, Lv Z, Wang Z. Propofol and sevoflurane alleviate malignant biological behavior and cisplatin resistance of Xuanwei lung adenocarcinoma by modulating the Wnt/ β -catenin pathway and PI3K/AKT pathway. *Anticancer Agents Med Chem* 2022; **22**: 2098-2108. doi: 10.2174/1871520621666211026092405
47. Yap A, Lopez-Olivo MA, Dubowitz J, Hiller J, Riedel B; Global Onco-Anesthesia Research Collaboration Group. Anesthetic technique and cancer outcomes: a meta-analysis of total intravenous versus volatile anesthesia. *Can J Anaesth* 2019; **66**: 546-61. doi: 10.1007/s12630-019-01330-x
48. Hovaguimian F, Braun J, Z'graggen BR, Schläpfer M, Dumrese C, Ewald C, et al. Anesthesia and circulating tumor cells in primary breast cancer patients: a randomized controlled trial. *Anesthesiology* 2020; **133**: 548-58. doi: 10.1097/ALN.0000000000003409
49. Buggy DJ, Riedel B, Sessler DI. Can anaesthetic technique influence cancer outcome? The next steps.... *Br J Anaesth* 2021; **127**: 5-7. doi: 10.1016/j.bja.2021.04.005
50. Maalouf M, Reddy AJ, Mazboudi P, Min M, Rawal R, Curow CA, et al. An analysis of lidocaine usage in the treatment of squamous cell carcinoma. *Cureus* 2023; **15**: e35614. doi: 10.7759/cureus.35614
51. Xing W, Chen DT, Pan JH, Chen YH, Yan Y, Li Q, et al. Lidocaine induces apoptosis and suppresses tumor growth in human hepatocellular carcinoma cells in vitro and in a xenograft model in vivo. *Anesthesiology* 2017; **126**: 868-81. doi: 10.1097/ALN.0000000000001528
52. Zhao L, Ma N, Liu G, Mao N, Chen F, Li J. Lidocaine inhibits hepatocellular carcinoma development by modulating circ_ITCH/miR-421/CPEB3 axis. *Dig Dis Sci* 2021; **66**: 4384-97. doi: 10.1007/s10620-020-06787-1
53. Zhang H, Yang L, Zhu X, Zhu M, Sun Z, Cata JP, et al. Association between intraoperative intravenous lidocaine infusion and survival in patients undergoing pancreatotomy for pancreatic cancer: a retrospective study. *Br J Anaesth* 2020; **125**: 141-8. doi: 10.1016/j.bja.2020.03.034
54. Diaz-Cambroner O, Mazzinari G, Cata JP. Perioperative opioids and colorectal cancer recurrence: a systematic review of the literature. *Pain Manag* 2018; **8**: 353-61. doi: 10.2217/pmt-2018-0029
55. Boudreau DM, Chen L, Yu O, Bowles EJA, Chubak J. Risk of second breast cancer events with chronic opioid use in breast cancer survivors. *Pharmacoepidemiol Drug Saf* 2019; **28**: 740-53. doi: 10.1002/pds.4779
56. Shavit Y, Ben-Eliyahu S, Zeidel A, Beilin B. Effects of fentanyl on natural killer cell activity and on resistance to tumor metastasis in rats. Dose timing study. *Neuroimmunomodulation* 2004; **11**: 255-60. doi: 10.1159/000078444
57. Saeed I, La Caze A, Hollmann MW, Shaw PN, Parat MO. New insights on tramadol and immunomodulation. *Curr Oncol Rep* 2021; **23**: 123. doi: 10.1007/s11912-021-01121-y
58. Cata JP, Singh V, Lee BM, Villarreal J, Mehran JR, Yu J, et al. Intraoperative use of dexmedetomidine is associated with decreased overall survival after lung cancer surgery. *J Anaesthesiol Clin Pharmacol* 2017; **33**: 317-23. doi: 10.4103/joacp.JOACP_299_16
59. Lavon H, Matzner P, Benbenishty A, Sorski L, Rossene E, Haldar R, et al. Dexmedetomidine promotes metastasis in rodent models of breast, lung, and colon cancers. *Br J Anaesth* 2018; **120**: 188-96. doi: 10.1016/j.bja.2017.11.004
60. Forget P, Berlière M, Poncelet A, De Kock M. Effect of clonidine on oncological outcomes after breast and lung cancer surgery. *Br J Anaesth* 2018; **121**: 103-4. doi: 10.1016/j.bja.2018.04.020
61. Zhang Y, Li M, Cui E, Zhang H, Zhu X, Zhou J, et al. Dexmedetomidine attenuates sevoflurane induced neurocognitive impairment through α 2 adrenoceptors. *Mol Med Rep* 2021; **23**: 38. doi: 10.3892/mmr.2020.11676
62. Zappavigna S, Cossu AM, Grimaldi A, Bocchetti M, Ferraro GA, Nicoletti GF, et al. Anti-inflammatory drugs as anticancer agents. *Int J Mol Sci* 2020; **21**: 2605. doi: 10.3390/ijms21072605
63. Musselman RP, Bennett S, Li W, Mamdani M, Gomes T, van Walraven C, et al. Association between perioperative beta blocker use and cancer survival following surgical resection. *Eur J Surg Oncol* 2018; **44**: 1164-69. doi: 10.1016/j.ejso.2018.05.012
64. Kalleist L, Galland L, Ledys F, Ghiringhelli F, Limagne E, Ladoire S. Impact of glucocorticoid use in oncology in the immunotherapy era. *Cells* 2022; **11**: 770. doi: 10.3390/cells11050770
65. Ristescu AI, Tiron CE, Tiron A, Grigoras I. Exploring hyperoxia effects in cancer-from perioperative clinical data to potential molecular mechanisms. *Biomedicines* 2021; **9**: 1213. doi: 10.3390/biomedicines9091213

Detection performance and prognostic value of initial bone marrow involvement in diffuse large B-cell lymphoma: a single centre ¹⁸F-FDG PET/CT and bone marrow biopsy evaluation study

Andrej Doma^{1,2}, Katarina Zevnik^{1,2}, Andrej Studen^{3,4}, Veronika Kloboves Prevodnik^{5,6}, Gorana Gasljevic^{6,7}, Barbara Jezersek Novakovic^{2,8}

¹ Department of Nuclear Medicine, Institute of Oncology Ljubljana, Ljubljana, Slovenia

² Faculty of Medicine, University of Ljubljana, Ljubljana, Slovenia

³ Experimental Particle Physics Department, Jožef Stefan Institute, Ljubljana, Slovenia

⁴ Faculty of Mathematics and Physics, University of Ljubljana, Ljubljana, Slovenia

⁵ Department of Cytopathology, Institute of Oncology Ljubljana, Ljubljana, Slovenia

⁶ Faculty of Medicine, University of Maribor, Maribor, Slovenia

⁷ Department of Pathology, Institute of Oncology Ljubljana, Ljubljana, Slovenia

⁸ Division of Medical Oncology, Institute of Oncology Ljubljana, Ljubljana, Slovenia

Radiol Oncol 2024; 58(1): 15-22.

Received 15 October 2023

Accepted 3 January 2024

Correspondence to: Andrej Doma, M.D., Department of Nuclear Medicine, Institute of Oncology Ljubljana, Zaloška 2, SI-1000 Ljubljana, Slovenia. E-mail: adoma@onko-i.si

Disclosure: No potential conflicts of interest were disclosed.

This is an open access article distributed under the terms of the CC-BY license (<https://creativecommons.org/licenses/by/4.0/>).

Funding: This research was funded by Slovenian Research Agency (ARRS), grant P3-0321.

Background. Detection of bone marrow involvement (BMI) in diffuse large B-cell lymphoma (DLBCL) typically relies on invasive bone marrow biopsy (BMB) that faces procedure limitations, while ¹⁸F-FDG PET/CT imaging offers a non-invasive alternative. The present study assesses the performance of ¹⁸F-FDG PET/CT in DLBCL BMI detection, its agreement with BMB, and the impact of BMI on survival outcomes.

Patients and methods. This retrospective study analyzes baseline ¹⁸F-FDG PET/CT and BMB findings in 145 stage II-IV DLBCL patients, evaluating both performance of the two diagnostic procedures and the impact of BMI on survival.

Results. DLBCL BMI was detected in 38 patients (26.2%) using PET/CT and in 18 patients (12.4%) using BMB. Concordant results were seen in 79.3% of patients, with 20.7% showing discordant results. Combining PET/CT and BMB data, we identified 29.7% of patients with BMI. The sensitivity, specificity, positive predictive value (PPV), negative predictive value (NPV), and accuracy of PET/CT for detecting DLBCL BMI were 88.4%, 100%, 100%, 95.3%, and 96.5%, respectively, while BMB showed lower sensitivity (41.9%) and NPV (46.8%). The median overall survival (OS) was not reached in any gender subgroup, with 5-year OS rates of 82% (total), 84% (female), and 80% (male) ($p = 0.461$), while different International Prognostic Index (IPI) groups exhibited varied 5-year OS rates: 94% for low risk (LR), 91% for low-intermediate risk (LIR), 84% for high-intermediate risk (HIR), and 65% for high risk (HR) ($p = 0.0027$). Bone marrow involvement did not impact OS significantly ($p = 0.979$).

Conclusions. ¹⁸F-FDG PET/CT demonstrated superior diagnostic accuracy compared to BMB. While other studies reported poorer overall and BMI 5-year OS in DLBCL, our findings demonstrated favourable survival data.

Key words: ¹⁸F-FDG PET/CT; Diffuse Large B-Cell Lymphoma; bone marrow; biopsy; overall survival

Introduction

Diffuse Large B-Cell Lymphoma (DLBCL) is the most common type of Non-Hodgkin lymphoma

(NHL), comprising approximately 30–40% of all cases of NHL. DLBCL most frequently occurs in lymph nodes, but it can also affect other organs such as the spleen, liver, gastrointestinal tract,

central nervous system, or bone marrow (BM).¹ BM involvement (BMI) in DLBCL indicates a more advanced stage of the disease, playing a critical role in determining treatment strategies² and predicting patient outcomes.³ The detection of BMI in DLBCL can be achieved through Positron Emission Tomography combined with Computed Tomography using the radiotracer fluorodeoxyglucose (¹⁸F-FDG PET/CT) and with BM aspiration and trephine biopsy (BMB). BMB has traditionally been considered as a gold standard for detecting BMI in DLBCL.^{4,5} BMB provides high diagnostic accuracy and allows for detailed morphological assessment of lymphoma cells, including their infiltration patterns within the bone marrow. Advantages of BMB include its ability to detect even focal or low-grade involvement, as well as its potential for identifying other concurrent bone marrow disorders or non-lymphoid malignancies.⁶ However, BMB is an invasive procedure associated with discomfort and possible complications.⁷ It may also be limited by the possible sampling errors, as the distribution of lymphoma cells can be heterogeneously within the BM, resulting in false negative BMB reports.⁴

¹⁸F-FDG PET/CT is a non-invasive imaging technique that provides functional and anatomical information, relying on the increased glucose metabolism of cancer cells including lymphoma cells.⁸ Several studies have evaluated the utility of ¹⁸F-FDG PET/CT in detecting BMI in DLBCL. ¹⁸F-FDG PET/CT can identify areas of increased glucose uptake, indicating the presence of lymphoma cells in the BM and ¹⁸F-FDG PET/CT has shown promising results in terms of sensitivity and specificity, with a high accuracy rate for detecting BMI in DLBCL patients.⁹⁻¹¹

The aim of our study was to assess the performance of ¹⁸F-FDG PET/CT and its concordance with BMB results in patients with DLBCL and to evaluate consequential survival outcome.

Patients and methods

Patients population

Medical records of all patients, who were appointed to our institution with referral diagnosis of suspected DLBCL between January 2016 and December 2020 were retrospectively reviewed. Inclusion criteria were: histological confirmation of DLBCL; stage II to IV disease; BMB and ¹⁸F-FDG PET/CT prior to start of treatment. Exclusion criteria were: age <18 and >80 years; disease stage I;

CNS involvement; history of prior or present other malignancies, including a low-grade lymphoma.

Patients were treated with 6 or 8 cycles of standard therapy according to local guidelines. The effect of treatment was assessed according to the Lugano classification with either CT or ¹⁸F-FDG PET/CT at the end of treatment, followed by the radiotherapy of the residual disease (determined by PET/CT), if applicable. All patients provided written informed consent for PET/CT and BMB and for the usage of medical data for the research purposes. This study has been approved by the Ethics Committee of the Institute of Oncology Ljubljana, number: ERIDEK-0104/2019 and the National Medical Ethics Committee of the Republic of Slovenia, number: 0120-104/2021/3.

The collected clinical information included: sex, age, history of previous diseases, BMB report, stage, IPI score, serum LDH level, WHO performance status, type of therapy, date of progression, date of death.

PET/CT

PET/CT acquisitions were performed using a Siemens Biograph mCT40 PET/CT, according to current guidelines.¹² In short, all patients fasted for the last 6 hours before the examination. The blood sugar level prior to the injection of ¹⁸F-FDG was <7 mmol/L and if necessary, i.v. Insulin was applied. FDG activity of 3.7 MBq/kg was administered intravenously 1 hour prior to imaging. A tip-of-the-head to mid-thigh PET/CT acquisition was performed with the following settings: the system regulated current and voltage for each subject based on the reference kV value of 100 kV and reference mAs value of 80 mAs; beam width: 16 x 1.2 mm; Pitch: 1.2; PET acquisition time 2 min/bed position.

All ¹⁸F-FDG PET/CT images were assessed by two experienced nuclear medicine physicians, blinded for BMB reading, and conclusions for discrepant cases were made with consensus.

Bone marrow biopsy

According to the International Guidelines, BM trephine biopsy and aspiration were performed either by medical oncologist or by surgeon (performing the lymph node biopsy) according to standard protocol in all patients included in the study.¹³ All BM trephine biopsies were fixed in 10% buffered formalin overnight. Each specimen was then cut into two halves parallel to the longitudinal axis.

TABLE 1. The six-colour antibody panel used for flow-cytometric immunophenotyping of bone marrow (BM) aspirates

	Tube	FITC	PE	PerCP-Cy5.5	APC	PE-Cy7	APC-Cy7
1.	mAb	κ	λ	CD19	CD5	CD10	CD45
	V ^e	5 µl	5 µl	5 µl	3 µl	2 µl	3 µl
2.	mAb	CD34	CD117	CD33	HLA-DR	CD14	CD45
	V ^e	3 µl	3 µl	2 µl	2 µl	3 µl	3 µl
3.	mAb	CD3	CD56	CD5	CD20	CD19	CD45
	V ^e	1 µl	3 µl	3 µl	6 µl	3 µl	3 µl
4.	mAb			CD19			CD45
	V ^e			5 µl			3 µl
5.	mAb	FMC7	CD23	CD19	CD5	CD10	CD45
	V ^e	6 µl	6 µl	5 µl	3µl		
6.	mAb	CD52	CD11c	CD19	CD38		CD45
	V ^e	3 µl	5 µl	5 µl	3 µl		3 µl
7.	mAb	CD103	CD22	CD19	CD25		CD45
	V ^e	5 µl	4 µl	5 µl	2 µl		3 µl
8.	mAb	CD38	CD56	CD19	CD138		CD45
	V ^e	5 µl	3 µl	5 µl	5 µl		3 µl
9.	mAb	CD4	CD8	CD3	CD7	CD5	CD45
	V ^e	3 µl	4 µl	3 µl	2 µl	5 µl	3 µl

APC = allophycocyanin; APC-Cy7 = allophycocyanin-cyanine 7; FITC = fluorescein isothiocyanate; mAb = monoclonal antibody; PE = phycoerythrin; PerCP-Cy5.5 = peridinin-chlorophyll-protein-complex-Cy5.5; PerCP = peridinin-chlorophyll-protein-complex; PE-Cy7 = phycoerythrin-cyanine7; V = volume; V^e = the volume of the antibodies was adjusted according to the results of titration measurements

One half of the specimen was embedded into a resin and stained by Giemsa, H&E, chloroacetate esterase, PAS, Pearls and Gomory. The other half was decalcified in EDTA and used for immunohistochemical analysis. Standard immunohistochemistry panel consisting of CD20 (DAKO, 1:500), CD3 (DAKO, 1:400), PAX-5 (DAKO, 1:40), MIB-1 (DAKO, 1:200), MPO (DAKO, 1:4000), CD61 (Cell Marque, 1:200), CD71 (Roche, ready-to-use) was applied and was executed on 2–4 µm thick FFPE tissue sections dried at 56°C for 2 h using the fully automated IHC staining platform Benchmark Ultra (Manufacturer Ventana ROCHE Inc., Tucson, AZ, USA). Pathohistological examination of BM was performed by a skilled hematopathologist. From all BM aspirates, May-Grunwald-Giemsa smears were prepared for microscopic evaluation and flow-cytometric immunophenotyping was carried out. Before flow-cytometric analysis, the cell count was automatically determined using the Sysmex XP-300 hematological analyser (Sysmex). Sample preparation for flow-cytometric analysis was carried out as previously described by our group.^{14,15} Antibodies presented in Table 1 were divided in 9 tubes and half a million cells were put in each tube.

After 20 min incubation, erythrocyte lysis was carried out using a commercial lysing solution (BD Biosciences). Flow-cytometric data were acquired by a 10-color BD FACSCanto™ II Flow Cytometer and FACSDiva 8.0.2 software (BD Bioscience).

PET scan interpretation

BMI on ¹⁸F-FDG PET/CT was evaluated using semi-quantitative analysis by measuring the maximum standardized uptake values (SUV_{max}) in BM DLBCL infiltrates and normal non-infiltrated liver and comparing the two values. Additionally, a pattern of BM uptake of ¹⁸F-FDG was considered in the analysis.

Positive BMI on ¹⁸F-FDG PET/CT was defined in case of focal or multifocal pattern of increased BM ¹⁸F-FDG uptake, greater than normal liver uptake, which could not be explained as a benign aetiology by CT or clinical correlation. Negative BMI on ¹⁸F-FDG PET/CT was considered in case of diffuse BM ¹⁸F-FDG uptake, irrespective of the degree of uptake, in case of no detectable uptake in BM, and in case of a putative benign aetiology of increased ¹⁸F-FDG uptake.^{16,17}

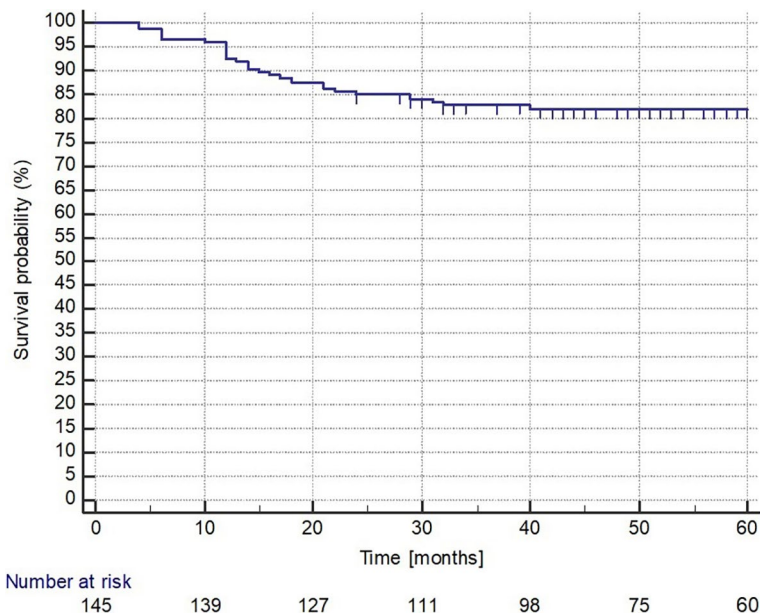


FIGURE 1. Overall survival.

BMI determination

BMB was considered the reference standard to detect BMI. Concordant positive and negative ^{18}F -FDG PET/CT BM findings and BMB results were considered as true positive and true negative results, and negative ^{18}F -FDG PET/CT scan results in patients with a positive DLBCL BMB were considered as false-negative results.

Discordant ^{18}F -FDG PET/CT BM findings and BMB results in which PET/CT results were positive and BMB results were negative were correlated

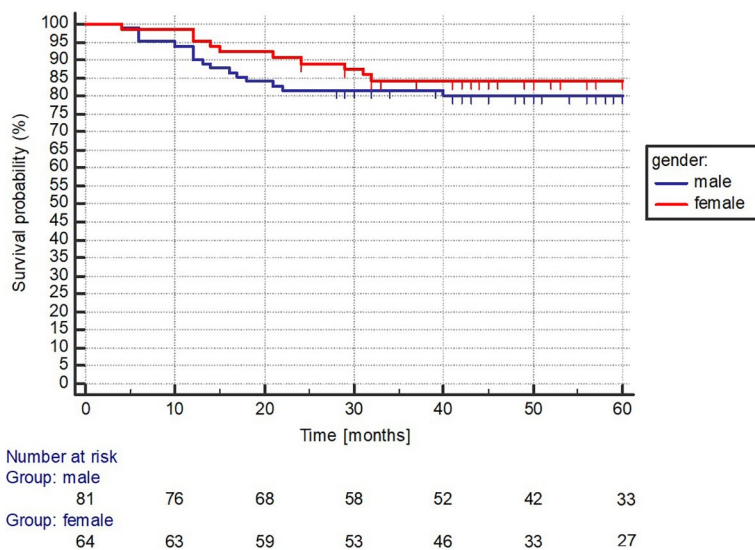


FIGURE 2. Gender based survival analysis.

with evaluation PET/CT at the end of the treatment: BM was defined as positive on ^{18}F -FDG PET CT in case of disappearance or decrease of activity comparable to nodal DLBCL infiltrates on evaluation PET/CT scans, and negative in case of unchanged persistent activity on post-treatment evaluation PET/CT scans, when the activity of nodal DLBCL infiltrates would noticeably decrease.

Statistical analysis

Statistical analysis of sensitivity, specificity, accuracy, positive and negative predictive values of BMB and ^{18}F -FDG PET/CT for detection of BMI was performed. Survival analysis was performed with Kaplan-Meier curves and log-rank tests, differences between groups for the continuous variables were compared with Mann-Whitney U test, and the Chi-squared test was used to measure the association or independence between categorical variables; p values <0.05 were considered significant. Statistical analysis was performed using MedCalc 19.2.6 (MedCalc Software, Belgium).

Results

Medical records of 507 patients were retrospectively reviewed. DLBCL was histologically confirmed in 371 patients. Of those, 194 patients were excluded from analysis (stage I disease n = 33; CNS involvement n = 15; palliative care n = 11; no FDG PET/CT performed n = 126; age >80 years n = 9). Another 32 patients did not have a BMB. Thus, 145 patients were included in the analysis. Patients' characteristics are presented in Table 2.

DLBCL BMI was detected in 38 patients (26.2%) by PET/CT and in 18 patients (12.4%) by BMB; concordant results between PET/CT and BMB were observed in 115 (79.3%) patients; in 102 (70.3%) negative and 13 (9.0%) positive. Discordant results were seen in 30 (20.7%) patients; in 25 (17.2%) with true positive PET/CT and false negative BMB and in 5 (3.4%) with false negative PET/CT and true positive BMB.

Through a combined analysis of PET/CT and BMB data, we determined the absence of BMI in 102 patients (70.3%) and its presence in 43 patients (29.7%), with all 30 discordant results being acknowledged as BMI positive.

The sensitivity, specificity, positive predictive value (PPV), negative predictive value (NPV), and accuracy for ^{18}F -FDG PET/CT for the detection of DLBCL BMI was 88.4% (95% confidence interval

TABLE 2. Patients' characteristics

Age (median, range), years	65 (20–79)	
Gender, female/male, n (%)	64 (44.1%)/ 81 (55.9%)	
	BMI -	BMI +
Age (median) [years]; BMI-: BMI+	66 (25–79)	63(20–78); p = 0.524
Gender, female/male, n;	48/54	16/27; p = 0.277
IPI score, n (%)		
IPI Low risk group (LR): 33 (22.8%)	32	1
IPI Low-intermediate risk group (LIR): 32 (22.1%)	22	10
IPI High-intermediate risk group (HIR): 33 (22.8%)	24	9
IPI High risk group (HR): 47 (32.4%)	24	23
Stage at diagnosis, n (%)	II: 39 (26.9%)	
	III: 19 (13.1%)	
	IV: 87 (60.0%)	
Chemotherapy regimen, n (%)	R-CHOP: 119 (82.1%)	
	R-EPOCH: 9 (6.2%)	
	R-ACVBP: 6 (4.1%)	
	RCOEP: 3 (2.1%)	
	Other: 8 (5.5%)	
Radiotherapy after chemotherapy, n (%)	52 (35.9%)	
Death in 60 months follow-up period, n (%)	29 (20.0%)	
Bone marrow involvements present- overall, n (%)	43 (29.7%)	
Extranodal sites: 0, n (%)	26 (17.9%)	
Extranodal sites: 1, n (%)	48 (33.1%); of those BMI n = 11 (7.6%)	
Extranodal sites more than 1, no. (%)	71 (49.0%)	

BMI = bone marrow involvement; IPI = international prognostic index; R-ACVBP = rituximab, doxorubicin, cyclophosphamide, vindesine, bleomycin, prednisone (R-ACVBP); R-CEOP = rituximab, cyclophosphamide, doxorubicin, vincristine, and prednisone; R-CHOP = rituximab, cyclophosphamide, doxorubicin, vincristine, prednisolone (a steroid) – (pred-ni-suh-lown); R-EPOCH = rituximab, etoposide, prednisone, vincristine, cyclophosphamide, hydroxydaunorubicin

[CI]; 74.9–96.1), 100% (95% CI; 96.4–100), 100% (95% CI; 0–0), 95.3% (95% CL; 89.9–97.9) and 96.5% (95% CI; 92.1–98.9). Regarding the BMB, the sensitivity, specificity, PPV, NPV, and accuracy for the detection of DLBCL BMI was 41.9% (95% CI; 27.0–57.9), 100% (95% CI; 84.6–100), 100% (95% CI; 0–0), 46.8% (9 5% CI; 40.6–53.1), and 61.5% (95% CI; 48.6–73.3).

No significant association was found between the gender and BMI ($\chi^2[1] = 1.182$, $p = 0.277$), however statistically significant association was observed between different IPI groups and BMI ($\chi^2[3] = 19.718$, $p = 0.0002$).

The median OS has not been reached in any of the total (Figure 1), female and male group with a 5-year OS rate of 82%, 84%, and 80%, respectively ($p = 0.461$) (Figure 2). The median OS has not been reached in any of the IPI LR, LIR, HIR, and HR

groups with a 5-year OS rate of 94%, 91%, 84%, and 65%, respectively, while the association between the IPI groups and the 5-year OS rates was statistically significant ($P = 0.0027$) (Figure 3).

The median OS was not yet reached in the BM non-involved (absent) and BM involved (present) groups with a 5-year OS rate of 82%, and 81%, respectively ($p = 0.979$) (Figure 4).

Discussion

The presence of BMI in DLBCL upstages the disease to stage IV, underscoring the critical importance of accurately assessing BMI for determining appropriate treatment strategies and predicting patient outcomes.¹⁸

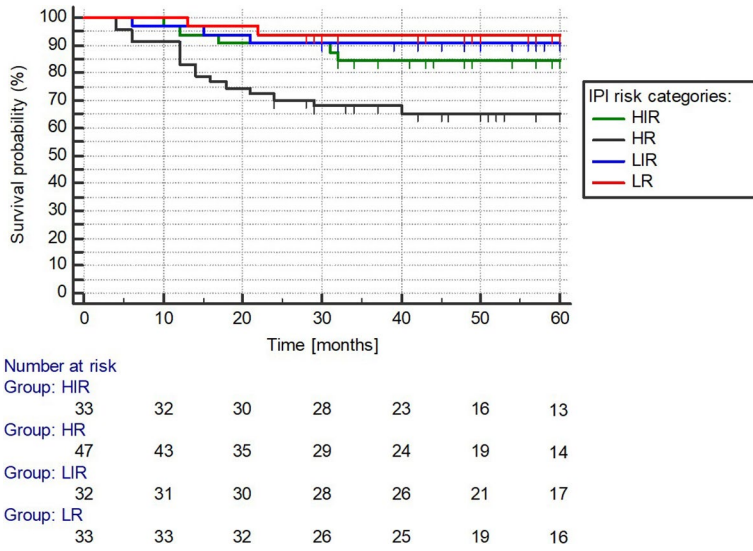


FIGURE 3. International prognostic index (IPI) survival analysis.

HR = high risk; HIR = high-intermediate risk; LIR = low-intermediate risk; LR = low risk

Historically, BMB has been regarded as the gold standard for assessing BMI. However, recent studies have demonstrated superior results with ¹⁸F-FDG PET/CT. Blind, unifocal BMB procedures come with several drawbacks, including the potential to miss a patchy pattern of BMI.¹⁹ Additionally, BMB can induce discomfort, pain, and potential bleeding in patients.²⁰

In contrast, ¹⁸F-FDG PET/CT, as a whole-body imaging modality, is known for providing highly

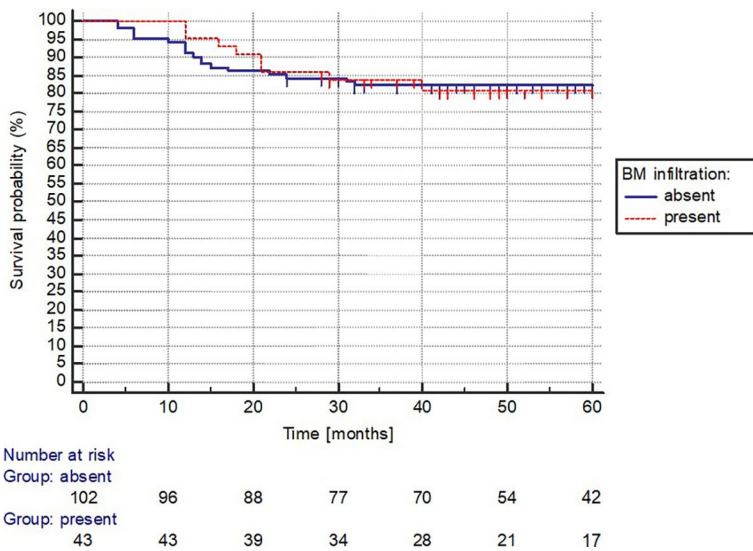


FIGURE 4. Bone marrow involvement status survival analysis.

BM = bone marrow

accurate staging data across various malignancies while maintaining safety and causing only moderate levels of anxiety for patients.²¹ As a result, current guidelines no longer recommend BMB when a PET/CT scan reveals bone or marrow involvement, indicating advanced-stage disease. However, BMB is still advisable in cases where PET results are negative, when a shift in BMI status would impact prognosis and treatment decisions, and to exclude discordant low-grade lymphoma.¹⁸

In our retrospective study, we found that ¹⁸F-FDG PET/CT exhibited significantly higher accuracy compared to BMB as a diagnostic modality. This observation aligns with several other studies^{5,9,22-24}, that reported superior sensitivity of ¹⁸F-FDG PET/CT over BMB, with only one study²⁵ indicating similar accuracy between the two diagnostic methods.

Our study's findings regarding sensitivity and specificity are consistent with the results of a systematic review conducted by Almainani *et al.* in 2022, which analysed 20 studies involving 2336 DLBCL patients.²⁶ The authors reported combined sensitivity and specificity values of 77% and 92% for ¹⁸F-FDG PET/CT and 47% and 100% for BMB, respectively.

In our dataset, ¹⁸F-FDG PET/CT produced false-negative results in 5 out of 43 (11.6%) BMI+ patients which is consistent with the findings of a previous large multicentre study by Pelosi *et al.*²⁴ Our data support the notion that ¹⁸F-FDG PET/CT can effectively replace BMB for determining BMI status in DLBCL patients.

False positive BMI findings on FDG PET/CT can be caused by a variety of factors, such as focal uptake of other types of cancer or septic diseases, and diffuse BM uptake due to inflammation.^{27,28} By implementing rigorous inclusion and interpretation criteria, we achieved perfect specificity and a positive predictive rate of 100%.

Several studies have reported poor OS rates in DLBCL patient cohorts, with BMI being associated with further reductions in OS. Recent studies by Yao *et al.* and Alonso-Alvarez *et al.* demonstrated statistically significant differences in 5-year OS rates between BMI- and concordant BMI+ patients (67.7% vs. 42% and 72% vs. 51%, respectively).^{29,30} However, our study showed significantly better OS outcomes, with 5-year OS rates of 94%, 91%, 84%, and 65% for IPI LR, LIR, HIR, and HR groups, respectively. Interestingly, we did not find a statistically significant difference in 5-year OS between BMI- and BMI+ groups.

The discrepancies in OS results among studies could be attributed to variations in patient characteristics. For example, our study excluded patients with CNS involvement, whereas Alonso-Alvarez's study included such cases.³⁰ Other differences include variations in the frequency of IPI high-risk patients and the inclusion of stage I disease. Additionally, discrepancies may arise from the different methods used to determine BMI status; some studies relied solely on BMB results, while our analysis incorporated both BMB and PET/CT-based BMI assessments.

Our study's impressive survival data is consistent with previous reports from a large cohort of patients treated at our institution between 2004 and 2013, where 5-year OS ranged from 86% in IPI LR patients to 45% in IPI HR patients.³¹ The high-quality clinical care provided by our dedicated lymphoma department likely contributes to these favourable outcomes.

It is important to acknowledge the limitations of our study, inherent from its retrospective design and potential selection bias. Future research on the prognostic value of baseline PET/CT in lymphoma, including the impact of BMI on survival, should move beyond binary qualitative PET/CT results (present/ absent) and incorporate tumour burden analysis using advanced radiomics quantitative segmentation methods such as metabolic tumour volume (MTV) and total lesion glycolysis (TLG).

Conclusions

In conclusion, the findings of our study suggest that ¹⁸F-FDG PET/CT may be a more accurate method for detecting BMI in DLBCL patients, and that BMI may not be a significant prognostic factor for OS in this population.

References

- Sehn LH, Salles G. Diffuse large B-cell lymphoma. *N Engl J Med* 2021; **384**: 842-58. doi: 10.1056/NEJMra2027612
- Cheson BD, Ansell S, Schwartz L, Gordon LI, Advani R, Jacene HA, et al. Refinement of the Lugano Classification lymphoma response criteria in the era of immunomodulatory therapy. *Blood* 2016; **128**: 2489-96. doi: 10.1182/blood-2016-05-718528
- Sehn LH, Scott DW, Chhanabhai M, Berry B, Ruskova A, Berkahn L, et al. Impact of concordant and discordant bone marrow involvement on outcome in diffuse large B-cell lymphoma treated with R-CHOP. *J Clin Oncol* 2011; **29**: 1452-7. doi: 10.1200/JCO.2010.33.3419
- Adams HJ, Niveststein RA, Kwee TC. Opportunities and limitations of bone marrow biopsy and bone marrow FDG-PET in lymphoma. *Blood Rev* 2015; **29**: 417-25. doi: 10.1016/j.blre.2015.06.003
- Khan AB, Barrington SF, Mikhaeel NG, Hunt AA, Cameron L, Morris T, et al. PET-CT staging of DLBCL accurately identifies and provides new insight into the clinical significance of bone marrow involvement. *Blood* 2013; **122**: 61-7. doi: 10.1182/blood-2012-12-473389
- Cheson BD, Fisher RI, Barrington SF, Cavalli F, Schwartz LH, Zucca E, et al. Recommendations for initial evaluation, staging, and response assessment of Hodgkin and non-Hodgkin lymphoma: the Lugano classification. *J Clin Oncol* 2014; **32**: 3059-68. doi: 10.1200/JCO.2013.54.8800
- Bain BJ. Bone marrow biopsy morbidity and mortality. *Br J Haematol* 2003; **121**: 949-51. doi: 10.1046/j.1365-2141.2003.04329.x
- Basu S, Alavi A. SPECT-CT and PET-CT in oncology – an overview. *Curr Med Imaging Rev* 2011; **7**: 202-9. doi: 10.2174/157340511796411168
- Berthel L, Cochet A, Kanoun S, Berriolo-Riedinger A, Humbert O, Toubeau M, et al. In newly diagnosed diffuse large B-cell lymphoma, determination of bone marrow involvement with 18F-FDG PET/CT provides better diagnostic performance and prognostic stratification than does biopsy. *J Nucl Med* 2013; **54**: 1244-50. doi: 10.2967/jnumed.112.114710
- El Karak F, Bou-Orm IR, Ghosn M, Kattan J, Farhat F, Ibrahim T, et al. PET/CT scanner and bone marrow biopsy in detection of bone marrow involvement in diffuse large B-cell lymphoma. *PLoS One* 2017; **12**: e0170299. doi: 10.1371/journal.pone.0170299
- Hao B, Zhao L, Luo NN, Ruan D, Pang YZ, Guo W, et al. Is it sufficient to evaluate bone marrow involvement in newly diagnosed lymphomas using ¹⁸F-FDG PET/CT and/or routine iliac crest biopsy? A new approach of PET/CT-guided targeted bone marrow biopsy. *BMC Cancer* 2018; **18**: 1192. doi: 10.1186/s12885-018-5104-0
- Boellaard R, Delgado-Bolton R, Oyen WJ, Giammarile F, Tatsch K, Eschner W, et al. FDG PET/CT: EANM procedure guidelines for tumour imaging: version 2.0. *Eur J Nucl Med Mol Imaging* 2015; **42**: 328-54. doi: 10.1007/s00259-014-2961-x
- Lee SH, Erber WN, Porwit A, Tomonaga M, Peterson LC. International Council for Standardization in hematology. ICSH guidelines for the standardization of bone marrow specimens and reports. *Int J Lab Hematol* 2008; **30**: 349-64. doi: 10.1111/j.1751-553X.2008.01100.x
- Brozic A, Pohar Marinsek Z, Novakovic S, Kloboves Prevodnik V. Inconclusive flow cytometric surface light chain results; can cytoplasmic light chains, Bcl-2 expression and PCR clonality analysis improve accuracy of cytological diagnoses in B-cell lymphomas? *Diagn Pathol* 2015; **10**: 191. doi: 10.1186/s13000-015-0427-5
- Brožič A. [Clonality and antigenic properties of reactive and neoplastic lymphocytic proliferations]. [Slovenian]. [Doctoral dissertation]. Ljubljana: University of Ljubljana. [cited 2023 Jul 27]. Available at: <https://repositorij.uni-lj.si/izpisGradiva.php?lang=slv&id=84423>
- Salaun PY, Gastinne T, Bodet-Milin C, Campion L, Cambefort P, Moreau, et al. Analysis of 18F-FDG PET diffuse bone marrow uptake and splenic uptake in staging of Hodgkin's lymphoma: a reflection of disease infiltration or just inflammation? *Eur J Nucl Med Mol Imaging* 2009; **36**: 1813-21. doi: 10.1007/s00259-009-1183-0
- Zwarthoed C, El-Galaly TC, Canepari M, Ouvrier MJ, Viotti J, Ettaiche M, et al. Prognostic value of bone marrow tracer uptake pattern in baseline PET scans in Hodgkin lymphoma: results from an International Collaborative Study. *J Nucl Med* 2017; **58**: 1249-54. doi: 10.2967/jnumed.116.184218
- Tilly H, Gomes da Silva M, Vitolo U, Jack A, Meignan M, Lopez-Guillermo A, et al. ESMO Guidelines Committee. Diffuse large B-cell lymphoma (DLBCL): ESMO Clinical Practice Guidelines for diagnosis, treatment and follow-up. *Ann Oncol* 2015; **26**: v116-25. doi: 10.1093/annonc/mdv304
- Wang J, Weiss LM, Chang KL, Slovak ML, Gaal K, Forman SJ, et al. Diagnostic utility of bilateral bone marrow examination: significance of morphologic and ancillary technique study in malignancy. *Cancer* 2002; **94**: 1522-31. doi: 10.1002/cncr.10364
- Salem P, Wolverson MK, Reimers HJ, Kudva GC. Complications of bone marrow biopsy. *Br J Haematol* 2003; **121**: 821. doi: 10.1046/j.1365-2141.2003.04328.x
- Vieira L, Pires A, Grilo A. Anxiety experienced by oncological patients who undergo 18F-FDG PET CT: a systematic review. *Radiography* 2021; **27**: 1203-10. doi: 10.1016/j.radi.2021.06.001
- Elamir Y, Elazab M, Owis AS, Elsayed HF. PET/CT and bone marrow biopsy (BMB) in evaluating bone marrow in lymphoma. *Egypt J Radiol Nucl Med* 2020; **51**: 201. doi: 10.1186/s43055-020-00318-8

23. Büyüksimşek M, Kolsuz İ, Yetişir AE, Tohumcuoğlu M, Oğul A, Mirili C, et al. Performance of positron emission tomography-computed tomography and bone marrow biopsy in detecting bone marrow infiltration in lymphoma cases. *Turk J Haematol* 2020; **37**: 220-25. doi: 10.4274/tjh.galenos.2020.2019.0361
24. Pelosi E, Penna D, Douroukas A, Bellò M, Amati A, Arena V, et al. Bone marrow disease detection with FDG-PET/CT and bone marrow biopsy during the staging of malignant lymphoma: results from a large multicentre study. *Q J Nucl Med Mol Imaging* 2011; **55**: 469-75. PMID: 21150862
25. Kandeel AA, Hussein M, Zidan L, Younis J, Edesa W, Alsayed Y. Diagnostic performance of 18F-2-fluoro-2-deoxy-D-glucose PET/computerized tomography in identifying bone marrow infiltration in new patients with diffuse large B-cell lymphoma and Hodgkin lymphoma. *Nucl Med Commun* 2020; **41**: 269-79. doi: 10.1097/MNM.0000000000001139
26. Almainani J, Tsoumpas C, Feltbower R, Polycarpou I. FDG PET/CT versus bone marrow biopsy for diagnosis of bone marrow involvement in non-hodgkin lymphoma: a systematic review. *Applied Sciences* 2022; **12**: 540. doi: 10.3390/app12020540
27. Chang JM, Lee HJ, Goo JM, Lee HY, Lee JJ, Chung JK, et al. False positive and false negative FDG-PET scans in various thoracic diseases. *Korean J Radiol* 2006; **7**: 57-69. doi: 10.3348/kjr.2006.7.1.57
28. Aoki J, Watanabe H, Shinozaki T, Takagishi K, Ishijima H, Oya N, et al. FDG PET of primary benign and malignant bone tumors: standardized uptake value in 52 lesions. *Radiology* 2001; **219**: 774-7.
29. Yao Z, Deng L, Xu-Monette ZY, Manyam GC, Jain P, Tzankov A, et al. Concordant bone marrow involvement of diffuse large B-cell lymphoma represents a distinct clinical and biological entity in the era of immunotherapy. *Leukemia* 2018; **32**: 353-63. doi: 10.1038/leu.2017.222.
30. Alonso-Álvarez S, Alcoceba M, García-Álvarez M, Blanco O, Rodríguez M, Baile M, et al. Biological features and prognostic impact of bone marrow infiltration in patients with diffuse large b-cell lymphoma. *Cancers* 2020; **12**: 474. doi: 10.3390/cancers12020474
31. Horvat M, Zadnik V, Južnič Šetina T, Boltežar L, Pahole Goličnik J, Novaković S, et al. Diffuse large B-cell lymphoma: 10 years' real-world clinical experience with rituximab plus cyclophosphamide, doxorubicin, vincristine and prednisolone. *Oncol Lett* 2018; **15**: 3602-9. doi: 10.3892/ol.2018.7774

Looking through the imaging perspective: the importance of imaging necrosis in glioma diagnosis and prognostic prediction – single centre experience

Hui Ma, Shanmei Zeng, Dingxiang Xie, Wenting Zeng, Yingqian Huang, Liwei Mazu, Nengjin Zhu, Zhiyun Yang, Jianping Chu, Jing Zhao

Department of Radiology, The First Affiliated Hospital, Sun Yat-sen University, Guangzhou, Guangdong Province, China

Radiol Oncol 2024; 58(1): 23-32.

Received 19 September 2023
Accepted 01 December 2023

Correspondence to: Zhao Jing, Chu Jianping and Yang Zhiyun, Department of Radiology, The First Affiliated Hospital, Sun Yat-sen University, No. 58 Zhongshan Er Road, Guangzhou, 510080, Guangdong Province, People's Republic of China. E-mail: zhaoj23@mail.sysu.edu.cn

Ma Hui, Zeng Shanmei and Xie Dingxiang contributed equally.

Disclosure: No potential conflicts of interest were disclosed.

This is an open access article distributed under the terms of the CC-BY license (<https://creativecommons.org/licenses/by/4.0/>).

Background. The aim of the study was to investigate the diagnostic value of imaging necrosis ($Im_{necrosis}$) in grading, predict the genotype and prognosis of gliomas, and further assess tumor necrosis by dynamic contrast-enhanced MR perfusion imaging (DCE-MRI).

Patients and methods. We retrospectively included 150 patients (104 males, mean age: 46 years old) pathologically proved as adult diffuse gliomas and all diagnosis was based on the 2021 WHO central nervous system (CNS) classification. The pathological necrosis ($Pa_{necrosis}$) and gene mutation information were collected. All patients underwent conventional and DCE-MRI examinations and had been followed until May 31, 2021. The $Im_{necrosis}$ was determined by two experienced neuroradiologists. DCE-MRI derived metric maps have been post-processed, and the mean value of each metric in the tumor parenchyma, peritumoral and contralateral area were recorded.

Results. There was a strong degree of inter-observer agreement in defining $Im_{necrosis}$ (Kappa = 0.668, $p < 0.001$) and a strong degree of agreement between $Im_{necrosis}$ and $Pa_{necrosis}$ (Kappa = 0.767, $p < 0.001$). Compared to low-grade gliomas, high-grade gliomas had more $Im_{necrosis}$ (85.37%, $p < 0.001$), and $Im_{necrosis}$ significantly increased with the grade of gliomas increasing. And $Im_{necrosis}$ was significantly more identified in *IDH*-wildtype, *1p19q*-non-codeletion, and *CDKN2A/B*-homozygous-deletion gliomas. Using multivariate Cox regression analysis, $Im_{necrosis}$ was an independent and unfavorable prognosis factor (Hazard Ratio = 2.113, $p = 0.046$) in gliomas. Additionally, extravascular extracellular volume fraction (*ve*) in tumor parenchyma derived from DCE-MRI demonstrated the highest diagnostic efficiency in identifying $Pa_{necrosis}$ and $Im_{necrosis}$ with high specificity (83.3% and 91.9%, respectively).

Conclusions. $Im_{necrosis}$ can provide supplementary evidence beyond $Pa_{necrosis}$ in grading, predicting the genotype and prognosis of gliomas, and *ve* in tumor parenchyma can help to predict tumor necrosis with high specificity.

Key words: glioma; necrosis; MRI; molecular markers; prognosis

Introduction

Necrosis is a common feature of human cancer and is often related to a poor prognosis, especially in glioblastomas.¹⁻³ Though the importance of necro-

sis in gliomas has already been addressed, necrosis was first incorporated into the determinant of the diagnosis for glioma grade in the fifth edition of the 2021 WHO classification of Tumors of the central nervous system (CNS), which highlighted

and underlined the significant value of necrosis in the diagnosis and prognosis of adult diffuse gliomas.⁴ According to the latest classification, once histological necrosis is identified, a diagnosis of WHO grade 4 astrocytoma or glioblastoma is suggested. However, there is a diagnostic dilemma in grading gliomas by identifying necrosis.

Presently, necrosis is primarily determined by pathological examination, in which partial tumor specimens from specific sites of tumors obtained by surgery or biopsy at a single point in time are generally inspected.⁵ However, due to tumor heterogeneity and incompleteness of the pathological sample, some pathological necrosis is likely to be missed, which may result in an underestimation of tumor grades, especially when the molecular analysis is not available. As tumor grades influence therapeutic decisions and prognosis, it is imperative to make up for the problem of a missed diagnosis of necrosis on pathological evaluation.

Magnetic resonance imaging (MRI) is utilized for routine, noninvasive, preoperative examination in diagnosing gliomas. Pathological necrosis usually has corresponding imaging features.^{6,7} Imaging necrosis has been defined as a region within the tumor that does not enhance or shows markedly diminished enhancement, high signal intensity on T2WI, low signal intensity on T1WI, and an irregular border.⁶ Hence necrosis in gliomas, when substantially present, can be detected by conventional MRI and plays a vital role in diagnosing gliomas and predicting prognosis.^{6,8-13} Moreover, conventional and advanced MRI can acquire comprehensive morphological and pathophysiological images of entire tumors, which is impossible with pathological examinations.

Taking all of this into account, we speculated whether necrosis diagnosed by MRI (hereafter termed “imaging necrosis”, abbreviated as $Im_{necrosis}$) could be used as a correction or a supplement to necrosis diagnosed by pathological evaluation (hereafter termed “pathological necrosis”, abbreviated as $Pa_{necrosis}$), especially when there is no evidence of $Pa_{necrosis}$ owing to limited sampling sites and sampling amounts. Consequently, herein, we retrospectively reviewed MRI findings of adult diffuse gliomas that were diagnosed based on the 2021 WHO CNS classification and assessed the role of $Im_{necrosis}$ in grading, predicting the genotype and prognosis of gliomas. We also attempted to analyse tumor necrosis by dynamic contrast-enhanced MR perfusion imaging (DCE-MRI) to validate quantitative imaging markers for probing tumor necrosis.

Patients and methods

Study participants

Patients with a primary diagnosis of glioma (June 2013–May 2021) were retrospectively included. Inclusion and exclusion criteria are presented in Supplementary Figure 1. Clinical information of patients was retrieved from the electronic medical records, and follow-up information was obtained through clinical interviews. Follow-up survival data were available until May 31, 2021. Overall survival (OS) was calculated from the initial surgery date to the date of death, or the date of the last follow-up visit if the patient was alive or lost to follow-up.

This retrospective analysis was in accordance with the ethical standards of the institutional and national research committee and was approved by the ethics committee of our institution ([2021]209). The requirement for written informed consent was waived due to the retrospective nature of this study.

MRI parameters

Participants underwent conventional (T1/T2-weighted images [T1WI/T2WI], T2-weighted fluid-attenuated inversion recovery [T2WI-FLAIR] and sagittal view of contrast-enhanced three-dimensional T1 MPRAGE images) and DCE-MRI imaging using a 3.0T MR system (Magnetom Verio, Siemens Medical Solutions, Erlangen, Germany) with a 64-channel head-neck coil. The parameter details of the conventional MRI and the DCE-MRI were elaborated in Supplementary Appendix 1.

Image processing

All DCE-MRI data were transferred to the post-processing workstation (detailed in Supplementary Appendix 2). Pharmacokinetic parameters, including the transfer constant (k_{trans}), extravascular extracellular volume fraction (ve), rate constant ($kep = k_{trans}/ve$), and initial area under the curve in the first 60 s ($iauc$), were automatically generated. Regions of interest (ROIs) were selected across three consecutive maximum tumor parenchyma slices. At each slice, one ROI was put in tumor parenchyma (hereafter termed “tumor”), according to T2WI-FLAIR, and enhanced T1WI, avoiding necrosis, cystic, and vessel areas. Another two approximate 2-mm-diameter ROIs were put in tumor peripheral zones (hereafter termed “edema”, within a 1-cm distance from the outer enhancing tumor

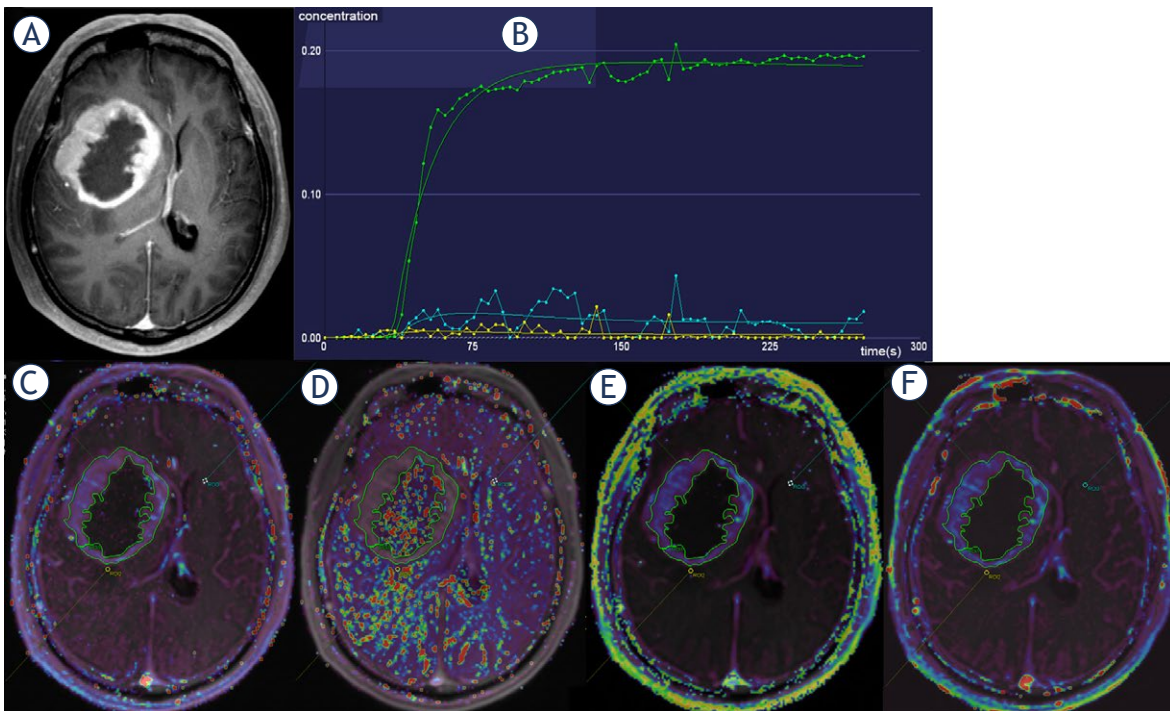


FIGURE 1. Representative ROI delineations. A 53-year-old man was diagnosed with glioblastoma, IDH-wildtype. (A) contrast-enhanced T1-weighted image (T1WI-CE); (B) the time-signal intensity curve; (C) the transfer constant (k_{trans}) image; (D) rate constant (k_{ep}) image; (E) extravascular extracellular volume fraction (v_e) image; (F) initial area under the curve in the first 60 s ($iauc$) image. On images, B-F, ROI 1 marked green represented tumor parenchyma, ROI 2 marked yellow represented the peripheral zones, and ROI 3 marked blue-turquoise represented contralateral normal-appearing brain tissues.

margin) and contralateral normal-appearing brain tissues (hereafter termed “control”) (Figure 1). The mean values of each DCE-MRI metric was recorded.

As mentioned in the introduction, examples of imaging necrosis, defined as a region within the tumor that does not enhance or shows markedly diminished enhancement, high signal intensity on T2WI, low signal intensity on T1WI, and an irregular border, are shown in Figure 2 and Supplementary Figure 2. Two experienced radiologists reviewed all conventional MRIs. Then they determined whether there was $Im_{necrosis}$ by consensus. One of these two experienced radiologists and a third radiologist repeatedly assessed 68 cases after the initial assessment to assess the inter-observer agreement. The assessed images were randomized within each type of pathology, and the observers were blinded to the clinical and pathological information and thoroughly acquainted with the criteria.

Pathological and molecular analysis

$Pa_{necrosis}$ was defined according to pathological reports provided by the Pathology department of our

hospital, if available. The status of $1p19q$ codeletion, $EGFR$ amplification, chr7 gain/10 loss (+7/-10), and $CDKN2A/B$ homozygous deletion were determined by fluorescence *in situ* hybridization with a specific probe. IDH mutation was determined by high-throughput sequencing, including $IDH1$ and $IDH2$ mutations. The pathological diagnosis and grading of gliomas were reassigned according to the 2021 WHO CNS classification (Supplementary Figure 3).^{4,14,15}

Statistical analysis

Statistical Analysis Data were analyzed using IBM SPSS Statistics 26 software, the SPSSAU data scientific analysis platform (<https://spssau.com/>), and the R programming language (version 4.1.2, The R Foundation for Statistical Computing). Normally distributed continuous variables were compared using unpaired t-tests, whereas non-parametric tests were used for non-normally distributed variables. Descriptive data are expressed as mean \pm SD, except where otherwise stated. Unpaired t-tests, non-parametric tests, and chi-squared tests were used to compare differences between parameters. Receiver Operating Characteristics (ROC) curves

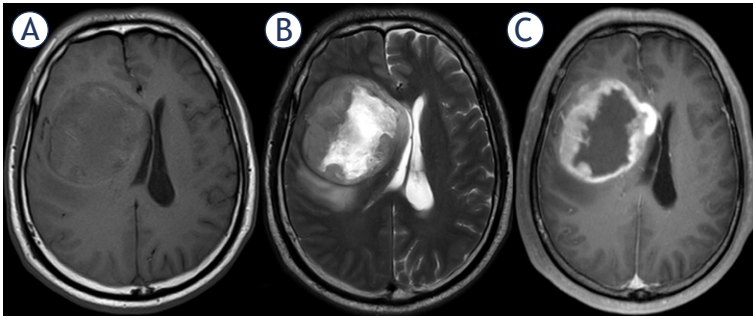


FIGURE 2. Representative MR images with imaging necrosis derived from a 53-year-old man with glioblastoma, IDH-wildtype. Shown from left to right by the order are T1WI (A), T2WI (B), and T1WI-CE (C).

were used to evaluate diagnostic efficacy. Simple kappa was calculated to assess the consistency of different diagnoses and inter-observer agreement. Kaplan–Meier survival analysis was used to analyze survival data. Hazard ratios (HR) were estimated according to the Cox proportional hazard method. A two-sided p value < 0.05 was considered significant. Detailed statistical methods are shown in Supplementary Appendix 3.

Results

Patients' demographic and clinical findings

We initially identified 150 eligible patients (median age = 46 years, range 21–79 years), and 104 (69.33%) were male (Table 1). All the diagnoses assigned to the patients according to the latest integrated histomolecular classification criterion were presented in Supplementary Figure 3 and Supplementary Table 1. Pa_{necrosis} was identified in 70/76 of high-grade gliomas (HGGs, CNS WHO grade 4) and 3/43 of low-grade gliomas (LGGs, CNS WHO grade 2 and 3) which were oligodendrogliomas, IDH-mutant and 1p/19q-deleted, while Im_{necrosis} was identified in 70/76 of HGGs and 12/43 of LGGs.

There was 1/77 HGG without enhancement but with positive status of *EGFR* amplification, thus diagnosed as glioblastomas, IDH-wildtype, while there were 32/45 LGGs with enhancement diagnosed as oligodendrogliomas, IDH-mutant and 1p/19q-deleted ($n = 15$) and astrocytoma, IDH-mutant ($n = 17$). And most HGGs were manifested as ring enhancement, and most LGGs had patchy and punctate enhancement. All the clinical information was presented in Table 1 and Supplementary Appendix 4.

Interobserver agreement of imaging necrosis and correlation between imaging and pathological necrosis

In this study, the following four groups were determined: $Im+Pa_{\text{necrosis}}$ group (representing patients with both Im_{necrosis} and Pa_{necrosis} , $n = 74$), no_{necrosis} group (representing patients without Im_{necrosis} nor Pa_{necrosis} , $n = 28$), *Only* Im_{necrosis} group (representing patients with Im_{necrosis} but without Pa_{necrosis} , $n = 7$), and *Only* Pa_{necrosis} group (representing patients with Pa_{necrosis} but without Im_{necrosis} , $n = 4$) groups. Detailed clinical, imaging and psychological information of *Only* Im_{necrosis} group and *Only* Pa_{necrosis} group were shown in Table 2. We found strong agreement between Im_{necrosis} and Pa_{necrosis} (Kappa = 0.767, $p < 0.001$, 95%CI: 0.637–0.897).

Besides, there was strong inter-observer agreement in identifying imaging necrosis (Kappa = 0.668, $p < 0.001$, 95%CI: 0.489–0.846). And the spot-like, dotted, long-strip, long tubular, and fissural enhancements (Figure 3) which were easily misdiagnosed as imaging necrosis should be avoided.

Association of imaging necrosis with integrated glioma grading

Most HGGs (85.37%) were found to have Im_{necrosis} while most LGGs (83.78%) were without Im_{necrosis} . There were 4/30 WHO grade 2 patients with Im_{necrosis} . Of those, two were diagnosed as oligodendrogliomas, IDH-mutant and 1p/19q-deleted, and two as astrocytomas, IDH-mutant.

Significant differences in the presence of Im_{necrosis} with a large effect size were found between HGGs and LGGs and among different grades of gliomas (Table 1, $p < 0.001$). Cochran–Armitage tests showed an upward trend in Im_{necrosis} from lower to higher grades of gliomas ($p < 0.001$). Multiple comparisons with Bonferroni correction showed that the difference between WHO grades (any two grades) and Im_{necrosis} was significant (all $p < 0.01$).

Association of imaging necrosis and molecular profiles of gliomas

There were significant correlations between the expression of other molecular markers such as *IDH*, *1p19q*, and *CDKN2A/B* and the presence of Im_{necrosis} . According to Table 1, the proportion of *IDH*-wildtype, *1p19q*-non-codeletion, or *CDKN2A/B*-positive cases with Im_{necrosis} was significantly higher than that of cases without Im_{necrosis} with a medium effect size, respectively (75.82% *vs.*

TABLE 1. Participant demographic findings

Parameters	Type	Imaging necrosis		Sum	t/χ2b	p
		Negative n (%)	Positive n (%)			
Age (n = 150)	-	40.54±11.08 (n = 54)	50.39±12.47 (n = 96)	-	-4.829&	p < 0.001
Sex (n = 150)	male	36(66.67)	68(70.83)	104	0.282	0.595
	female	18(33.33)	28(29.17)	46		
IDH (n = 144)	wildtype	17(32.08)	69(75.82)	86	26.649	p < 0.001
	mutant	36(67.92)	22(24.18)	58		
1p19q (n = 109)	non-codeletion	23(51.11)	55(85.94)	78	15.746	p < 0.001
	codeletion	22(48.89)	9(14.06)	31		
CDKN2A/B homozygous deletion (n = 63)	non-deletion	38(100.00)	20(80.00)	58	5.745b	0.017*
	deletion	0(0.00)	5(20.00)	5		
EGFR amplification (n = 81)	non-amplification	8(66.67)	45(65.22)	53	0.054a	0.817
	amplification	4(33.33)	24(34.78)	28		
chr7 gain/10 loss (n = 26)	negative	10(83.33)	13(92.86)	23	0.552b	0.457
	positive	2(16.67)	1(7.14)	3		
Grade (n = 119)	high-grade	6(16.22)	70(85.37)	76	52.828	p < 0.001
	low-grade	31(83.78)	12(14.63)	43		
WHO grade (n = 119)	WHO grade 2	26(70.27)	4(4.88)	30	62.664a	p < 0.001
	WHO grade 3	5(13.51)	8(9.76)	13		
	WHO grade 4	6(16.22)	70(85.37)	76		
Integrated histo-molecular diagnoses (n = 116)	Oligodendroglioma, IDH-mutant and 1p/19q-deleted	17(45.95)	7(8.86)	24	41.238	p < 0.001
	Astrocytoma, IDH-mutant	15(40.54)	12(15.19)	27		
	Glioblastoma, IDH-wildtype	5(13.51)	60(75.95)	65		

& = Student's t statistic in this cell, and other cells in the same column represent Chi-square values. a and b = chi-square tests with continuity correction and Fisher's exact tests, respectively; * = p < 0.05

32.08%, 85.94% vs. 51.11%, 20% vs. 0, respectively). However, no significant correlation was found between Im_{necrosis} and EGFR amplification or +7/-10 cytogenetic signature (p > 0.05) (Table 1).

Association of imaging necrosis with patient prognosis

One-hundred and thirty patients were included in the final survival analysis. Compared with gliomas with Im_{necrosis} patients without Im_{necrosis} had a significantly longer survival time (p < 0.001, Figure 4A). By reference to the gliomas with Pa_{necrosis} patients without Pa_{necrosis} had a sig-

nificantly longer survival time as well (p < 0.001, Figure 4B).

The differences among the OS of Im+Pa_{necrosis}/no_{necrosis}, Only Im_{necrosis} and Only Pa_{necrosis} groups were statistically significant (p < 0.01, Figure 4C). Further, after Bonferroni correction, there were significant differences between Im+Pa_{necrosis} and no_{necrosis} groups (p < 0.001). According to Figure 4C, the OS of the Only Pa_{necrosis} group (n = 2) was shorter than the OS of no_{necrosis} group (n = 28) and Only Im_{necrosis} group (n = 7). Between the two survival curves of no_{necrosis} and the Only Im_{necrosis} groups, there were marked crossovers, but within a certain period (time spanning about from 5-month

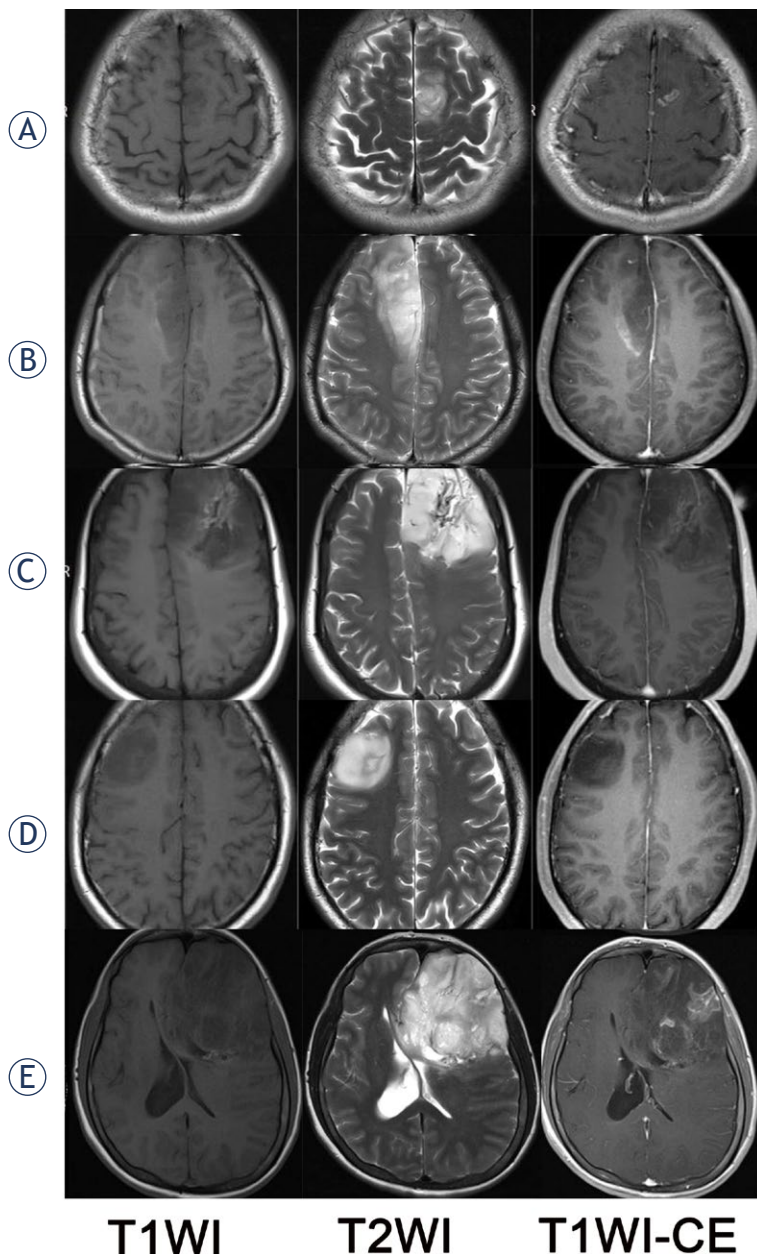


FIGURE 3. Some representative MRI images without imaging necrosis which was exactly confused in diagnosing imaging necrosis. Shown from left to right by the order are T1WI, T2WI, and T1WI-CE. (A) a 24-year-old man with an oligodendroglioma, IDH-mutant and 1p/19q-deleted, CNS WHO grade 2; (B) a 39-year-old man with an oligodendroglioma, IDH-mutant and 1p/19q-deleted, CNS WHO grade 2; (C) a 55-year-old woman with an oligodendroglioma, IDH-mutant and 1p/19q-deleted, CNS WHO grade 2; (D) a 45-year-old man with an astrocytoma, CNS IDH-mutant, WHO grade 2; (E) a 36-year-old woman with an oligodendroglioma, IDH-mutant and 1p/19q-deleted, CNS WHO grade 2. In this case (E), it showed multiple long tubular and filiform enhancement and there were some tumor areas with remarked decrease of reinforcement. But these areas are hyperintense, not hypointense, on the T1-weighted image. Comparing with CT images (not provided), calcification on these areas were just observed. So, there was no imaging necrosis in these conditions.

to 40-month postoperatively), the OS of the *Only* $Im_{necrosis}$ group was shorter than the OS of $no_{necrosis}$ group.

Further, when added significant variables such as age, *IDH*, *1p19q*, and $Im_{necrosis}$ into the multivariate Cox proportional hazards regression analyses, only $Im_{necrosis}$ (HR = 2.113, 95% CI: 1.015–4.402, $p = 0.046$) was significant and independently related to the patients' outcome, indicating that $Im_{necrosis}$ is an independent and unfavourable prognostic factor.

Correlation of tumor necrosis and DCE-MRI metrics

Since pathology is the golden standard for necrosis diagnosis, we analyzed the associations with $Pa_{necrosis}$ and DCE-MRI metrics. Most DCE-MRI metrics demonstrated a significant difference in identifying gliomas with $Pa_{necrosis}$ with a very large effect size (Table 3). *Kep* was significantly higher for gliomas with $Pa_{necrosis}$ than those without $Pa_{necrosis}$, while other DCE-MRI metrics showed the opposite trend. ROCs analysis showed that the Tumor-*ve*-Mean displayed the best diagnostic performance with the largest AUC of 0.891 (95%CI: 0.788–0.995, $p < 0.0001$), and the optimal cut-off point was 0.17 with a sensitivity of 96% and specificity of 83.3%.

Similarly, we performed the analysis regarding $Im_{necrosis}$ (Table 3), and the Tumor-*ve*-Mean displayed the best diagnostic performance as well, with the most significant AUC of 0.929 (95%CI: 0.872–0.986, $p < 0.0001$) and the optimal cut-off point was 0.17 with a sensitivity of 89.2% and specificity of 91.9%.

Discussion

In this study, we investigated the clinical implication of imaging necrosis in the preoperative evaluation of glioma. We found strong agreement between $Im_{necrosis}$ and $Pa_{necrosis}$. Moreover, $Im_{necrosis}$ was found to be significantly related to glioma-related key gene mutations, such as *1p19q* non-codeletion and *CDKN2A/B* homozygous deletion. And it is an independent imaging marker for predicting tumor prognosis. Additionally, tumor parenchyma *ve* derived from DCE-MRI can help to predict tumor necrosis with high specificity.

Our study indicated strong agreement between the inter-observer agreement of $Im_{necrosis}$ and $Pa_{necrosis}$. And during the analysis, we found that

TABLE 2. Detailed clinical, imaging and pathological information of Only Im_{necrosis} group and Only Pa_{necrosis} group

Group	Grade	Sex	Age	OS (month)	IDH (0:wild; 1:mutant)	1p19q (0:non-codeletion; 1:codeletion)	CDKN2A/B (0:non-deletion; 1:deletion)	EGFR amplification (0:non-amplification; 1:amplification)	chr7 gain/10 loss(0:negative; 1:positive)	Pathology
Only Pa _{necrosis} group	WHO CNS grade 4	female	63	2.5	1	0	0	NA	NA	Astrocytoma, IDH-mutant
Only Pa _{necrosis} group	WHO CNS grade 4	female	55	20	0	0	NA	0	NA	Glioblastoma, IDH-wildtype
Only Pa _{necrosis} group	WHO CNS grade 2	female	36	NA	1	1	0	NA	NA	Oligodendroglioma, IDH-mutant and 1p/19q-deleted
Only Pa _{necrosis} group	NA	female	34	NA	1	NA	NA	NA	NA	IDH-mutation, NOS
Only Im _{necrosis} group	WHO CNS grade 4	male	64	5	0	0	NA	1	NA	Glioblastoma, IDH-wildtype
Only Im _{necrosis} group	WHO CNS grade 2	male	40	25	1	0	0	NA	NA	Astrocytoma, IDH-mutant
Only Im _{necrosis} group	WHO CNS grade 3	female	55	60.06	1	1	0	NA	NA	Oligodendroglioma, IDH-mutant and 1p/19q-deleted
Only Im _{necrosis} group	WHO CNS grade 2	male	26	5.39	1	0	0	0	0	Astrocytoma, IDH-mutant
Only Im _{necrosis} group	NQ	male	40	7.19	0	0	NA	0	NA	IDH-wildtype, NOS
Only Im _{necrosis} group	NA	male	28	19.68	0	0	NA	0	0	IDH-wildtype, NOS
Only Im _{necrosis} group	WHO CNS grade 3	male	26	34.42	1	0	0	NA	NA	Astrocytoma, IDH-mutant

CNS = central nervous system; NA = not available; NOS = not otherwise specified

the regions with an absence or marked decrease of enhancement inside the intensified areas were easily mistaken as Im_{necrosis}. While considering pathological samples were partial, imaging observation can capture full tumors. There was a pathologically proven astrocytoma, IDH-mutant, CNS WHO grade 2, with a very short OS (5 months). We reviewed the raw data and identified that this patient had a small extent of Im_{necrosis} indicating high grade gliomas. The situation mentioned above can be avoided if a judgement of Im_{necrosis} is made, which is one unique advantage of radiographic examination. Besides, we identified seven patients with Im_{necrosis} who were diagnosed as oligodendrogliomas, IDH-mutant and 1p/19q-deleted, CNS WHO grade 2 or 3, indicating that necrosis plays a limited predictive value in oligodendrogliomas. Hence, if there is evidence of oligodendrogliomas, such as calcification and filiform or localized internal homogeneous enhancement, Im_{necrosis} does not indicate a high-grade tumor. Besides, Waqar *et al.* reported this kind of reinforcement as a “chicken

wire” appearance with the explanation that oligodendroglioma vasculature often was described as a network of regular fine branching capillaries.^{16,17}

Previous studies have highlighted that Im_{necrosis} is an independent unfavorable prognosis factor.^{5,6,10,18-20} Our results were in accordance with their findings. Besides, the latest WHO CNS classification emphasizes the role of molecular markers, such as IDH, 1p19q, CDKN2A/B, 7+/10-, and EGFR, in the diagnosis and prediction of the prognosis of gliomas.⁴ From this prospect, Im_{necrosis} might be more critical than Pa_{necrosis} since it can be non-invasively obtained before operation. However, there was no significant difference between the expressions of 7+/10- cytogenetic signature or EGFR amplification and the presence of Im_{necrosis}. This negative result might be due to the small sample size and insufficient number of events.

In this study, we also sought quantitative metrics for indicating tumor necrosis. Our results revealed that, compared with tumor without Im_{necrosis}/Pa_{necrosis}, DCE-derived metrics in tumor

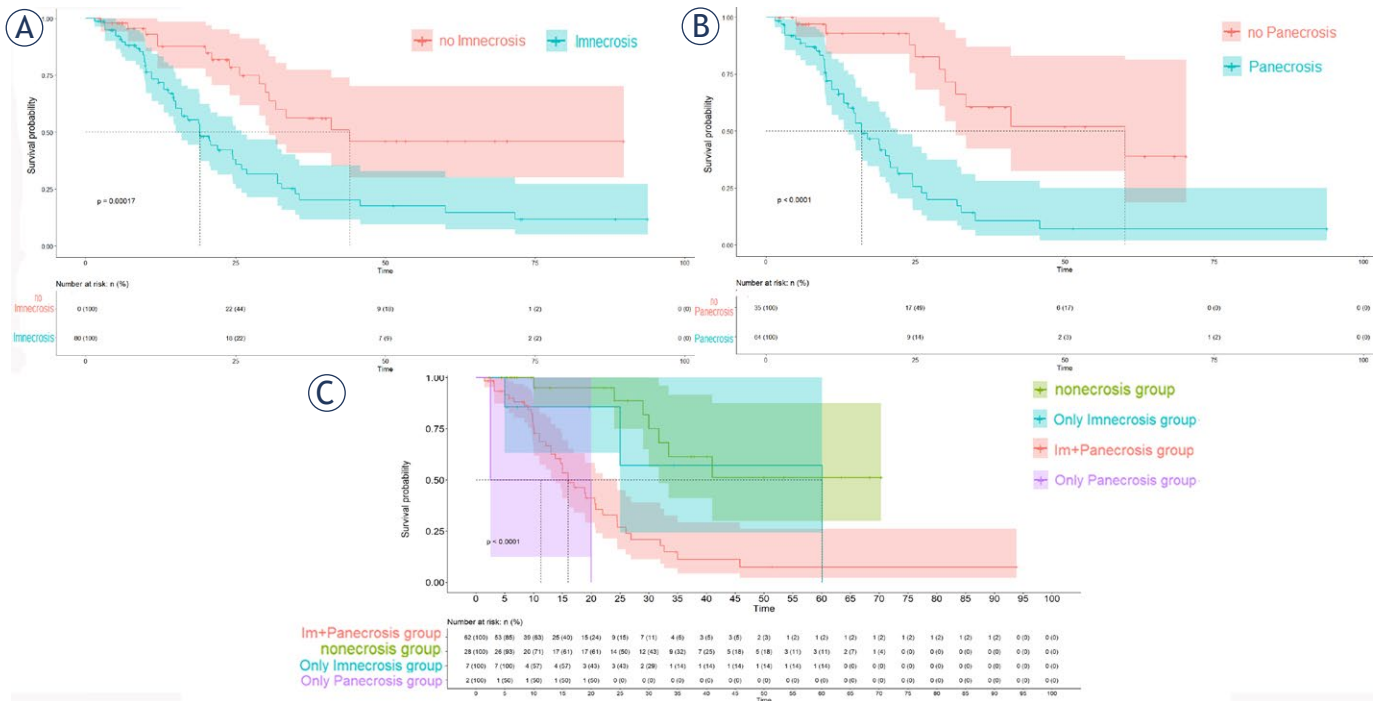


FIGURE 4. Survival curves for cases of imaging necrosis (A), cases of pathological necrosis (B), and cases of both pathological and imaging necrosis (C).

parenchyma, except *kep*, were significantly higher in gliomas with $Im_{necrosis}/Pa_{necrosis}$. And *ve* in tumor parenchyma demonstrated the highest diagnostic efficiency in identifying tumor necrosis with high sensitivity and specificity. Significantly high

DCE-MRI metrics may be attributed to gliomas growing uncontrollably fast, resulting in severe hypoxia and necrosis. Thus, an extensively hyper-permeable vasculature is generated, resulting in inadequate oxygen and supplements delivery. The

TABLE 3. Representative results of non-parametric tests and ROC analyses between DCE-related data for gliomas with or without pathological necrosis/imaging necrosis

Parameter	p	AUC (95% CI)	Sensitivity	Specificity	Cut-off
$Pa_{necrosis}$					
Tumor- <i>ktrans</i> -Mean	< 0.001	0.824 (0.711 ~ 0.936)	0.94	0.625	0.07
Edema- <i>ktrans</i> -Mean	0.031*	0.655 (0.527 ~ 0.783)	0.833	0.46	0.03
Tumor- <i>ve</i> -Mean	< 0.001	0.891 (0.788 ~ 0.995)	0.96	0.833	0.17
Edema- <i>ve</i> -Mean	0.002**	0.728 (0.613 ~ 0.842)	0.34	1	0.16
Tumor- <i>kep</i> -Mean	< 0.001	0.872 (0.761 ~ 0.983)	0.833	0.86	2.48
Tumor- <i>iauc</i> -Mean	< 0.001	0.899 (0.803 ~ 0.996)	1	0.75	0.07
$Im_{necrosis}$					
Tumor- <i>ktrans</i> -Mean	< 0.001	0.856 (0.772 ~ 0.939)	0.877	0.757	0.08
Tumor- <i>ve</i> -Mean	< 0.001	0.929 (0.872 ~ 0.986)	0.892	0.919	0.17
Edema- <i>ve</i> -Mean	0.005**	0.667 (0.558 ~ 0.776)	0.708	0.595	0.06
Tumor- <i>kep</i> -Mean	< 0.001	0.914 (0.857 ~ 0.971)	0.946	0.831	2.74
Tumor- <i>iauc</i> -Mean	< 0.001	0.909 (0.844 ~ 0.974)	0.8	0.946	0.13

* = p < 0.05; ** = p < 0.01

greater the levels of perfusion and permeability in the tumor tissue, the higher the k_{trans} and ve and the higher the degree of tumor malignancy.²¹⁻²³ Hence, DCE-MRI metrics, especially ve in tumor parenchyma (cut-off value: 0.17), might be a supplementary metric to the morphological observation for delineating tumor necrosis.

The current study has some limitations. First, since evidence of pathological necrosis was obtained from pathology reports of the same hospital, there may be an observation bias. However, this study, based on clinical real-world evidence, can exactly address the current clinical deficits. Second, this is a single-center study; subgroups analysis had a small sample, which might result in insufficient power to reach definite conclusions. Further multicenter studies with large sample sizes will help improve the efficacy of $Im_{necrosis}$ in predicting the expression of molecular markers and prognosis.

Conclusions

Based on the latest WHO CNS guidelines, the present study depicted the importance of imaging necrosis in diagnosing gliomas. Detection of imaging necrosis in gliomas probably suggests an HGG unless there is imaging evidence for oligodendrogliomas, IDH-mutant and 1p/19q-deleted. Imaging necrosis was significantly associated with glioma-related key gene mutations, such as *1p19q* non-codeletion and *CDKN2A/B* homozygous deletion. And it is an independent imaging marker for predicting tumor prognosis. Additionally, the Tumor- ve -Mean derived from DCE-MRI can help to predict necrosis with high sensitivity and specificity. Overall, in this study, we re-evaluated the imaging necrosis in the assessment of gliomas and provided a feasible solution to solve the frequent diagnostic dilemma of gliomas.

Acknowledgments

This study was funded in part by the National Natural Science Foundation of China (grant numbers 82172015, 82202217), the Natural Science Foundation of Guangdong Province (grant numbers 2021A1515012279, 2022A1515011264), and the Science and Technology Program of Guangzhou, China (grant number 202201011244).

References

1. Yee PP, Wei Y, Kim SY, Lu T, Chih SY, Lawson C, et al. Neutrophil-induced ferroptosis promotes tumor necrosis in glioblastoma progression. *Nat Commun* 2020; **11**: 5424. doi: 10.1038/s41467-020-19193-y
2. Hou J, Zhao R, Xia W, Chang CW, You Y, Hsu JM, et al. PD-L1-mediated gasdermin C expression switches apoptosis to pyroptosis in cancer cells and facilitates tumour necrosis. *Nat Cell Biol* 2020; **22**: 1264-75. doi: 10.1038/s41556-020-0575-z
3. Jiao D, Cai Z, Choksi S, Ma D, Choe M, Kwon HJ, et al. Necroptosis of tumor cells leads to tumor necrosis and promotes tumor metastasis. *Cell Res* 2018; **28**: 868-70. doi: 10.1038/s41422-018-0058-y
4. Wen PY, Packer RJ. The 2021 WHO classification of tumors of the central nervous system: clinical implications. *Neuro Oncol* 2021; **23**: 1215-7. doi: 10.1093/neuonc/noab120
5. Shao Y, Xiong S, Sun G, Dou W, Hu X, Yang W, et al. Prognostic analysis of postoperative clinically nonmetastatic renal cell carcinoma. *Cancer Med* 2020; **9**: 959-70. doi: 10.1002/cam4.2775
6. Wu CX, Lin GS, Lin ZX, Zhang JD, Chen L, Liu SY, et al. Peritumoral edema on magnetic resonance imaging predicts a poor clinical outcome in malignant glioma. *Oncol Lett* 2015; **10**: 2769-76. doi: 10.3892/ol.2015.3639
7. Seidel C, Dörner N, Osswald M, Wick A, Platten M, Bendszus M, et al. Does age matter? - a MRI study on peritumoral edema in newly diagnosed primary glioblastoma. *BMC Cancer* 2011; **11**: 127. doi: 10.1186/1471-2407-11-127
8. Pierallini A, Bonamini M, Pantano P, Palmeggiani F, Raguso M, Osti MF, et al. Radiological assessment of necrosis in glioblastoma: variability and prognostic value. *Neuroradiology* 1998; **40**: 150-3. doi: 10.1007/s002340050556
9. Yee PP, Wang J, Chih SY, Aregawi DG, Glantz MJ, Zacharia BE, et al. Temporal radiographic and histological study of necrosis development in a mouse glioblastoma model. *Front Oncol* 2022; **12**: 993649. doi: 10.3389/fonc.2022.993649
10. Hammoud MA, Sawaya R, Shi W, Thall PF, Leeds NE. Prognostic significance of preoperative MRI scans in glioblastoma multiforme. *J Neurooncol* 1996; **27**: 65-73. doi: 10.1007/BF00146086
11. Nowosielski M, Gorlia T, Bromberg JEC, Sahm F, Harting I, Kickingereder P, et al. Imaging necrosis during treatment is associated with worse survival in EORTC 26101 study. *Neurology* 2019; **92**: e2754-63-e63. doi: 10.1212/WNL.0000000000007643
12. Pope WB, Sayre J, Perlina A, Villablanca JP, Mischel PS, Cloughesy T. MR imaging correlates of survival in patients with high-grade gliomas. *AJNR Am J Neuroradiol* 2005; **26**: 2466-74. PMID: 16286386
13. Liu S, Wang Y, Xu K, Wang Z, Fan X, Zhang C, et al. Relationship between necrotic patterns in glioblastoma and patient survival: fractal dimension and lacunarity analyses using magnetic resonance imaging. *Sci Rep* 2017; **7**: 8302. doi: 10.1038/s41598-017-08862-6
14. Weller M, van den Bent M, Preusser M, Le Rhun E, Tonn JC, Minniti G, et al. Author Correction: EANO guidelines on the diagnosis and treatment of diffuse gliomas of adulthood. *Nat Rev Clin Oncol* 2022; **19**: 357-8. doi: 10.1038/s41571-022-00623-3
15. Weller M, van den Bent M, Preusser M, Le Rhun E, Tonn JC, Minniti G, et al. EANO guidelines on the diagnosis and treatment of diffuse gliomas of adulthood. *Nat Rev Clin Oncol* 2021; **18**: 170-86. doi: 10.1038/s41571-020-00447-z
16. Waqar M, Lewis D, Agushi E, Gittins M, Jackson A, Coope D. Cerebral and tumoral blood flow in adult gliomas: a systematic review of results from magnetic resonance imaging. *Br J Radiol* 2021; **94**: 20201450. doi: 10.1259/bjr.20201450
17. Cha S, Tihan T, Crawford F, Fischbein NJ, Chang S, Bollen A, et al. Differentiation of low-grade oligodendrogliomas from low-grade astrocytomas by using quantitative blood-volume measurements derived from dynamic susceptibility contrast-enhanced MR imaging. *AJNR Am J Neuroradiol* 2005; **26**: 266-73. PMID: 15709123
18. Hong EK, Choi SH, Shin DJ, Jo SW, Yoo RE, Kang KM, et al. Comparison of genetic profiles and prognosis of high-grade gliomas using quantitative and qualitative MRI features: a focus on G3 gliomas. *Korean J Radiol* 2021; **22**: 233-42. doi: 10.3348/kjr.2020.0011

19. Shen G, Wang R, Gao B, Zhang Z, Wu G, Pope W. The MRI features and prognosis of gliomas associated with IDH1 mutation: a single center study in southwest China. *Front Oncol* 2020; **10**: 852. doi: 10.3389/fonc.2020.00852
20. Li Y, Qin Q, Zhang Y, Cao Y. Noninvasive determination of the IDH status of gliomas using MRI and MRI-based Radiomics: impact on diagnosis and prognosis. *Curr Oncol* 2022; **29**: 6893-907. doi: 10.3390/curroncol29100542
21. Cosma I, Tennstedt-Schenk C, Winzler S, Psychogios MN, Pfeil A, Teichgraber, et al. The role of gadolinium in magnetic resonance imaging for early prostate cancer diagnosis: a diagnostic accuracy study. *PLOS ONE* 2019; **14**: e0227031
22. ncoronato M, Grimaldi AM, Mirabelli P, Cavaliere C, Parente CA, Franzese M, et al. Circulating miRNAs in untreated breast cancer: an exploratory multimodality morpho-functional study. *Cancers* 2019; **11**: 876. doi: 10.3390/cancers11060876
23. Tao WJ, Zhang HX, Zhang LM, Gao F, Huang W, Liu Y, et al. Combined application of pharamcokinetic DCE-MRI and IVIM-DWI could improve detection efficiency in early diagnosis of ductal carcinoma in situ. *J Appl Clin Med Phys* 2019; **20**: 142-50. doi: 10.1002/acm2.12624.

Role of diffusion-weighted imaging in response prediction and evaluation after high dose rate brachytherapy in patients with colorectal liver metastases

Salma Karim¹, Ricarda Seidensticker¹, Max Seidensticker^{1,2}, Jens Ricke^{1,2}, Regina Schinner¹, Karla Treitl¹, Johannes Rübenthaler^{1,2}, Maria Ingenerf¹, Christine Schmid-Tannwald^{1,2}

¹ Department of Radiology, University Hospital, LMU Munich, Germany

² ENETS Centre of Excellence, Interdisciplinary Center of Neuroendocrine Tumours of the GastroEntero-Pancreatic System at the University Hospital of Munich (GEPNET KUM), University Hospital of Munich, Munich, Germany

Radiol Oncol 2024; 58(1): 33-42.

Received 10 November 2023
Accepted 4 January 2024

Correspondence to: Christine Schmid-Tannwald, Department of Radiology, University Hospital, LMU Munich, Germany; Email: Christine.schmid-tannwald@med.uni-muenchen.de

Maria Ingenerf and Christine Schmid-Tannwald contributed equally to this work and share last authorship

Disclosure: No potential conflicts of interest were disclosed.

This is an open access article distributed under the terms of the CC-BY license (<https://creativecommons.org/licenses/by/4.0/>).

Background. The aim of the study was to assess the role of diffusion-weighted imaging (DWI) to evaluate treatment response in patients with liver metastases of colorectal cancer.

Patients and methods. In this retrospective, observational cohort study, we included 19 patients with 18 responding metastases (R-Mets; follow-up at least one year) and 11 non-responding metastases (NR-Mets; local tumor recurrence within one year) who were treated with high-dose-rate brachytherapy (HDR-BT) and underwent pre- and post-interventional MRI. DWI (qualitatively, mean apparent diffusion coefficient [ADC_{mean}], ADC_{min}, intraindividual change of ADC_{mean} and ADC_{min}) were evaluated and compared between pre-interventional MRI, first follow-up after 3 months and second follow-up at the time of the local tumor recurrence (in NR-Mets, mean: 284 ± 122 d) or after 12 months (in R-Mets, mean: 387+/-64 d). Sensitivity, specificity, positive predictive values (PPVs), and negative predictive values (NPVs) for detection of local tumor recurrence were calculated on second follow up, evaluating (1) DWI images only, and (2) DWI with Gd-enhanced T1-weighted images on hepatobiliary phase (contrast-enhanced [CE] T1-weight [T1w] hepatobiliary phase [hb])

Results. ADC_{mean} significantly increased 3 months after HDR-BT in both groups (R-Mets: 1.48 ± 0.44 and NR-Mets: 1.49 ± 0.19 × 10⁻³ mm²/s, p < 0.0001 and p = 0.01), however, intraindividual change of ADC_{mean} (175% vs. 127%, p = 0.03) and ADC_{min} values (0.44 ± 0.24 to 0.82 ± 0.58 × 10⁻³ mm²/s) significantly increased only in R-Mets (p < 0.0001 and p < 0.001). ADC_{min} was significant higher in R-Mets compared to NR-Mets on first follow-up (p = 0.04). Sensitivity (1 vs. 0.72), specificity (0.94 vs. 0.72), PPV (0.91 vs. 0.61) and NPV (1 vs. 0.81) could be improved by combining DWI with CE T1w hb compared to DWI only.

Conclusions. DW-MRI seems to be helpful in the qualitative and quantitative evaluation of treatment response after HDR-BT of colorectal metastases in the liver.

Key words: liver; HDR-brachytherapy; diffusion-weighted imaging; apparent diffusion coefficient; colorectal liver metastases

Introduction

Image-guided interstitial high-dose-rate brachytherapy (HDR-BT) supported by CT or MR fluoroscopic-guided catheter implantation and dose calculation is a relatively new percutaneous ablation technique. It has shown promising results with consideration to safety, local tumor control, efficiency and overall survival (OS) in patients with unresectable liver metastases.¹⁻⁴ HDR-BT can be performed repeatedly as therapy for recurrent liver metastases while maintaining liver function as high irradiation doses with steep dose gradients are being precisely applied to tumor tissue assuring the sparing of surrounding liver parenchyma.⁵

High-dose-rate brachytherapy (HDR-BT)⁶ of unresectable liver metastases leads to post-radiogenic changes such as post-radiogenic margins and vascularization, resulting in limited ability to assess morphological images^{6,7} similar to other loco-regional treatment (LRT) methods like radiofrequency ablation (RFA)^{8,9} or selective internal radiotherapy (SIRT).^{10,11}

Currently, the modified response evaluation criteria in solid tumors (mRECIST) is used to evaluate treatment response of Hepatocellular carcinoma (HCC) after loco-regional treatment (LRT) strategies, based on tumor size and contrast agent enhancement.^{12,13} However, studies have shown that these criteria might be limited because post-treatment contrast enhancement are not exclusive characteristics of viable tumor and may also be seen in benign tissue as a result of inflammation or due to post-radiogenic changes. Thus, mRECIST may underestimate treatment response.¹⁴⁻¹⁶ However, tumor response evaluated by the RECIST 1.1 is a morphologically-based by assessing the change in the size of the tumor and do not take into account information about the intra-lesional features.¹⁷ On the other hand side colorectal liver metastases demonstrate peripheral rim enhancement on the arterial phase and appear hypointense in the portal venous phase with delayed phase of enhancement.¹⁸ If a tumor has residual rim enhancement on the post-treatment contrast-enhanced CT (CE-CT), it may have viable tumor components, as confirmed by pathological correlation.¹⁹

Diffusion-weighted imaging (DWI) reflects motion of free water molecules and allows qualitative and quantitative (on apparent diffusion coefficient [ADC] map) evaluation of changes in tissue cellularity.^{9,20,21} Therefore, it seems promising as a complement for evaluation of treatment response. Previous studies have already demonstrated the

ability of DWI to assess tumor response in the liver after RFA as well as after SIRT to monitor different anticancer therapies.^{10,22-26} In addition, there are also studies showing that DWI may be an additional tool for predicting tumor response in patients with colorectal cancer liver metastases.^{24,27,28}

However, there is limited data reflecting the role of diffusion-weighted imaging in evaluation of tumor response in patients with liver metastases treated with HDR-BT. Wybranski *et al.* showed that DWI is an important parameter for early prediction of treatment response after HDR-BT in patients with colorectal liver metastases.⁵ However, the study had an observation interval of only three months after therapy, and did not differentiate between responding and non-responding lesions.⁵

Therefore, the purpose of this study was to assess the role of diffusion-weighted imaging in response prediction and evaluation after HDR-BT in patients with colorectal liver metastases over short and long-term intervals.

Patients and methods

Patients

This retrospective observational cohort study was approved by the local research ethics committee and the need for written informed patient consent was waived. The reporting of this study conforms to the Strengthening the Reporting of Observational Studies in Epidemiology STROBE guidelines.²⁹

Consecutively selected patients with liver metastases of colorectal cancer who were treated by HDR-BT at our department between August 2017 and December 2018 and who underwent MRI with DWI before, three months after HDR-BT and a second follow-up MRI at time of local tumor recurrence in nonresponding metastases (NR-Mets) and 12 months after therapy in responding metastases (R-Mets) were evaluated. Exclusion criteria were severe motion artefacts, lesion size less than 1cm, an incomplete MRI protocol, locoregional ablative therapy of treated metastases before and after HDR-BT.

CT-guided interstitial HDR-BT

Patient selection for treatment with CT-guided HDR-BT was based on a consensus decision in an interdisciplinary tumor conference. If multiple lesions were treated by brachytherapy in a patient, all treated lesions were included in the study. The

procedure was performed in one single session as described before.^{6,30} After analgesia and sedation, CT-guided brachytherapy catheters were positioned inside the tumor volume, followed by a planning CT scan. The HDR-BT in after-loading technique was then performed using a ¹⁹²Ir source. After irradiation, the catheters were removed while Gelfoam was administered to seal the puncture tract.^{6,30} The applied dose was at least 15 Gy surrounding the tumor.

MR imaging

Standardized pretreatment and posttreatment liver MRI were performed on a 1.5 T MR system (Magnetom Avanto, Magnetom Aera Siemens Healthcare, Erlangen, Germany or Ingenia, Ingenia S, Philips Healthcare, Best, Netherlands). Liver MRI included unenhanced T1w gradient-echo (GRE) (2D Flash) sequences in- and out-of-phase, a single shot T2w sequence (HASTE), T1w 3D GRE sequences with fat suppression (VIBE) before and 20, 50, and 120 seconds (depending on circulation time) after intravenous contrast injection (Gd-EOB-DTPA; Primovist, Eovist, Bayer Schering Pharma, Germany; 25 µmol/kg body weight), a multishot T2w turbo spin echo sequence with fat saturation, diffusion-weighted sequences with b-values of 50, 400 and 800 s/mm² and, after a delay of 15 minutes, an additional T1w GRE sequence with fat saturation (2D FLASH) and a fat suppressed T1w VIBE 3D GRE sequence identical to those performed earlier. Parallel imaging with an acceleration factor of 2 was utilized for all sequences. ADC maps were automatically computed from acquired DWI-MR images including all b-values.

Image analysis

Standard of reference

Diagnosis of the primary tumor was established by histopathology. The evaluation of treatment response was lesion-based and based on mRECIST criteria on longterm follow-up imaging in consensus. Treatment evaluation was based on mRECIST but also included enhancement not only in the arterial but also in the portalvenous phase with corresponding hypointensity in the hepatobiliary phase:

Complete response (CR): Disappearance of any intratumoral enhancement

Partial response (PR): (a) A decrease of vascularization of at least 30% or (b) a decrease of vas-

cularization of at least 30% without washout or (c) decreasing defect/ size (at least 30%) in the hepatobiliary phase

Progressive disease (PD): (a) over time increasing size and enhancement (at least 20%) or (b) new nodular enhancement with corresponding hypointensity

Stable disease (SD): Treated lesions were in between the three categories mentioned above.

R-Mets were defined as lesions (a) without vascularization in the sense of a disappearance of any intratumoral enhancement (CR) or (b) a decrease of vascularization of at least 30% without washout or (c) decreasing defect/ size (at least 30%) in the hepatobiliary phase (PR) 12 months after therapy. Whereas NR-Mets were defined as treated lesions with (a) persisting (SD) and over time increasing (PD) size and enhancement (at least 20%) or (b) new nodular enhancement with corresponding hypointensity (PD) in the hepatobiliary phase.

Quantitative and qualitative image analysis

Image analysis was performed in consensus by two radiologists. The review was conducted in three separate sessions by two radiologists in consensus: (1) preinterventional MRI and (2) 1st postinterventional MRI and (3) 2nd post-interventional MRI with 2-week interval between the review sessions.

Location and size measurements

The location of each metastasis was recorded, and size measurements were performed on T1-weighted postcontrast imaging in the hepatobiliary phase on the slice with the largest tumor extent, excluding post-radiogenic changes, in consensus with all other acquired sequences.

Evaluation of metastases and normal liver on DWI

In each session, DWI was evaluated whether (1) metastases exhibited visually restricted diffusion or (2) showed no diffusion restriction (invisible on high b-value images or T2 shine through).

Mean ADC values of tumor-free hepatic parenchyma were measured on pre- and post-interventional DWI-MR images by placing circular ROIs, as large as possible, in areas of normal liver parenchyma.

For ADC measurements of the metastases circular regions-of-interest (ROI) were manually drawn on the slice with the largest tumor extent on diffusion-weighted images while excluding neigh-

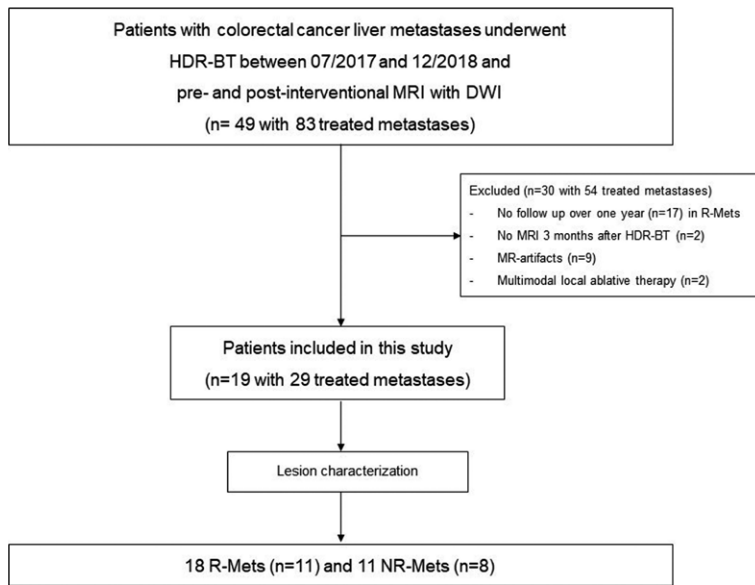


FIGURE 1. Flow diagram for this study

DWI = diffusion-weighted imaging; HDR-BT = high-dose-rate brachytherapy; NR-Mets = non-responding metastases; R-Mets = responding metastases; HDR-BT = high-dose-rate brachytherapy

boring structures or regions close to the rim of the lesion to avoid partial volume effects. Then, ROIs were transferred to the same slice of the ADC map to calculate intralesional ADC values including minimal (ADC_{min}), and mean (ADC_{mean}) ADC values (below noted as 10^{-3} mm²/s).

Evaluation of DWI for local tumor recurrence assessment

Furthermore, in two additional separate sessions, a third reviewer recorded the presence of local tumor recurrence on second follow up evaluating (1) DWI images only, (2) DWI with Gd-enhanced T1-weighted images on hepatobiliary phase (contrast-enhanced [CE] T1-weight [T1w] hepatobiliary phase [hb]) with a four points confidence scale: 1 = no local tumor recurrence, 2 = probably no local tumor recurrence, 3 = probably local tumor recurrence, 4 = definite local tumor recurrence.

On DWI, local tumor recurrence was defined as new or increasing nodular diffusion restriction over time. On CE T1w hb, local tumor recurrence was recorded if hypointense, treated metastasis either increased in size or new hypointense lesions appeared directly adjacent to the boarder of treated lesion.

Statistical analysis

Statistical analysis was performed with IBM SPSS Statistics 22 (IBM Corporation) and SAS (version 9.4) for Windows (SAS Institute, Inc.).

All ADC values and size measurements by both readers were averaged for further statistical analysis. Statistical significance level was set at $p \leq 0.05$. For normally distributed data, such as mean and min ADC of target lesions, paired t-tests were used for comparisons between study visits (before *vs.* after HDR-BT) and two-sample t-tests were used for comparisons between response groups (intraindividual changes in responders *vs.* non-responders). For non-normally distributed continuous data, such as lesion size, Mann-Whitney U test and Wilcoxon test were used instead of two-sample t-test and paired t-test. For categorical data, such as diffusion restriction McNemar's test was used for comparisons between study visits, and Fisher's exact test or Chi-square test was used for comparisons between response groups. Sensitivity, specificity, positive predictive values (PPVs), negative predictive values (NPVs) for detection of local tumor recurrence were calculated by means of cross tabulation. Significance levels of sensitivity and specificity of each review session were calculated using a McNemar Test. The Wilcoxon signed rank test for nonparametric paired samples was used for comparison of multiple confidence scores.

Results

Patients, MR interval, tumor location and size

The final study population consisted of 19 patients (6 males, 13 females; mean age: 70 years, SD: 10.7) with a total of 29 treated liver metastases (Figure 1). According to reference standard, 18 metastases were rated as R-Mets in 11 patients and 11 metastases as NR-Mets in 8 patients. 11 patients were responders: 6 patients each had one responding lesion, 3 patients each had two responding lesions and 2 patients each had 3 responding metastases after treatment with brachytherapy. 8 patients were non-responders: 5 patients each had one NR-Mets, 3 patients each had two NR-Mets. There were no patients with both, responding and non-responding lesions.

Baseline imaging in R-Mets was performed 11 days (\pm 17 days) (MRI) before therapy, 1st and 2nd follow-up imaging were acquired 93 d (\pm 22 days) and 378 d (\pm 64 days) after HDR-BT, respectively.

TABLE 1. Quantitative and qualitative results on baseline, 1. follow up and 2. follow up after local therapy of colorectal liver metastases with brachytherapy

Target lesions	Responding metastases			Non-responding metastases		
	Baseline	1. follow-up	2. follow-up	Baseline	1. follow-up	2. follow-up
Size (cm)	2.2 +/- 1.2	1.7 +/- 0.9	1.0 +/- 0.4	4.1 +/- 2.2	3.3 +/- 2.0	4.1 +/- 2.3
ADCmean	0.84 +/- 0.34	1.44 +/- 0.19	1.48 +/- 0.44	1.21 +/- 0.34	1.49 +/- 0.35	1.28 +/- 0.32
ADCmin	0.44 +/- 0.24	0.82 +/- 0.25	0.9 +/- 0.38	0.44 +/- 0.23	0.54 +/- 0.41	0.4 +/- 0.32
Visually diffusion restriction	11/18 (61.11%)	2/18 (11.11%)	0/18 (0%)	8/11 (72.38%)	4/11 (36.36%)	8/11 (72.38%)
Intraindividual increase in	between baseline and 1. follow-up	between baseline and 2. follow up		between baseline and 1.follow-up	between baseline and 2. follow up	
ADCmean (%)	175	187		127	106	
ADCmin (%)	208	281		146	115	

Baseline imaging in NR-Mets was performed 21 days (\pm 17 days) before therapy, and 1st and 2nd follow-up imaging were acquired 96 d (\pm 36 days) and 284 d (\pm 122 days) (= at time of local recurrence) after HDR-BT, respectively.

11 lesions were located in the right lobe, and 18 lesions were located in the left.

The mean size of R-Mets was 2.2 ± 1.2 cm on preinterventional MRI and decreased significantly to 1.7 ± 0.9 cm on the first postinterventional images ($p = 0.004$) and showed another significant decrease (mean size 1.0 ± 0.4 cm) on the second postinterventional MRI ($p = 0.0002$). The mean size of NR-Mets also significantly decreased between pre-interventional MR images and the first postinterventional images (4.1 ± 2.2 cm and 3.3 ± 2.0 cm, respectively). However, on second follow-up, there was again a significant increase in size (mean size: 4.1 ± 2.3 cm, $p = 0.02$) (Table 1).

The size of R-Mets was significantly smaller than the size of NR-Mets on the pre-, 1st post- and 2nd postinterventional MRI ($p = 0.007$, 0.001 and $p < 0.001$, respectively).

ADC measurements

ADC of normal liver

Mean ADCmean of normal liver parenchyma for patients with R-Mets was $0.93 \pm 0.11 \times 10^{-3}$ mm²/s on preinterventional images and $0.99 \pm 0.16 \times 10^{-3}$ mm²/s on 1st postinterventional images and $0.88 \pm 0.23 \times 10^{-3}$ mm²/s on 2nd follow up. Mean ADCmean of normal liver parenchyma for patients with NR-Mets was $0.92 \pm 0.18 \times 10^{-3}$ mm²/s on the preinter-

ventional images and $0.84 \pm 0.24 \times 10^{-3}$ mm²/s on the 1st post-interventional images and $0.96 \pm 0.24 \times 10^{-3}$ mm²/s on the 2nd follow up. There were neither a statistically significant change in mean ADC values of non-tumorous liver parenchyma between baseline and follow-up MRIs ($p > 0.05$) nor between responders and non-responders.

ADCmean of metastases

ADCmean of R-Mets (Table 1) was $0.84 \pm 0.34 \times 10^{-3}$ mm²/s on preinterventional images and $1.44 \pm 0.19 \times 10^{-3}$ mm²/s on the 1st postinterventional images and $1.48 \pm 0.44 \times 10^{-3}$ mm²/s on the 2nd follow up. There was a significant increase between baseline and the 1st follow-up examination and between baseline and the 2nd follow-up ($p < 0.0001$)

ADCmean of NR-Mets (Table 1) also increased significantly between pre- and 1st postinterventional MRI (ADCmean: $1.21 \pm 0.34 \times 10^{-3}$ mm²/s to $1.49 \pm 0.35 \times 10^{-3}$ mm²/s) ($p = 0.01$); however, there was a significant decrease of ADCmean between 1st and 2nd follow up (ADCmean on 2. follow up: $1.28 \pm 0.32 \times 10^{-3}$ mm²/s, $p = 0.04$).

The intra-individual increase in ADCmean values of R-Mets after HD-BRT was 175% on first follow-up and 187% on second follow up compared to preinterventional MRI (Figure 2). The average increase in ADCmean values of R-Mets after HD-BRT was 12% between first and second follow-up.

The intra-individual increase in ADCmean values of NR-Mets after HD-BRT was 127% on first follow-up and 106% on second follow-up compared to preinterventional MRI (Figure 2). In contrast to R-Mets (Figure 3), there was a decrease of 21% in

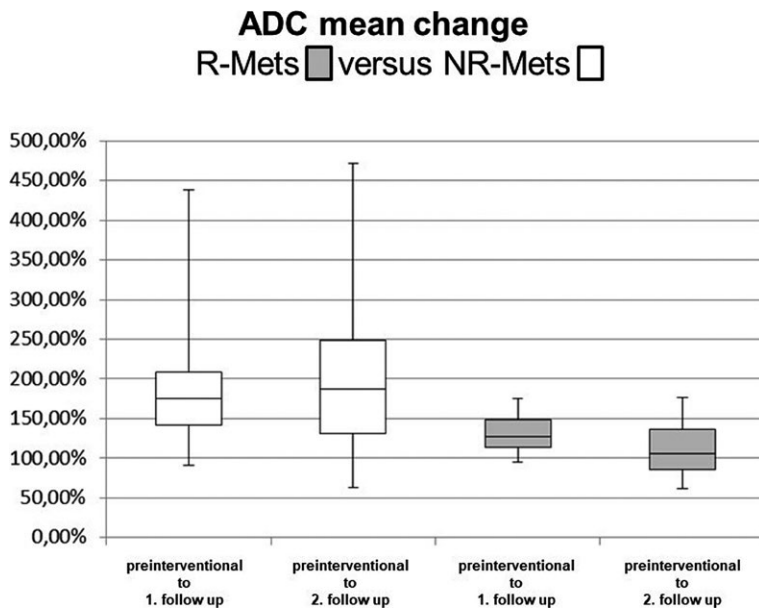


FIGURE 2. Mean apparent diffusion coefficient (ADCmean) change in responding metastases (R-Mets) and NR-Mets between preinterventional MRI and first and second follow-up, respectively

ADC = apparent diffusion coefficient; NR-Mets = non-responding metastases, R-Mets = responding metastases

ADCmean values of NR-Mets (Figure 4) after HD-BRT between first and second follow-up.

A cut-off value of a change of ADCmean less than 39% yielded a sensitivity of 0.82 (95% CI: 0.52-0.97) and a specificity of 0.72 (95% CI: 0.49-0.88).

Comparing the intra-individual change in ADCmean values between both groups, we found a significant difference between preinterventional ADCmean to ADCmean of the first and second follow up: ($p = 0.03$ and 0.01 retrospectively).

There was a significant difference of ADCmean between R-Mets and NR-Mets on preinterventional MRI ($p = 0.008$).

ADCmin of metastases

ADCmin of R-Mets (Table 1) increased significantly from $0.44 \pm 0.24 \times 10^{-3} \text{ mm}^2/\text{s}$ before treatment to $0.82 \pm 0.25 \times 10^{-3} \text{ mm}^2/\text{s}$ after treatment on the first follow up and to $0.9 \pm 0.38 \times 10^{-3} \text{ mm}^2/\text{s}$ on the second follow-up ($p < 0.0001$ and $p = 0.001$), but there was no significant increase of ADCmin between the first and second follow up ($p = 0.49$). In NR-Mets (Table 1) there was no significant change of ADCmin (from $0.44 \pm 0.23 \times 10^{-3} \text{ mm}^2/\text{s}$ to $0.54 \pm 0.41 \times 10^{-3} \text{ mm}^2/\text{s}$ to $0.40 \pm 0.32 \times 10^{-3} \text{ mm}^2/\text{s}$) over time.

The intra-individual increase in ADCmin values of R-Mets after HD-BRT was 208% on first follow up and 281% on second follow up compared to preinterventional MRI.

The intra-individual increase in ADCmin values of NR-Mets after HD-BRT was 146% on the first follow up and 115% on the second follow up compared to preinterventional MRI.

There were no significant difference between preinterventional ADCmin to ADCmin of the second follow up: ($p = 0.03$) but not compared to first follow up ($p = 0.1$).

There was no significant differences of preinterventional ADCmin between R-Mets and NR-Mets, however ADCmin was significantly higher in R-Mets compared to NR-Mets on the first follow-up ($p = 0.04$).

Qualitative analysis of metastases

In R-Mets, there was a significant loss of diffusion restriction over time (pre- to first postinterventional MRI $p = 0.012$ and pre- to second postinterventional $p = 0.001$): On preinterventional MRI, 11/18 (61.11%) R-Mets were diffusion-restricted. On the first follow-up, only 2/18 (11.11%) showed diffusion restriction and on the second follow up, no responding metastasis showed restricted diffusion. In contrast, 8/11 (72.73%) NR-Mets showed restricted diffusion on preinterventional, 4/11 (36.36%) on the first follow up and then again 8/11 (72.73%) showed restricted diffusion on the second follow-up.

Detection of local tumor recurrence on DWI

There were 11 recurrent lesions in total on the second follow-up. On DWI only, 8 of 11 NR-Mets and 13 of 18 R-Mets were correctly detected. Combining DWI with the hepatobiliary phase 11 of 11 NR-Mets and 17 of 18 R-Mets were identified. It was not differentiated whether the lesions showed enhancement in the first follow-up and therefore showed a stable disease in the short-term interval (SD) or whether the lesions showed a completely new nodular enhancement with corresponding hypointensity on the hepatobiliary phase in the second follow-up (PD), since both types of lesions were classified as NR Mets.

The presence of local tumor recurrence on the second follow up evaluating DW-images only resulted in a sensitivity of 0.72, a specificity of 0.72, a positive predictive value (PPV) of 0.61 and a negative predictive value (NPV) of 0.81.

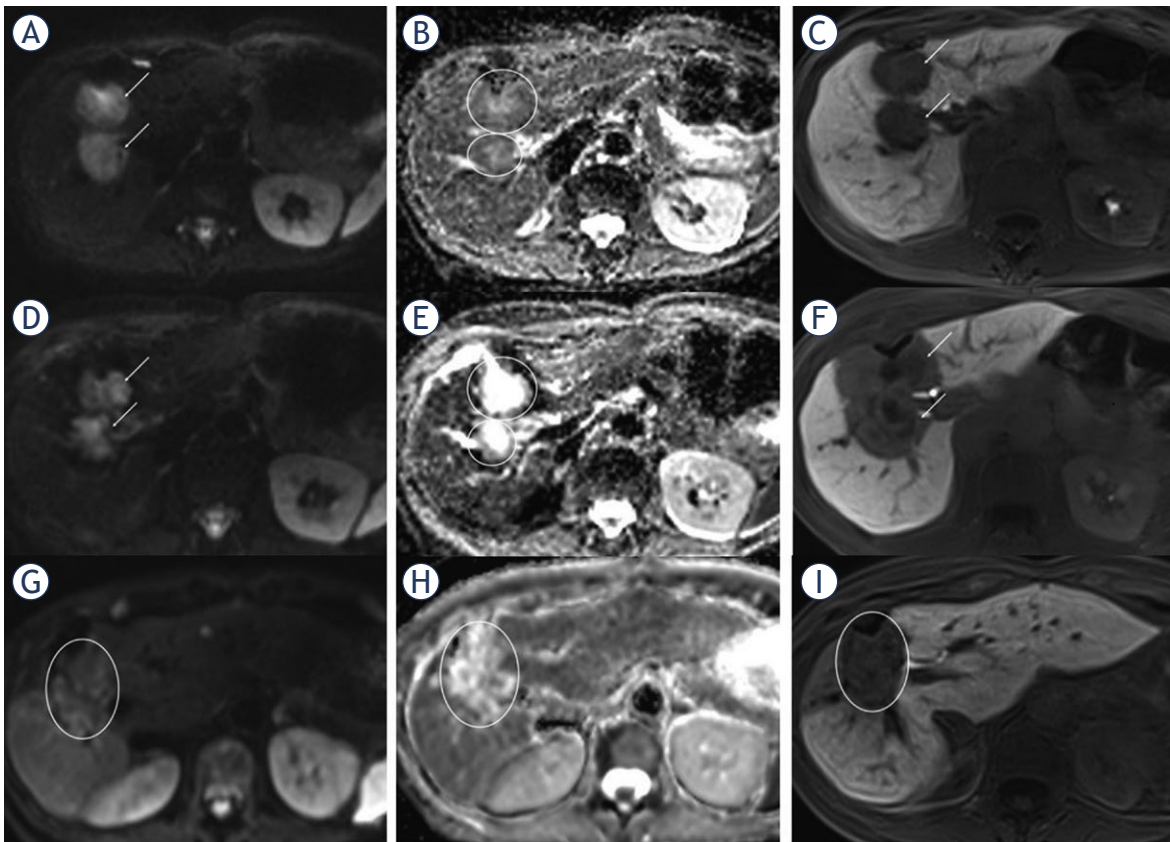


FIGURE 3. R-Met in a 62-year-old female. The pre-interventional diffusion-weighted imaging (DWI) shows two diffusion-restricted liver metastases with high signal on axial diffusion-weighted (DW)-MR image $b = 800 \text{ s/mm}^2$ (A) and low signal on apparent diffusion coefficient (ADC) map (B). The pre-interventional ADCmean of the metastases were 0.83 and $0.86 \times 10^{-3} \text{ mm}^2/\text{s}$. In the hepatobiliary phase (C) both metastases showed a hypointense signal. After high-dose-rate brachytherapy (HDR-BT), the metastases demonstrated a hyperintense signal on the axial DW-MR image (D) and a hyperintense signal on the ADC map (E) indicating less restricted diffusion compared to the pre-interventional image. The ADCmean increased to 1.41 and $1.53 \times 10^{-3} \text{ mm}^2/\text{s}$ in the hepatobiliary phase (F). The lesion showed central necrosis with a peripheral post-radiogenic hypointense rim. In the second follow-up the lesions showed no restricted diffusion (G) with a further increasing ADC (H) value of 2.09 and $2.07 \times 10^{-3} \text{ mm}^2/\text{s}$. There was a shrinkage in size of the metastases without a new hypointense defect in the hepatobiliary phase (I).

Combining DWI with Gd-enhanced T1-weighted images on hepatobiliary phase improved diagnostic performance: Sensitivity: 1, specificity 0.94, PPV: 0.91, NPV: 1.

Discussion

Loco-regional treatment methods like SBRT or HDR-BT lead to post-radiation changes such as cell swelling, transudation of plasma components to the extravascular-extracellular and space of tumor but also cellular necrosis and changes in microvasculature.^{5,6} DWI reflects changes in tumor cellularity and cell membrane integrity but also vascular capillary perfusion.²⁰ In the current literature quantitative and qualitative evaluation

of DWI seems to be a promising tool in evaluating tumor response after loco-regional treatment; to the best of our knowledge there are no studies determining the role of DWI in patients with colorectal metastases treated with HDR-BT to stratify responding from non-responding metastases and therefore, determining the role of DWI for prediction of tumor response.

In the early follow-up, three months after treatment with HDR-BT, we found in both groups a significant increase of ADCmean. We suggest that high dose rate brachytherapy induces loss of cell membrane integrity, increased extracellular space and ultimately tumor cell lysis. However, regarding the intraindividual change of ADCmean, only responding lesions showed a significant increases in ADCmean which correlates with other studies

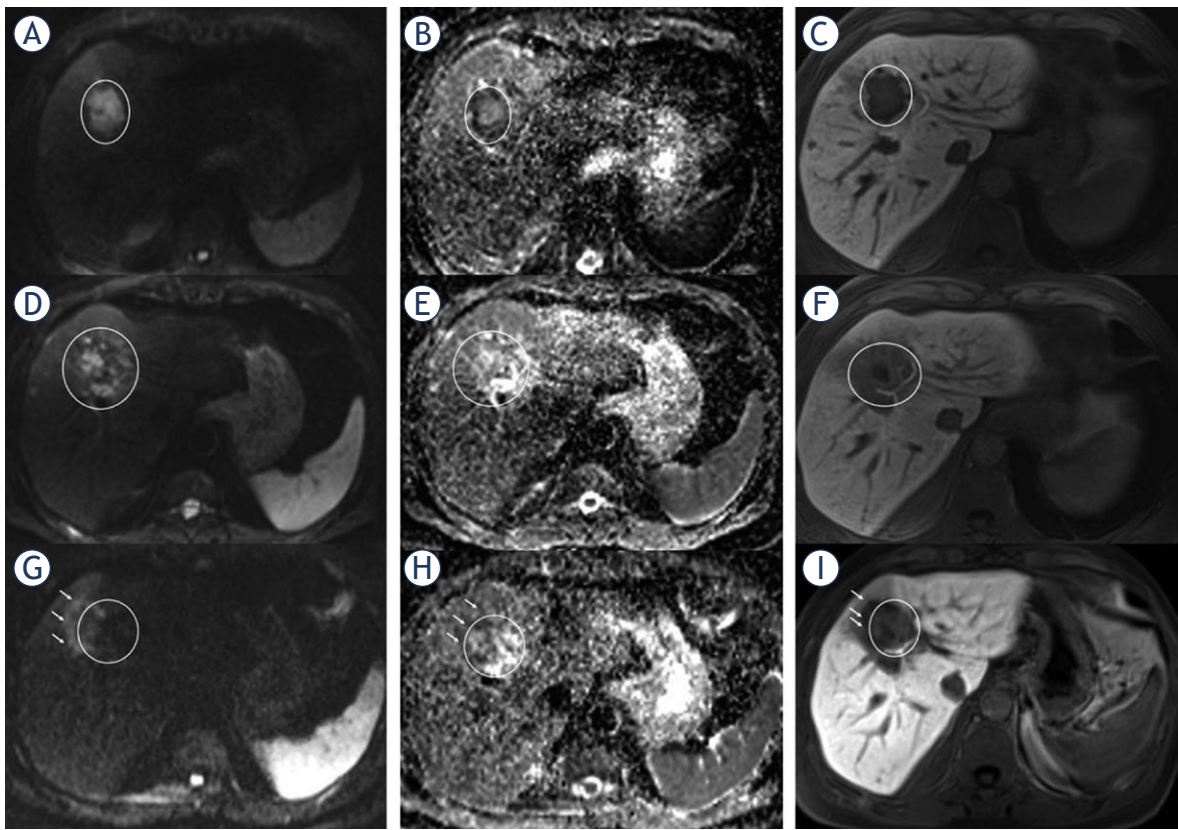


FIGURE 4. Non-responding metastases (NR-met) in a 56-year-old male. In pre-interventional MRI, metastasis (circle) shows restricted diffusion (**A+B**) with an mean apparent diffusion coefficient (ADC_{mean}) of $0.86 \times 10^{-3} \text{ mm}^2/\text{s}$ and a hypointense pattern on the liver-specific phase (**C**). Three months after high-dose-rate brachytherapy (HDR-BT), the metastasis showed visually partial restricted diffusion (**D+E**), but, with an increasing ADC_{mean} of $1.52 \times 10^{-3} \text{ mm}^2/\text{s}$ and hypointensity in the hepatobiliary phase (**F**). After 11 months, the lesion increased in size, shows a visually an increasing diffusion restriction (**K+L**) at the boarder (arrow) with a persistently ADC_{mean} value of $1.53 \times 10^{-3} \text{ mm}^2/\text{s}$ and a new defect in the hepatobiliary phase (arrow) (**I**) indicating local tumor recurrence.

in the literature.^{25,31} Furthermore ADC_{min} significantly increased in the responding lesions indicating necrosis induction in the tumor periphery beyond the already pre-interventional persisting central necrosis which is well known in colorectal metastases.^{25,29-32} It seems that DWI may be also used in long-term evaluation of tumor response. We found that over time (12months) a significant increase of ADC_{mean} and ADC_{min} as well as loss of diffusion restriction could only be observed in responding metastases. In contrast, non-responding metastases even showed at time of local recurrence a decrease in ADC_{mean} and ADC_{min} and consecutively increasing visual diffusion restriction compared to the first/early follow-up.

In the current literature there seems to be a disagreement regarding the role of pretreatment ADC values in predicting tumor response, depending on treatment techniques applied:

Cui *et al.* as well as Koh *et al.* demonstrated that pretreatment ADC_{mean} values in non-responding lesions of patients with colorectal and gastric hepatic metastases treated by chemotherapy were significantly higher than those of nonresponding lesions.^{22,24} Before chemotherapy, the presence of necrosis (resulting in higher ADC values) may lead to less delivery of chemotherapeutic drugs to these less perfused regions.²⁴

Similar results were found by Lahrsow *et al.*²⁸: Responding colorectal liver metastases had significant lower ADC values than non-responding metastases before treatment with conventional lipiodol-based transarterial chemoembolization.

In contrast, Schmeel *et al.* showed that ADC_{mean} in responding hepatic metastases of colorectal origin treated with ⁹⁰Y-microsphere radioembolization were significantly higher than ADC_{mean} of non-responding lesions.²⁷ This might be attributed

to the higher tumor grade and tumor aggressiveness associated with highly diffusivity restricted tumors.^{27,33}

We found that preinterventional ADC_{mean} was significantly lower in responding lesions compared to non-responding lesions. However, this result can only be seen as a marginal result and was not the central issue. In addition, as a limiting factor with regard to the value of our result, it must be noted that in our group the size of the metastases differed significantly between the responders and non-responders in the baseline examination.

In this study we could achieve good sensitivity and specificity in detection of local tumor recurrence; however, combining DWI with T1-weighted images in the hepatobiliary phase increased sensitivity, specificity and PPV and NPV as well. Still, it must be noted, that there is a certain bias in the evaluation of combining DWI with T1-weighted images in the hepatobiliary phase, since T1-weighted images in the hepatobiliary phase was part of the gold standard that we have defined. However, at least one lesion was scored as a false positive combining DWI with T1-weighted images in the hepatobiliary phase, i.e. NR-Met, underlining that the contrast media behavior of the lesions should be part of the response assessment if possible. On the other hand, DWI alone achieves good but also worse results than the contrast-enhanced-based evaluation. Similar results were found by Liu *et al.* in detecting residual HCC after drug-eluting bead transarterial chemoembolization using DWI.³⁴ Especially in very severe renal function impaired patients or in case of general avoidance of gadolinium exposure taking into account the frequent examinations over years in typical cases or in case of contraindication for contrast media administration DWI might be a valid alternative at imaging follow up after HDR-BT.

Our study has limitations due to its retrospective design, single center study and small sample size, which generally limits the conclusions to be drawn due to the lack of reproducibility. On the other hand, the evaluation was lesion-based with at least a total of 29 lesions were evaluated. Furthermore, the timing of imaging acquisition before and especially after treatment between the responder and non-responder group was not entirely similar. Moreover, mRECIST is limited by post-interventional changes that simulate a local recurrence. However, to overcome this limitation, we chose a long period after the intervention for the final evaluation. DWI is already routinely used to assess a treatment response of liver me-

tastases and has been evaluated in many studies. Nevertheless, the use of DWI to assess a treatment response after brachytherapy in the liver has not yet been evaluated in short- and long-term studies; the post-radiogenic changes, especially after brachytherapy, can be delineated in a circular hypointensity in the hepatobiliary phase around the lesion for a relatively long time and thus the assessment of response is difficult, as a result providing the study basis.

In conclusion, our results indicate that DWI-MRI may be a useful adjunct to morphologic MRI for detection of local tumor recurrence in patients with colorectal liver metastases treated with HDR-BT.

References

- Ricke J, Wust P, Stohlmann A, Beck A, Cho CH, Pech M, et al. CT-guided interstitial brachytherapy of liver malignancies alone or in combination with thermal ablation: phase I-II results of a novel technique. *Int J Radiat Oncol Biol Phys* 2004; **58**: 1496-505. doi: 10.1016/j.ijrobp.2003.09.024
- Ricke J, Wust P, Wieners G, Beck A, Cho CH, Seidensticker M, et al. Liver malignancies: CT-guided interstitial brachytherapy in patients with unfavorable lesions for thermal ablation. *J Vasc Interv Radiol* 2004; **15**: 1279-86. doi: 10.1097/O1.Rvi.0000141343.43441.06
- Seidensticker M, Wust P, Rühl R, Mohnike K, Pech M, Wieners G, et al. Safety margin in irradiation of colorectal liver metastases: assessment of the control dose of micrometastases. *Radiat Oncol* 2010; **5**: 24. doi: 10.1186/1748-717x-5-24
- Ricke J, Mohnike K, Pech M, Seidensticker M, Rühl R, Wieners G, et al. Local response and impact on survival after local ablation of liver metastases from colorectal carcinoma by computed tomography-guided high-dose-rate brachytherapy. *Int J Radiat Oncol Biol Phys* 2010; **78**: 479-85. doi: 10.1016/j.ijrobp.2009.09.026
- Wybranski C, Zeile M, Löwenthal D, Fischbach F, Pech M, Röhl FW, et al. Value of diffusion weighted MR imaging as an early surrogate parameter for evaluation of tumor response to high-dose-rate brachytherapy of colorectal liver metastases. *Radiat Oncol* 2011; **6**: 43. doi: 10.1186/1748-717x-6-43
- Bretschneider T, Ricke J, Gebauer B, Streitparth F. Image-guided high-dose-rate brachytherapy of malignancies in various inner organs – technique, indications, and perspectives. *J Contemp Brachytherapy* 2016; **8**: 251-61. doi: 10.5114/jcb.2016.61068
- Omari J, Drewes R, Orthmer M, Hass P, Pech M, Powerski M. Treatment of metastatic gastric adenocarcinoma with image-guided high-dose rate, interstitial brachytherapy as second-line or salvage therapy. *Diagn Interv Radiol* 2019; **25**: 360-7. doi: 10.5152/dir.2019.18390
- Chow DH, Sinn LH, Ng KK, Lam CM, Yuen J, Fan ST, et al. Radiofrequency ablation for hepatocellular carcinoma and metastatic liver tumors: a comparative study. *J Surg Oncol* 2006; **94**: 565-71. doi: 10.1002/jso.20674
- Le Bihan D, Turner R, Douek P, Patronas N. Diffusion MR imaging: clinical applications. *AJR Am J Roentgenol* 1992; **159**: 591-9. doi: 10.2214/ajr.159.3.1503032
- Dudeck O, Zeile M, Wybranski C, Schulmeister A, Fischbach F, Pech M, et al. Early prediction of anticancer effects with diffusion-weighted MR imaging in patients with colorectal liver metastases following selective internal radiotherapy. *Eur Radiol* 2010; **20**: 2699-706. doi: 10.1007/s00330-010-1846-z
- Welsh JS, Kennedy AS, Thomadsen B. Selective internal radiation therapy (SIRT) for liver metastases secondary to colorectal adenocarcinoma. *Int J Radiat Oncol Biol Phys* 2006; **66**(2 Suppl): S62-73. doi: 10.1016/j.ijrobp.2005.09.011

12. Lencioni R, Llovet JM. Modified RECIST (mRECIST) assessment for hepatocellular carcinoma. *Semin Liver Dis* 2010; **30**: 52-60. doi: 10.1055/s-0030-1247132
13. Kim MN, Kim BK, Han KH, Kim SU. Evolution from WHO to EASL and mRECIST for hepatocellular carcinoma: considerations for tumor response assessment. *Expert Rev Gastroenterol Hepatol* 2015; **9**: 335-48. doi: 10.1586/17474124.2015.959929
14. Vouche M, Kulik L, Atassi R, Memon K, Hickey R, Ganger D, et al. Radiological-pathological analysis of WHO, RECIST, EASL, mRECIST and DWI: imaging analysis from a prospective randomized trial of Y90 ± Sorafenib. *Hepatol* 2013; **58**: 1655-66. doi: 10.1002/hep.26487
15. Vossen JA, Buijs M, Kamel IR. Assessment of tumor response on MR imaging after locoregional therapy. *Tech Vasc Interv Radiol* 2006; **9**: 125-32. doi: 10.1053/j.tvir.2007.02.004
16. Ludwig JM, Camacho JC, Kokabi N, Xing M, Kim HS. The role of diffusion-weighted imaging (DWI) in Locoregional therapy outcome prediction and response assessment for hepatocellular carcinoma (HCC): the new era of functional imaging biomarkers. *Diagnostics* 2015; **5**: 546-63. doi: 10.3390/diagnostics5040546
17. Eisenhauer EA, Therasse P, Bogaerts J, Schwartz LH, Sargent D, Ford R, et al. New response evaluation criteria in solid tumours: revised RECIST guideline (version 1.1). *Eur J Cancer* 2009; **45**: 228-47. doi: 10.1016/j.ejca.2008.10.026
18. Hamm B, Thoeni RF, Gould RG, Bernardino ME, Lüning M, Saini S, et al. Focal liver lesions: characterization with nonenhanced and dynamic contrast material-enhanced MR imaging. *Radiology* 1994; **190**: 417-23. doi: 10.1148/radiology.190.2.8284392
19. Ishida K, Tamura A, Kato K, Uesugi N, Osakabe M, Eizuka M, et al. Correlation between CT morphologic appearance and histologic findings in colorectal liver metastasis after preoperative chemotherapy. *Abdom Radiol (NY)* 2018; **43**: 2991-3000. doi: 10.1007/s00261-018-1588-y
20. Koh DM, Collins DJ. Diffusion-weighted MRI in the body: applications and challenges in oncology. *AJR Am J Roentgenol* 2007; **188**: 1622-35. doi: 10.2214/ajr.06.1403
21. Le Bihan D, Breton E, Lallemand D, Grenier P, Cabanis E, Laval-Jeantet M. MR imaging of intravoxel incoherent motions: application to diffusion and perfusion in neurologic disorders. *Radiology* 1986; **161**: 401-7. doi: 10.1148/radiology.161.2.3763909
22. Cui Y, Zhang XP, Sun YS, Tang L, Shen L. Apparent diffusion coefficient: potential imaging biomarker for prediction and early detection of response to chemotherapy in hepatic metastases. *Radiology* 2008; **248**: 894-900. doi: 10.1148/radiol.2483071407
23. Eccles CL, Haider EA, Haider MA, Fung S, Lockwood G, Dawson LA. Change in diffusion weighted MRI during liver cancer radiotherapy: preliminary observations. *Acta Oncol* 2009; **48**: 1034-43. doi: 10.1080/02841860903099972
24. Koh DM, Scurr E, Collins D, Kanber B, Norman A, Leach MO, et al. Predicting response of colorectal hepatic metastasis: value of pretreatment apparent diffusion coefficients. *AJR Am J Roentgenol* 2007; **188**: 1001-8. doi: 10.2214/ajr.06.0601
25. Marugami N, Tanaka T, Kitano S, Hirohashi S, Nishiofuku H, Takahashi A, et al. Early detection of therapeutic response to hepatic arterial infusion chemotherapy of liver metastases from colorectal cancer using diffusion-weighted MR imaging. *Cardiovasc Intervent Radiol* 2009; **32**: 638-46. doi: 10.1007/s00270-009-9532-8
26. Schraml C, Schwenzer NF, Clasen S, Rempp HJ, Martirosian P, Claussen CD, et al. Navigator respiratory-triggered diffusion-weighted imaging in the follow-up after hepatic radiofrequency ablation-initial results. *J Magn Reson Imaging* 2009; **29**: 1308-16. doi: 10.1002/jmri.21770
27. Schmeel FC, Simon B, Luetkens JA, Traber F, Meyer C, Schmeel LC, et al. Prognostic value of pretreatment diffusion-weighted magnetic resonance imaging for outcome prediction of colorectal cancer liver metastases undergoing 90Y-microsphere radioembolization. *J Cancer Res Clin Oncol* 2017; **143**: 1531-41. doi: 10.1007/s00432-017-2395-5
28. Lahrswow M, Albrecht MH, Bickford MW, Vogl TJ. Predicting treatment response of colorectal cancer liver metastases to conventional lipiodol-based transarterial chemoembolization using diffusion-weighted MR imaging: value of pretreatment apparent diffusion coefficients (ADC) and ADC changes under therapy. *Cardiovasc Intervent Radiol* 2017; **40**: 852-9. doi: 10.1007/s00270-017-1634-0
29. von Elm E, Altman DG, Egger M, Pocock SJ, Gøtzsche PC, Vandenbroucke JP. The Strengthening of Reporting of Observational Studies in Epidemiology (STROBE) statement: guidelines for reporting observational studies. *J Clin Epidemiol* 2008; **61**: 344-9. doi: 10.1016/j.jclinepi.2007.11.008
30. Mohnike K, Wieners G, Schwartz F, Seidensticker M, Pech M, Ruehl R, et al. Computed tomography-guided high-dose-rate brachytherapy in hepatocellular carcinoma: safety, efficacy, and effect on survival. *Int J Radiat Oncol Biol Phys* 2010; **78**: 172-9. doi: 10.1016/j.ijrobp.2009.07.1700
31. Ingenerf MK, Karim H, Fink N, Ilhan H, Ricke J, Treitl KM, et al. Apparent diffusion coefficients (ADC) in response assessment of transarterial radioembolization (TARE) for liver metastases of neuroendocrine tumors (NET): a feasibility study. *Acta Radiol* 2022; **63**: 877-88. doi: 10.1177/02841851211024004
32. Outwater E, Tomaszewski JE, Daly JM, Kressel HY. Hepatic colorectal metastases: correlation of MR imaging and pathologic appearance. *Radiology* 1991; **180**: 327-32. doi: 10.1148/radiology.180.2.2068294
33. Curvo-Semedo L, Lambregts DM, Maas M, Beets GL, Caseiro-Alves F, Beets-Tan RG. Diffusion-weighted MRI in rectal cancer: apparent diffusion coefficient as a potential noninvasive marker of tumor aggressiveness. *J Magn Reson Imaging* 2012; **35**: 1365-71. doi: 10.1002/jmri.23589
34. Liu Z, Fan JM, He C, Li ZF, Xu YS, Li Z, et al. Utility of diffusion weighted imaging with the quantitative apparent diffusion coefficient in diagnosing residual or recurrent hepatocellular carcinoma after transarterial chemoembolization: a meta-analysis. *Cancer Imaging* 2020; **20**: 3. doi: 10.1186/s40644-019-0282-9

Quantitative assessment of bone marrow infiltration and characterization of tumor burden using dual-layer spectral CT in patients with multiple myeloma

Xing Xiong¹, Rong Hong¹, Xu Fan¹, Zhengmei Hao¹, Xiaohui Zhang², Yu Zhang³, Chunhong Hu¹

¹ Department of Radiology, The First Affiliated Hospital of Soochow University, Suzhou, Jiangsu, China

² Department of Clinical Science, Philips Healthcare Greater China, Shanghai, China

³ Department of Radiology, Dushu Lake Hospital Affiliated to Soochow University, Suzhou, China

Radiol Oncol 2024; 58(1): 43-50.

Received 18 August 2023

Accepted 31 October 2023

Correspondence to: Yu Zhang M.D., Department of Radiology, Dushu Lake Hospital Affiliated to Soochow University, Suzhou, 215163, China. E-mail: zhangyusdfyy@163.com and Chunhong Hu M.D., Department of Radiology, The First Affiliated Hospital of Soochow University, Suzhou, 215006, Jiangsu, China. E-mail: sudahuchunhong@163.com

Xing Xiong and Rong Hong contributed equally to this work.

Disclosure: No potential conflicts of interest were disclosed.

This is an open access article distributed under the terms of the CC-BY license (<https://creativecommons.org/licenses/by/4.0/>).

Background. The aim of the study was to evaluate whether virtual calcium subtraction (VNCA) image extracted from dual-layer spectral CT could estimate bone marrow (BM) infiltration with MRI as the reference standard and characterize tumor burden in patients with multiple myeloma (MM).

Patients and methods. Forty-seven patients with newly diagnosed MM were retrospectively enrolled. They had undergone whole-body low-dose dual-layer spectral CT (DLCT) and whole-body MRI within one week. VNCA images with calcium-suppressed (CaSupp) indices ranging from 25 to 95 at an interval of 10 and apparent diffusion coefficient (ADC) maps were quantitatively analyzed on vertebral bodies L1–L5 at the central slice of images. The optimal combination was selected by correlation analysis between CT numbers and ADC values. Then, it was used to characterize tumor burden by correlation analysis and receiver operating characteristic (ROC) curves analysis, including plasma cell infiltration rate (PCIR), high serum-free light chains (SFLC) ratio and the high-risk cytogenetic (HRC) status.

Results. The most significant quantitative correlation between CT numbers of VNCA images and ADC values could be found at CaSupp index 85 for averaged L1–L5 ($r = 0.612$, $p < 0.001$). It allowed quantitative evaluation of PCIR ($r = 0.835$, $p < 0.001$). It could also anticipate high SFLC ratio and the HRC status with *area under the curve* (AUC) of 0.876 and 0.760, respectively.

Conclusions. The VNCA measurements of averaged L1–L5 showed the highest correlation with ADC at CaSupp index 85. It could therefore be used as additional imaging biomarker for non-invasive assessment of tumor burden if ADC is not feasible.

Key words: bone marrow; tumor burden; virtual non-calcium; dual energy CT; multiple myeloma

Introduction

Multiple myeloma (MM) is one of the malignant hematological diseases with monoclonal proliferation of plasma cells which primarily involves bone marrow (BM).¹ “Myeloma bone disease” forms

when malignant proliferation of plasma cells displaces the healthy BM, and then results in activation of osteoclasts and inhibition of osteoblastic activity.^{2,3} The characterization of BM tumor burden has important indications for treatment regimens, treatment response and surveillance. It has

been exclusively accomplished by BM biopsy and serologic/urine markers such as plasma cell infiltration rate (PCIR), serum-free light chains (SFLC) ratio, paraproteins (M-protein) in serum/urine and cytogenetic status.⁴⁻⁶ However, these biomarkers examinations suffer unavoidable deficits such as invasive, painful and expensive.

As first introduced by Durie and Salmon in 1975, conventional radiographic survey of the skeleton was applied to stage MM bone disease.⁷ However, owing to low sensitivity in detecting osteolytic lesions and unable to evaluate therapy response, it calls for more practical techniques to be used. With the development of imaging techniques such as monoenergetic computed tomography (MECT), magnetic resonance imaging (MRI), and fluorodeoxyglucose positron-emission-tomography CT (FDG PET/CT), direct evaluation of BM infiltration has become possible.⁸ MECT is widespread available and economic efficient, so MM patients are commonly first assessed with whole body MECT scans.⁹ The major limitation of MECT is low sensitivity for detecting nonlytic BM infiltration in the axial skeleton, which is more common for MM patients. MRI is confirmed to be “imaging golden standard” for BM infiltration which has proven higher sensitivity in detecting MM lesions than any other modality.¹⁰ Whereas, it takes long time to accomplish examination for patients which may cause unbearable pain and claustrophobia.^{11,12} FDG PET/CT has been lately recommended to evaluate response and residual activity in treated patients as it could respond to BM changes quickly.¹³ However, the associated radiation and economic cost should be considered.

Dual-layer spectral CT (DLCT) is a novel CT technique with two different detector layers atop each other to absorb different parts of the polychromatic-attenuated X-ray spectrum. It could construct various parameter images e.g., uric acid, iodine, or calcium according to the aim of research retrospectively. Recent studies showed that DLCT, especially virtual non-calcium (VNCA) image, shows significant improvements in comparison to MECT and comparable to FDG PET/CT and MRI in the evaluation of MM.¹⁴⁻¹⁶ Hence, our study had two objectives: firstly, to explore the potential of VNCA image in estimating BM infiltration with MRI as the reference standard in MM patients. Secondly, to identify if VNCA image could characterize tumor burden by correlate with established biomarkers (PCIR, SFLC ratio and cytogenetic status).

Patients and methods

Patient characteristics

The study was approved by ethics committee of local institution and the need for written informed consent was waived due to retrospective nature of the study (registration number: 000/2021). All scans were performed for conventional clinical requirements.

We have collected the information of MM patients from 6/2021 to 10/2022 admitted to our institution consecutively. The inclusion criteria were as follows: (1) histologically confirmed diagnosis of MM; (2) the interval between clinical data, whole-body low-dose DLCT and whole-body MRI examination no more than two weeks; (3) received no specific therapy for MM before. The exclusion criteria were as follows: (1) patient's age below 18 years; (2) no complete clinical data, neither DLCT nor MRI examination; (3) obvious metal or motion artifacts affecting the lumbar vertebral segmentation.

Imaging acquisition and post-processing

All scans were performed on a commercially available spectral detector DLCT scanner (IQon Spectral CT, Philips Healthcare), following the most recent recommendations of the International Myeloma Working Group (IMWG).¹⁷ Patients were placed in a head-first supine position. The scan ranges from vertex of the skull to the knees. No contrast agent was given. Scan parameters were as follows: tube voltage, 120 kV; tube current, 70 mAs; collimation, 64×0.625 mm; pitch, 0.990; rotation time, 0.75 s; volumetric computed tomography dose index, 7.4 mGy. Mean dose length product was 1069.2 ± 205.9 mGy*cm. The field of view (FOV) was adjusted depending on patient body volume.

The corresponding MRI examination was performed on a 3.0 T scanner (Magnetic Verio, Siemens Healthcare, Erlangen Germany). The patients were also placed in a head-first supine position. Phased-array surface coils were installed to cover from the head to the upper femur. No contrast medium was given. The protocol parameters were as follows: T2 turbo inversion recovery magnitude (TIRM) sequence [echo time (TE), 84 ms; repetition time (TR), 7110 ms; slice thickness, 5 mm; slice gap, 1.5 mm; FOV, 480 mm] was acquired on the coronal plane from the head to the upper femur. On the same coverage area, axial DWI sequences were acquired using two values ($b = 50, 700 \text{ s/mm}^2$) with

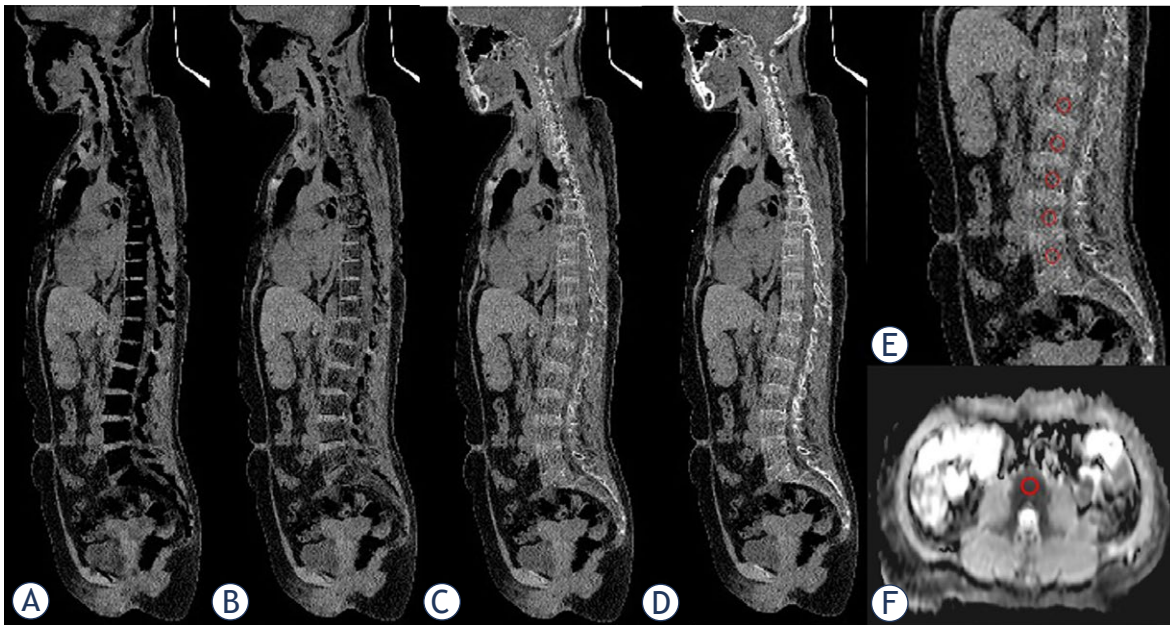


FIGURE 1. An example of bone marrow (BM) segmentation in multiple myeloma (MM) patient. An oval regions of interests (ROIs) of 100 mm² was drawn at the central slice of sagittal vertebral bodies L1–L5 in different virtual calcium subtraction (VNCA) images and the corresponding location was manually displayed on the axial apparent diffusion coefficient (ADC) map. (A) calcium-suppressed (CaSupp) index 25, (B) CaSupp index 55, (C) CaSupp index 85, (D) CaSupp index 95, (E) magnification of (C), (F) ADC map.

the following parameters: TR, 4000 ms; TE, 46 ms; slice thickness, 5 mm; slice gap, 0; FOV, 450 mm.

Post-processing of spectral-based image (SBI) data was performed with the vendor's software (IntelliSpace Portal Version 11, Philips Healthcare). First, all SBI images were reconstructed in a 512 × 512 matrix, slice thickness 2 mm with an overlap of 1 mm. Then, VNCA images were created from SBI data by exploiting the material specific attenuation of X-rays in different energy levels to simulate each voxels attenuation in Hounsfield units without the calcium-specific contribution. The intelligent post-processing vendor allows calcium suppression in seamlessly adjustable factors. In our study, VNCA images were reconstructed with calcium-suppressed (CaSupp) indices ranging from 25 to 95 in steps of 10. Among them, CaSupp indice 25 means images has minimum visibility of bony structures and 95 means maximum visibility.

Segmentation of the bone marrow

Although the MM lesions were scattered, it involved typical location such as lumbar vertebra, pelvis and ribs. So, we chose to focus on L1–L5 due to the large size of those vertebrae with maximized reliable measurement, typical sites of BM infiltra-

tion and minimally affected by the intrauterine device.^{18,19} Using the same software, regions of interests (ROIs) were positioned manually in the sagittal vertebral bodies L1–L5 to measure the respective CT numbers and basivertebral vein was avoided from the ROIs. Since the lumbar vertebra were wide, a standard circular ROI which size set to 100 mm² was placed at the central slice. To ensure comparability, ROIs were copied between different CaSupp indices. At the same time, the corresponding location was contoured manually on the axial apparent diffusion coefficient (ADC) map (Figure 1). The images were analyzed by two radiologists with more than 5 years of experience who were blinded to any patient information. The intraclass correlation coefficient (ICC) was calculated for determining the interrater reliability of the quantitative assessment. The final CT number and ADC values were averaged. The analysis of VNCA and ADC images was conducted for 10 min per person.

Assessment of established biomarkers

PCIR was obtained through BM biopsy on the wing of ilium and assessed by our in-house pathologists. Immunoturbidimetry was used to detect the expression levels of SFLC kappa and

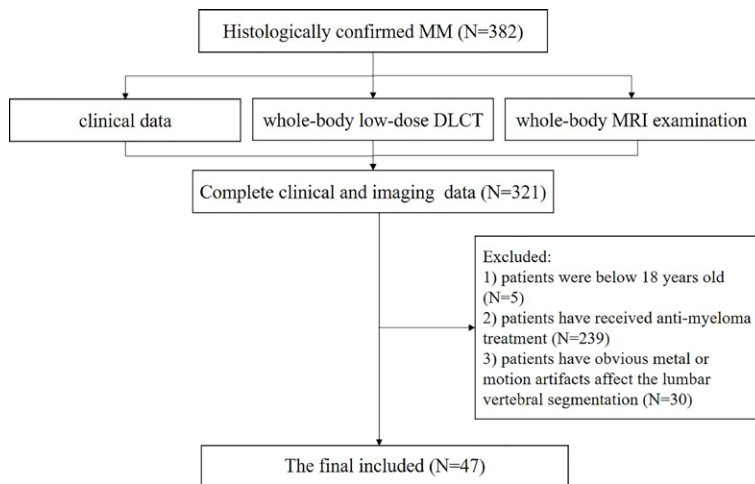


FIGURE 2. Flow chart of patients' selection.

DLCT = low-dose dual-layer spectral CT; MM = multiple myeloma

lambda. SFLC ratio were classified as high (<0.01 or >100) or low (0.01–100) according to the IMWG criteria and the practical experience of our institution.^{20,21} Cytogenetic status was performed by fluorescence in situ hybridization (FISH) in interphase cells to overcome the problem of karyotyping. MM patients were divided into high-risk cytogenetic (HRC) and standard risk cytogenetic (SRC) groups on the basis of FISH results. Patients who pre-

TABLE 1. Patient characteristics

Characteristics	n
Age*	57.9 ± 8.1
Sex#	
Males	26 (55.3%)
Females	21 (44.7%)
Myeloma subtypes#	
IgG	32 (68.1%)
IgA	10 (21.3%)
Light chain	5 (10.6%)
Plasma cell infiltration ratio obtained from the wing of ilium*	0.54 ± 0.30
Kappa/lambda SFLC ratio#	
High (< 0.01 or > 100)	27 (57.4%)
Low (0.01–100)	20 (42.6%)
Cytogenetic status#	
HRC	26 (55.3%)
SRC	21 (44.7%)

*represented as Mean ± SD; # represented as number (percentage)

HRC = high-risk cytogenetic; SD = Standard deviation; SFLC = serum-free light chains; SRC = standard risk cytogenetics

sented with any of the following cytogenetic abnormalities (CAs) were categorized into the HRC group: del(17p), t(4;14), t(14;16), t(14;20), gain(1p), or p53 mutation. Other MM patients were allocated into the SRC group.

Statistic assessment

Statistical analysis was performed by either SPSS 22.0 software (Chicago, IL, USA) or MedCalc statistical software version 16.4.3 (Ostend, Belgium). Correlations between different VNCa CT numbers (combined L1–L5 with different CaSupp indices) and ADC values were calculated. Since VNCa CT numbers and ADC values were normally distributed, Pearson's correlation analysis was applied. Then the optimal combination was used to characterize PCIR by correlation analysis and receiver operating characteristic curves (ROC) analysis was carried out to predict binary outcomes "high SFLC ratio" and "HRC status". Statistical significance was defined as $p \leq 0.05$.

Results

Patient characteristics

A total of 382 MM patients were admitted at the hematology center in our institution for whole-body DLCT. Of these, 5 patients had to be excluded because they were under 18 years old. 239 patients had to be excluded because they have received anti-myeloma treatment. 61 patients had no complete clinical data, neither DLCT nor MRI examination. Another 30 patients had obvious metal or motion artifacts that affected the lumbar vertebral segmentation. Consequently, 47 MM patients were included. Enrollment results of MM patients after exclusion were shown in the Figure 2. The average interval between the clinical examination and DLCT scan was 10 days [interquartile range 3.0–13.5 days]. The clinical characteristics are shown in Table 1. The interrater reliability of all quantitative measurements was very high with ICC ranged from 0.824–0.970.

Correlation analysis

1880 and 235 ROIs were derived from VNCa images for different CaSupp indices and ADC maps, respectively. Table 2 shows the mean ADC values and CT numbers (combination of different vertebral bodies and CaSupp indices). Regardless of the measured location, CT numbers in VNCa

TABLE 2. Means and standard deviations of MRI apparent diffusion coefficient (ADC) and CT numbers in virtual calcium subtraction (VNCA) images for all measured locations

	L1	L2	L3	L4	L5	Averaged L1-L5
ADC	554.12 ±177.42	520.02 ±171.74	546.19 ±179.75	523.20 ±175.14	524.3 ±173.17	536.30 ±163.93
CaSupp 25	-236.58±77.07	-227.60 ±73.00	-217.83 ±83.35	-225.40 ±82.36	-244.67 ±79.27	-221.19 ±78.89
CaSupp 35	-138.15±46.58	-131.15 ±43.86	-127.11 ±51.4	-133.38 ±49.30	-143.10 ±48.23	-128.84 ±47.37
CaSupp 45	-82.04 ±30.19	-77.33 ±28.86	-75.38 ±34.45	-81.01 ±31.32	-85.24 ±31.31	-76.42 ±30.10
CaSupp 55	-45.12 ±20.87	-41.925 ±20.70	-41.32 ±24.80	-46.57 ±20.95	-47.08 ±21.44	-41.92 ±19.91
CaSupp 65	-18.50 ±16.35	-16.38 ±17.05	-16.79 ±19.89	-21.71 ±15.83	-19.71 ±16.14	-17.07 ±14.58
CaSupp 75	2.03 ±15.39	3.29 ±16.53	2.12 ±18.3	-2.58 ±14.9	1.42 ±14.54	2.08 ±13.26
CaSupp 85	18.63 ±16.60	19.22 ±17.75	17.45 ±18.93	12.93 ±16.52	18.55 ±15.37	17.61 ±14.59
CaSupp 95	32.46 ±19.15	32.46 ±20.12	30.25 ±20.75	25.98 ±19.16	33.00 ±17.41	30.59± 17.20

CaSupp = calcium-suppressed index

images at CaSupp indices from 75 to 95 were significantly correlated with ADC (Pearson’s r ranges from 0.342–0.612, with all p < 0.05). Inversely, CT numbers in VNCA images at CaSupp indices from 35 to 45 showed no correlation with ADC for all locations. The highest correlation of VNCA-CT numbers and ADC values was averaged L1-L5 at CaSupp indices 85 (Pearson’s r = 0.612, p < 0.001). Figure 3 provides the statistical results regarding the correlation between CT numbers (combined different CaSupp indices with measured locations) and ADC values.

Characterize tumor burden with optimal combination of CaSupp index and vertebral body

The CT number of averaged L1-L5 at CaSupp index 85 showed significant correlation with the PCIR (r = 0.835, p < 0.001) confirmed by BM biopsy

(Figure 4). It showed a mean infiltration ratio of 54% (range, 10%–95%; median 60%).

We performed ROC analysis with the predictor binary outcome “SFLC ratio” and “cytogenetic status” using the CT number of averaged L1-L5 at CaSupp index 85. Expectedly, it exhibited satisfying performance for discriminating high and low SFLC ratio with area under the curve (AUC) of 0.876 (0.736–0.958). The corresponding sensitivity, specificity and cutoff value were 0.952, 0.800, 10.66, respectively. Also, AUC for prediction of the “cytogenetic status” was 0.760 (0.603–0.878). The corresponding sensitivity, specificity and cutoff value were 0.714, 0.762, 20.43, respectively (Figure 5A, B).

Discussion

Our results showed that VNCA images derived from DLCT could estimate BM infiltration with

	L1		L2		L3		L4		L5		Average L1-L5	
	r	p	r	p	r	p	r	p	r	p	r	p
CaSupp 25	-0.03052	0.8478	-0.1441	0.3508	-0.1111	0.4783	-0.3013	0.0469	-0.1658	0.2941	-0.134	0.369
CaSupp 35	0.04731	0.7661	-0.09898	0.5227	-0.03702	0.8137	-0.2544	0.0956	-0.09565	0.5468	-0.06698	0.6546
CaSupp 45	0.1586	0.3159	0.000739	0.9962	0.0664	0.6723	-0.1748	0.2564	0.009092	0.9544	0.03848	0.7973
CaSupp 55	0.3105	0.0454	0.1407	0.3622	0.2027	0.1924	-0.04001	0.7965	0.1653	0.2955	0.2015	0.1744
CaSupp 65	0.4725	0.0016	0.2914	0.055	0.3527	0.0204	0.1602	0.2988	0.3613	0.0187	0.4156	0.0037
CaSupp 75	0.5631	0.0001	0.398	0.0075	0.4662	0.0016	0.3424	0.0229	0.5247	0.0004	0.5762	< 0.0001
CaSupp 85	0.568	<0.0001	0.4448	0.0025	0.5165	0.0004	0.4358	0.0031	0.5894	<0.0001	0.6118	<0.0001
CaSupp 95	0.5362	0.0003	0.4549	0.0019	0.5234	0.0003	0.4675	0.0014	0.5911	<0.0001	0.5868	<0.0001

FIGURE 3. Heat map of Pearson's correlation r and p value between CT numbers (combined different calcium-suppressed [CaSupp] indices with measured locations) and apparent diffusion coefficient (ADC) values.

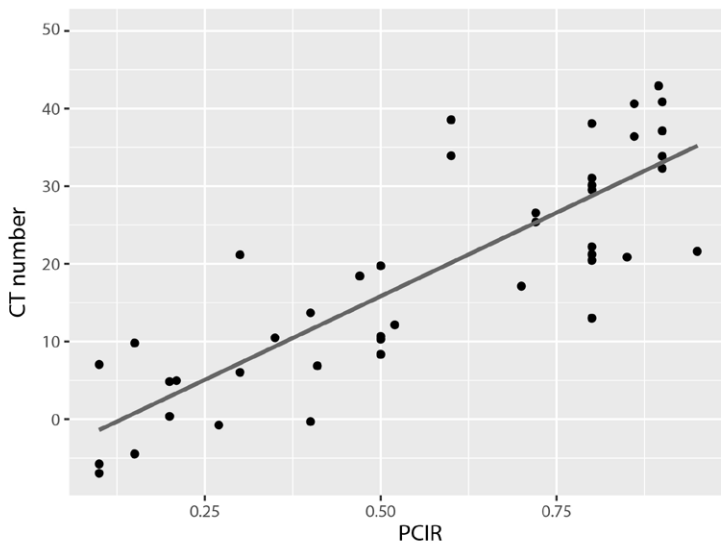


FIGURE 4. Bivariate correlation between CT number (averaged L1–L5 at calcium-suppressed [CaSupp] index 85) and plasma cell infiltration rate (PCIR) confirmed by bone marrow biopsy. The Pearson's r yields 0.835 with p value < 0.001.

MRI as the reference, especially the CT number of averaged L1–L5 at CaSupp index 85 showed the highest correlation with ADC. What's more, it allowed quantitative evaluation of tumor burden by correlating with PCIR and anticipating high SFLC ratio and the HRC status.

Instead of activating a second X-ray tube or rapid-voltage switching tube before performing the examination, DLCT adopts two different detector layers to decrease X-ray dose. For postprocessing, the flexible vendor could construct different parameters. VNca image is a common parameter in musculoskeletal system^{9,22,23}, in which the osseous component is removed from the spectral base data in order to improve visualization of BM. The degree of calcium suppression depends on the CaSupp index, which defines the calcium composition level. Several documents have confirmed the importance of VNca image. Fervers *et al.* assumed that the pathologic BM was defined as voxels >0 HU and concluded that it could significantly predict BM infiltration, osteolytic lesions and the clinical diagnosis of MM.¹⁴ However, there is no consensus for the CT cutoff number of pathologic BM. Brandelik *et al.* assessed the potential of VNca images to reflect BM infiltration.¹⁶ They evaluated the different regions (C7, T12, L1–L5) and infiltration patterns (non-diffuse and diffuse). However, C7 is not the typical region for BM infiltration and could be influenced by beam hardening artifacts easily as far as we know.²⁴ Fervers *et al.* also inves-

tigated if VNca images might discriminate metabolically vital, focal lesions from avital lesions in MM patients with FDG PET/CT as the standard of reference.¹⁵ Best result was yielded by high calcium suppression, followed by medium and low calcium suppression. However, the median interval time between DECT and FDG PET/CT was 53 days which was so long to leave time window for possible change in tumor biology between two images. In our study, the CaSupp indices ranged from 25 to 95 with an interval of 10 to search for the optimal CaSupp index, which may be more scientific and comprehensive. There is a growing tendency of the importance for increased CaSupp index that high CaSupp index could provide more information for BM infiltration and tumor burden than low CaSupp index. This might due to gradual exposure of underlying plasma cell cluster by increasing calcium suppression, which further validates VNca images as a measurement tool for tumor burden. The averaged L1–L5 seems to be more representative than single lumbar vertebra due to the large size of those vertebrae with maximized reliable measurement avoiding sclerosis, fractures, or disc herniations. We did not divide the infiltration pattern according to MRI performance and we believe that this “agnostic” approach provides a more reliable marrow sample for evaluation of BM infiltration.²⁵

We have included laboratory biomarkers to evaluate MM tumor burden. Among them, PCIR was obtained through BM biopsy on the iliac crest clinically, which is painful and uncomfortable for most patients. Despite IMWG recommendation²⁶, a recent large-scale clinical analysis was performed to explore whether BM biopsy is necessary in all patients diagnosed with monoclonal protein since in some cases it did not contribute to the diagnosis. In our study, PCIR was correlated well with CT number of averaged L1–L5 at CaSupp index 85. Thus, it's promising to obtain PCIR results by measuring CT number noninvasively. Due to different thresholds for the serum paraproteins of MM subtypes (e.g., IgA, IgG, IgM), only SFLC ratio was taken into consideration which is also an important indicator of tumor burden. In 2014, the IMWG included the SFLC ratio in the diagnostic criteria for MM, and SFLC ratio >100 is considered as a biomarker for ultrahigh-risk smoldering MM patient.⁴ However, some MM patients are non-secretory or hypo-secretory and are therefore difficult to surveil by means of serologic/urine markers alone which influences patient management at primary diagnosis and during therapy.²⁷

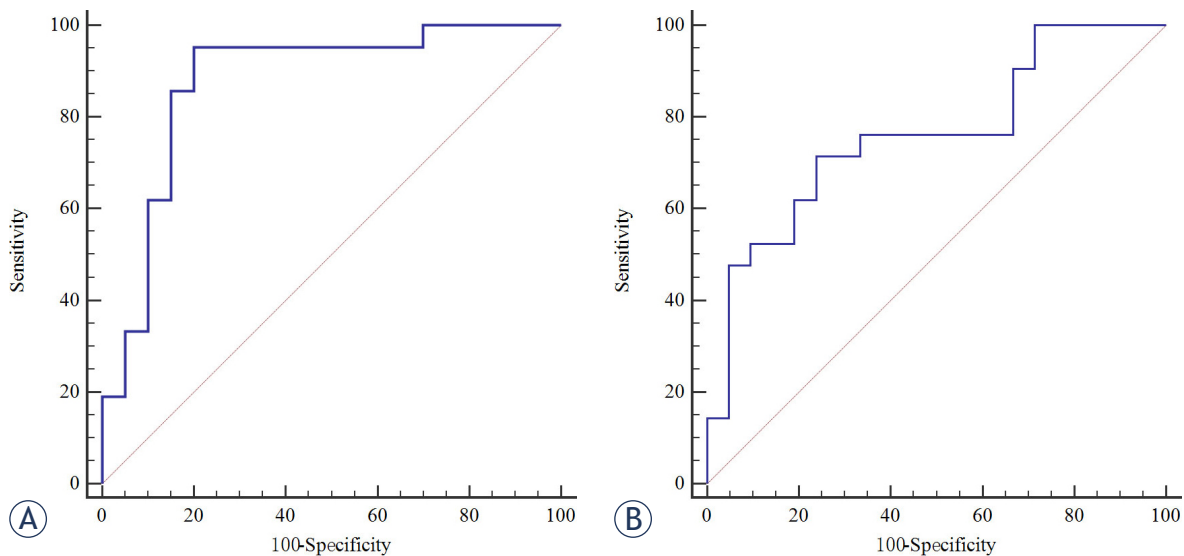


FIGURE 5. Receiver operating characteristic curves for CT number (averaged L1–L5 at calcium-suppressed [CaSupp] index 85) to predict "high serum-free light chains (SFLC) ratio" (A) and "cytogenetic status" (B).

What's more, myeloma may escape hematologic diagnosis if it extends outside the marrow cavities (extramedullary).²⁸ Similarly, ROC analysis indicates satisfactory performance for VNCA images to discriminate high and low SFLC ratio with AUC 0.876. Some studies have found that CAs are significantly associated with the proliferation and secretion of tumor cells.^{29–31} It was obtained through different invasive methods such as FISH. However, this technique suffers some drawbacks. For example, the patients may experience the pain of biopsy and bear the expensive expenses. What's more, the BM results may be influenced by intratumoral heterogeneity and poor sample quality.^{32–33} So, developing a convenient and noninvasive method to predict cytogenetic status is critical for clinicians and patients. The results showed that VNCA images could anticipate HRC status with preferable AUC, sensitivity and specificity of 0.760, 0.714 and 0.762. Since the above specific situations may exist in clinical practice, such as painful and unbearable biopsy for some patients, non-secretory or hypo-secretory M protein, extramedullary infiltration et al., DLCT could be employed to evaluate tumor burden additionally.

There are some limitations that needed to be discussed. First, the number of patients was rather small. Since the incidence rate of MM is lower than other diseases and is complex to deal with, so patients are usually admitted to specialized hospitals. Second, it was validated in the lumbar vertebra which were considered as the representative

region of BM infiltration and minimally affected by the intrauterine device. But this needs to be up-scaled across the body and also has more robust measurement of technique accuracy. Third, correlation with PCIR was possible only for the pelvic bones, but this reflects the deficit of daily practice. Finally, this study investigated the ability of DLCT acquired by specific scanner, imaging protocols, and post-processing tools which may not widely applied in other institutions. In the future, more studies are needed for definitive evaluation of this powerful technological equipment.

Conclusions

Quantitative assessment of VNCA images in DLCT is a potential determination of BM infiltration extent in MM for radiologists and would be promising incorporated into the daily clinical practice, especially when the gold standard MRI is not accessible. Therefore, VNCA images could be used as additional imaging biomarkers for non-invasive assessment of tumor burden.

Acknowledgement

This study has received funding by Gusu health talent project of Suzhou (GSWS2020003) and Suzhou Science and Technology Project (SKJY2021025).

References

- Kazandjian D. Multiple myeloma epidemiology and survival: a unique malignancy. *Semin Oncol* 2016; **43**: 676-81. doi: 10.1053/j.seminoncol.2016.11.004
- Panaroni C, Yee AJ, Raju NS. Myeloma and bone disease. *Curr Osteoporos Rep* 2017; **15**: 483-98. doi: 10.1007/s11914-017-0397-5
- O'Donnell EK, Raju NS. Myeloma bone disease: pathogenesis and treatment. *Clin Adv Hematol Oncol* 2017; **15**: 285-95. PMID: 28591104
- Rajkumar SV, Dimopoulos MA, Palumbo A, Blade J, Merlini G, Mateos MV, et al. International Myeloma Working Group updated criteria for the diagnosis of multiple myeloma. *Lancet Oncol* 2014; **15**: e538-48. doi: 10.1016/S1470-2045(14)70442-5
- Duvauferrier R, Valence M, Patrat-Delon S, Brillet E, Niederberger E, Marchand A, et al. Current role of CT and whole body MRI in multiple myeloma. *Diagn Interv Imaging* 2013; **94**: 169-83. doi: 10.1016/j.diii.2012.12.001
- Dimopoulos M, Terpos E, Comenzo RL, Tosi P, Beksac M, Sezer O, et al. International Myeloma Working Group consensus statement and guidelines regarding the current role of imaging techniques in the diagnosis and monitoring of multiple myeloma. *Leukemia* 2009; **23**: 1545-56. doi: 10.1038/leu.2009.89
- Durie BG, Salmon SE. A clinical staging system for multiple myeloma. Correlation of measured myeloma cell mass with presenting clinical features, response to treatment, and survival. *Cancer* 1975; **36**: 842-54. doi: 10.1002/1097-0142(197509)36:3<842::aid-cnrcr2820360303>3.0.co;2-u
- Portet M, Owens E, Howlett D. The use of whole-body MRI in multiple myeloma. *Clin Med* 2019; **19**: 355-6. doi: 10.7861/clinmedicine.19-4-355
- Kosmala A, Weng AM, Heidemeier A, Krauss B, Knop S, Bley TA, et al. Multiple myeloma and dual-energy CT: diagnostic accuracy of virtual non-calcium technique for detection of bone marrow infiltration of the spine and pelvis. *Radiology* 2018; **286**: 205-13. doi: 10.1148/radiol.2017170281
- Hillengass J, Usmani S, Rajkumar SV, Durie BGM, Mateos MV, Lonial S, et al. International Myeloma Working Group consensus recommendations on imaging in monoclonal plasma cell disorders. *Lancet Oncol* 2019; **20**: e302-e312. doi: 10.1016/S1470-2045(19)30309-2
- Shah LM, Hanrahan CJ. MRI of spinal bone marrow: part I, techniques and normal age-related appearances. *AJR Am J Roentgenol* 2011; **197**: 1298-308. doi: 10.2214/AJR.11.7005
- Padhani AR, Koh DM, Collins DJ. Whole-body diffusion-weighted MR imaging in cancer: current status and research directions. *Radiology* 2011; **261**: 700-18. doi: 10.1148/radiol.11110474
- Cavo M, Terpos E, Nanni C, Moreau P, Lentzsch S, Zweegman S, et al. Role of (18)F-FDG PET/CT in the diagnosis and management of multiple myeloma and other plasma cell disorders: a consensus statement by the International Myeloma Working Group. *Lancet Oncol* 2017; **18**: e206-e217. doi: 10.1016/S1470-2045(17)30189-4
- Fervers P, Fervers F, Kottlors J, Lohneis P, Pollman-Schweckhorst P, Zaytoun H, et al. Feasibility of artificial intelligence-supported assessment of bone marrow infiltration using dual-energy computed tomography in patients with evidence of monoclonal protein - a retrospective observational study. *Eur Radiol* 2022; **32**: 2901-11. doi: 10.1007/s00330-021-08419-2
- Fervers P, Glauner A, Gertz R, Täger P, Kottlors J, Maintz D, et al. Virtual calcium-suppression in dual energy computed tomography predicts metabolic activity of focal MM lesions as determined by fluorodeoxyglucose positron-emission-tomography. *Eur J Radiol* 2021; **135**: 109502. doi: 10.1016/j.ejrad.2020.109502
- Brandelik SC, Skornitzke S, Mokry T, Sauer S, Stiller W, Nattenmüller J, et al. Quantitative and qualitative assessment of plasma cell dyscrasias in dual-layer spectral CT. *Eur Radiol* 2021; **31**: 7664-73. doi: 10.1007/s00330-021-07821-0
- Moulopoulos LA, Koutoulidis V, Hillengass J, Zamagni E, Querretta JD, Roche CL, et al. Recommendations for acquisition, interpretation and reporting of whole body low dose CT in patients with multiple myeloma and other plasma cell disorders: a report of the IMWG Bone Working Group. *Blood Cancer J* 2018; **8**: 95. doi: 10.1038/s41408-018-0124-1
- Reinert CP, Krieg E, Esser M, Nikolaou K, Bösmüller H, Horger M. Role of computed tomography texture analysis using dual-energy-based bone marrow imaging for multiple myeloma characterization: comparison with histology and established serologic parameters. *Eur Radiol* 2021; **31**: 2357-67. doi: 10.1007/s00330-020-07320-8
- Hu C, Zhang Y, Xiong X, Meng Q, Yao F, Ye A, et al. Quantitative evaluation of bone marrow infiltration using dual-energy spectral computed tomography in patients with multiple myeloma. *J Xray Sci Technol* 2021; **29**: 463-75. doi: 10.3233/XST-200811
- Mosebach J, Thierjung H, Schlemmer HP, Delorme S. Multiple myeloma guidelines and their recent updates: implications for imaging. *Rofo* 2019; **191**: 998-1009. doi: 10.1055/a-0897-3966
- Cowan AJ, Green DJ, Kwok M, Lee S, Coffey DG, Holmberg LA, et al. Diagnosis and management of multiple myeloma: a review. *JAMA* 2022; **327**: 464-77. doi: 10.1001/jama.2022.0003
- Thomas C, Schabel C, Krauss B, Weisel K, Bongers M, Claussen CD, et al. Dual-energy CT: virtual calcium subtraction for assessment of bone marrow involvement of the spine in multiple myeloma. *AJR Am J Roentgenol* 2015; **204**: W324-31. doi: 10.2214/AJR.14.12613
- Ekert K, Hinterleitner C, Baumgartner K, Fritz J, Horger M. Extended texture analysis of non-enhanced whole-body MRI image data for response assessment in multiple myeloma patients undergoing systemic therapy. *Cancers* 2020; **12**: 761. doi: 10.3390/cancers12030761
- Yu Z, Leng S, Jorgensen SM, Li Z, Gutjahr R, Chen B, et al. Evaluation of conventional imaging performance in a research whole-body CT system with a photon-counting detector array. *Phys Med Biol* 2016; **61**: 1572-95. doi: 10.1088/0031-9155/61/4/1572
- Koutoulidis V, Terpos E, Papanikolaou N, Fontara S, Seimenis I, Gavriatopoulou M, et al. Comparison of MRI features of fat fraction and ADC for early treatment response assessment in participants with multiple myeloma. *Radiology* 2022; **304**: 137-44. doi: 10.1148/radiol.211388
- Sidiqi MH, Aljama M, Kumar SK, Jevremovic D, Buadi FK, Warsame R, et al. The role of bone marrow biopsy in patients with plasma cell disorders: should all patients with a monoclonal protein be biopsied? *Blood Cancer J* 2020; **10**: 52. doi: 10.1038/s41408-020-0319-0
- Dupuis MM, Tuchman SA. Non-secretory multiple myeloma: from biology to clinical management. *Onco Targets Ther* 2016; **9**: 7583-90. doi: 10.2147/OTT.S122241
- Wale A, Pawlyn C, Kaiser M, Messiou C. Frequency, distribution and clinical management of incidental findings and extramedullary plasmacytomas in whole body diffusion weighted magnetic resonance imaging in patients with multiple myeloma. *Haematologica* 2016; **101**: e142-4. doi: 10.3324/haematol.2015.139816
- Hamdaoui H, Benlarroubia O, Ait Boujmia OK, Mossafa H, Ouldin K, Belkhatay A, et al. Cytogenetic and FISH analysis of 93 multiple myeloma Moroccan patients. *Mol Genet Genomic Med* 2020; **8**: e1363. doi: 10.1002/mgg3.1363
- Saxe D, Seo EJ, Bergeron MB, Han JY. Recent advances in cytogenetic characterization of multiple myeloma. *Int J Lab Hematol* 2019; **41**: 5-14. doi: 10.1111/ijlh.12882
- Zhao XQ, Zhao SY, Chen WX, Liu XW, Yan HX, Lou YJ. Correlation between clinical factors and prognosis in newly diagnosed multiple myeloma. *J Coll Physicians Surg Pak* 2020; **30**: 601-5. doi: 10.29271/jcpsp.2020.06.601
- Usmani SZ, Crowley J, Hoering A, Mitchell A, Waheed S, Nair B, et al. Improvement in long-term outcomes with successive total therapy trials for multiple myeloma: are patients now being cured? *Leukemia* 2013; **27**: 226-32. doi: 10.1038/leu.2012.160
- Ross FM, Avet-Loiseau H, Ameye G, Gutiérrez NC, Liebisch P, O'Connor S, et al. Report from the European Myeloma Network on interphase FISH in multiple myeloma and related disorders. *Haematologica* 2012; **97**: 1272-7. doi: 10.3324/haematol.2011.056176

The equivalence of different types of electric pulses for electrochemotherapy with cisplatin – an *in vitro* study

Maria Scuderi¹, Janja Dermol-Cerne¹, Janez Scancar^{2,3}, Stefan Markovic^{2,3}, Lea Rems¹, Damijan Miklavcic¹

¹ Faculty of Electrical Engineering, University of Ljubljana, Ljubljana, Slovenia

² Department of Environmental Sciences, Jožef Stefan Institute, Ljubljana, Slovenia

³ Jožef Stefan International Postgraduate School, Ljubljana, Slovenia

Radiol Oncol 2024; 58(1): 51-66.

Received 20 November 2023

Accepted 5 December 2023

Correspondence to: Prof. Damijan Miklavčič, Ph.D., Faculty of Electrical Engineering, University of Ljubljana, Tržaška cesta 25, SI-1000 Ljubljana, Slovenia. E-mail: damijan.miklavcic@fe.uni-lj.si

Disclosure: No potential conflicts of interest were disclosed.

This is an open access article distributed under the terms of the CC-BY license (<https://creativecommons.org/licenses/by/4.0/>).

Background. Electrochemotherapy (ECT) is a treatment involving the administration of chemotherapeutic drugs followed by the application of 8 square monopolar pulses of 100 μ s duration at a repetition frequency of 1 Hz or 5000 Hz. However, there is increasing interest in using alternative types of pulses for ECT. The use of high-frequency short bipolar pulses has been shown to mitigate pain and muscle contractions. Conversely, the use of millisecond pulses is interesting when combining ECT with gene electrotransfer for the uptake of DNA-encoding proteins that stimulate the immune response with the aim of converting ECT from a local to systemic treatment. Therefore, the aim of this study was to investigate how alternative types of pulses affect the efficiency of the ECT.

Materials and methods. We performed *in vitro* experiments, exposing Chinese hamster ovary (CHO) cells to conventional ECT pulses, high-frequency bipolar pulses, and millisecond pulses in the presence of different concentrations of cisplatin. We determined cisplatin uptake by inductively coupled plasma mass spectrometry and cisplatin cytotoxicity by the clonogenic assay.

Results. We observed that the three tested types of pulses potentiate the uptake and cytotoxicity of cisplatin in an equivalent manner, provided that the electric field is properly adjusted for each pulse type. Furthermore, we quantified that the number of cisplatin molecules, resulting in the eradication of most cells, was $2-7 \times 10^7$ per cell.

Conclusions. High-frequency bipolar pulses and millisecond pulses can potentially be used in ECT to reduce pain and muscle contraction and increase the effect of the immune response in combination with gene electrotransfer, respectively.

Key words: electrochemotherapy; electroporation; cisplatin uptake; phenomenological model; equivalent pulse parameters

Introduction

Electrochemotherapy (ECT) is a highly effective local treatment used in clinics to treat superficial tumors, specifically various types of skin tumors when standard treatments such as surgery, chemotherapy, and radiotherapy are not sufficient or ap-

plicable.^{1,2} Over the past decade, ECT has also been successfully used for the treatment of deep-seated tumors, including tumors in the liver, bone, and pancreas.³⁻⁹

ECT essentially consists of two main steps.^{10,11} First, a chemotherapeutic drug is injected intratumorally or intravenously. Second, short high-

intensity electric pulses that result in cell membrane electroporation are delivered to the tumor. Electroporation transiently increases the cell membrane permeability through the formation of pores/defects in the membrane and enhances the intracellular uptake of the chemotherapeutic drug. The drugs most often used in ECT are bleomycin and cisplatin, which kill cancerous cells by acting on DNA but poorly permeate the cell membrane.^{1,12} Electroporation potentiates the uptake, and consequently the cytotoxicity, of bleomycin by several hundred to thousand folds and of cisplatin by several ten folds compared to nonelectroporated controls.¹³⁻¹⁵ In addition to increased intracellular drug delivery, drug entrapment due to the blood flow modifying effect of electric pulses¹⁶, the vascular disrupting effect^{17,18} and immune system response^{19,20} were identified to critically contribute to the success of ECT.²¹

Electroporation can be achieved with a wide range of pulse parameters (pulse shape, polarity, duration, amplitude, number, repetition rate, etc.). In ECT, conventionally 8 square monopolar pulses of 100 μ s duration at a repetition frequency of 1 Hz or 5000 Hz are applied.^{10,11,22} However, the use of 100 μ s long pulses causes pain and muscle contractions^{23,24} in the patient during the treatment. Furthermore, muscle contraction might lead to the displacement of the electrodes resulting in undertreatment²⁵ and in potential harm for the vital structures when treating deep-seated tumors.²⁶ Thus, there is a need to use local or general anesthesia and muscle relaxants and, when performing ECT of deep-seated tumors in proximity to the heart, the pulses need to be synchronized with the heart rhythm.²⁷⁻³¹ To overcome these drawbacks, recent studies suggest the use of bursts of short high-frequency bipolar pulses (1-10 μ s pulse duration), which minimize pain and muscle contractions.^{23,32,33} Such pulses are already used for the ablation of tumors³⁴ and cardiac tissue³⁵⁻³⁷ by irreversible electroporation. Furthermore, *in vitro* and *in vivo* studies show that high-frequency bipolar pulses can potentially be used in ECT.^{38,39} Recent reports demonstrated the safety, tolerability, and efficacy of using high-frequency bipolar pulses for the treatment of cutaneous tumors with ECT.⁴⁰⁻⁴²

In ECT preclinical and clinical studies have shown that immune response critically contributes to tumor eradication.^{19,43,44} Thus, ECT has been tested in combination with gene electrotransfer (GET) which delivers protein-encoding DNA into tumor cell/tissue to induce immune stimulation.⁴⁵⁻⁴⁷ Even if the combined ECT+GET treat-

ment was applied only to some of the cutaneous metastases, this combination successfully evoked a systemic immune response and in some cases succeeded in producing a partial response or complete response of distant, non-treated nodules (i.e., abscopal effect).⁴⁸ GET, which is also based on electroporation, is traditionally achieved by the application of millisecond-duration electric pulses as it is believed that different transmembrane pathways/mechanisms are involved in chemotherapeutic vs. pDNA transport.⁴⁹ When ECT is used in combination with GET traditionally two different types of pulses would be necessary (conventional 8 \times 100 μ s pulses for ECT and millisecond duration pulses for GET).

Changing the conventional 8 \times 100 μ s pulses to an alternative type of pulse such as high-frequency bipolar pulses or millisecond pulses could thus be advantageous in ECT. However, it is not well understood whether the use of alternative types of pulses would compromise the efficiency of the ECT treatment. Recently, *in vitro* study by Radzevičiūtė *et al.*⁵⁰ and *in vivo* study by Novickij *et al.*⁵¹ demonstrated that pulses of sub-microsecond duration can be as effective as the conventional pulses for ECT with bleomycin. Moreover, *in vitro* study by Vižintin *et al.*⁵² demonstrated that sub-microsecond pulses can be as effective as the conventional 8 \times 100 μ s pulses for ECT with cisplatin. The study⁵² also quantified the number of internalized cisplatin molecules needed for decreasing cell survival.

In this study, we expanded upon Vižintin *et al.*⁵² and investigated how high-frequency bipolar pulses and millisecond duration pulses affect the uptake and cytotoxicity of cisplatin compared with conventional 8 \times 100 μ s pulses. We performed *in vitro* ECT experiments, quantified the number of internalized cisplatin molecules and determined cisplatin cytotoxicity for the selected types of pulses. Our results demonstrated that the tested types of pulses resulted in equivalent drug uptake and cytotoxicity, provided that the electric field strength was adjusted for each pulse type separately. The quantified number of internalized cisplatin molecules producing a cytotoxic effect was in agreement with the Vižintin *et al.*⁵² study. We also tested a simple phenomenological model to describe the uptake of cisplatin molecules following cell exposure to different types of pulses. We discussed how the development of such models describing electroporative cisplatin uptake could provide a tool for treatment planning, using arbitrary types of pulses.

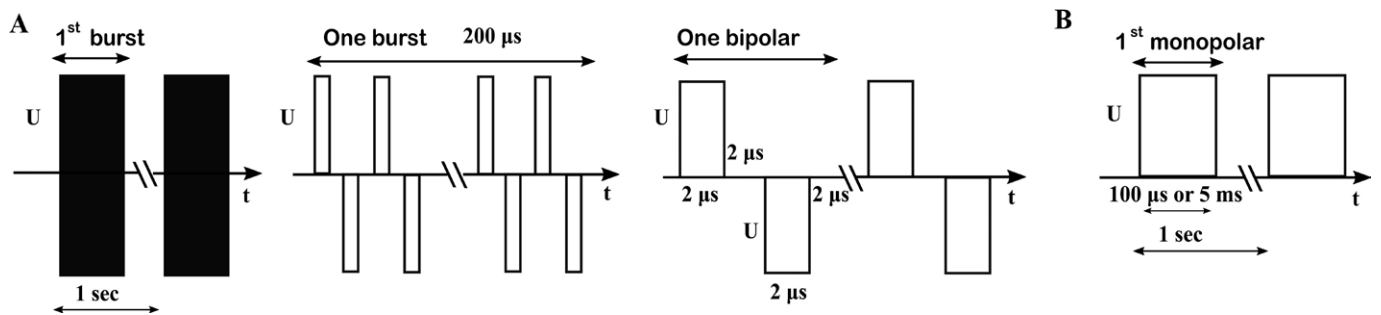


FIGURE 1. (A) 50×50 HF pulses. From left to right: 50 bursts were applied with a repetition frequency of 1 Hz; one burst with 200 μ s total pulse on time and consisted of 50 bipolar pulses; one bipolar pulse of amplitude U consisted of a 2 μ s long positive pulse, and a 2 μ s long negative pulse (both of voltage U) with a 2 μ s long interpulse delay. **(B)** $8 \times 100 \mu$ s or 8×5 ms monopolar pulse of amplitude U and pulse duration of 100 μ s or 5 ms were applied with a repetition frequency of 1 Hz

Materials and methods

Cell preparation

We used Chinese hamster ovary cell line (CHO-K1; cat. no. 85051005, European Collection of Authenticated Cell Cultures, United Kingdom). Cells were grown in 25 cm² culture flasks (no. 90026, TPP, Switzerland) for 2–4 days in an incubator at 37°C, in a humidified atmosphere with 5% CO₂. CHO cells were cultured in Ham-F12 growth medium (cat.no. N6658, Sigma Aldrich, Germany) supplemented with 10% fetal bovine serum (cat. No. F9665, Sigma Aldrich, Germany), L-glutamine (cat. No. G7513, Sigma Aldrich, Germany), antibiotics penicillin/streptomycin (cat.no. P0781, Sigma Aldrich, Germany), and gentamycin (cat.no. G1397, Sigma Aldrich, Germany). The cell suspension was prepared by detaching the cells in the exponential growth phase with 10x trypsin-EDTA (cat. no. T4174, Sigma Aldrich, Germany), diluted 1:9 in Hank's basal salt solution (cat. no. H4641, Sigma Aldrich, Germany). After no more than 2 minutes, trypsin was inactivated by adding Ham-F12, and cells were transferred to a 50 ml centrifuge tube. Then, the cells were centrifuged (5 min, 180 g, 21°C) and re-suspended in Dulbecco's Modified Eagle Medium (DMEM, cat. no. D5671, Sigma-Aldrich, Missouri, United States) supplemented with 10% FBS (cat. no. F9665, Sigma-Aldrich), 2.0 mM L-glutamine, 1 U/ml penicillin-streptomycin and 50 μ g/ml gentamycin. The CHO cells were re-suspended at concentrations of 4×10^6 cells/ml (permeability and survival experiments for determination of the optimal electric field) and 4.2×10^6 cells/ml (for the clonogenic assay experiments and intracellular platinum concentration experiments).

Pulse parameters and pulse application

Three different types of pulses were used to perform experiments. For brevity, we refer to the three types of pulses used as 50×50 HF pulses, $8 \times 100 \mu$ s pulses, and 8×5 ms pulses, and they are described in detail as follows. (i) The first type consisted of high-frequency bipolar pulses, specifically 50 bursts with a repetition frequency of 1 Hz. Each burst contained 50 short bipolar pulses having a pulse duration of 2 μ s for the positive as well as for the negative pulse. The interpulse delay between consecutive bipolar pulses was 2 μ s (Figure 1A). These high-frequency bipolar pulses were delivered by the pulse generator L-POR V0.1 (mPOR, Slovenia) at various voltages ranging from 80 V to 320 V with a step of 40 V. (ii) The second type of pulses consists of eight 100 μ s monopolar pulses delivered at a repetition frequency of 1 Hz. These pulses were delivered by a prototype pulse generator based on H-bridge digital amplifier with 1 kV MOSFETs developed in our lab and described previously.³⁹ The voltage of these pulses varied from 80 V to 320 V with a step of 40 V, Figure 1B. (iii) The third type consists of eight 5 ms long monopolar pulses, delivered at a repetition frequency of 1 Hz. These pulses were delivered by BTX Gemini X2 pulse generator (Harvard Apparatus, USA). Note that the pulse on time (the time when the voltage was different than zero) was 20 ms for 50×50 HF pulses, 800 μ s for $8 \times 100 \mu$ s, and 40 ms for 8×5 ms pulses. The voltage of these pulses varied from 80 V to 160 V with a step of 20 V (Figure 1B). The electric pulses were applied to cells in suspension placed in 2 mm aluminium cuvette. To ensure the quality of the delivered pulses the voltage and the current were monitored in all

experiments with an oscilloscope Wavesurfer 422, 200 MHz, a differential voltage probe ADP305, and a current probe CP030 (from LeCroy, USA), according to the recommendations.⁵³

Permeability and survival curves for determination of the optimal electric field strength

To select the optimal electric field strength, i.e., where the highest cell membrane permeability and highest survival are achieved, we determined the so-called permeability and survival curves for each of the tested types of pulses. The selected optimal electric field strength was later used in the experiments with cisplatin.

To determine the permeability curve, the cell suspension was mixed with YO-PRO-1 iodide (cat. no Y3603, Thermo Fisher Scientific, Massachusetts, USA) to a final concentration of 1 μ M. 150 μ l of cells-YO-PRO-1 mixture was transferred in a 2 mm aluminum cuvette and then pulses were applied. 20 μ l of the treated sample was transferred to a 1.5 ml centrifuge tube. Three minutes after pulse delivery the treated sample was diluted in 150 μ l of DMEM and vortexed. The uptake of YO-PRO-1 was measured on the flow cytometer (Attune NxT; Life Technologies, Carlsbad, CA, USA). Cells were excited with a blue laser at 488 nm, and the emitted fluorescence was detected through a 530/30 nm band-pass filter. For each measurement, we acquired 10,000 events. Single cells were separated from all events by gating. Obtained data were analyzed using the Attune NxT software. The percentage of permeabilized cells was determined from the histogram of YO-PRO-1 fluorescence (see Supplementary Info S1).

To determine the survival curve, 150 μ l of cell suspension was transferred to a 2 mm aluminum cuvette and then pulses were applied. 20 μ l of the treated sample was transferred to a 1.5 ml centrifuge tube, and 25 minutes after pulse delivery, the samples were diluted in 380 μ l Ham-F12. The cell suspension was gently mixed and 100 μ l were transferred per well of a 96-well plate in triplicates. After 24 h of incubation in a humidified atmosphere at 37°C and 5% CO₂, the MTS assay (CellTiter 96® Aqueous One Solution Cell Proliferation Assay (MTS), Promega, USA⁵⁴) was performed. The MTS assay was used to quantify the number of viable cells by evaluating their metabolic activity by measuring the formazan absorbance at 490 nm on a microplate reader (Tecan Infinite 200 pro; Tecan, Grödig, Austria). Cell survival was de-

termined by first subtracting the background (signal from blank wells containing medium without cells) from all measurements and then normalizing the absorbance of the treated samples to the absorbance of the control sample.

Clonogenic assay

We determined cisplatin cytotoxicity in combination with electroporation pulses using the clonogenic assay which is based on the ability of a single cell to divide and grow into colonies.⁵⁵ On the day of the experiment, saline solution was used to dilute cisplatin (Cisplatin Kabi, 1 mg/ml, Fresenius Kabi, Germany or Cisplatin Accord, 1 mg/ml, Accord, UK) and prepare working solutions. The final concentrations of cisplatin during electroporation were 0 μ M, 10 μ M, 30 μ M, and 50 μ M. First, 150 μ l of cell suspension with added specific cisplatin concentration was transferred to a 2 mm aluminum cuvette and then the suspension was exposed to the selected type of pulses of the optimal electric field as described in the subsection *Permeability and survival curves for determination of the optimal electric field strength*. Control samples received no pulses and no cisplatin. 25 minutes after pulse delivery, 5 μ l of each sample (treated and control) was diluted in 495 μ l Ham-F12 and mixed. Then, the number of cells in suspension was counted using Countess 3 Automated Cell Counter (Thermo Fisher Scientific). For each sample, specific dilutions were prepared to transfer ~100 live cells in each well of a 6-well plate in triplicates. Note that a higher number of cells was plated for the treated samples compared to the control sample⁵⁵ to compensate for the cells which died immediately after the treatment. After 7 days of incubation at 37 °C and humidified atmosphere with 5% CO₂, the growth medium was removed. The attached cells/colonies were fixed with methanol and stained with crystal violet for 10 minutes and washed. The colonies in each well were manually counted. First, we determined the average plating efficiency by dividing the number of counted colonies with the number of plated cells (specific for each experimental group). Then we determined cell survival by normalizing the average plating efficiency to the plating efficiency of the control sample.

Determination of intracellular platinum concentration

Cells were prepared and treated with electric pulses in the presence of different concentra-

tions of cisplatin, as described in previous section 25 minutes after pulse delivery, each sample was diluted in Ham-F12, centrifuged, and washed twice. The cell pellet was separated from the supernatant and the intracellular concentration of platinum was analyzed using inductively coupled plasma mass spectrometry (ICP-MS). To aid sample digestion, 0.1 ml of H₂O₂ and 0.1 ml of HNO₃ (both from Merck, Darmstadt, Germany), were added to the cell pellets. The tubes were then sealed with caps and Teflon tape and left overnight at 80°C. Following digestion, 1.8 ml of Milli-Q water (Direct-Q 5 Ultrapure water system; Merck Millipore, Massachusetts, USA) was added. The platinum content in the samples was then measured using ICP-MS (7900 ICP-MS; Agilent Technologies, California, USA) with ¹⁹³Ir (Merck, Darmstadt, Germany) used as an internal standard during the measurement.

To determine the amount of Pt per cell, the number of cells in the pellet was divided with the measured Pt in the cell pellet of each sample. To assess the number of cisplatin molecules per cell, it was assumed that 1 mol of Pt is equivalent to 1 mol of cisplatin. Control samples (not electroporated cells that were not incubated with cisplatin) were used for blank subtraction for all cisplatin-treated samples. To reduce cross-contamination of the instrument during the measurement, a mixture containing 1% HNO₃ and 1% HCl (Merck, Darmstadt, Germany) was used as a rinse between the sample runs.

Statistical analysis

Statistical analysis was performed using Prism 9.4.1 (GraphPad Software, USA). For permeability and survival experiments we performed one-way ANOVA if the normality test passed, or the ANOVA on ranks if the normality test failed with the Shapiro-Wilk test. For cisplatin cytotoxicity and cisplatin uptake experiments, we performed two-way ANOVA (independent variables: cisplatin concentration and pulse type). The normality test passed with the D'Agostino-Pearson test. Statistically significant difference was analyzed with respect to the control group (no cisplatin, no pulses) for all experiments. In the figures, the asterisk (*) indicates $p < 0.05$.

Modeling

To model the intracellular uptake of cisplatin molecules, we used the phenomenological model de-

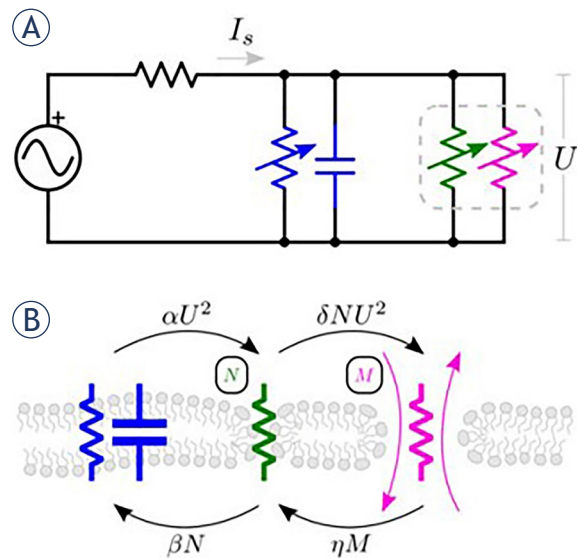


FIGURE 2. Schematic of the model that describes electroperoration and molecular transport. (A) The equivalent circuit, which considers electroperoration (membrane pore/defect formation) to be a two-step process, as depicted in (B). The blue capacitance and resistance represent the intact cell membrane. When the electric field is applied, the cell membrane becomes permeable first to small ions, indicating the first porous state (N) of the membrane represented by green resistance. Then the membrane becomes permeable to small molecules, indicating the second porous state (M) of the membrane represented by magenta resistance. Reproduced from Sweeney *et al.*⁵⁶ with permission.

veloped by Sweeney *et al.*⁵⁶, which is based on an equivalent circuit (Figure 2). The model considers a spherical cell exposed to electric pulses between parallel plate electrodes (homogenous electric field distribution), describes pores/defects formation as a two-state process, and considers diffusion as the only mechanism of transmembrane molecular transport. The model does not describe the cell spatially thus, the parameters used in the model are representative of the whole cell.

The source current I_s describes how the electric field induces a voltage on the cell membrane. This induced transmembrane voltage (U) and I_s are described by:

$$\frac{dU}{dt} = I_s - U(1 + \gamma(N + M)) \quad [1]$$

$$I_s = \frac{\tau_{RC} \sigma_{EXT} h E_0}{U_0 \epsilon_m} \quad [2]$$

The term σ_{EXT} is the conductivity of the electroperoration medium, h is the membrane thickness, E_0 is the applied electric field, U_0 is the electropo-

TABLE 1. Model parameters

Parameter	Symbol	Value	Reference
Electroporation threshold voltage	U_0	258 mV	56
Membrane thickness	h	5 nm	56
Cell radius	r	7.5 μm	56
Membrane time constant	τ_{RC}	1 μs	56
Membrane permittivity	ϵ_m	$12 \times 8.85 \times 10^{-12} \text{ F/m}$	56
Solute radius	ρ_s	0.58 nm	58
Defect radius	ρ_d	0.8 nm	56
Solute radius/Defect radius	$\lambda_m = \rho_s / \rho_d$	0.7250	56
Solute diffusivity	D	$1.670 \times 10^{-9} \text{ m}^2/\text{s}$	58,59
Parameter in N formation rate	α	2×10^{-6}	56
N relaxation rate	β	4×10^{-8}	56
Relative permeabilized conductance	γ	1×10^4	56
Parameter in M formation rate	δ	1×10^{-3}	56
M relaxation rate	η	4×10^{-9}	56
Permeability coefficient	ξ	8.45×10^{-4}	56
Electroporation medium conductivity	σ	1.4 S/m	*

* Measured conductivity of DMEM using a conductometer (Mettler Toledo, S230)

ration threshold voltage and ϵ_m is the membrane dielectric permittivity.

The increase of the transmembrane voltage results in the formation of small pores/defects (first porous state N) allowing the transmembrane transport of ions only. The presence of ionic currents decreases the value of the transmembrane voltage. The formed pores/defects can expand radially to allow transmembrane uptake of small molecules (second porous state M). The transport of small molecules into the cell is assumed to be governed by diffusion only, i.e., due to a concentration gradient between the extracellular and intracellular environment. The first porous state N , where only small ions can pass through the cell membrane, and the second porous state M , where also small molecules can pass through the cell membrane, are described by equations [3] and [4], respectively. The normalized intracellular concentration (X) of a selected molecule (here cisplatin) that crosses the membrane in the M state is described by equation [5]. All the differential equations are expressed as a function of the normalized time (τ), which is defined as $\tau = t/\tau_{RC}$, where t is the real-time and τ_{RC} is the membrane charging time constant.

$$\frac{dN}{d\tau} = \alpha U^2 - \delta U^2 N - \beta N + \eta M \quad [3]$$

$$\frac{dM}{d\tau} = \delta U^2 N - \eta M \quad [4]$$

$$\frac{dX}{d\tau} = \xi M(1 - X) \quad [5]$$

We implemented the model using a custom script in Matlab 2019b (MathWorks, Natick, MA, USA) and verified that the model in its original form reproduces the published results.⁵⁶ The model was developed using the same cell line as in this study (CHO-K1) but based on quantitative measurements of propidium iodide uptake. Therefore, we modified the parameters related to the transported molecule, in our case cisplatin. Specifically, we changed the value of the solute radius (ρ_s), solute diffusivity (D), the permeability coefficient (ξ). The latter was determined by:

$$\xi = \frac{3 H(\lambda_m) D \tau_{RC}}{r h} \quad [6]$$

The term $H(\lambda_m)$ is the hindrance factor evaluated using the Renkin equation⁵⁷, D is the diffusion constant of cisplatin, and r is the cell radius. We also adapted the conductivity of the electroporation medium (σ) to correspond to DMEM used in our experiments. The final model parameters are shown in Table 1. We performed calculations for

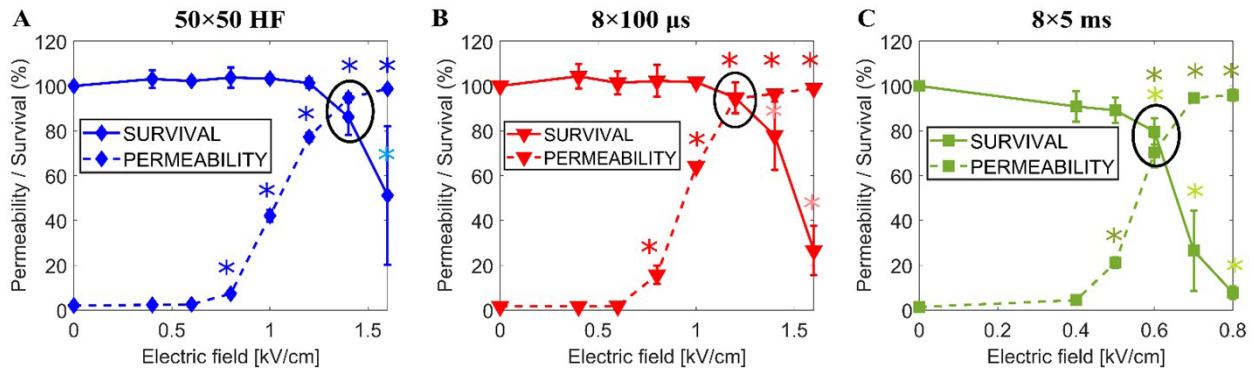


FIGURE 3. Cell survival (solid) and cell membrane permeability (dashed) as a function of the electric field when (A) 50×50 HF pulses; (B) $8 \times 100 \mu\text{s}$ pulses; (C) 8×5 ms pulses are used. The chosen optimal electric fields are encircled. Each data point presents the mean \pm standard deviation from 3–4 experiments. * = statistically significant differences from control ($p < 0.05$) performing one-way ANOVA if the normality test passed or otherwise ANOVA on ranks. The light blue, red, and green asterisks are related to survival experiments.

pulse parameters used in our present and preceding⁵² studies: 50×50 HF pulses, $8 \times 100 \mu\text{s}$ pulses, 8×5 ms pulses, and 1×200 ns pulse of 12.6 kV/cm and 25×400 ns pulses of 3.9 kV/cm applied at 10 Hz repetition frequency.

The output of the model is the time course of the intracellular concentration of cisplatin ($X_i = X \times X_e$, where X_e is the extracellular concentration of cisplatin) following the application of the electric pulses. We calculated the number of intracellular cisplatin molecules at time 25 minutes using:

$$N = X_i \frac{4}{3} \pi r^3 N_A \quad [7]$$

where $\frac{4}{3} \pi r^3$ is the average volume of a cell and N_A is the Avogadro number. The number of cisplatin molecules obtained with the model was then compared with the corresponding experimental measurements.

Results

The optimal electric field strength for each type of pulse

First, we performed experiments to determine the optimal electric field strength for each of the three tested types of pulses, to be later used in the experiments with cisplatin. As the optimal electric field strength, we consider the one in which the highest permeability and highest cell survival are achieved.

Figure 3 shows the experimentally determined permeability (dashed) and survival (solid) curves as a function of the applied electric field for A) 50

$\times 50$ HF pulses, B) $8 \times 100 \mu\text{s}$ pulses, and C) 8×5 ms pulses. Permeability curves show how the percentage of permeabilized cells increases with increasing electric field strength, whereas the survival curves show how the percentage of viable cells decreases with increasing electric field strength. The chosen optimal electric fields (i.e., highest permeability and highest survival) are 1.4 kV/cm for 50×50 HF pulses, 1.2 kV/cm for $8 \times 100 \mu\text{s}$ pulses, and 0.6 kV/cm for 8×5 ms pulses.

Cytotoxicity vs. the number of intracellular cisplatin molecules

We next used the clonogenic assay to determine the cytotoxicity of cisplatin when exposing cells to the three types of pulses at their optimal electric field strength. Figure 4A shows how cell survival decreases as the extracellular concentration of cisplatin increases. In the absence of applied pulses, the tested cisplatin concentrations (0 μM , 10 μM , 30 μM , and 50 μM) do not affect cell viability (black curve). However, cytotoxicity is strongly potentiated with all three types of pulses, decreasing the cell survival to $\sim 0.8\%$ for 50×50 HF pulses, $\sim 2.7\%$ for $8 \times 100 \mu\text{s}$ pulses, and $\sim 4\%$ for 8×5 ms pulses at the highest cisplatin concentration (50 μM) – note the logarithmic scale. Results for all three types of pulses are similar and are not statistically significantly different. Qualitatively similar results were obtained when measuring cell viability with the metabolic MTS assay (see Supplementary Info S2). However, as well known, the MTS assay reported better cell viability than the clonogenic assay for the same experimental conditions.^{52,60}

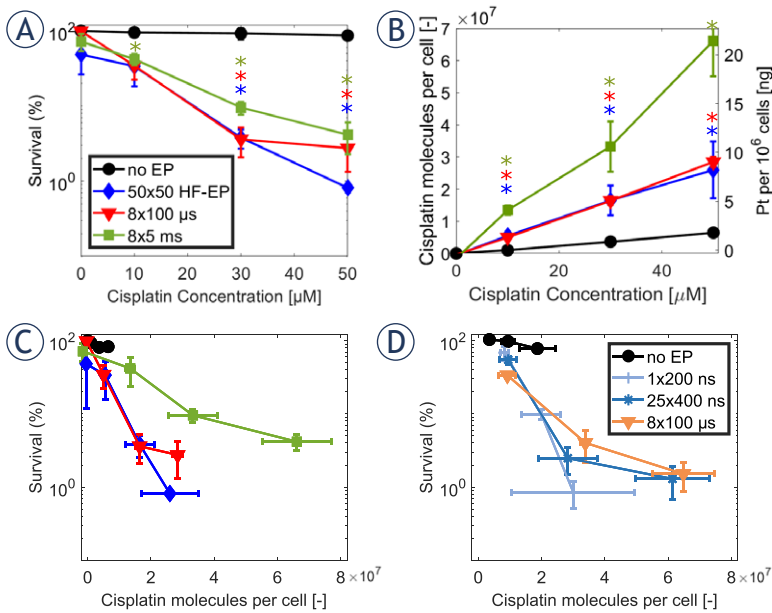


FIGURE 4. Cytotoxicity of cisplatin (A) and cisplatin molecules per cell (B) at different concentrations of cisplatin at a fixed electric field: 1.4 kV/cm for 50×50 HF pulses, 1.2 kV/cm for $8 \times 100 \mu\text{s}$ pulses and 0.6 kV/cm for 8×5 ms pulses. Each data point presents the mean \pm standard deviation from 3–4 experiments. * = statistically significant differences from control ($p < 0.05$) performing two-way ANOVA test. The color of the asterisk corresponds to the line color for a specific type of tested pulse. Cell survival as a function of cisplatin molecules per cell in combination with electroporation (C) our experimental data and (D) experimental data replotted from Vižintin *et al.*⁵² with permission.

We also measured the mass of intracellular Pt for each tested condition using ICP-MS and determined the average number of intracellular cisplatin molecules per cell, assuming that 1 mol of Pt is equivalent to 1 mol of cisplatin (Figure 4B). When no electric pulses are applied (black line), the number of cisplatin molecules increases slightly with increasing cisplatin concentration due to passive (i.e., diffusion), and active (i.e., membrane transporters^{61–63}, endocytosis, pinocytosis, macrocytosis^{64,65}) transport of cisplatin. However, when electric pulses are applied, the number of cisplatin molecules increases considerably. The greatest increase is observed for 8×5 ms pulses (up to 6.7×10^7 at $50 \mu\text{M}$). Roughly 2 times lower increase is observed for both 50×50 HF pulses and $8 \times 100 \mu\text{s}$ pulses. There is a statistically significant difference between 8×5 ms pulses and the other two types of tested pulses when extracellular cisplatin concentration is $50 \mu\text{M}$.

To determine the number of intracellular cisplatin molecules needed to achieve a cytotoxic effect, we combined the data from Figures 4A and 4B and

plotted cell survival as a function of the number of cisplatin molecules in Figure 4C. Consistent with previous observations^{13,52}, electroporation potentiates the cytotoxicity of cisplatin, as much lower survival is obtained with any of the three types of pulses compared with control for the same number of cisplatin molecules. The curves for 50×50 HF pulses and $8 \times 100 \mu\text{s}$ pulses are almost overlapping, demonstrating that practically the same number of cisplatin molecules results in the same cytotoxic effect. Interestingly, in spite of two times higher Pt content for 8×5 ms pulses the cytotoxicity is lower than when using 50×50 HF pulses or $8 \times 100 \mu\text{s}$ pulses.

A previous study by Vižintin *et al.*⁵² used the same experimental protocols and analysis as here, but compared two other types of pulses with conventional $8 \times 100 \mu\text{s}$ pulses, namely, 1×200 ns pulse of 12.6 kV/cm and 25×400 ns pulses applied at 10 Hz repetition frequency of 3.9 kV/cm. Their results are replotted in Figure 4D. This comparison demonstrates that the number of intracellular cisplatin molecules required to achieve a certain cytotoxic effect can be achieved with different types of pulses, if the electric field is properly adjusted.

Modeling cisplatin uptake

Experimental data in previous section suggests that any type of pulses can be used for ECT, if it results in the same average number of internalized cisplatin molecules. Therefore, it would be useful to have a mathematical model for predicting the uptake of cisplatin molecules as a function of the pulse parameters. Figure 5 compares the measured uptake of cisplatin with prediction from a phenomenological model developed by Sweeney *et al.*⁵⁶ for all types of pulses used in this and previous study.⁵² Note that the experimental data plotted in Figure 5 refer to the number of cisplatin molecules due to electroporation (i.e., we subtracted the uptake of cisplatin when no pulses were applied, black line Figure 4B). The model correctly predicts a proportional increase in the number of internalized molecules with increasing cisplatin concentration. The model also very well quantitatively predicts the number of cisplatin molecules experimentally obtained for 8×5 ms pulses, 1×200 ns pulses, and 25×400 ns pulses, but overestimates by ~ 2.5 and ~ 2 times the number of cisplatin molecules obtained for 50×50 HF pulses and $8 \times 100 \mu\text{s}$ pulses, respectively. Nevertheless, for all pulse types, the model correctly captures the order of magnitude of the internalized cisplatin molecules.

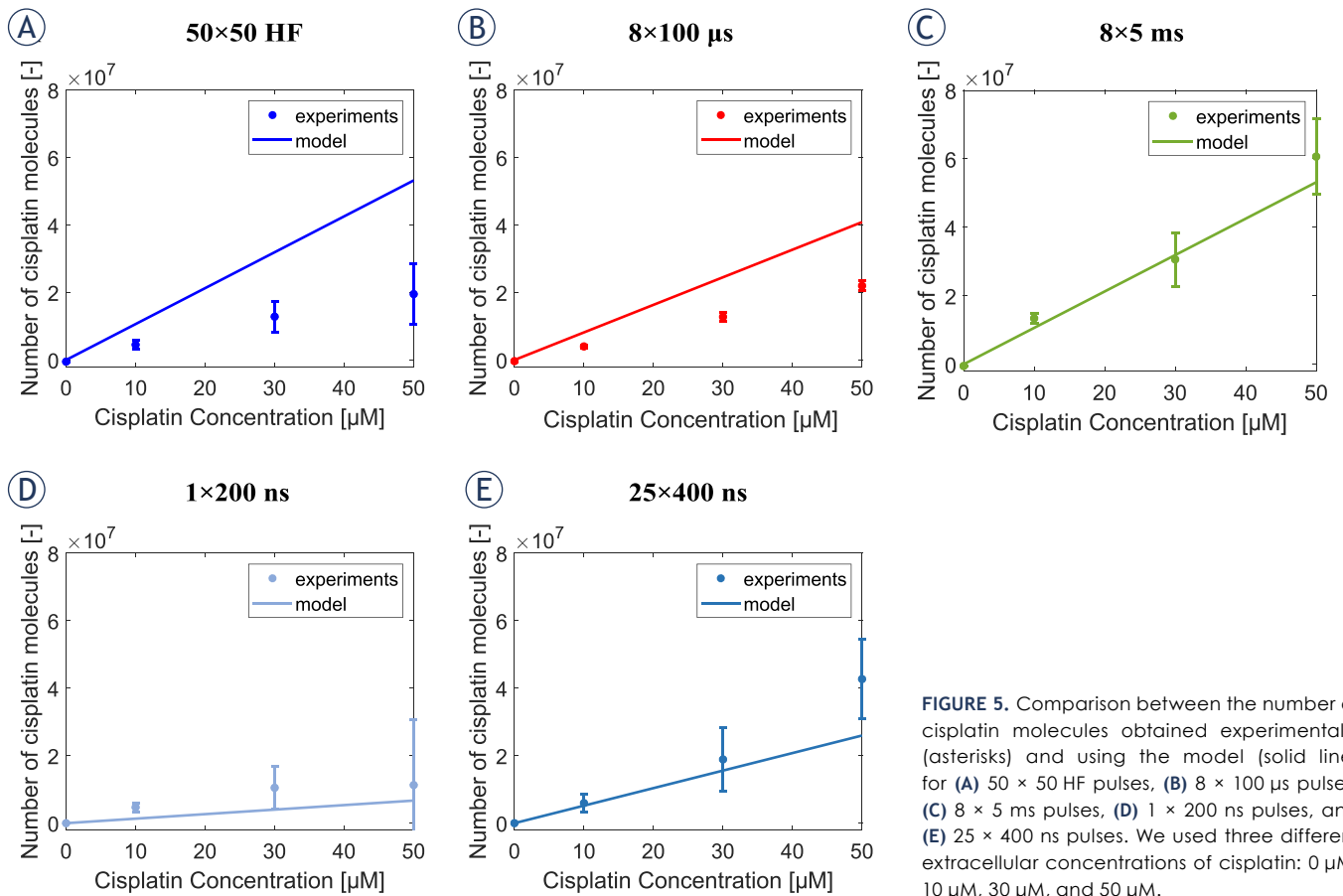


FIGURE 5. Comparison between the number of cisplatin molecules obtained experimentally (asterisks) and using the model (solid line) for (A) 50×50 HF pulses, (B) $8 \times 100 \mu\text{s}$ pulses, (C) 8×5 ms pulses, (D) 1×200 ns pulses, and (E) 25×400 ns pulses. We used three different extracellular concentrations of cisplatin: 0 μM , 10 μM , 30 μM , and 50 μM .

Discussion

In this study, we investigated how different types of pulses affect ECT *in vitro*. Specifically, we determined cisplatin uptake and cytotoxicity using CHO cells. We also tested a model that describes electroporation and the associated transmembrane molecular transport to predict the number of cisplatin molecules in an individual cell.

Electroporation potentiates cisplatin uptake and cytotoxicity in a similar way for all tested types of pulses

Different types of pulses can be considered equivalent for electroporation when the electric field strength is adjusted for each type of pulses separately.⁶⁶ We thus first determined, for each selected type of pulses, how the electric field strength affects the percentage of cells that become permeable to YO-PRO-1 and the percentage of cells that survive the exposure to electric pulses in the absence of cisplatin. YO-PRO-1 is a nucleic acid stain that

allows rapid screening of permeabilized cells using flow cytometry. The size of YO-PRO-1 (630 Da) is somewhat larger, but nevertheless comparable to cisplatin (300 Da). Therefore, cells that become permeable to YO-PRO-1 are expected to also become permeable to cisplatin. Cell survival was measured 24 hours after electroporation with the metabolic MTS assay. An *in vitro* study by Peng *et al.*⁶⁷ showed that 24 h is the adequate incubation time to measure cell survival following electroporation. The electric field strength, with the highest percentage of permeable cells and the highest percentage of viable cells, was 1.4 kV/cm for 50×50 HF pulses, 1.2 kV/cm for $8 \times 100 \mu\text{s}$ pulses, and 0.6 kV/cm for 8×5 ms pulses. Consistent with Pucihar *et al.*⁶⁶, longer pulses (8×5 ms) require lower electric fields to obtain a similar fraction of permeabilized cells than shorter pulses ($8 \times 100 \mu\text{s}$). *In vitro* studies^{38,39} have observed that a higher electric field is needed for high-frequency bipolar pulses than for monopolar pulses of 100 μs duration, with equivalent treatment time, to achieve a similar fraction of permeabilized cells. However, in this study, a similar elec-

tric field of 1.2 kV/cm and 1.4 kV/cm is required for $8 \times 100 \mu\text{s}$ and $50 \times 50 \text{ HF}$ pulses, respectively, to achieve a similar fraction of permeabilized cells. This is due to the use of a higher number of bursts and bipolar pulses that reduce the required pulse amplitude. The average cell survival at the optimal electric field was for all pulse types above 80% and was not statistically significantly different from control except for $8 \times 5 \text{ ms}$ pulses. Overall, in terms of electroporation, all the three tested types of pulses of the optimal electric field strength can be considered equivalent.

We then performed *in vitro* ECT experiments. We measured the cytotoxicity and the uptake of cisplatin when exposing cells to all three types of pulses with the optimal electric field strength in the presence of different extracellular concentrations of cisplatin (0 μM , 10 μM , 30 μM , 50 μM). For all three types of pulses, we observed that an increase in cisplatin concentration increased cell cytotoxicity and intracellular uptake of cisplatin, which is in agreement with previous studies using mouse skin melanoma cells.^{13,38,52,68} Furthermore, the results for both cisplatin uptake and cytotoxicity were very similar for all three types of pulses, demonstrating that these pulse types can be considered, not only equivalent in terms of electroporation and transmembrane molecular transport, but also in terms of potentiation of cisplatin cytotoxicity and ECT. We also observed in Figures 4A and 4B that ~2 times higher amount of cisplatin molecules is needed for $8 \times 5 \text{ ms}$ pulses to achieve a similar cytotoxic effect as when using $50 \times 50 \text{ HF}$ pulses and for $8 \times 100 \mu\text{s}$ pulses. Vižintin *et al.*⁵² reported that the structure of cisplatin is not affected when nanosecond and $8 \times 100 \mu\text{s}$ pulses are used. However we cannot completely exclude that the structure of cisplatin might be affected by the higher amount of electrochemical reaction caused by ms pulses (we saw bubble formation during experiments) which might lead to a lower cytotoxic effect of cisplatin.^{62,69,70} Furthermore an *in vitro* study by Rols *et al.*⁷¹ showed that electroporation, using millisecond pulses, can induce long term micropinocytosis, thus cisplatin molecules might be entrapped in vesicles and not express their cytotoxic effect.

By combining the results on cisplatin cytotoxicity and cisplatin uptake, we were able to determine the number of internalized cisplatin molecules needed to achieve a cytotoxic effect. For all tested types of pulses, this number was in the range of $2\text{--}7 \times 10^7$ cisplatin molecules per cell. Same range was obtained by Vižintin *et al.*⁵², who studied cis-

platin cytotoxicity following exposure of cells to $1 \times 200 \text{ ns}$ and $25 \times 400 \text{ ns}$ pulses. Altogether the results suggest that, as long as the electric field is appropriately adjusted, different types of pulses can be used for potentiating cisplatin cytotoxicity, and consequently different types of pulses can be used for ECT. Thus, the $50 \times 50 \text{ HF}$ pulses, $8 \times 100 \mu\text{s}$, $8 \times 5 \text{ ms}$ pulses, $1 \times 200 \text{ ns}$ pulses, and $25 \times 400 \text{ ns}$ pulses of properly adjusted electric field strength can be considered for ECT.

Clinical relevance

ECT has been demonstrated as a locally effective treatment of tumors of various histotypes.⁷² The consistent clinical success of ECT has been achieved through the meticulous development of pulse protocols, electrodes, and the publication of Standard Operating Procedures for cutaneous and subcutaneous tumors.¹¹ It has been later demonstrated that also deep-seated tumors can be successfully treated by ECT provided the tumor is covered by sufficiently high electric fields either as intraoperative⁵ or percutaneous procedure.^{31,73–75} Accordingly, Standard Operating Procedures have been updated.¹⁰ With good success and acceptance by patients, larger tumors and patients with more extensive diseases were treated. Pain and muscle contraction-related high voltage pulse delivery became the most often reported side effects and alternative pulse waveforms that would maintain ECT efficacy but reduce pain and muscle contraction.²⁴ In this respect, high-frequency bipolar short pulses^{33,34} and also nanosecond pulses^{76,77} were suggested. Furthermore, recent studies investigate how high-frequency bipolar pulses and nanosecond pulses affect ECT. Our previous *in vitro* study³⁸ showed that similar cisplatin cytotoxicity is obtained by comparing high-frequency bipolar pulses and conventionally ECT pulses as soon as the electric field is properly adjusted. Lyons *et al.*⁴⁰ have recently demonstrated the safety and efficiency of using high-frequency bipolar pulses in ECT using bleomycin for the treatments of 97 lesions of different histological subtypes of cutaneous malignancies in 25 patients. The authors observed an overall response rate of 86% (complete response rate 63.6%) three months after the treatment which is in agreement with the overall response rate of 85% (complete response rate 73.7%) determined in the ESOPE study of 2006²² and in a follow-on study using InspECT database in which the overall response is 85% (complete response rate 70%, partial response rate 15%).⁷² Thus, the data published

by Lyons *et al.*⁴⁰ showed that the use of high frequency bipolar pulses is equivalent regarding the overall response rate to the use of classical ECT pulses. Furthermore, the patients that were treated with local anesthesia showed excellent tolerability to the treatment. Thus, the use of high frequency bipolar pulses might possibly reduce the need to use general anesthesia during ECT shortening the overall hospital stay, reducing the time needed to recover and the costs and increasing the safety of the treatment.⁷⁸

A study by Vižintin *et al.*⁵² compared the effects of conventional $8 \times 100 \mu\text{s}$ pulses with nanosecond pulses on cisplatin uptake and cytotoxicity in cell lines *in vitro*. The authors showed that nanosecond pulses can be equally effective for ECT as conventional $8 \times 100 \mu\text{s}$ pulses.^{52,79} These results are in agreement with *in vitro* studies on a tumor model, murine Lewis lung carcinoma (LLC1) cell line, by Radzevičiūtė *et al.*⁵⁰ and *in vivo* study by Novickij *et al.*⁵¹ which show that nanosecond pulses can be as effective as when using the conventional ECT pulses in ECT when using bleomycin as chemotherapeutic drug.

Considerable efforts are also focused on making ECT a systemic treatment by combining it with immunotherapy.^{20,48,80,81} Electrochemotherapy can induce immunogenic cell death through the release of damage-associated molecular patterns (DAMP) which serve as a signal to stimulate the immune system.⁸²⁻⁸⁴ Massive liberation of tumor antigens together with DAMPs can activate the antigen-presenting dendritic cells.^{85,86} Multiple studies in canine⁸⁷⁻⁸⁹, in mice⁴⁷ and human patients⁹⁰ have thus been testing ECT in combination with gene electrotransfer (GET) of plasmid DNA encoding for interleukin-12 (IL-12), which stimulates the immune system.⁴⁵⁻⁴⁷ Traditionally in GET millisecond duration pulses are used to deliver DNA into the cells.⁹¹⁻⁹³ Thus, when ECT is used in combination with GET two different types of pulses $8 \times 100 \mu\text{s}$ pulses and millisecond pulses are used, respectively. However, it might be beneficial to use the same type of pulses when ECT is combined with GET as this would allow the use of simpler pulse generators.

In order to capitalize on a significant body of clinical evidence we tested equivalence of such pulses by *in vitro* test, specifically determining the amount of chemotherapeutic drug delivery by electroporation pulses. In this way equivalent pulses are determined by delivering the same drug amount into cells, thus producing the same cytotoxicity. Therefore, the replacement of classical

ECT pulses with nanosecond and high frequency bipolar pulses would be beneficial to reduce muscle contractions and pain, potentially avoiding the need for anesthetics and muscle relaxants during the treatment. Furthermore, using the same pulses (either long or short, or bipolar) for delivering cytotoxic drugs into the cells, as well as pDNA to achieve simultaneous gene electrotransfer, is an attractive idea that may be within reach.⁹⁴

Further development of mathematical models that can predict cisplatin uptake can help with electrochemotherapy treatment planning

For the success of ECT, all the tumor needs to be covered by an electric field of sufficient amplitude to permeabilize the cells/tissue, and a sufficient amount of chemotherapeutic drug is needed in the tumor.

In the Standard Operating Procedures all information related to the types of electrodes i.e., of fixed geometry, pulse parameters, and pulse generators^{10,11,22} which guarantee a complete coverage of the tumor are provided. However, to treat deep-seated tumors long needles with variable configuration electrodes are used.⁹⁵ Thus, there is a need to determine the optimal position of the electrodes and the optimal pulse parameters for complete coverage of the tumor tissue. It is not trivial to determine how the electric field is distributed in biological tissues due to tissue-specific properties, the use of different types of electrode geometries, and pulse parameters. Treatment planning using numerical models helps clinicians to determine the optimal parameters to treat a specific tumor. Currently, in treatment planning a fixed threshold electric field is used to deem tissue permeabilized or not.^{3,96} However, just a high-enough electric field does not guarantee cell death as simultaneously a high-enough extracellular cisplatin concentration is needed to obtain enough internalized cisplatin molecules for cell death. Our model presents a missing link in the complete model for treatment planning, connecting the external electric field, the number of internalized cisplatin molecules, and cell death. The first building block for the multiscale model of tissue electroporation was published in Dermol-Černe *et al.* 2018⁶⁸ where a model connecting extracellular and intracellular cisplatin concentration as a function of electric pulses was developed. Now, we went one step further and connected the intracellular cisplatin concentration with cell death.

A mathematical model that can also predict the uptake of molecules such as chemotherapeutics drugs (e.g., cisplatin and bleomycin) is needed to be determined for treatment planning for different pulse types is useful. Now we only need the final piece, and this is a model of cisplatin transport across the cell membrane as a function of electric pulses. Our previous study demonstrated that existing mechanistic models of electroporation have limited reliability for predicting the transmembrane transport of small molecules across a wide range of pulse parameters.⁹⁷ We observed that the contribution of electrophoretic transport during pulse delivery is often overestimated. Therefore, we decided to test a phenomenological model developed by Sweeney *et al.*⁵⁶ that neglects electrophoresis and takes into account only diffusion during and after pulse delivery. Furthermore, we selected this model since it is the simplest model that allows computation of the transmembrane transport of small molecules for arbitrary types of pulses. Indeed, the model is based on quantitative measurements of transmembrane transport of propidium iodide uptake (not cisplatin) induced by a single pulse of different pulse lengths (1, 10, 100, 1000 μ s) and electric field strengths (1.7, 2.5, 3.2, 4 kV/cm) that are different from the ones used in our study. Despite its simplicity, and without any considerable model modifications (see the Modeling section), the model was able to predict the order of magnitude of cisplatin uptake for all tested pulse parameters. However, a basic parametric analysis (see Supplementary Info S3) showed that the results for different types of pulses depend in a different way on the model parameters. Therefore, a comprehensive parametric analysis and additional model development would be required, which is out of the scope of the present study (see the Clinical Relevance section). Based on the results obtained, we nevertheless expect that relatively simple models could be developed in the future as a tool for predicting cisplatin uptake.

Limitation of the study

The drawback of our study is the use of only one cell line i.e., the Chinese hamster ovary cells (CHO-K1) non-cancerous cells to perform *in vitro* ECT experiments. It was observed *in vitro* that cancer cells behave differently than normal cells.⁹⁸ However, an *in vitro* study published by Vižintin *et al.*⁵² showed a similar platinum uptake when using CHO-K1 cells or mouse skin melanoma B16-F1 cells and applying $8 \times 100 \mu$ s pulses. Thus, we expect that the

observed equivalence of different pulse types observed in CHO-K1 cells would also be observed in different cancer cells.

It has been shown that the immune system plays an important role in the efficiency of ECT. Electroporation can potentiate the cytotoxicity and uptake of cisplatin but can also stimulate the immune response by releasing damage-associated molecular patterns (DAMP). In our *in vitro* study we demonstrated the equivalence of different types of pulses on cisplatin uptake and cytotoxicity. Similarly, a recent *in vitro* study by Polajžer *et al.*⁹⁹ showed the release of DAMP molecules (e.g. ATP, HMGB1, Calreticulin) albeit with some differences observed with different types of pulses.

We have focused on equivalent drug delivery to cells *in vitro* but this may be different *in vivo*. Thus, further studies in animals are needed to investigate the equivalence of different pulse types for drug entrapment by tumor blood flow modification, for the vascular disrupting action, and for the immune response in ECT.

Conclusions

Our study focused on the effect of different types of electric pulses in ECT, particularly in terms of cisplatin uptake and cisplatin cytotoxicity, using CHO cells *in vitro*. We demonstrate that different types of pulses such as classical ECT pulses, high frequency bipolar pulses and millisecond pulses potentiate cisplatin uptake and cisplatin cytotoxicity. Moreover, we observed similar cisplatin uptake and cisplatin cytotoxicity when using different types of pulses i.e., considered equivalent provided that the electric field is properly adjusted. Thus, equivalent electric pulses such as high frequency bipolar pulses and nanosecond can potentially be used in ECT to reduce pain and muscle contraction while maintaining the same efficacy in cisplatin uptake and cisplatin cytotoxicity as when using the classical ECT pulses. Moreover, our results show that using one type of pulse when combining ECT with EGT is a concept that might be readily achievable considering the equivalent pulse parameters.

In addition, we experimentally determine the number of cisplatin molecules needed to achieve a cytotoxic effect which is in the range of $2-7 \times 10^7$ cisplatin molecules per cell in agreement with previous study.⁵² We also used a mathematical model describing electroporation and transmembrane molecular transport, as a tool to predict the number of cisplatin molecules into individual cells

when different types of pulses need to be tested. The future goal is to improve treatment planning by including a model that predicts the uptake of molecules such as cisplatin or bleomycin.

Acknowledgments

This research was funded by Slovenian Research and Innovation Agency (ARIS) research core funding No. P2-0249 and P1-0143. The work was performed within the network of the research and infrastructural center of the University of Ljubljana, which is financially supported by the Slovenian Research Agency through infrastructural grant I0-0022. The authors would like to thank Duša Hodžič for her help with cell culture, Angelika Vižintin for her help with the protocols for the experiments, and Daniel C. Sweeney for help with his published model.

References

- Campana LG, Miklavčič D, Bertino G, Marconato R, Valpione S, Imarisio I, et al. Electrochemotherapy of superficial tumors – current status: basic principles, operating procedures, shared indications, and emerging applications. *Semin Oncol* 2019; **46**: 173-91. doi: 10.1053/j.seminoncol.2019.04.002
- Campana LG, Edhemović I, Soden D, Perrone AM, Scarpa M, Campanacci L, et al. Electrochemotherapy – emerging applications technical advances, new indications, combined approaches, and multi-institutional collaboration. *Eur J Surg Oncol* 2019; **45**: 92-102. doi: 10.1016/j.ejso.2018.11.023
- Miklavcic D, Snoj M, Zupanic A, Kos B, Cemazar M, Kropivnik M, et al. Towards treatment planning and treatment of deep-seated solid tumors by electrochemotherapy. *Biomed Eng Online* 2010; **9**: 1-12. doi: 10.1186/1475-925X-9-10
- Cindrič H, Miklavčič D, Cornelis FH, Kos B. Optimization of transpedicular electrode insertion for electroporation-based treatments of vertebral tumors. *Cancers* 2022; **14**: 5412. doi: 10.3390/cancers14215412
- Edhemovic I, Breclj E, Gasljevic G, Marolt Music M, Gorjup V, Mali B, et al. Intraoperative electrochemotherapy of colorectal liver metastases. *J Surg Oncol* 2014; **110**: 320-7. doi: 10.1002/jso.23625
- Bianchi G, Campanacci L, Ronchetti M, Donati D. Electrochemotherapy in the treatment of bone metastases: a phase II trial. *World J Surg* 2016; **40**: 3088-94. doi: 10.1007/s00268-016-3627-6
- Granata V, Fusco R, Piccirillo M, Palaia R, Petrillo A, Lastoria S, et al. Electrochemotherapy in locally advanced pancreatic cancer: preliminary results. *Int J Surg* 2015; **18**: 230-6. doi: 10.1016/j.ijsu.2015.04.055
- Simioni A, Valpione S, Granziera E, Rossi CR, Cavallin F, Spina R, et al. Ablation of soft tissue tumours by long needle variable electrode-geometry electrochemotherapy: final report from a single-arm, single-centre phase-2 study. *Sci Rep* 2020; **10**: 2291. doi: 10.1038/s41598-020-59230-w
- Tarantino L, Busto G, Nasto A, Nasto RA, Tarantino P, Fristachi R, et al. Electrochemotherapy of cholangiocellular carcinoma at hepatic hilum: a feasibility study. *Eur J Surg Oncol* 2018; **44**: 1603-9. doi: 10.1016/j.ejso.2018.06.025
- Gehl J, Sersa G, Matthiessen LW, Muir T, Soden D, Occhini A, et al. Updated standard operating procedures for electrochemotherapy of cutaneous tumours and skin metastases. *Acta Oncol* 2018; **57**: 874-82. doi: 10.1080/0284186X.2018.1454602
- Mir LM, Gehl J, Sersa G, Collins CG, Garbay JR, Billard V, et al. Standard operating procedures of the electrochemotherapy: instructions for the use of bleomycin or cisplatin administered either systemically or locally and electric pulses delivered by the Cliniporator™ by means of invasive or non-invasive electrodes. *Eur J Cancer Suppl* 2006; **4**: 14-25. doi: 10.1016/j.ejcsup.2006.08.003
- Sersa G, Miklavcic D, Cemazar M, Rudolf Z, Pucihar G, Snoj M. Electrochemotherapy in treatment of tumours. *Eur J Surg Oncol EJSO* 2008; **34**: 232-40. doi: 10.1016/j.ejso.2007.05.016
- Sersa G, Cemazar M, Miklavcic D. Antitumor effectiveness of electrochemotherapy with cis-diamminedichloroplatinum (II) in mice. *Cancer Res* 1995; **55**: 3450-5. PMID: 7614485
- Orlowski S, Belehradek Jr J, Paoletti C, Mir LM. Transient electroporation of cells in culture: increase of the cytotoxicity of anticancer drugs. *Biochem Pharmacol* 1988; **37**: 4727-33. doi: 10.1016/0006-2952(88)90344-9
- Mir LM. Bases and rationale of the electrochemotherapy. *Eur J Cancer Suppl* 2006; **4**: 38-44. doi: 10.1016/j.ejcsup.2006.08.005
- Jarm T, Cemazar M, Miklavcic D, Sersa G. Antivascular effects of electrochemotherapy: implications in treatment of bleeding metastases. *Expert Rev Anticancer Ther* 2010; **10**: 729-46. doi: 10.1586/era.10.43
- Sersa G, Jarm T, Kotnik T, Coer A, Podkrajsek M, Sentjurc M, et al. Vascular disrupting action of electroporation and electrochemotherapy with bleomycin in murine sarcoma. *Br J Cancer* 2008; **98**: 388-98. doi: 10.1038/sj.bjc.6604168
- Markelc B, Sersa G, Cemazar M. Differential mechanisms associated with vascular disrupting action of electrochemotherapy: intravital microscopy on the level of single normal and tumor blood vessels. *PLoS One* 2013; **8**: e59557. doi: 10.1371/journal.pone.0059557
- Serša G, Miklavčič D, Čemažar M, Belehradek Jr J, Jarm T, Mir LM. Electrochemotherapy with CDDP on LPB sarcoma: comparison of the anti-tumor effectiveness in immunocompetent and immunodeficient mice. *Bioelectrochem Bioenerg* 1997; **43**: 279-83. doi: 10.1016/S0302-4598(96)05194-X
- Calvet CY, Mir LM. The promising alliance of anti-cancer electrochemotherapy with immunotherapy. *Cancer Metastasis Rev* 2016; **35**: 165-77. doi: 10.1007/s10555-016-9615-3
- Miklavčič D, Mali B, Kos B, Heller R, Serša G. Electrochemotherapy: from the drawing board into medical practice. *Biomed Eng Online* 2014; **13**: 1-20. doi: 10.1186/1475-925X-13-29
- Marty M, Sersa G, Garbay JR, Gehl J, Collins CG, Snoj M, et al. Electrochemotherapy – an easy, highly effective and safe treatment of cutaneous and subcutaneous metastases: results of ESOPE (European Standard Operating Procedures of Electrochemotherapy) study. *Eur J Cancer Suppl* 2006; **4**: 3-13. doi: 10.1016/j.ejcsup.2006.08.002
- Sano MB, Fan RE, Cheng K, Saenz Y, Sonn GA, Hwang GL, et al. Reduction of muscle contractions during irreversible electroporation therapy using high-frequency bursts of alternating polarity pulses: a laboratory investigation in an ex vivo swine model. *J Vasc Interv Radiol* 2018; **29**: 893-8.e4. doi: 10.1016/j.jvir.2017.12.019
- Fusco R, Di Bernardo E, D'Alessio V, Salati S, Cadossi M. Reduction of muscle contraction and pain in electroporation-based treatments: an overview. *World J Clin Oncol* 2021; **12**: 367. doi: 10.5306/wjco.v12.i5.367
- Miklavcic D, Corovic S, Pucihar G, Pavselj N. Importance of tumour coverage by sufficiently high local electric field for effective electrochemotherapy. *Eur J Cancer Suppl* 2006; **4**: 45-51. doi: 10.1016/j.ejcsup.2006.08.006
- Martin RC, Schwartz E, Adams J, Farah I, Derhake BM. Intra-operative anesthesia management in patients undergoing surgical irreversible electroporation of the pancreas, liver, kidney, and retroperitoneal tumors. *Anesthesiol Pain Med* 2015; **5**: e22786. doi: 10.5812/aapm.22786
- Deodhar A, Dickfeld T, Single GW, Hamilton Jr WC, Thornton RH, Sofocleous CT, et al. Irreversible electroporation near the heart: ventricular arrhythmias can be prevented with ECG synchronization. *Am J Roentgenol* 2011; **196**: W330-5. doi: 10.2214/AJR.10.4490

28. Mali B, Jarm T, Corovic S, Paulin-Kosir MS, Cemazar M, Sersa G, et al. The effect of electroporation pulses on functioning of the heart. *Med Biol Eng Comput* 2008; **46**: 745-57. doi: 10.1007/s11517-008-0346-7
29. Ball C, Thomson KR, Kavnaudias H. Irreversible electroporation: a new challenge in "out of operating theater" anesthesia. *Anesth Analg* 2010; **110**: 1305-9. doi: 10.1213/ane.0b013e3181d27b30
30. Cannon R, Ellis S, Hayes D, Narayanan G, Martin RC. Safety and early efficacy of irreversible electroporation for hepatic tumors in proximity to vital structures. *J Surg Oncol* 2013; **107**: 544-9. doi: 10.1002/jso.23280
31. Spallek H, Bischoff P, Zhou W, de Terlizzi F, Jakob F, Kovács A. Percutaneous electrochemotherapy in primary and secondary liver malignancies—local tumor control and impact on overall survival. *Radiol Oncol* 2022; **56**: 102-10. doi: 10.2478/raon-2022-0003
32. Cvetkoska A, Maček-Lebar A, Trdina P, Miklavčič D, Reberšek M. Muscle contractions and pain sensation accompanying high-frequency electroporation pulses. *Sci Rep* 2022; **12**: 1-15. doi: 10.1038/s41598-022-12112-9
33. Arena CB, Sano MB, Rossmeisl JH, Caldwell JL, Garcia PA, Rylander MN, et al. High-frequency irreversible electroporation (H-FIRE) for non-thermal ablation without muscle contraction. *Biomed Eng Online* 2011; **10**: 1-21. doi: 10.1186/1475-925X-10-102
34. Dong S, Wang H, Zhao Y, Sun Y, Yao C. First human trial of high-frequency irreversible electroporation therapy for prostate cancer. *Technol Cancer Res Treat* 2018; **17**: 1533033818789692. doi: 10.1177/1533033818789692
35. van Es R, Konings MK, Du Pré BC, Neven K, van Wessel H, van Driel VJ, et al. High-frequency irreversible electroporation for cardiac ablation using an asymmetrical waveform. *Biomed Eng Online* 2019; **18**: 1-13. doi: 10.1186/s12938-019-0693-7
36. Ye X, Liu S, Yin H, He Q, Xue Z, Lu C, et al. Study on optimal parameter and target for pulsed-field ablation of atrial fibrillation. *Front Cardiovasc Med* 2021; **8**: 690092. doi: 10.3389/fcvm.2021.690092
37. Hartl S, Reinsch N, Fütting A, Neven K. Pearls and pitfalls of pulsed field ablation. *Korean Circ J* 2022; **53**: 273-93. doi: 10.4070/kcj.2023.0023
38. Scuderi M, Reberšek M, Miklavčič D, Dermol-Cerne J. The use of high-frequency short bipolar pulses in cisplatin electrochemotherapy in vitro. *Radiol Oncol* 2019; **53**: 194-205. doi: 10.2478/raon-2019-0025
39. Sweeney DC, Reberšek M, Dermol J, Rems L, Miklavčič D, Davalos RV. Quantification of cell membrane permeability induced by monopolar and high-frequency bipolar bursts of electrical pulses. *Biochim Biophys Acta BBA-Biomembr* 2016; **1858**: 2689-98. doi: 10.1016/j.bbame.2016.06.024
40. Lyons P, Polini D, Russell-Ryan K, Clover AJP. High-frequency electroporation and chemotherapy for the treatment of cutaneous malignancies: evaluation of early clinical response. *Cancers* 2023; **15**: 3212. doi: 10.3390/cancers15123212
41. Pfeifferle V, Häfner HM, Saur A, Kofler K, Kofler L. Electrochemotherapy in analgesedation for patients with reduced ability to receive general anesthesia. *JDDG J Dtsch Dermatol Ges* 2022; **20**: 1384-6. doi: 10.1111/ddg.14855
42. Pfeifferle V, Leiter U, Grünke T, Kofler K, Häfner HM, Kofler L. Electrochemotherapy under analgesedation – case report of a patient with Kaposi's sarcoma. *J Eur Acad Dermatol Venereol* 2023; **37**: e209-11. doi: 10.1111/jdv.18518
43. Mir LM, Orlowski S, Belehradec Jr J, Paoletti C. Electrochemotherapy potentiation of antitumor effect of bleomycin by local electric pulses. *Eur J Cancer Clin Oncol* 1991; **27**: 68-72. doi: 10.1016/0277-5379(91)90064-k
44. Trotošek B, Djokić M, Čemažar M, Serša G. New era of electrochemotherapy in treatment of liver tumors in conjunction with immunotherapies. *World J Gastroenterol* 2021; **27**: 8216. doi: 10.3748/wjg.v27.i48.8216
45. Heller R, Gilbert R, Jaroszeski MJ. Electrochemotherapy of murine melanoma using intratumor drug administration. *Methods Mol Med* 2000; **37**: 253-7. doi: 10.1385/1-59259-080-2:253.
46. Sedlar A, Jesenko T, Markelc B, Prosen L. Potentiation of electrochemotherapy by intramuscular IL-12 gene electrotransfer in murine sarcoma and carcinoma with different immunogenicity. *Radiol Oncol* 2012; **46**: 302-11. doi: 10.2478/v10019-012-0044-9
47. Ursic K, Kos S, Kamensek U, Cemažar M, Miceska S, Markelc B, et al. Potentiation of electrochemotherapy effectiveness by immunostimulation with IL-12 gene electrotransfer in mice is dependent on tumor immune status. *J Controlled Release* 2021; **332**: 623-35. doi: 10.1016/j.jconrel.2021.03.009
48. Sersa G, Teissie J, Cemazar M, Signori E, Kamensek U, Marshall G, et al. Electrochemotherapy of tumors as in situ vaccination boosted by immunogene electrotransfer. *Cancer Immunol Immunother* 2015; **64**: 1315-27. doi: 10.1007/s00262-015-1724-2
49. Rosazza C, Haberl Meglic S, Zumbusch A, Rols MP, Miklavčič D. Gene electrotransfer: a mechanistic perspective. *Curr Gene Ther* 2016; **16**: 98-129. doi: 10.2174/1566523216666160331130040
50. Radzevičiūtė E, Malyško-Ptašinskė V, Kulbacka J, Rembiałkowska N, Novickij J, Girkontaitė I, et al. Nanosecond electrochemotherapy using bleomycin or doxorubicin: influence of pulse amplitude, duration and burst frequency. *Bioelectrochemistry* 2022; **148**: 108251. doi: 10.1016/j.bioelechem.2022.108251
51. Novickij V, Balevičiūtė A, Malyško V, Želvys A, Radzevičiūtė E, Kos B, et al. Effects of time delay between unipolar pulses in high frequency nano-electrochemotherapy. *IEEE Trans Biomed Eng* 2021; **69**: 1726-32. doi: 10.1109/TBME.2021.3129176
52. Vizintin A, Markovic S, Scancar J, Kladnik J, Turel I, Miklavčič D. Nanosecond electric pulses are equally effective in electrochemotherapy with cisplatin as microsecond pulses. *Radiol Oncol* 2022; **56**: 326-35. doi: 10.2478/raon-2022-0028
53. Cemazar M, Sersa G, Frey W, Miklavčič D, Teissie J. Recommendations and requirements for reporting on applications of electric pulse delivery for electroporation of biological samples. *Bioelectrochemistry* 2018; **122**: 69-76. doi: 10.1016/j.bioelechem.2018.03.005
54. Protocol AG. CellTiter 96® Aqueous One Solution Cell Proliferation Assay. Promega USA. [Internet]. [cited 2023 Oct 15]. Available at: <https://www.promega.com/-/media/files/resources/protocols/technical-bulletins/0/celltiter-96-aqueous-one-solution-cell-proliferation-assay-system-protocol.pdf>
55. Franken NA, Rodermond HM, Stap J, Haveman J, Van Bree C. Clonogenic assay of cells in vitro. *Nat Protoc* 2006; **1**: 2315-19. doi: 10.1038/nprot.2006.339
56. Sweeney DC, Douglas TA, Davalos RV. Characterization of cell membrane permeability in vitro part II: computational model of electroporation-mediated membrane transport. *Technol Cancer Res Treat* 2018; **17**: 1533033818792490. doi: 10.1177/1533033818792490
57. Mahnič-Kalamiza S, Miklavčič D, Vorobiev E. Dual-porosity model of solute diffusion in biological tissue modified by electroporation. *Biochim Biophys Acta BBA-Biomembr* 2014; **1838**: 1950-66. doi: 10.1016/j.bbame.2014.03.004
58. Nejad MA, Urbassek HM. Diffusion of cisplatin molecules in silica nanopores: molecular dynamics study of a targeted drug delivery system. *J Mol Graph Model* 2019; **86**: 228-34. doi: 10.1016/j.jmgm.2018.10.021
59. Panczyk T, Jagusiak A, Pastorin G, Ang WH, Narkiewicz-Michalek J. Molecular dynamics study of cisplatin release from carbon nanotubes capped by magnetic nanoparticles. *J Phys Chem C* 2013; **117**: 17327-36. doi: 10.1021/jp405593u
60. Jakštys B, Ruzgys P, Tamošiūnas M, Šatkauskas S. Different cell viability assays reveal inconsistent results after bleomycin electrotransfer in vitro. *J Membr Biol* 2015; **248**: 857-63. doi: 10.1007/s00232-015-9813-x
61. Huckle A, Ciarimboli G. The role of transporters in the toxicity of chemotherapeutic drugs: focus on transporters for organic cations. *J Clin Pharmacol* 2016; **56**: S157-72. doi: 10.1002/jcph.706
62. Makovec T. Cisplatin and beyond: molecular mechanisms of action and drug resistance development in cancer chemotherapy. *Radiol Oncol* 2019; **53**: 148-58. doi: 10.2478/raon-2019-0018
63. Howell SB, Safaei R, Larson CA, Sailor MJ. Copper transporters and the cellular pharmacology of the platinum-containing cancer drugs. *Mol Pharmacol* 2010; **77**: 887-94. doi: 10.1124/mol.109.063172

64. Spreckelmeyer S, Orvig C, Casini A. Cellular transport mechanisms of cytotoxic metalldrugs: an overview beyond cisplatin. *Molecules* 2014; **19**: 15584-610. doi: 10.3390/molecules191015584
65. Shen DW, Pouliot LM, Hall MD, Gottesman MM. Cisplatin resistance: a cellular self-defense mechanism resulting from multiple epigenetic and genetic changes. *Pharmacol Rev* 2012; **64**: 706-21. doi: 10.1124/pr.111.005637
66. Pucihar G, Krmelj J, Reberšek M, Napotnik TB, Miklavčič D. Equivalent pulse parameters for electroporation. *IEEE Trans Biomed Eng* 2011; **58**: 3279-88. doi: 10.1109/TBME.2011.2167232
67. Peng W, Polajžer T, Yao C, Miklavčič D. Dynamics of cell death due to electroporation using different pulse parameters as revealed by different viability assays. *Ann Biomed Eng* 2023. [Internet]. doi: 10.1007/s10439-023-03309-8. Available at: https://www.researchgate.net/publication/373911137_Dynamics_of_Cell_Death_Due_to_Electroporation_Using_Different_Pulse_Parameters_as_Revealed_by_Different_Viability_Assays
68. Dermol-Černe J, Vidmar J, Ščančar J, Uršič K, Serša G, Miklavčič D. Connecting the *in vitro* and *in vivo* experiments in electrochemotherapy—a feasibility study modeling cisplatin transport in mouse melanoma using the dual-porosity model. *J Controlled Release* 2018; **286**: 33-45. doi: 10.1016/j.jconrel.2018.07.021
69. Daley-Yates PT, McBrien DC. Cisplatin metabolites in plasma, a study of their pharmacokinetics and importance in the nephrotoxic and antitumour activity of cisplatin. *Biochem Pharmacol* 1984; **33**: 3063-70. doi: 10.1016/0006-2952(84)90610-5
70. Gately DP, Howell SB. Cellular accumulation of the anticancer agent cisplatin: a review. *Br J Cancer* 1993; **67**: 1171-6. doi: 10.1038/bjc.1993.221
71. Rols MP, Femenia P, Teissie J. Long-lived macrophocytosis takes place in electroporabilized mammalian cells. *Biochem Biophys Res Commun* 1995; **208**: 26-35. doi: 10.1006/bbrc.1995.1300
72. Clover AJP, de Terlizzi F, Bertino G, Curatolo P, Odili J, Campana LG, et al. Electrochemotherapy in the treatment of cutaneous malignancy: outcomes and subgroup analysis from the cumulative results from the pan-European International Network for Sharing Practice in Electrochemotherapy database for 2482 lesions in 987 patients (2008–2019). *Eur J Cancer* 2020; **138**: 30-40. doi: 10.1016/j.ejca.2020.06.020
73. Cornelis FH, Ben Ammar M, Nouri-Neuville M, Matton L, Benderra MA, Gligorov J, et al. Percutaneous image-guided electrochemotherapy of spine metastases: initial experience. *Cardiovasc Intervent Radiol* 2019; **42**: 1806-9. doi: 10.1007/s00270-019-02316-4
74. Tarantino L, Busto G, Nasto A, Fristachi R, Cacace L, Talamo M, et al. Percutaneous electrochemotherapy in the treatment of portal vein tumor thrombosis at hepatic hilum in patients with hepatocellular carcinoma in cirrhosis: a feasibility study. *World J Gastroenterol* 2017; **23**: 906. doi: 10.3748/wjg.v23.i5.906
75. Djokic M, Cemazar M, Stabuc M, Petric M, Smid LM, Jansa R, et al. Percutaneous image guided electrochemotherapy of hepatocellular carcinoma: technological advancement. *Radiol Oncol* 2020; **54**: 347-52. doi: 10.2478/raon-2020-0038
76. Gudvangen E, Kim V, Novickij V, Battista F, Pakhomov AG. Electroporation and cell killing by milli-to nanosecond pulses and avoiding neuromuscular stimulation in cancer ablation. *Sci Rep* 2022; **12**: 1-15. doi: 10.1038/s41598-022-04868-x
77. Kim V, Gudvangen E, Kondratiev O, Redondo L, Xiao S, Pakhomov AG. Peculiarities of neurostimulation by intense nanosecond pulsed electric fields: how to avoid firing in peripheral nerve fibers. *Int J Mol Sci* 2021; **22**: 7051. doi: 10.3390/ijms22137051
78. Jung J, Kim DH, Son J, Lee SK, Son BS. Comparative study between local anesthesia and general anesthesia in the treatment of primary spontaneous pneumothorax. *Ann Transl Med* 2019; **7**: 553. doi: 10.21037/atm.2019.09.89
79. Vižintin A, Marković S, Ščančar J, Miklavčič D. Electroporation with nanosecond pulses and bleomycin or cisplatin results in efficient cell kill and low metal release from electrodes. *Bioelectrochemistry* 2021; **140**: 107798. doi: 10.1016/j.bioelechem.2021.107798
80. Bendix MB, Houston A, Forde PF, Brint E. Electrochemotherapy and immune interactions; a boost to the system? *Eur J Surg Oncol* 2022; **48**: 1895-900. doi: 10.1016/j.ejso.2022.05.023
81. Groselj A, Bosnjak M, Jesenko T, Cemazar M, Markelc B, Strojjan P, et al. Treatment of skin tumors with intratumoral interleukin 12 gene electrotransfer in the head and neck region: a first-in-human clinical trial protocol. *Radiol Oncol* 2022; **56**: 398-408. doi: 10.2478/raon-2022-0021
82. Napotnik TB, Polajžer T, Miklavčič D. Cell death due to electroporation—a review. *Bioelectrochemistry* 2021; **141**: 107871. doi: 10.1016/j.bioelechem.2021.107871
83. Kesar U, Markelc B, Jesenko T, Ursic Valentinuzzi K, Cemazar M, Strojjan P, et al. Effects of electrochemotherapy on immunologically important modifications in tumor cells. *Vaccines* 2023; **11**: 925. doi: 10.3390/vaccines11050925
84. Calvet CY, Famin D, André FM, Mir LM. Electrochemotherapy with bleomycin induces hallmarks of immunogenic cell death in murine colon cancer cells. *Oncol Immunology* 2014; **3**: e28131. doi: 10.4161/onci.28131
85. Gerlini G, Di Gennaro P, Borgognoni L. Enhancing anti-melanoma immunity by electrochemotherapy and *in vivo* dendritic-cell activation. *Oncimmunology* 2012; **1**: 1655-7. doi: 10.4161/onci.21991
86. Gerlini G, Sestini S, Di Gennaro P, Urso C, Pimpinelli N, Borgognoni L. Dendritic cells recruitment in melanoma metastasis treated by electrochemotherapy. *Clin Exp Metastasis* 2013; **30**: 37-45. doi: 10.1007/s10585-012-9505-1
87. Cemazar M, Ambrozic Avgustin J, Pavlin D, Sersa G, Poli A, Krhac Levacic A, et al. Efficacy and safety of electrochemotherapy combined with peritumoral IL-12 gene electrotransfer of canine mast cell tumours. *Vet Comp Oncol* 2017; **15**: 641-54. doi: 10.1111/vco.12208
88. Reed SD, Fulmer A, Buckholz J, Zhang B, Cutrera J, Shiomitsu K, et al. Bleomycin/interleukin-12 electrochemogene therapy for treating naturally occurring spontaneous neoplasms in dogs. *Cancer Gene Ther* 2010; **17**: 457-64. doi: 10.1038/cgt.2010.6
89. Tratar UL, Milevoj N, Cemazar M, Znidar K, Valentinuzzi KU, Brozic A, et al. Treatment of spontaneous canine mast cell tumors by electrochemotherapy combined with IL-12 gene electrotransfer: comparison of intratumoral and peritumoral application of IL-12. *Int Immunopharmacol* 2023; **120**: 110274. doi: 10.1016/j.intimp.2023.110274
90. Daud AI, DeConti RC, Andrews S, Urbas P, Riker AI, Sondak VK, et al. Phase I trial of interleukin-12 plasmid electroporation in patients with metastatic melanoma. *J Clin Oncol* 2008; **26**: 5896. doi: 10.1200/JCO.2007.15.6794
91. Sachdev S, Potočnik T, Rems L, Miklavčič D. Revisiting the role of pulsed electric fields in overcoming the barriers to *in vivo* gene electrotransfer. *Bioelectrochemistry* 2022; **144**: 107994. doi: 10.1016/j.bioelechem.2021.107994
92. Bulysheva A, Heller L, Francis M, Varghese F, Boye C, Heller R. Monopolar gene electrotransfer enhances plasmid DNA delivery to skin. *Bioelectrochemistry* 2021; **140**: 107814. doi: 10.1016/j.bioelechem.2021.107814
93. Smith TR, Patel A, Ramos S, Elwood D, Zhu X, Yan J, et al. Immunogenicity of a DNA vaccine candidate for COVID-19. *Nat Commun* 2020; **11**: 2601. doi: 10.1038/s41467-020-16505-0
94. Potočnik T, Maček Lebar A, Kos Š, Reberšek M, Pirc E, Serša G, et al. Effect of experimental electrical and biological parameters on gene transfer by electroporation: a systematic review and meta-analysis. *Pharmaceutics* 2022; **14**: 2700. doi: 10.3390/pharmaceutics14122700
95. Geboers B, Scheffer HJ, Graybill PM, Ruarus AH, Nieuwenhuizen S, Puijk RS, et al. High-voltage electrical pulses in oncology: irreversible electroporation, electrochemotherapy, gene electrotransfer, electrofusion, and electroimmunotherapy. *Radiology* 2020; **295**: 254-72. doi: 10.1148/radiol.2020192190
96. Cindric H, Mariappan P, Beyer L, Wiggermann P, Moche M, Miklavcic D, et al. Retrospective study for validation and improvement of numerical treatment planning of irreversible electroporation ablation for treatment of liver tumors. *IEEE Trans Biomed Eng* 2021; **68**: 3513-24. doi: 10.1109/TBME.2021.3075772

97. Scuderi M, Dermol-Černe J, da Silva CA, Muralidharan A, Boukany PE, Rems L. Models of electroporation and the associated transmembrane molecular transport should be revisited. *Bioelectrochemistry* 2022; **147**: 108216. doi: 10.1016/j.bioelechem.2022.108216
98. Frandsen SK, Gehl J. A review on differences in effects on normal and malignant cells and tissues to electroporation-based therapies: a focus on calcium electroporation. *Technol Cancer Res Treat* 2018; **17**: 1533033818788077. doi: 10.1177/1533033818788077
99. Polajžer T, Miklavčič D. Immunogenic cell death in electroporation-based therapies depends on pulse waveform characteristics. *Vaccines* 2023; **11**: 1036. doi: 10.3390/vaccines11061036

RAD54B promotes gastric cancer cell migration and angiogenesis via the Wnt/ β -catenin pathway

Jianchao Li, Hui Geng, Xin Li, Shenshan Zou, Xintao Xu

Department of General Surgery, Changzhou TCM Hospital, Changzhou, Jiangsu, China

Radiol Oncol 2024; 58(1): 67-77.

Received 28 July 2023

Accepted 06 November 2023

Correspondence to: Xintao Xu, Department of General Surgery, Changzhou TCM Hospital, No. 25 Heping North Road, Changzhou, Jiangsu, China. E-mail: xintao_x@163.com

Disclosure: No potential conflicts of interest were disclosed.

This is an open access article distributed under the terms of the CC-BY license (<https://creativecommons.org/licenses/by/4.0/>).

Background. Gastric cancer is an epidemic malignancy that is commonly diagnosed at the late stage. Evidence has elucidated that RAD54B exerts a crucial role in the progress of various tumors, but its specific role and mechanism in gastric cancer remain gloomy.

Materials and methods. The level of RAD54B was detected by western blot. RAD54B expression was downregulated or upregulated in both MKN45 and AGS cells by the transfection of shRAD54B or overexpression plasmid, respectively. The role of RAD54B in the growth, migration, invasion and tube formation of gastric cancer was evaluated by Edu, colony formation, transwell and tube formation assays. In addition, the molecular mechanism of RAD54B in gastric cancer was also determined by western blot. Moreover, *in vivo* experiment was conducted in xenografted mice.

Results. The expression of RAD54B was discovered to be upregulated in gastric cancer based on the ATGC and GEPIA databases, which was also confirmed in gastric cancer cell lines. Moreover, overexpression of RAD54B enhanced the growth, migration, invasion, tube formation and Wnt/ β -catenin signaling axis in AGS and MKN45 cells. As expected, knockdown of RAD54B in AGS and MKN45 cells reversed these promotions. More importantly, *in vivo* assay also verified that RAD54B accelerated the growth of gastric cancer and Wnt/ β -catenin signaling pathway.

Conclusions. Both loss-of-function and gain-of-function assays demonstrated that RAD54B facilitated gastric cancer cell progress and angiogenesis through the Wnt/ β -catenin axis.

Key words: gastric cancer; RAD54B; migration; angiogenesis; Wnt/ β -catenin

Introduction

Gastric cancer is a category of prevalent malignancy with high invasiveness that has been demonstrated to be the fifth diagnosed cancer and fourth cause of cancer death.¹ It has been recognized that several risk factors, including *Helicobacter pylori* infection, alcohol consumption, obesity and cigarette smoking, are strongly involved in gastric cancer.² Although its incidence has been steadily decreased in the last century, a majority of gastric cancer cases are diagnosed at advanced stages nowadays.³ Moreover, the existence of tumor behaviors, such as metastasis and invasion forces

immensely poor prognosis on the gastric cancer patients.⁴ Accordingly, the 5-year survival rate of advanced gastric cancer remains under 30% in spite enormous advance has been achieved in the therapies.⁵ Thus, discovering potential therapeutic targets and identifying the underlying molecular mechanism are of great importance for improving the gastric cancer.

RAD54 Homolog B (RAD54B) located on chromosome 8p22.1, is a member of SWI2/SNF2 heliase superfamily.⁶ Evidence has revealed that RAD54B is associated with the homologous recombination repair and the regulation of the DNA damage checkpoint response.^{7,8} Thus, plenty of

studies verify the implication between RAD54B and the progress of various cancers. For instance, upregulation of RAD54B indicates a poor survival of patients with luminal A subtype breast cancer, thus knockdown of RAD54B inhibits the growth of luminal A subtype breast cancer both *in vitro* and *in vivo*.⁹ Similarly, RAD54B is highly expressed in hepatocellular carcinoma (HCC), which has negative effects on the 5-year disease-free survival and 5-year overall survival of HCC patients. Overexpression of RAD54B greatly enhanced the cell viability and migration of HCC cells and the metastasis in xenografted mice.¹⁰ Also, Xu C *et al.*¹¹ reported that downregulation of RAD54B attenuated the proliferation with increased apoptosis of lung cancer cells. RAD54B was highly expressed in colorectal cancer that was identified as an independent predictor of postoperative distant recurrence in patients with colorectal cancer.¹² RAD54B is revealed to be related to the pathogenic or likely pathogenic (P/LP) germline variants in melanoma.¹³ However, the role of RAD54B in gastric cancer is still unknown.

Hence, the role and underlying molecular mechanism of RAD54B were explored in gastric cancer in the current study. We hope the results can establish an academic foundation for the development of therapeutic strategies of gastric cancer.

Materials and methods

Analysis of the expression profile of RAD54B in gastric cancer based on the online databases

The expression level of RAD54B in the gastric cancer samples and normal samples, as well as the pan-cancer RAD54B expression were analyzed by The Cancer Genome Atlas (TCGA). In addition, the level of RAD54B in the gastric cancer samples and normal samples was also determined by the Gene Expression Profiling Interactive Analysis (GEPIA; <http://gepia2.cancer-pku.cn>), an online open-access RNA-seq analysis tool¹⁴, in which the cutoff mRNA/transcript value and *p* value were the default values with 1 and 0.01, respectively.

Cell culture

Human gastric cancer lines, including AGS (CL-0022), MKN45 (CL-0292), NCI-N87 (CL-0169), HGC-27 (CL-0107), human gastric epithelial cells GES-1 (CL-0563) and human umbilical vein endothelial cells (HUVECs, CL-0122) were bought

from Procell (Wuhan, China). All the cell lines except for HUVECs were cultured in RPMI-1640 media (PM150110, Procell), while HUVECs were maintained in DMEM/F12 basic media (PM150312, Procell) with 10% fetal bovine serum (FBS, 1600044, Gibco, Rockville, MD, USA) and 1% penicillin/streptomycin (PB180120, Procell) at 37°C with 5% carbon dioxide (CO₂).

Cell transfection

Two short hairpin RNAs (shRNAs) targeting RAD54B (sh-RAD54B#1 and sh-RAD54B#2) and negative controls (sh-NC) were purchased from GenePharma (Shanghai, China). Overexpression of RAD54B was achieved via the transfection of pcDNA vector plasmids containing the sequences of RAD54B (pcDNA-RAD54B). The transfection assays were conducted with Lipofectamine 3000 (L3000015, Invitrogen, Carlsbad, CA, USA). Briefly, sh-RAD54B#1, sh-RAD54B#2, sh-NC, pcDNA-RAD54B and empty pcDNA vector plasmids (pcDNA), as well as Lipofectamine 3000 reagents were diluted with Opti-MEM™ (31985070, Invitrogen), and then mixed with a ratio of 1:1. AGS and MKN45 cells were inoculated into 6-well plates with 6×10⁵ cells per well and cultured at 37°C with 5% CO₂. When the convergence reached 70%-90%, the mixtures were added into AGS and MKN45 cells for transfection. Cells were harvested for the subsequent examination after transfection for 48 h.

Western blot

Total proteins from transfected AGS and MKN45 cells were isolated by RIPA buffer (R0010, Solarbio, Beijing, China) and quantified with the BCA protein quantification kit (ab102536, Abcam, Cambridge, UK) in line with the operating instructions. 20 µg protein samples were dissolved and electrically transferred onto a PVDF membrane (IPVH00010, EMD Millipore, Billerica, MA, USA). After blocking with 5% skim milk (D8340, Solarbio) at room temperature for 1 h, the membranes were incubated with primary antibodies against diverse proteins (RAD54B, 1:1000, ab168463; β-catenin, 1:500, ab16051; Axin, 1:1000, ab32197; c-myc, 1:20000, ab152146; MMP-7, 1:1000, ab216631; GAPDH, 1:2500, ab9485; all from Abcam) at 4°C overnight. Subsequently, the membranes were incubated with corresponding secondary antibodies for 2 h at room temperature and visualized by an ECL assay (P0018S, Beyotime, Shanghai, China).

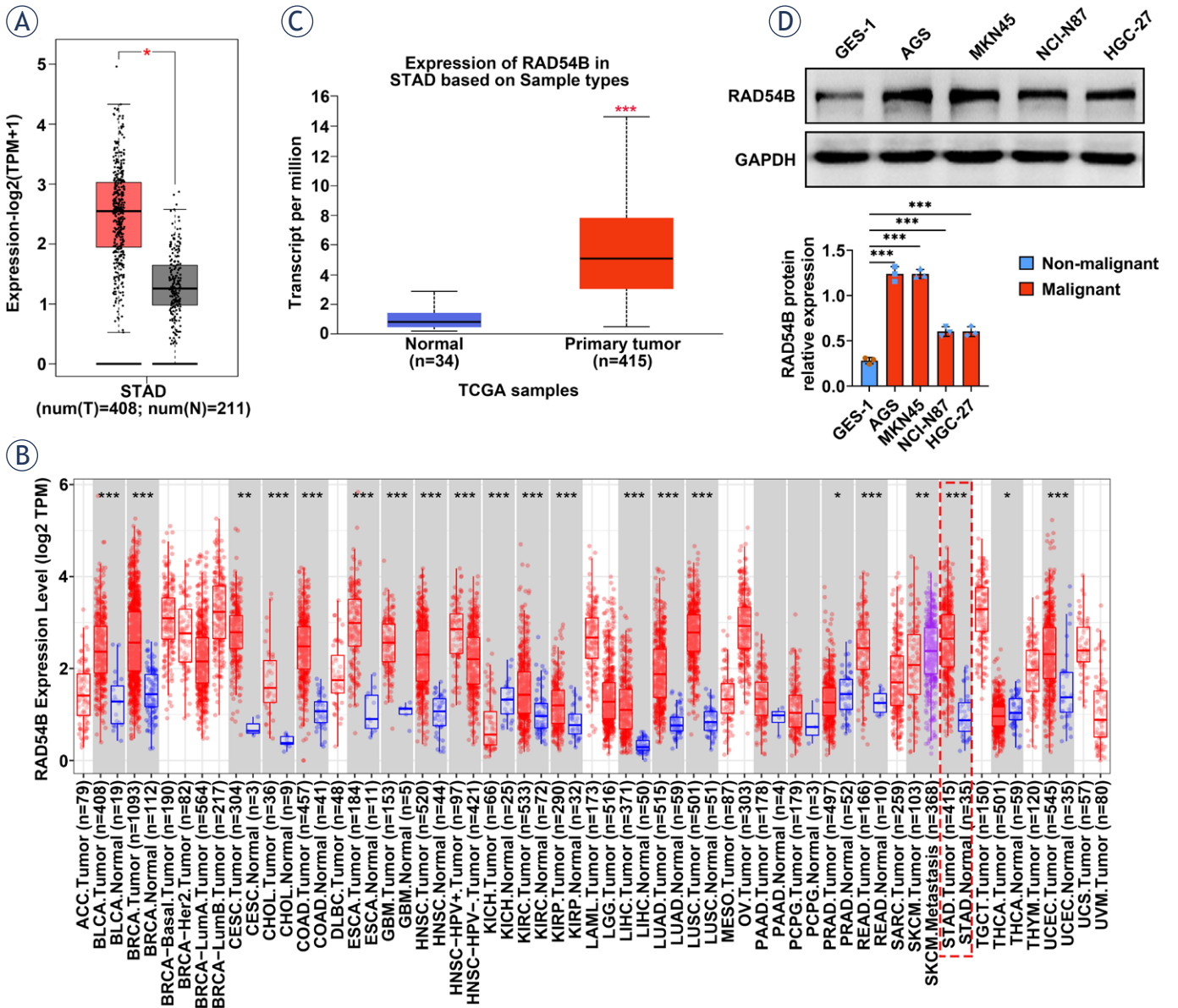


FIGURE 1. RAD54B expression was increased in gastric cancer. **(A)** The expression of RAD54B in gastric cancer was enhanced compared to normal samples according to ATGC database. **(B)** The pan-cancer analysis confirmed an increase in gastric cancer. **(C)** RAD54B expression was upregulated in gastric cancer based on GEPIA. **(D)** The expression level of RAD54B was also augmented in gastric cancer cell lines.

*p < 0.05; **p < 0.01; ***p < 0.001

T = tumor tissues, N = normal tissues

The band intensity was determined by ImageJ software (National Institutes of Health, USA).

The 5-ethynyl-2'-deoxyuridine (EdU) incorporation assay

Transfected AGS and MKN45 cells with 6×10⁵ cells per well were seeded into 6-well plates and maintained at 37°C for 12 h with 5% CO₂. Following the incubation with 1 ml of EdU working solution (20

μM) for 2 h at 37°C, cells were immobilized with immunol-staining fix solution (P0098, Beyotime), permeated with 0.3% Triton X-100 (ST795, Beyotime) and incubated with the anti-EdU Click reaction solution in dark for 30 min. Hoechst 33342 (5 μg/mL, C1022, Beyotime) was utilized for the stain of cell nucleus. The stained cells were photographed under a fluorescence microscopy (Olympus, Tokyo, Japan) and five random fields were chosen for the analysis of the EdU-positive cell percentage.

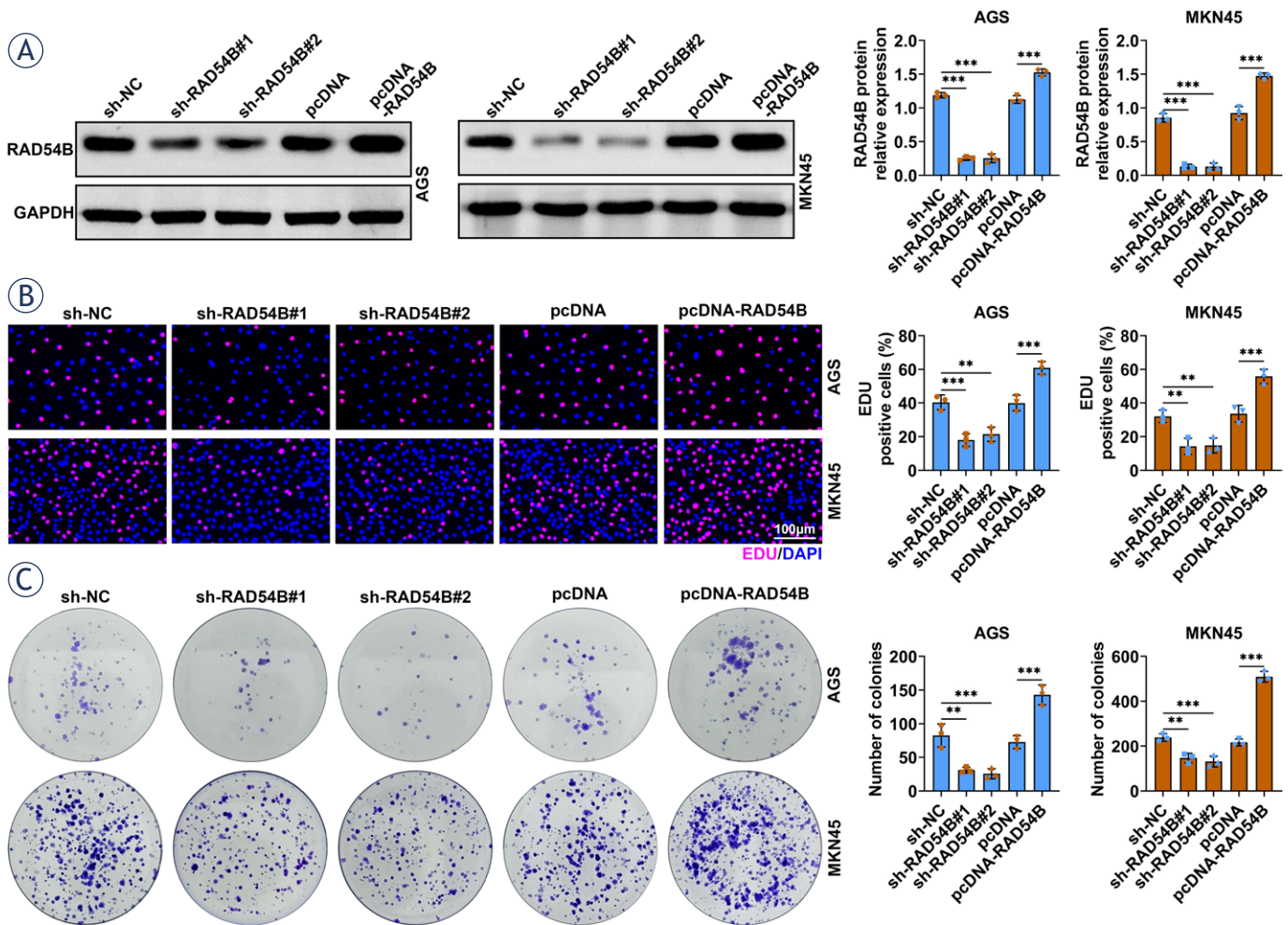


FIGURE 2. RAD54B facilitated the proliferation of gastric cancer cells. (A) The expression of RAD54B was downregulated or upregulated in AGS and MKN45 cells by the transfection of shRAD54B or overexpression plasmid respectively. (B) Transfected AGS and MKN45 cells were seeded into 6-well plates at a density of 6×10^5 cells per well and maintained at 37 °C for 12 h with 5% CO₂. The proliferation of AGS and MKN45 cells was assessed by Edu assays. (C) Transfected AGS and MKN45 cells with 6×10^5 cells per well were plated into 6-well plates and cultured at 37°C for 14 days. The proliferation of AGS and MKN45 cells was determined by colony formation assay.

** $p < 0.01$; *** $p < 0.001$

Colony formation assay

Transfected AGS and MKN45 cells with 6×10^5 cells per well were plated into 6-well plates. Cells were hatched at 37°C for 14 days and then immobilized with 4% paraformaldehyde (P0099, Beyotime) and stained with 0.1% crystal violet (C0121, Beyotime) for 30 min, separately. The clone numbers were manually counted.

Transwell assay

The mobility and invasion of transfected AGS and MKN45 cells were assessed by transwell assay using 24-well transwell chambers with 8.0- μ m

pore size polycarbonate membranes. Briefly, 200 μ l of cell suspension with a total of 2×10^5 cells and 600 μ l of RPMI-1640 with 10% FBS were severally appended into the upper and lower chamber for the cell migration determination. Additionally, Matrigel matrix was filled in the transwell chamber with serum-free medium dilution for the cell invasion detection. The upper and lower chambers were diffused with 200 μ l of cell suspension with a total of 2×10^5 cells and 600 μ l of RPMI-1640 with 10% FBS, respectively. After the continuous culture for 24 h, cells were immobilized with 4% paraformaldehyde and stained with 0.1% crystal violet for 30 min orderly, and then photographed under an inverted microscope (Olympus). Five random

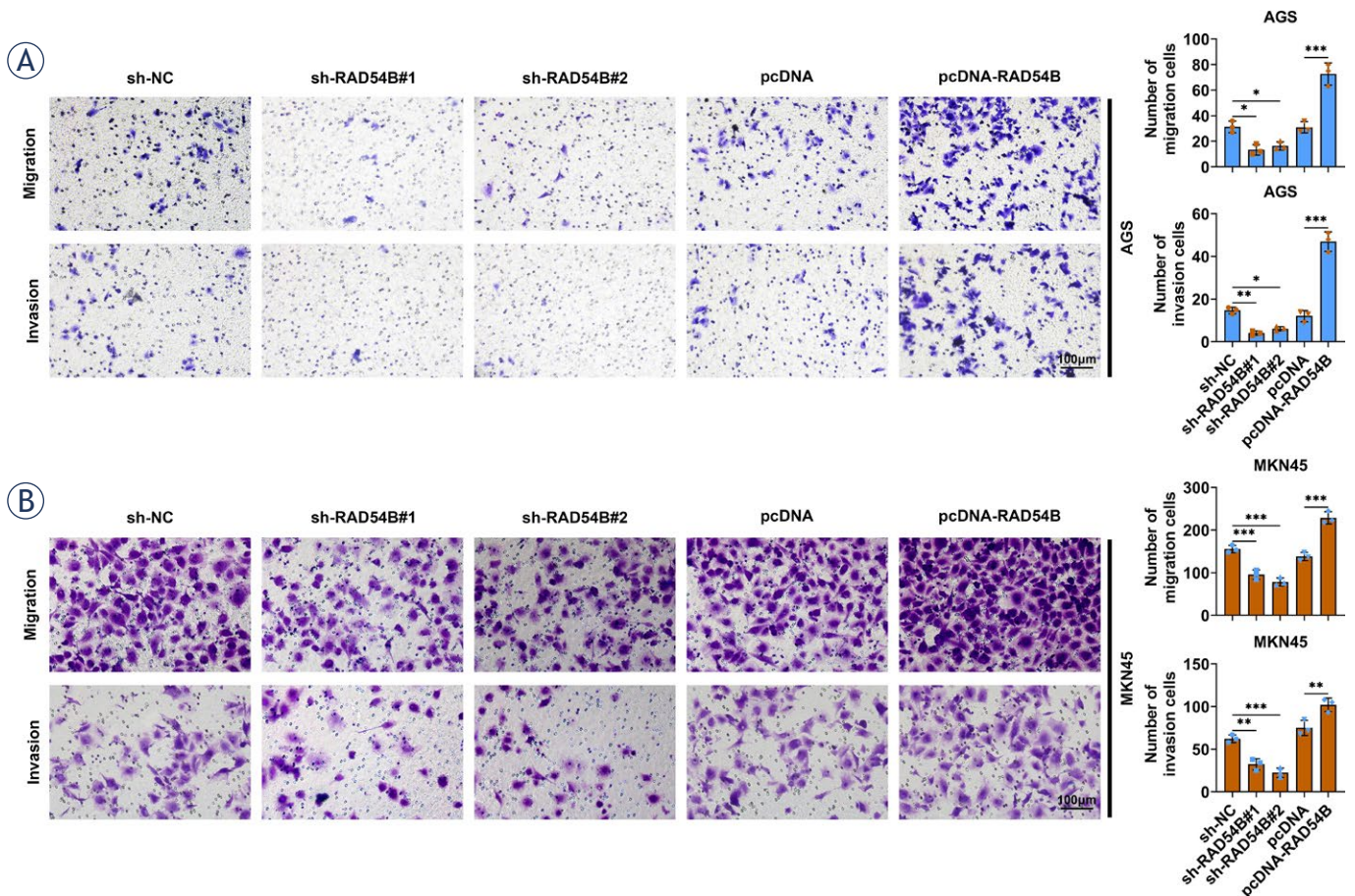


FIGURE 3. RAD54B promoted the migration and invasion of gastric cancer cells. The mobility and invasion of AGS and MKN45 cells were assessed by transwell assay using 24-well Transwell chambers with 8.0 μm pore size polycarbonate membranes. 200 μl of cells suspension with a total of 2×10^5 cells was appended into the upper chamber and cultured for 24 h at 37 $^{\circ}\text{C}$. The migration and invasion of AGS and MKN45 cells were examined by transwell assay.

* $p < 0.05$; ** $p < 0.01$; *** $p < 0.001$

fields were selected for the analysis of the number of migrated and invasive cells by using the Image J software (National Institutes of Health, USA).

Tube formation assay

sh-RAD54B#1, sh-RAD54B#2, sh-NC, pcDNA-RAD54B and empty pcDNA vector plasmids (pcDNA) were transfected into AGS and MKN45 cell lines. Supernatant was collected for the tube formation assay after transfection for 48 h. In brief, HUVECs were cultured in conditioned medium containing supernatant. Then, HUVECs were plated in a 6-well plate coated with matrigel (354248, Corning Company, New York, NY, USA) at a density of 6×10^5 cells per well. Following 4 h, cells were examined with a phase-contrast microscopy, and the tube formation capacity was evaluated by the number of branching points.

Animal experiment

4 weeks-old BALB/c nude mice were bought from Vital River (Beijing, China). Mice were raised in a temperature-controlled SPF animal room with the 12-h cycle of light-dark. Ten mice were randomly divided into two groups, including sh-NC group and sh-RAD54B#1 group. Mice in both groups were subcutaneously injected with a total of 2×10^6 MKN45 cells transfected with sh-NC and sh-RAD54B#1, severally. Tumor volume was monitored every seven days for continuous five weeks and calculated based on the formula: $1/2 \times \text{length} \times \text{width}^2$. After consecutive five weeks, mice were intraperitoneally injected with 120 mg/kg sodium pentobarbital for euthanasia based on the previous study¹⁵, and the tumors samples were enucleated and weighed. The sh-NC group was served as a negative control. MKN45 cells trans-

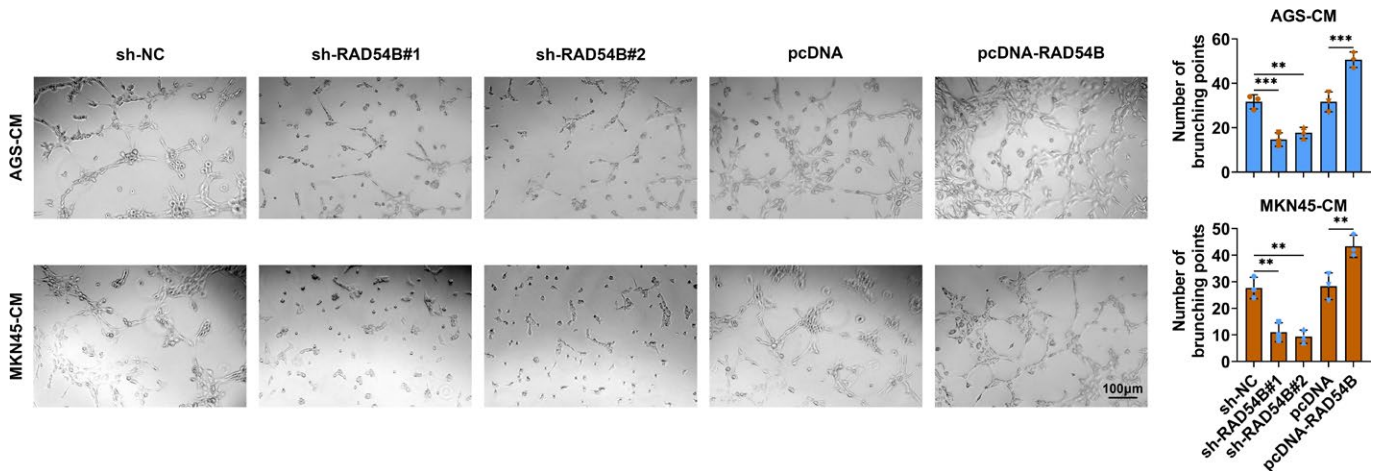


FIGURE 4. RAD54B enhanced the tube formation of gastric cancer cells. After HUVECs were inoculated into conditioned medium containing supernatant harvested from transfected AGS and MKN45 cells for co-culture, the tube formation of HUVECs was assessed by tube formation assay.

** $p < 0.01$; *** $p < 0.001$

ected with sh-NC was not affecting tumor growth compared to untreated tumors that could be supported with *in vitro* results showing no differences in cell proliferation (the percent EDU positive cells

and number of colonies) between control untreated and sh-NC group (Supplementary Figure 1A and B). All animal experiments were authorized by the Animal Research Ethics Committee of Changzhou TCM Hospital.

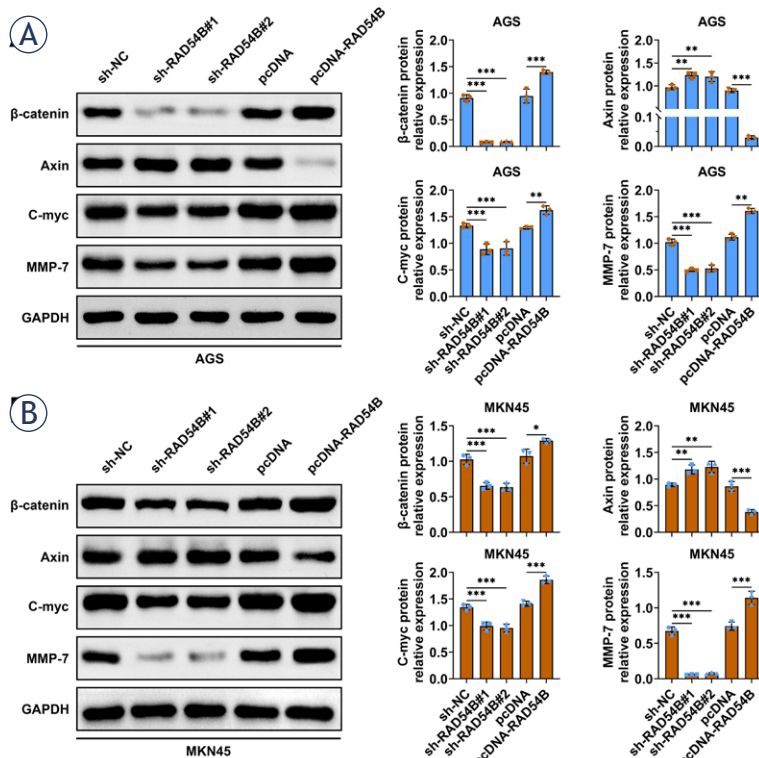


FIGURE 5. RAD54B enhanced activation of Wnt/ β -catenin signaling pathway in gastric cancer cells. The relative protein expressions of β -catenin, Axin, c-myc and MMP-7 were detected by western blot. The data was expressed after being normalized to GAPDH.

* $p < 0.05$; ** $p < 0.01$; *** $p < 0.001$

Immunohistochemistry (IHC)

Tumor tissues were fixed in 4% formaldehyde, dehydrated with gradient concentrations ethanol, embedded into paraffin (YA0011, Solarbio) and cut into sections with a thick of 5 μ m. Sections were retrieved in 10 mM sodium citrate buffer (pH 6.0, P0083, Beyotime) for 15 min at 94°C. Following cooling to room temperature, sections were blocked with 1% bovine serum albumin (BSA, ST2249, Beyotime) for 30 min and then incubated with primary antibodies against RAD54B (1:200, ab238579, Abcam), Ki-67, c-myc (1:1000, ab32072, Abcam) and MMP-7 (1:500, ab216631, Abcam) respectively. Subsequently, sections were incubated with biotinylation-labeled secondary antibody (1:1000, ab207996, Abcam), re-stained with hematoxylin, and captured under a light microscope (Olympus). The relative level of RAD54B, Ki-67, c-myc and MMP-7 was determined as the ratio of the number of positive cells to the total number of cells.

Statistical analysis

Three technical replicates with three independent experimental replicates were conducted in the cell experiments, while five technical replicates with three independent experimental replicates were performed in the animal experiments. Results

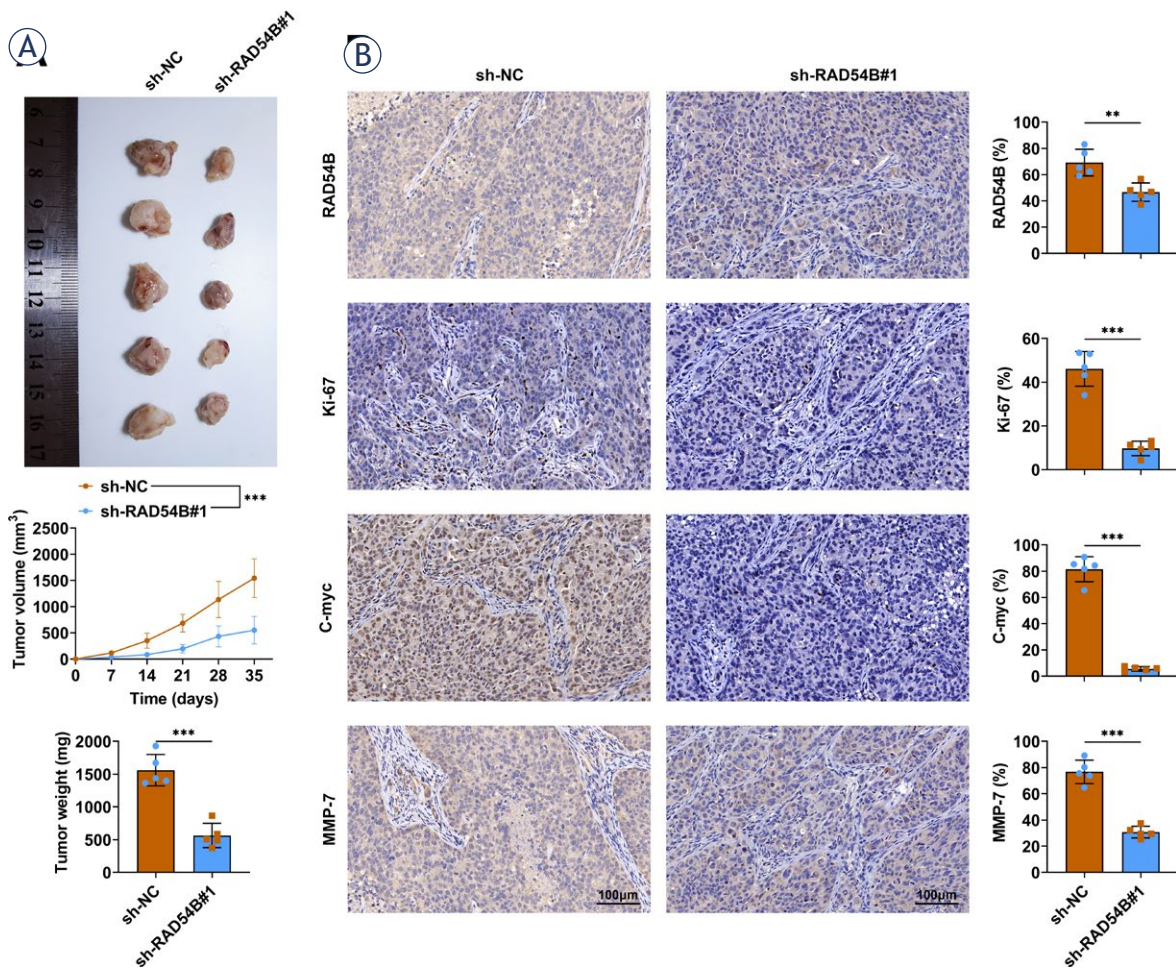


FIGURE 6. RAD54B enhanced the growth of gastric cancer and activation of Wnt/ β -catenin signaling pathway *in vivo*. (A) Nude mice were injected with MKN45 transfected with sh-NC or sh-RAD54B#1 and then the tumor volume and weight were monitored for consecutive five weeks after the treatment. (B) The expression levels of RAD54B, Ki-67, c-myc and MMP-7 were determined by IHC.

*** $p < 0.001$

were expressed as mean \pm standard deviation (SD). Statistical differences were determined through the Student's t-test between two groups followed by *Post Hoc* Bonferroni test by SPSS 26.0 software (IBM, Armonk, New York, USA). $P < 0.05$ was considered as significant difference.

Results

RAD54B was highly expressed in gastric cancer

As presented in Figure 1A, the level of RAD54B in stomach adenocarcinoma (STAD) was significantly increased compared with that in normal samples. Besides, the pan-cancer analysis revealed

that RAD54B expression was also prominently enhanced in the majority of cancers, including STAD (Figure 1B). Moreover, the level of RAD54B was confirmed to be enhanced in the STAD primary tumor samples relative to that in normal samples based on the GEPIA (Figure 1C). Furthermore, a prominent increase in RAD54B expression was also observed in the gastric cancer cell lines, including AGS, MKN45, NCI-N87 and HGC-27, relative to that in human gastric epithelial cells GES-1. Among them, the expression level of RAD54B in AGS and MKN45 was significantly higher than that in NCI-N87 and HGC-27, thus the first two cell lines were chosen for subsequent assays (Figure 1D). Briefly, RAD54B expression was up-regulated in gastric cancer.

RAD54B enhanced the growth of gastric cancer cells

Upregulated expression of RAD54B indicated that RAD54B might exert a crucial effect during the progress of gastric cancer. Hence, the expression of RAD54B was first downregulated or upregulated in both MKN45 and AGS cells with transfection of shRAD54B or overexpression plasmid respectively (Figure 2A). The Edu positive cells and numbers of colonies were observably decreased with silencing of RAD54B, while markedly increased by overexpression of RAD54B in both AGS and MKN45 cells based on the Edu (Figure 2B and C) and colony formation assays (Figure 2D and E). Moreover, no statistical difference was found in the percent EDU positive cells and number of colonies in MKN45 cells between untreated control group and sh-NC group (Supplementary Figure 1A and B). Therefore, RAD54B increased the viability of gastric cancer cells.

RAD54B promoted the mobility and invasion of gastric cancer cells

In addition, the effect of RAD54B on the mobility and invasion of gastric cancer was also assessed by transwell assay. Both the numbers of migrated and invasive cells were notably reduced in both AGS and MKN45 cells transfected with shRAD54B (Figure 3). On the other hand, upregulation of RAD54B markedly enhanced the numbers of both migrated and invasive cells in both AGS and MKN45 cells (Figure 3). Besides, no statistical difference was found in the numbers of both migrated and invasive cells in MKN45 cells between untreated control group and sh-NC group (Supplementary Figure 1C and D). Thus, RAD54B expedited the mobility and invasion of gastric cancer cells.

RAD54B facilitated the tube formation of gastric cancer cells

Moreover, supernatants from cultured AGS and MKN45 cells with the knockdown of RAD54B or with the overexpression of RAD54B were used to incubate with HUVEC. The results showed that the number of branching points of HUVECs was significantly diminished after HUVECs were cultured with supernatants from cultured AGS and MKN45 cells with the knockdown of RAD54B, while that was prominently increased after HUVECs were cultured with supernatants from

cultured AGS and MKN45 cells with the overexpression of RAD54B (Figure 4), indicating that RAD54B promoted the tube formation of gastric cancer cells.

RAD54B activated Wnt/ β -catenin signaling axis in gastric cancer cells

To explore the molecular mechanism of RAD54B in the progress of gastric cancer, the relative protein levels of β -catenin, Axin, c-myc and MMP-7 were examined via western blot. As displayed in Figure 5, the relative protein expressions of β -catenin, c-myc and MMP-7 were significantly decreased in both AGS and MKN45 cells with transfection of shRAD54B, while notably augmented in both AGS and MKN45 cells transfected with RAD54B overexpression plasmid. On the contrary, downregulation of RAD54B markedly enhanced the relative protein expression of Axin, whereas upregulation of RAD54B observably decreased the relative protein expression of Axin in both AGS and MKN45 cells. Therefore, these results manifested that RAD54B facilitated the activation of Wnt/ β -catenin signaling axis in gastric cancer cells.

RAD54B accelerated the growth of gastric cancer *in vivo*

To further verify the role of RAD54B in gastric cancer, nude mice were injected with MKN45 transfected with sh-NC or sh-RAD54B#1 and then monitored for sequential five weeks. As shown in Figure 6A, results exhibited that knockdown of RAD54B significantly decreased the tumor volume and weight (Figure 6A). In addition, silencing of RAD54B also prominently reduced the expression levels of RAD54B, Ki-67, c-myc and MMP-7 relative to sh-NC group (Figure 6B). Thus, these outcomes demonstrated that RAD54B accelerated the proliferation of gastric cancer and activation of Wnt/ β -catenin signaling axis *in vivo*.

Discussion

Gastric cancer is an epidemic malignancy, which is always diagnosed at the late stage.³ Thus, despite the advance and survival of gastric cancer have been prominently increased in recent decades, the prognosis remains discontented due to its high recurrence rate.¹⁶ Evidence has elaborated that RAD54B exerts a significant role in a variety

of cancers¹⁷, but its specific role and mechanism in gastric cancer are still unknown. In the current study, the level of RAD54B was discovered to be enhanced in gastric cancer based on the ATGC and GEPIA databases, which was also confirmed in gastric cancer cell lines. Moreover, overexpression of RAD54B enhanced the growth, migration, invasion, tube formation and activation of Wnt/ β -catenin signaling axis in AGS and MKN45 cells, which was reversed by knockdown of RAD54B in AGS and MKN45 cells. More importantly, *in vivo* assay also verified that RAD54B accelerated the growth of gastric cancer and activation of Wnt/ β -catenin signaling pathway. Based on these outcomes, we concluded that RAD54B facilitated gastric cancer cell progress and angiogenesis through activating the Wnt/ β -catenin pathway.

High expression of RAD54B has been founded in a series of cancers, such as breast cancer and its subtype^{9,18}, HCC^{10,19}, lung cancer¹¹, and colorectal cancer¹², which has been verified in our pan-cancer analysis, as indicated by a remarkable increase of RAD54B expression in BRCA, LIHC, LUAD, LUSC, COAD and READ. In line with these findings, RAD54B expression was also upregulated in gastric cancer according to the ATGC and GEPIA databases, which has been confirmed in gastric cancer cell lines as well. Zhang Z *et al.*⁹ demonstrated that enrichment of RAD54B in luminal A breast cancer promoted tumor cell proliferation, apoptosis and cell cycle arrest. Feng S *et al.*¹⁰ validated that high-expression of RAD54B facilitated the growth and mobility of HCC cells, as well as the metastasis ability *in vivo*. Xu C *et al.*¹¹ reported that upregulation of RAD54B enhanced lung cancer signatures involved in proliferation and apoptosis. In the current study, overexpression of RAD54B consistently promoted the proliferation, migration and invasion of both AGS and MKN45 cells through gain-of-function examination, *vice versa*. Moreover, the suppressive effect of shRAD54B on the tumor volume and weight was also verified in xenografted mice. Thus, these findings clarified that RAD54B expression was notably enhanced in gastric cancer, which accelerated the growth, mobility and invasion of gastric cancer cells.

Angiogenesis is a pivotal process involved in the blood vessels formation that follows a sequence of serial steps for vascular branching.²⁰ Angiogenesis is required for the growth, development, wound healing and regeneration, thus it is generally associated with various physiological and pathological processes.²¹ A growing number of studies has demonstrated that angiogenesis is

implicated with tumorigenesis, in which angiogenesis is imperative for the tumor proliferation and metastasis through the nutrient supply.^{21,22} Hence, strategies targeting anti-angiogenesis are significant for cancer treatment. Here, downregulation of RAD54B notably reduced the number of branching points, and upregulation of RAD54B prominently enhanced the number of branching points of both AGS and MKN45 cells. Therefore, both loss-of-function and gain-of-function assays expounded that RAD54B promoted the tube formation of gastric cancer cells. However, the method used in the present study for the detection of angiogenesis was only the tube formation assay, which may lead to potential bias or imprecision. Thus, more abundant methods should be utilized to assess the role of RAD54B in the angiogenesis in the future.

Mechanically, RAD54B facilitated activation of Wnt/ β -catenin signaling pathway both *in vitro* and *in vivo*. Wnt/ β -catenin signaling axis is associated with a variety of physiological processes, such as embryonic development, regeneration, growth and homeostasis, hence unusual activation Wnt/ β -catenin signaling is always observed in the different cancers.²³ Extensive studies have reported that Wnt/ β -catenin signaling is associated with the progress of diverse cancers. For instance, IFIT1 activates Wnt/ β -catenin signaling in pancreatic cancer to enhance its growth, mobility and invasion.²⁴ Inhibin subunit beta A modulates the proliferation, migration and invasion via activation of Wnt/ β -catenin signaling in breast cancer.²⁵ Inhibition of Wnt/ β -catenin pathway through C644-0303 also impedes the growth of colorectal cancer.²⁶ In the current study, the expression levels of β -catenin, c-myc and MMP-7 were notably diminished in both AGS and MKN45 cells with transfection of shRAD54B and notably increased in both AGS and MKN45 cells transfected with RAD54B overexpression plasmid, which also confirmed *in vivo*. However, the contrary results were obtained in the relative protein expression of Axin in both AGS and MKN45 cells. Axin is a dominating constituent of the canonical Wnt signaling axis, and it contains functional domains that bind to many members involved in the Wnt signaling axis, such as adenomatous polyposis coli (APC), glycogen synthase kinase 3 β (GSK3 β) and β -catenin.²⁷ Axin owns a dual role in regulating Wnt signaling.²⁷ On the one hand, Axin, as a scaffold protein with multiple domains, can form a β -catenin destruction complex (APC-Axin-GSK-3 β), which facilitates the degradation of β -catenin, and effectively regulates

β -catenin to maintain a very low concentration in normal cells, thereby inhibiting Wnt signaling. Additionally, Axin interacts with low-density lipoprotein receptor-related proteins 5 or 6 (LRP5/6) and promotes the recruitment of GSK3 to the plasma membrane to enhance LRP5/6 phosphorylation and activation of Wnt signaling. Accumulated β -catenin within the nucleus can interact with T-cell factor-lymphoid enhancer-binding factor (Tcf-Lef) to enable Wnt-respondent gene transcription, containing c-Myc and Cyclin D1, eventually causing the alterations in the proliferation.²³ MMP-7 is transcriptionally modulated by β -catenin and also one of primary downstream regulator of canonical Wnt signaling reported in diverse cancers, such as ovarian endometrial carcinoma²⁸, intestinal adenoma²⁹ and colorectal cancer.³⁰ Moreover, it has been demonstrated that RAD54B facilitated the progression of HCC via regulating the Wnt/ β -catenin signaling axis.¹⁰ Altogether, these findings elaborated that RAD54B facilitated gastric cancer progression and angiogenesis through activating the Wnt/ β -catenin axis. Nevertheless, a direct connection between the Wnt/ β -catenin signaling and the progression of gastric cancer should be validated in the subsequent studies through the pharmacological block or other effective interference.

In summary, the results in the current study clarified that RAD54B level was significantly upregulated in gastric cancer. Both loss-of-function and gain-of-function assays illustrated that RAD54B promoted the growth, mobility, invasion and tube formation of gastric cancer. Mechanically, RAD54B activated Wnt/ β -catenin signaling. Therefore, RAD54B accelerated gastric cancer progress and angiogenesis by activating the Wnt/ β -catenin pathway. Briefly, our findings can lay a theoretical basic for the development of diagnosis biomarker and therapy target for gastric cancer treatment.

References

- Sung H, Ferlay J, Siegel RL, Laversanne M, Soerjomataram I, Jemal A, et al. Global Cancer Statistics 2020: GLOBOCAN estimates of incidence and mortality worldwide for 36 cancers in 185 countries. *CA Cancer J Clin* 2021; **71**: 209-49. doi: 10.3322/caac.21660
- Rawla P, Barsouk A. Epidemiology of gastric cancer: global trends, risk factors and prevention. *Prz Gastroenterol* 2019; **14**: 26-38. doi: 10.5114/pg.2018.80001
- Smyth EC, Nilsson M, Grabsch HI, van Grieken NC, Lordick F. Gastric cancer. *Lancet* 2020; **396**: 635-48. doi: 10.1016/s0140-6736(20)31288-5
- Lina X, Haiyanga Z, Boa Y, Haia H, Kea Z, Zoub K, et al. Plasma cell-free DNA for screening patients with benefit-assisted neoadjuvant chemotherapy for advanced gastric cancer. *ScienceAsia* 2020; **46**: 462-71. doi: 10.2306/scienceasia1513-1874.2020.056
- Katai H, Ishikawa T, Akazawa K, Ito Y, Miyashiro I, Oda I, et al. Five-year survival analysis of surgically resected gastric cancer cases in Japan: a retrospective analysis of more than 100,000 patients from the nationwide registry of the Japanese Gastric Cancer Association (2001-2007). *Gastric Cancer* 2018; **21**: 144-54. doi: 10.1007/s10120-017-0716-7
- Pazin MJ, Kadonaga JT. SWI2/SNF2 and related proteins: ATP-driven motors that disrupt protein-DNA interactions? *Cell* 1997; **88**: 737-40. doi: 10.1016/s0092-8674(00)81918-2
- Miyagawa K, Tsuruga T, Kinomura A, Usui K, Katsura M, Tashiro S, et al. A role for RAD54B in homologous recombination in human cells. *Embo J* 2002; **21**: 175-80. doi: 10.1093/emboj/21.1.175
- Yasuhara T, Suzuki T, Katsura M, Miyagawa K. Rad54B serves as a scaffold in the DNA damage response that limits checkpoint strength. *Nat Commun* 2014; **5**: 5426. doi: 10.1038/ncomms6426
- Zhang Z, Li X, Han Y, Ji T, Huang X, Gao Q, et al. RAD54B potentiates tumor growth and predicts poor prognosis of patients with luminal A breast cancer. *Biomed Pharmacother* 2019; **118**: 109341. doi: 10.1016/j.biopha.2019.109341
- Feng S, Liu J, Hailiang L, Wen J, Zhao Y, Li X, et al. Amplification of RAD54B promotes progression of hepatocellular carcinoma via activating the Wnt/ β -catenin signaling. *Transl Oncol* 2021; **14**: 101124. doi: 10.1016/j.tranon.2021.101124
- Xu C, Liu D, Mei H, Hu J, Luo M. Knockdown of RAD54B expression reduces cell proliferation and induces apoptosis in lung cancer cells. *J Int Med Res* 2019; **47**: 5650-9. doi: 10.1177/0300060519869423
- Nagai Y, Yamamoto Y, Yasuhara T, Hata K, Nishikawa T, Tanaka T, et al. High RAD54B expression: an independent predictor of postoperative distant recurrence in colorectal cancer patients. *Oncotarget* 2015; **6**: 21064-73. doi: 10.18632/oncotarget.4222
- Amaral T, Schulze M, Sinnberg T, Nieser M, Martus P, Battke F, et al. Are pathogenic germline variants in metastatic melanoma associated with resistance to combined immunotherapy? *Cancers* 2020; **12**. doi: 10.3390/cancers12051101
- Tang Z, Kang B, Li C, Chen T, Zhang Z. GEPIA2: an enhanced web server for large-scale expression profiling and interactive analysis. *Nucleic Acids Res* 2019; **47**: W556-60. doi: 10.1093/nar/gkz430
- Deng T, Zhong P, Lou R, Yang, X. RNF220 promotes gastric cancer growth and stemness via modulating the USP22/wnt/ β -catenin pathway. *Tissue Cell* 2023; **83**: 102123. doi: 10.1016/j.tice.2023.102123
- Matsuoka T, Yashiro M. Biomarkers of gastric cancer: Current topics and future perspective. *World J Gastroenterol* 2018; **24**: 2818-32. doi: 10.3748/wjg.v24.i26.2818
- McAndrew EN, McManus KJ. The enigmatic oncogene and tumor suppressor-like properties of RAD54B: Insights into genome instability and cancer. *Genes Chromosomes Cancer* 2017; **56**: 513-23. doi: 10.1002/gcc.22458
- Wang M, Liao J, Tan C, Zhou H, Wang J, Wang K, et al. Integrated study of miR-215 promoting breast cancer cell apoptosis by targeting RAD54B. *J Cell Mol Med* 2021; **25**: 3327-38. doi: 10.1111/jcmm.16402
- Wang R, Li Y, Chen Y, Wang L, Wu Q, Guo Y, et al. Inhibition of RAD54B suppresses proliferation and promotes apoptosis in hepatoma cells. *Oncol Rep* 2018; **40**: 1233-42. doi: 10.3892/or.2018.6522
- Ucuzian AA, Gassman AA, East AT, Greisler HP. Molecular mediators of angiogenesis. *J Burn Care Res* 2010; **31**: 158-75. doi: 10.1097/BCR.0b013e3181c7ed82
- Carmeliet P, Jain RK. Angiogenesis in cancer and other diseases. *Nature* 2000; **407**: 249-57. doi: 10.1038/35025220
- Katayama Y, Uchino J, Chihara Y, Tamiya N, Kaneko Y, Yamada T, et al. Tumor neovascularization and developments in therapeutics. *Cancers* 2019; **11**. doi: 10.3390/cancers11030316
- Chatterjee A, Paul S, Bisht B, Bhattacharya S, Sivasubramaniam S, Paul MK. Advances in targeting the WNT/ β -catenin signaling pathway in cancer. *Drug Discov Today* 2022; **27**: 82-101. doi: 10.1016/j.drudis.2021.07.007
- Li TH, Zhao BB, Qin C, Wang YY, Li ZR, Cao HT, et al. IFIT1 modulates the proliferation, migration and invasion of pancreatic cancer cells via Wnt/ β -catenin signaling. *Cell Oncol* 2021; **44**: 1425-37. doi: 10.1007/s13402-021-00651-8

25. Xueqin T, Jinhong M, Yuping H. Inhibin subunit beta A promotes cell proliferation and metastasis of breast cancer through Wnt/ β -catenin signaling pathway. *Bioengineered* 2021; **12**: 11567-75. doi: 10.1080/21655979.2021.1971028
26. Yan Y, Zhang Y, Li M, Zhang Y, Zhang X, Zhang X, et al. C644-0303, a small-molecule inhibitor of the Wnt/ β -catenin pathway, suppresses colorectal cancer growth. *Cancer Sci* 2021; **112**: 4722-35. doi: 10.1111/cas.15118
27. Song X, Wang S, Li L. New insights into the regulation of Axin function in canonical Wnt signaling pathway. *Protein Cell* 2014; **5**: 186-93. doi: 10.1007/s13238-014-0019-2
28. Machin P, Catus L, Pons C, Muñoz J, Matias-Guiu X, Prat J. CTNNB1 mutations and beta-catenin expression in endometrial carcinomas. *Hum Pathol* 2002; **33**: 206-12. doi: 10.1053/hupa.2002.30723
29. Crawford HC, Fingleton B, Gustavson MD, Kurpios N, Wagenaar RA, Hassell JA, et al. The PEA3 subfamily of Ets transcription factors synergizes with beta-catenin-LEF-1 to activate matrilysin transcription in intestinal tumors. *Mol Cell Biol* 2001; **21**: 1370-83. doi: 10.1128/mcb.21.4.1370-1383.2001
30. Brabletz T, Jung A, Dag S, Hlubek F, Kirchner T. beta-catenin regulates the expression of the matrix metalloproteinase-7 in human colorectal cancer. *Am J Pathol* 1999; **155**: 1033-8. doi: 10.1016/s0002-9440(10)65204-2

Role of endoscopic ultrasound-guided fine needle aspiration biopsies in diagnosing pancreatic neoplasms in the paediatric population: experience from a tertiary center and review of the literature

Maja Kebe Radulovic¹, Jernej Breclj², Andrej Gruden³, Margareta Strojan Flezar¹

¹ Institute of Pathology, Faculty of Medicine, University of Ljubljana, Ljubljana, Slovenia.

² Department of Gastroenterology, Hepatology and Nutrition, University Children's Hospital Ljubljana, and Department of Pediatrics, Faculty of Medicine, University of Ljubljana, Ljubljana, Slovenia

³ University Medical Centre Ljubljana, Service of Internal Medicine, Department of Gastroenterology, Ljubljana, Slovenia.

Radiol Oncol 2024; 58(1): 78-86.

Received 14 July 2023

Accepted 7 October 2023

Correspondence to: Maja Kebe Radulovic, M.D., Institute of Pathology, Faculty of Medicine, University of Ljubljana, Korytkova 2, SI-1000 Ljubljana, Slovenia. E-mail: maja.kebe-radulovic@mf.uni-lj.si

Disclosure: No potential conflicts of interest were disclosed.

This is an open access article distributed under the terms of the CC-BY license (<https://creativecommons.org/licenses/by/4.0/>).

Background. Endoscopic ultrasound-guided fine needle aspiration biopsy (EUS FNAB) is a well established diagnostic method in adult patients, but is rarely used in the paediatric population. The Clinical Department of Gastroenterology at the University Clinical Centre Ljubljana and the Department of Cytopathology at the Institute of Pathology, Faculty of Medicine, University of Ljubljana, Slovenia, have been closely collaborating on EUS FNAB since the introduction in 2010. The aim of the study was to review the cases of EUS FNAB of pancreatic neoplasms in children.

Patients and methods. In the digital archive of the Institute of Pathology (IP), Faculty of Medicine (FM), University of Ljubljana (UL), we found 6 cases of EUS FNAB in children, 3 had EUS FNAB of the pancreas, 2 of whom had a cytopathologic diagnosis of a tumour. In the first case, the lesion was ultrasonographically solid, and the cell sample contained branching papillary structures surrounded by aggregates of small cells with nuclear grooves. In the second case, the lesion was ultrasonographically cystic, and predominantly necrosis was seen, with only single preserved cells. Positive nuclear reaction for β -catenin was found in both cases by immunohistochemical staining.

Results. In both cases, the cytopathological diagnosis of solid pseudopapillary neoplasm of the pancreas was made, the cases represent the totality of paediatric cases of pancreatic neoplasms from the Children's Hospital Ljubljana since 2010. There were no adverse events during and after EUS FNAB. A histopathological examination of the tumour resection specimens confirmed the cytopathological diagnosis.

Conclusions. Our experience indicates that EUS FNAB is a safe and effective method for diagnosing pancreatic neoplasms in the pediatric population, as supported by the findings in the literature.

Key words: fine needle aspiration biopsy; endoscopic ultrasound; pancreatic neoplasm, paediatric pathology

Introduction

Endoscopic ultrasonography (EUS) is a well-established diagnostic method for the evaluation of a di-

verse range of pancreatic lesions in adult patients, however it is a relatively new technique in paediatric pancreatology.^{1,2}

Studies have also shown that EUS is a better diagnostic procedure than transabdominal ultrasound (TUS), CT scan or endoscopic retrograde cholangiopancreatography for smaller pancreatic lesions, mainly because of the proximity of the EUS probe, making possible a better evaluation of the lesion.^{1,2} EUS enables a detailed evaluation of pancreatic parenchyma and the ductal system, especially in paediatric patients with pancreatic masses, suspected autoimmune pancreatitis or fluid collections.^{3,4}

In addition, it allows for the intervention procedures, namely sampling of lesions with fine-needle aspiration biopsy (FNAB) or core tissue biopsies, or performing drainage procedures in cystic lesions while using Doppler to assess and avoid the vasculature.³ However, the methods of cell or tissue sampling depend on the size and location of the pancreatic lesion and the professional expertise.

Pancreatic neoplasms are exceptionally rare in children, with malignant tumours having an estimated incidence of 0.02 per 100,000.³ It is estimated that solid pseudopapillary neoplasm (SPN) accounts for up to 71% of pancreatic tumours in children and adolescents, followed in order of frequency by pancreatic neuroendocrine tumour, serous cystadenoma and pancreatoblastoma, which is the most common malignant tumour in the patients under 10 years old.^{3,5,6}

The radiologic preoperative diagnosis usually starts with a TUS, which allows a diagnosis of most paediatric pancreatic tumours, except for functional neuroendocrine tumours like insulinomas and gastrinomas, which may cause symptoms even though they're small.³ This is especially true in the case of SPN, which presents as a well demarcated lesion, with cystic or necrotic components and with occasional calcifications within solid tumour.^{3,4}

The Clinical Department of Gastroenterology at the University Clinical Centre Ljubljana and the Department of Cytopathology at the Institute of Pathology (IP), Faculty of Medicine (FM), University of Ljubljana (UL), Slovenia, have been closely collaborating on endoscopic ultrasound-guided fine needle aspiration biopsies (EUS FNAB) since the introduction of the method in 2010. The aim of present study was to analyse the cases of EUS FNAB of pancreatic neoplasms in children in a tertiary care centre and to incorporate a review of the existing literature.

Patients and methods

Study design

A retrospective institutional case series with a literature review was made to assess the outcomes of EUS FNAB in our tertiary referral centre. From January 2010 to December 2021, 6 EUS FNAB of gastrointestinal lesions were performed on paediatric patients (age < 18 years), coming from the Department of Gastroenterology, Hepatology and Nutrition (GHN) of the Children's Hospital Ljubljana. The study was approved by Review Board of the Institute of Pathology UL FM (ID 4/23).

Endoscopic ultrasound-guided fine needle aspiration biopsy

EUS FNAB procedures were done by experienced gastroenterologists specialized in endosonography and US guided FNAB. Three children had EUS FNAB of the pancreas because of a TUS detected tumour: in one, only normal pancreatic tissue was retrieved, with no tumour on follow-up, the other two had a tumour. A primary cytopathological diagnosis in both cases was that of a solid pseudopapillary neoplasm (SPN) (Table 1). According to the search of the hospital and institute's databases, these were also the only cases of pancreatic neoplasms diagnosed at GHN.

In all the cases written informed consent from the parents was obtained for the procedure. The procedures were done in general anaesthesia with a linear probe echoendoscope (EG-580UT, Fujifilm, Japan). FNAB was performed with a 22-gauge Boston Acquire FNAB needle (Boston Scientific, Marlborough, MA, USA).

In all the cases, a cytopathologist was present for a rapid on-site evaluation (ROSE) of the sample cellularity. For ROSE, one direct smear was prepared at the patient's side, fixed in Delaunay fixative (absolute ethanol:acetone 1:1 with 0.05 % 0.5M trichloroacetic acid) and stained with Hemacolor for immediate cytomorphological examination (and later Papanicolaou stained in the laboratory). The second direct smear was air-dried (for later Giemsa staining). The remaining sample was rinsed and stored in an in-house made cell medium.⁷ There was a maximum of 5 passes in one case with initial unsatisfactory samples (e.g. samples without diagnostic cells). Subsequently, all the samples were sent to the cytopathology laboratory for further preparation. If necessary, the samples were filtered to remove blood, concentrated or diluted to obtain uniform monolayers of diagnostic

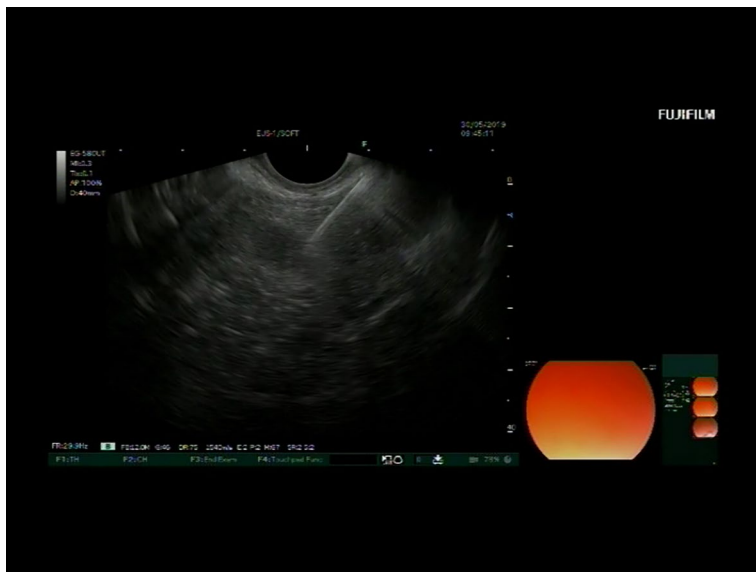


FIGURE 1. Case 1 during endoscopic ultrasound-guided fine needle aspiration biopsy (EUS FNAB). Linear probe echoendoscope localised in duodenum showing a round, well circumscribed, isoechoic lesion in the pancreatic neck that was punctured transduodenally. Tip of the needle (upper right) is in the lesion.

cells by subsequent cytocentrifugation (Shandon Cytospin 4, ThermoScientific, UK). In both cases with a neoplasm, tissue fragments were present and cell blocks were prepared by transferring clots and/or any visible tissue fragments into standard tissue cassettes. Samples were further fixed in formalin and then processed according to the standard procedures for tissue samples. After the cytopathological examination of the slides, the immunocytochemical staining was conducted using the automated immunostaining system ULTRA by Ventana Medical Systems Inc., Tucson, Arizona, USA, on the cytospins and formalin-fixed, paraffin embedded tissue sections from the cell blocks. The detection of bound primary antibodies was carried out with the optiView detection kit, except for CD 10 and NSE which were detected by iView, all from the same company.

The antibody panels utilised on cytospins consisted of following markers:

Vimentin (Recombinant Anti-Vimentin antibody, clone EPR3776, Cytoskeleton Marker, ABCAM), CD56 (Rabbit monoclonal antibody, Clone MRQ-42, Cell Marque), CD10 (clone 56C6) and CKAE1/AE3 from the same producer (Leica Biosystems), NSE (Monoclonal mouse anti-human neuron specific enolase, clone BBS) and Ki67 (Monoclonal mouse antihuman antigen, clone MIB-1) from the same producer (Agilent Technologies), chromogranin (anti-chromogranin

A, primary antibody, clone LK2H10) and synaptophysin (Rabbit monoclonal antibody, clone MRQ-40) and PR (Anti-progesterone receptor, Rabbit monoclonal primary antibody, clone 1E2) and CyclinD (Anti-Cyclin D1, Rabbit monoclonal primary antibody, clone SP4-R), all from Ventana Medical Systems Inc.

Reactions with additional antibodies were performed on the cell block sections using following reagents: E-Cadherin (Mouse monoclonal antibody, clone NCH-38, Agilent Technologies), β -catenin (Mouse monoclonal antibody, clone 14) and SOX11 (Mouse monoclonal antibody, clone MRQ-58), all from the same producer (Cell Marque).

For our literature review, we conducted a comprehensive search on PubMed to identify cases of SPN diagnosed through EUS-FNAB. We employed the following key terms during the search process: 'EUS-FNAB (in full) and pediatric patients' and 'EUS-FNAB (in full) and solid pseudopapillary neoplasia.' Given the rarity of pediatric SPN cases, we opted to include all relevant results, ranging from research articles to case reports. The gathered information has been compiled in Table 2 for a thorough examination of the available data.

Results

The first case was a 8-year-old female patient, weighting 40 kg, who was referred to EUS FNAB from GHN due to a dense lesion in the pancreas found by TUS when searching for the cause of increased liver function tests (AST 1.19 μ kat/L [normal up to 0.52 μ kat/L], ALT 1.19 μ kat/L [normal up to 0.52 μ kat/L], normal gamma-GT, alkaline phosphatase and bilirubin) performed due to nonspecific disease signs (fatigue, nausea, headache).

EUS showed a round, well circumscribed, isoechoic lesion in the pancreatic neck with a diameter of 15 mm (Figures 1, 2A). The cell sample was highly cellular, with abundant eosinophilic stroma, around which the tumour cells were arranged in rounded clusters (Figure 2B-C). The individual cells had moderate, basophilic cytoplasm. The nuclei were round to elongated, with grooves, the chromatin was pale with inconspicuous nucleoli (Figure 2D-E). The background of the specimen contained blood and a few siderophages. Only a few tumour cell nuclei were positive for the proliferation marker Ki67 (less than 1%), the rest of the immunocytochemical reactions were consistent with the final cytopathological diag-

nosis of SPN (Table 1) (Figure 2F). Additional immunohistochemical reactions revealed positive results for Vimentin, CD56, CD10, and NSE, while E-Kadherin showed a negative result.

Eighteen days after EUS FNAB, a partial resection of the pancreas with the lymph node dissection at a. hepatica communis and cholecystectomy followed. The frozen section and definitive specimens showed a solid pseudopapillary tumour confined to the pancreas, measuring 18x10 mm in the largest diameter, lobulated, homogeneous, removed 3 mm from the pancreatic surgical margin (Figure 2B). There was no perineural or lymphovascular invasion, and no tumour tissue was present in the resected lymph node. The patient reported no problems at the outpatient follow-up, the weight gain was adequate, postoperative US showed no additional abnormalities and a fecal elastase, which assesses exocrine pancreatic function, was normal. Thirty-nine months after the EUS FNAB she had acute pancreatitis, which resolved with conservative treatment. Magnetic resonance imaging of the pancreas and abdominal MR with contrast showed no recurrence. At the last follow-up 50 months after the initial diagnosis, she had no medical complaints.

The second case was a 7-year-old female patient, weighting 43 kg, who came to EUS FNAB from the GHN where she presented with abdominal pain. A pancreatic cystic lesion was noted on TUS exam, which could represent a tumour or pseudocyst. EUS showed a 40x40 mm hypoechogenic tumour in the head of the pancreas, pressing the portal system and causing dilatation of the ductus choledochus to 9 mm (Figure 3A). On ROSE the EUS FNAB samples were all non-diagnostic (only blood), except for one pass, where numerous lymphocytes, histiocytes and a necrotic background was retrieved. In the filtered and concentrated sample, there were few preserved tumour cells.

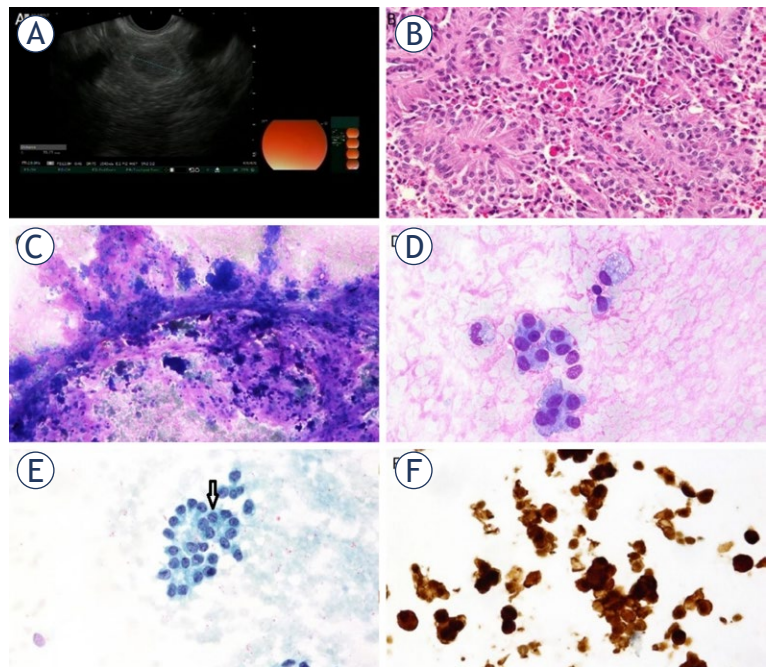


FIGURE 2. Case 1 (A) Endoscopic ultrasound (EUS). A well demarcated, isoechogenic tumour with more echogenic thin border, probably representing a solid pseudopapillary neoplasm (SPN). (B) Pseudopapillary structures in a resected specimen (HE, X200). (C) Endoscopic ultrasound-guided fine needle aspiration biopsy (EUS FNAB). Branching pseudopapillary structures with cohesive cellular clusters and a pinkish substance in the background (MGG, X100). (D) EUS FNAB. Small clusters of bland cells with a foamy macrophage and eosinophilic substance in the background (MGG, X400). (E) Cytospin showing a group of monomorphous cells with round/oval nuclei with smooth, indented nuclear membrane and grooves (arrow) (Pap, X400). (F) Positive nuclear β -Catenin reaction in the cell block (X400).

They were monomorphous, small, with a round, regular nuclei, single nucleoli and focally spiculated chromatin (Figure 3D). The cytoplasm was coarsely granular. In the background, poorly preserved branched capillaries, surrounded by predominantly necrotic cells were visible (Figure 3C).

TABLE 1. Results of the immunochemical reactions in both cases, on cytological and histological samples

Case	β - Catenin	Cyclin D1	Synapto physin	Chromo granin	CD56	PR	CD10	CKAE1/AE3	SOX11
1 cyto	+	+	-+	-	+	/	+	-	+
1 histo	+	/	/	/	/	/	/	/	+
2 cyto	+	+	+-	-	-+	-	+	-+	+
2 histo	+	+	Focally +	/	/	/	/	/	+

Cyto = cytology samples obtained by endoscopic ultrasound-guided fine needle aspiration biopsy (EUS FNAB); Histo: histology samples from the tumour resection specimen

+ = positive immunostaining reaction; - = negative immunostaining reaction; / = immunostaining was not performed; +- = immunostaining reaction predominantly positive; -+ = immunostaining reaction predominantly negative

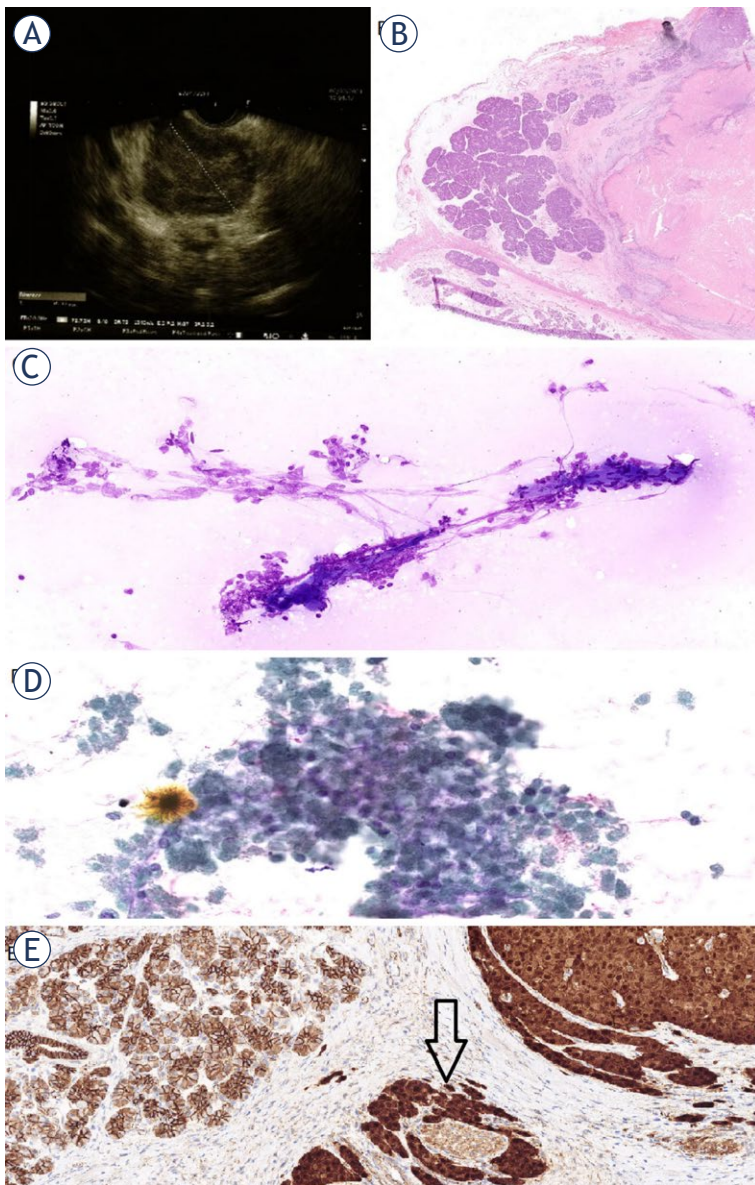


FIGURE 3. Case 2 (A) Endoscopic ultrasound (EUS). A well demarcated, hypoechoic tumour. (B) A slide of a resected pancreas at low magnification showing an area of normal pancreatic tissue (left) and an area of eosinophilic degenerative necrosis (right) (HE, X3). (C) Endoscopic ultrasound-guided fine needle aspiration biopsy (EUS FNAB). Naked capillaries surrounded by necrotic cells and a group of cells with preserved nuclei (MGG X100). (D) EUS FNAB. A group of mainly necrotic cells and a few cells with preserved nuclei in between. (E) A slide of a resected pancreas at high magnification as in (B) with a positive nuclear β -Catenin reaction in the tumour (right) with a perineural invasion (arrow) (X100).

According to the immunochemical reactions in the rare preserved cells, the cytopathologic diagnosis was SPN (Table 1). Thirteen days after EUS FNAB, a partial resection of the pancreas with duodenum, excision of the lymph node adjacent to the a. hepatica communis and cholecystectomy followed. Histopathologic examination confirmed

SPN with extensive necrosis of the pancreatic head, with the largest diameter of 30 mm, at a distance of 0.1 mm from the nearest retropancreatic surgical margin (Figure 3B). There were perineural as well as lymphatic and vascular invasions (Figure 3E). No involvement with tumour cells was present in the excised lymph node and 6 regional lymph nodes. The gallbladder and duodenum were unremarkable. Given the extensive tumour necrosis and lymphovascular invasion, the report mentioned the possibility of a more aggressive clinical course. Postoperative follow-up was uneventful. TUS showed changes consistent with the post-operation state. The stool elastase was reduced. Despite the absence of clinical signs, pancreatic enzyme therapy was initiated to ensure adequate nutrient resorption. She has gained considerable weight and has grown appropriately. The girl was presented to the haemato-oncology multidisciplinary team, which advised MRI of the abdomen every 3 months for the first 2 years and then every 6 months for up to 5 years, which she regularly undergoes. At the last follow-up, 31 months after the initial diagnosis, she had no complaints, the laboratory results and the abdomen MRI showed no signs of disease recurrence.

The third case, which ultimately did not involve a pancreatic tumor, pertained to a 17-year-old boy with trisomy 21, weighing 46 kg. He exhibited an enlarged and inhomogeneous pancreatic head on TUS and magnetic resonance cholangiopancreatography following treatment for biliary pancreatitis that resolved without the need for endoscopic retrograde cholangiopancreatography. EUS-FNAB revealed no tumor cells. Consequently, a pancreatic biopsy was recommended, but the patient's mother declined. Subsequent TUS follow-ups showed no evidence of tumor growth or disease progression.

Given the patient's concurrent mild exocrine pancreatic insufficiency (faecal elastase 88 $\mu\text{g/g}$, normal $> 200 \mu\text{g/g}$), pancreatic enzyme replacement therapy was initiated. However, a more comprehensive diagnosis of the pancreatic disease, such as autoimmune or hereditary pancreatitis, proved unattainable as the family withheld consent, and the patient failed to attend follow-up visits.

Discussion

The use of EUS FNAB in the paediatric population is limited, even though it is a well-established diag-

nostic procedure for the assessment of suspicious pancreatic tumours in adult patients. In paediatric cases, the primary indication for EUS-guided pancreatic tissue sampling is pancreatic mass or suspected autoimmune pancreatitis. These conditions often manifest as inhomogeneous lesions of the pancreas, detectable through TUS or EUS.³ Our retrospective study spanned the whole period since the introduction of EUS FNAB in the tertiary health care centre in 2010 until the end of the review period in December 2021. During that period, we had the first case of EUS FNAB in a child in 2019 followed by 5 more cases with complete cytopathological reports and corresponding archival slides. Among the total of 6 children with EUS FNAB of gastrointestinal lesions, two had pancreatic neoplasm, diagnosed as SPN by cytopathological examination.

According to the reviewed literature (Table 2), the adoption of EUS for children with pancreaticobiliary diseases was delayed due to different reasons, among them the low incidence of tumorous lesions and even rarer malignancies.⁸ Other important reasons were also the size limitation of EUS equipment relative to pediatric anatomy, the low number of skilled pediatric endoscopists with

EUS expertise, the need for sedation or general anesthesia, and a limited awareness among pediatric practitioners of EUS diagnostic and therapeutic possibilities.^{3,8} In our patients, the procedure and equipment used was similar to the adult population, apart from the use of general anaesthesia. The endoscopists were very experienced in the management of adult patients, enabling the procedure to be safe and efficient also in the pediatric patients, which corresponds well with other studies.^{1,3,8-11,16-18} While EUS was shown previously as a safe diagnostic method in the pediatric population, covering the age range of our patients (age 8 and 9 years, respectively), there is limited experience with EUS especially in smaller children (< 15 kg) due to the fear of an esophageal rupture associated with the large diameter (adult) EUS scope. Therefore, for smaller children (< 15 kg) endobronchial ultrasound has been used instead and a few studies have shown that EUS can be performed safely and with a high diagnostic accuracy even in these children.^{1,3,8-11,16-18}

The initial diagnostic radiologic assessment of pancreatic lesions is usually conducted by a TUS, which was also the approach in our two paediatric patients. In one patient, a solid isoechoic lesion

TABLE 2. Pancreatic neoplasms diagnosed by FNAB in the pediatric population: cases in the literature

Study	No of cases/ No with tumour	Sex/age (y)	EUS-FNAB non tumour diagnosis	EUS-FNAB tumour diagnosis	EUS-FNAB complications	Tumour histology	Follow-up
Nabi Z <i>et al.</i> ⁸	34/23	NA/Median age 15 (8-18)	Inflammatory mass, Pseudocyst, Lymphoepithelial cyst, Epithelial cyst	SPN (21), Pancreatoblastoma (1), Round cell tumor (1)	Throat pain (7), abdominal pain (2), self-limiting bleeding (2), fever (1)	88% confirmed EUS-FNA diagnosis	NA
Al Rashdan A <i>et al.</i> ⁹	9/3	NA/Median age 16 (4-18)	Cysts, Inflammation	SPN (2), Carcinoid tumour (1)	None	SPN	Uneventful (SPN), Died of metastatic disease (Carcinoid tumour)
Gordon K <i>et al.</i> ¹⁰	6/3	NA/ Average weight 70 kg	Pseudocyst (4), multiple unilocular cysts (1)	SPN (2), Insulinoma	Mild pancreatitis (1)	NA	Multiple endocrine neoplasia 1 (Insulinoma)
Jia Y <i>et al.</i> ¹¹	1/0	F/13	Simple pancreatic cyst	None	None	None	None
Mahida JB <i>et al.</i> ¹²	1/1	F/13	None	SPN (1)	None	SPN	No recurrence
Attila T <i>et al.</i> ¹³	6/2(3)*	4M,2F/10-16	Focal pancreatitis, Chronic pancreatitis	B-cell lymphoma, Islet cell tumour, Suspicious of malignancy	None	B-cell lymphoma, Islet cell tumour, Sclerosing pancreatitis	Multiple endocrine neoplasia 1 (1), NA
Bardales RH <i>et al.</i> ¹⁴	2/2	F/13, 18	None	SPN (2)	NA	SPN	None
Nadler EP <i>et al.</i> ¹⁵	1/1	F/13	None	SPN (1)	None	SPN	No recurrence.

EUS FNAB = endoscopic ultrasound-guided fine needle aspiration biopsy; F = female; M = male; NA = not available; SPN = solid pseudopapillary neoplasm

suspicious for tumour was found in the neck of the pancreas. For radiologically solid lesions, the differential diagnoses include autoimmune pancreatitis, neuroendocrine tumours, microcystic serous adenoma, pancreatoblastoma and acinar cell carcinoma.¹⁹ Autoimmune pancreatitis can also closely mimic radiologic impression of a tumour, so tissue acquisition for light microscopic morphological evaluation is a crucial step in reaching a diagnosis.^{1,3,16} However, a cytologic impression can also be false positive.¹³

In the second patient, a pancreatic cystic lesion was noted on TUS, which was interpreted as either a tumor or a pseudocyst. Cystic lesions of the pancreas may represent benign or malignant processes and are identified incidentally during abdominal cross-sectional imaging or TUS performed for other indications.^{3,8} The main radiologic differential diagnoses in the case of predominantly cystic lesions in children are pseudocysts after a blunt pancreatic injury, retention cysts in cystic fibrosis patients, congenital anomalies (duplication cyst), a part of syndromes like von Hippel Lindau or a tumour pathology of a cystic appearance, such as SPN, neuroendocrine tumours, macrocystic serous adenoma, or mucinous cystic neoplasm.^{3,8,19}

SPN is a low-grade tumour that mainly affects younger women and, to a lesser extent, children. It accounts for up to 30% of pancreatic tumours in patients under 40 years of age.²⁰

It may be clinically silent as in case 1 or presents as an abdominal pain for its mass effect as in case 2, or rarely as jaundice.²⁰ Usually it does not have an endocrine function and the tumorous markers are negative.²⁰

The radiologic imaging in our cases covered the ends of the spectrum of the adult SPN presentation which is illustrated by its old name of "solid-cystic tumour" reflecting its radiological picture of a solid tumor with necrotic cystic areas, which are more common in larger tumours.²⁰ However, we present a pediatric case of one completely solid and one almost completely cystic lesion, without the predominant solid-cystic appearance. Another difference was also the location of the lesions, with one located in the pancreatic head and one in the pancreatic neck, as opposed to the usual body or tail presentation.²⁰

The demographics matched the incidence of pediatric SPN with exclusively female patients, the youngest being 8 years old, as is also the case in the literature.²⁰ Nevertheless there are anecdotal cases of tumors in pediatric males.²¹⁻²³

With EUS one gains the ability to better characterise pancreatic cystic and less common solid lesions also in children and, when performed in combination with FNAB, the discrimination between the various types of cysts and solid tumors can be made, that may direct treatment from a surgical resection to chemotherapy.¹³ In our cases, ROSE was used to assure diagnostic cell samples and a specific diagnosis of SPN could be made in both cases based on cytomorphology supplemented by relevant immunocytochemical stainings.

The morphological and immunocytochemical features of SPN in paediatric population don't differ from adult population. In the cytopathological specimens, SPN comprises pseudopapillary clusters, acinar groups and single cells, delicate capillaries and globules of amorphous myxoid material which was well presented in case 1, but not in case 2 which was mainly necrotic.²⁴⁻²⁵ Histomorphologically and cytomorphologically, the tumour is most commonly composed of unimorphic cells, with sparse to moderately abundant cytoplasm, which may be pale or oncocytic, with vacuoles and round to oval nuclei, with grooves and a fine chromatin structure, which also presented in our cases.²⁴⁻²⁵ There is however an exception, where a few large pleomorphic atypical multinucleated giant cells could be intermingled with more typical ones, which was not found in our cases.²⁵

Main cytopathologic differential diagnosis of SPN in children depends on the age, comprising neuroendocrine neoplasms in patients older than 10 years and a pancreatoblastoma in younger patients.³ In comparison to neuroendocrine neoplasms, SPNs have hyaline-mucinous stroma, cytoplasmic vacuoles, nuclei with grooves and negative reactions to chromogranin and cytokeratin.^{20,26,27} Pancreatoblastoma, which occurs in younger children (median age 5 years) combines several types of differentiation, namely acinar, endocrine and ductal with morulae, with corresponding immunoprofile. Cells are positive for cytokeratin AE1/AE3, BCL 10, neuroendocrine markers, EMA, and have PAS-D positive granules in the cytoplasm.^{20,26,27}

For the concordant final cytopathological diagnosis of SPN, a combination of cytomorphological and immunohistochemical findings is widely recommended.²⁶ To differentiate between neuroendocrine tumours, the recently proposed β -catenin, CD10, and PR were used, but not CD99, which is not specific for SPN.^{19,26} Instead, the CyclinD1, chromogranin and an additional, SOX11 were uti-

lised (Table 1). The clue marker β -Catenin showed a consistent reaction between cytopathological (cell block) and resection samples. The differential diagnosis of pancreatoblastoma was dismissed with a negative CKAE1/ AE3 reaction.

A diagnostic challenge arises because of the positive nuclear reaction to β -catenin, which is the marker of a somatic point mutation of the β -catenin gene (CCTNB), a driving mutation in more than 90% of SPN, but also present in most pancreatoblastomas and in 15% of pancreatic neuroendocrine neoplasms of higher stage (III/IV) but not in lower stage neoplasms.^{19,20} That is the reason why the adjunctive immunohistochemical staining to SOX11 is recommended, which is positive in SPNs and negative in normal pancreatic tissue and in neuroendocrine neoplasms. Additionally, it does not stain background cells and it does not have non-specific membranous or cytoplasmic staining as opposed to β -catenin.²⁴

In general, the histopathological features make it difficult to predict the future behaviour of SPN, and radical resection is recommended in all cases, usually followed by an excellent prognosis, as in our cases.²⁰ A more aggressive course is expected in tumours with high-grade malignant transformation, a higher number of mitoses and severe nuclear atypia.²⁰ Vascular, lymphatic and perineural invasion or infiltrative growth into surrounding structures are not yet associated with a higher likelihood of relapse, as is also consistent with our second case.²⁰ Overall, disease recurs in up to 15% of cases, most commonly in the local lymph nodes, liver and peritoneum, possibly years after the removal of the primary tumour and the metastasis.²⁸ Compared to the adult population, the paediatric population with SPN has a better survival rate at all stages, despite the same treatment.^{18,20, 23} The 5-year survival rate of paediatric patients after completely resected SPN is 95%.⁵ In our institution both cases are without recurrence with a 31 and 50 months follow-up.

The sensitivity of EUS FNAB in diagnosing SPN in the adult population is estimated to be above 80%.⁹ In our institution, EUS-guided fine-needle aspiration biopsy (EUS FNAB) in diagnosing solid pseudopapillary neoplasms (SPN) in pediatric patients was so far accurate, based on two documented cases. In cases with necrotic samples, as in case 2, cytopathology specific techniques like filtration of cell sample to discard necrotic debris, and concentration are very helpful in detecting any individual viable cells, that can further undergo im-

munochemical stains. Unfortunately, necrosis and degenerated samples may also show a significant number of non-specific positive or false negative immunochemical reactions, making the diagnosis less reliable. The techniques that enable selection of viable diagnostic cells are not available in histology, which is yet another advantage of EUS FNAB.

The main drawback of the present study is the small sample size, connected to the rarity of the neoplasm, that could be avoided only by a multicentric study.

Conclusions

Solid pseudopapillary neoplasm (SPN) is a low-grade tumour that mainly affects young women and very rarely female pediatric patients. In the study, we documented two cases, successfully diagnosed by EUS FNAB, without any complications regarding the procedure. Main differential possibilities, neuroendocrine tumours and pancreatoblastomas, were both excluded by several immunochemical reactions, essential for the correct diagnosis. The caveat of one almost completely necrotic sample was overcome with an aid of filtration, the cytopathology specific technique, retrieving the sparse viable cells.

To sum it up, the diagnosis of SPN in the paediatric population requires a high level of suspicion and good collaboration of all specialties (paediatricians, gastroenterologists, radiologists, pathologists and surgeons) due to the wide spectrum of symptoms, the variety of radiological presentations and (cyto)pathological morphology. EUS FNAB proved to be a safe and efficient technique even at paediatric population.

References

1. Piester TL, Liu QY. EUS in pediatrics: a multicenter experience and review. *Front Pediatr* 2021; **9**: 709461. doi: 10.3389/fped.2021.709461
2. Dumonceau JM, Deprez PH, Jenssen C, Iglesias-Garcia J, Larghi A, Vanbiervliet G, et al. Indications, results, and clinical impact of endoscopic ultrasound (EUS)-guided sampling in gastroenterology: European Society of Gastrointestinal Endoscopy (ESGE) Clinical Guideline – Updated January 2017. *Endoscopy* 2017; **49**: 695-714. doi: 10.1055/s-0043-109021
3. Lin TK, Troendle DM, Wallihan DB, Barth B, Fox VL, Fishman DS, et al. Specialized imaging and procedures in pediatric pancreatology: A North American Society for Pediatric Gastroenterology, Hepatology, and Nutrition Clinical Report. *J Pediatr Gastroenterol Nutr* 2017; **64**: 472-84. doi:10.1097/MPG.0000000000001371
4. Eloubeidi MA, Decker GA, Chandrasekhara V, Chathadi KV, Early DS, Evans JA, et al. The role of endoscopy in the evaluation and management of patients with solid pancreatic neoplasia. *Gastrointest Endosc* 2016; **83**: 17-28. doi: 10.1016/j.gie.2015.09.009

5. Mirminachi B, Farrokhzad S, Sharifi AH, Nikfam S, Nikmanesh A, Malekzadeh R, et al. Solid pseudopapillary neoplasm of pancreas; a case series and review literature. *Middle East J Dig Dis* 2016; **8**: 102-8. doi: 10.15171/mejdd.2016.14
6. Sacco Casamassima MG, Gause CD, Goldstein SD, Abdullah F, Meoded A, Lukish JR et al. Pancreatic surgery for tumors in children and adolescents. *Pediatr Surg Int* 2016; **32**: 779-88. doi: 10.1007/s00383-016-3925-y
7. Srebotnik Kirbis I, Prosen L, Strojnar Flezar M. Time-related changes in cell morphology and biomarker immunoreactivity for cells stored in a buffer-based cell medium. *Cytopathology* 2021; **32**: 513-8. doi:10.1111/cyt.12980
8. Nabi Z, Lakhtakia S, Chavan R, Asif S, Basha J, Gupta R, et al. Diagnostic utility of EUS-guided tissue acquisition in children: a tertiary care center experience. *Endosc Ultrasound* 2021; **10**: 288-93. doi: 10.4103/EUS-D-20-00203
9. Al-Rashdan A, LeBlanc J, Sherman S, McHenry L, DeWitt J, Al-Haddad M. Role of endoscopic ultrasound for evaluating gastrointestinal tract disorders in pediatrics: a tertiary care center experience. *J Pediatr Gastroenterol Nutr* 2010; **51**: 718-22. doi: 10.1097/MPG.0b013e3181dac094
10. Gordon K, Conway J, Evans J, Petty J, Fortunato JE, Mishra G. EUS and EUS-guided interventions alter clinical management in children with digestive diseases. *J Pediatr Gastroenterol Nutr* 2016; **63**: 242-6. doi: 10.1097/MPG.0000000000001101
11. Jia Y, Maspons A, Othman MO. The therapeutic use of endoscopic ultrasonography in pediatric patients is safe: a case series. *Saudi J Gastroenterol* 2015; **21**: 391-5. doi: 10.4103/1319-3767.167191
12. Mahida JB, Thakkar RK, Walker J, Shen R, Kenney BD, Prasad V, et al. Solid pseudopapillary neoplasm of the pancreas in pediatric patients: a case report and institutional case series. *J Ped Surg Case Reports* 2015; **3**: 149-53. doi: 10.1016/j.epsc.2015.02.006
13. Attila T, Adler DG, Hilden K, Faigel DO. EUS in pediatric patients. *Gastrointest Endosc* 2009; **70**: 892-8. doi: 10.1016/j.gie.2009.04.012
14. Bardales RH, Centeno B, Mallery JS, Lai R, Pochapin M, Guitier G, et al. Endoscopic ultrasound-guided fine-needle aspiration cytology diagnosis of solid-pseudopapillary tumor of the pancreas: a rare neoplasm of elusive origin but characteristic cytomorphic features. *Am J Clin Pathol* 2004; **121**: 654-62. doi: 10.1309/DKK2-B9V4-NOW2-6A8Q
15. Nadler EP, Novikov A, Landzberg BR, Pochapin MB, Centeno B, Fahey TJ, et al. The use of endoscopic ultrasound in the diagnosis of solid pseudopapillary tumors of the pancreas in children. *J Pediatr Surg* 2002; **37**: 1370-3. doi: 10.1053/jpsu.2002.35028
16. Keane MG, Kumar M, Cieplik N, Thorburn D, Johnson GJ, Webster GJ, et al. Paediatric pancreaticobiliary endoscopy: a 21-year experience from a tertiary hepatobiliary centre and systematic literature review. *BMC pediatrics* 2018; **18**: 42. doi: 10.1186/s12887-017-0959-9
17. Jia Y, Maspons A, Othman MO. The therapeutic use of endoscopic ultrasonography in pediatric patients is safe: a case series. *Saudi J Gastroenterol* 2015; **21**: 391-5. doi:10.4103/1319-3767.167191
18. Waters AM, Russell RT, Maizlin II; CDDR Group, Beierle EA. Comparison of pediatric and adult solid pseudopapillary neoplasms of the pancreas. *J Surg Res* 2019; **242**: 312-7. doi: 10.1016/j.jss.2019.04.070
19. Weiss V, Dueber J, Wright JP, Cates J, Revetta F, Parikh AA, et al. Immunohistochemical analysis of the Wnt/ β -catenin signaling pathway in pancreatic neuroendocrine neoplasms. *World J Gastrointest Oncol* 2016; **8**: 615-22. doi: 10.4251/wjgo.v8.i8.615
20. Gill AJ, Klimstra DS, Lam AK, Washington MK. Tumours of the pancreas. In: WHO Classification of Tumours Editorial Board. *WHO classification of tumours: digestive system tumours*, Vol. 1, 5th edition. Lyon: International Agency for Research on Cancer; 2019. p. 295-370.
21. Speer AL, Barthel ER, Patel MM, Grikscheit TC. Solid pseudopapillary tumor of the pancreas: a single-institution 20-year series of pediatric patients. *J Pediatr Surg* 2012; **47**: 1217-22. doi: 10.1016/j.jpedsurg.2012.03.026
22. Aki B, Erdogan-Durmus S, Yalcin O, Atamanalp RS. A solid pseudopapillary neoplasm in a 10-years-old boy diagnosed by fine-needle-aspiration: a case report. In: Abstracts of the 44th European Congress of Cytopathology, Budapest, 1-4 October 2023. *Cytopathology* 2023; **34(Suppl 1)**: 5-55. doi: 10.1111/cyt.13293
23. Lee SE, Jang JY, Hwang DW, Park KW, Kim SW. Clinical features and outcome of solid pseudopapillary neoplasm: differences between adults and children. *Arch Surg* 2008; **143**: 1218-21. doi: 10.1001/archsurg.143.12.1218
24. Dinarvand P, Wang WL, Roy-Chowdhuri S. Utility of SOX11 for the diagnosis of solid pseudopapillary neoplasm of the pancreas on cytological preparations. *Cytopathology* 2022; **33**: 216-21. doi: 10.1111/cyt.13080
25. Brant GW, Hareesh M, Zoe QW, Wenping L. Cytological diagnosis of pancreatic solid-pseudopapillary neoplasm: a single-institution community practice experience. *Diagnostics* 2022; **12**: 449. doi: 10.3390/diagnostics12020449
26. Ardengh JC, Lopes CV, Venco FE, Machado MA. Diagnosis of pancreatic solid pseudopapillary neoplasms using cell-blocks and immunohistochemical evaluation of endoscopic ultrasound-guided fine needle aspiration biopsy specimens. *Cytopathology* 2021; **32**: 50-6. doi: 10.1111/cyt.12905
27. Granados R, Stelow EB. Solid pseudo papillary neoplasm. In: IAC-IARC-WHO joint editorial board. IAC-IARC-WHO Cytopathology Reporting Systems: WHO Reporting System for Pancreaticobiliary Cytopathology, Vol. 2, 1st edition. Lyon: International Agency for Research on Cancer; 2022. p. 295-370.
28. Lamps L. Pancreas and ampullary region. In: Goldblum J, Lamps L, McKenney J, Myers J. Rosai and Ackerman's Surgical Pathology, Vol. 2, 11th edition. Philadelphia: Elsevier. 2017. p. 912-3.

Telomere length and *TERT* polymorphisms as biomarkers in asbestos-related diseases

Ana Mervic¹, Katja Goricar², Tanja Blagus², Alenka Franko^{1,3}, Katarina Trebusak-Podkrajsek^{2,4}, Metoda Dodic Fikfak^{1,3}, Vita Dolzan^{1,2*}, Viljem Kovac^{1,5*}

¹ Faculty of Medicine, University of Ljubljana, Ljubljana, Slovenia

² Institute of Biochemistry and Molecular Genetics, Faculty of Medicine, University of Ljubljana, Ljubljana, Slovenia

³ Clinical Institute of Occupational Medicine, University Medical Centre Ljubljana, Ljubljana, Slovenia

⁴ Clinical Institute for Special Laboratory Diagnostics, University Children's Hospital, University Medical Centre Ljubljana, Ljubljana, Slovenia

⁵ Institute of Oncology Ljubljana, Ljubljana, Slovenia

Radiol Oncol 2024; 58(1): 87-98.

Received 25 August 2023

Accepted 13 September 2023

Correspondence to: Assoc. Prof. Viljem Kovač, M.D., Ph.D., Institute of Oncology Ljubljana, Zaloška cesta 2, 1000 Ljubljana, Slovenia; Phone: +386 1 5879 622; Email: vkovac@onko-i.si; Prof. Vita Dolžan, M.D., Ph.D., Pharmacogenetics Laboratory, Institute of Biochemistry and Molecular Genetics, Faculty of Medicine, University of Ljubljana, Vrazov trg 2, 1000 Ljubljana, Slovenia; Phone: +386 1 543 7670; Email: vita.dolzan@mf.uni-lj.si

Disclosure: No potential conflicts of interest were disclosed.

This is an open access article under the CC BY-NC-ND license (<http://creativecommons.org/licenses/by-nc-nd/4.0/>).

Background. Asbestos exposure has been proposed as a risk factor for shorter telomere length. The aim of our study was to investigate whether telomere length in leukocytes and *hTERT* genetic polymorphisms may serve as potential biomarkers for the risk of developing asbestos-related diseases and as biomarkers of progression and chemotherapy response rate in malignant mesothelioma (MM).

Subjects and methods. We conducted two retrospective studies. In the first study, a case-control study, telomere length and *hTERT* polymorphisms were determined in patients with MM, subjects with pleural plaques and controls without the asbestos related disease, who were occupationally exposed to asbestos. In the second study, a longitudinal observational study, telomere length was also determined in samples from MM patients before and after chemotherapy. Telomere length was determined by monochromatic multiplex quantitative polymerase chain reaction (PCR), while competitive allele-specific PCR was used to genotype *hTERT* rs10069690, rs2736100 and rs2736098. Logistic regression and survival analysis were used in statistical analysis.

Results. Patients with MM had shorter telomere length than subjects with pleural plaques ($p < 0.001$). After adjustment for age, rs2736098 CT, and rs10069690 TT and CT+TT genotypes were significantly associated with a higher risk of MM ($p_{\text{adj}} = 0.023$; $p_{\text{adj}} = 0.026$ and $p_{\text{adj}} = 0.017$), while rs2736100 AA and CA+AA genotypes conferred to a lower risk for MM compared to all other subjects ($p_{\text{adj}} = 0.017$, and $p_{\text{adj}} = 0.026$). Telomere length was not associated with a response to chemotherapy ($p > 0.05$) or time to disease progression ($p > 0.05$). Carriers of one or two polymorphic rs10069690 T alleles had a good response to chemotherapy ($p = 0.039$, and $p = 0.048$), these associations remained statistically significant after adjustment for age ($p_{\text{adj}} = 0.019$; $p_{\text{adj}} = 0.017$). Carriers of two polymorphic rs2736100 A alleles had a longer time to disease progression ($p = 0.038$).

Conclusions. Shorter telomere length and *hTERT* polymorphisms may serve as a biomarker for the risk of developing MM. Additionally, rs10069690 and rs2736100 polymorphisms, but not telomere length, were associated with a chemotherapy response or MM progression.

Key words: malignant mesothelioma; asbestos; telomere length; *hTERT* polymorphisms

Introduction

Asbestos consists of mineral fibres with a high malignant potential, listed among carcinogens by the

World Health Organisation in 1987.¹ The malignant potential of asbestos fibres lies within their capability to deeply infiltrate the respiratory system

and persist there for extended durations.² There is no known safe level of asbestos exposure.³

Inhaled asbestos fibres induce oxidative stress due to the presence of iron as well as frustrated phagocytosis by macrophages, what in turn stimulates Fenton and Haber-Weiss reactions, ultimately resulting in the generation of reactive oxygen species (ROS). Asbestos further elicits the upregulation of the heavy chain of ferritin, consequently leading to an augmented iron burden and increased production of ROS.⁵ Oxidative stress is closely associated with chronic inflammation. The asbestos deposits contribute to the production of iron-rich asbestos bodies, that are accountable for sustaining chronic inflammation.⁴ The pro-inflammatory microenvironment fosters cell survival by inhibiting apoptosis, promoting mesothelial cell proliferation despite DNA damage, activating fibroblasts and inducing immunosuppression.^{2,5} Furthermore, asbestos fibres also have a detrimental impact on chromosomes. All of these mechanisms eventually contribute to the induction of carcinogenesis.^{6,7}

Asbestos exposure causes several diseases. In the lung, asbestosis and lung cancer carcinoma affect the lung parenchyma, while pleural plaques (PP) and malignant mesothelioma (MM) affect the pleura, but other serous membranes such as peritoneum may also be affected.⁸

Malignant mesothelioma arises from the malignant transformation of mesothelial cells and is a rare, yet highly aggressive cancer with a poor prognosis. In over 80% of cases, the development of MM is associated with asbestos exposure.⁹ The majority of patients who develop MM have been exposed to asbestos through occupational exposure; however, para-occupational, domestic and environmental exposure have also been associated with MM development.⁸ Due to its long latency period, which can extend up to 40 years or even longer, the MM epidemic continues to rise in Central Europe.^{8,10,11} Malignant mesothelioma occurs more often in males, with a median age of 70 years.³ In 2018, the incidence of MM in Slovenia was 3.0/100 000 in males and 1.5/100 000 in females, resulting in a total of 45 new cases that year. At the time of diagnosis, 31.1% of patients had MM in an early localized stage, 55.6% had cancer spread to lymph nodes and in 11.1% it already presented with metastasis.¹² Malignant mesothelioma can be histologically classified into subgroups: epithelioid, biphasic and sarcomatoid subtypes. The epithelioid subtype is the most common and also exhibits the most favourable prognosis, while patients with sarcomatoid MM tend to have the worst prognosis.⁹

The diagnosis of MM is accomplished through clinical examination, thorax CT or MRI, and PET-CT. The prevailing clinical presentation often involves progressive dyspnoea, accompanied by non-pleuritic chest pain. Additional symptoms include cough, fever, asthenia, hypoxia, weight loss, and night sweats. Typically, the disease is detected 3-6 months after the initial clinical presentation.² The therapeutic strategy is tailored based on the tumour resectability and the patient's performance status. In resectable disease, the treatment involves the combination of surgery, chemotherapy and radiotherapy, while patients with unresectable disease receive systemic treatment. Chemotherapy with pemetrexed/cisplatin doublet has not been changed as a standard treatment since 2004 and immunotherapy with ipilimumab and nivolumab was approved for the first line treatment in late 2020.¹³ Although different chemotherapy (gemcitabine/cisplatin, pemetrexed single, vinorelbine weekly) and immunotherapy (nivolumab/ipilimumab) regimens are used in relapsed MM, there is still no standard of care.^{2,13,14}

The increasing incidence of MM and the poor prognosis call for the identification of novel non-invasive biomarkers that will enable an earlier diagnosis, will have a prognostic value and/or will predict the response to treatment. Despite the growing numbers of potential biomarkers, there is no reliable diagnostic or prognostic biomarker available yet. Telomerase reactivation may play a crucial role in cancer development and progression, and telomeres could serve both as a potential biomarker and as a therapeutic target in cancer. In somatic cells telomeres shorten with each cell division, ultimately leading to senescence or apoptosis.^{15,16} Cancer cells gain the ability to sustain their telomere length by reactivating telomerase, a process typically suppressed under physiological circumstances.¹⁵⁻¹⁸

The regulation of the expression of the human telomerase reverse transcriptase (hTERT) subunit of telomerase occurs predominantly at the transcriptional level.¹⁹⁻²¹ Numerous single nucleotide polymorphisms (SNP) in the *hTERT* gene may also have an impact on telomerase expression levels and activity, and may thus play a role in the risk of carcinogenesis, as well as the prognosis and survival of cancer patients.^{18,19,22}

Telomere length is influenced by cellular senescence, chronic inflammation and oxidative stress. Telomere shortening itself serves as one of the main markers for senescence, as telomeres typically shorten by 50-200 base pairs (bp) with each

TABLE 1. Characteristics of subjects included in the study

Characteristics	Category/unit	Total participants (N = 774)	Control group (N = 86)	Cases with PP (N = 386)	Patients with MM (N = 302)	P
Gender	Male, N (%)	555 (71.7)	63 (73.3)	269 (69.7)	223 (73.8)	0.467 ^a
	Female, N (%)	219 (28.3)	23 (26.7)	117 (30.3)	79 (26.2)	
Age	Years, median (25%–75%)	59.1 (51.1–67.5)	53.3 (48.1–59.5)	55.0 (48.8–62.7)	66.0 (59.0–73.0)	< 0.001 ^b
Smoking	No, N (%)	398 (52.0) [8]	47 (54.7)	189 (49.0)	162 (55.1)	0.254 ^a
	Yes, N (%)	368 (48.0)	39 (45.3)	197 (51.0)	132 (44.9)	

Number of missing data is presented in [] brackets. Statistically significant values are printed in bold.

^a Calculated using Fisher exact test; ^b Calculated using Kruskal-Wallis test.

MM = malignant mesothelioma; N = number of samples; PP = pleural plaques

cell cycle.²³ Chronic inflammation is associated with elevated *hTERT* expression, which, in turn, maintains telomere length.⁷ On the other hand, the cellular turnover stimulated by chronic inflammation leads to an increased number of cell divisions, resulting in telomere shortening.¹⁹ Furthermore, oxidative stress causes DNA damage, which subsequently stops telomere elongation.^{7,18}

Cancer cells exhibit shorter, yet stable, telomeres compared to non-neoplastic cells.^{18,20,21} Malignant mesothelioma is considered to be a telomerase dependant cancer.²² The impact of asbestos exposure on telomere length was also established in pleural effusion cells, showing that non-neoplastic cells had longer telomeres than neoplastic MM cells and that telomere shortening and genomic instability play significant roles in MM pathogenesis, and may also serve as biomarkers for disease development, treatment response, and prognosis.²³

To the best of our knowledge, the association between telomere length and *hTERT* polymorphisms and asbestos-related diseases has not been evaluated yet. Thus, the aim of the present study was to analyse the role of telomere length in leukocytes and *hTERT* polymorphisms as a biomarker for asbestos-related diseases, in particular MM, its response to treatment and prognosis.

Subjects and methods

Subjects

We conducted two retrospective studies. In the first study, a case-control study, telomere length and *hTERT* polymorphisms were determined in 340 patients with MM, 380 subjects with pleural plaques and 94 control subjects without any dis-

TABLE 2. Clinical characteristics of patients with malignant mesothelioma (MM) (N = 302)

Characteristics	Category	N (%)
Location [1]	Pleura	267 (88.7)
	Peritoneum	34 (11.3)
Histology type	Epithelioid	227 (75.2)
	Biphasic	27 (8.9)
	Sarcomatoid	27 (8.9)
	Undifferentiated	21 (6.9)
		1
Stage (pleural MM)	2	65 (24.3)
	3	89 (33.3)
	4	93 (34.8)
		0
ECOG performance status [1]	1	154 (51.2)
	2	111 (36.9)
	3	18 (6.0)
Asbestos exposure [8]	No	79 (26.9)
	Yes	215 (73.1)
Pain [29]	No	114 (41.8)
	Yes	159 (58.2)
Weight loss [34]	No	97 (36.2)
	Yes	171 (63.8)
CRP [mg/mL] [48]	Median (25%–75%)	22 (7–63.5)
Chemotherapy [21]	No chemotherapy	17 (6.1)
	Gemcitabine with cisplatin	161 (57.3)
	Pemetrexed with cisplatin	92 (31.6)
	Other	11 (3.9)
		CR
Chemotherapy response [46]	PR	73 (28.5)
	SD	128 (50.0)
	PD	45 (17.6)
		Poor response (SD+PD)
Response rate	Good response (PR+CR)	83 (32.4)

Number of missing data is presented in [] brackets.

CRP = C-reactive protein; ECOG = Eastern Cooperative Oncology Group; CR = complete response; N = number of samples; SD = stable disease; PD = progressive disease; PR = partial response

TABLE 3. Telomere length in patients with malignant mesothelioma (MM) at different time points during chemotherapy

Time point	N	Median (25%-75%)	P	N shortens/ N prolongs
A	79	1.23 (1.01-1.37)		
B	66	1.23 (1.10-1.38)		
C	66	1.27 (1.08-1.36)		
Comparison B vs. A	66		0.480	28 shortens 38 prolongs
Comparison C vs. A	66		0.423	32 shortens 34 prolongs
Comparison C vs. B	53		0.733	26 shortens 27 prolongs

A = telomere length before first chemotherapy cycle; B = telomere length at third chemotherapy cycle; C = telomere length after completed chemotherapy or at disease progression; N = number of samples; P = p value

eases related to asbestos exposure. The cases with PP and controls had a history of occupational asbestos exposure while working at the Salonit Anhovo factory, Slovenia and were presented before the State Board for the Recognition of Occupational Asbestos Diseases between January 1999 and December 2003. The patients with MM were treated at the Institute of Oncology Ljubljana from 2008 and 2018. Among MM patients, 94 had blood samples available from at least two different time points during chemotherapy treatment (211 samples available in total).

The diagnosis of MM, PP, or “no asbestos related disease” was confirmed by the experts of the

State Board for the Recognition of Occupational Asbestos Diseases.²⁴⁻²⁶ In all subjects of the study high-resolution computed tomography (HRCT) was performed. Pleural MM was histologically confirmed based on samples obtained through thoracoscopy or video-assisted thoracic surgery, while samples for confirming peritoneal MM were collected via laparoscopy. The histopathologic samples were classified as epithelioid, sarcomatoid, biphasic or undifferentiated types of MM.^{2,27,28} The TNM classification was used for staging pleural MM.²⁹ Additionally, clinical data on MM patients, such as a performance status based on The Eastern Cooperative Oncology Group (ECOG), weight loss and C-reactive protein (CRP) levels were also collected.

Data on the chemotherapy protocol (gemcitabine with cisplatin, pemetrexed with cisplatin, other, or no chemotherapy) and chemotherapy response (classified as complete response [CR], partial response [PR], stable disease [SD], progressive disease [PD]) were collected from patients' medical records at The Institute of Oncology Ljubljana and the Cancer Registry of the Republic of Slovenia.

Data on asbestos exposure were available from our previous studies.³⁰ A standardized questionnaire-based interview was conducted with cases having PP and control group to gather data on their smoking status, whereas data for patients with MM was extracted from medical records at The Institute of Oncology Ljubljana.³¹

TABLE 4. Comparison of genotype frequencies in control group, cases with pleural plaques (PP) and patients with malignant mesothelioma (MM)

SNP	Genotype	Control group (N = 86)	Cases with PP (N = 386)	Patients with MM (N = 302)	P
		N (%)	N (%)	N (%)	
rs2736098	CC	45 (56.3)	215 (56.3)	139 (46.8)	Padd = 0.018
	CT	28 (35.0)	133 (34.8)	140 (47.1)	
	TT	7 (8.8)	34 (8.9)	18 (6.1)	
	CT+TT	35 (43.8)	167 (43.7)	158 (53.2)	
rs2736100	CC	17 (20.0)	103 (26.8)	93 (30.8)	Padd = 0.362
	CA	48 (56.5)	194 (50.4)	147 (48.7)	
	AA	20 (23.5)	88 (22.9)	62 (20.5)	
	CA+AA	68 (80.0)	282 (73.2)	209 (69.2)	
rs10069690	CC	48 (63.2)	233 (61.0)	160 (54.6)	Padd = 0.107
	CT	26 (34.2)	131 (34.3)	107 (36.5)	
	TT	2 (2.6)	18 (4.7)	26 (8.9)	
	CT+TT	28 (36.8)	149 (39.0)	133 (45.4)	

A = adenine; C = cytosine; N = number of samples; Padd = p value of additive genetic model; Pdom = p value of dominant genetic model; SNP = single nucleotide polymorphism; T = thymine. Statistically significant values are printed in bold.

TABLE 5. Association between selected polymorphisms and the risk of developing malignant mesothelioma (MM): comparison of patients with MM and other participants (control group and cases with pleural plaques [PP])

SNP	Genotype	Patients with MM		OR (95% CI)	P	OR (95% CI) _{adj}	P _{adj}
		N (%)	Others N (%)				
rs2736098	CC	139 (46.8)	260 (56.3)	Reference		Reference	
	CT	140 (47.1)	161 (34.8)	1.63 (1.20–2.21)	0.002	1.49 (1.06–2.10)	0.023
	TT	18 (6.1)	41 (8.9)	0.82 (0.46–1.48)	0.514	0.78 (0.40–1.54)	0.470
	CT+TT	158 (53.2)	202 (43.7)	1.46 (1.09–1.96)	0.011	1.36 (0.98–1.88)	0.070
rs2736100	CC	93 (30.8)	120 (56.3)	Reference		Reference	
	CA	147 (48.7)	242 (51.5)	0.78 (0.56–1.10)	0.160	0.71 (0.48–1.04)	0.076
	AA	62 (20.5)	108 (23.0)	0.74 (0.49–1.12)	0.155	0.56 (0.35–0.90)	0.017
	CA+AA	209 (69.2)	350 (74.5)	0.77 (0.56–1.06)	0.111	0.66 (0.46–0.95)	0.026
rs10069690	CC	160 (54.6)	281 (61.4)	Reference		Reference	
	CT	107 (36.5)	157 (34.3)	1.20 (0.88–1.64)	0.261	1.41 (0.99–2.01)	0.058
	TT	26 (8.9)	20 (4.4)	2.28 (1.24–4.22)	0.008	2.22 (1.10–4.48)	0.026
	CT+TT	133 (45.4)	177 (38.6)	1.32 (0.98–1.78)	0.067	1.52 (1.08–2.12)	0.017

A = adenine; adj = adjustment for age; C = cytosine; CI = confidence interval; OR = odds ratio; Others = control group and cases with pleural plaques; SNP = single nucleotide polymorphism; T = thymine. Statistically significant values are printed in bold.

All participants were fully informed about the purpose of the study and willingly provided their informed written consent to participate. The study was part of the comprehensive studies approved by the Slovenian Ethics Committee for Research in Medicine (KME 41/02/09, 36/02/04 and 31/07/04). The study adhered to the principles outlined in the Declaration of Helsinki.

Molecular genetic analysis

Peripheral venous blood samples from MM patients were collected in Tempus tubes and frozen at -80°C until the analysis. DNA extraction was performed using the MagMax 96DNA Multi Sample Kit and the MagMax protocol for stabilized Blood Tub RNA isolation (all, Applied Biosystems [ABI]). For the purpose of our study, only DNA was extracted, while the remaining sample was stored for later RNA extraction. Genomic DNA of cases with PP and control group had been isolated during our previous studies from peripheral venous blood collected in ethylenediaminetetraacetic acid (EDTA) containing tubes and DNA was extracted with the QIAmp DNA Mini Kit (QIAGEN). The concentration of DNA samples was measured using the Perkin Elmer Lambda BIO+ UV/VIS spectrophotometer. Telomere length was assessed using monochrome multiplex quantitative polymerase chain reaction (MMQ-PCR), relatively as the

ratio between the telomere product (Tel) and albumin gene product (Alb) as previously described.³² Genotyping of *hTERT* rs10069690, rs2736100 and rs2736098 polymorphisms was performed using the competitive allele-specific polymerase chain reaction (KASP) SNP Genotyping Assay (LGC Group).

Statistics

Descriptive statistics were used to depict the variables. Continuous variables were described using the median and interquartile range, while categorical variables were presented as frequencies. To compare the distribution of continuous variables, the non-parametric Kruskal-Wallis test was performed; for categorical variables, Fisher's exact test was used.

The association between telomere length and categorical variables was analyzed using the Mann-Whitney test and the Kruskal-Wallis test. The Wilcoxon test for related samples was used to evaluate the longitudinal change in telomere length. Additionally, the correlation between continuous variables and longitudinal telomere length change was assessed using Spearman's Rho correlation coefficient.

Minor allele frequency (MAF) was analysed for each investigated polymorphism. The deviation from the Hardy-Weinberg equilibrium (HWE) was

TABLE 6. Association between selected polymorphisms and risk of developing malignant mesothelioma (MM): comparison of patients with MM and cases with pleural plaques (PP)

SNP	Genotype	OR (95% CI)	P	OR (95% CI) _{adj}	P _{adj}
rs2736098	CC	Reference		Reference	
	CT	1.63 (1.18–2.24)	0.003	1.52 (1.06–2.16)	0.022
	TT	0.82 (0.45–1.51)	0.521	0.76 (0.38–1.53)	0.445
	CT+TT	1.46 (1.08–1.99)	0.014	1.37 (0.98–1.93)	0.069
rs2736100	CC	Reference		Reference	
	CA	0.84 (0.59–1.19)	0.330	0.77 (0.52–1.15)	0.196
	AA	0.78 (0.51–1.20)	0.257	0.58 (0.36–0.94)	0.028
	CA+AA	0.82 (0.59–1.15)	0.245	0.71 (0.48–1.03)	0.070
rs10069690	CC	Reference		Reference	
	CT	1.19 (0.86–1.65)	0.296	1.39 (0.96–2.01)	0.078
	TT	2.10 (1.12–3.96)	0.021	2.11 (1.02–4.34)	0.043
	CT+TT	1.30 (0.96–1.78)	0.096	1.48 (1.05–2.10)	0.027

A = adenine; C = cytosine; CI = confidence interval; OR = odds ratio; SNP = single nucleotide polymorphism; T = thymine. Statistically significant values are printed in bold.

tested using a chi-square test. A p-value less than 0.05 indicated that the distribution did not adhere to HWE. Both additive and dominant genetic models were used in statistical analyses. Univariate logistic regression was used to assess the association between telomere length and polymorphisms with asbestos-related diseases and the response to chemotherapy.

Cox regression was utilized to evaluate the association of telomere length and genotypes with progression-free survival (PFS) and overall survival (OS). Kaplan-Meier method was used to illustrate the PFS function over time.

All statistical analyses were conducted using the IBM SPSS Statistics, version 27.0 (IBM Corporation,

Armonk, NY, USA). The threshold for statistical significance in all tests performed was set at 0.05.

Results

Subjects

In total, 302 patients with MM, 386 cases with PP and 86 controls were included in our study. The characteristics of patients with MM, cases with PP and the control group are shown in Table 1. There were statistically significant differences between the groups in respect to age ($p < 0.001$) and asbestos exposure ($p < 0.001$). Patients with MM (66.0 (59.0–73.0) years) were significantly older than cases with PP (55.0 (48.8–62.7) years) and control subjects (53.3 (48.1–59.5) years). Asbestos exposure was available for the control group, 379 cases with PP and 42 patients with MM. Among subjects with known asbestos exposure, 52.7% of patients with MM had medium or high exposure, compared to 28.5% of cases with PP and 24.4% of the control group. However, the three study groups did not differ significantly with regards to gender ($p = 0.467$) and smoking status ($p = 0.254$) (Table 1).

The clinical characteristics of patients with MM are summarized in Table 2. The majority had pleural MM (267; 88.7%) of the epithelioid type (227; 75.2%) and had stage four (93; 34.8%) or stage three (89; 33.3%) of the disease. According to the ECOG

TABLE 7. Association between telomere length and chemotherapy response rate in patients with malignant mesothelioma (MM)

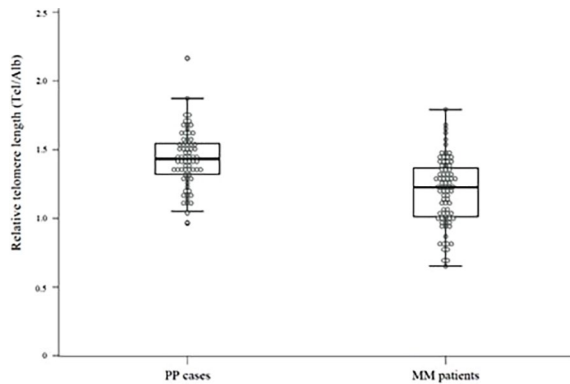
Telomere length	Poor response Median (25–75%)	Good response Median (25–75%)	P
A	1.20 (1.01–1.37)	1.28 (1–1.39)	0.576
B	1.21 (1.05–1.37)	1.28 (1.13–1.35)	0.601
C	1.29 (1.07–1.37)	1.23 (1.02–1.34)	0.369
Comparison B vs. A	0.04 (-0.1 to 0.1)	-0.01 (-0.11 to 0.07)	0.317
Comparison C vs. A	0.01 (-0.09 to 0.22)	-0.04 (-0.16 to 0.15)	0.241
Comparison C vs. B	0.03 (-0.09 to 0.13)	-0.01 (-0.12 to 0.07)	0.353

A = telomere length before first chemotherapy cycle; B = telomere length at third chemotherapy cycle; C = telomere length after completed chemotherapy or at disease progression

TABLE 8. Association between selected polymorphism and chemotherapy response rate in patients with malignant mesothelioma (MM)

SNP	Genotype	Poor response N (%)	Good response N (%)	OR (95% CI)	P	OR (95% CI) _{adj}	P _{adj}
rs2736098	CC	81 (68.6)	37 (31.4)	Reference		Reference	
	CT	76 (65.5)	40 (34.5)	1.15 (0.67–1.99)	0.611	1.20 (0.67–2.16)	0.542
	TT	11 (64.7)	6 (35.3)	1.19 (0.41–3.47)	0.745	1.27 (0.42–3.87)	0.671
	CT+TT	87 (65.4)	46 (34.6)	1.16 (0.68–1.96)	0.587	1.21 (0.69–2.14)	0.511
rs2736100	CC	53 (67.1)	26 (32.9)	Reference		Reference	
	CA	89 (70.6)	37 (29.4)	0.85 (0.46–1.55)	0.592	0.85 (0.45–1.63)	0.625
	AA	31 (60.8)	20 (39.2)	1.32 (0.63–2.74)	0.463	1.16 (0.53–2.57)	0.709
	CA+AA	120 (67.8)	57 (32.2)	0.97 (0.55–1.70)	0.911	0.94 (0.51–1.71)	0.831
rs10069690	CC	94(72.9)	35 (27.1)	Reference		Reference	
	CT	58 (59.8)	39 (40.2)	1.81 (1.03–3.17)	0.039	2.08 (1.13–3.84)	0.019
	TT	14 (66.7)	7 (33.3)	1.34 (0.50–3.60)	0.558	1.85 (0.64–5.31)	0.255
	CT+TT	72 (61.0)	46 (39.0)	1.72 (1.00–2.93)	0.048	2.04 (1.13–3.67)	0.017

A = adenine; Adj = adjustment for weight loss and ECOG performance status; C = cytosine; CI = confidence interval; OR = odds ratio; SNP = single nucleotide polymorphism; T = thymine. Statistically significant values are printed in bold.

**FIGURE 1.** Relative telomere length in cases with pleural plaques (PP) and patients with malignant mesothelioma (MM).

Alb = albumin gene product Tel = telomere product

performance status (PS), most patients with MM had PS 1 (154; 51.2%) or PS 2 (111; 36.9%).

Telomere length

There was a statistically significant difference in telomere length between patients with MM and cases with PP ($p < 0.001$) (Figure 1). Patients with MM had shorter median telomere length of 1.23 (1.01–1.37) compared to 1.43 (1.32–1.56) in cases with PP. The difference in telomere length remained statistically significant ($p < 0.001$) after adjustment for age.

TABLE 9. Association between telomere length and progression-free survival in patients with malignant mesothelioma (MM)

Telomere length	HR (95% CI)	P	HR (95% CI) _{adj}	P _{adj}
A	2.15 (0.69–6.68)	0.185	1.66 (0.50–5.47)	0.408
B	1.02 (0.28–3.76)	0.976	0.92 (0.22–3.76)	0.905
C	1.69 (0.46–6.16)	0.430	1.49 (0.40–5.48)	0.551
Comparison B vs. A	0.16 (0.03–1.01)	0.052	0.23 (0.03–1.67)	0.145
Comparison C vs. A	1.01 (0.25–4.18)	0.985	1.36 (0.31–5.92)	0.682
Comparison C vs. B	1.57 (0.26–9.58)	0.624	2.16 (0.31–14.83)	0.435

Ad = adjustment for C-reactive protein (CRP); CI = confidence interval; HR = hazard ratio

The analysis of the association between telomere length and age revealed a statistically significant influence of age on telomere length, indicating that older patients with MM had longer telomeres (Spearman's rho = 0.370; $p < 0.001$).

The dynamics of telomere length during chemotherapy

Among the patients with MM, no specific trend was observed in telomere length changes at different time points during chemotherapy. Approximately the same number of cases exhibited telomere elongation or shortening (Table 3, Figure 2).

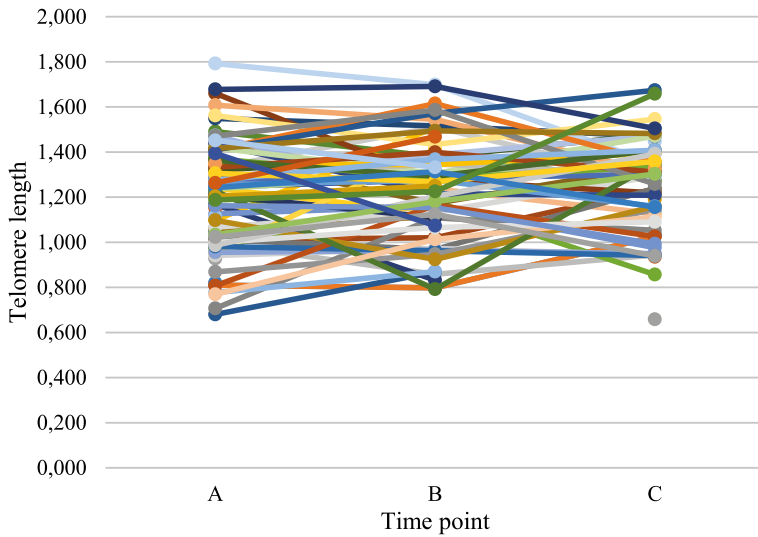


FIGURE 2. Relative telomere length at different time points A, B and C.

A = telomere length before first chemotherapy cycle; B = telomere length at third chemotherapy cycle; C = telomere length after completed chemotherapy or at disease progression

hTERT polymorphisms and the risk for asbestos-related diseases

We investigated three *hTERT* polymorphisms: rs2736098, rs2736100 and rs10069690. The distribution of all genotypes followed the Hardy-Weinberg equilibrium (HWE) ($p_{HWE} > 0.05$). Genotype frequencies in different study groups are presented in Table 4.

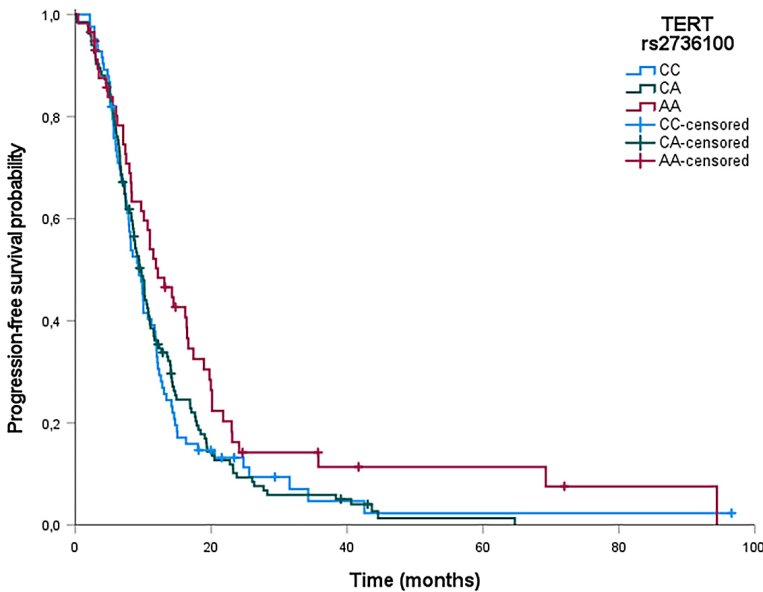


FIGURE 3. Kaplan Meier survival plot.

Step = disease progression; cross = censored patient; AA = adenine-adenine; CA = cytosine-adenine; CC = cytosine-cytosine; *hTERT* = telomerase reverse transcriptase

For further analysis, the most common CC genotype was used as the reference.

For rs2736098, the genotype distribution differed significantly between groups association with MM (P value of additive genetic model [P_{add}] = 0.018; P value of dominant genetic model [P_{dom}] = 0.039). Carriers of polymorphic rs2736098 T alleles were more common among patients with MM compared to cases with PP and control subjects. There were no significant differences in the distribution of other investigated polymorphisms among the groups (Table 4).

When MM patients were compared to all other subjects combined, polymorphic rs2736098 T allele was statistically significantly associated with an increased risk of developing MM (CT genotype: odds ratio [OR] = 1.63; 95% confidence interval [CI] = 1.20-2.21; $p = 0.002$; CT+TT genotype: OR = 1.46; CI = 1.09-1.96; $p = 0.011$) (Table 5). After adjustment for age, only the association of CT genotype remained significant (OR_{adj} = 1.49; CI_{adj} = 1.06-2.10; $p_{adj} = 0.023$). The presence of at least one polymorphic rs2736100 A allele was associated with a lower risk for developing MM after age adjustment (AA genotype: OR_{adj} = 0.56; CI_{adj} = 0.35-0.90; $p_{adj} = 0.017$; CA+AA genotype: OR_{adj} = 0.66; CI_{adj} = 0.46-0.95; $p_{adj} = 0.026$). Carriers of two polymorphic rs10069690 T alleles had a higher risk of MM development (TT genotype: OR = 2.28; CI = 1.24-4.22; $p = 0.008$). After adjustment for age, the risk for MM was significantly higher in carriers of at least one polymorphic allele (CT+TT genotype: OR_{adj} = 1.52; CI_{adj} = 1.08-2.12; $p_{adj} = 0.017$) as well as in carriers of two polymorphic alleles (TT genotype: OR_{adj} = 2.2; CI_{adj} = 1.10-4.48; $p_{adj} = 0.026$) (Table 5).

When the group of MM patients was compared with the cases with PP, polymorphic rs2736098 T allele remained statistically significantly associated with an increased risk of developing MM (CT genotype: OR = 1.63; CI = 1.18-2.24; $p = 0.003$; CT+TT genotype: OR = 1.46; CI = 1.08-1.99; $p = 0.014$) (Table 6). After adjustment for age, only CT genotype remained associated with significantly higher MM risk (OR_{adj} = 1.52; CI_{adj} = 1.06-2.16; $p_{adj} = 0.022$). Carriers of two polymorphic rs2736100 A alleles had a lower risk for developing MM, but only after adjustment for age (OR_{adj} = 0.58; CI_{adj} = 0.36-0.94; $p_{adj} = 0.028$). On the other hand, carriers of two polymorphic rs10069690 T alleles had a higher risk of MM development (OR = 2.10; CI = 1.12-3.96; $p = 0.021$). After adjustment for age, the risk for MM remained significant in carriers of two polymorphic alleles (OR_{adj} = 2.11; CI_{adj} = 1.02-4.34; $p_{adj} = 0.043$). Additionally, in the multivariable analysis

TABLE 10. Association between selected polymorphisms and progression-free survival in patients with malignant mesothelioma (MM)

SNP	Genotype	PFS Median (25%–75%)	HR (95% CI)	P	HR (95% CI) _{adj}	P _{adj}
rs2736098	CC	10.2 (6.5–18.9)	Reference		Reference	
	CT	9.4 (6.1–14.5)	1.21 (0.93–1.57)	0.163	1.31 (0.98–1.76)	0.073
	TT	10.0 (6.6–14.2)	1.32 (0.79–2.20)	0.294	1.46 (0.82–2.59)	0.194
	CT+TT	9.7 (6.3–14.3)	1.22 (0.95–1.57)	0.127	1.33 (1.00–1.77)	0.051
rs2736100	CC	9.4 (5.9–13.4)	Reference		Reference	
	CA	9.7 (6.4–14.9)	0.98 (0.74–1.30)	0.879	0.83 (0.60–1.14)	0.250
	AA	12.2 (7.1–20.1)	0.68 (0.47–0.98)	0.038	0.68 (0.45–1.03)	0.070
	CA+AA	10.2 (6.5–17.6)	0.87 (0.67–1.15)	0.328	0.78 (0.57–1.06)	0.113
rs10069690	CC	10.7 (6.3–16.5)	Reference		Reference	
	CT	9.3 (6.1–15.0)	1.09 (0.83–1.42)	0.552	1.06 (0.79–1.43)	0.699
	TT	11.8 (7.3–13.4)	0.85 (0.52–1.38)	0.502	0.81 (0.48–1.38)	0.443
	CT+TT	9.4 (6.6–15.0)	1.04 (0.80–1.34)	0.791	1.01 (0.76–1.33)	0.963

A = adenine; Adj = adjustment for smoking, asbestos exposure, weight loss, C-reactive protein (CRP), and histology type of MM; C = cytosine; CI = confidence interval; HR = hazard ratio; PFS = progression free survival; SNP = single nucleotide polymorphism; T = thymine. Statistically significant values are printed in bold.

the association was also significant in the dominant model (CT+TT genotype: OR_{adj} = 1.48; CI_{adj} = 1.05–2.10; p_{adj} = 0.027) (Table 6).

Treatment response rate in patients with malignant mesothelioma

The data on chemotherapy treatment and response are presented in Table 2. The majority of patients with MM received chemotherapy based on gemcit-

abine with cisplatin (N = 161; 57.3%). Complete and partial responses were achieved only in 3.9% and 28.5% of patients, respectively, while in 50.0% of patients, the disease was stable. Disease progression occurred in 17.6% of patients. The majority of patients thus had a poor chemotherapy response rate (N = 173; 67.6%).

We observed no significant associations between telomere length or their dynamics with a chemotherapy response rate (p > 0.05) (Table 7).

TABLE 11. Association between selected polymorphisms and overall survival in patients with malignant mesothelioma (MM)

SNP	Genotype	OS Median (25%–75%)	HR (95% CI)	P	HR (95% CI) _{adj}	P _{adj}
rs2736098	CC	18.2 (10.1–28.6)	Reference		Reference	
	CT	19.3 (9.6–31.4)	1.01 (0.76–1.35)	0.944	1.02 (0.75–1.39)	0.899
	TT	24.4 (22.0–31.1)	0.84 (0.46–1.54)	0.573	0.94 (0.48–1.83)	0.859
	CT+TT	20.3 (9.9–31.2)	0.99 (0.75–1.31)	0.924	1.01 (0.75–1.36)	0.945
rs2736100	CC	17.5 (11.6–28.1)	Reference		Reference	
	CA	19.3 (10.7–32.5)	0.87 (0.64–1.20)	0.404	0.88 (0.62–1.24)	0.460
	AA	20.6 (9.6–31.4)	0.79 (0.53–1.17)	0.229	0.86 (0.56–1.31)	0.478
	CA+AA	19.5 (10.0–32.5)	0.85 (0.63–1.14)	0.270	0.87 (0.63–1.21)	0.410
rs10069690	CC	20.3 (9.6–31.4)	Reference		Reference	
	CT	19.3 (11.1–25.9)	1.09 (0.81–1.47)	0.578	1.13 (0.82–1.55)	0.455
	TT	16.0 (13.1–29.0)	1.01 (0.60–1.72)	0.958	0.74 (0.41–1.35)	0.321
	CT+TT	18.5 (11.4–29.0)	1.08 (0.81–1.43)	0.619	1.04 (0.77–1.41)	0.780

A = adenine; Adj = adjustment for asbestos exposure, ECOG performance status, C-reactive protein (CRP), histology type of MM; C = cytosine; CI = confidence interval; HR = hazard ratio; OS = overall survival; SNP = single nucleotide polymorphism; T = thymine

When we analysed the associations between *hTERT* polymorphisms and a chemotherapy response rate, only rs10069690 influenced the chemotherapy response rate in MM patients. Carriers of at least one polymorphic rs10069690 allele had a significantly better response rate to chemotherapy (CT genotype: OR = 1.18; CI = 1.03-3.17; $p = 0.039$; CT+TT genotype: RO = 1.72; CI = 1.00-2.93; $p = 0.048$). Both associations became even stronger after adjustment for weight loss and ECOG performance status (CT genotype: OR_{adj} = 2.08; CI_{adj} = 1.13-3.84; $p_{adj} = 0.019$; CT+TT genotype: RO_{adj} = 2.04; CI_{adj} = 1.13-3.67; $p_{adj} = 0.017$) (Table 8).

Survival of patients with malignant mesothelioma

Within the median follow-up time of the patients of 41.7 (22.8-77.3) months, median PFS was 10.0 (6.3-16.4) months and the median overall survival (OS) was 19.3 (10.0-30.3) months.

Telomere length or their dynamics were not associated with PFS, even after adjustment for CRP (all $p > 0.05$) (Table 9).

In Cox regression analysis (Table 10), patients with the rs2736100 AA genotype had significantly longer PFS compared to patients with the reference CC genotype (hazard ratio [HR] = 0.68; CI = 0.47-0.98; $p = 0.038$). The association of rs2736100 with PFS in patients with MM is illustrated as a function of time (Kaplan Meier plot) in Figure 3. None of other investigated polymorphisms were associated with PFS, not even after the adjustment for smoking status, asbestos exposure, weight loss, CRP level and histology type ($p > 0.05$) (Table 10).

Additionally, the investigated polymorphisms were not associated with OS of patients with MM neither in univariable analysis, nor after the adjustment for asbestos exposure, ECOG performance status, CRP level, and histologic type (all $p > 0.05$) (Table 11).

Discussion

In our study, we evaluated whether telomere length or their dynamics and *hTERT* polymorphisms could serve as a biomarker for the risk of developing asbestos-related diseases, chemotherapy response, and progression in MM patients. Consistent with previous studies, we observed that patients with MM had shorter telomeres compared to cases with PP. Previous studies stated that the telomeres in cancer patients are shorter but sta-

ble when compared to healthy individuals.^{18,20,21} Also, a study analysing telomere length in pleural effusion cells reported shorter telomeres in 12 MM patients compared to 35 cases with non-neoplastic disease.²³

Interestingly, older patients with MM had longer telomeres than younger patients with MM. According to our knowledge, telomere shortening is one of the most important markers of ageing.^{19,33,34} Furthermore, cancer cells have typically short telomeres^{18,20,21}, as also shown for MM.²³ However, the presence of telomerase reactivation in MM²² allows for an unlimited cell division potential and telomere length maintenance, which, on the contrary, does not occur in non-neoplastic cells,³⁵ potentially contributing to the observed results.

In the first part of the study, we evaluated the association of *TERT* SNPs with a risk for MM. We observed rather consistent associations of the polymorphic rs2736098 T allele with an increased risk of MM in the additive or in the dominant genetic model. Although no specific studies on this association with MM have been conducted, recent studies have shown associations between rs2736098 and lung cancers^{36,37} as well as an increased risk for bladder cancer, while the risk was decreased for breast and colon cancers.³⁶

Another important finding of this study was the decreased risk of MM associated with homozygosity for polymorphic rs2736100 A allele after adjustment for age. This observation emphasizes the importance of age as a contributing factor to carcinogenesis, although further investigation is needed to determine whether this association is coincidental. Our results are in agreement with previous studies indicating that carriers of two reference rs2736100 C alleles generally have a higher risk of developing idiopathic lung fibrosis, chronic obstructive pulmonary disease (COPD) and laryngeal cancer.^{18,39,40}

Furthermore, we observed a significantly higher risk for MM in carriers of two polymorphic rs10069690 T alleles. To our knowledge, there are no other studies investigating this association in MM; however, rs10069690 has been linked to a higher overall cancer risk, specifically in breast, ovarian, lung and thyroid cancers.⁴¹

In the second part of the study, we evaluated the association of telomere length and *TERT* SNPs with a treatment outcome in MM. We did not find any associations between telomere length and MM chemotherapy response. While studies on breast cancer reported that chemotherapy can lead

to telomere shortening in the short term, telomere length was shown to return to its pre-treatment level after two years.⁴² Given that our findings are based on a limited number of participants and that studies in MM patients are lacking, further analyses and investigations are necessary to gain a deeper understanding of the relationship between telomere length and a chemotherapy response in MM.

In our study, polymorphic rs10069690 T allele was associated with a good chemotherapy response. Moreover, this association became even more statistically significant after adjustment for age. Interestingly, our findings differ from a previous study in breast cancer, which is also telomerase-dependent cancer, where rs10069690 was associated with poor chemotherapy outcome.⁴³ As there are currently no studies specifically exploring this relationship in MM, further studies are required to fully understand the impact of rs10069690 on a chemotherapy response in MM.

No significant associations were identified between telomere length and PFS in patients with MM. To our knowledge, there are no other studies that investigated the association between telomere length and survival in MM, and the existing survival analyses conducted for other cancer types yield contradictory results. An extensive study examining the effect of telomere length on survival in various benign and malignant diseases found no influence on cancer patients' survival.⁴⁴ Conversely, an American study on pancreatic cancer observed that shorter telomeres were linked to poorer OS, while *hTERT* polymorphisms had no statistically significant impact on OS.⁴⁵ Similarly, our study showed no significant associations between the investigated *hTERT* polymorphisms and overall survival of MM patients. Due to the inconsistent knowledge in this field, further studies should be performed to better define the factors influencing the outcome of MM.

Finally, our study has shown that carriers of two polymorphic rs2736100 A alleles had a lower risk for MM progression. However, this area of research is still limited, and our finding contrasts with a kidney cancer study that identified rs2736100 as an independent factor associated with a poor prognosis.⁴⁶ Similarly, an Indian study reported that rs2736100 contributes to a poorer prognosis of glioma patients.⁴⁷ On the other hand, a Chinese study did not seem to validate the relationship between this polymorphism and a poor prognosis in papillary thyroid carcinoma.⁴⁸ It is essential to consider that the mentioned studies

did not focus on MM and were not conducted on Caucasians, thus caution should be applied when interpreting the data. Therefore, future studies investigating these associations with a specific focus on MM are required.

In conclusion, our results suggest that telomere length and genetic polymorphisms in the *hTERT* gene have a limited role as a biomarker for the risk of developing asbestos-related diseases. Collectively, our study did not demonstrate the role of telomere length as a biomarker for a MM chemotherapy response; however, with a cautious interpretation, *hTERT* polymorphisms may represent a biomarker for the chemotherapy outcome in MM. Similarly, telomere length does not seem to impact PFS, while *hTERT* polymorphisms may be used as a biomarker for the risk of MM progression. So far, our findings have been encouraging, yet further studies are necessary to validate these associations in independent patient cohorts and elucidate the role of telomere length and genetic variants of the *hTERT* gene in MM.

Acknowledgements

This work was financially supported by the Slovenian Research and Innovation Agency (ARIS Grants No. P1-0170 and L3-2622).

References

1. Toyokuni S. Commentary on "mechanisms of asbestos-induced carcinogenesis" published in 2009. *Nagoya J Med Sci* 2023; **85**: 13-5. doi: 10.18999/najms.85.1.13
2. Hajj GNM, Cavarson CH, Pinto CAL, Venturi G, Navarro JR, de Lima VCC. Malignant pleural mesothelioma: an update. *J Bras Pneumol* 2021; **47**: e20210129. doi: 10.36416/1806-3756/e20210129
3. Brims F. Epidemiology and clinical aspects of malignant pleural mesothelioma. *Cancers* 2021; **13**: 4194. doi: 10.3390/cancers13164194.
4. Gaudino G, Xue J, Yang H. How asbestos and other fibers cause mesothelioma. *Transl Lung Cancer Res* 2020; **9**(Suppl 1): S39-46. doi: 10.21037/tlcr.2020.02.01
5. Tallet A, Nault JC, Renier A, Hysi I, Galateau-Sallé F, A Cazes A, et al. Overexpression and promoter mutation of the *TERT* gene in malignant pleural mesothelioma. *Oncogene* 2014; **33**: 3748-52. doi: 10.1038/onc.2013.351
6. Rossiello F, Jurk D, Passos JF, di Fagagna FA. Telomere dysfunction in ageing and age-related diseases. *Nat Cell Biol* 2022; **24**: 135-47. doi: 10.1038/s41556-022-00842-x
7. Lin J, Epel E. Stress and telomere shortening: insights from cellular mechanisms. *Ageing Res Rev* 2022; **73**: 101507. doi: 10.1016/j.arr.2021.101507
8. Wadowski B, De Rienzo A, Bueno R. The molecular basis of malignant pleural mesothelioma. *Thorac Surg Clin* 2020; **30**: 383-93. doi: 10.1016/j.thorsurg.2020.08.005
9. Berry TA, Belluso E, Vigliaturo R, Gieré R, Emmett EA, Testa JR, et al. Asbestos and other hazardous fibrous minerals: potential exposure pathways and associated health risks. *Int J Environ Res Public Health* 2022; **19**: 4031. doi: 10.3390/ijerph19074031

10. Pouliquen DL, Kopecka J. Malignant mesothelioma. *Cancers* 2021; **13**: 3447. doi: 10.3390/cancers13143447
11. Zhu W, Liu J, Li Y, Shi Z, Wei S. Global, regional, and national trends in mesothelioma burden from 1990 to 2019 and the predictions for the next two decades. *SSM Popul Health* 2023; **23**: 101441. doi: 10.1016/j.ssmph.2023.101441
12. *Cancer in Slovenia 2018*. Annual report. Zadnik V, Gašljević G, Hočevar M, Jarm K, Pompe-Kirn V, Strojjan P, et al, editors. Ljubljana: Institute of Oncology Ljubljana, Epidemiology and Cancer Registry, Slovenian Cancer Registry; 2020.
13. Štrbac, D, Dolžan V. Novel and future treatment options in mesothelioma: a systematic review. *Int J Mo Sci* 2022; **23**: 1975. doi: 10.3390/ijms23041975
14. Guo X, Lin L, Zhu J. Immunotherapy vs. chemotherapy in subsequent treatment of malignant pleural mesothelioma: which is better? *J Clin Med* 2023; **12**: 2531. doi:10.3390/jcm12072531
15. Okamoto K, Seimiya H. Revisiting telomere shortening in cancer. *Cells* 2019; **8**: 107. doi: 10.3390/cells8020107
16. Razgonova MP, Zakharenko AM, Golokhvast KS, Thanasoula M, Sarandi E, Nikolouzakis K, et al. Telomerase and telomeres in aging theory and chronographic aging theory (review). *Mol Med Rep* 2020; **22**: 1679-94. doi: 10.3892/mmr.2020.11274
17. Rampazzo E, Cecchin E, Del Bianco P, Menin C, Spolverato G, Giunco S, et al. Genetic variants of the *TERT* gene, telomere length, and circulating *TERT* as prognostic markers in rectal cancer patients. *Cancers* 2020; **12**: 3115. doi: 10.3390/cancers12113115
18. Yuan X, Dai M, Xu D. Telomere-related markers for cancer. *Curr Top Med Chem* 2020; **20**: 410-32. doi: 10.2174/1568026620666200106145340
19. Levstek T, Redenšek S, Trošt M, Dolžan V, Trebušak Podkrajšek K. Assessment of the telomere length and its effect on the symptomatology of parkinson's disease. *Antioxidants* 2021; **10**: 137. doi: 10.3390/antiox10010137
20. Borges G, Criqui M, Harrington L. Tying together loose ends: telomere instability in cancer and aging. *Mol Oncol* 2022; **16**: 3380-96. doi: 10.3390/antiox10010137
21. Cigan SS, Meredith JJ, Kelley AC, Yang T, Langer EK, Hooten AJ, et al. Predicted leukocyte telomere length and risk of germ cell tumours. *Br J Cancer* 2022; **127**: 301-12. doi: 10.1038/s41416-022-01798-3
22. Au AY, Hackl T, Yeager TR, Cohen SB, Pass HI, Harris CC, et al. Telomerase activity in pleural malignant mesotheliomas. *Lung Cancer* 2011; **73**: 283-8. doi: 10.1016/j.lungcan.2010.12.023
23. Aida S, Aida J, Naoi M, Kato M, Tsuura Y, Natsume I, et al. Measurement of telomere length in cells from pleural effusion: asbestos exposure causes telomere shortening in pleural mesothelial cells. *Pathol Int* 2018; **68**: 503-8. doi: 10.1111/pin.12710
24. Alfiduhii KM, Lynch DA, Laurent F, Ferretti GR, Dunet V, Beigelman-Aubry C, et al. Focal pleural thickening mimicking pleural plaques on chest computed tomography: tips and tricks. *Br J Radiol* 2016; **89**: 20150792. doi: 10.1259/bjr.20150792
25. Kim Y, Myong JP, Lee JK, Kim JS, Kim YK, Jung SH, et al. CT characteristics of pleural plaques related to occupational or environmental asbestos exposure from South Korean asbestos mines. *Korean J Radiol* 2015; **16**: 1142-52. doi: 10.3348/kjr.2015.16.5.1142
26. Wolff H, Vehmas T, Oksa P, Rantanen J, Vainio H. Asbestos, asbestosis, and cancer, the Helsinki criteria for diagnosis and attribution 2014: recommendations. *Scand J Work Environ Health* 2015; **41**: 5-15. doi: 10.5271/sjweh.3462
27. Chapel DB, Schulte JJ, Husain AN, Krausz T. Application of immunohistochemistry in diagnosis and management of malignant mesothelioma. *Transl Lung Cancer Res* 2020; **9**(Suppl 1): S3-27. doi: 10.21037/tlcr.2019.11.29
28. Munkholm-Larsen S, Cao CQ, Yan TD. Malignant peritoneal mesothelioma. *World J Gastrointest Surg* 2009; **1**: 38-48. doi: 10.4240/wjgs.v1.i1.38
29. Berzenji L, Van Schil PE, Carp L. The eighth TNM classification for malignant pleural mesothelioma. *Transl Lung Cancer Res* 2018; **7**: 543-9. doi: 10.21037/tlcr.2018.07.05
30. Franko A, Goricar K, Kovac V, Dodic-Fikfak M, Dolzan V. NLRP3 and CARD8 polymorphisms influence risk for asbestos-related diseases. *J Med Biochem* 2020; **39**: 91-9. doi: 10.2478/jomb-2019-0025
31. Klebe S, Leigh J, Henderson DW, Nurminen M. Asbestos, smoking and lung cancer: an update. *Int J Environ Res Public Health* 2019; **17**: 258. doi: 10.3390/ijerph17010258
32. Levstek T, Redenšek S, Trošt M, Dolžan V, Trebušak Podkrajšek K. Assessment of the telomere length and its effect on the symptomatology of Parkinson's disease. *Antioxidants* 2021; **10**: 137. doi: 10.3390/antiox10010137.
33. Lulkiewicz M, Bajsert J, Kopczyński P, Barczak W, Rubis B. Telomere length: how the length makes a difference. *Mol Biol Rep* 2020; **47**: 7181-8. doi: 10.1007/s11033-020-05551-y
34. Havas A, Yin S, Adams PD. The role of aging in cancer. *Mol Oncol* 2022; **16**: 3213-9. doi: 10.1002/1878-0261.13302
35. Kusamura S, Baratti D, De Simone M, Pasqual EM, Ansaloni L, Marrelli D, et al. Diagnostic and therapeutic pathway in diffuse malignant peritoneal mesothelioma. *Cancers* 2023; **15**: 662. doi: 10.3390/cancers15030662
36. Zhou M, Jiang B, Xiong M, Zhu X. Association between *TERT* rs2736098 polymorphisms and cancer risk-a meta-analysis. *Front Physiol* 2018; **9**: 377. doi: 10.3389/fphys.2018.00377
37. Wang M, Sun Y. Telomerase reverse transcriptase rs2736098 polymorphism is associated with lung cancer: a meta-analysis. *J Int Med Res* 2020; **48**: 300060520936173. doi: 10.1177/0300060520936173
38. Holesova Z, Krasnicanova L, Saade R, Pös O, Budis J, Gazdarica J, et al. Telomere length changes in cancer: insights on carcinogenesis and potential for non-invasive diagnostic strategies. *Genes* 2023; **14**: 715. doi: 10.3390/genes14030715
39. Arimura-Omori M, Kiyohara C, Yanagihara T, Yamamoto Y, Ogata-Suetsugu S, Harada E, et al. Association between telomere-related polymorphisms and the risk of IPF and COPD as a precursor lesion of lung cancer: findings from the Fukuoka tobacco-related lung disease (FOLD) registry. *Asian Pac J Cancer Prev* 2020; **21**: 667-73. doi: 10.31557/APJCP.2020.21.3.667
40. Cornean CI, Catana A, Maniu AA. Do polymorphisms of the *TERT*, *GSTM1*, and *GSTT1* genes increase laryngeal cancer susceptibility in smokers of Romanian descent? *Medicina (Kaunas)* 2022; **58**: 1106. doi: 10.3390/medicina5808110
41. He G, Song T, Zhang Y, Chen X, W, Chen H, et al. *TERT* rs10069690 polymorphism and cancers risk: a meta-analysis. *Mol Genet Genomic Med* 2019; **7**: e00903. doi: 10.1002/mgg3.903
42. Benitez-Buelga C, Sanchez-Barroso L, Gallardo M, Apellániz-Ruiz M, Inglada-Pérez L, Yanowski K, et al. Impact of chemotherapy on telomere length in sporadic and familial breast cancer patients. *Breast Cancer Res Treat* 2015; **149**: 385-94. doi: 10.1007/s10549-014-3246-6
43. Zins K, Peka E, Miedl H, Ecker S, Abraham D, Schreiber M. Association of the telomerase reverse transcriptase rs10069690 polymorphism with the risk, age at onset and prognosis of triple negative breast cancer. *Int J Mol Sci* 2023; **24**: 1825. doi: 10.3390/ijms24031825
44. Schneider CV, Schneider KM, Teumer A, Rudolph KL, Hartmann D, Rader DJ, et al. Association of telomere length with risk of disease and mortality. *JAMA Intern Med* 2022; **182**: 291-300. doi: 10.1001/jamainternmed.2021.7804
45. Hamada T, Yuan C, Bao Y, Mingfeng Zhang, Natalia Khalaf, Ana Babic, et al. Prediagnostic leukocyte telomere length and pancreatic cancer survival. *Cancer Epidemiol Biomarkers Prev* 2019; **28**: 1868-75. doi: 10.1158/1055-9965.EPI-19-0577
46. Ma R, Liu C, Lu M, Yuan X, Cheng G, Kong F, et al. The *TERT* locus genotypes of rs2736100-CC/CA and rs2736098-AA predict shorter survival in renal cell carcinoma. *Urol Oncol* 2019; **37**: 301.e1-10. doi: 10.1016/j.urolonc.2019.01.014
47. Pandith AA, Wani ZA, Qasim I, Afroze D, Manzoor U, Amin I, et al. Association of strong risk of hTERT gene polymorphic variants to malignant glioma and its prognostic implications with respect to different histological types and survival of glioma cases. *J Gene Med* 2020; **22**: e3260. doi: 10.1002/jgm.3260
48. Nie X, Shang J, Wang W. *TERT* genetic polymorphism rs2736100 is associated with an aggressive manifestation of papillary thyroid carcinoma. *Front Surg* 2022; **9**: 1019180. doi: 10.3389/fsurg.2022.1019180

The prognostic significance of programmed cell death protein 1 and its ligand on lymphoma cells and tumor-immune cells in diffuse large B-cell lymphoma, not otherwise specified

Teja Cas Slak^{1,2}, Simona Miceska^{1,2}, Gorana Gasljevic^{3,4}, Lucka Boltezar^{2,5},
Veronika Kloboves Prevodnik^{1,4}

¹ Department of Cytopathology, Institute of Oncology Ljubljana, Ljubljana, Slovenia

² Faculty of Medicine, University of Ljubljana, Ljubljana, Slovenia

³ Department of Pathology, Institute of Oncology Ljubljana, Ljubljana, Slovenia

⁴ Faculty of Medicine, University of Maribor, Maribor, Slovenia

⁵ Department of Medical Oncology, Institute of Oncology Ljubljana, Ljubljana, Slovenia

Radiol Oncol 2024; 58(1): 99-109.

Received 7 November 2023

Accepted 25 November 2023

Correspondence to: Assoc. Prof. Veronika Kloboves-Prevodnik, M.D., Ph.D., Institute of Oncology Ljubljana, Zaloška 2, SI-1000 Ljubljana, Slovenia. E-mail: vkloboves@onko-i.si

Disclosure: No potential conflicts of interest were disclosed.

This is an open access article distributed under the terms of the CC-BY license (<https://creativecommons.org/licenses/by/4.0/>).

Background. Diffuse large B-cell lymphoma, not otherwise specified (DLBCL, NOS) is the most common type non-Hodgkin's lymphoma, where the treatment of relapsed/refractory cases is the major challenge. Programmed cell death protein 1 (PD-1) and its ligand PD-L1 play a crucial role in the negative regulation of the immune response against the disease. The aim of the study was to analyze the expression of PD-1 and PD-L1 on lymphoma cells (LCs) and tumor-immune cells (TICs) and to investigate their correlation with outcome.

Patients and methods. Samples from 283 patients diagnosed with DLBCL, NOS (both germinal center B cell like [GCB] and non-GCB subtypes) were included in the study. Expression of PD-1 and PD-L1 was determined using double immunohistochemical staining (D-IHC) for PD-1/PAX5 and PD-L1/PAX5 on tissue microarrays. LCs were highlighted by D-IHC to obtain more accurate results. Clinical data and histologic diagnoses were obtained from electronic data records. We correlated clinical characteristics, and PD-1 and PD-L1 expression on LCs and TICs with progression-free survival (PFS) and overall survival (OS).

Results. Expression of PD-1 on TICs was observed in 38.4% and on LCs in 8.8% of cases, while PD-L1 was expressed on TICs in 46.8% and on LCs in 6.5% of cases. PD-L1 expression on LCs was more frequent in non-GCB subtype ($p = 0.047$). In addition, patients with PD-L1 expression on LCs had significantly shorter PFS ($p = 0.015$), and the expression retained significant in the multivariate model ($p = 0.034$).

Conclusions. PD-L1 was more frequently expressed in LCs of the non-GCB subtype. Additionally, PD-L1 in LCs may predict shorter PFS time. D-IHC staining for PD-L1/PAX5 is a feasible method to assess PD-L1 expression on LCs of DLBCL, NOS patients and can be used to identify patients who may benefit from targeted immunotherapy with checkpoint inhibitors.

Key words: diffuse large B-cell lymphoma; immunohistochemistry; PD-1; PD-L1; PAX5

Introduction

Diffuse large B-cell lymphoma, not otherwise specified (DLBCL, NOS) is the most prevalent type

of non-Hodgkin's lymphoma (NHL) arising from a complex interplay of genetic and molecular factors. This heterogeneity results in approximately 35% of DLBCL, NOS cases not responding to

standard treatment method that combines rituximab with anthracycline-based chemotherapy. As a result, patients who do not respond to standard therapy experience relapsed or refractory disease, which remains the leading cause of mortality.^{1,2} In recent years, a variety of novel therapies, including immunotherapies, have emerged that may provide effective treatment strategies for DLBCL, NOS patients, particularly for relapsed or refractory disease. Identifying additional biomarkers and carefully assessing them to precisely define the effectiveness of immunotherapy are therefore critical for improved treatment outcomes, which are being investigated in several ongoing studies.³⁻⁵

The programmed cell death protein 1 (PD-1)/programmed cell death ligand 1 (PD-L1) immune checkpoint pathway, which is crucial for maintaining self-tolerance and excessive immune responses, has emerged as a novel biomarker target for various malignant neoplasms to suppress the anti-tumor immune response and evade immune surveillance.⁶ Immunotherapy based on the PD-1/PD-L1 signaling pathway has already been included in standard treatment guidelines for various carcinomas such as melanoma, non-small cell lung cancer, urothelial carcinoma, triple negative breast cancer and many others.⁷ Moreover, it has also attracted wide attention for the treatment of lymphomas, with the greatest success achieved in classical Hodgkin's lymphoma and T-cell lymphoma.⁸⁻¹³ However, in DLBCL, NOS, immunotherapy based on the PD-1/PD-L1 pathway has not yet become part of the standard treatment approach. Expression of PD-1 and PD-L1 in DLBCL, NOS is often elevated, leading to impaired immune cell function and tumor growth. The expression of PD-1 has been reported mainly on immune cells, emphasizing tumor-immune cells (TICs), while PD-L1 expression on lymphoma cells (LCs) and TICs. Some studies have already shown that increased PD-1 expression on TICs is associated with favorable overall survival (OS) of DLBCL, NOS patients.¹⁴ In contrast, increased PD-L1 expression on LCs has been associated with poorer prognosis and increased resistance to chemotherapy⁸, which also correlates with the DLBCL, NOS non-germinal center B-cell like (non-GCB) DLBCL, NOS subtype defined by the Hans algorithm.¹⁵ These data confirm their pivotal role in the tumor microenvironment of DLBCL, NOS and also their contribution to the poor clinical outcomes.^{8,14} However, to date, reported data have yielded conflicting results, particularly in relation to PD-1 expression on TICs, which has been by some authors associ-

ated with better progression-free survival (PFS) and OS, while some other studies have found no association with survival.^{1,6,16-20} On the other hand, some findings revealed an association of PD-L1 expression on LCs with worse OS^{1,6,8,14,16,18-21}, although there are data disputing the prognostic significance of PD-L1 or even showing a correlation with better rather than worse outcomes. It is also worth noting that most studies on the expression of PD-1 and PD-L1 in DLBCL, NOS have focused on the Asian population, where there is a higher prevalence of non-GCB DLBCL, NOS subtypes²², which has led to a lack of comprehensive research in the European population. Furthermore, almost all published studies have generally included only a very small number of DLBCL, NOS patients in their analyses.^{1,18,19,23-25}

Moreover, the majority of published research on DLBCL, NOS has merely focused on analyzing PD-1 and PD-L1 expression on LCs or TICs, and when this has been the case, the analyses had been based on only a single immunohistochemical (IHC) staining assessment. To our knowledge, the use of markers to accurately identify LCs, such as PAX5, has rarely been reported.¹⁴ PAX5, a member of the paired box gene family of transcription factors, is a B cell-specific activator protein that plays an important role during B lymphopoiesis. It shows consistent expression across various stages of B-cell maturation and can be identified in the majority of B-cell neoplasms, even in cases where mature B-cell markers are not expressed.²⁶ Furthermore, no studies have investigated the simultaneous expression of PD-1 and PD-L1 on both LCs and TICs and their prognostic significance.

Therefore, our aim was to evaluate the simultaneous expression of PD-1 and PD-L1 on LCs and TICs in a Slovenian cohort of DLBCL, NOS patients using double IHC staining in combination with PAX5 and to investigate their association with prognosis.

Patients and methods

Patients

Patients who were diagnosed with *de novo* DLBCL, NOS at the Institute of Oncology Ljubljana (IOL), Slovenia, between February 2004 and May 2018, were included in the study. All patients were older than 18 years, tested negative for HIV and underwent lymph node biopsy and histology assessment before receiving any specific oncologic treatment. In addition, all patients were treated with stand-

TABLE 1. Description of the PAX5, PD-1 And PD-L1 antibodies and immunohistochemistry staining protocols

Primary Ab	Clone	Vendor	Reaction type	Antigen retrieval [100°C]	Ab dilution	Ab incubation time [min]	IHC detection kit
PAX5	SP34	Ventana	Nuclear	CC1 56 min	RTU	32 (37°C)	UltraView Universal Alkaline Phosphatase Red
PD-1	NAT105	Dako	Cytoplasmic, Membranous	CC1 88 min	1:200	60 (37°C)	OptiView DAB
PD-L1	SP263	Ventana	Cytoplasmic, Membranous	CC1 64 min	RTU	16 (37°C)	OptiView DAB

Ab = antibody; CC1 = cell conditioning solution 1; DAB = diaminobenzidine; IHC = immunocytochemistry; RTU = ready to use

ard treatment (R-CHOP: rituximab-cyclophosphamide, vincristine, doxorubicin and prednisone or an R-CHOP-like protocol) and radiotherapy of residual disease if needed. Each patient has given written informed consent.

Study design

The study was conducted retrospectively, and representative lymph node excision biopsy samples were utilized. All DLBCL, NOS patients were diagnosed and subtyped according to the Hans algorithm²⁷, as was previously described²⁸ (classifying DLBCL, NOS by the cell-of-origin into germinal center B-cell [GCB] and non-germinal center B-cell like [non-GCB]). Double PD-1/PAX5 and double PD-L1/PAX5 IHC staining were performed on tissue microarrays (TMAs). Results were evaluated by one experienced haemato-pathologist (GG), following an already published criteria.^{14,16,17,25,29,30} Clinical data were obtained from the patients' electronic medical record and were used to calculate

the correlation with the survival outcomes, as well as with PD-1 and PD-L1 expression. International Prognostic Score (IPI) was calculated for each patient.³¹ Survival analysis was based on a minimum of a 5-year patient follow-up. The study was conducted in accordance with the Declaration of Helsinki and was also approved by the Republic of Slovenia National Medical Ethics Committee (No. 0120-151/2019/4).

Immunohistochemical staining

Double IHC staining was performed for PAX5 and PD-1 as well as for PAX5 and PD-L1 to determine PD-1 and PD-L1 expression on LCs and TICs, respectively. PAX5 nuclear staining was visualized by the presence of red chromogen in B cells, including DLBCL cells, while PD-1 and PD-L1 membranous staining was visualized by the presence of brown (diaminobenzidine, DAB) chromogen. IHC staining was performed using Benchmark XT and Benchmark Ultra automated immunostainers

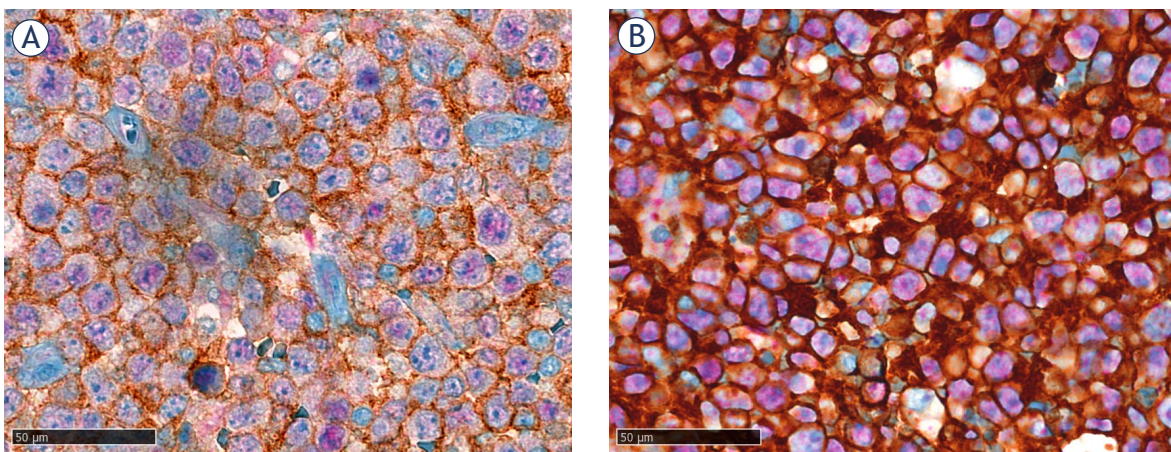


FIGURE 1. Representative images of the double immunohistochemical staining for (A) PD-1/PAX5 and (B) PD-L1/PAX5. Red chromogen indicates PAX5 in DLBCL, NOS nuclei of LCs, with brown chromogen is labeled PD-1 (A) or PD-L1 (B), respectively (40x magnification).

DLBCL = diffuse large B-cell lymphoma; LCs = lymphoma cells; NOS = not otherwise specified; PD-1 = programmed cell death protein 1; PD-L1 = PD-1 ligand

TABLE 2. Clinicopathological characteristics of the Slovenian patient cohort (N = 216) included in the analysis

Age at diagnosis (years)	
Median	64
Range	27-89
≤60	84
>60	132
Sex, N (%)	
Male	104 (48)
Female	112 (52)
Ann Arbor stage, N (%)	
I	37 (17)
II	47 (22)
III	45 (21)
IV	87 (40)
Involvement of an extranodal organ, N (%)	
Yes	72 (33)
No	103 (48)
No data	41 (19)
Involvement of spleen, N (%)	
Yes	34 (16)
No	129 (60)
No data	53 (24)
B symptoms, N (%)	
Yes	76 (35)
No	116 (54)
No data	24 (11)
IPI score, N (%)	
0, 1	63 (29.2)
2	51 (23.6)
3	50 (23.1)
4, 5	54 (24.1)
Classification according to Hans Algorithm, N (%)	
Non-GCB	92 (43)
GCB	124 (57)
Survival status of the patients, N (%)	
Alive	102 (47)
Dead	114 (53)

GCB = germinal center B-cell diffuse large B-cell lymphoma (DLBCL) subtype; IPI = International Prognostic Index; N = number; non-GCB = non-germinal center B-cell like DLBCL subtype

(Ventana Medical Systems, Inc., Tucson, AZ, USA). A detailed description of the used antibodies and IHC staining protocols are shown in Table 1.

Evaluation of PD-1 and PD-L1 expression

TICs and LCs were defined by re-evaluating hematoxylin and eosin H&E slides and IHC slides stained for Bcl-6, CD5, CD10, CD20, and MUM1. LCs were recognized according to PAX5 expression and morphology. The expression of PD-1 and PD-L1 was assessed semi-quantitatively for both LCs and TICs, using already published cut-off values. PD-1 and PD-L1 expression on TICs was assessed in three high-powered fields (HPF), and the score was categorized in four groups: score 0 (no positive cells), score 1 (less than 10 cells), score 2 (10-30 cells) and score 3 (more than 30 cells). According to the references^{16,17,25} we considered scores 0 and 1 as negative and 2 and 3 as positive. PD-1 and PD-L1 expression on LCs was categorized into negative and positive group by using cut-off of 10% and 30%, respectively.^{14,29,30}

Statistical analysis

Descriptive statistics were used to describe the basic characteristic of the data. The median and range were calculated for the age of the patients, OS, PFS, and observation time. The Chi-square test or Fisher's exact test were used to analyze if there is a difference between PD-1 and PD-L1 expression and clinicopathological characteristics of the patients. PFS was calculated as the time from diagnosis until disease progression or death from any cause, and OS was calculated as the time from diagnosis to death from any cause. The median survival of the patients was expressed in months. Kaplan Maier with log-rank test was used to compare PFS and OS between two groups. Hazard ratio (HR) and 95% confidence interval (CI) were calculated for both univariate and multivariate analysis (Cox regression model). Parameters that proved to be significant in the univariate analysis were included in the multivariate analysis. $p < 0.05$ was considered significant. IBM SPSS Statistics (version 28.0.1.0, IBM, Armonk, NY, USA) was used for the analysis.

Results

Patients' characteristics

The study included 283 Slovenian patients diagnosed with DLBCL, NOS. However, due to incomplete data on patients' treatment, lost follow-up or inadequate biological material, 67 patients were excluded, resulting in a final cohort of 216 patients

TABLE 3. Clinicopathological characteristics of the Slovenian patient cohort (N = 216) included in the analysis

(N, %)	PD-1 on TICs Expression		PD-1 on LCs Expression		PD-L1 on TICs Expression		PD-L1 on LCs Expression	
	Positive	Negative	Positive	Negative	Positive	Negative	Positive	Negative
All cases (N = 216)	83	133	19	197	135	81	14	202
Non-GCB subtype (N = 92)	31 (37.3)	61 (45.9)	11 (57.9)	81 (41.1)	58 (43.0)	34 (42.0)	10 (71.4)	82 (40.6)
GCB subtype (N = 142)	52 (62.7)	72 (54.1)	8 (42.1)	116 (58.9)	77 (57.0)	47 (58.0)	4 (28.6)	120 (59.4)
Non-GCB versus GCB subtype (p value)	0.258		0.224		0.887		0.047	

GCB = germinal center B-cell DLBCL subtype; LCs = lymphoma cells; N = number; non-GCB = non-germinal center B-cell like DLBCL subtype; PD-1 = programmed cell death protein 1; PD-L1 = PD-1 ligand; TICs = tumor-immune cells

for subsequent analyses. The median observation time for the analyzed patients was 162 months (range 60-234 months). Clinicopathological characteristics of our patient’s cohort are presented in Table 2.

The expression of PD-1 and PD-L1

PD-1 was expressed on TICs in 38.4% of cases and on LCs in 8.8% of cases, while PD-L1 was expressed on TICs in 62.5% of cases and on LCs in 6.5% of cases (Figure 1). We also investigated whether there was a difference between the non-GCB and GCB subtypes regarding PD-1 and PD-L1 expression on both TICs and LCs. Our results showed no difference in the expression of PD-1 on TICs and LCs (p = 0.291 and p = 0.224, respectively), nor for PD-L1 on TICs (p = 0.393). Interestingly, we confirmed significantly increased PD-L1 expression on LCs within the non-GCB subtype compared to the GCB subtype (p = 0.047). The detailed results of PD-1 and PD-L1 expression analysis can be found in Table 3.

Regarding clinicopathological characteristics of the patients (Table 4), no significant differences were observed in PD-1 and PD-L1 expression on TICs or LCs when analyzed in relation with variables such as the age, sex, Ann Arbor stage, involvement of an extranodal organ, involvement of spleen, presence of B symptoms or IPI score.

Clinicopathological characteristics and correlation with progression free-survival and overall survival

The results of the survival analysis, which was performed on the basis of the clinicopathological characteristics of the patients, are summarized in Figure 2 and Table 5. The median PFS was 77.4 months (range 0.23-224.89) and the median OS

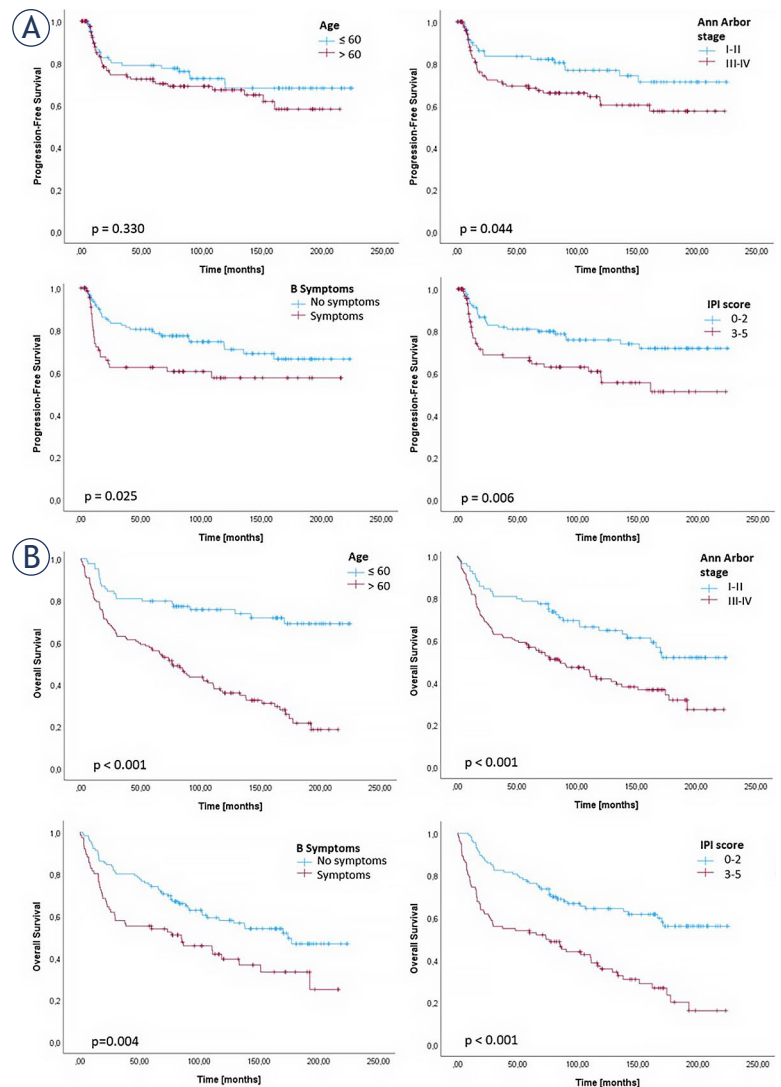


FIGURE 2. Kaplan-Meier curves for (A) progression-free survival and (B) overall survival, representing only significant differences among all analyzed clinicopathological characteristics of diffuse large B-cell lymphoma, not otherwise specified patients.

was 83.3 months (range 0.23-224.89). In the group of patients under 60 years of age, the OS was sig-

TABLE 4. PD-1 and PD-L1 expression in association with clinicopathological characteristics of patients with diffuse large B-cell lymphoma, not otherwise specified

[N, (%)]	PD-1 expression on TICs			PD-1 expression on LCs			PD-L1 expression on TICs			PD-L1 expression on LCs		
	Positive	Negative	p value	Positive	Negative	p value	Positive	Negative	p value	Positive	Negative	p value
Total	83 (38.4)	133 (61.6)		19 (8.8)	197 (91.2)		135 (62.5)	81 (37.5)		14 (6.5)	202 (93.5)	
Age			0.775			0.466			0.885			0.406
≤60	31 (14.4)	53 (24.5)		9 (4.2)	75 (34.7)		53 (24.5)	31 (14.4)		7 (3.2)	77 (35.6)	
>60	52 (24.1)	80 (37.0)		10 (4.6)	122 (56.5)		82 (38.0)	50 (23.1)		7 (3.2)	125 (57.9)	
Sex			0.889			0.811			0.265			1.000
Male	39 (18.1)	65 (30.1)		10 (4.6)	94 (43.5)		61 (28.8)	43 (19.9)		7 (3.2)	97 (44.9)	
Female	44 (20.4)	68 (31.5)		9 (4.2)	103 (47.7)		74 (34.2)	38 (17.6)		7 (3.2)	1.5 (48.6)	
Ann Arbor stage			1.000			1.000			0.116			0.134
I-II	32 (14.8)	52 (24.1)		7 (3.2)	77 (35.6)		47 (21.8)	37 (17.1)		3 (1.4)	81 (37.5)	
III-IV	51 (23.6)	81 (37.5)		12 (5.6)	120 (55.6)		88 (40.7)	44 (20.4)		11 (5.1)	121 (56.0)	
Involvement of an extranodal organ			0.643			0.412			0.332			0.738
Yes	33 (18.9)	39 (22.3)		8 (4.6)	64 (36.6)		44 (25.1)	28 (16.0)		3 (1.7)	69 (39.4)	
No	43 (24.6)	60 (34.3)		7 (4.0)	96 (54.9)		71 (40.6)	32 (18.3)		6 (3.4)	97 (55.4)	
Involvement of spleen			0.847			1.000			0.540			1.000
Yes	15 (9.2)	19 (11.7)		3 (1.8)	31 (19.0)		25 (15.3)	9 (5.5)		1 (0.6)	33 (20.2)	
No	61 (37.4)	68 (41.7)		11 (6.7)	118 (72.4)		87 (53.4)	42 (25.8)		7 (4.3)	122 (74.8)	
B symptoms			0.366			0.598			0.536			0.085
Yes	27 (14.1)	49 (25.5)		5 (2.6)	71 (37.0)		52 (27.1)	24 (12.5)		9 (4.7)	67 (34.9)	
No	50 (26.0)	66 (34.4)		11 (5.7)	105 (54.7)		73 (38.0)	43 (22.4)		5 (2.6)	111 (57.8)	
IPI score			0.780			0.228			0.575			1.000
0-2	45 (20.8)	69 (31.9)		13 (6.0)	101 (46.8)		69 (31.9)	45 (20.8)		7 (3.2)	107 (49.5)	
3-5	38 (17.6)	64 (29.6)		6 (2.8)	96 (44.4)		66 (30.6)	36 (16.7)		7 (3.2)	95 (44.0)	
Hans Algorithm classification			0.258			0.224			0.887			0.047
Non-GCB	31 (14.4)	61 (28.2)		11 (5.1)	88 (37.5)		58 (26.9)	34 (15.7)		10 (4.6)	82 (38.0)	
GCB	52 (24.1)	72 (33.3)		8 (3.7)	116 (53.7)		77 (35.6)	47 (21.8)		4 (1.9)	120 (55.6)	
Patients' outcome			0.124			0.639			0.779			0.788
Alive	45 (20.8)	57 (26.4)		10 (4.6)	92 (42.6)		65 (30.1)	37 (17.1)		6 (2.8)	96 (44.4)	
Dead	38 (17.6)	76 (35.2)		9 (4.2)	105 (48.6)		70 (32.4)	44 (20.4)		8 (3.7)	106 (49.1)	

GCB = germinal center B-cell DLBCL subtype; IPI = International Prognostic Index; LCs = lymphoma cells; N = number; non-GCB = non-germinal center B-cell like DLBCL subtype; PD-1 = programmed cell death protein 1; PD-L1 = PD-1 ligand; TICs = tumor-immune cells; % = percentage

nificantly longer than in the group of patients over 60 years of age ($p < 0.001$). At the same time, we did not find age to be statistically significant for PFS. Moreover, patients in Ann Arbor stages I or II showed a significant association with longer PFS ($p = 0.044$) and OS ($p < 0.001$) compared to patients in stages III and IV. In addition, a longer PFS ($p = 0.025$) and OS ($p = 0.004$) were observed in patients without B-symptoms compared to patients with B-symptoms. A low IPI score (score between 0 and 2) was associated with a longer PFS ($p = 0.003$) and

a longer OS ($p < 0.001$). No correlation with PFS and OS was observed for the other clinicopathological characteristics such as Hans algorithm, gender, an extranodal organ and spleen involvement.

Correlation of PD-1 and PD-L1 expression with progression free-survival and overall survival

We conducted individual survival analyses for PD-1 and PD-L1 on TICs. The results were obtained

while classifying the samples into four groups, as well as grouping them in two categories: negative (0 and 1) and positive (2 and 3). However, no statistically significant differences were found in either data set (Figure 3).

Correlation analysis between PD-L1 expression on LCs and patient survival showed a significant correlation for patients who had no PD-L1 expression on LCs (i.e. less than 30% of LCs were PD-L1 positive), with significantly longer progression-free survival (PFS) ($p = 0.015$) compared to patients who had detectable PD-L1 expression (77.7 months *vs.* 15.6 months). However, no correlation with OS was observed. Furthermore, correlation PD-1 expression on LCs cell showed no correlation with PFS and OS. Detailed results of the correlation analysis for PD-1 and PD-L1 expression with PFS and OS are summarized in Table 4 and Figure 4.

Multivariate analysis of the significant parameters in the univariate analysis

Only the significant clinicopathological features from the univariate analysis were included in the multivariate analysis: the Ann Arbor stage, presence of B symptoms, IPI score, and PD-L1 expression on LCs were used for the PFS analysis, and the age, Ann Arbor stage, presence of B symptoms, and IPI score were used for the OS analysis. Our results showed that the IPI score ($p = 0.048$, HR = 1.945) and the presence of PD-L1 on the LCs ($p = 0.034$, HR = 2.393) retained their significant prognostic impact for PFS. As expected, patient age ($p < 0.001$, HR = 2.907) was found to be a significant prognostic factor for OS, while the other variables, including IPI score, remained non-significant. The results of the multivariate analysis are shown in Table 5.

Discussion

In the present study, we investigated the expression of PD-1 and PD-L1 on LCs and TICs in the tumor microenvironment of DLBCL, NOS patients in relation to non-GCB and GCB subtypes and patients' survival.

The expression of PD-1 and PD-L1 has drawn great attention to the impact of lymphoma treatment, particularly in aggressive lymphomas such as DLBCL, NOS, where they evade immune response and drive aggressiveness.²¹ Identification of patients for PD-1/PD-L1 immunotherapy, possibly through IHC evaluation, holds promise for

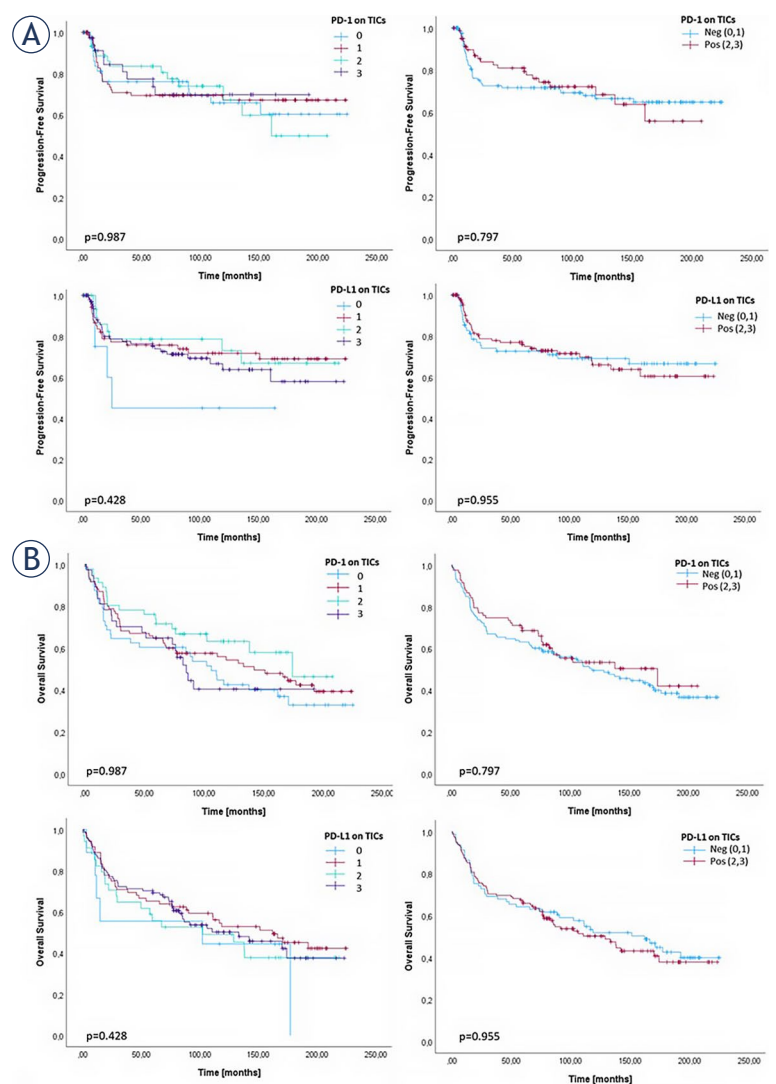


FIGURE 3. Kaplan-Meier curves for (A) progression-free survival (PFS) and (B) overall survival (OS) for PD-1 and PD-L1 on tumor-immune cells. The cases were divided into four groups based on the cell count per high-power field. Furthermore, these cases were stratified into two classifications: negative (cell counts 0 and 1) and positive (cell counts 2 and 3).

PD-1 = programmed cell death protein 1; PD-L1 = PD-1 ligand; TICs = tumor immune cells.

better patient outcomes and further research in checkpoint inhibitor treatment. Currently, there are few ongoing clinical trials investigating the use of anti-PD-1 and anti-PD-L1 treatments in patients with relapsed or refractory DLBCL, NOS. Preliminary results in small patient cohorts show promising results for prolonged disease-free intervals.²⁹ However, the selection criteria for patient enrollment are not dependent on PD-1 or PD-L1 expression on either TICs or LCs. One of the explanations for this could be the lack of consensus in the

TABLE 5. Univariate and multivariate analysis of the patients' survival based on their clinicopathological characteristics and PD-1 and PD-L1 expressions on lymphoma cells and tumor-infiltrating immune cells in tissue samples of diffuse large B-cell lymphoma, not otherwise specified

		Univariate analysis				Multivariate analysis			
		PFS		OS		PFS		OS	
		p value	Median when patients have relapse [months]	p value	Median when patients died [months]	p value	HR (95% CI)	p value	HR (95% CI)
Age	≤ 60 vs. > 60	0.330	91.8 vs. 59.7	< 0.001	110.1 vs. 73.5			< 0.001	2.907 (1.710-4.940)
Sex	Male vs. Female	0.945	69.1 vs. 80.9	0.324	78.3 vs. 90.8				
Ann Arbor stage	I-II vs. III-IV	0.044	91.3 vs. 59.7	< 0.001	113.8 vs. 72.0	0.845	1.072 (0.532-2.130)	0.073	1.654 (0.955-2.865)
Involvement of an extranodal organ	(-) vs. (+)	0.886	77.4 vs. 74.1	0.451	81.8 vs. 82.3				
Involvement of the spleen	(-) vs. (+)	0.915	69.9 vs. 81.8	0.844	80.1 vs. 81.8				
B symptoms	(-) vs. (+)	0.025	85.3 vs. 30.8	0.004	91.8 vs. 65.3	0.338	1.319 (0.748-2.326)	0.170	1.354 (0.879-2.087)
IPI score	0-2 vs. 3-5	0.006	88.8 vs. 29.3	< 0.001	101.2 vs. 62.7	0.048	1.945 (1.005-3.767)	0.494	1.205 (0.706-2.058)
Hans classification	Non-GCB vs. GCB	0.914	66.5 vs. 80.7	0.095	77.6 vs. 85.9				
PD-1 on TICs	(-) vs. (+)	0.797	81.6 vs. 76.0	0.478	85.9 vs. 80.7				
PD-1 on LCs	(-) vs. (+)	0.657	77.8 vs. 76.0	0.882	84.9 vs. 76.3				
PD-L1 on TICs	(-) vs. (+)	0.955	85.9 vs. 76.2	0.623	111.0 vs. 79.2				
PD-L1 on LCs	(-) vs. (+)	0.015	77.7 vs. 15.6	0.373	85.1 vs. 22.3	0.034	2.393 (1.070-5.352)		

GCB = germinal center B-cell DLBCL subtype; IPI = International Prognostic Index; LCs = lymphoma cells; N = number; non-GCB = non-germinal center B-cell like DLBCL subtype; OS = overall survival; PD-1 = programmed cell death protein 1; PD-L1 = PD-1 ligand; PFS = progression-free survival; TICs = tumor-immune cells

evaluation criteria, especially for PD-1 expression, as it is less frequently assessed and less defined. Different evaluation criteria are used to assess cell positivity, and we have used the most commonly used ones.^{8,14,16,17,25,29,32} We found only a few studies investigating whether there is a correlation between the expression of PD-1 or PD-L1 on TICs or LCs and patient outcomes. For the assessment of PD-1 and PD-L1 on LCs and TICs in our study, we performed double staining for PD-1/PAX5 and PD-L1/PAX5 to simplify the assessment of PD-1 and PD-L1 expression and obtain more reliable results. Indeed, PAX5 was required for accurate identification of B cells, including LCs, because PAX5 is expressed in mature B cells and LCs.^{14,24,25,33} The use of PAX5 increased the accuracy of LC identification, which in combination with the simultaneous staining of PD-1 and PD-L1 is one of the major advantages of this study. This double staining was so far reported in Kiyasu's study of 1091 patients with DLBCL¹⁴, NOS and Chen's study of various lymphoma subtypes, including 66 patients with DLBCL, NOS³³, but both studies used only PD-L1/

PAX5 staining. To the best of our knowledge, our study is the first to perform PD-L1 and PD-1 staining simultaneously with PAX5.

In this way, we confirmed a PD-1 expression of 38.4% on TICs and 8.8% on LCs. Our results were similar to the already published data, where PD-1 expression on TICs ranged from 22.2-60.0%. For PD-1 on LCs, we observed a slightly lower expression rate compared to the expression levels of PD-1 reported in the literature (22.2-65.0%).^{16,24,25,29,34} Using the same assessment method as in the other published studies^{14,16,17,25,29,30}, we reported 62.4% PD-L1 expression on TICs and 6.5% on LCs. Our data again differed from already reported PD-L1 expression levels, where expression ranged from 15.3-37.0% on TICs and 8.9-61.1% on LCs.^{14,17,24,29} In summary, we observed a lower expression of PD-L1 and PD-1 on LCs and a higher expression of PD-L1 on TICs. We speculate that the major reason for the low expression on LCs is the additional staining with PAX5. With the double staining, we were able to recognize PD-1/PD-L1 positive LCs more precisely, so the numbers are probably more

reliable than in other studies where other cells such as macrophages could be misinterpreted as LCs and resulted in higher expression of PD-L1 and PD-1 on LCs. Two already published studies using PAX5 staining reported 8.9%¹⁴ and 11% PD-L1 positivity on LCs³³, which is comparable to our results.

We also speculate that a possible reason for this discrepancy in PD-L1 and PD-1 expression rates could be a consequence of several other factors. One reason might be the different inclusion criteria of the patients. Almost all published studies included patients with Epstein-Barr virus (EBV) positive DLBCL, NOS, which typically exhibit PD-L1 positive status due to the association between PD-L1 expression and EBV infection. EBV positive patients were not a part of our patient cohort, so this could be one of the reasons for the discrepant results. In addition, different algorithms were used to define the DLBCL, NOS subtypes. The majority of the studies have used Hans' algorithm^{14,16,17,25,29,30}, but some have applied Choi's algorithm.³⁵ The choice of one of these algorithms may contribute to different percentages of GCB and non-GCB subtypes, as well as different percentages of PD-L1 positive LCs and TICs within each subtype.³⁵ Furthermore, different antibody clones were used in different studies, and in some cases the clones used were not clearly stated.^{8,25} Additionally, some studies lacked a clear description of the criteria used for the assessment of PD-L1 positivity.²⁴ Since the major focus was on the Asian population, where non-GCB subtypes of DLBCL, NOS, were more common than GCB subtypes, a higher number of PD-L1 positive cases was expected.²²

The second aim of our study was to investigate the association of PD-1 and PD-L1 expression on TICs or LCs with clinicopathological characteristics. We investigated the potential differences between various clinicopathological characteristics of patients such as age at diagnosis, gender, Ann Arbor stage, extranodal organ involvement, involvement of the spleen, presence of B symptoms, and IPI score, but our results showed no difference in PD-1 and/or PD-L1 expression on LCs and/or TICs between these groups. Additionally, we examined the histological subtypes determined by the Hans algorithm and found that PD-L1 positive expression was more frequent in the non-GCB subtype, as already reported.^{14,15,17,19} However, in a univariate analysis, the Hans algorithm showed no significant impact on PFS or OS. Regarding patient survival, we found that patients with PD-L1

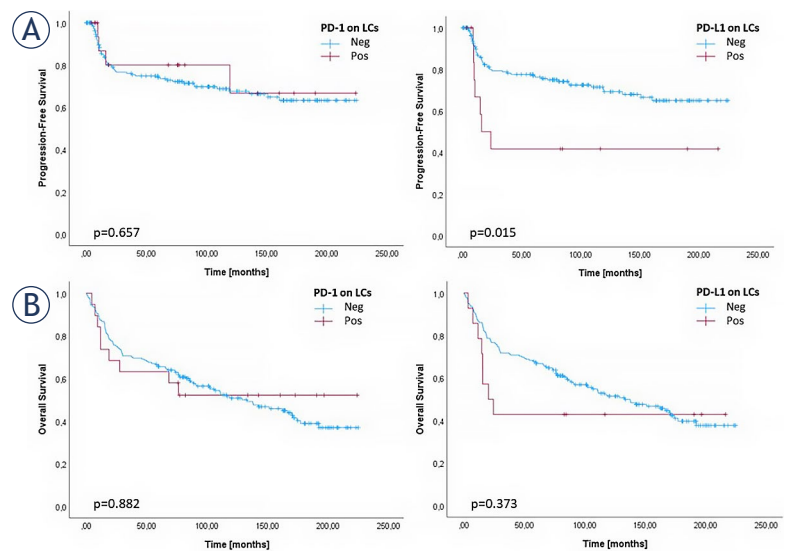


FIGURE 4. Kaplan-Meier curves for (A) progression-free survival and (B) overall survival representing the influence of PD-1 and PD-L1 expression on lymphoma cells (LCs). PD-1 expression on LCs was categorized as negative below 10%. PD-L1 expression on LCs was categorized as negative below 30%.

PD-1 = programmed cell death protein 1; PD-L1 = PD-1 ligand

expression on the LCs are correlated with shorter PFS, which also had a significant impact in the multivariate analysis including the IPI score. This indicates that although the number of patients with PD-L1 positive expression on the LCs is small, their survival is worse in comparison with the patients with no PD-L1 expression, regardless of the IPI score. Since the IPI score is still one of the strongest and most reliable prognostic markers in DLBCL, NOS, even in the era of novel therapies, we believe this is an interesting conclusion that requires further research.

In the multivariate analysis for PFS, where the Ann Arbor stage, presence of B symptoms, IPI score, and PD-L1 expression on LCs for PFS were included as significant parameters from the univariate analyses, PD-L1 expression on LCs was found to be an independent prognostic marker for PFS. As expected, the IPI score also proved to be an independent prognostic marker for PFS. In the multivariate analysis of OS, where the age, Ann Arbor stage, B symptoms and IPI score were included, we showed that age remained as an individual marker for OS. This result was consistent with already published data based on 5-year follow-up analyses for PFS and OS of DLBCL, NOS patients.⁸

Noteworthy, there are some limitations of our study that need to be considered. For example, due

to the retrospective nature of the study, the longer archiving time of FFPE tissue blocks may potentially influence the staining results. In addition, it is still unclear whether the expression of PD-1 and PD-L1 on tumors and TICs is a key factor for the clinical prognosis of DLBCL, NOS patients treated with PD-1/PD-L1 blockade therapy. On the other hand, our study has certain advantages, such as centralized evaluation of specimens, homogeneous treatment and long follow-up time. To the best of our knowledge, we are the first to simultaneously assess the expression of PD-1 and PD-L1 on both TICs and LCs from the same cohort of patients using a double immunostaining approach and their impact on PFS and OS, as well as their association with other clinicopathological characteristics. Our results were consistent with individual studies on the European population as well as studies on the Asian population.

In conclusion, we demonstrated that PD-L1 expression on LCs was associated with shorter PFS and was more frequently observed in the non-GCB subtype. Double IHC staining with PAX5 proved to be a feasible method to assess PD-1 and PD-L1 expression in tissue samples. Further research and clinical studies are required to assess the importance of assessing PD-1 and PD-L1 in DLBCL, NOS patients as well as methods to determine their expression, particularly with regard to planning immunotherapy treatments. It is also important to understand the mechanisms of tumor immune evasion induced by PD-1/PD-L1 and to explore approaches to modulate the host immune response accordingly, which requires further research.

Acknowledgments

We would like to thank to the Department of Pathology and the Department of Cytopathology at the Institute of Oncology Ljubljana for their support, contributions and collaboration.

The publication of this article was financed by Slovenian Research and Innovation Agency (ARIS), grant No. P3-0289. The founder had no role in study design, data collection and analysis, decision to publish, or preparation of the manuscript.

References

- Qiu L, Zheng H, Zhao X. The prognostic and clinicopathological significance of PD-L1 expression in patients with diffuse large B-cell lymphoma: a meta-analysis. *BMC Cancer* 2019; **19**: 273. doi: 10.1186/s12885-019-5466-y
- Minghan Q, Shan W, Xinrui C, Huaqing W. Update on diffuse large B-cell lymphoma: highlights from the 2022 ASCO Annual Meeting. *Cancer Biol Med* 2022; **19**: 1117-20. doi: 10.20892/j.issn.2095-3941.2022.0403
- Wang C, Shi F, Liu Y, Zhang Y, Dong L, Li X, et al. Anti-PD-1 antibodies as a salvage therapy for patients with diffuse large B cell lymphoma who progressed/relapsed after CART19/20 therapy. *J Hematol Oncol* 2021; **14**: 106. doi: 10.1186/s13045-021-01120-3
- Lu T, Zhang J, Xu-Monette ZY, Young KH. The progress of novel strategies on immune-based therapy in relapsed or refractory diffuse large B-cell lymphoma. *Exp Hematol Oncol* 2023; **12**: 72. doi: 10.1186/s40164-023-00432-z
- Guan J, Zhang J, Zhang X, Yuan Z, Cheng J, Chen B. Efficacy and safety of PD-1/PD-L1 immune checkpoint inhibitors in treating non-Hodgkin lymphoma: A systematic review and meta-analysis of clinical trials. *Medicine* 2022; **101**: e32333. doi: 10.1097/MD.00000000000032333
- Xie M, Huang X, Ye X, Qian W. Prognostic and clinicopathological significance of PD-1/PD-L1 expression in the tumor microenvironment and neoplastic cells for lymphoma. *Int Immunopharmacol* 2019; **77**: 105999. doi: 10.1016/j.intimp.2019.105999
- Boydell E, Sandoval JL, Michielin O, Obeid M, Addeo A, Friedlaender A. Neoadjuvant immunotherapy: A promising new standard of care. *Int J Mol Sci* 2023; **24**: 11849. doi: 10.3390/ijms241411849
- Hu LY, Xu XL, Rao HL, Chen J, Lai RC, Huang HQ, et al. Expression and clinical value of programmed cell death-ligand 1 (PD-L1) in diffuse large B cell lymphoma: a retrospective study. *Chin J Cancer* 2017; **36**: 94. doi: 10.1186/s40880-017-0262-z
- Goodman A, Patel SP, Kurzrock R. PD-1-PD-L1 immune-checkpoint blockade in B-cell lymphomas. *Nat Rev Clin Oncol* 2017; **14**: 203-20. doi: 10.1038/nrclinonc.2016.168
- Jelinek T, Mihalyova J, Kascak M, Duras J, Hajek R. PD-1/PD-L1 inhibitors in haematological malignancies: update 2017. *Immunology* 2017; **152**: 357-71. doi: 10.1111/imm.12788
- Ok CY, Young KH. Checkpoint inhibitors in hematological malignancies. *J Hematol Oncol* 2017; **10**: 103. doi: 10.1186/s13045-017-0474-3
- Wang Y, Wu L, Tian C, Zhang Y. PD-1-PD-L1 immune-checkpoint blockade in malignant lymphomas. *Ann Hematol* 2018; **97**: 229-37. doi: 10.1007/s00277-017-3176-6
- Annibali O, Crescenzi A, Tomarchio V, Pagano A, Bianchi A, Grifoni A, et al. PD-1/PD-L1 checkpoint in hematological malignancies. *Leuk Res* 2018; **67**: 45-55. doi: 10.1016/j.leukres.2018.01.014
- Kiyasu J, Miyoshi H, Hirata A, Arakawa F, Ichikawa A, Niino D, et al. Expression of programmed cell death ligand 1 is associated with poor overall survival in patients with diffuse large B-cell lymphoma. *Blood* 2015; **126**: 2193-201. doi: 10.1182/blood-2015-02-629600
- Swerdlow SH, Campo E, Harris NL, Jaffe ES, Pileri SA, Stein H, et al. *WHO classification of tumours of haematopoietic and lymphoid tissues, WHO classification of tumours, Revised 4th edition, Volume 2. France: International Agency for Research on Cancer; 2017.*
- Fang X, Xiu B, Yang Z, Qiu W, Zhang L, Zhang S, et al. The expression and clinical relevance of PD-1, PD-L1, and TP63 in patients with diffuse large B-cell lymphoma. *Medicine* 2017; **96**: e6398. doi: 10.1097/MD.0000000000006398
- Kwon D, Kim S, Kim PJ, Go H, Nam SJ, Paik JH, et al. Clinicopathological analysis of programmed cell death 1 and programmed cell death ligand 1 expression in the tumour microenvironments of diffuse large B cell lymphomas. *Histopathology* 2016; **68**: 1079-89. doi: 10.1111/his.12882
- Gravelle P, Burroni B, Péricart S, Rossi C, Bezombes C, Tosolini M, et al. Mechanisms of PD-1/PD-L1 expression and prognostic relevance in non-Hodgkin lymphoma: a summary of immunohistochemical studies. *Oncotarget* 2017; **8**: 44960-75. doi: 10.18632/oncotarget.16680
- Zeng Q, Liu Z, Liu T. Prognostic value and clinicopathological characteristics of PD-L1 overexpression in non-Hodgkin lymphoma: a meta-analysis. *BMC Cancer* 2020; **20**: 59. doi: 10.1186/s12885-020-6550-z
- Xie W, Medeiros LJ, Li S, Yin CC, Khoury JD, Xu J. PD-1/PD-L1 pathway and its blockade in patients with classic Hodgkin lymphoma and Non-Hodgkin large-cell lymphomas. *Curr Hematol Malig Rep* 2020; **15**: 372-81. doi: 10.1007/s11899-020-00589-y

21. Xing W, Dresser K, Zhang R, Evens AM, Yu H, Woda BA, Chen BJ. PD-L1 expression in EBV-negative diffuse large B-cell lymphoma: clinicopathologic features and prognostic implications. *Oncotarget* 2016; **7**: 59976-86. doi: 10.18632/oncotarget.11045
22. Shiozawa E, Yamochi-Onizuka T, Takimoto M, Ota H: The GCB subtype of diffuse large B-cell lymphoma is less frequent in Asian countries. *Leuk Res* 2007; **31**: 1579-83. doi: 10.1016/j.leukres.2007.03.017
23. Muenst S, Hoeller S, Willi N, Dirnhofera S, Tzankov A. Diagnostic and prognostic utility of PD-1 in B cell lymphomas. *Dis Markers* 2010; **29**: 47-53. doi: 10.3233/DMA-2010-0725
24. Laurent C, Charmpi K, Gravelle P, Tosolini M, Franchet C, Ysebaert L, et al. Several immune escape patterns in non-Hodgkin's lymphomas. *Oncoimmunology* 2015; **4**: e1026530. doi:10.1080/2162402X.2015.1026530
25. Karakatsanis S, S Papadatos S, Syrigos N, Marinou L, Pouliou E, Papanikolaou A. Clinical significance of PD-1 and PD-L1 molecules in patients with diffuse large B-cell lymphoma, not otherwise specified: Correlation with clinical and pathological findings. *J BUON* 2021; **26**: 569-79.
26. Desouki MM, Post GR, Cherry D, Lazarchick J. PAX-5: a valuable immunohisto-chemical marker in the differential diagnosis of lymphoid neoplasms. *Clin Med Res* 2010; **8**: 84-8. doi: 10.3121/cm.2010.891
27. Hans CP, Weisenburger DD, Greiner TC, Gascoyne RD, Delabie J, Ott G, et al. Confirmation of the molecular classification of diffuse large B-cell lymphoma by immunohistochemistry using a tissue microarray. *Blood* 2004; **103**: 275-82. doi: 10.1182/blood-2003-05-1545
28. Boltezar L, Kloboves-Prevodnik V, Pohar-Perme M, Gasljevic G, Jezersek-Novakovic B. Comparison of the algorithms classifying the ABC and GCB subtypes in diffuse large B-cell lymphoma. *Oncol Lett* 2018; **15**: 6903-12. doi: 10.3892/ol.2018.8243
29. Chen BJ, Dashnamoorthy R, Galera P, Makarenko V, Chang H, Ghosh S, et al. The immune checkpoint molecules PD-1, PD-L1, TIM-3 and LAG-3 in diffuse large B-cell lymphoma. *Oncotarget* 2019; **10**: 2030-40. doi: 10.18632/oncotarget.26771
30. Xu-Monette ZY, Xiao M, Au Q, Padmanabhan R, Xu B, Hoe N, et al. Immune profiling and quantitative analysis decipher the clinical role of immune-checkpoint expression in the tumor immune microenvironment of DLBCL. *Cancer Immunol Res* 2019; **7**: 644-57. doi: 10.1158/2326-6066.CIR-18-0439
31. International Non-Hodgkin's Lymphoma Prognostic Factors Project. A predictive model for aggressive non-Hodgkin's lymphoma. *N Engl J Med* 1993; **329**: 987-94. doi: 10.1056/NEJM199309303291402
32. McCord R, Bolen CR, Koeppen H, Kadel EE 3rd, Oestergaard MZ, Nielsen T, et al. PD-L1 and tumor-associated macrophages in de novo DLBCL. *Blood Adv* 2019; **3**: 531-40. doi: 10.1182/bloodadvances.2018020602
33. Chen BJ, Chapuy B, Ouyang J, Sun HH, Roemer MG, Xu ML, et al. PD-L1 expression is characteristic of a subset of aggressive B-cell lymphomas and virus-associated malignancies. *Clin Cancer Res* 2013; **19**: 3462-73. doi: 10.1158/1078-0432.CCR-13-0855
34. Zhang T, Xie J, Arai S, Wang L, Shi X, Shi N, et al. The efficacy and safety of anti-PD-1/PD-L1 antibodies for treatment of advanced or refractory cancers: a meta-analysis. *Oncotarget* 2016; **7**: 73068-79. doi: 10.18632/oncotarget.12230
35. Kwon HJ, Yang JM, Lee JO, Lee JS, Paik JH. Clinicopathologic implication of PD-L1 and phosphorylated STAT3 expression in diffuse large B cell lymphoma. *J Transl Med* 2018; **16**: 320. doi: 10.1186/s12967-018-1689-y

Influence of nutritional status and body composition on postoperative events and outcome in patients treated for primary localized retroperitoneal sarcoma

Manuel Ramanovic¹, Marko Novak², Andraz Perhavec^{2,3}, Taja Jordan^{3,4}, Karteek Popuri⁵, Nada Rotovnik Kozjek^{3,6}

¹ Biotechnical Faculty, University of Ljubljana, Ljubljana, Slovenia

² Department of Surgical Oncology, Institute of Oncology Ljubljana, Ljubljana, Slovenia

³ Medical Faculty, University of Ljubljana, Ljubljana, Slovenia

⁴ Department for Radiology, University Medical Centre Ljubljana, Ljubljana, Slovenia

⁵ Department of Computer Science, Memorial University of Newfoundland, Newfoundland, Canada

⁶ Department of Clinical Nutrition, Institute of Oncology Ljubljana, Ljubljana, Slovenia

Radiol Oncol 2024; 58(1): 110-123.

Received 26 July 2023

Accepted 3 November 2023

Correspondence to: Manuel Ramanović, M.D., Biotechnical Faculty, University of Ljubljana, Jamnikarjeva ul. 101, 1000 Ljubljana, Slovenia.
E-mail: mako_manuel1@yahoo.com

Disclosure: No potential conflicts of interest were disclosed.

This is an open access article under the CC BY-NC-ND license (<http://creativecommons.org/licenses/by-nc-nd/4.0/>).

Background. Retroperitoneal sarcomas (RPS) are rare tumours of mesenchymal origin, commonly presented as a large tumour mass at time of diagnosis. We investigated the impact of body composition on outcome in patients operated on for primary localized RPS.

Patients and methods. We retrospectively analysed data for all patients operated on for primary RPS at our institution between 1999 and 2020. Preoperative skeletal muscle area (SMA), visceral and subcutaneous adipose tissue area (VAT and SAT) and muscle radiation attenuation (MRA) were calculated using computed tomography scans at the level of third lumbar vertebra. European Working Group on Sarcopenia in Older People (EWGSOP2) criteria were applied to define myopenia. Using maximum log-rank statistic method we determined the optimal cut-off values of body composition parameters. Myosteatosis was defined based on determined MRA cut-offs.

Results. In total 58 patient were eligible for the study. With a median follow-up of 116 months, the estimated 5-year overall survival (OS) and local-recurrence free survival (LRFS) were 66.8% and 77.6%, respectively. Patients with myopenia had significantly lower 5-year OS compared to non-myopenic ($p = 0.009$). Skeletal muscle index and subcutaneous adipose tissue index predicted LRFS on univariate analysis ($p = 0.052$ and $p = 0.039$, respectively). In multivariate analysis high visceral-to-subcutaneous adipose tissue area ratio (VSR) independently predicted higher postoperative complication rate (89.2% vs. 10.8%, $p = 0.008$). Myosteatosis was associated with higher postoperative morbidity.

Conclusions. Myopenia affected survival, but not postoperative outcome in RPS. Visceral obesity, VSR (> 0.26) and myosteatosis were associated with higher postoperative morbidity. VSR was better prognostic factor than VAT in RPS.

Key words: body composition; myopenia; cancer cachexia; myosteatosis; obesity; retroperitoneal sarcoma

Introduction

Retroperitoneal sarcomas (RPS) are soft tissue tumours of mesenchymal origin accounting for

approximately 15% of all sarcomas and less than 1% of all tumour malignancy.¹⁻³ Most patients develop large tumour mass before diagnosis is clinically confirmed. Imaging techniques, CT and MRI

are primarily used in clinical evaluation of RPS.^{1,4} Surgical resection with removal of all gross disease is the cornerstone of curative therapy and optimal results are achieved with *en bloc* resection at the time of primary presentation.^{4,5} The role of radiation therapy and chemotherapy in management of RPS is still under investigation. Following the STRASS trial and STREXIT study, it seems that preoperative radiotherapy might influence the local control in liposarcoma (LPS) patients, while the evaluation of chemotherapy remains ongoing for high-grade LPS and leiomyosarcoma.⁶⁻⁸ There are no currently available data supporting the use of routine neoadjuvant or adjuvant chemotherapy for these patients.¹ Optimal management is achieved in specialized sarcoma centres^{4,9} with multidisciplinary approach.¹⁰⁻¹³ Institute of Oncology Ljubljana is the only referral sarcoma centre in Slovenia.¹⁴

Body composition changes are related to nutrition status and associated with perioperative outcome and influence management of surgical oncology patients.¹⁵ Ongoing catabolic processes, systemic inflammation, as well as decreased protein synthesis, as part of often presented cancer-associated cachexia, together contribute to loss of lean body mass and pose a risk of malnutrition in sarcoma patients.¹⁶⁻¹⁸ Sarcopenia is a clinical syndrome in which involuntary loss of skeletal muscle mass and function is progressive and generalized, together or without increased fat mass.^{19,20} Another clinically important body composition abnormality, myosteatosis, is characterized by excess accumulation of adipose tissue within muscle, resulting in impaired muscle strength and physical ability, as well as increased frailty.^{21,22} Recent studies demonstrated that both sarcopenia and myosteatosis pose a greater risk for postoperative complications and decrease overall survival (OS) in a variety of different cancers, including soft tissue sarcomas.²²⁻²⁷ Visceral obesity (VO) is the fat accumulation in visceral adipose tissue and serves as a clinical marker for adiposopathy.²⁸ Number of recent studies reported that VO is more reliable clinical marker for predicting outcome than traditional view on obesity defined by BMI.²⁹⁻³³ The useful predictor of VO is visceral-to-subcutaneous adipose tissue area ratio (VSR), and high VSR is associated with poor oncologic outcome.³⁴⁻³⁷ Also, another body composition abnormality, the new concept of sarcopenic obesity (SO), a combination of excess adiposity and sarcopenia, seems to have powerful negative prognostic impact in oncology treatment and is gaining increased attention in

cancer research.^{38,39} Loss of muscle mass or myopenia is a critical determinant of sarcopenia.

CT has been shown to be a precise and feasible method to evaluate body composition parameters.⁴⁰⁻⁴³ There is a lack of literature data regarding the impact of body composition on postoperative and oncologic outcome in patients operated on for primary RPS.

The aim of our study is to investigate the impact of low muscle mass or myopenia, myosteatosis, visceral obesity and cancer cachexia on OS, local recurrence-free survival (LRFS) and postoperative morbidity in patients operated for primary localized RPS. Additionally, we aimed to investigate the predictive value of preoperative body composition parameters for OS, LRFS and postoperative morbidity.

Patients and methods

Study design and population

Retrospective study was conducted on patients operated on for primary RPS at Department of Surgical Oncology at the Institute of Oncology Ljubljana between September 1999 and June 2020 (Figure 1). A total of 58 patients met the inclusion criteria, 24 females (41.4%) and 34 males (58.6%). The Slovenian National Medical Ethical Committee (decision number: 0120-530/2020/3), Institutional Review Board (ERID-KSOPKR-0081/2020) and Institutional Ethical Committee (ERIDEK-0079/2020) approved the study. Due to the retrospective nature of the study the need to obtain informed consent from participants was waived.

Clinical data collection

Patient's histories including anesthesiologic preoperative reports, operative reports, hospital records, and follow-up data were reviewed. Clinical and pathological data were collected (Figure 1). Postoperative complications were evaluated in accordance with Clavien–Dindo classification.⁴⁴ Tumour features of interest were as follows: histopathological diagnosis, stage (according to American Joint Committee on Cancer [AJCC] 8th Edition), grade (according to National Federation of Centers for the Fight Against Cancer grading system)⁴⁵ and tumour size (largest diameter value). Resection quality was recorded as either complete (R0), incomplete (R1) with microscopic involvement of resection margins or macroscopic residual tumour (R2).

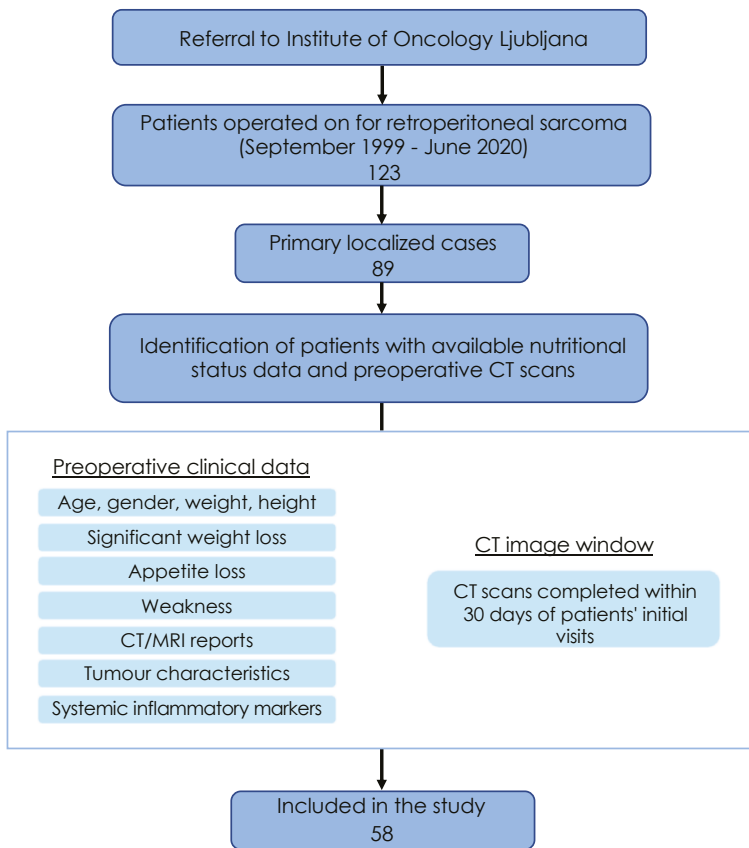


FIGURE 1. Patients' flow diagram. Out of 123 patients, 58 (47.1%) with primary localized retroperitoneal sarcomas (RPS) were included in the study and 65 were excluded. 34 (27.6%) were excluded as they presented as primary metastatic cases (6), locally recurrent cases (14) or cases with residual disease after operation elsewhere (14), and 31 patients (25.2%) were excluded as they had CT performed > 30 days from initial assessment or CT image was not technically adequate for analysis

Body composition assessment

The assessment of body composition was conducted using images from CT scans taken within 30 days preoperatively at the level of the third lumbar vertebra using the "Automated Body Composition Analyzer using Computed tomography image Segmentation" (ABACS) software.⁴⁶ This method uses predefined CT Hounsfield units (HU) values to recognize different tissues. The CT HU thresholds were 29 to 150 for skeletal muscles, 190 to 30 for subcutaneous adipose tissue, and 150 to 50 for visceral adipose tissue. The following body composition parameters were measured: total cross-sectional skeletal muscle area (SMA, cm²), subcutaneous adipose tissue area (SAT, cm²) and visceral adipose tissue area (VAT, cm²). After normalization by patient's height (m²), we used these

parameters as lumbar skeletal muscle index (SMI, cm²/m²), subcutaneous adipose tissue index (SATI, cm²/m²), and visceral adipose tissue index (VATI, cm²/m²). VSR was calculated by dividing VAT by SAT. To assess the muscle density and myosteatosis, skeletal muscle radiation attenuation (MRA) has also been recorded in HUs. All measurements were performed by experienced researcher, accredited for complex image analysis and segmentation techniques. Additionally, we used previously reported and validated equations to calculate appendicular skeletal muscle index (ASMI), lean body mass (LBM) and fat mass (FM)^{26,29,43,47}:

$$\text{ASMI (kg/m}^2\text{)} = 0.11 \times \text{SMI (cm}^2\text{/m}^2\text{)} + 1.17$$

$$\text{LBM (kg)} = 0.030 \times \text{Lean Tissue Area (cm}^2\text{)} + 6.06$$

$$\text{FM (kg)} = 0.042 \times \text{Total Fat Area (cm}^2\text{)} + 11.2$$

Based on a single abdominal CT image per patient, LBM and FM properly reflect appropriate dual-energy X-ray absorptiometry (DXA) derived whole-body fat-free mass (FFM) and whole-body fat mass (FM), respectively.

Assessment of myopenia, myopenic and visceral obesity, myosteatosis and cancer cachexia

Myopenia was defined based on the new recommendations of The European Working Group on Sarcopenia in Older People (EWGSOP2), as follows: SMI < 43 cm²/m² for men with BMI < 25, SMI < 53 cm²/m² for men with BMI ≥ 25, and SMI < 41 cm²/m² for women.⁴⁸

Muscle mass in patients with obesity was assessed according to The European Society for Clinical Nutrition and Metabolism (ESPEN) and the European Association for the Study of Obesity (EASO) consensus report for sarcopenic obesity.³⁹ Previously reported diagnostic criteria for visceral obesity were applied: VAT > 163.8 cm² for men and VAT > 80.1 cm² for women.^{29,39,47}

Preoperative cancer cachexia was defined using Fearon *et al.* criteria.⁴⁹

In order to establish optimal cut-off values for SMI, VATI, SATI, VSR and MRA which would best reflect our study cohort in relationship to defined outcome (maximum OS), we performed optimal stratification analysis based on maximally selected rank statistics using *maxstat* package implemented in R statistics.^{50,51} This approach is widely used and validated in cancer patients.^{26,52-55} The presence of myosteatosis was then confirmed based on established optimal threshold for MRA: < 35.88 HU in patients with a BMI ≥ 25 kg/m² and < 47.41 HU in those with a BMI < 25 kg/m².

TABLE 1. Clinical characteristics of study population

Clinical characteristic (N = 58)	Median (IQR); n (%)	Clinical characteristic (N = 58)	Median (IQR); n (%)
Age, years	61.0 (46.0 – 67.0)	Pathologic characteristics and postoperative outcome data	
Gender		Postoperative (90 day) complication rate	37 (64%)
Male	34 (58.6%)	Abdominal complication	24 (41%)
Female	24 (41.4%)	Systemic complication	17 (29%)
ASA grade		Abdominal and systemic complications	5 (9.0%)
1	9 (16%)	Clavien-Dindo > IIIa	
2	30 (52%)	Yes	17 (29%)
3	16 (28%)	No	41 (71%)
4	3 (5.2%)	Comprehensive Complication Index	20.92 (0.0–32.55)
Baseline albumin, g/L	41.0 (34.2 – 45.0)	Histologic type	
Baseline C-reactive protein, mg/L	13.5 (2.0 – 66.5)	Liposarcoma	35 (60%)
Neutrophil-lymphocyte ratio	3.3 (2.1 – 4.7)	Leiomyosarcoma	9 (16%)
Body Mass Index, kg/m ²	26.0 (24.7 – 29.7)	Pleomorphic sarcoma	1 (1.7%)
Nutrition and body composition characteristics		Other	13 (22%)
Nutritional team support before operation	28(48.3%)	Tumour size, cm	20 (11–30)
Skeletal Muscle Area, cm ²	45.5 (115.9 – 170.1)	FNCLCC grade	
Visceral Fat Area, cm ²	104.5 (53.6 – 168.7)	1	15 (26%)
Subcutaneous Adipose Tissue Area, cm ²	167.9 (127.9 – 231.6)	2	11 (19%)
Total Fat Area, cm ²	23.6 (19.8 – 29.1)	3	23 (40%)
Total Body Fat, %	30.6 (26.8 – 32.4)	Unknown	9 (16%)
Lean Body Mass, kg	52.7 (50.0 – 57.2)	Stage AJCC (8 th edition)	
Skeletal Muscle Index, cm ² /m ²	50.2 (44.0 – 55.6)	1A	1 (1.7%)
Appendicular Skeletal Muscle Index, cm ² /m ²	6.70 (6.00 – 7.3)	1B	23 (40%)
Myopenia based on estimated cut-off value for SMI ^a	18 (31.0%)	3A	6 (10%)
Myopenia based on EWGSOP2 criteria for SMI	19 (32.8%)	3B	28 (48%)
Cancer cachexia	13 (22.4%)	Completeness of surgical resection	
Visceral obesity	21 (36.2%)	R0	47 (81%)
Myopenic obesity	4 (6.9%)	R1/R2	11 (19%)
Myosteatorsis ^a	37 (63.7%)		

AJCC = The American Joint Committee on Cancer; ASA = American Society of Anesthesiologists classification; EWGSOP2 = The European Working Group on Sarcopenia in Older People; FNCLCC = Fédération Nationale des Centres de Lutte Contre Le Cancer

Summary for continuous variables is presented as median (interquartile range) and the statistical test is Kruskal-Wallis/Mann-Whitney; ^a cut-off values displayed in Table 3

Survival and statistical analysis

Final survival follow-up time was set as last follow-up date in the study period or the event of death. OS was defined as time between the date of the operation and date of death from any cause or last follow-up. LRFS was defined as the time interval between operation date and date of first

documented local progression, and instances involving deaths without evidence of disease and the occurrence of distant metastases considered as competing events. Survival curves were estimated using Kaplan-Meier method. Log-rank test, linear regression and Cox proportional hazard regression models were used to analyse the relationship between clinicopathological parameters

TABLE 2. Comparison of clinical and body composition parameters between myopenic and non-myopenic patients (EGSWOP2 criteria)

Clinicopathological factor	Level ^a	Myopenic ^b	Non Myopenic ^b	p
Age, years	Median (IQR)	66.0 (50.5–71.5)	61.0 (46.0–64.8)	0.236
Gender	Male	11 (57.9)	23 (60.5)	1
	Female	8 (42.1)	15 (39.5)	
ASA Grade, 2–3 vs. 1	1	3 (15.8)	6 (15.8)	1
	2–3	16 (84.2)	32 (84.2)	
FNCLCC Grade	1	5 (29.4)	10 (32.3)	0.547
	2	5 (29.4)	5 (16.1)	
	3	7 (41.2)	16 (51.6)	
	(Missing)	7 (18.4)	2 (10.5)	
Tumour size, cm	Median (IQR)	26.0 (20.5–34.0)	17.5 (10.0–24.8)	0.005
Clavien-Dindo > IIIa	Yes	3 (15.8)	14 (36.8)	0.183
	No	16 (84.2)	24 (63.2)	
Neutrophil-lymphocyte ratio	Median (IQR)	3.9 (2.4–4.7)	3.0 (2.1–4.7)	0.504
Baseline albumin, g/L	Median (IQR)	40.0 (32.0–42.5)	43.0 (35.0–45.8)	0.232
Baseline C-reactive protein, mg/L	Median (IQR)	44.0 (7.5–99.5)	6.0 (2.0–45.0)	0.088
Haemoglobin level, g/L	Median (IQR)	128.0 (101.5–136.5)	132.5 (115.2–145.8)	0.141
Preoperative radiotherapy	No	19 (100.0)	37 (97.4)	1
	Yes	0 (0.0)	1 (2.6)	
Resection status	R0	17 (89.5)	29 (76.3)	0.406
	R1	2 (10.5)	9 (23.7)	
Intraoperative blood loss, ml	Median (IQR)	1300.0 (425.0–4100.0)	1350.0 (500.0–2075.0)	0.78
Stage AJCC, 8th edition	1A–1B	7 (36.8)	17 (44.7)	0.776
	3A–3B	12 (63.2)	21 (55.3)	
Histology subtype	Pleomorphic	1 (5.3)	0 (0.0)	0.184
	Liposarcoma	14 (73.7)	21 (55.3)	
	Leiomyosarcoma	2 (10.5)	6 (15.8)	
	Other	2 (10.5)	11 (28.9)	
Nutrition team before surgery	Yes	12 (63.2)	16 (42.1)	0.223
	No	7 (36.8)	22 (57.9)	
Length of hospital stay, days	Median (IQR)	20.0 (11.0–28.8)	15.0 (11.5–27.0)	0.593
Visceral obesity	Yes	4 (21.1)	16 (42.1)	0.202
	No	15 (78.9)	22 (57.9)	
Myosteotosis	Yes	16 (84.2)	21 (56.8)	0.079
	No	3 (15.8)	16 (43.2)	
Cancer cachexia	No	12 (63.2)	31 (83.8)	0.163
	Yes	7 (36.8)	6 (16.2)	
Body Mass Index, kg/m ²	Median (IQR)	25.7 (23.3–27.2)	26.9 (24.8–30.9)	0.071
Skeletal Muscle Area, HU	Median (IQR)	115.8 (106.5–153.3)	149.9 (130.6–177.1)	0.019
Skeletal Muscle Index, cm ² /m ²	Median (IQR)	41.0 (38.3–46.8)	53.5 (46.2–58.8)	< 0.001
Muscle Radiation Attenuation, HU	Median (IQR)	35.6 (31.8–43.2)	38.1 (29.9–42.2)	0.959
Subcutaneous Adipose Tissue Area, cm ²	Median (IQR)	156.4 (103.2–194.4)	185.4 (131.4–254.1)	0.078
Visceral Adipose Tissue Area, cm ²	Median (IQR)	64.6 (38.1–131.6)	125.5 (66.1–201.7)	0.07
Visceral-to-subcutaneous adipose tissue area ratio	Median (IQR)	0.5 (0.2–0.9)	0.8 (0.3–1.1)	0.393
Body fat, %	Median (IQR)	28.3 (21.3–31.6)	31.1 (28.1–33.3)	0.024
Lean Body Mass, kg	Median (IQR)	52.5 (50.4–57.7)	52.8 (49.8–56.4)	0.684
Subcutaneous Adipose Tissue Index, cm ² /m ²	Median (IQR)	46.8 (30.6–67.2)	64.6 (43.9–95.0)	0.048
Visceral Adipose Tissue Index, cm ² /m ²	Median (IQR)	20.6 (13.2–43.8)	42.3 (24.2–63.6)	0.025

^a Summary for continuous variables is median (interquartile range) and the statistical test is Kruskal-Wallis/Mann-Whitney; ^b Median (IQR); n (%);

AJCC = The American Joint Committee on Cancer; ASA = American Society of Anesthesiologists; EGSWOP2 = The European Working Group on Sarcopenia in Older People; FNCLCC = Fédération Nationale des Centres de Lutte Contre Le Cancer; HU = Hounsfield units

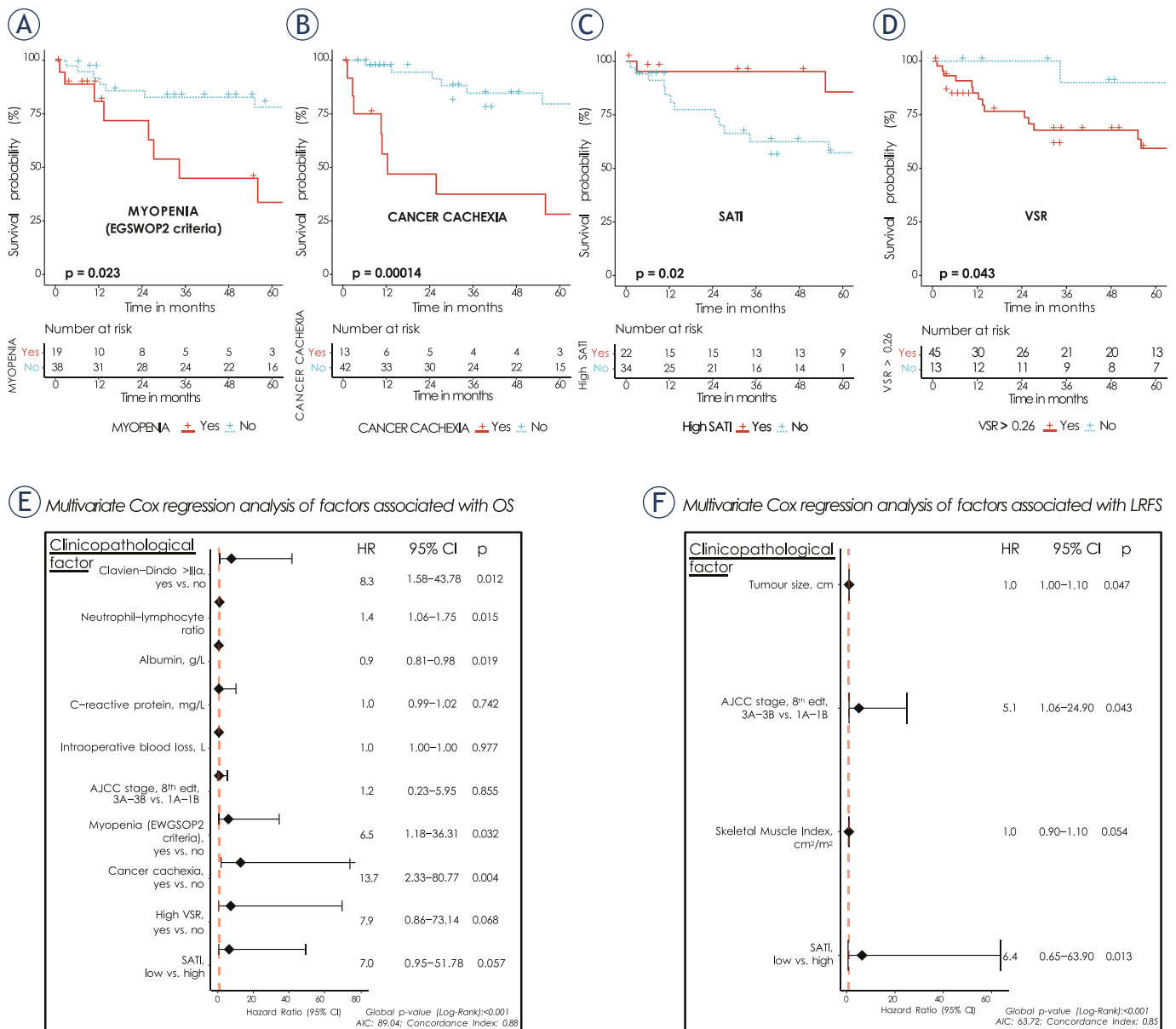


FIGURE 2. Kaplan-Meier curves for OS (A-D) and forest plots of multivariate Cox regression analysis of factors associated with OS (E) and LRFS (F). Kaplan-Meier curves for OS according to presence of: (A) myopenia based on EWGSOP2 criteria (red = myopenic, blue = non-myopenic), (B) cancer cachexia (red = cachectic, blue = non-cachectic), (C) high SATI (red = SATI above estimated cohort cut-off, blue = SATI below estimated cohort cut-off) and (D) high VSR (red = VSR > 0.26, blue = VSR < 0.26);

EWGSOP2 = The European Working Group on Sarcopenia in Older People revised criteria from 2018; SATI = Subcutaneous Adipose Tissue Index, cm²/m²; SMI = Skeletal Muscle Index; VSR = Visceral-to-subcutaneous adipose tissue area ratio; OS = Overall survival; LRFS = Local recurrence-free survival; HR = Hazard ratio; AIC = Akaike Information Criterion

and survival. Hosmer-Lemeshow test assessed the prediction accuracy (goodness of fit) of regression models. Hazard ratios (HRs) and 95% confidence intervals (CIs) were obtained.

In addition to body composition parameters, following known prognostic factors or other clinical features were considered: age, gender, American Society of Anesthesiologists (ASA) classification,

Albumin level (g/dL), C-reactive protein (mg/L), neutrophil-to-lymphocyte ratio (NLR), preoperative radiotherapy, tumour size (cm), and intraoperative blood loss (ml). Results were statistically significant if two-sided p value < 0.05 was achieved. R statistical software (version 4.2.1, R core Team) was used.

TABLE 3. Results of optimal stratification analysis for body composition parameters

BMI, kg/m ²	Skeletal Muscle Index ^a , cm ² /m ²		Visceral Adipose Tissue Index ^b , cm ² /m ²		Subcutaneous Adipose Tissue Index ^b , cm ² /m ²		Visceral to subcutaneous ratio ^c		Muscle Radiation Attenuation ^d , HU	
	Male	Female	Male	Female	Male	Female	Male	Female	Male	Female
< 25	49.21	49.21								47.41
≥ 25	49.90	50.64	61.38	25.55	49.23	86.89	0.26			35.88

BMI = body mass index; HU = Hounsfield Unit; ^a adjusted for gender and BMI; ^b adjusted for gender only; ^c cut-off determined on the level of whole cohort, not stratified for BMI nor gender; ^d adjusted for BMI only.

Results

Demographic and clinical characteristics

Out of 89 primary localized RPS cases, clinical and pathological characteristics and preoperative abdominal CT scans technically adequate for analysis were available for 58 patients, representing the final study cohort (Figure 1). The demographic and clinical characteristics of the patients are provided in Table 1. In the cohort, 34 (58.6%) were males and 24 (41.4%) were females. Median age at diagnosis was 61.0 (46.0–67.0). Loss of muscle mass according to EWGSOP2 criteria, was present in 19 patients (32.8%). Applying our cut-off values for low SMI, comparable number of myopenic patients was detected, 12 males (66.7%) and 6 females (33.33%). Significant difference between myopenic and non-myopenic group was detected in tumour size (median 26 *vs.* 17.5 cm, $p = 0.005$), SMA (median 115.8 *vs.* 149.9 cm², $p = 0.019$), SMI (median 41 *vs.* 53.5 cm²/m², $p < 0.001$), SATI (46.8 *vs.* 64.6 cm²/m², $p = 0.048$) and VATI (20.6 *vs.* 42.3 cm²/m², $p = 0.025$) (Table 2). There was no significant difference in clinical management among myopenic and non-myopenic group.

Males had significantly higher mean values of SMA (163.7 *vs.* 120 cm², $p < 0.001$), SMI (52.8 *vs.* 45.3 cm²/m², $p = 0.006$), VAT (153.9 *vs.* 96 cm², $p = 0.045$) and VSR (1.0 *vs.* 0.5, $p = 0.001$), while in females SAT (227.2 *vs.* 155.1 cm², $p = 0.003$) and SATI (85.0 *vs.* 49.8 cm²/m², $p = 0.001$) were significantly higher (Supplemental Table 1).

The results of optimal stratification analysis for finding cut-off values for SMI, VATI, SATI, VSR and MRA are presented in Table 3 and Supplemental Figures 1–4.

Survival analysis

Overall survival

In the cohort, median follow up time was 116 months, with 5-year OS of 66.8% (95% CI 53.9–82.7).

The result of univariate analysis of OS is presented in Supplemental Table 2. Of the nutritional and body composition features, myopenia (HR 3.18, 95% CI 1.11–8.56, $p = 0.020$), cancer cachexia (HR 6.07, 95% CI 2.24–16.46, $p < 0.001$), high VSR (HR 4.32, $p = 0.043$) and low SATI (HR 4.91, 95% CI 1.11–21.65, $p = 0.02$) were associated with elevated risk for overall mortality. SMI and BMI had small protective impact on OS in univariate analysis (HR 0.95, $p = 0.040$ and HR 0.83, $p = 0.036$, respectively). Of the known prognostic factors, preoperative levels of albumin, CRP, NLR, and AJCC stage were associated with OS. Major postoperative morbidity (CD > IIIa) was significantly correlated with shorter OS (HR 3.16, 95% CI, 1.24–8.04, $p = 0.016$). Multivariate analysis of OS confirmed the significance of myopenia (myopenic *vs.* non-myopenic: adjusted HR 6.5, $p = 0.032$), cancer cachexia (cachectic *vs.* non-cachectic: adjusted HR 13.7, $p = 0.004$) and high SATI (adjusted HR 7.00, $p = 0.057$). Major postoperative morbidity, NLR and albumin level also remained significant in multivariate OS analysis (Figure 2 A–E).

Local-recurrence free survival

The 5-year LRFS for whole study cohort was 77.6% (95% CI, 65.2–92). In univariate analysis among all body composition parameters, only SMI and SATI (low *vs.* high) showed association with LRFS (HR 0.94, 95% CI 0.88–1.00, $p = 0.052$ and HR 8.77, 95% CI 1.12–68.69, $p = 0.039$, respectively). Tumour size (HR 1.05, 95% CI 1.01–1.09, $p = 0.016$) and AJCC stage (3A–3B *vs.* 1A–1B, HR 4.46, 95% CI, 0.95–20.95, $p = 0.058$) were also associated with LRFS. However, SMI and SATI lost statistical significance in multivariate model, while tumour size and AJCC stage remained significant (Figure 2 F and Supplemental Table 2).

Postoperative outcome and morbidity

We performed univariate and multivariate risk factor analysis to evaluate factors associated with

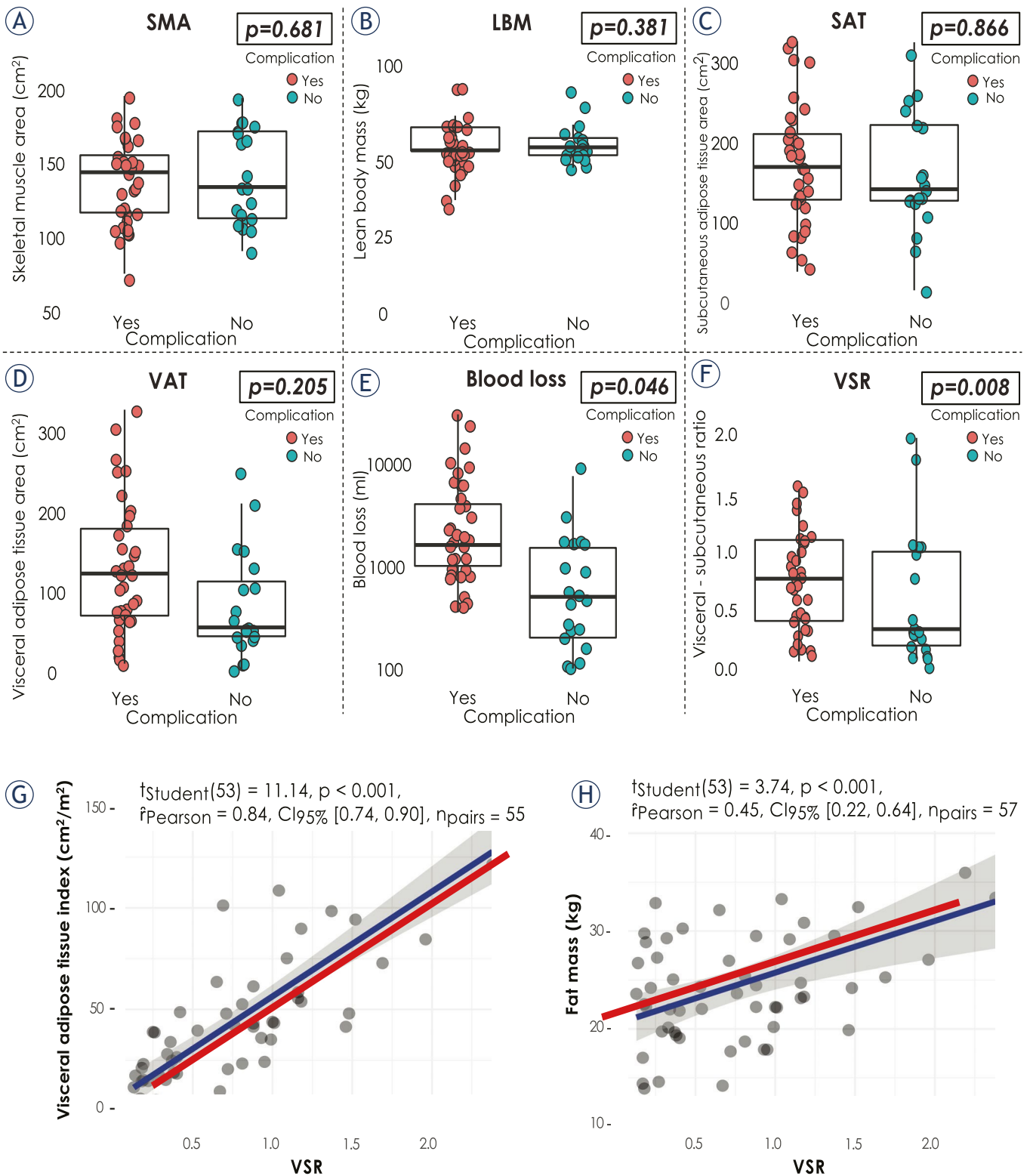


FIGURE 3. Association between overall morbidity following surgery for primary RPS and body composition (A-F) and linear correlation analysis between VSR and VATI (G) and VSR and fat mass (H). VSR (F) and intraoperative blood loss (E) independently predicted worse postoperative outcome. In multivariate analysis skeletal muscle index (SMA), lean body mass (LBM), subcutaneous adipose tissue area (SAT) and visceral adipose tissue area (VAT) were not associated with statistically higher overall postoperative morbidity (A-D).

VATI = Visceral Adipose Tissue Index; VSR = Visceral-to-subcutaneous adipose tissue area ratio. $r_{Pearson}$ = Pearson Correlation Coefficient; $t_{Student}$ = result of t-test for correlation

TABLE 4. Summary of univariate and multivariate analysis of association between body composition and outcome following surgery for primary RPS

Clinico-pathological factor	Length of hospital stay (> 10 days)				Clavien-Dindo > IIIa				Any complication (overall morbidity)			
	Uni-variable		Multi-variable		Uni-variable		Multi-variable		Uni-variable		Multi-variable	
	OR (95% CI)	P	OR (95% CI)	P	OR (95% CI)	P	OR (95% CI)	P	OR (95% CI)	P	OR (95% CI)	P
Myopenia, yes vs. no ^a	1.34 (0.38-5.54)	0.664	-	-	0.32 (0.07-1.18)	0.112	-	-	3.11 (0.85-15.08)	0.112	-	-
Visceral obesity, yes vs. no	2.54 (0.68-12.40)	0.196	-	-	0.65 (0.18-2.13)	0.49	-	-	3.61 (1.09-14.44)	0.047	-	-
Myopenic obesity, yes vs. no	0.01 (0.00-0.001)	0.993	-	-	20090605.83 (0.00-NA)	0.993	-	-	279.10 (0.00-NA)	0.993	-	-
Myosteatosis, yes vs. no	1.39 (0.39-5.76)	0.626	-	-	2.17 (0.58-10.58)	0.282	-	-	5.05 (1.39-24.41)	0.023	4.63 (1.03-28.42)	0.063
Cancer cachexia, yes vs. no	0.68 (0.18-2.94)	0.585	-	-	2.83 (0.76-10.59)	0.117	-	-	0.95 (0.27-3.60)	0.935	-	-
Body mass index, kg/m ²	1.00 (0.89-1.14)	0.992	-	-	0.94 (0.81-1.06)	0.351	-	-	0.95 (0.27-3.60)	0.935	-	-
Skeletal Muscle Area, HU	1.00 (0.99-1.02)	0.869	-	-	1.00 (0.98-1.01)	0.679	-	-	1.00 (0.99-1.02)	0.681	-	-
Skeletal Muscle Index, cm ² /m ²	1.00 (0.95-1.07)	0.88	-	-	1.00 (0.95-1.06)	0.909	-	-	1.04 (0.98-1.10)	0.230	-	-
Muscle Radiation Attenuation, HU	0.98 (0.92-1.04)	0.526	-	-	0.99 (0.93-1.05)	0.775	-	-	0.94 (0.88-1.00)	0.076	-	-
SAT, cm ²	1.00 (0.99-1.00)	0.336	-	-	1.00 (0.99-1.00)	0.48	-	-	1.00 (0.99-1.01)	0.866	-	-
VAT, cm ²	1.00 (1.00-1.01)	0.769	-	-	1.00 (0.99-1.00)	0.622	-	-	1.00 (1.00-1.01)	0.205	-	-
VSR	1.55 (0.53-5.51)	0.456	-	-	1.09 (0.39-2.861)	0.861	-	-	1.72 (0.66-5.19)	0.292	-	-
High VSR ^b , yes vs. no	2.50 (0.63-9.52)	0.179	-	-	2.75 (0.63-19.26)	0.224	-	-	6.19 (1.69-26.52)	0.008	5.05 (1.08-29.74)	0.05
Body fat, %	0.96 (0.87-1.05)	0.380	-	-	1.00 (0.92-1.09)	0.962	-	-	1.00 (0.93-1.09)	0.912	-	-
Lean Body Mass, kg	1.01 (0.96-1.07)	0.765	-	-	1.02 (0.97-1.08)	0.381	-	-	1.02 (0.97-1.08)	0.381	-	-
SATI, cm ² /m ²	0.99 (0.97-1.01)	0.279	-	-	0.99 (0.97-1.01)	0.344	-	-	1.00 (0.99-1.02)	0.794	-	-
VATI, cm ² /m ²	1.00 (0.99-1.02)	0.625	-	-	1.00 (0.98-1.01)	0.706	-	-	1.01 (1.00-1.04)	0.122	-	-
High SATI ^c , yes vs. no	1.80 (0.52-6.25)	0.346	-	-	0.90 (0.26-2.93)	0.863	-	-	1.50 (0.49-4.81)	0.481	-	-
High VATI ^d , yes vs. no	0.49 (0.10-1.87)	0.327	-	-	0.38 (0.08-1.44)	0.184	-	-	2.83 (0.84-11.45)	0.111	-	-

OR = Odds Ratio; SAT = Subcutaneous Adipose Tissue Area; SATI = Subcutaneous Adipose Tissue Index; VAT = Visceral Adipose Tissue Area; VATI = Visceral Adipose Tissue Index; VSR = Visceral-to-subcutaneous adipose tissue area ratio;

^a assessed by the European Working Group on Sarcopenia in Older People revised criteria from 2018; ^b defined as VSR > 0.26; ^c defined as SATI > 49.23 for males and SATI > 86.89 for females; ^d defined as VATI > 61.38 for males and VATI > 25.55 for females

Only significant variables (p < 0.05) were included in multivariate analysis.

postoperative morbidity, intrahospital length of stay (LOS) and major postoperative complications.

The median postoperative LOS was 18 days (IQR: 11.25–28.75). In univariate analysis, higher ASA grade (2–3 vs. 1, OR 5.56, p = 0.025) and tumour size (OR 1.12, p = 0.007) showed correlation with prolonged LOS. Preoperative CRP (OR 1.02, p = 0.007), resection status (R1–R2 vs. R0 OR 4.87, p = 0.046) and intraoperative blood loss (OR 1.10, p = 0.065) were associated with major postoperative morbidity (Table 4 and Supplementary Table 3).

In univariate analysis of overall postoperative morbidity, the presence of myosteatosis (OR 5.05, p = 0.023), VO (OR 3.61, p = 0.047) and high VSR (OR 6.19, p = 0.008) were associated with signifi-

cantly higher overall complication rate. Adjusted for other covariates in multivariate analysis, high VSR maintained significant impact (adjusted OR 5.05, p = 0.05). We omitted VO from multivariate analysis to avoid multicollinearity. Figure 3 (panels A–F) summarises our analysis of morbidity following surgery for primary RPS.

Discussion

Our study provided new insight into the association between preoperative body composition and postoperative and oncologic outcome in primary RPS patients. We focused on evaluation of the sig-

nificance of preoperative nutrition status-related syndromes. Furthermore, we examined the predictive value of SMI and MRA, measures of muscular quantity and quality, as well as, VATI, SATI and VSR, measures of adiposity, for possible clinical use in preoperative clinical assessment of patients diagnosed with this rare malignancy. To address the lack of literature and inconsistency in used body composition cut points, we used maximally selected rank statistics to defined cohort – specific cut point. This method incorporated follow-up time and time-to-event outcomes, dividing the patients into two groups with the most significant statistics between each other in term of survival.⁵⁶

In our cohort, both myopenia and VO were associated with poorer OS. Patients with myopenia had 5-year OS of 33.7%, compared to significantly higher 78.3% 5-year OS for non-myopenic patients ($p = 0.009$). SMI predicted LRFS on univariate analysis and lost prognostic value in multivariate analysis.

These findings are in line with knowledge that sarcopenic surgical oncology patients are at greater risk for poor operative outcome because of underlying muscle mass loss which is an integral component of sarcopenia and also facilitates the impairment of muscle function and physical performance.⁵⁷ Therefore we used the cut-off values for diagnosis of myopenia which are the component of diagnostic criteria and tools that define and characterize sarcopenia in EWGSOP2 Revised European Consensus.⁴⁸ Our optimal fitting method analysis for establishing the cut-off value for defining low SMI (used for comparative and descriptive purposes) resulted in slightly different cut-off values: SMI $< 49.21 \text{ cm}^2/\text{m}^2$ for males and females with BMI < 25 , and SMI $< 49.9 \text{ cm}^2/\text{m}^2$ for males with BMI ≥ 25 and SMI $< 50.64 \text{ cm}^2/\text{m}^2$ for females with BMI ≥ 25 . Both EWGSOP2 criteria for low SMI and our cut-off values were able to predict poor prognosis. It seems, that difference is generated because our cohort consisted of only patients with primary RPS with resectable disease rather than a heterogeneous cohort. We also found that SMI analysed as continuous variable was not able to predict poor outcome. This is another proof that in clinical practice SMI should be evaluated as body composition (myopenia) parameter defined with cut-off values below which the risk of poor prognosis is increased significantly, rather than discretionary decrease.⁵⁸

Several studies demonstrated the superior predictive value of myosteatosis to sarcopenia or myopenia for poor survival.⁵⁹⁻⁶¹ Most of this data is

founded on reports about patients operated on for gastrointestinal cancers. In our study cohort myosteatosis was also associated with greater overall complication rate (OR 5.05, 95% CI 1.39-24.41, $p = 0.023$) in univariate analysis, but it was not confirmed in multivariate analysis. Myosteatosis was not associated with OS, LRFS or postoperative outcome. However, recently a group of authors reported significant association between myosteatosis and major complication rate and OS in retroperitoneal and trunk soft tissue sarcoma.²⁹ They used preoperative MRA as continuous variable to define myosteatosis, not providing any cut-off point for reference. We defined myosteatosis based on optimal cut point analysis for MRA, and determined cut-offs are comparable to most commonly used range of MRA cut-offs for myosteatosis.⁶²

In order to evaluate obesity and the distribution of fat tissue, we calculated VAT, SAT and corresponding height-adjusted indexes VATI and SATI. We also considered BMI. Higher value of BMI (≥ 25) was not associated with oncologic or postoperative outcome. This is in line with number of studies suggesting that BMI is not reliable prognostic parameter for predicting perioperative outcome in cancer patients.⁶³⁻⁶⁵ Stratified for myopenia, comparison of the subgroups revealed that body fat and VATI were significantly higher in non-myopenic patients (median 31.1 *vs.* 28.1%, $p = 0.024$ and 42.3 *vs.* 20.6 cm^2/m^2 , $p = 0.025$, respectively) (Table 2). Further on, we used VAT to assess VO applying the ESPEN/EASO criteria.³⁹ VO predicted poorer OS and higher postoperative complication rate. VAT alone had no impact on OS or postoperative outcome. Recent study on soft tissue sarcoma patients reported identical findings.²⁹ We considered VSR into adiposity analysis defining subgroup of patients with normal and high VSR (> 0.26) based on optimal cut-off analysis. In multivariate analysis VSR was an independent predictor for overall complication rate following surgery. High VSR group experienced significantly more complications compared to normal VSR group (33 (89.2%) *vs.* 4 (10.8%), $p = 0.008$). These results are comparable with previous reports in which VSR was superior to VAT as independent risk factor for death and local recurrence.^{34,35,58,66,67} Linear regression analysis showed significant correlation between VSR and both VATI and fat mass (Figure 3 – panels G–H and Supplementary Figure 5), confirming the importance of balance between visceral and subcutaneous adipose tissue. Recent studies demonstrated that predictive values of VSR for cardiovascular and metabolic disease incidence is superior to

VAT.^{34,36,37,68} However, to our knowledge, only a few studies investigated the impact of VSR and VAT on survival and postoperative outcome in patients operated on for primary RPS.²⁹ Our study underlined that high VSR is not only superior to VAT but also to BMI in predicting poor oncologic and perioperative outcome. These findings suggest that VSR better estimates adipose tissue distribution and poses an additional difficulty for performing the surgery itself. High VSR is strong independent predictor for overall postoperative morbidity (multivariable-adjusted OR 5.05, $p = 0.05$). On the other hand, in the context of survival analysis, the multivariate regression model was not able to confirm the statistical significance of VSR ($p = 0.068$). This suggests that the impact of VSR on survival of RPS patients may be attenuated when considered alongside the broader set of predictors. One of the reasons may be the fact that, the presence of high VSR, as determined by specific gender-independent cut-off criteria, exhibited a statistically significant gender difference, with females having higher odds (OR = 4.5, $p = 0.027$) compared to males. Furthermore, we found a statistically significant difference in the distribution of SMI, between the two groups defined by VSR (high VSR *vs.* low VSR OR = 0.926, $p = 0.047$). Logistic regression model revealed significant association of SMI with a reduced odds of the specified outcome within the “high VSR” group. Based on our initial hypothesis that “high VSR” has a negative impact on survival, supported by univariate analysis, this implies that SMI (approximation of myopenia) may be a factor that mitigates the negative impact of “high VSR” on patient survival or serves as a positive influence, hence confounding the effect of VSR in multivariate settings. Further prospective studies need to be developed to confirm the importance of preoperative VSR for poor postoperative survival. In contrast to high VAT, low SATI, independently predicted poorer OS (adjusted HR 7.00, $p = 0.057$). Recent study reported similar protective effect of higher subcutaneous fat in RPS patients²⁹, which confirms the known benefits of SATI in processes of carcinogenesis and metabolism.^{30,69-71}

The multivariate analysis demonstrated that, when assessed as a continuous variable, albumin levels (HR 0.9, 95% CI 0.81–0.98, $p = 0.019$) and NLR (HR 1.4, 95% CI 1.06–1.75, $p = 0.015$) were independently associated with overall survival. This finding underscores the pivotal role of these inflammatory biomarkers in clinical practice and management of surgical oncology patients. Our results align with previous findings.^{17,18,72-77} Furthermore,

our observation suggests that hypoalbuminemia identifies a high-risk cohort that may derive greater benefits from enhanced nutritional support preoperatively. The omission of descriptive statistical analysis for serum albumin and NLR, in term of patients’ outcome, limits the depth of our data exploration.

Our study had some limitations. It was a single center report including relatively small number of patients which might influence the power of drawn conclusions. Another weakness was the fact that we didn’t assess all comorbidities in our analyses, as they were considered negligible in patients with soft tissue sarcoma. However, since our Institution is the only referral sarcoma center in Slovenia, having population of 2.1 million, our study cohort consisted of unique set of primary RPS patients eligible for curative surgery. We reported the most distinguishable, cohort – specific, cut points for CT measured body composition (muscle and adipose tissue) parameters in regard to long term prognosis. And finally, providing a unique and new insight into the association between preoperative body composition and postoperative and oncologic outcome in primary RPS patients was the main strength of the study.

Conclusions

Patients with primary RPS are in a great risk for nutritional disorders for number of reasons such as: requirement for demanding abdominal surgery in their management, long preclinical history and tumour size.^{4,10,18,78,79} In our study cohort there was a high prevalence of myopenia (32.8%) and visceral obesity (36.2%). Myopenia, cancer cachexia and low SATI were strongly associated with poor OS. High VSR was strong independent predictor for overall postoperative morbidity. Additional prospective studies are required to substantiate the role of preoperative VSR as independent prognostic factor for postoperative survival. Our findings suggest that clinical nutrition interventions towards improving visceral adiposity and myopenia may benefit surgical and oncologic outcome in primary RPS patients.

References

1. Van Tine BA. 90 - Sarcomas of soft tissue. In: Niederhuber JE, Armitage JO, Kastan MB, Doroshow JH, Tepper JE, editors. *Abeloff's clinical oncology* (Sixth Edition). Philadelphia: Elsevier; 2019. p. 1655-93.e11.

2. Stiller CA, Trama A, Serraino D, Rossi S, Navarro C, Chirilaque MD, et al. Descriptive epidemiology of sarcomas in Europe: report from the RARECARE project. *Eur J Cancer* 2013; **49**: 684-95. doi: 10.1016/j.ejca.2012.09.011
3. Gholami S, Jacobs CD, Kapp DS, Parast LM, Norton JA. The value of surgery for retroperitoneal sarcoma. *Sarcoma* 2009; **2009**: 605840. doi: 10.1155/2009/605840
4. Trans-Atlantic RPSWG. Management of primary retroperitoneal sarcoma (RPS) in the adult: a consensus approach from the Trans-Atlantic RPS Working Group. *Ann Surg Oncol* 2015; **22**: 256-63. doi: 10.1245/s10434-014-3965-2
5. Trans-Atlantic RPSWG. Erratum to: Management of recurrent retroperitoneal sarcoma (RPS) in the adult: a consensus approach from the Trans-Atlantic RPS Working Group. *Ann Surg Oncol* 2017; **24**: 688-9. doi: 10.1245/s10434-017-5889-0
6. Bonvalot S, Gronchi A, Le Pêcheux C, Swallow CJ, Strauss D, Meeus P, et al. Preoperative radiotherapy plus surgery versus surgery alone for patients with primary retroperitoneal sarcoma (EORTC-62092: STRASS): a multicentre, open-label, randomised, phase 3 trial. *Lancet Oncol* 2020; **21**: 1366-77. doi: 10.1016/s1470-2045(20)30446-0
7. Bonvalot S, Gronchi A, Le Pêcheux C, Swallow CJ, Strauss DC, Meeus P, et al. STRASS (EORTC 62092): a phase III randomized study of preoperative radiotherapy plus surgery versus surgery alone for patients with retroperitoneal sarcoma. [abstract]. *J Clin Oncol* 2019; **37(15 Suppl)**: 11001. doi: 10.1200/JCO.2019.37.15_suppl.11001
8. Callegaro D, Raut CP, Ajayi T, Strauss D, Bonvalot S, Ng D, et al. Preoperative radiotherapy in patients with primary retroperitoneal sarcoma: EORTC-62092 Trial (STRASS) versus off-trial (STREXIT) results. *Ann Surg* 2023; **278**: 127-34. doi: 10.1097/sla.0000000000005492
9. Bonvalot S, Raut CP, Pollock RE, Rutkowski P, Strauss DC, Hayes AJ, et al. Technical considerations in surgery for retroperitoneal sarcomas: position paper from E-Surge, a master class in sarcoma surgery, and EORTC-STBSG. *Ann Surg Oncol* 2012; **19**: 2981-91. doi: 10.1245/s10434-012-2342-2
10. Bonvalot S, Rivoire M, Castaing M, Stoeckle E, Le Cesne A, Blay JY, et al. Primary retroperitoneal sarcomas: a multivariate analysis of surgical factors associated with local control. *J Clin Oncol* 2009; **27**: 31-7. doi: 10.1200/jco.2008.18.0802
11. Gutierrez JC, Perez EA, Moffat FL, Livingstone AS, Franceschi D, Koniaris LG. Should soft tissue sarcomas be treated at high-volume centers? An analysis of 4205 patients. *Ann Surg* 2007; **245**: 952-8. doi: 10.1097/01.sla.0000250438.04393.a8
12. van Dalen T, Hennipman A, Van Coevorden F, Hoekstra HJ, van Geel BN, Slootweg P, et al. Evaluation of a clinically applicable post-surgical classification system for primary retroperitoneal soft-tissue sarcoma. *Ann Surg Oncol* 2004; **11**: 483-90. doi: 10.1245/aso.2004.09.005
13. Andritsch E, Beishon M, Bielack S, Bonvalot S, Casali P, Crul M, et al. EOCO Essential Requirements for Quality Cancer Care: soft tissue sarcoma in adults and bone sarcoma. A critical review. *Crit Rev Oncol Hematol* 2017; **110**: 94-105. doi: 10.1016/j.critrevonc.2016.12.002
14. Novak M, Perhavec A, Povšič M, Arnuš M, Eržen D. Primary localized retroperitoneal sarcomas: report from Slovenian sarcoma referral center. *World J Surg Oncol* 2020; **18**: 277. doi: 10.1186/s12957-020-02038-9
15. Balderas-Pena LM, Gonzalez-Barba F, Martinez-Herrera BE, Palomares-Chacon UR, Duran-Anguiano O, Salazar-Paramo M, et al. Body composition and biochemical parameters of nutritional status: correlation with health-related quality of life in patients with colorectal cancer. *Nutrients* 2020; **12**: 2110. doi: 10.3390/nu12072110
16. Arends J, Baracos V, Bertz H, Bozzetti F, Calder PC, Deutz NEP, et al. ESPEN expert group recommendations for action against cancer-related malnutrition. *Clin Nutr* 2017; **36**: 1187-96. doi: 10.1016/j.clnu.2017.06.017
17. Kirov KM, Xu HP, Crenn P, Goater P, Tzani D, Bouhadiba MT, et al. Role of nutritional status in the early postoperative prognosis of patients operated for retroperitoneal liposarcoma (RLS): a single center experience. *Eur J Surg Oncol* 2019; **45**: 261-7. doi: 10.1016/j.ejso.2018.07.001
18. Previtali P, Fiore M, Colombo J, Arendar I, Fumagalli L, Pizzocri M, et al. Malnutrition and perioperative nutritional support in retroperitoneal sarcoma patients: results from a prospective study. *Ann Surg Oncol* 2020; **27**: 2025-32. doi: 10.1245/s10434-019-08121-0
19. Nipp RD, Fuchs G, El-Jawahri A, Mario J, Troschel FM, Greer JA, et al. Sarcopenia is associated with quality of life and depression in patients with advanced cancer. *Oncologist* 2018; **23**: 97-104. doi: 10.1634/theoncologist.2017-0255
20. Chen LK, Lee WJ, Peng LN, Liu LK, Arai H, Akishita M. Recent advances in sarcopenia research in Asia: 2016 update from the Asian Working Group for Sarcopenia. *J Am Med Dir Assoc* 2016; **17**: 767.e1-7. doi: 10.1016/j.jamda.2016.05.016
21. Czigany Z, Kramp W, Bednarsch J, van der Kroft G, Boecker J, Strnad P, et al. Myosteatosis to predict inferior perioperative outcome in patients undergoing orthotopic liver transplantation. *Am J Transplant* 2020; **20**: 493-503. doi: 10.1111/ajt.15577
22. Aro R, Mäkäräinen-Uhlbäck E, Ämmälä N, Rautio T, Ohtonen P, Saarnio J, et al. The impact of sarcopenia and myosteatosis on postoperative outcomes and 5-year survival in curatively operated colorectal cancer patients – a retrospective register study. *Eur J Surg Oncol* 2020; **46**: 1656-62. doi: 10.1016/j.ejso.2020.03.206
23. Rier HN, Jager A, Sleijfer S, Maier AB, Levin MD. The prevalence and prognostic value of low muscle mass in cancer patients: a review of the literature. *Oncologist* 2016; **21**: 1396-409. doi: 10.1634/theoncologist.2016-0066
24. Deng CY, Lin YC, Wu JS, Cheung YC, Fan CW, Yeh KY, et al. Progressive sarcopenia in patients with colorectal cancer predicts survival. *AJR Am J Roentgenol* 2018; **210**: 526-32. doi: 10.2214/ajr.17.18020
25. Jung AR, Roh JL, Kim JS, Kim SB, Choi SH, Nam SY, et al. Prognostic value of body composition on recurrence and survival of advanced-stage head and neck cancer. *Eur J Cancer* 2019; **116**: 98-106. doi: 10.1016/j.ejca.2019.05.006
26. Prado CM, Lieffers JR, McCargar LJ, Reiman T, Sawyer MB, Martin L, et al. Prevalence and clinical implications of sarcopenic obesity in patients with solid tumours of the respiratory and gastrointestinal tracts: a population-based study. *Lancet Oncol* 2008; **9**: 629-35. doi: 10.1016/S1470-2045(08)70153-0
27. Strassmann D, Hensen B, Grünwald V, Stange K, Eggers H, Länger F, et al. Impact of sarcopenia in advanced and metastatic soft tissue sarcoma. *Int J Clin Oncol* 2021; **26**: 2151-60. doi: 10.1007/s10147-021-01997-7
28. Bays H. Central obesity as a clinical marker of adiposopathy; increased visceral adiposity as a surrogate marker for global fat dysfunction. *Curr Opin Endocrinol Diabetes Obes* 2014; **21**: 345-51. doi: 10.1097/med.0000000000000093
29. Boyle EA, Elliott JA, McIntyre TV, Barnes ME, Donlon NE, Umair M, et al. Body composition is associated with operative and oncologic outcomes in the management of retroperitoneal and trunk soft tissue sarcoma. *Am J Surg* 2022; **223**: 729-37. doi: 10.1016/j.amjsurg.2021.08.005
30. O'Sullivan J, Lysaght J, Donohoe CL, Reynolds JV. Obesity and gastrointestinal cancer: the interrelationship of adipose and tumour microenvironments. *Nat Rev Gastroenterol Hepatol* 2018; **15**: 699-714. doi: 10.1038/s41575-018-0069-7
31. Shirazipour CH, Freedland SJ. Obesity, visceral adiposity, and prostate cancer: what is the role of lifestyle interventions? *Cancer* 2019; **125**: 2730-1. doi: 10.1002/cncr.32165
32. Bastrup NN, Christensen JK, Jensen KK, Jørgensen LN. Visceral obesity and short-term outcomes after laparoscopic rectal cancer resection. *Surg Endosc* 2020; **34**: 177-85. doi: 10.1007/s00464-019-06748-4
33. Silveira EA, Kliemann N, Noll M, Sarrafzadegan N, de Oliveira C. Visceral obesity and incident cancer and cardiovascular disease: an integrative review of the epidemiological evidence. *Obes Rev* 2021; **22**: e13088. doi: 10.1111/obr.13088
34. Hamaguchi Y, Kaido T, Okumura S, Kobayashi A, Shirai H, Yagi S, et al. Impact of skeletal muscle mass index, intramuscular adipose tissue content, and visceral to subcutaneous adipose tissue area ratio on early mortality of living donor liver transplantation. *Transplantation* 2017; **101**: 565-74. doi: 10.1097/tp.0000000000001587
35. Okamura A, Watanabe M, Mine S, Nishida K, Imamura Y, Kuroguchi T, et al. Clinical impact of abdominal fat distribution on prognosis after esophagectomy for esophageal squamous cell carcinoma. *Ann Surg Oncol* 2016; **23**: 1387-94. doi: 10.1245/s10434-015-5018-x

36. Hamaguchi Y, Kaido T, Okumura S, Kobayashi A, Shirai H, Yao S, et al. Preoperative visceral adiposity and muscularity predict poor outcomes after hepatectomy for hepatocellular carcinoma. *Liver Cancer* 2019; **8**: 92-109. doi: 10.1159/000488779
37. Grignol VP, Smith AD, Shlapak D, Zhang X, Del Campo SM, Carson WE. Increased visceral to subcutaneous fat ratio is associated with decreased overall survival in patients with metastatic melanoma receiving anti-angiogenic therapy. *Surg Oncol* 2015; **24**: 353-8. doi: 10.1016/j.suronc.2015.09.002
38. Baracos VE, Arribas L. Sarcopenic obesity: hidden muscle wasting and its impact for survival and complications of cancer therapy. *Ann Oncol* 2018; **29**: ii1-9. doi: 10.1093/annonc/mdx810
39. Donini LM, Busetto L, Bischoff SC, Cederholm T, Ballesteros-Pomar MD, Batsis JA, et al. Definition and diagnostic criteria for sarcopenic obesity: ESPEN and EASO consensus statement. *Clin Nutr* 2022; **41**: 990-1000. doi: 10.1016/j.clnu.2021.11.014
40. Vehmas T, Kairemo KJ, Taavitsainen MJ. Measuring visceral adipose tissue content from contrast enhanced computed tomography. *Int J Obes Relat Metab Disord* 1996; **20**: 570-3. PMID: 8782734
41. Mitsiopoulos N, Baumgartner RN, Heymsfield SB, Lyons W, Gallagher D, Ross R. Cadaver validation of skeletal muscle measurement by magnetic resonance imaging and computerized tomography. *J Appl Physiol* 1998; **85**: 115-22. doi: 10.1152/jappl.1998.85.1.115
42. Maurovich-Horvat P, Massaro J, Fox CS, Moselewski F, O'Donnell CJ, Hoffmann U. Comparison of anthropometric, area- and volume-based assessment of abdominal subcutaneous and visceral adipose tissue volumes using multi-detector computed tomography. *Int J Obes* 2007; **31**: 500-6. doi: 10.1038/sj.ijo.0803454
43. Mourtzakis M, Prado CM, Lieffers JR, Reiman T, McCargar LJ, Baracos VE. A practical and precise approach to quantification of body composition in cancer patients using computed tomography images acquired during routine care. *Appl Physiol Nutr Metab* 2008; **33**: 997-1006. doi: 10.1139/H08-075
44. Dindo D, Demartines N, Clavien PA. Classification of surgical complications: a new proposal with evaluation in a cohort of 6336 patients and results of a survey. *Ann Surg* 2004; **240**: 205-13. doi: 10.1097/01.sla.0000133083.54934.ae
45. Trojani M, Contesso G, Coindre JM, Rouesse J, Bui NB, de Mascarel A, et al. Soft-tissue sarcomas of adults; study of pathological prognostic variables and definition of a histopathological grading system. *Int J Cancer* 1984; **33**: 37-42. doi: 10.1002/ijc.2910330108
46. Popuri K, Cobzas D, Esfandiari N, Baracos V, Jägersand M. Body composition assessment in axial CT images using FEM-based automatic segmentation of skeletal muscle. *IEEE Trans Med Imaging* 2016; **35**: 512-20. doi: 10.1109/tmi.2015.2479252
47. Doyle SL, Bennett AM, Donohoe CL, Mongan AM, Howard JM, Lithander FE, et al. Establishing computed tomography – defined visceral fat area thresholds for use in obesity – related cancer research. *Nutr Res* 2013; **33**: 171-9. doi: 10.1016/j.nutres.2012.12.007
48. Cruz-Jentoft AJ, Bahat G, Bauer J, Boirie Y, Bruyere O, Cederholm T, et al. Sarcopenia: revised European consensus on definition and diagnosis. *Age Ageing* 2019; **48**: 601. doi: 10.1093/ageing/afz046
49. Fearon K, Strasser F, Anker SD, Bosaeus I, Bruera E, Fainsinger RL, et al. Definition and classification of cancer cachexia: an international consensus. *Lancet Oncol* 2011; **12**: 489-95. doi: 10.1016/s1470-2045(10)70218-7
50. Contal C, O'Quigley J. An application of changepoint methods in studying the effect of age on survival in breast cancer. *Comput Stat Data Anal* 1999; **30**: 253-70. doi: 10.1016/S0167-9473(98)00096-6
51. Caan BJ, Meyerhardt JA, Kroenke CH, Alexeeff S, Xiao J, Weltzien E, et al. Explaining the obesity paradox: the association between body composition and colorectal cancer survival (C-SCANS Study). *Cancer Epidemiol Biomarkers Prev* 2017; **26**: 1008-15. doi: 10.1158/1055-9965.Epi-17-0200
52. Hassen W, Kassambara A, Reme T, Sahota S, Seckinger A, Vincent L, et al. Drug metabolism and clearance system in tumor cells of patients with multiple myeloma. *Oncotarget* 2015; **6**: 6431-47. doi: 10.18632/oncotarget.3237
53. Kassambara A, Gourzones-Dmitriev C, Sahota S, Reme T, Moreaux J, Goldschmidt H, et al. A DNA repair pathway score predicts survival in human multiple myeloma: the potential for therapeutic strategy. *Oncotarget* 2014; **5**: 2487-98. doi: 10.18632/oncotarget.1740
54. He WZ, Jiang C, Liu LL, Yin CX, Rong YM, Hu WM, et al. Association of body composition with survival and inflammatory responses in patients with non-metastatic nasopharyngeal cancer. *Oral Oncology* 2020; **108**: 104771. doi: 10.1016/j.oraloncology.2020.104771
55. Caan BJ, Feliciano EMC, Prado CM, Alexeeff S, Kroenke CH, Bradshaw P, et al. Association of muscle and adiposity measured by computed tomography with survival in patients with nonmetastatic breast cancer. *JAMA Oncol* 2018; **4**: 798-804. doi: 10.1001/jamaoncol.2018.0137
56. Lausen B, Schumacher M. Maximally selected rank statistics. *Biometrics* 1992; **48**: 73-85. doi: 10.2307/2532740
57. Cederholm T, Barazzoni R, Austin P, Ballmer P, Biolo G, Bischoff SC, et al. ESPEN guidelines on definitions and terminology of clinical nutrition. *Clin Nutr* 2017; **36**: 49-64. doi: 10.1016/j.clnu.2016.09.004
58. Fujiwara N, Nakagawa H, Kudo Y, Tateishi R, Taguri M, Watadani T, et al. Sarcopenia, intramuscular fat deposition, and visceral adiposity independently predict the outcomes of hepatocellular carcinoma. *J Hepatol* 2015; **63**: 131-40. doi: 10.1016/j.jhep.2015.02.031
59. McSorley ST, Black DH, Horgan PG, McMillan DC. The relationship between tumour stage, systemic inflammation, body composition and survival in patients with colorectal cancer. *Clin Nutr* 2018; **37**: 1279-85. doi: 10.1016/j.clnu.2017.05.017
60. Martin L, Birdsell L, MacDonald N, Reiman T, Clandinin MT, McCargar LJ, et al. Cancer cachexia in the age of obesity: skeletal muscle depletion is a powerful prognostic factor, independent of body mass index. *J Clin Oncol* 2013; **31**: 1539-47. doi: 10.1200/jco.2012.45.2722
61. Srpcic M, Jordan T, Popuri K, Sok M. Sarcopenia and myosteatosis at presentation adversely affect survival after esophagectomy for esophageal cancer. *Radiol Oncol* 2020; **54**: 237-46. doi: 10.2478/raon-2020-0016
62. Aleixo GFP, Shachar SS, Nyrop KA, Muss HB, Malpica L, Williams GR. Myosteatosis and prognosis in cancer: systematic review and meta-analysis. *Crit Rev Oncol Hematol* 2020; **145**: 102839. doi: 10.1016/j.critrevonc.2019.102839
63. Prentice AM, Jebb SA. Beyond body mass index. *Obes Rev* 2001; **2**: 141-7. doi: 10.1046/j.1467-789x.2001.00031.x
64. Kobayashi A, Kaido T, Hamaguchi Y, Okumura S, Shirai H, Kamo N, et al. Impact of visceral adiposity as well as sarcopenic factors on outcomes in patients undergoing liver resection for colorectal liver metastases. *World J Surg* 2018; **42**: 1180-91. doi: 10.1007/s00268-017-4255-5
65. Rickles AS, Iannuzzi JC, Mironov O, Deeb AP, Sharma A, Fleming FJ, et al. Visceral obesity and colorectal cancer: are we missing the boat with BMI? *J Gastrointest Surg* 2013; **17**: 133-43; discussion p.43. doi: 10.1007/s11605-012-2045-9
66. Smith AD, Gray MR, del Campo SM, Shlapak D, Ganeshan B, Zhang X, et al. Predicting overall survival in patients with metastatic melanoma on antiangiogenic therapy and RECIST stable disease on initial posttherapy images using CT texture analysis. *AJR Am J Roentgenol* 2015; **205**: W283-93. doi: 10.2214/ajr.15.14315
67. Okumura S, Kaido T, Hamaguchi Y, Fujimoto Y, Masui T, Mizumoto M, et al. Impact of preoperative quality as well as quantity of skeletal muscle on survival after resection of pancreatic cancer. *Surgery* 2015; **157**: 1088-98. doi: 10.1016/j.surg.2015.02.002
68. He AQ, Li CQ, Zhang Q, Liu T, Liu J, Liu G. Visceral-to-subcutaneous fat ratio is a potential predictor of postoperative complications in colorectal cancer. *Med Sci Monit* 2021; **27**: e930329. doi: 10.12659/msm.930329
69. Tran TT, Yamamoto Y, Gesta S, Kahn CR. Beneficial effects of subcutaneous fat transplantation on metabolism. *Cell Metab* 2008; **7**: 410-20. doi: 10.1016/j.cmet.2008.04.004
70. Ebadi M, Martin L, Ghosh S, Field CJ, Lehner R, Baracos VE, et al. Subcutaneous adiposity is an independent predictor of mortality in cancer patients. *Br J Cancer* 2017; **117**: 148-55. doi: 10.1038/bjc.2017.149
71. Ebadi M, Baracos VE, Bathe OF, Robinson LE, Mazurak VC. Loss of visceral adipose tissue precedes subcutaneous adipose tissue and associates with n-6 fatty acid content. *Clin Nutr* 2016; **35**: 1347-53. doi: 10.1016/j.clnu.2016.02.014
72. Di Prata C, Renouf B, Tzanis D, Bouhadiba T, Watson S, Zein SE, et al. Significant predictors of postoperative morbidity after radical resection of retroperitoneal sarcoma in a tertiary center. *Ann Surg Oncol* 2023; **30**: 4515-26. doi: 10.1245/s10434-023-13459-7

73. Nasirishargh A, Grova M, Bateni CP, Judge SJ, Nuno MA, Basmaci UN, et al. Sarcopenia and frailty as predictors of surgical morbidity and oncologic outcomes in retroperitoneal sarcoma. *J Surg Oncol* 2023; **127**: 855-61. doi: 10.1002/jso.27199
74. Choi ES, Kim HS, Han I. Elevated preoperative systemic inflammatory markers predict poor outcome in localized soft tissue sarcoma. *Ann Surg Oncol* 2014; **21**: 778-85. doi: 10.1245/s10434-013-3418-3
75. Fiore M, Ljevar S, Pasquali S, Morelli D, Callegaro D, Sanfilippo R, et al. Preoperative neutrophil-to-lymphocyte ratio and a new inflammatory biomarkers prognostic index for primary retroperitoneal sarcomas: retrospective monocentric study. *Clin Cancer Res* 2023; **29**: 614-20. doi: 10.1158/1078-0432.CCR-22-2897
76. Schwartz PB, Poultsides G, Roggin K, Howard JH, Fields RC, Clarke CN, et al. PLR and NLR are poor predictors of survival outcomes in sarcomas: a new perspective from the USSC. *J Surg Res* 2020; **251**: 228-38. doi: 10.1016/j.jss.2020.01.008
77. Netanyahu Y, Gerstenhaber F, Shamai S, Sher O, Merimsky O, Klausner JM, et al. Innate inflammatory markers for predicting survival in retroperitoneal sarcoma. *J Surg Oncol* 2020; **122**: 1655-61. doi: 10.1002/jso.26178
78. Swallow CJ, Strauss DC, Bonvalot S, Rutkowski P, Desai A, Gladdy RA, et al. Management of primary retroperitoneal sarcoma (RPS) in the adult: an updated consensus approach from the transatlantic australasian RPS Working Group. *Ann Surg Oncol* 2021; **28**: 7873-88. doi: 10.1245/s10434-021-09654-z
79. Fearon KC, Luff R. The nutritional management of surgical patients: enhanced recovery after surgery. *Proc Nutr Soc* 2003; **62**: 807-11. doi: 10.1079/PNS2003299

A retrospective study on improving the accuracy of radiotherapy for patients with breast cancer with lymph node metastasis using Styrofoam

Jie Li, Lin Yang, Xiaowei Yao, Linlin Xu, Lina Zhao, Fei Bai

Department of Radiation Oncology, Xijing Hospital, Fourth Military Medical University, Xi'an, China

Radiol Oncol 2024; 58(1): 124-132.

Received 16 May 2023

Accepted 15 August 2023

Correspondence to: Dr. Fei Bai, Department of Radiation Oncology, Xijing Hospital, Fourth Military Medical University, 127 West Changle Road, Xi'an, Shaanxi, China. E-mail: baifei0912@163.com. and Dr. Lina Zhao, Department of Radiation Oncology, Xijing Hospital, Air Force Medical University, 127 West Changle Road, Xi'an, Shaanxi, China. E-mail: zhaolina@fmmu.edu.cn

Jie Li and Lin Yang are contributed equally to this work.

Disclosure: No potential conflicts of interest were disclosed.

This is an open access article distributed under the terms of the CC-BY license (<https://creativecommons.org/licenses/by/4.0/>).

Background. To retrospectively analyze the accuracy of radiotherapy using cone beam computed tomography (CBCT), Styrofoam fixation, and breast bracket fixation in the chest wall target area and supraclavicular lymphatic drainage area (supraclavicular target area) of patients with breast cancer and compare the setting efficiency and comfort satisfaction.

Patients and methods. A total of 65 patients with postoperative lymphatic metastasis of breast cancer, including 36 cases of Styrofoam fixation and 29 cases of breast bracket fixation, were recruited from March 2021 to August 2022 and retrospectively analyzed. All the patients underwent CBCT scans weekly, and the setup errors of the chest wall and supraclavicular target volume were compared and recorded. The planning target volume (PTV) margins of the two groups were calculated using the correlation $M_{PTV} = 2.5\sigma + 0.7\sigma$. The setup time and comfort satisfaction scores of the two groups were recorded and analyzed. The correlations among errors in each direction were analyzed using the Pearson correlation analysis.

Results. There was a significant difference in the left-right direction (X) axis of the chest wall target area between the Styrofoam and breast bracket groups (1.59 ± 1.47 mm vs. 2.05 ± 1.64 mm, $P = 0.012$). There were statistical differences in the ventrodorsal direction (Z) and bed angle of the supraclavicular target area, the data were (1.36 ± 1.27 mm vs. 1.75 ± 1.55 mm, $P = 0.046$; $0.47 \pm 0.47^\circ$ vs. $0.66 \pm 0.59^\circ$, $P = 0.006$, respectively). In the X, Y, and Z directions, the respective PTV margins of the two groups in the chest wall target area were 5.01 mm, 5.99 mm, and 5.47 mm in the Styrofoam group, while those in the breast bracket group were 6.10 mm, 6.34 mm, and 6.10 mm, respectively. Moreover, the PTV margins of the supraclavicular target in the three directions were 3.69 mm, 3.86 mm, and 4.28 mm in the Styrofoam group, while those in the breast bracket group were 3.99 mm, 3.72 mm, and 5.45 mm, respectively. The setup time of the two groups was 3.4 ± 1.1 min and 5.5 ± 3.1 min ($P = 0.007$). The subjective comfort satisfaction scores of the two groups were 27.50 ± 1.24 and 25.44 ± 1.23 ($P < 0.001$).

Conclusions. The application of Styrofoam fixation in radiotherapy of breast cancer in the supraclavicular lymph node area has several advantages as compared to breast bracket fixation, including higher positioning accuracy, smaller external expansion boundary, improved work efficiency, and patients' comfort, which might provide a reference for clinical work.

Key words: breast cancer; Styrofoam; setup error; planning target volume

Introduction

Since the 21st century, the incidence and mortality rates of female breast cancer have shown an overall increasing trend. In 2020, the rate of female breast cancer reached the top of the global cancer incidence spectrum and global female cancer death spectrum.¹ In China, a total of 420,000 new breast cancer cases have been reported in 2020.² Breast cancer is treated by a combination of different treatment strategies, including surgery, radiation therapy, chemotherapy, and endocrine therapy. The 10-year local recurrence rate in axillary node-positive patients is 46%, which can be decreased to 13% with postoperative radiotherapy.³ The intensity-modulated radiation therapy (IMRT) and cone-beam computed tomography (CBCT) have shown significant improvements with the advancements in radiotherapy technology. IMRT can achieve arbitrary dose distribution for breast cancer and improve dose uniformity of the irradiated area.^{4,5} Using imaging, the CBCT technology can guide radiation to accurately irradiate within the target area of the breast tissues.⁶

In breast cancer radiotherapy, the lungs and heart are the main organs at risk (OARs). Reducing the dose to these organs can reduce the radiation-induced long-term cardiovascular and lung damage.^{7,8} Accurate setup is one of the methods to reduce the exposure dose to OARs under the premise of advanced radiotherapy technology and Radiation Therapy Oncology Group (RTOG) guidelines. The accuracy of setup can be improved by selecting the professional level of therapists along with the optimization of position selection and position fixation mode during radiotherapy. The role of the therapists becomes increasingly important in this dynamic environment.⁹ Zhou *et al.*¹⁰ showed that fixation of the chest wall with a vacuum bag required CTV-PTV margins (PTV margin) of 12, 12.37, and 14.25 mm in X, Y, and Z directions, respectively, while 10.71 mm, 10.91 mm, and 13.87 mm margins were required for the supraclavicular target area. Dong *et al.*¹¹ found that when the fixation device with arm support was used, the PTV margins of 8.14 mm, 10.89 mm, and 6.29 mm were required in X, Y, and Z directions, respectively, while in the case of using cervicothoracic thermoplastic membrane combined with arm support, the PTV margins of 8.01 mm, 5.44 mm, and 5.45 mm were required in X, Y, and Z directions, respectively. Svestad *et al.*¹² positioned patients with breast cancer using WingSTEP™ and found that the patients needed margins of 5 mm, 10 mm, and 8 mm

in the three directions. Mulliez *et al.*¹³ compared two positioning systems, including Positrest-2 system (Civco Medical Solutions, Orange City, Ia, USA) in a supine position and AIO prone breast system (AIO Solution, Orfit Industries, Wijnegem, Belgium) in a prone position. The results showed that 9.4 mm, 9.4 mm, and 10.4 mm margins were required in the three directions for patients in a supine position, while 22.4 mm, 13.7 mm, and 10.5 mm margins were required in a prone position. It could be seen that the standard PTV margin of 5 mm in the chest wall target area in a fixed position was insufficient both in the supine and prone position under the existing vacuum bag, arm support, and cervicothoracic thermoplastic membrane fixation mode. Similar results were also observed for the supraclavicular lymphatic drainage area (supraclavicular target area). The repeatability of the neck and arm directly affects the accuracy of supraclavicular target irradiation as well as effects of radiotherapy. Currently, there are limited studies on supraclavicular target setup errors in breast cancer radiotherapy with a smaller sample size as compared to the chest wall, and the setup error of the conventional fixed method is larger. Therefore, it is necessary to develop and explore good repeatability of the fixation device. Styrofoam fixation (registered name: Body Positioning Mats, Guangzhou Fury, China) has the advantages of individualization and high comfort, and it has been confirmed in other tumor radiotherapy position fixation.^{14,15} Therefore, the current study focused on investigating the repeatability of the supraclavicular target irradiation setup of Styrofoam in patients with breast cancer.

This study retrospectively analyzed the setup error of each target volume in breast cancer radiotherapy fixed by Styrofoam glue using CBCT and compared it with the fixation device with arm support (Abbreviation: breast bracket). The setup repeatability and PTV margin of the two fixation devices were also compared. The current study also provided a reference basis for the fixation device with good repeatability for breast cancer radiotherapy target areas, including the supraclavicular lymphatic drainage area.

Patients and methods

Case selection

This was a single-institution retrospective study, which was approved by the institutional ethics committee (KY0202002-F-1). The study included



FIGURE 1. Making process of Styrofoam. (A) Glue. (B) Bags. (C) Unformed Styrofoam. (D) Making of molded Styrofoam (Individualized head fixation as well as arm fixation as shown in the red circle)

the patients, receiving IMRT radiotherapy after breast cancer surgery between March 2021 and August 2022. The inclusion criteria included (1) patients with breast cancer confirmed by pathology, (2) patients with postoperative radiotherapy tar-

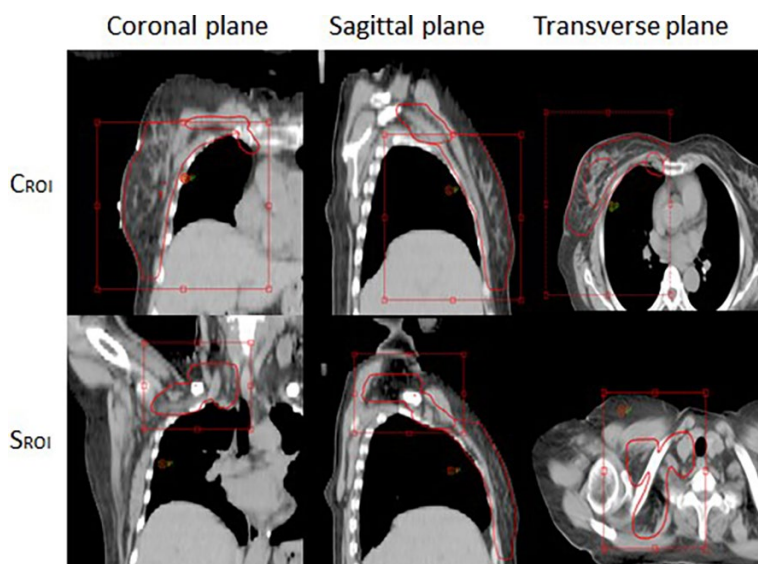


FIGURE 2. ROI Matching.

CROI = chest wall target; SROI = supraclavicular target

get, including supraclavicular lymphatic drainage area, (3) patients with good abduction and upper limb lifting function of the affected side, and (4) patients with KPS (Karnofsky) score greater than 80. The exclusion criteria were as follows: (1) the patients receiving chest wall radiotherapy only, (2) the patients with difficulty in upper arm support and unable to meet fixation, and (3) the patients who were unwilling or unable to complete the whole study process.

Patients' CT positioning and treatment plan formulation

According to the fixation mode (due to the introduction of Styrofoam postural fixation of breast cancer in routine practice in 2022, the previous fixation was terminated), the selected patients were divided into two groups, including the breast bracket and Styrofoam glue groups. The production process of Styrofoam is shown in Figure 1. In both groups, the mandible of the participants was raised as much as possible, their heads were inclined to the healthy side by 15 degrees, and their arms were raised naturally. The 16-slice large-aperture spiral Computer Tomography (CT) was used to simulate localization in the two groups. The scanning range was 5 cm from submandibular to subdiaphragmatic with a slice thickness and interval of 5 mm. The scanned images were sent to the doctor's workstation system, and the radiotherapist delineated the target area in the CT positioning image combined with other image data based on the RTOG standard, limited the surrounding organs at risk, and formulated a target dose. The CTV was enlarged to 5 mm to form a PTV. The sketched images were sent to the radiotherapy treatment planning system (TPS), and the radiotherapy plan was prepared by the radiotherapy physicist. The radiotherapy plan was transferred to the accelerator after verification.

CBCT image acquisition and matching

The CBCT images were obtained using the on-board image guidance system (OBI) of the Clinac IX linear accelerator purchased from Varian Medical Systems, California, US. The regions of interest were placed in the chest wall and supraclavicular target area, respectively, as shown in Figure 2. The CBCT image was compared with the positioning CT planning image. Then, the setup errors of the X-axis (left and right), Y-axis (head and foot), Z-axis (front and rear), and the foot of table (RTN)

were calculated. Moreover, the error data was recorded after manual adjustment according to the target area position.

CTV-PTV margin

According to International Commission on Radiation Units and Measurements (ICRU) reports 50 and 62, there should be a certain distance outside the CTV to reduce the setup error and effects of patient and tissue motion on the target volume. In our institution, Clinicians will follow unified standard for delineation and will delineate an ITV to address the effects of organ motion. For the setup error, a uniform 5 mm external margin is adopted. In this study, we mainly study the CTV (Including ITV)-PTV margin caused by setup error. The marginal calculation formula of Van Herk *et al.*¹⁶ was used in this study to ensure that at least 95% of the prescribed dose was given to 90% of the patients with CTVs. The marginal calculation formula is given in Eq. (A).

$$\text{MPTV} = 2.5\Sigma + 0.7\delta \quad (\text{A})$$

where the group systematic error (Σ) and random error (δ) were the standard deviations of individual systematic and random errors, respectively.

Comparison of setting efficiency and comfort satisfaction

The setup time for each fraction of the two fixation techniques was recorded and counted. The time required for the setup was defined as the time when the patient sat on the treatment couch until the therapist walked out of the treatment room after the setup. Each patient was investigated weekly. Subjective comfort A questionnaire survey was conducted for the first treatment to understand patients' subjective comfort satisfaction with the device. The satisfaction survey comprised eight items, each with a 5-point Likert scale. The dimensions of evaluation included head, neck, and back comfort, mask fit, tightness, temperature, color, anxiety about the fixture, general discomfort, and recommendation of the fixture.

Statistical analysis

The data were analyzed using SPSS25.0 statistical software. The data counts were expressed as frequencies (n) and percentages (%). The measurement data were expressed as mean \pm SD. All the

TABLE 1. Comparison of clinical data between the two groups

Group	Styrofoam n = 36	Bracket n = 29	P-value
Age ($x \pm s$, years)	48.34 \pm 9.58	48.90 \pm 10.92	0.837
Affected Side (n, %)			0.565
Left	20 (55.6)	11 (37.9)	
Right	16 (44.4)	18 (62.1)	
Type of operation (n, %)			0.053
Bcs	7 (16.7)	9 (31)	
Rm	29 (83.3)	20 (69)	
Stage (n, %)			0.146
II	7 (19.4)	4 (13.8)	
III	26 (72.2)	20 (68.9)	
IV	3 (8.4)	5 (17.3)	

BCS = Breast Conserving Surgery; RM = Radical Mastectomy

setup errors were taken as absolute values, and the data results were expressed as mean \pm standard deviation ($x \pm s$). Between the two groups, the differences in data counts were compared using the χ^2 test, while all the other comparisons were performed using t-tests. The correlation of errors in each direction was analyzed using the Pearson correlation analysis. A P-value of < 0.05 was considered statistically significant.

Results

Among 78 patients with breast cancer who received IMRT, 65 patients met the inclusion criteria. Among these 65 patients, 36 patients received Styrofoam fixation, and 29 patients received bracket fixation. A total of 281 CBCT verifications, including 147 Styrofoam and 134 breast bracket verifications, were performed. The clinical data of the two groups were analyzed, and the results are listed in Table 1. No significant differences between the indices were observed ($P > 0.05$).

Setup error

The setup error of the Styrofoam glue in the chest wall target area in the left-right direction was less than the breast bracket (1.59 \pm 1.47 mm *vs.* 2.05 \pm 1.64 mm, $t = 2.516$, $P = 0.012$), while that in the supraclavicular target area in the abdominal-dorsal direction was less than the breast bracket (1.36 \pm 1.27 mm *vs.* 1.75 \pm 1.55 mm), $t = 2.003$, $P = 0.046$. Moreover, the couch angle error of

TABLE 2. Comparison of setup errors of the two fixation methods in the chest wall target area and supraclavicular target area (mm, $\bar{x} \pm s$)

Group	Styrofoam	Bracket	t	P-value
CROI (X)	1.59 ± 1.47	2.05 ± 1.64	2.516	0.012
(Y)	1.99 ± 1.46	2.10 ± 1.59	0.611	0.541
(Z)	1.78 ± 1.47	2.00 ± 1.58	1.235	0.218
SROI (X)	1.23 ± 0.88	1.32 ± 1.16	0.620	0.536
(Y)	1.23 ± 1.21	1.16 ± 1.17	-0.445	0.657
(Z)	1.36 ± 1.27	1.75 ± 1.55	2.003	0.046
CRTN (°)	0.48 ± 0.46	0.53 ± 0.43	1.033	0.302
SRTN (°)	0.47 ± 0.47	0.66 ± 0.59	2.760	0.006

CROI = Chest Wall Target; SROI = supraclavicular target

Styrofoam rubber was less than that of the breast bracket ($0.47 \pm 0.47^\circ$ vs. $0.66 \pm 0.59^\circ$), $t = 2.760$, $P = 0.006$. The detailed results are provided in Table 2.

PTV margin comparison

In the breast bracket group, the PTV margins of the chest wall in the X, Y, and Z directions were 6.10 mm, 6.34 mm, and 6.10 mm, respectively, while those of the supraclavicular target area were 3.99 mm, 3.72 mm, and 5.45 mm, respectively. In the Styrofoam group, the PTV margins of the chest wall in the X, Y, and Z directions were 5.01 mm, 5.99 mm, and 5.47 mm, respectively, while those of

the supraclavicular target area were 3.69 mm, 3.86 mm, and 4.28 mm, respectively (Table 3). In the chest wall target area, the margin of the Styrofoam group was 17.87% smaller than that of the bracket group in the X direction. In the supraclavicular target area, the margin of the Styrofoam group was 21.47% less than that of the bracket group in the Z direction.

Note: Σ was the standard deviation of the systematic error of each patient, and the systematic error of each patient in each direction was the average value of the errors in each direction among all fractions; σ was the mean square value of the random error of each patient, and the random error of each patient in each direction was the standard deviation of the error in each direction among all fractions; and MPTV was the size of the outspread boundary from the clinical target volume to the planned target volume.

The comparison of the displacement frequency of the chest wall target area

The displacement distributions for < 3 mm, 3~5 mm, and > 5mm in the Styrofoam group in the X direction were 75.4%, 23.1%, and 1.5%, respectively, and those in the Y direction were 66.8%, 32.1%, and 1.1%, respectively. In the Z direction, the displacement distributions for the respective frequencies were 69.2%, 29.2%, and 1.6%. In the breast bracket group, the displacement distributions for <3 mm, 3~5 mm, and > 5mm in the X direction were 66.9%, 31.6%, and 1.5%, respectively, while those in the Y direction were 66.9%, 30.8%, and 2.3%, respectively. Moreover, in the Z direction, the displacement distributions for the respective were, 66.9%, 31.6%, and 1.5%, respectively. The probability of < 3 mm of Styrofoam in the left and right direction was significantly greater than that of the bracket group, as shown in Figure 3.

A comparison of the displacement frequency in the supraclavicular target area

The displacement distributions for < 3 mm, 3~5 mm, and > 5mm in the Styrofoam group in the X-direction were 89.7%, 9.1%, and 1.2%, respectively, and those in the Y-direction were 84.5%, 15.5%, and 0%, respectively. In the Z-direction, the displacement distributions of respective were 82.8%, 17.2%, and 0%. The displacement distributions for < 3 mm, 3~5 mm, and > 5mm in the breast bracket group in the X-direction were 87.3%, 10.8%, and 1.9%, respectively. In the Y-direction, the displace-

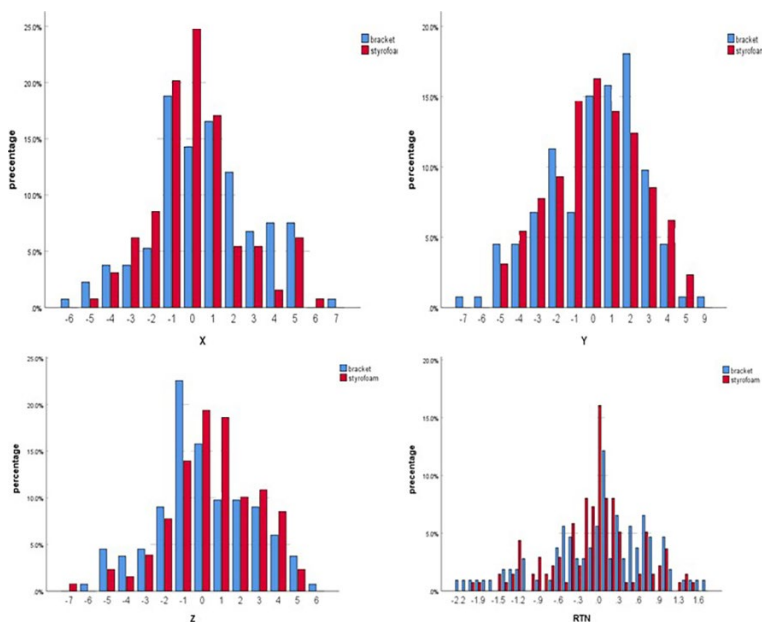


FIGURE 3. Bar chart of setup error of two fixation methods in chest wall target area.

TABLE 3. Target volume expansion boundary in the three-dimensional direction in 65 patients in the breast bracket and Styrofoam groups (mm)

		Styrofoam			Bracket		
		X	Y	Z	X	Y	Z
Σ Systematic error	CROI	1.59	1.99	1.78	2.05	2.10	2.00
	SROI	1.23	1.23	1.36	1.32	1.16	1.75
σ Random error	CROI	1.47	1.46	1.46	1.39	1.57	1.57
	SROI	0.88	1.12	1.26	0.98	1.17	1.54
M_{PTV}	CROI	5.01	5.99	5.47	6.10	6.34	6.10
	SROI	3.69	3.86	4.28	3.99	3.72	5.45

ment distributions were 87.7%, 12.3%, and 0%, while in the Z-direction, they were 76.5%, 20.6%, and 2.9%, respectively, as shown in Figure 4.

Comfort satisfaction score of a fixation device and comparison of setup efficiency

The subjective comfort satisfaction scores of patients in the Styrofoam and bracket groups were 27.50 ± 1.24 and 25.44 ± 1.23 points, respectively, showing a statistically significant difference ($P < 0.001$). The setup times of the Styrofoam and breast bracket groups were 3.4 ± 1.1 min and 5.5 ± 3.1 min, respectively ($P = 0.007$).

Correlation analysis of setup error between two groups of different directions

In the bracket group, the Pearson correlation analysis showed a moderate correlation between the Y-axis and Z-axis direction in the chest wall setup error ($r = -0.205$), while the supraclavicular target area X-axis setup error showed a weak correlation with the Y and Z-axis directions ($r = 0.190$ and 0.185). The Z-axis setup error in the Styrofoam group supraclavicular target area was moderately correlated with the X-axis direction and RTN ($r = -0.211$ and 0.235), as shown in Figure 5.

Discussion

The current study compared the Styrofoam fixation and breast bracket fixation in patients with breast cancer, who underwent postoperative radiotherapy. The results showed that Styrofoam fixation could significantly reduce inter-fractional displacement in the X direction of the chest wall and displacement in the Z and RTN directions of the supraclavicular region. The chest PTV margin

of the foam group was 17.87% (5.01 mm *vs.* 6.10 mm) less than that in the bracket group in the left and right directions. In the supraclavicular region, the Styrofoam group was 21.47% (4.28 mm *vs.* 5.45 mm) less exposed in the anteroposterior direction as compared to the bracket group. The Styrofoam fixation group showed a higher comfort satisfaction score and work efficiency.

The accuracy of radiotherapy directly affects the success or failure of radiotherapy.^{17,18} The setup error was relatively large due to the special physiological structure of breast cancer. Errors in breast cancer radiotherapy are related to factors, such as fixation devices, the patient's position, experience of the radiotherapy therapist, and the patient's body mass index.¹⁹ When the fixture is more comfortable, it reduces the setup error more effectively. Currently, the commonly used molds for breast cancer positioning in various radiotherapy centers include vacuum bags, thermoplastic body films, breast brackets, and Styrofoam. A vacuum bag poses a risk of air leakage and compression deformation during treatment. The thermoplastic phantom could significantly reduce inter-fraction error in IMRT for breast cancer as compared to a vacuum bag. However, it might increase the irradiated skin dose at the irradiated site, thereby exacerbating radiation skin reactions.^{20,21} Therefore, care should be taken while using thermoplastic masks for fixation. In the breast bracket (a conventional mechanical fixing device), the fixation of the neck and shoulder was uncertain, and it was easier to form a forced body position. Moreover, the repeatability of the clavicle area could not be guaranteed, and the degree of individualization of mold was not as high as that of Styrofoam.

Our results showed that the Styrofoam group had a smaller setup error than the bracket group in the X direction of the chest wall. Zhou C *et al.*²² compared the vacuum bag and Styrofoam fixation in 40 patients after breast-conserving radical mastectomy for breast cancer and revealed that

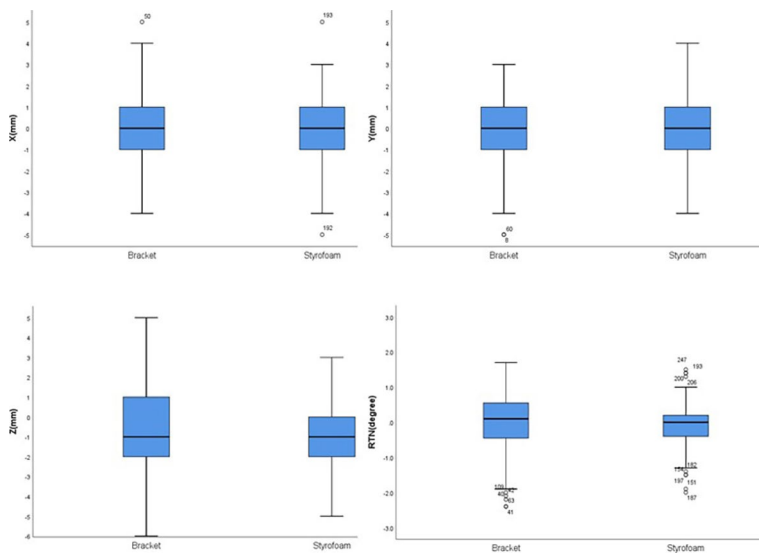


FIGURE 4. Box plot of setup error in supraclavicular region of two fixation methods.

the setup errors in the X, Y, and Z directions of the Styrofoam group were 1.63 ± 1.29 mm, 1.46 ± 1.51 mm, and 1.30 ± 1.35 mm, respectively, which were less than those of the vacuum bag group (1.83 ± 1.61

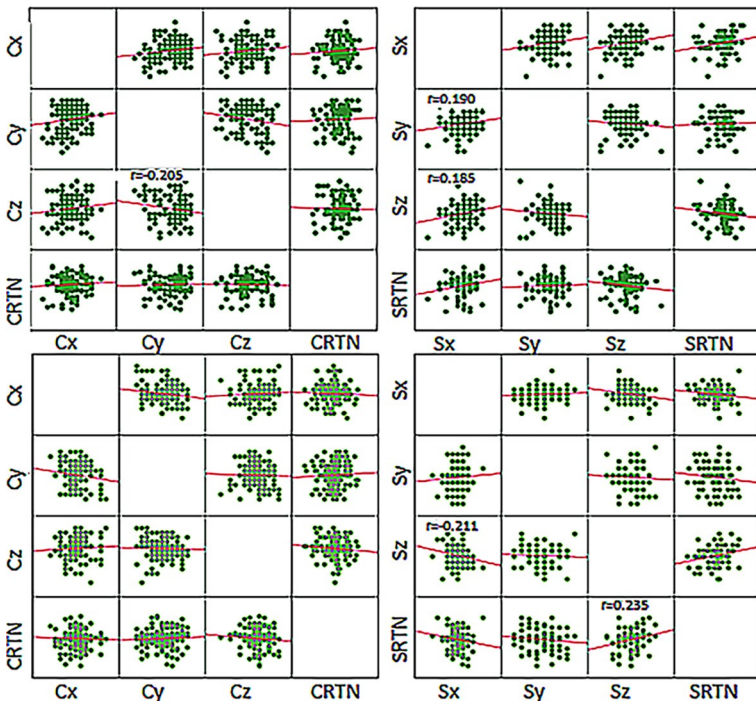


FIGURE 5. Scatter plot of setup error between two groups in different directions. The dark color in the upper figure shows the bracket group, and the light color in the lower figure shows the Styrofoam group. The r-values with P-values < 0.05 are indicated in the figure.

C = chest wall; S = supraclavicular

mm, 2.26 ± 2.03 mm, and 1.91 ± 1.67 mm, respectively). In their study, the Styrofoam and vacuum pad groups showed similar results to those of the Styrofoam and bracket groups in the current study in terms of errors in the X and Y directions errors. Fang Jiannan *et al.*²³ conducted a study on 24 patients treated with breast-conserving radiotherapy for breast cancer and showed that the Styrofoam rubber group exhibited a smaller setup error as compared to that of the breast bracket group in the Y direction (1.76 ± 1.78 mm *vs.* 3.28 ± 2.79 mm), X direction (2.36 ± 2.89 mm *vs.* 2.56 ± 2.05 mm), and Z direction (1.47 ± 1.49 mm *vs.* 1.73 ± 1.81 mm) with higher work efficiency. However, in the current study, the Styrofoam group showed smaller setup errors in the X direction while having similar setup errors in other directions. The differences between the two studies might be due to differences in sample size, treatment procedures in the respective centers, and experience levels of the therapists (the therapists in the current study had an experience of more than 10 years). In conclusion, the above studies demonstrated that the Styrofoam fixation could significantly improve the setup accuracy, repeatability, and setup efficiency of the fixation and might be a promising individualized fixation device.

This study found that Styrofoam fixation in the supraclavicular region had a significantly smaller setup error in the Z direction as compared to that in the bracket group. Zhang Y *et al.*²⁴ used cervicothoracic membrane in combination with breast bracket for fixation in 32 patients with breast cancer after the operation, and the respective setup errors on the supraclavicular target area were 1.98 ± 2.44 mm, 1.98 ± 2.48 mm, and 1.71 ± 1.79 mm. Except for the bracket group, which had similar setup errors in the Z orientation, the setup errors of other orientations were significantly greater than those of any of the fixation devices in this study. Shen K *et al.*²⁵ used vacuum bag fixation in 24 patients with radiotherapy after mastectomy and revealed that the standard deviations of the setup error on the supraclavicular target area were 1.6 mm, 1.4 mm, and 1.8 mm, which were similar to those of the bracket group in the current study. Based on the previous studies, it could be observed that Styrofoam fixation in the supraclavicular target area might have less error, which might be because the Styrofoam is an individualized fixation device, and the patient's comfort satisfaction scores were higher (27.50 ± 1.24 *vs.* 25.44 ± 1.23 points). In this study, individualized fixation was also performed on the patient's arm, and the arm showed better plasticity on Styrofoam, as shown in Figure 1 D. The patient

could quickly and accurately repeat positioning on his fixation device. The setup efficiency can also reflect (3.4 ± 1.1 vs. 5.5 ± 3.1) min.

The PTV margins of the IMRT target volume in most studies were 5 mm. The current study showed that the calculated PTV margins of the target volume fixed by Styrofoam in the X, Y, and Z directions of the chest wall were 5.01 mm, 5.99 mm, and 5.47 mm, respectively, while those of the supraclavicular target area were 3.69 mm, 3.86 mm, and 4.28 mm, respectively. Moreover, in the breast bracket group, the chest wall boundaries of the calculated PTV margins were 6.10 mm, 6.34 mm, and 6.10 mm in the three directions, while the supraclavicular margins were 3.99 mm, 3.72 mm, and 5.45 mm, respectively. It could be seen that for both fixation devices, a PTV margin of 5 mm was not sufficient on the chest wall, while it was sufficient for the supraclavicular target area. Yao W *et al.*²⁶ fixed 25 patients with breast cancer with Styrofoam and showed that the corresponding margins were 6.75 mm, 8.46 mm, and 8.73 mm. In comparison, the chest wall margins in the current study were smaller. Shen K *et al.*²⁵ showed that the chest wall systematic errors in the X, Y, and Z directions were 1.67 mm, 2.37 mm, and 1.31 mm with random errors of 1.70 mm, 1.83 mm, and 1.68 mm, respectively, while the supraclavicular target area systematic errors in the three directions were 1.02 mm, 0.90 mm, and 1.19 mm with the random errors of 1.22 mm, 1.20 mm, and 1.44 mm, respectively. The calculated PTV margins for the chest target area were 5.36 mm, 7.20 mm, and 4.46 mm, while those for the supraclavicular target area were 3.41 mm, 3.08 mm, and 3.98 mm, respectively. Zhang Y *et al.*²⁴ The calculated PTV margins were 6.2 mm, 6.7 mm, and 5.7 mm in the chest wall target area, while those in the supraclavicular target area were 6.6 mm, 6.7mm, and 5.5 mm. The PTV margin required for the set-up error in this study is slightly smaller than in other studies, which might be due to differences in the fixation devices and standards in different studies. Similarly, the differences in sample size and other factors could not be excluded. As a radiotherapy therapist, in this study, the CTV-PTV margins caused by set-up error was discussed, and in the ICRU report62, clinicians will delineate the ITV based on factors such as organ movement.

The current study showed that the setup errors of the two groups of fixation devices in the Y direction of the chest target area contained more positive values; this indicated that the position of the two groups of patients moved to the foot side. In addition, the couch angle in both groups had

extreme values, which might be due to a slightly greater number of patients enrolled after radical mastectomy on the right side. During the late-course treatment, the patient's arm could not be naturally lifted to the original positioning position due to irradiation and surgery, and the body was affected by traction to shift to the affected side, resulting in coronal rotation. Therefore, the radiotherapist must educate patients with breast cancer to do functional exercises of the affected upper limb after radiotherapy. The data in the supraclavicular target area showed more negative values in the Z direction in both groups, suggesting that both groups collapsed in the neck region. A similar phenomenon was also reported by Svestad JG *et al.*¹² However, in addition to the patient in the CT positioning of the body is too tight and the body relaxed during treatment reasons, cannot rule out the therapist in the setup process is not rigorous and caused by human error, radiation therapists should avoid this problem.

The current study analyzed the setup errors in all directions using the Pearson correlations analysis, which has been rarely studied in previous studies. The correlation analysis was used to analyze whether an increase in error in one direction would change the error in the other direction. The results showed that the setup error of bracket fixation in the Y direction in the chest wall region was negatively correlated with that in the Z direction, while the setup error in the X direction in the supraclavicular target area was weakly correlated with that in the Y and Z directions; this was also consistent with clinical practice. When the X direction error became larger, the side deformed the neck in the headrest, resulting in changing the neck error in the Y and Z directions. In the Styrofoam group, the setup error in the Z direction of the supraclavicular target area was negatively correlated with that in the X direction, while it was positively correlated with the RTN. This might be due to the relatively stronger head fixation of Styrofoam (Figure 1 D), and the error in the Z direction, which caused the coronal rotation of the neck. This also showed that the bracket fixation was not as good as the Styrofoam fixation for the patient's head.

The current study has several limitations. First, only two groups of fixation methods were discussed, and there were many factors, which affected the setup error. Secondly, van Herk's boundary calculation was performed only for the errors of three horizontal displacements. At larger target volumes, even small rotational errors can lead to dose uncertainty.²⁷ In clinical practice, it is difficult

to correct rotational errors and local setup errors using CBCT image guidance. However, a combination of a six-dimensional treatment couch²⁸ and an optical surface detection system (OSMS)²⁹ can be used to solve these problems in a qualified unit. Finally, the effects of breathing on positioning were not explored in this study and are needed to be studied further in the future. The use of artificial intelligence (AI) in radiotherapy is increasing; therefore, it is expected to apply AI techniques for error correction. Mathematical models or computerized deep learning might help in reducing the setup errors of breast cancer in the future. It is also possible to quantify the physical indicators, including weight and body mass index, which will be the subject of future studies. Future studies with larger sample sizes, multifactorial setup errors, and better fixation methods are needed.

In summary, the current study retrospectively analyzed the use of Styrofoam fixation in radiotherapy for patients with lymph node metastasis after breast cancer surgery. The study suggested that the use of Styrofoam could further improve the setup accuracy and setup efficiency of the chest wall and supraclavicular target area, improve patients' comfort and satisfaction, and decrease the PTV margin distance. This study might provide a reference for the clinical use of Styrofoam glue to fix the postoperative radiotherapy of patients with breast cancer.

References

1. Ferlay J, Ervik M, Lam F, Colombet M, Mery L, Piñeros M, et al. Global cancer observatory: cancer today [EB/OL]. (cited 2022 Nov 07). Available at: <https://gco.iarc.fr/today>.
2. Sung H, Ferlay J, Siegel RL, Laversanne M, Soerjomataram I, Jemal A, et al. Global cancer statistics 2020: GLOBOCAN estimates of incidence and mortality worldwide for 36 cancers in 185 countries. *CA Cancer J Clin* 2021; **71**: 209-49. doi: 10.3322/caac.21660.
3. Clarke M, Collins R, Darby S, Davies C, Elphinstone P, Evans V, et al. Effects of radiotherapy and of differences in the extent of surgery for early breast cancer on local recurrence and 15-year survival: an overview of the randomised trials. *Lancet* 2005; **366**: 2087-106. doi: 10.1016/S0140-6736(05)67887-7
4. Barnett GC, Wilkinson JS, Moody AM, Wilson CB, Twyman N, Wishart GC, et al. The Cambridge breast intensity-modulated radiotherapy trial: Patient- and treatment-related factors that influence late toxicity. *Clin Oncol (R Coll Radiol)* 2011; **23**: 662-73. doi: 10.1016/j.clon.2011.04.011
5. Mukesh MB, Qian W, Wilkinson JS, Dorling L, Barnett GC, Moody AM, et al. Patient reported outcome measures (PROMs) following forward planned field-in-field IMRT: Results from the Cambridge breast IMRT trial. *Radiation Oncol* 2014; **11**: 270-5. doi: 10.1016/j.radonc.2014.02.016
6. O'Connell AM, Karellas A, Vedantham S, Kawakyo-O'Connor DT. Newer technologies in breast cancer imaging: Dedicated cone-beam breast CT. *Semin Ultrasound CT MR* 2018; **39**: 106-13. doi: 10.1053/j.sult.2017.09.001
7. Taylor C, Correa C, Duane FK, Aznar MC, Anderson SJ, Bergh J, et al. Estimating the risks of breast cancer radiotherapy: Evidence from modern radiation doses to the lungs and heart and from previous randomized trials. *J Clin Oncol* 2017; **35**: 1641-9. doi: 10.1200/JCO.2016.72.0722
8. Vasiljevic D, Arnold C, Neuman D, Fink K, Popovscaia M, Kvitsaridze I, et al. Occurrence of pneumonitis following radiotherapy of breast cancer – A prospective study. *Strahlenther Onkol* 2018; **194**: 520-32. doi: 10.1007/s00066-017-1257-z
9. Duffton A, Li W, Forde E. The pivotal role of the therapeutic radiographer/radiation therapist in image-guided radiotherapy research and development. *Clin Oncol (R Coll Radiol)* 2020; **32**: 852-60. doi: 10.1016/j.clon.2020.09.009
10. Zhou J, Li S, Ye C, Shen K, Li A, Chen G, et al. Analysis of local setup errors of sub-regions in cone-beam CT-guided post-mastectomy radiation therapy. *J Radiat Res* 2020; **61**: 457-63. doi: 10.1093/jrr/rraa007
11. Dong F, Weng X, Deng X, Yang Y, Xu B, Li X. Clinical utility of a new immobilization method in image-guided intensity-modulated radiotherapy for breast cancer patients after radical mastectomy. *J Xray Sci Technol* 2022; **30**: 641-55. doi: 10.3233/XST-221127
12. Svestad JG, Heydari M, Mikalsen SG, Flote VG, Nordby F, Hellebust TP, et al. Surface-guided positioning eliminates the need for skin markers in radiotherapy of right sided breast cancer: A single center randomized crossover trial. *Radiation Oncol* 2022; **17**: 46-52. doi: 10.1016/j.radonc.2022.10.017
13. Mulliez T, Gulyban A, Vercauteren T, van Greveling A, Speleers B, De Neve W, et al. Setup accuracy for prone and supine whole breast irradiation. *Strahlenther Onkol* 2016; **192**: 254-9. doi: 10.1007/s00066-016-0943-6
14. Lin, CG, Xu, SK, Yao, WY, et al. Comparison of set up accuracy among three common immobilisation systems for intensity modulated radiotherapy of nasopharyngeal carcinoma patients. *J Med Radiat Sci* 2016; **64**: 106-13. doi: 10.1002/jmrs.189
15. Li B, Bai F, Yao X, Xu L, Zhao L. Clinical value of styrofoam fixation in intracranial tumor radiotherapy. *Front Oncol* 2023; **13**: 1131006. doi: 10.3389/fonc.2023.1131006
16. van Herk M, Remeijer P, Rasch C, Lebesque JV. The probability of correct target dosage: Dose-population histograms for deriving treatment margins in radiotherapy. *Int J Radiat Oncol Biol Phys* 2000; **47**: 1121-35. doi: 10.1016/S0360-3016(00)00518-6.
17. Matke M, Rath D, Häfner MF, Unterhinninghofen R, Sterzing F, Debus J, et al. Individual 3D-printed fixation masks for radiotherapy: first clinical experiences. *Int J Comput Assist Radiol Surg* 2021; **16**: 1043-9. doi: 10.1007/s11548-021-02393-2
18. Vilotte F, Antoine M, Bobin M, Latorzeff I, Supiot S, Richaud P, et al. Post-prostatectomy image-guided radiotherapy: The invisible target concept. *Front Oncol* 2017; **7**: 34. doi:10.3389/fonc.2017.00034
19. Zhang HJ, Zhang C, Ge RG, Liu XL, Cong XH, BL Qu, et al. Evaluation of positional error during radiotherapy for breast cancer after modified radical mastectomy. *J Biomed Res-india* 2017; **28**: 7526-33. doi: 10.1016/j.meddos.2016.02.002
20. Lv R, Yang G, Huang Y, Wang Y. Dosimetric effects of supine immobilization devices on the skin in intensity-modulated radiation therapy for breast cancer: a retrospective study. *BMC Cancer* 2021; **21**: 384. doi: 10.1186/s12885-021-08119-6.
21. Dinu A, Flonta T, Marcu LG. The impact of breast irradiation using thermoplastic mask on treatment delivery and acute effects. *Romanian Reports in Physics* 2020; **72**, 603.
22. Zhou C, Fang J, Huang X, Shi J, Ma Y. Preliminary study of accurate position fixation between polyurethane styrofoam and vacuum negative pressure pad in IMRT after radical mastectomy for breast cancer. *Chin J Radiat Oncol* 2019; **28**: 776-9. doi: 10.3760/cma.j.issn.1004-4221.2019.10.013
23. Fang J, Ma Y, Shi J, Huang J, Wu X, Ma S, et al. Comparison of immobilization accuracy between styrofoam and breast carrier in intensity-modulated radiotherapy after breast conservative surgery for breast cancer patients. *Chin J Radiat Oncol* 2019; **28**: 369-72. doi: 10.3760/cma.j.issn.1004-4221.2019.05.010
24. Zhang Y, Huan F, Zhu G, Zhou K, Feng X, Wan B, et al. Analysis of setup errors of postoperative intensity-modulated radiotherapy immobilized with integrated cervicothoracic board mask system in breast cancer patients. *Chin J Radiat Oncol* 2021; **30**: 835-40. doi: 10.3760/cma.j.cn113030-20200229-00081
25. Shen K, Xiong J, Wang Z, Wang W, Li W, Zhou J, et al. Design of a new breast vacuum bag to reduce the global and local setup errors and to reduce PTV margin in post-mastectomy radiation therapy. *J Radiat Res* 2020; **61**: 985-92. doi: 10.1093/jrr/rraa006
26. Yao W, Liu B, Fang J, Fang Y, Xiao L, Wang Y, et al. Breast bracket combined with polyurethane Styrofoam improves the accuracy of immobilization in breast cancer radiotherapy. *Chin J Radiat Oncol* 2022; **31**: 916-21. doi: 10.3760/cma.j.cn113030-20210812-00301
27. Harron EC, McCallum HM, Lambert EL, Lee D, Lambert GD. Dosimetric effects of setup uncertainties on breast treatment delivery. *Med Dosim* 2008; **33**: 293-8. doi: 10.1016/j.meddos.2008.01.003
28. Boman E, Kapanen M, Laaksomaa M, Mäenpää H, Hyödynmaa S, Kellokumpu-Lehtinen PL. Treatment accuracy without rotational setup corrections in intracranial SRT. *J Appl Clin Med Phys* 2016; **17**: 86-94. doi: 10.1120/jacmp.v17i4.6149
29. Wiant D, Pursley J, Sintay B. SU-D-213CD-02: The accuracy of AlignRT guided set-up for whole breast and chestwall irradiation. *J Med Phys* 2012; **39**(6Part3): 3617-8. doi: 10.1118/1.4734687

The influence of cytotoxic drugs on the immunophenotype of blast cells in paediatric B precursor acute lymphoblastic leukaemia

Tomaz Prelog^{1,2}, Simon Bucek³, Andreja Brozic³, Jakob Peterlin⁴, Marko Kavcic¹, Masa Omerzel⁵, Bostjan Markelc⁵, Tanja Jesenko^{2,5}, Veronika Kloboves Prevodnik^{2,3,6}

¹ Department of Haemato-Oncology, University Children's Hospital, University Medical Centre Ljubljana, Ljubljana, Slovenia

² Faculty of Medicine, University of Ljubljana, Ljubljana, Slovenia

³ Department of Cytopathology, Institute of Oncology Ljubljana, Ljubljana, Slovenia

⁴ Institute for Biostatistics and Medical Informatics, University of Ljubljana, Ljubljana, Slovenia

⁵ Department of Experimental Oncology, Institute of Oncology Ljubljana, Ljubljana, Slovenia

⁶ Institute of Pathology, Faculty of Medicine University of Maribor, Maribor, Slovenia

Radiol Oncol 2024; 58(1): 133-144.

Received 14 May 2023

Accepted 6 December 2023

Correspondence to: Prof. Veronika Kloboves Prevodnik, M.D., Ph.D., Institute of Pathology, Faculty of Medicine University of Maribor, Maribor, Slovenia. E-mail: vkloboves@onko-i.si

Disclosure: No potential conflicts of interest were disclosed.

This is an open access article distributed under the terms of the CC-BY license (<https://creativecommons.org/licenses/by/4.0/>).

Background. Flow cytometry plays an important role in the diagnosis of acute lymphoblastic leukaemia (ALL) and when antigen-specific immunotherapy is indicated. We have investigated the effects of prednisolone, vincristine, daunorubicin, asparaginase and methotrexate on the antigen expression on blast cells that could influence the planning of antigen-specific therapy as well as risk-based treatment assignment.

Patients and methods. Patients aged ≤ 17 years with *de novo* B-cell ALL (B-ALL) were enrolled in the study. Blast cells were isolated and exposed *in vitro* to 5 individual cytotoxic drugs in logarithmically increasing concentrations. Then, the expression of CD10, CD19, CD20, CD27, CD34, CD45, CD58, CD66c and CD137 antigens was determined by quantitative flow cytometry.

Results. Cytotoxic drugs caused dose-dependent or dose-independent modulation of antigen expression. Daunorubicin caused a dose-dependent down-modulation of CD10, CD19, CD34, CD45 and CD58 and an up-modulation of CD137. Vincristine caused a dose-dependent down-modulation of CD19 and CD58 and an up-modulation of CD45. Daunorubicin also caused dose-independent down-modulation of CD27 and prednisolone down-modulation of CD10, CD19, CD27, CD34 and CD58. Down-modulation of CD20 was detected only in relation to the specific dose of daunorubicin.

Conclusions. The results of the study have shown that cytotoxic drugs can alter the expression of antigens that are important for immunotherapy. Importantly, daunorubicin, prednisolone and vincristine caused down-modulation of CD19 and CD58, suggesting that these drugs are better avoided during bridging therapy prior to bispecific antibodies or CAR-T cell therapy. In addition, immunophenotypic changes on blast cells induced by different drugs could also influence risk-based treatment assignment.

Key words: immunophenotypic changes; chemotherapy; immunotherapy; paediatric B-ALL

Introduction

Flow cytometry is one of the methods used in the diagnosis of acute lymphoblastic leukaemia (ALL).

It provides important information about the expression of antigens on blast cells and is important for determining minimal residual disease (MRD),

which allows assessment of response to therapy and further planning of treatment.^{1,2}

According to the International Berlin-Frankfurt-Münster Study Group clinical trial (ALL IC BFM 2009) the intensity of therapy for childhood ALL is based on risk stratification.¹ The patients are divided into three risk groups, standard risk (SR), intermediate risk (IR) and high risk (HR). HR patient must fulfil at least one of the following criteria: presence of specific genetic alterations (t(9;22) or t(4;11)), hypodiploid blast cells, > 1000 blast cells in 1 mL peripheral blood on day 8 of therapy, MRD on day 15 > 10% and patients not in morphological remission on day 33.¹ SR patients are 1-6 years old, have a white blood cell count of < 20000/mL at the time of diagnosis, < 1000 blasts per mL of peripheral blood on day 8 of therapy, MRD on day 15 < 0.1% and are in morphological remission on day 33 of therapy.¹ All others are IR patients.¹

SR and IR patients are treated with 4 consecutive chemotherapy blocks: induction, early intensification, consolidation and reinduction, followed by maintenance therapy. HR patients receive more intensive consolidation with 6 blocks of chemotherapy or 3 blocks followed by bone marrow transplantation.¹ In induction prednisolone, vincristine, daunorubicin, asparaginase and intrathecal application of methotrexate are used.¹ In later phases, other cytostatic drugs are administered.¹

In relapsed or refractory disease, when immunotherapy with bispecific antibodies or chimeric antigen receptor T (CAR-T) cells is commonly in-

dicated, the choice of therapeutic approach is often based on the immunophenotype of the blast cells. For instance the expression of antigens such as CD19, CD20 and CD58 is essential for planning treatment with blinatumomab, rituximab and CAR-T therapy.²⁻⁶

Some studies have already investigated the impact of the cytotoxic drugs on antigen expression of blast cells and showed that chemotherapy can cause a change in their expression, which may be related to cell death, the efficacy of therapy and the overall prognosis of the disease.⁷⁻¹⁰ Moreover, chemotherapy may also influence expression of antigens which are essential for effective treatment with bispecific antibodies and CAR-T cells.¹⁰

Certain antigens expressed on blast cells may also be associated with the prognosis of the ALL patients. Expression of CD27, CD34, CD45 and CD66c antigens has already been reported to be associated with prognosis of ALL.¹¹⁻¹⁸ Additionally, expression of CD66c strongly correlates with BCR/ABL rearrangement.¹⁷ To our knowledge there is no data about the influence of chemotherapeutic drugs on expression of these prognostic markers in the literature. In Table 1 we present the antigens which are important for planning the treatment of ALL patients or are associated with the prognosis of the ALL.

The aim of the study was to assess the influence of drugs included in ALL induction therapy on antigen expression of blast cells which are common targets for immunotherapy (CD19, CD20) or

TABLE 1. Antigens expressed on acute lymphoblastic leukaemia (ALL) blasts which are essential for planning the treatment or may influence the prognosis of the disease

Antigen	Expression of the antigen in normal and pathological conditions	Clinical significance
CD10	Normal lymphoid progenitors, neutrophils and blast cells of B-ALL ¹⁹	Associated with favourable presenting features in paediatric B-ALL and possible target for emerging CAR-T ¹⁹⁻²¹
CD19	Normal and malignant B lymphocytes ²²	Target of blinatumomab and CAR-T ²²⁻²⁴
CD20	Normal and malignant B lymphocytes ²¹	Target of rituximab, up-modulated in B-ALL patients with poor prognosis ^{7,21}
CD27	T cells, natural killer cells and thymocytes, also memory B cells, and in some subsets of B-ALL ¹¹	Positive in B-ALL with BCR/ABL or CRLF2 rearrangement, high positivity was associated with poor prognosis ¹¹⁻¹³
CD34	Pluripotent stem cells ¹⁴	Lack of expression associated with worse event free and overall survival of ALL ¹⁵
CD45	Cells of hematopoietic origin ²⁵	High expression associated with high risk disease and worse event free survival, and worse rate of complete remission after the induction therapy ^{16,26}
CD58	Hematopoietic and nonhematopoietic cells ²⁷	Lack of expression reduces the efficacy of blinatumomab and anti-CD19 CAR-T ^{4,5}
CD66c	Granulocytes and their precursors, most common myeloid antigen on malignant B lymphoblasts ¹⁷	Associated with specific genetic alterations such as BCR/ABL, hypodiploidy, hypodiploidy and CRLF2-positivity in B-ALL ^{17,18}
CD137	T lymphocytes and natural killer cells but also on activated B cells of naive origin ²⁸	Enhances B cell survival ²⁸

B-ALL = B-cell ALL; CAR-T = chimeric antigen receptor T; CRLF2 = cytokine receptor-like factor 2

possess the potential to impact its effectiveness (CD58). Additionally, we have studied the antigens that could play a role in categorizing patients into distinct treatment risk groups, enhancing the precision of patient stratification (CD10, CD27, CD34, CD45, CD66c and CD137). Importantly, we analysed the influence of drugs and their dosage separately.

Patients and methods

Patients

Between March 2018 and November 2021, we performed bone marrow aspiration or peripheral blood withdrawal in case of extreme leukocytosis in all children with suspected acute leukaemia. Informed consent was obtained from the patient and parents or consent from a proxy before enrolment in the study. The National Medical Ethics Committee approved the study (protocol number: KME 25/05/15).

First, we performed all routine diagnostic procedures, and if B-cell ALL was confirmed, the remaining bone marrow sample was further cultivated *in vitro*. In total, we recruited 35 patients and collected 34 bone marrow samples and one peripheral blood sample. Six samples were not included in the final analysis because the number of cells after isolation was too low to perform the treatment with cytostatic drugs (4 cases) or because viable cells in the control group were lost during the treatment with cytostatic drugs (2 cases). In total, we treated and analysed blast cells from the remaining 29 samples.

Twenty-seven of the included patients older than one year were treated according to the ALL IC-BMF 09 protocol¹, more than half of them according to the intermediate risk arm. Two patients younger than 1 year were treated according to the Interfant 06 protocol.²⁹ None of the included patients had blasts in the cerebrospinal fluid at the time of diagnosis. One patient who failed induction therapy received anti-CD19 CAR-T cell therapy, followed by bone marrow transplantation. Two other high-risk patients were treated with allogeneic stem cell transplantation. The clinical characteristics and outcome of all included patients are summarised in Table 2.

The response to therapy in patients treated according to the ALL IC-BMF 09 protocol is summarised in Table 3.

Among two patients, who were treated according to Interfant 06 protocol one of them had ex-

TABLE 2. Clinical characteristics of all included patients

No. of all included patients with B-ALL	N = 29
Male/female	N 17/12
Mean age at diagnosis	Years 4.76 (newborn 17)
Flow cytometric findings at diagnosis	N (%)
Pro-B	3 (10)
Pre-B	6 (21)
Common type	20 (69)
Cytogenetic and molecular finding at diagnosis	N (%)
normal karyotype	6 (21)
hyperdiploid	10 (34)
t(12;21)	(28)
complex karyotype	(3)
MLL	1 (3)
changes of unknown risk potential	3 (10)
Outcome	N (%)
Alive	93)
Died	2 (7)
Cause of death	N
pancreatitis*	1
progressive disease**	1

* = treated according to ALL IC-BMF 2009 protocol; ** = treated according to Interfant 06 protocol; MLL = mixed-lineage leukaemia rearrangement; N = number of patients; Pro-B, Pre-B and common B = stage of differentiation

treme hyperleukocytosis, finished the therapy and is in a remission. The other patient died of progressive disease.

Isolation and cultivation of blast cells

After confirming B-ALL diagnosis, blast cells from bone marrow or peripheral blood were isolated by density gradient centrifugation using Ficoll-Paque (GE HealthCare Technologies Inc, Chicago, IL, USA) media and SepMate™-15 centrifugation tubes (STEMCEL Technologies, Vancouver, Canada). After centrifugation and harvesting from the top of the Ficoll layer, cells were washed 2 times in RPMI 1640 medium containing 10 mM HEPES buffer (Gibco, Thermo Fisher Scientific, Waltham, MA, USA). Medium was supplemented with 10% (v/v) fetal bovine serum (FBS, Gibco), Gluta-MAX (100 x, Gibco), and penicillin-streptomycin (100 x, Sigma-Aldrich, Merck, Darmstadt, Germany). Cells were plated at high density in T-75 or T-182 flasks (VWR, Radnor, PA, USA) in cell culture media and incubated in a humidified incubator with 5% CO₂ at 37°C until the treatment with cytotoxic drugs (maximum 3 days).

TABLE 3. Response to the therapy in patients treated according ALL IC BFM 09 protocol

Patients treated according to ALL IC-BFM 2009 protocol	
No. of patients	27
Treatment arm	N (%)
SR	6 (22)
IR	18 (66)
HR	3 (11)
Response to prednisolone on day 8	N (%)
good response*	27 (100)
poor response**	0 (0)
Minimal residual disease on day 15	N (%)
< 0.1%	10 (37)
0.1–10%	15 (56)
> 10%	2 (7)
Minimal residual disease on day 33	N (%)
neg	16 (59)
< 0.1%	6 (22)
0.1–10%	3 (11)
> 10%	2 (7)
Outcome	N (%)
alive	26 (96)
died	1 (4)

* = prednisolone good response is defined as blast count of less than 1000 per mL of peripheral blood on the day 8 of induction therapy; ** = prednisolone poor response is defined as blast count of more than 1000 per mL of peripheral blood on the day 8 of induction therapy; HR = high risk; IR = intermediate risk; N = number of patients; SR = standard risk

Treatment of blast cells with cytotoxic drugs

Cells were collected and a suspension of 1×10^6 cells in 1.8 mL of fresh culture medium was plated in each well of the 24-well plate (Corning Inc., Corning, NY, USA). Then, 0.2 mL of different concentrations of cytotoxic drugs (prednisolone, daunorubicin, methotrexate, asparaginase or vincristine) diluted in saline were added to the cells. Each drug was used in three logarithmically increasing concentrations, which were determined before the beginning of the study. Few logarithmically increasing concentrations were tested and final concentrations used in the study were selected based on blast viability. More specifically, the lowest concentration was chosen such that it was not significantly cytotoxic. In the experiments, prednisolone (Predisolut, MIBE GmbH Arzneimittel, Brehna, Germany) was used at final concentrations of 1, 0.1 and 0.01 mM, daunorubicin (Daunoblastin, Pfizer, New York, NY, USA) at concentrations of 1, 0.1 and 0.01 $\mu\text{g}/\text{mL}$, methotrexate (Methotrexate, Medac Pharma, Wedel, Germany) at concentrations of 1, 0.1 and 0.01 mg/mL and asparaginase (Oncaspar Pegaspargase, Servier Pharmaceuticals

LLC, Boston, MA; USA) at concentrations of 1, 0.1 and 0.01 units/mL. Vincristine (Vincristine, Teva Pharmaceuticals, Tel Aviv, Israel) was used at concentrations of 0.1, 0.01 and 0.001 $\mu\text{g}/\text{mL}$, with the exception of two experiments, performed at the time when optimal concentration was to be determined. In those two experiments vincristine was used at concentration of 10, 1 and 0.1 $\mu\text{g}/\text{mL}$. Each experiment also included a population of blast cells not exposed to any cytotoxic drug (addition of 0.2 mL saline), which was used as a control. After the addition of the cytotoxic drugs, the cells were incubated in a 5% CO_2 humidified incubator at 37 °C for three days and then prepared for immunophenotypic analysis by quantitative flow cytometry.

Quantitative flow cytometric measurements

To quantify the antigen expression a calibration chart was used. It was based on Quantum™ Simply Cellular® beads (Bangs Laboratories Inc., Fishers, IN, USA) and was generated at the time of each experiment. The sample and bead measurements were performed on the same day under the same conditions. The measured fluorescence of each antibody on the surface of the blast cells was converted to an antibody count using the calibration chart and expressed as antibody binding capacity. Measurements, analysis and interpretation of the results were performed according to the Instructions for Use of Quantum™ Simply Cellular® Beads (Bangs Laboratories Inc.).

Cell count and sample preparation for flow-cytometric analysis was carried out as previously described by our group.^{30,31} The sample aliquot containing half a million cells was first put in a test tube. Antibodies against CD10, CD19, CD20, CD27, CD34, CD45 CD58, CD66c and CD137 antigens were added at saturation concentrations (Table 4). 1 μL of propidium iodide (concentration 200 $\mu\text{g}/\text{mL}$) was also added to determine the viability of cells. After 20 min incubation, erythrocyte lysis was carried out using a commercial lysing solution (BD Biosciences, Franklin Lakes, NJ, USA). The samples were then acquired using a FACSCanto 10-colour flow cytometer (BD Biosciences) with three lasers (405, 488 and 633 nm) and FACSDiva 8.0.2 software (BD Bioscience). The flow cytometer was routinely set up and calibrated by measuring FACSDiva™ CS &T IVD beads (BD Biosciences) and Sphero™ Rainbow Calibration particles (Spherotech Inc., Lake Forest, IL, USA).

TABLE 4. The description of the antibodies used for flow cytometry

	Antibody	Antibody clone	Antibody vendor	Antibody volume (µL)
CD10	Anti-CD10 Horizon™ BV605	HI10a	BD Biosciences	5
CD19	CD19-BD Horizon™ V450 Mouse Anti-Human CD19	SJ25C1	BD Biosciences	5
CD20	CD20-BD™ CD20 APC	L27	BD Biosciences	7
CD27	CD27-BD Horizon™ APC-R700 Mouse Anti-Human CD27	M-T271	BD Biosciences	5
CD34	CD34-BD™ CD34 PE -Cy™7	8G12	BD Biosciences	5
CD45	CD45-BD™ CD45 APC-Cy™7	2D1	BD Biosciences	3
CD58	CD58-BD Pharmingen™ FITC Mouse Anti-Human CD58	1C3	BD Biosciences	3
CD66c	CD66c-BD OptiBuild™ BV510 Mouse Anti-Human CD66c	B6.2/ CD66	BD Biosciences	5
CD137	CD137-BD Pharmingen™ PE Mouse Anti-Human CD137	4B4-1	BD Biosciences	7

For the final analyses, the software BD FlowJo 10.8.1 (BD Biosciences) was used. First a gate for mononuclear cells on the forward versus side scatter plot was selected. In the next step, single cells were selected by gating on the height against the area for forward scatter. Gating on propidium iodide was used to select only viable cells. In the final step, blast cells were gated according to their immunophenotype, in most cases by selecting CD10-positive cells on CD10 versus CD45 plots. An example of a gating procedure is shown in Figure 1. Finally, we determined the fluorescence of each antigen analysed from the histogram.

Statistical analysis

The analysis was performed using R (R version 4.1.0)³² and Julia (version 19.2).³³ Linear mixed models were fitted using R package nlme (version 3.1-157)³⁴ and using MixedModels.jl (version 4.13.1)³⁵ in Julia. The optimal transformation of the dependent variables and the assessment of the goodness of fit of linear mixed models were performed with the help of the goodness of fit procedure described in publication by Peterlin *et al.*³⁶ The significance of the parameters was assessed with Wald's test in the nlme package, and the confidence intervals were computed with the help of the parametric bootstrap with 10^6 repetitions in MixedModels.jl. All p values and confidence intervals are two-sided and were adjusted with the Bonferonni-Holm procedure, with a significance level of 0.05. The marginal effects were calculated with the help of the lmeresampler package (version 0.2.4) with residual bootstrap with 10^4 repetitions. The 95% confidence intervals for these marginal effects are unadjusted and provided only in graphic form, serving as a

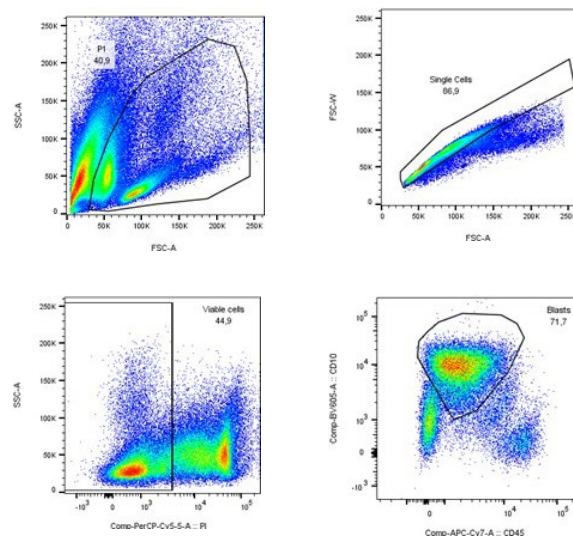


FIGURE 1. Example of a gating procedure. Mononuclear cells were selected on the forward versus side scatter plot (A) and single cells by gating on the area against the width for forward scatter (B). Propidium iodide (PI) was used to select viable cells (C). The final selection of blasts was based on their immunophenotype, in this case by selecting CD10-positive cells on the CD10 versus CD45 plots (D).

tool to aid in understanding the results rather than as definitive statistical result.

We have analyzed every single antigen expression (CDn) with a separate linear mixed model. Before analyzing the data with linear mixed models, we transformed the dependent variables CDn and the number of cytotoxic drugs given. We have done this to improve the resulting models' goodness of fit. We have used 9 models described by the formula:

$$\log(CDn + 0.1) \sim 1 + 1_{con} * con + \sum_{d \in drugs} 1_d * (d + k_d * \log_{10}(amount)) + (1|id).$$

In the above formula, the term **CDn** indicates the antigen expression, **con** indicates control, **drugs** indicates the cytotoxic drugs that were present in this study, **id** determines the patient and $\mathbf{x} \rightarrow \mathbf{1}_x$ indicates an indicator function (**0** if **0** is not true and **1** if **x** is true). The fixed effects parameters of the above model are then **con** - base value for units in the data that were not exposed to any cytotoxic drugs, **d** and **k_d** are the - base value and the slope for the units that were exposed to the cytotoxic drug **d**. We assessed the significance of the parameters **d** and **k_d**.

Results

For every drug **d** and marker CDn antigen, we have primarily been focused on the statistical significance of the coefficients **d**, which signifies the effect that we observed that was independent of the amount (for the amounts that we have examined), and the coefficient **k_d**, which describes how the value of the $\log(CD + 0.1)$ changes with respect to the \log_{10} (amount) of a drug **d**, which signifies the effect that we observed that was dependent on the amount. For a given CDn and drug **d** that appear in the same row in Table 5, one of four things can happen:

A) Both coefficients (**d**, **k_d**) were statistically significantly different from 0. In this case, which we highlight with red in Table 5, we can interpret this as merely giving a drug to a cell culture, significantly changing observed antigen expression on blast cells, and that it also matters in which amount the drug is given to the culture. One such example was CD19 and vincristine. In the case of CD19 and vincristine, we can therefore expect that the value of the $\log(CD + 0.1)$ will decrease by $0.56 - 0.17 * \log_{10}(amount)$ for a given patient and amount in the range examined by our study. Note that the amounts of vincristine examined by our analysis ranged from 0.001 to 10. Hence, depending on the amount, we expect the decrease of $\log(CD19 + 0.1)$ to be between $-0.56 - 0.17 * \log_{10}(10) = -0.73$ to $0.56 - 0.17 * \log_{10}(0.001) = -0.05$ and it decreases linearly with respect to $\log_{10}(amount)$. Other combinations of drug and observed CDn antigen with the same pattern of influence are daunorubicin and CD10, CD137, CD19, CD34, CD45 and CD58, as well as vincristine and CD45 and CD58.

B) If just the coefficient **d** was significant, which we highlight with blue in Table 5, we can interpret that giving a drug **d** to cell culture significantly changes antigen expression. However, the amount of drug **d** that is used, if the amount is within the range of the drug **d** given in this study, does not significantly alter the expression of observed CDn antigen. One such example is CD19 and prednisolone.

In the case of prednisolone and CD19, we can say that we expect that the patient's value of $\log(CD19 + 0.1)$ decreases by 0.61, regardless of the amount of prednisolone, as long as this amount is in the range examined by our study, which was 0.01 and 1.0.

Other combinations of drug and observed antigen with the same pattern of influence were daunorubicin and CD27, as well as prednisolone and CD10, CD27, CD34 and CD58.

C) If only the coefficient **k_d** was significant, which we highlight with green in Table 5, we cannot say that just giving some amount (in the range examined by our study) of drug **d** to blast cells is either up or downmodulating the CDn antigen expression without specifying the amount of this drug. Example of this is CD20 and daunorubicin.

In the case of daunorubicin and CD20, we can say that the value of patients' $\log(CD20 + 0.1)$ changes by $-0.22 * \log_{10}(amount)$ when the amount is between 0.01 and 1, which is the range examined by our study. This means that the value of $\log(CD20 + 0.1)$ can either change by $-0.22 * \log_{10}(1) = 0$ or increase by $-0.22 * \log_{10}(0.01) = 0.44$, depending on the value of $\log_{10}(amount)$, with respect to which, it changes linearly.

D) If neither the coefficient **d** nor **k_d** is statistically significantly different from 0, we cannot say that the drug **d** affects the CDn marker—an example is vincristine and CD10 (Table 5).

Marginal effects for these nine models are shown in Figure 2A and Figure 2B. From these figures, we can easily see which cytotoxic drugs change a specific CDn antigen expression. However, since this study is primarily concerned with the effects of cytotoxic drugs conditionally on the individual and these figures are primarily informative, the confidence intervals in these two figures are not adjusted.

Discussion

Our *in vitro* study has shown that prednisolone, methotrexate, vincristine, daunorubicin and asparaginase used in the induction treatment of ALL cause up- or down-modulation of some antigens on ALL blast cells. The effect of the drugs was dose-dependent or dose-independent. We showed that the drugs used in induction therapy influence antigen expression which has been not yet described in the literature such as CD27, CD45, CD137 and CD66c. Moreover, the results of our study showed that cytotoxic drugs used in the induction treatment of ALL can influence CD19, CD20 and CD58 antigen expression on blast cells that can play an essential role in the treatment of resistant or relapsed disease or antigens that could potentially influence the future stratification of patients into risk groups important for planning the treatment.

CD20 expression was stable with all cytotoxic drugs except daunorubicin. When the effect of daunorubicin was analysed with our statistical model, there were no changes in CD20 expression. However, when only the role of dose was examined, a modulation of CD20 expression was observed. Accordingly, we cannot say that just giving some amount of daunorubicin to blast cells causes an up- or down-modulation of CD20 expression without specifying the amount of the drug. These results are difficult to interpret, but as our study was not designed to explain the isolated effect of the dose when there is no effect of the drug in the model. To clarify the discrepancy between the effect of the drug and its dose, further analyses with a larger number of patients and a larger number of different concentrations of daunorubicin are needed.

Dworzak *et al.* have published that CD20 is up-modulated in the early phases of therapy, especially in patients with poor prognosis and high MRD at the end of induction treatment.⁷ Similar changes also occurred after blasts were exposed to different cytotoxic drugs *in vitro*.⁷ Prednisolone and a single intrathecal dose of methotrexate are usually the only drugs used in the first week of ALL therapy and in some protocols, the response to prednisolone is one of the criteria for stratifying patients into risk groups. It is defined by the number of blast cells in the peripheral blood on day 8 of treatment. If the patient has more than 1000 blasts per millilitre of blood, they are defined as a prednisolone poor responder and thus a high-risk patient.¹ If the number of blasts is very high at the start of treatment, a patient may not reach

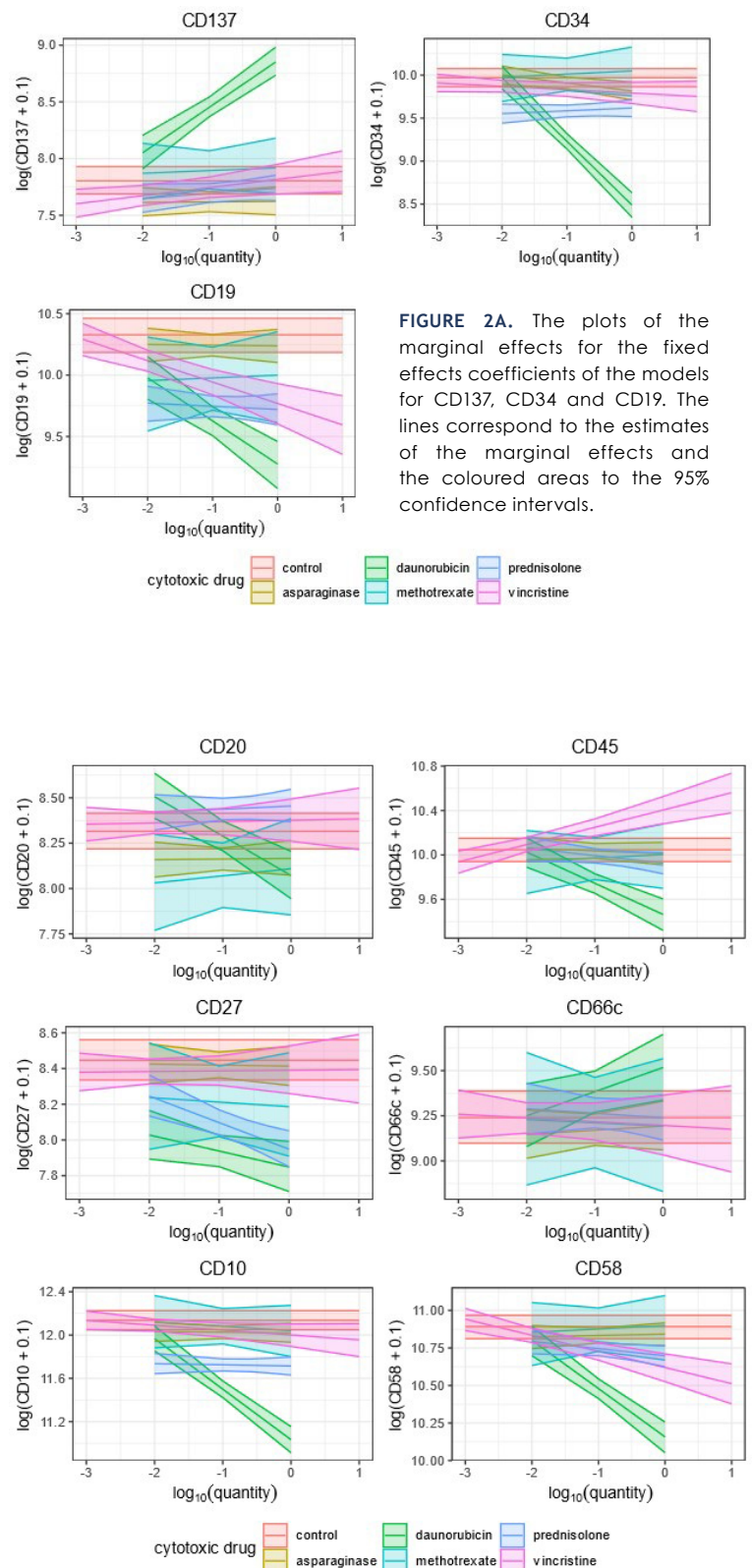


TABLE 5. The coefficients obtained by using separate mixed model which showed the effect of single drug in CDn antigen expression. The coefficient d showed the presence of CDn antigen and coefficient of k_d the influence of drug dose on antigen expression. The way how the given drug influences the antigen expression is shown in different colours: **RED** (coefficients d and k_d are statistically significantly different from 0), **BLUE** (the coefficient d is significantly different from 0), **GREEN** (coefficient k_d is significantly different from 0) and **WHITE** (neither the coefficient d nor k_d is statistically significantly different from 0). 95% confidence intervals, and corresponding p values are also shown. All confidence intervals and p values were adjusted with Holm's method

Drug	CD	Coefficient d (presence)	p value for d	Coefficient k_d (log(amount))	p value for k_d
Asparaginase	CD10	-0.12, [-0.33, 0.1]	1	-0.01, [-0.11, 0.1]	1
	CD137	-0.18, [-0.46, 0.1]	1	0, [-0.11, 0.12]	1
	CD19	-0.09, [-0.42, 0.24]	1	-0.01, [-0.14, 0.13]	1
	CD20	-0.15, [-0.39, 0.09]	1	0, [-0.09, 0.1]	1
	CD27	-0.03, [-0.28, 0.22]	1	-0.01, [-0.12, 0.11]	1
	CD34	-0.15, [-0.4, 0.09]	1	-0.09, [-0.23, 0.04]	1
	CD45	-0.04, [-0.27, 0.2]	1	-0.02, [-0.16, 0.11]	1
	CD58	-0.05, [-0.23, 0.13]	1	0.01, [-0.08, 0.1]	1
	CD66c	-0.05, [-0.36, 0.27]	1	0.02, [-0.15, 0.19]	1
Daunorubicin	CD10	-1.1, [-1.38, -0.83]	< 0.001	-0.47, [-0.63, -0.31]	< 0.001
	CD137	1.05, [0.72, 1.37]	< 0.001	0.4, [0.21, 0.59]	< 0.001
	CD19	-1.05, [-1.48, -0.62]	< 0.001	-0.35, [-0.6, -0.1]	< 0.001
	CD20	-0.24, [-0.53, 0.05]	0.35	-0.22, [-0.39, -0.05]	0.002
	CD27	-0.6, [-0.92, -0.27]	< 0.001	-0.09, [-0.27, 0.09]	1
	CD34	-1.48, [-1.8, -1.16]	< 0.001	-0.74, [-0.93, -0.55]	< 0.001
	CD45	-0.58, [-0.9, -0.27]	< 0.001	-0.28, [-0.47, -0.1]	< 0.001
	CD58	-0.73, [-0.97, -0.5]	< 0.001	-0.32, [-0.46, -0.19]	< 0.001
	CD66c	0.28, [-0.13, 0.69]	1	0.13, [-0.1, 0.37]	1
Methotrexate	CD10	-0.1, [-0.52, 0.33]	1	-0.04, [-0.32, 0.24]	1
	CD137	0.11, [-0.33, 0.56]	1	0.02, [-0.24, 0.29]	1
	CD19	-0.33, [-1, 0.35]	1	0.02, [-0.38, 0.42]	1
	CD20	-0.21, [-0.68, 0.27]	1	0.04, [-0.26, 0.34]	1
	CD27	-0.26, [-0.79, 0.27]	1	-0.03, [-0.34, 0.29]	1
	CD34	0.08, [-0.4, 0.56]	1	0.04, [-0.28, 0.35]	1
	CD45	-0.04, [-0.5, 0.41]	1	0.03, [-0.29, 0.35]	1
	CD58	0.01, [-0.25, 0.27]	1	0.02, [-0.21, 0.26]	1
	CD66c	-0.05, [-0.64, 0.54]	1	-0.02, [-0.4, 0.37]	1
Prednisolone	CD10	-0.42, [-0.64, -0.21]	< 0.001	-0.01, [-0.12, 0.1]	1
	CD137	-0.06, [-0.32, 0.19]	1	0.05, [-0.1, 0.19]	1
	CD19	-0.61, [-0.94, -0.27]	< 0.001	-0.03, [-0.2, 0.15]	1
	CD20	0.14, [-0.09, 0.37]	1	0.02, [-0.1, 0.14]	1
	CD27	-0.5, [-0.76, -0.23]	< 0.001	-0.15, [-0.3, 0]	0.055
	CD34	-0.35, [-0.6, -0.11]	< 0.001	0.03, [-0.1, 0.16]	1
	CD45	-0.12, [-0.36, 0.12]	1	-0.07, [-0.2, 0.07]	1
	CD58	-0.19, [-0.38, -0.01]	0.034	-0.05, [-0.15, 0.05]	1
	CD66c	0, [-0.19, 0.19]	1	-0.02, [-0.2, 0.15]	1
Vincristine	CD10	-0.14, [-0.37, 0.1]	1	-0.05, [-0.14, 0.05]	1
	CD137	0.01, [-0.22, 0.25]	1	0.07, [-0.04, 0.18]	1
	CD19	-0.56, [-0.94, 0]	< 0.001	-0.17, [-0.32, -0.03]	0.004
	CD20	0.06, [-0.19, 0.31]	1	0.01, [-0.08, 0.09]	1
	CD27	-0.06, [-0.34, 0.23]	1	0, [-0.09, 0.09]	1
	CD34	-0.18, [-0.45, 0.1]	1	-0.04, [-0.14, 0.06]	1
	CD45	0.36, [0.07, 0.64]	0.002	0.16, [0.05, 0.26]	< 0.001
	CD58	-0.27, [-0.48, -0.06]	0.001	-0.11, [-0.19, -0.03]	< 0.001
	CD66c	-0.04, [-0.39, 0.3]	1	-0.02, [-0.15, 0.11]	1

the threshold despite a relatively good response to therapy, resulting in a classification in a high-risk group with a more aggressive and toxic treatment. None of our patients was classified as HR due to a poor response to prednisolone and CD20 expression remained stable in the *in vitro* settings after the addition of prednisolone. Those results are consistent with the publication by Dworzak *et al.* showing that CD20 up-modulation in early treatment phases is associated with a worse prognosis.⁷ However, since all patients in our experiment responded well to prednisolone, we cannot confirm that CD20 modulation could be a stratification criterion replacing the number of blasts in peripheral blood on day 8 of therapy. To confirm this hypothesis, we would need to include more patients.

Rituximab, an anti-CD20 antibody, has been shown to improve survival in adult patients with CD20-positive B-cell ALL.² Based on the data published by van der Sluijs-Gelling *et al.* describing CD20 up-modulation after *in vitro* exposure of blast cells to prednisolone, dexamethasone, vincristine or asparaginase¹⁰, one might assume that rituximab has the best efficacy when one of these drugs is used prior to initiation of the therapy. In contrast to the published results, our study suggests that the use of rituximab is equally justified in all phases of therapy that include steroids, vincristine, methotrexate or asparaginase.

CD19 expression in ALL is of clinical importance due to the efficacy of anti-CD19 therapies such as blinatumomab or CAR-T cells.^{23,24} According to our results, daunorubicin, vincristine and prednisolone can induce down-modulation of CD19, which is partly consistent with data published by Van der Sluijs-Gelling *et al.* showing that CD19 is down-modulated after exposure to prednisolone, dexamethasone, vincristine or asparaginase.¹⁰ These changes may have implications for the treatment of children with resistant or relapsed ALL who receive blinatumomab or anti-CD19 CAR-T therapy. In the 4–6 weeks between leukapheresis and CAR-T administration, bridging therapy reduces the disease burden and keeps the patient's clinical condition stable. After reviewing the patient's medical history and response to previous treatment, a multidisciplinary team usually selects cytotoxic drugs for bridging therapy. There are no specific recommendations for the choice of therapeutic approach at this crucial stage.³ Our results show that daunorubicin, vincristine and prednisolone can induce down-modulation of CD19 on blast cells suggesting these drugs and especially prednisolone, whose effect is dose-independent,

should be better avoided in bridging therapy so as not to impair the effectiveness of anti-CD19 immunotherapy.

The presence of CD58 has been shown to be very important for the efficacy of bispecific anti-CD19 antibodies and anti-CD19 CAR-T cell therapy, as the lack of CD58 decreases T-lymphocyte activation and reduces the success of treatment.^{4,5} In our experiment, CD58 was down-modulated when daunorubicin, prednisolone or vincristine was added. The effect of prednisolone was dose-independent, while the dose of daunorubicin and vincristine was also important. Gaipa *et al.* described the down-modulation of CD58 expression on day 33 of treatment in patients with ALL, and these changes were considered to be prognostically significant.⁸ Our results and the data from Gaipa's study suggest that it may be useful to avoid daunorubicin, prednisolone or vincristine immediately before specific anti-CD19 therapy as well as for bridging therapy to prevent CD58 down-modulation and a possible decrease in treatment efficacy.

Specific changes in CD10 and CD34 expression during ALL therapy is controversial, but it has been shown that CD10 positivity in B-ALL had been associated with disease prognosis.¹⁵ CD10, also known as the common acute lymphoblastic leukaemia antigen, can be detected in the blast cells of most patients with B-ALL.¹⁵ The prognostic significance of CD10 expression is associated with several favourable features such as a hyperdiploid karyotype, age less than nine years and a standard risk group.^{15,19} Our study showed down-modulation of CD10 after treatment with daunorubicin or prednisolone, and the effect of prednisolone was dose-independent. This is consistent with published data showing a transient down-modulation of CD10 in the early phase of ALL treatment, with the changes being more pronounced in patients with a good response to prednisolone and a better prognosis of the disease.^{8–10,37}

CD34, the pluripotent stem cell antigen, plays an important role in stem cell attachment to the extracellular matrix and its presence on blast cells has been shown to be a good prognostic factor in adult patients with ALL, who have undergone stem cell transplantation in the first remission.¹⁴ Its positivity in ALL is also associated with a lower leukocyte count, a favourable karyotype and a better prognosis compared to CD34-negative ALL.¹⁵ In our experiment, prednisolone and daunorubicin triggered a significant down-modulation of CD34, which again is partly consistent with published da-

ta, where down-modulation of CD34 on blast cells after *in vitro* exposure to prednisolone and *in vivo* during the early phase of ALL therapy has been shown, especially in patients with a better prognosis.^{9,10,37} According to our data, methotrexate, vincristine and asparaginase, drugs also used in induction therapy, had no effect on CD34 expression.

In our study CD10 and CD34 were shown to be down-modulated in blast cells after exposure to prednisolone and daunorubicin, which is partly consistent with data published by Gaipa *et al.* showing correlation between a better response to prednisolone and down-modulation of CD10 and CD34.⁹ Since our study included only a small number of patients and all responded well to prednisolone, our data do not allow us to draw any conclusions about the importance of changes in antigen expression as a prognostic marker. Therefore, a larger number of patients, including prednisolone-poor responders would need to be enrolled in the study to confirm changes in CD10 and CD34 expression as stratification parameters.

In addition to CD10, CD19, CD20, CD34 and CD58, we analysed other antigens whose modulation significance in patients with B-ALL has, to our knowledge, not yet been described. The experiment allowed us to assess shifts in the expression of CD27, CD45, CD66c and CD137.

Lower expression of CD45, an essential modulator of signal transduction pathways in blast cells, is associated with a higher rate of complete remissions at day 29 of B-ALL treatment and high expression of CD45 was associated with unfavourable prognostic factors and worse event free survival of the disease.^{10,16,26,38} In our experiment, CD45 was down-modulated after exposure to increasing concentrations of daunorubicin, and a dose-dependent up-modulation was observed after the addition of vincristine to the blast cells. Since it was shown that CD45 expression is higher in immature pro-B-ALL than in pre-B-ALL we could speculate that vincristine causes modulation of antigen expression towards the immunophenotype of pro-B-ALL.¹⁶ Additionally, it has been shown that increased CD45 expression in blast cells is associated with decreased cell proliferation and treatment resistance but to determine the importance of changes in CD45 expression after exposure to daunorubicin and vincristine, further test would be needed.¹⁶

CD137 is known to be present in T lymphocytes and natural killer cells.³⁹ The antigen is also expressed in human B lymphocytes, particularly on activated B cells.²⁸ Despite the low expression

of CD137 (data not shown), we were able to detect an up-modulation of the antigen, but only after exposure to daunorubicin. Zhang *et al.* has published that CD137 mediates cell proliferation and that B cell survival was improved by CD137 ligation.²⁸ Potentially in case of CD137 up-modulation on blast cells after exposure to daunorubicin, the survival of blast cells could be improved, influencing the response to therapy. To evaluate the clinical impact of CD137 modulation, further analysis would be needed.

CD27, a member of the tumour necrosis factor receptor superfamily, is mainly present on T cells, natural killer cells and thymocytes.⁴⁰ It can also be detected on the surface of memory B cells as well as on high risk B-ALL with Philadelphia chromosome, cytokine receptor-like factor 2 (CRLF2) rearrangement or in B-other ALL with unknown or not classifying genetic aberrations, where it is additional poor prognostic factor.^{11,13,41} In oncology, CD27 is important in induction of cytotoxic T lymphocyte activation and CD27 agonists were proven to induce antitumor immunity.^{13,42} Additionally Vitale *et al.* have shown that anti-CD27 antibodies have also a direct effect against CD27 positive blast cells.⁴³ Our study showed a dose-independent down-modulation of CD27 on blast cells after exposure to daunorubicin or prednisolone. Our results suggest that down-modulation of CD27 may attenuate the efficacy of a direct anti-CD27 antibody against blast cells. Since we have shown that CD27 is down-modulated in blast cells, it would be very interesting to investigate the effect of daunorubicin and prednisolone on CD27 expression and activation of cytotoxic T lymphocytes, for which further studies are needed.

Patients diagnosed with Philadelphia chromosome positive ALL are usually treated with a combination of tyrosine kinase inhibitors and standard chemotherapy.⁴⁴ CD66c is the myeloid antigen commonly expressed on malignant B lymphoblasts, has no clear prognostic significance but is associated with important genetic alterations such as the presence of a Philadelphia chromosome, hyperdiploidy, hypodiploidy and CRLF2-positivity in B-ALL.^{17,18} After analysing the effects of chemotherapy, we found that CD66c expression was mostly low but quantifiable and that none of the drugs had an impact on its expression. Importantly, none of the included patients had Philadelphia chromosome positive ALL. Since the expression of CD66c was stable after the exposure to all tested drugs, CD66c could be a good candidate to MRD detection in patients with CD66c positive B-ALL.

Conclusions

The present *in vitro* study and statistical model allowed us to determine the effects of each drug and its dose separately. We were able to show that cytotoxic drugs can induce changes in the expression of antigens that play an important role in planning immunotherapy or that are prognostically important. Importantly we have shown that CD19 and CD58 were down-modulated after exposure to daunorubicin, prednisolone or vincristine, suggesting that these drugs are better avoided during bridging therapy prior to CAR-T cell therapy or bispecific antibodies. Furthermore, we have shown that in some cases the dose of the drug, as opposed to the addition of the drug itself, had no effect on antigen expression. An example of this is prednisolone, where all antigen modulations were dose-independent, meaning that even low doses of the drug can induce immunophenotypic changes.

Moreover, according to our results, cytotoxic drugs trigger other changes in the expression of antigens that could be prognostically important. However, further analyses with a larger number of patients are required to determine the clinical significance of these changes.

Acknowledgement

The research was supported by the Slovenian Research and Innovation Agency (ARIS) [grant numbers P3-0003, P3-0289 and P3-0154] and by the University Medical Centre Ljubljana grant 20200252.

References

- Campbell M, Castillo L, Riccheri C, Janic D, Jazbec J, Kaiserova E, et al. ALL IC-BFM 2009. A randomized trial of the I-BFM-SG for the management of childhood non-B acute lymphoblastic leukemia. Final version of therapy protocol from August 14 2009. [Internet]. [cited 2023 Mar 15]. Available at https://www.bialaczk.org/wp-content/uploads/2016/10/ALLIC_BFM_2009.pdf
- Maury S, Chevret S, Thomas X, Heim D, Leguay T, Huguot F, et al. Rituximab in B-lineage adult acute lymphoblastic leukemia. *N Engl J Med* 2016; **375**: 1044-53. doi: 10.1056/nejmoa1605085
- Hayden PJ, Roddie C, Bader P, Basak GW, Bonig H, Bonini C, et al. Management of adults and children receiving CAR T-cell therapy: 2021 best practice recommendations of the European Society for Blood and Marrow Transplantation (EBMT) and the Joint Accreditation Committee of ISCT and EBMT (JACIE) and the European Haematology Association (EHA). *Ann Oncol* 2022; **33**: 259-75. doi: 10.1016/j.annonc.2021.12.003
- Li Y, Moriyama T, Yoshimura S, Zhao X, Li Z, Yang X, et al. PAX5 epigenetically orchestrates CD58 transcription and modulates blinatumomab response in acute lymphoblastic leukemia. *Sci Adv* 2022; **8**: eadd6403. doi: 10.1126/sciadv.add6403
- Yan X, Chen D, Ma X, Wang Y, Guo Y, Wei J, et al. CD58 loss in tumor cells confers functional impairment of CAR T cells. *Blood Adv* 2022; **6**: 5844-56. doi: 10.1182/bloodadvances.2022007891
- Hunger SP, Raetz EA. How I treat relapsed acute lymphoblastic leukemia in the pediatric population. *Blood* 2020; **136**: 1803-12. doi: 10.1182/blood.2019004043
- Dworzak MN, Schumich A, Printz D, Pötschger U, Husak Z, Attarbaschi A, et al. CD20 up-regulation in pediatric B-cell precursor acute lymphoblastic leukemia during induction treatment: setting the stage for anti-CD20 directed immunotherapy. *Blood* 2008; **112**: 3982-88. doi: 10.1182/blood-2008-06-164129
- Gaipa G, Basso G, Maglia O, Leoni V, Faini A, Cazzaniga G, et al. Drug-induced immunophenotypic modulation in childhood ALL: implications for minimal residual disease detection. *Leukemia* 2005; **19**: 49-56. doi: 10.1038/sj.leu.2403559
- Gaipa G, Basso G, Aliprandi S, Migliavacca M, Vallinoto C, Maglia O, et al. Prednisone induces immunophenotypic modulation of CD10 and CD34 in nonapoptotic B-cell precursor acute lymphoblastic leukemia cells. *Cytometry B Clin Cytom* 2008; **74**: 150-5. doi: 10.1002/cyto.b.20408
- van der Sluijs-Gelling AJ, van der Velden VHJ, Roeffen ETJM, Veerman AJP, van Wering ER. Immunophenotypic modulation in childhood precursor-B-ALL can be mimicked in vitro and is related to the induction of cell death. *Leukemia* 2005; **19**: 1845-7. doi: 10.1038/sj.leu.2403911
- Chen D, Gerasimčik N, Camponeschi A, Tan Y, Wu Q, Brynjolfsson S, et al. CD27 expression and its association with clinical outcome in children and adults with pro-B acute lymphoblastic leukemia. *Blood Cancer J* 2017; **7**: e575. doi: 10.1038/bcj.2017.55
- Riether C, Schürch CM, Bühner ED, Hinterbrandner M, Huguenin AL, Hoepner S, et al. CD70/CD27 signaling promotes blast stemness and is a viable therapeutic target in acute myeloid leukemia. *J Exp Med* 2017; **214**: 359-80. doi: 10.1084/jem.20152008
- Starzer AM, Berghoff AS. New emerging targets in cancer immunotherapy: CD27 (TNFRSF7). *ESMO Open* 2020; **4**(Suppl 3): e000629. doi: 10.1136/esmoopen-2019-000629
- Aljurf M, Chaudhri NA, Almhareb F, Walter CU, Nounou R, Khalil S, et al. CD34 expression in adult acute lymphoblastic leukemia (ALL) is a favorable prognostic factor in patients treated with stem cell transplant in first remission. *Blood* 2011; **118**: 4091. doi: 10.1182/blood.v118.21.4091.4091
- Dakka N, Bellaoui H, Bouzid N, Khattab M, Bakri Y, Benjouad A. CD10 and CD34 expression in childhood acute lymphoblastic leukemia in morocco: clinical relevance and outcome. *Pediatr Hematol Oncol* 2009; **26**: 216-31. doi: 10.1080/07357900902897557
- Cario G, Rhein P, Mitlöchner R, Zimmermann M, Bandapalli OR, Romey R, et al. High CD45 surface expression determines relapse risk in children with precursor B-cell and T-cell acute lymphoblastic leukemia treated according to the ALL-BFM 2000 protocol. *Haematologica* 2014; **99**: 103-10. doi: 10.3324/haematol.2013.090225
- Guillaume N, Penther D, Vaida I, Gruson B, Harrivel V, Claisse JF, et al. CD66c expression in B-cell acute lymphoblastic leukemia: strength and weakness. *Int J Lab Hematol* 2011; **33**: 92-6. doi: 10.1111/j.1751-553X.2010.01254.x
- Kiyokawa N, Iijima K, Tomita O, Miharu M, Hasegawa D, Kobayashi K, et al. Significance of CD66c expression in childhood acute lymphoblastic leukemia. *Leuk Res* 2014; **38**: 2-48. doi: 10.1016/j.leukres.2013.10.008
- Consolini R, Legitimo A, Rondelli R, Guguelmi C, Barisone E, Lippi A, et al. Clinical relevance of CD10 expression in childhood ALL. The Italian Association for Pediatric Hematology and Oncology (AIEOP). *Haematologica* 1998; **83**: 967-73. PMID: 9864914
- Mitwasi N, Arndt C, Loureiro LR, Kegler A, Fassrinner F, Berndt N, et al. Targeting CD10 on B-cell leukemia using the universal CAR T-cell platform (UniCAR). *Int J Mol Sci* 2022; **23**: 4912. doi: 10.3390/ijms23094920
- Gökbuğut N, Hoelzer D. Treatment with monoclonal antibodies in acute lymphoblastic leukemia: Current knowledge and future prospects. *Ann Hematol* 2004; **83**: 201-5. doi: 10.1007/s00277-003-0752-8
- Wang K, Wei G, Liu D. CD19: a biomarker for B cell development, lymphoma diagnosis and therapy. *Exp Hematol Oncol* 2012; **1**: 1-7. doi: 10.1186/2162-3619-1-36

23. Brown PA, Ji L, Xu X, Devidas M, Hogan L, Borowitz JB, et al. A randomized phase 3 trial of blinatumomab vs. chemotherapy as post-reinduction therapy in high and intermediate risk (HR/IR) first relapse of B-acute lymphoblastic leukemia (B-ALL) in children and adolescents/young adults (AYAs) demonstrates superior efficacy and tolerability of blinatumomab: a report from children's oncology group study AALL1331. *Blood* 2019; **134**(Suppl 2): LBA-1. doi: 10.1182/blood-2019-132435
24. Fabrizio VA, Phillips CL, Lane A, Baggott C, Prabhu S, Egeler E, et al. Tisagenlecleucel outcomes in relapsed/refractory extramedullary ALL: A Pediatric Real World CAR Consortium Report. *Blood Adv* 2022; **6**: 600-10. doi: 10.1182/bloodadvances.2021005564
25. Schnitzlein WM, Zuckermann FA. Determination of the specificity of CD45 and CD45R monoclonal antibodies through the use of transfected hamster cells producing individual porcine CD45 isoforms. *Vet Immunol Immunopathol* 1998; **60**: 389-401. doi: 10.1016/S0165-2427(97)00113-X
26. Balasubramanian P, Singh J, Verma D, Kumar R, Bakshsi S, Tanwar P, et al. Prognostic significance of CD45 antigen expression in pediatric acute lymphoblastic leukemia. *Blood Cells Mol Dis* 2021; **89**: 102562. doi: 10.1016/j.bcmd.2021.102562
27. Zhang Y, Liu Q, Yang S, Liao Q. CD58 Immunobiology at a glance. *Front Immunol* 2021; **12**: 1-20. doi: 10.3389/fimmu.2021.705260
28. Zhang X, Voskens CJ, Sallin M, Maniar A, Montes CL, Zhang Y, et al. CD137 promotes proliferation and survival of human B cells. *J Immunol* 2010; **184**: 787-95. doi: 10.4049/jimmunol.0901619
29. Pieters R, Schrappe M, Valsecchi MG, Biondi A, de Rossi G, Suppiah R, et al. International collaborative treatment protocol for the infants under one year with acute lymphoblastic or biphenotypic leukemia - INTERFANT 06. 2008; version 11(17 July 2007). *Cochrane Central Register of Controlled Trials*. Available at: <https://www.cochranelibrary.com/central/doi/10.1002/central/CN-01834165/full>
30. Brozic A, Pohar Marinsek Z, Novakovic S, Kloboves Prevodnik V. Inconclusive flow cytometric surface light chain results; can cytoplasmic light chains, Bcl-2 expression and PCR clonality analysis improve accuracy of cytological diagnoses in B-cell lymphomas? *Diagn Pathol* 2015; **10**: 1-10. doi: 10.1186/s13000-015-0427-5
31. Brožič A. [Clonality and antigenic properties of reactive and neoplastic lymphocytic proliferations]. [Slovenian]. *Doctoral Dissertation*; 2016. [Internet]. Available at: <https://repozitorij.uni-lj.si/lzpis/Gradiva.php?lang=slv&id=84423>
32. Team RC. *A Language and environment for statistical computing*. Vienna: R Foundation for Statistical Computing; 2020. [Internet]. [cited 2023 Feb 15]. Available at: www.r-project.org/
33. Bezanson J, Edelman A, Karpinski S, Shah VB. Julia: a fresh approach to numerical computing. *SIAM Rev* 2017; **59**: 65-98. doi: 10.1137/141000671
34. Pinheiro J, Bates D, DebRoy S, Sarkar D. Team, R.C. Nlme: Linear and Nonlinear Mixed Effects Models. *R Package Version* Nov 27 2023. [Internet]. [cited 2023 Dec]. Available at: <https://cran.r-project.org/web/packages/nlme/nlme.pdf>
35. Bates D, Alday P, Kleinschmidt D, Calderón JBS, Noack A, Kelman T, et al. JuliaStats/MixedModels.jl: v2.3.0 (v2.3.0). Zenodo; 2020 [Internet]. [cited 2023 Feb 16]. Available at: <https://doi.org/10.5281/ZENODO.3727845>
36. Peterlin J, Kežar N, Blagus R. Correct specification of design matrices in linear mixed effects models: tests with graphical representation. *TEST* 2023; **32**: 184-210. doi: 10.1007/s11749-022-00830-1
37. Dworzak MN, Gaipa G, Schumich A, Maglia O, Ratei R, Veltroni M, et al. Modulation of antigen expression in B-cell precursor acute lymphoblastic leukemia during induction therapy is partly transient: evidence for a drug-induced regulatory phenomenon. Results of the AIEOP-BFM-ALL-FLOW-MRD-study group. *Cytometry B Clin Cytom* 2010; **78**: 147-53. doi: 10.1002/cyto.b.20516
38. Espinoza-Gutierrez MR, Agarwal P, Ferrer L, Czader M, Dave U. Relationship between CD45 expression and outcomes in B lymphoblastic leukemia/lymphoma. *Blood* 2020; **136**(Suppl 1): 24. doi: 10.1182/blood-2020-142085
39. Schwarz H, Valbracht J, Tuckwell J, Von Kempis J, Lotz M. ILA the human 4-1BB homologue, is inducible in lymphoid and other cell lineages. *Blood* 1995; **85**: 1043-52. doi: 10.1182/blood.v85.4.1043.bloodjournal8541043
40. Borst J, Hendriks J, Xiao Y. CD27 and CD70 in T cell and B cell activation. *Curr Opin Immunol* 2005; **17**: 275-81. doi: 10.1016/j.coi.2005.04.004
41. Agematsu K, Hokibara S, Nagumo H, Komiya A. CD27: a memory B-cell marker. *Immunol Today* 2000; **21**: 204-6. doi: 10.1016/S0167-5699(00)01605-4
42. Taraban VY, Rowley TF, Kerr JP, Willoughby JE, Johnson PM, Al-Shamkhani A, et al. CD27 costimulation contributes substantially to the expansion of functional memory CD8+ T cells after peptide immunization. *Eur J Immunol* 2013; **43**: 3314-23. doi: 10.1002/eji.201343579
43. Vitale LA, He LZ, Thomas LJ, Widger J, Weidlick J, Crocker A, et al. Development of a human monoclonal antibody for potential therapy of CD27-expressing lymphoma and leukemia. *Clin Cancer Res* 2012; **18**: 3812-21. doi: 10.1158/1078-0432.CCR-11-3308
44. Biondi A, Schrappe M, De Lorenzo P, Castor A, Lucchini G, Gandemer V, Pieters R, et al. Imatinib after induction for treatment of children and adolescents with Philadelphia-chromosome-positive acute lymphoblastic leukaemia (EsPhALL): a randomised, open-label, intergroup study. *Lancet Oncol* 2012; **13**: 936-45. doi: 10.1016/S1470-2045(12)70377-7

Multi-institutional study of ‘Sandwich treatment’ for motor area large brain metastases (LBM) with diameter over 3 cm

Zheng Wang¹, Haining Chen², Qun Chen³, Yucun Zhu⁴, Min Li¹, Jia Zhou¹

¹ Cancer Center, Gamma Knife Treatment Center, Zhejiang Provincial People’s Hospital, Affiliated People’s Hospital of Hangzhou Medical College, Hangzhou, China

² Gamma Knife Treatment Center, Anhui Provincial Hospital, The First Affiliated Hospital of University of Science and Technology of China, Hefei, China

³ Gamma Knife Treatment Center, Jiangsu Province People’s Hospital, the First Affiliated Hospital of Nanjing Medical University Nanjing, China

⁴ Gamma Knife Treatment Center, Ming ji Hospital, Affiliated to Nanjing Medical University, Nanjing, China

Radiol Oncol 2024; 58(1): 145-152.

Received 3 July 2023

Accepted 23 September 2023

Correspondence to: Jia Zhou, Cancer Center, Gamma Knife Treatment Center, Zhejiang Provincial People’s Hospital, Affiliated People’s Hospital of Hangzhou Medical College, Hangzhou 310014, China. E-mail: cneagles@sina.com

Disclosure: No potential conflicts of interest were disclosed.

This is an open access article distributed under the terms of the CC-BY license (<https://creativecommons.org/licenses/by/4.0/>).

Background. The objective of the present study was to explore the effectiveness and safety of ‘Sandwich treatment’ strategy for large brain metastases (LBM) with diameter over 3 cm (minimum volume $\geq 15 \text{ cm}^3$) located in motor area.

Patients and methods. Patients from four gamma knife center that received ‘Sandwich treatment’ were retrospectively studied from January 2016 to March 2023. The strategy was one-week treatment course including 2 stages of stereotactic radiosurgery (SRS) and using bevacizumab once during SRS gap. The tumor volume and peri-tumor edema changes were analyzed before and after ‘Sandwich treatment’. Manual muscle testing (MMT) score and Barthel Index (BI) score were used to evaluate the changes of patients’ movement and physical strength rehabilitation. The patients’ overall survival (OS) and tumor local control (TLC) rate was calculated. Cox regression model was used to analyze the risk factors that related to TLC.

Results. 61 patients with 72 lesions received the ‘Sandwich treatment’. The median prescription dose was 13.0 Gy and 12.5 Gy at the first- and second-stage SRS. The mean tumor volume at the time of ‘Sandwich treatment’ and 3 months later was 20.1 cm^3 and 12.3 , respectively ($P < 0.01$). The mean peri-tumor edema volume at the first- and second-stage SRS was 12.6 cm^3 and 5.2 cm^3 , respectively ($P < 0.01$). Patients’ median MMT score improved from 6 at the beginning to 8 at the end of ‘Sandwich treatment’ ($P < 0.01$), BI score was also greatly improved from 45 at the time of ‘Sandwich treatment’ to 95 after 3 months ($P < 0.01$). Patients’ median OS was 14.0 months, and the 3, 6, 12 months OS rate was 92.0%, 86.0% and 66.0%, respectively. The TLC rate at 3, 6, 12 months was 98.4%, 93.4%, and 85.3%, respectively. Patients with lung cancer had lower risk of tumor relapse. The cumulative incidence of patient’s hemorrhage and radiation necrosis was 4.92% (3/61) and 13.11% (8/61) after ‘Sandwich treatment’.

Conclusions. ‘sandwich treatment’ strategy is safe and effective for LBM located in motor area. The strategy could rapidly improve the patients’ movement and enhance their physical strength rehabilitation.

Key words: Sandwich treatment; bevacizumab; two-staged SRS; motor area; large brain metastases

Introduction

Brain metastases (BM) is the most common intracranial malignant tumor in adults, and is also the

main cause of mortality of cancer patients.¹ The current guidelines suggest that patient with limited number of BM with good performance can be treated with stereotactic radiosurgery (SRS)

alone.²⁻⁵ For patients with BM number less than 10, or the total volume smaller than 4 cm³, fractionated radiosurgery or two-staged stereotactic radiosurgery (2-SSRS) could control the tumor growth with low neurotoxicity and not delay the consequent systemic treatment.⁶⁻¹¹

However, for large BM (LBM) with diameter over 3 cm (minimum volume ≥ 15 cm³) and located in motor area, even 2-SSRS is still challenging.¹² The risk mainly comes from the compression of LBM and consequent peri-tumor edema to the brain, results in devastating intracranial hypertension. Further, the SRS-induced edema would add to the risk of intracranial hypertension, limb hemiplegia and refractory epilepsy.^{13,14} Meanwhile, SRS would cause the brain radiation necrosis (RN).¹⁵⁻¹⁷ These potential risks make it difficult for patients with LBM to receive 2-SSRS in outpatient department. Patient after SRS needs long-term inpatient steroids therapy to control peri-tumor and SRS-induced edema to improve their symptoms, and lower the potential risk of RN. Bevacizumab, an anti-VEGF monoclonal molecular drug, has been utilized by practitioners in anti-tumor therapy for cancer patients.^{18,19} Also, its anti-angiogenesis effect could be used for SRS-edema and RN control.^{20,21} To help patient with motor area LBM and shorten their treatment course, the practitioners from four gamma knife center developed the

'Sandwich treatment' strategy. The strategy was one-week treatment course that includes 2-SSRS and using bevacizumab once during SRS gap. In the present study, the authors retrospectively reviewed the patients that received 'Sandwich treatment'. The purpose of this study was to evaluate the efficacy of and safety of this strategy.

Patients and methods

Patients

From January 2016 to March 2023, patients with LBM that received the 'Sandwich treatment' were retrospectively studied. The inclusion criteria are as follows: patients had (1) at least one newly diagnosed BM in the motor area; (2) tumor diameter larger than 3 cm and no previous whole brain radiation therapy; (3) received steroid therapy for tumor or peri-tumor edema controlling; (4) not ongoing systemic therapy. Because the retrospective observation study was focused mainly on the effectiveness and safety of 'Sandwich treatment' for LBM in motor area, patients fitted the inclusion criteria were all included despite they received treatment for previous primary tumor or not. The present study was approved by the Institutional Ethics Committee of Zhejiang Provincial People's Hospital (ZHRYRS 2022 No. 005).

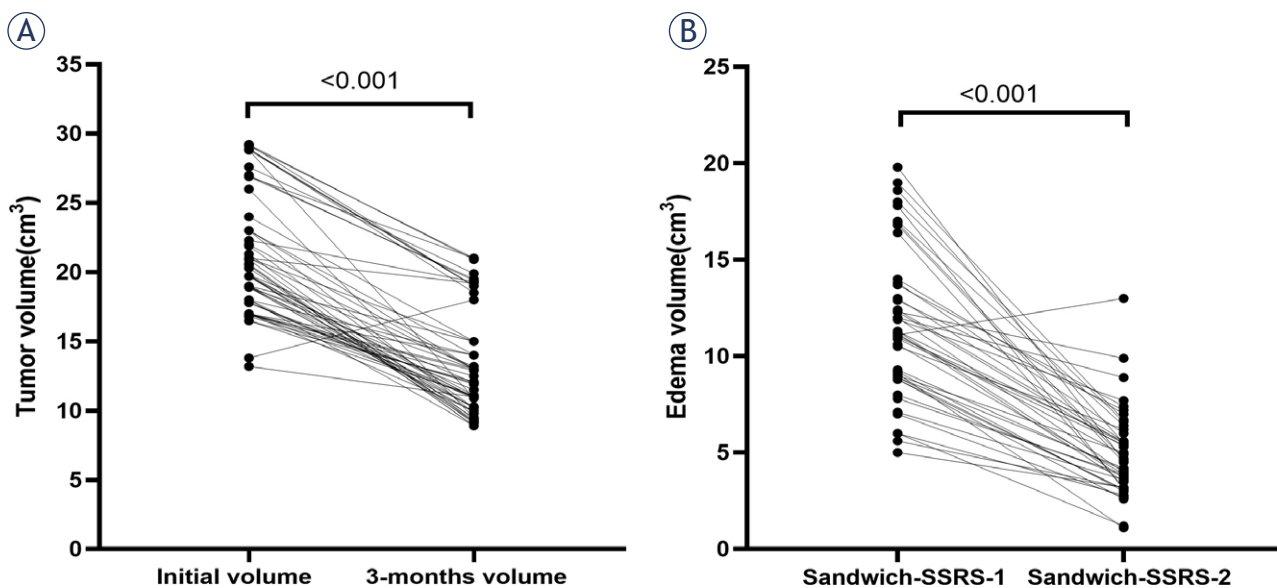


FIGURE 1. The mean tumor and peri-tumor edema volume changes. (A) The mean tumor volume decreased dramatically from 20.1 cm³ (range: 17.2–29.7 cm³) at the time of 'Sandwich treatment' to 12.3 cm³ (range: 7.7–22.4 cm³) 3 months later ($P < 0.001$); (B) The mean peri-tumor edema volume at first-stage SRS and second-stage SRS of 'Sandwich treatment' was 12.6 cm³ (range: 4.9–19.6 cm³) and 5.2 cm³ (range: 1.2–13.2 cm³) ($P < 0.001$).

2-SSRS = two-staged stereotactic radiosurgery

'Sandwich treatment' strategy

The 'Sandwich treatment' was a one-week treatment course. Two-SSRS were delivered to patients with mean dose of 13 Gy and 12.5 Gy at first and second SRS respectively. At each stage of SRS, the 45% – 60% isodose line covered the whole lesion. The bevacizumab was used once 3 days later after the first-stage SRS, for the purpose of tumor growth and peri-tumor edema control. The dose of bevacizumab was 5 mg/kg according to previous studies had suggested of 5–10 mg/kg.^{22,23} Target volumes were obtained from Gadolinium enhanced T1-weighted magnetic resonance images (MRI). The edema volume was accessed from MRI T2-FLAIR.

Evaluation of efficacy and adverse events

Tumor local control (TLC) failure was defined as 20% increase in product of perpendicular diameter on T1-enhanced MR after 'Sandwich treatment' according to the revised RANO guidelines.²⁴ Radiation necrosis (RN) was determined MRI perfusion and PET results and clinical symptoms.^{25,26} The manual muscle testing (MMT) score was used for the evaluation of patients' muscle strength change.²⁷ The scale proposed by the Medical Research Council (MRC) uses the numeral grades 0–5, 0: No contraction; 1) Flicker or trace contraction; 2) Active movement, with gravity eliminated; 3) Active movement against gravity; 4) Active movement against gravity and resistance; 5) Normal power. The total score of upper limb and lower limb was summed up as the baseline standard for the evaluation of patients' muscle strength. The Barthel Index (BI) is used to assess patients' early rehabilitation after radiosurgery.²⁸ Overall survival (OS) was defined as the time interval from patients finished the 'Sandwich treatment' to their death.

Statistical analysis

Follow-up time were defined as the time from completion of 'Sandwich strategy' to the time of most recent follow-up. End-point events were illustrated using Kaplan-Meier method. Categorical data were presented as percentages and compared by Mann-Wittney U test. Continuous data using t-test. Cox regression model was used to analyze the risk factors that related to TLC. All statistical analyses were performed using SPSS version 19.0 (IBM Corp., Armonk, New York) or GraphPad Prism 8.0

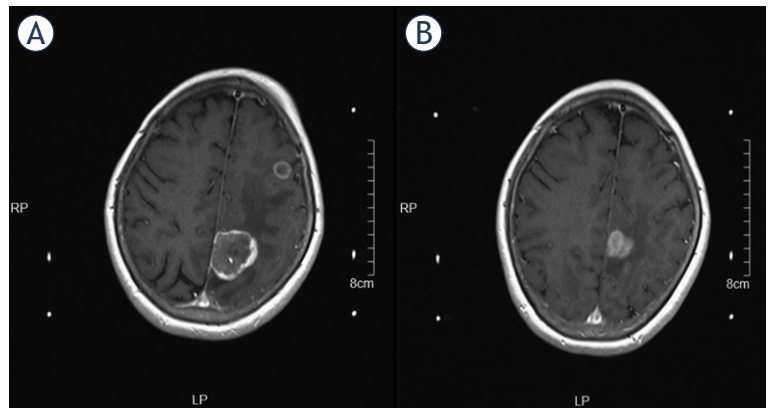


FIGURE 2. A typical case with LBM located in motor area that received 'Sandwich treatment'. **(A)** The lesion had severe peri-tumor edema and invading towards the frontal lobe; **(B)** 3 months after 'Sandwich treatment', peri-tumor edema and tumor volume significantly reduced.

(La Jolla, California, United States). Values with $P < 0.05$ were considered statistically significant.

Results

Patient characteristics

A total of 61 patients with 72 LBM located in the motor area received the 'Sandwich treatment' from January 2016 to March 2023. 36 patients were female and 35 were male. Patients' median age was 62 years (range: 34–81 years). The median

TABLE 1. Patient characteristics

Characteristic	Value	Range
Age (median, years)	62	34–81
Sex		
Female	36	
Male	25	
Primary tumor		
Lung	39	
Breast	13	
Gastric-intestinal tract	9	
KPS (median)	60	50–80
Dose at first-stage SRS (median, Gy)	13.0	11–15
Dose at second-stage SRS (median, Gy)	12.5	11–14
Total tumor volume (mean, cm ³)	20.1	17.2–29.7
Peri-tumor edema volume (mean, cm ³)	12.6	4.9–19.6
Follow-up time (median, months)	18.3	6.3–47.9

KPS = Karnofsky performance status

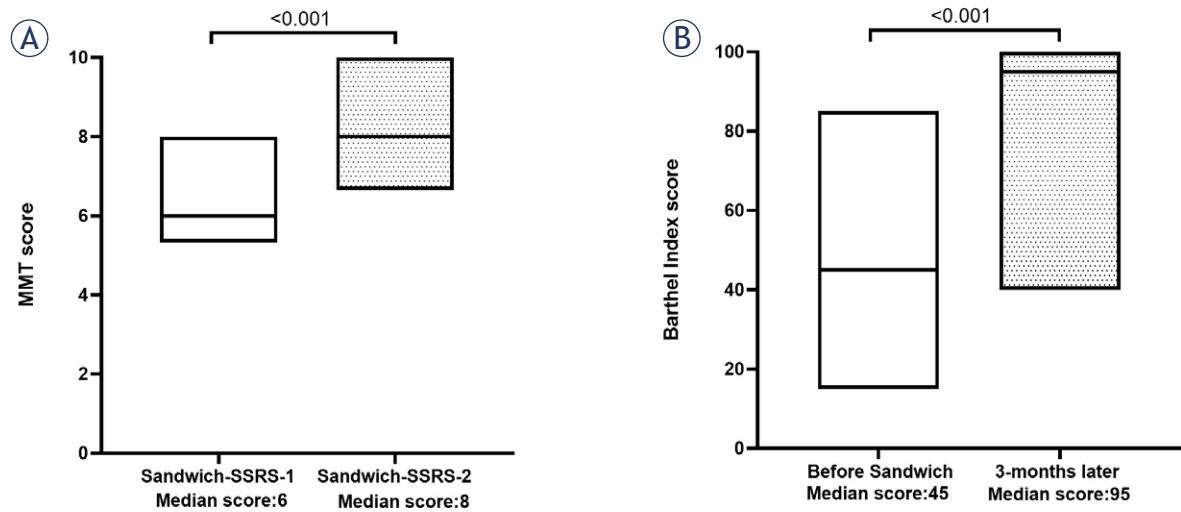


FIGURE 3. Patients' median MMT and BI score. (A) MMT score at the beginning and the end of 'Sandwich treatment' ($P < 0.001$); (B) BI score before 'Sandwich treatment' and at 3 months later ($P < 0.001$).

BI score = Barthel Index score; MMT score = manual muscle testing score; 2-SSRS = two-staged stereotactic radiosurgery

Karnofsky performance status (KPS) score before treatment was 60 (range: 50–80). The median dose at the first and second SSRS was 13 Gy (range: 11–15 Gy) and 12.5 Gy (range: 11–14 Gy), respectively. The median follow-up time of 61 patients was 18.3 months (range: 6.3–47.9 months). None of the treated patients had accidental intracranial hemorrhage after bevacizumab treatment. Detailed general patient characteristics are presented in Table 1.

The volume changes of tumor and peri-tumor edema

There was no statistical tumor volume change at first-stage SRS and second-stage SRS during the 'Sandwich treatment'. However, the mean tumor volume decreased dramatically from 20.1 cm³ (range: 17.2–29.7 cm³) at the time of 'Sandwich treatment' to 12.3 cm³ (range: 7.7–22.4 cm³) 3 months later ($P < 0.001$, Figure 1 A). The mean peri-tumor edema volume at the 1-SSRS and the 2-SSRS of 'Sandwich treatment' was 12.6 cm³ (range: 4.9–19.6 cm³) and 5.2 cm³ (range: 1.2–13.2 cm³), with significant statistical difference ($P < 0.001$, Figure 1 B). Figure 2 shows a patient that received 'Sandwich treatment' for LBM located in motor area, the peri-tumor edema and tumor volume significantly reduced 3 months later.

Patients' MMT score and BI score changes

Patients' median MMT score improved from 6 (range: 5–8) at the beginning to 8 (range: 7–10) at

the end of 'Sandwich treatment' ($P < 0.001$, Figure 3 A). Patients' median BI score was also greatly improved from 45 (range: 15–85) at the time of 'Sandwich treatment' to 95 (range: 40–100) after 3 months ($P < 0.001$, Figure 3 B).

Patients' OS, TLC and prognostic factors for TLC

As Kaplan - Meyer curve showed in Figure 4A, the patient's median survival time was 14.0 months, and the overall survival rates at 3, 6, 12 months was 92.0%, 86.0% and 66.0%, respectively. The TLC rate at 3, 6, 12 months was 98.4%, 93.4%, and 85.3%, respectively (Figure 4B). Primary tumor types (Lung/Breast/GI tract cancer) were prognostic factors for TLC in Univariate analysis. Multivariate analysis revealed that patients with lung cancer had lower risk of tumor relapse [Lung/Breast: HR = 0.539, 95% CI:(0.339–0.812); Lung/GI tract: HR = 0.784, 95%CI:(0.498–0.987)] (Table 2).

Side effects of 'Sandwich treatment'

The side effects of 'Sandwich treatment' mainly consist of hemorrhage hazard by bevacizumab and radiation necrosis (RN) by SRS. However, no patients had accidental intracranial hemorrhage after 'Sandwich treatment', and the cumulative incidence of hemorrhage was 4.92% (3/61), mainly oral and nasal bleeding. The cumulative radiation necrosis was 13.11% (8/61) in all patients, only 3.3% (2/61) presented with symptoms.

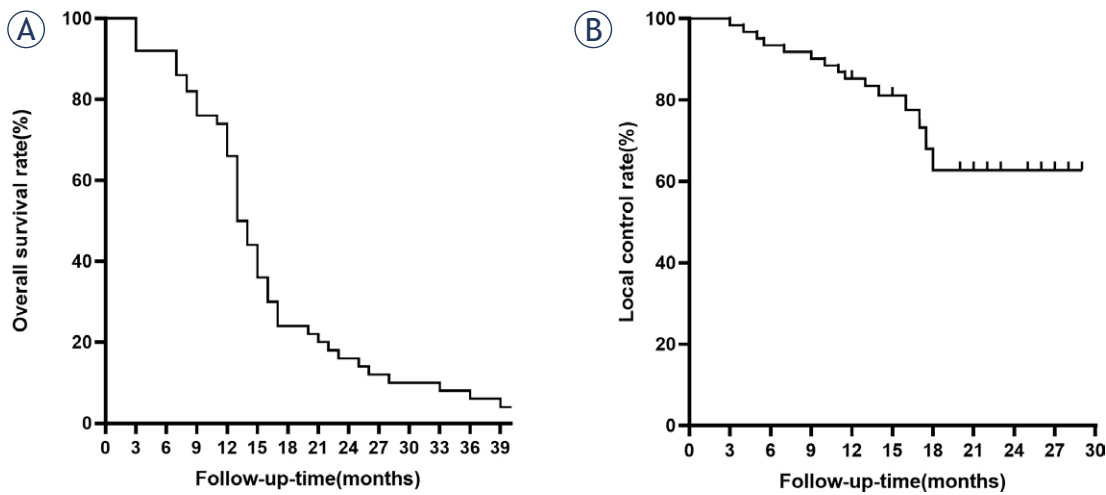


FIGURE 4. Kaplan - Meier curve of the patient's (A) Overall survival (OS) and (B) tumor local control (TLC) rate.

TABLE 2. Risk factors of TLC for LBM in motor area after 'Sandwich treatment'

	Univariate analysis			Multivariate analysis		
	HR ratio	95%CI	P-value	HR ratio	95%CI	P-value
Age	0.978	(0.598–1.686)	0.697			
>=62						
<62						
Sex	1.678	(0.913–2.174)	0.781			
Male						
Female						
Primary tumor						
Lung/Breast	0.459	(0.359–0.898)	< 0.01	0.539	(0.339–0.812)	0.007
Lung/GL tract	0.913	(0.478–1.316)	< 0.01	0.784	(0.498–0.987)	0.006
Breast/GI tract	1.987	(0.878–1.974)	0.411			
KPS score	2.113	(1.159–6.733)	0.139			
>= 60						
<60						
Total tumor volume	0.719	(0.419–1.598)	0.211			
>=20.1cm ³						
<20.1cm ³						
Peri-tumor edema volume	1.589	(0.973–2.894)	0.566			
>=12.6cm ³						
<12.6cm ³						
Dose at first-stage SRS	1.325	(0.53–1.734)	0.989			
>= 13.0 Gy						
< 13.0 Gy						
Dose at second-stage SRS	0.845	(0.356–1.250)	0.593			
>= 12.5 Gy						
< 12.5 Gy						

KPS = Karnofsky performance status; LBM = large brain metastases; 2-SSRS = two-staged stereotactic radiosurgery; TLC = tumor local control

TABLE 3. Comparison between 'Sandwich treatment' and other reports of 2-SSRS strategy for BM

Author	Year	Case number	Median diameter/ volume of BM	Total dose	2-SSRS interval	6 Months OS/ median OS	6 Months TLC/ median TLC	Radiation necrosis
Yomo <i>et al.</i> ⁹	2012	27	17.8 cm ³	27 Gy	3-4 weeks	8.8 months	89.8%	11.1%
Yomo and Hayashi ²⁹	2014	58	16.4 cm ³	28 Gy	3-4 weeks	63%	85.0%	8.6%
Angelov <i>et al.</i> ¹⁰	2018	54	Diameter>=2cm	30 Gy	34 days	65%	88.0%	11.0%
Dohm <i>et al.</i> ⁸	2018	33	LBM	29 Gy	30 days	65%	96.8%	6.06%
Hori <i>et al.</i> ³¹	2020	181	4 cm ³	N/A	N/A	14.6 months	91.0%	N/A
Ito <i>et al.</i> ³²	2020	178	10 cm ³	26 Gy	7-38 days	6.6 months	93.2%	6.20%
Damron <i>et al.</i> ³⁰	2022	24	8.1 cm ³	30 Gy	32 days	9.1 months	80%	N/A
Cho <i>et al.</i> ³³	2022	142	Median 7.4 cm ³	27-28 Gy	32 days	14 months	88-90%	17%
Present study	2023	51	20.1 cm ³	25.5 Gy	7 days	91.8%, 14 months	93.4%	13.11%

N/A = not available; BM = brain metastases; 2-SSRS = two-staged stereotactic radiosurgery

Study limitations

This study has several limitations. Firstly, the number of patients is not large and would interfere the results of statistical analysis. Secondly, patients received 'Sandwich treatment' may receive different consequent systemic therapy, so the influence weight of these different therapies on the local control of BM cannot be precisely accessed. However, it cannot be avoided in other similar researches and commonly exists in the treatment cause of patients. Finally, there are still disputes about the personalized dose of bevacizumab for edema control after SRS. A larger cohort and prospective studies are needed to provide more thrilling results.

Discussion

In recent years, SRS has been recognized as effective alternative treatment for BM.²⁻⁴ For BM with diameter at 2-3 cm, fractionated or staged SRS is preferable.^{9,11,29} One of the representative study on 2-SSRS method for BM is reported by Angelov *et al.* in 2018.¹⁰ In their case series, the volume of 63 BMs in 54 patients reduced significantly, and the TLC rate in 3, 6 months after treatment reaches 95% and 88%, respectively; the incidence of overall radiation side effects was 11%. Another representative study was conducted by Serizawa T *et al.*¹¹ They compared the treatment results between 3- and 2-stage Gamma Knife radiosurgery for large BM and found no differences between in terms of patients' overall survival, tumor progression, neuro-

logical death, and radiation-related adverse events. Dohm Amoren *et al.* reported 2-SRSS for BM that are difficult to be removed by surgery⁸, the cumulative incidence of local treatment failure at 6 and 12 months was 3.2% and 13.3% respectively. The study of Damron *et al.* in 2022 also supports the effectiveness and safety of 2-SSRS for BM patients.³⁰ According to the results of these studies, 2-SSRS for the BM treatment is satisfactory and local control failure rate is low. Table 3 listed 8 studies that adopted 2-SSRS strategy for BM.

The listed studies mainly focused on the optimal prescription doses of the 2-SSRS. The researchers suggested dose reduction strategy was suitable for lessening of SRS-induced edema and RN. However, the 2-SSRS strategy might not be enough for the LBM located in motor area. Meanwhile, these conventional 2-SSRS strategy have treatment course longer than 1 month. Patients may have to receive even longer time of inpatient dehydration and steroid treatment during the 2-SSRS when the diameter of BM was over 3 cm and located in the motor area. The long-term usage of mannitol and steroid hormones would bring a series of side effects to the patient, delay their consequent systemic treatment, increase their treatment cost. On the other hand, patient's intracranial hypertension, neuro-dysfunction symptoms and the risk of suffering from refractory epilepsy would make them hardly to receive SRS at outpatient department.

The side effect of 2-SSRS should not be neglected as well. The SRS-induced edema would aggravate the edema caused by LBM compression in the motor area, patients would experience de-

terioration of limb movement and their life quality. Cho *et al.* pointed out even 2-SSRS strategy for BM could cause RN as high as 17% and affects the life quality of patients.³³ Considering these tough issues, we introduce bevacizumab. Juan *et al.* had applied bevacizumab for the treatment of SRS related edema, and found the edema volume reduction at 49.0%–66.0% on MRI-T2FLAIR.³⁴ As bevacizumab could reduce the angiogenesis around the lesion, it could also lower the brain RN risk.³⁵ Its anti-angiogenesis effect could be used to control tumor growth had synergies with SRS. Therefore, the ‘Sandwich treatment’ strategy would have obvious advantage in the treatment of LBM in motor area, especially for those with primary lung adenocarcinoma.³⁶

The results of this retrospective study confirmed the effectiveness and safety of ‘Sandwich treatment’. The results indicated that using bevacizumab during SRS gap could reduce the median volume of peri-tumor edema by 38.8% (from 12.6 cm³ to 5.2 cm³). Meanwhile, patient’s muscle strength score that reflecting the patients’ physical activities also significantly improved. The strategy would shorten the whole treatment course while preserve patients’ neuro-function or improve their life quality. Patients with primary lung adenocarcinoma had significant lower risk of tumor relapse. Compared to previous 2-SSRS reports as showed in Table 3, the present study had the largest median tumor volume, shortest treatment course, while the TLC were similar compared to other studies. The 6-month OS rate and median survival in our present study exceeded 6 of the 8 studies.

The incidence of RN in this study was higher than other eight 2-SSRS cohorts listed in Table 3. The main reason may be that in these cohort the patient’s median OS was short and they failed to report the potential RN symptoms. On contrary, the LBM in the present study were all located in the motor area, and patients’ SRS-induced symptoms could be much more obvious.

Conclusions

As far as we know, this is the first report of ‘Sandwich treatment’ strategy for the LBM with diameter over 3 cm at motor area. The statistical results verified the effectiveness and safety of this strategy. This strategy could significantly improve patients’ life quality and greatly shortened treatment interval. However, a larger cohort is still needed for prospective study.

Funding statement

Zhejiang Provincial Department of Education Research Support Project (Y202249332); Zhejiang Provincial Medical and Health Research Project (2022KY570; 2023KY475).

References

- Cagney DN, Martin AM, Catalano PJ, Redig AJ, Lin NU, Lee EQ, et al. Incidence and prognosis of patients with brain metastases at diagnosis of systemic malignancy: A population-based study. *Neuro Oncol* 2021; **19**: 1511-21. doi: 10.1093/neuonc/nox077
- Graber JJ, Cobbs CS, Olson JJ. Congress of neurological surgeons systematic review and evidence-based guidelines on the use of stereotactic radiosurgery in the treatment of adults with metastatic brain tumors. *Neurosurgery* 2019; **84**: E168-E170. doi: 10.1093/neuros/nyy543
- Han JH, Kim DG, Chung HT, Paek SH, Park CK, Jung HW. Radiosurgery for large brain metastases. *Int J Radiat Oncol Biol Phys* 2012; **83**: 113-20. doi: 10.1016/j.ijrobp.2011.06.1965
- Arvold ND, Lee EQ, Mehta MP, Margolin K, Alexander BM, Lin NU, et al. Updates in the management of brain metastases 2016; *Neuro Oncol* 2016; **18**: 1043-65. doi: 10.1093/neuonc/nov127
- Devoid HM, McTyre ER, Page BR, Metheny-Barlow L, Ruiz J, Chan MD. Recent advances in radiosurgical management of brain metastases. *Front Biosci* 2016; **8**: 203-14. doi: 10.2741/s458
- Milano MT, Chiang VLS, Soltys SG, Wang TJC, Lo SS, Brackett, et al. Executive summary from American Radium Society’s appropriate use criteria on neurocognition after stereotactic radiosurgery for multiple brain metastases. *Neuro Oncol* 2020; **22**: 1728-41. doi: 10.1093/neuonc/noaa192
- Hasegawa T, Kato T, Yamamoto T, Iizuka H, Nishikawa T, Ito H, et al. Multisession gamma knife surgery for large brain metastases. *J Neurooncol* 2017; **131**: 517-24. doi: 10.1007/s11060-016-2317-4
- Dohm AE, Hughes R, Wheless W, Lecompte M, Lanier C, Ruiz J. Surgical resection and postoperative radiosurgery versus staged radiosurgery for large brain metastases. *J Neurooncol* 2018; **140**: 749-56. doi: 10.1007/s11060-018-03008-8
- Yomo S, Hayashi M, Nicholson C. A prospective pilot study of two-session Gamma Knife surgery for large metastatic brain tumors. *J Neurooncol* 2012; **109**: 159-65. doi: 10.1007/s11060-012-0882-8
- Angelov L, Mohammadi AM, Bennett EE, Abbassy M, Elson P, Chao ST, et al. Impact of 2-staged stereotactic radiosurgery for treatment of brain metastases ≥ 2 cm. *J Neurosurg* 2018; **129**: 366-82. doi: 10.3171/2017.3.JNS162532
- Serizawa T, Higuchi Y, Yamamoto M, Matsunaga S, Nagano O, Sato Y, et al. Comparison of treatment results between 3- And 2-stage Gamma Knife radiosurgery for large brain metastases: A retrospective multi-institutional study. *J Neurosurg* 2018; **131**: 227-37. doi: 10.3171/2018.4.JNS172596
- Vogelbaum MA, Brown PD, Messersmith H, Brastianos PK, Burri S, Cahill D, et al. Treatment for brain metastases: ASCO-SNO-ASTRO guideline. *J Clin Oncol* 2022; **40**: 492-516. doi: 10.1200/JCO.21.02314
- Lehrer EJ, Peterson JL, Zaorsky NG, Brown PD, Sahgal A, Chiang VL, et al. Single versus multifraction stereotactic radiosurgery for large brain metastases: An international meta-analysis of 24 trials. *Int J Radiat Oncol Biol Phys* 2019; **103**: 618-30. doi: 10.1016/j.ijrobp.2018.10.038
- Pinteá B, Baumert B, Kinfe TM, Gousias K, Parpaley Y, Boström JP. Early motor function after local treatment of brain metastases in the motor cortex region with stereotactic radiotherapy/radiosurgery or microsurgical resection: A retrospective study of two consecutive cohorts. *Radiat Oncol* 2017; **12**: 177. doi: 10.1186/s13014-017-0917-6
- Loganadane G, Dhermain F, Louvel G, Kaur P, Deutsch E, Le Pêchoux C, et al. Brain radiation necrosis: Current management with a focus on non-small cell lung cancer patients. *Front Oncol* 2018; **8**: 336. doi: 10.3389/fonc.2018.00336

16. Miller JA, Bennett EE, Xiao R, Kotecha R, Chao ST, Vogelbaum MA, et al. Association between radiation necrosis and tumor biology after stereotactic radiosurgery for brain metastasis. *Int J Radiat Oncol Biol Phys* 2016; **96**: 1060-9. doi: 10.1016/j.ijrobp.2016.08.039
17. Linskey ME, Andrews DW, Asher AL, Burri SH, Kondziolka D, Robinson PD, et al. The role of stereotactic radiosurgery in the management of patients with newly diagnosed brain metastases: A systematic review and evidence-based clinical practice guideline. *J Neurooncol* 2010; **96**: 45-68. doi: 10.1007/s11060-009-0073-4
18. Desai B, Rassam D, Ezeh P, et al. Phase III trial of PF-06439535 or bevacizumab-eu plus paclitaxel/ carboplatin in NSCLC. *J Thorac Oncol* 2015; **10**: S665.
19. Tamura R, Tanaka T, Miyake K, Yoshida K, Sasaki H. Bevacizumab for malignant gliomas: current indications, mechanisms of action and resistance, and markers of response. *Brain Tumor Pathol* 2017; **34**: 62-77. doi: 10.1007/s10014-017-0284-x
20. Lubelski D, Abdullah KG, Weil RJ, Marko NF. Bevacizumab for radiation necrosis following treatment of high grade glioma: A systematic review of the literature. *J Neurooncol* 2013; **115**: 317-22. doi: 10.1007/s11060-013-1233-0
21. Delishaj D, Ursino S, Pasqualetti F, Cristaudo A, Cosottini M, Fabrini MG, et al. Bevacizumab for the treatment of radiation-induced cerebral necrosis: A systematic review of the literature. *J Clin Med Res* 2017; **9**: 273-80. doi: 10.14740/jocmr2936e
22. Alanin MC, Klausen C, Caye-Thomasen P, Thomsen C, Fugleholm K, Poulsgaard L, et al. Effect of bevacizumab on intracranial meningiomas in patients with neurofibromatosis type 2 – a retrospective case series. *Int J Neurosci* 2016; **126**: 1002-6. doi: 10.3109/00207454.2015.1092443
23. Hawasli AH, Rubin JB, Tran DD, Adkins DR, Waheed S, Hullar TE, et al. Antiangiogenic agents for nonmalignant brain tumors. *J Neurol Surg B Skull Base* 2013; **74**: 136-41. doi: 10.1055/s-0033-1338262
24. Lin NU, Lee EQ, Aoyama H, Barani IJ, Barboriak DP, Baumert BG, et al. Response assessment criteria for brain metastases: Proposal from the RANO group. *Lancet Oncol* 2015; **16**: e270-e8. doi: 10.1016/S1470-2045(15)70057-4
25. Kano H, Kondziolka D, Lobato-Polo J, Zorro O, Flickinger JC, Lunsford LD. T1/T2 matching to differentiate tumor growth from radiation effects after stereotactic radiosurgery. *Neurosurgery* 2010; **66**: 486-91. doi: 10.1227/01.NEU.0000360391.35749.A5
26. Minamimoto R, Saginoya T, Kondo C, Tomura N, Ito K, Matsuo Y, et al. Differentiation of brain tumor recurrence from post-radiotherapy necrosis with 11C-methionine PET: Visual assessment versus quantitative assessment. *PLoS One* 2015; **10**: e0132515. doi: 10.1371/journal.pone.0132515
27. Paternostro-Sluga T, Grim-Stieger M, Posch M, Schuhfried O, Vacariu G, Mittermaier C, et al. Reliability and validity of the Medical Research Council (MRC) scale and a modified scale for testing muscle strength in patients with radial palsy. *J Rehabil Med* 2008; **40**: 665-71. doi: 10.2340/16501977-0235
28. Hankemeier A, Rollnik JD. The Early Functional Abilities (EFA) scale to assess neurological and neurosurgical early rehabilitation patients. *BMC Neurol* 2015; **15**: 207. doi: 10.1186/s12883-015-0469-z
29. Yomo S, Hayashi M. A minimally invasive treatment option for large metastatic brain tumors: Long-term results of two-session Gamma Knife stereotactic radiosurgery. *Radiat Oncol* 2014; **9**: 132. doi: 10.1186/1748-717X-9-132
30. Damron EP, Dono A, Chafi H, Martir M, Yu TK, Khwaja S, et al. Metastatic neoplasm volume kinetics following 2-stage stereotactic radiosurgery. *World Neurosurg* 2022; **161**: e210-e9. doi: 10.1016/j.wneu.2022.01.109
31. Hori Y, Muhsen B, Joshi K, Wei W, Borghei-Razavi H, Chao S et al. The efficacy and safety of two-staged stereotactic radiosurgery for large posterior fossa metastases: post-treatment volumetric changes in tumor size, peri-tumoral edema, and fourth ventricle. *Neuro Oncol* 2020; **22** Suppl2: ii181. doi: 10.1093/neuonc/noaa215.756
32. Ito D, Aoyagi K, Nagano O, Serizawa T, Iwadata Y, Higuchi Y. Comparison of two-stage Gamma Knife radiosurgery outcomes for large brain metastases among primary cancers. *J Neurooncol* 2020; **147**: 237-46. doi: 10.1007/s11060-020-03421-y
33. Cho A, Medvedeva K, Kranawetter B, Untersteiner H, Hirschmann D, Lepillina O, et al. How to dose-stage large or high-risk brain metastases: an alternative two-fraction radiosurgical treatment approach. *J Neurosurg* 2022; **137**: 1666-75. doi: 10.3171/2022.2.JNS212440
34. Li J, He J, Cai L, Lai M, Hu Q, Ren C, et al. Bevacizumab as a treatment for radiation necrosis following stereotactic radiosurgery for brain metastases: clinical and radiation dosimetric impacts. *Ann Palliat Med* 2021; **10**: 2018-26. doi: 10.21037/apm-20-2417
35. Erpolat OP, Demircan NV, Saribas GS, Kuzucu P, Senturk E, Elmas C, et al. A comparison of Ramipril and Bevacizumab to mitigate radiation-induced brain necrosis: An experimental study. *World Neurosurg* 2020; **144**: e210-e20. doi: 10.1016/j.wneu.2020.08.081
36. Ai B, Zhang L, Huang D, Chen J, Liu Z, Hu X, et al. Efficacy and safety of bevacizumab in advanced lung adenocarcinoma patients with stable disease after two cycles of first-line chemotherapy: A multicenter prospective cohort study. *Thorac Cancer* 2020; **11**: 3641-4. doi: 10.1111/1759-7714.13687

Radiol Oncol 2024; 58(1): 1-8.
doi: 10.2478/raon-2024-0011

Sarkopenična debelost in rak

Jurdana M, Čemažar M

Izhodišča. Sarkopenična debelost je razmeroma nov izraz, ki opisuje klinično stanje, za katerega je značilen soobstoj sarkopenije (izguba mišične mase in moči) in debelosti (povečan delež maščobne mase), ki prizadene predvsem starejše odrasle. Ker se pojavnost sarkopenije in debelosti v svetu povečuje, postaja sarkopenična debelost vse večji problem pri rakavih bolnikih. Sarkopenična debelost je namreč povezana s slabšimi izidi zdravljenja, daljšimi hospitalizacijami, telesno nezmogljivostjo in krajšim preživetjem pri različnih oblikah raka. Oksidativni stres, lipotoksičnost in sistemsko vnetje ter zmanjšano izražanje protivnetnih miokinov skeletnih mišic so mehanizmi, ki potekajo tako pri sarkopenični debelosti, kakor tudi pri raku.

Zaključki. Razširjenost sarkopenične debelosti je pri rakavih bolnikih precej heterogena, vzrok je v različnih definicijah in variabilnosti diagnostičnih preiskav, ki jih uporabljajo za oceno sarkopenije in debelosti. Zato je namen pričujočega pregleda prikazati na novo sprejeta diagnostična merila ter mehanizme, ki so skupni raku in sarkopenični debelosti.

Radiol Oncol 2024; 58(1): 9-14.
doi: 10.2478/raon-2024-0012

Vpliv anestezije na rast tumorjev

Potočnik I, Kerin-Povšič M, Markovič-Božič J

Izhodišča. Onkološki bolniki predstavljajo velik delež vseh operirancev. Izbira anestezijske tehnike ima posredno, preko vpliva na vnetje in imunski sistem bolnika velik vpliv na zdravje posameznega bolnika in tudi javno zdravje. Pri metastaziranju ima namreč tako specifični kot nespecifični imunski sistem velik vpliv. Patofiziološka podlaga za razrast in metastaziranje rakastih celic po operaciji je fiziološki odziv na stres. Univerzalni odgovor organizma na stres pa je vnetje. Z vnetjem odgovori organizem na katerikoli škodljiv dejavnik in s tem vpliva na tumorsko rast. Anestetične učinkovine in adjuvanti na različne načine vplivajo na perioperativno vnetje in posredno na razrast ter metastaziranje tumorja. Raziskave in vitro so pokazale, kako posamezne anestezijske učinkovine vplivajo na razsoj, vendar klinične raziskave tega niso potrdile. Kljub temu je priporočljiva uporaba anestezijske tehnike in učinkovine, ki je in vitro pokazala manjši učinek na razrast rakavih celic.

Zaključki. V preglednem članku osvetljuje področje vpliva anestezije na razrast tumorja in navedemo, katere učinkovine in anestezijske tehnike se glede na dosedanje izsledke raziskav najbolj priporočljive, kadar operiramo bolnike z rakom. Vendar je področje še dokaj neraziskano, malo je kliničnih randomiziranih prospektivnih raziskav, njihovi rezultati pa so kontroverzni.

Radiol Oncol 2024; 58(1): 15-22.
doi: 10.2478/raon-2024-0004

Uspešnost odkrivanja in napovedni pomen izhodiščne infiltracije kostnega mozga pri difuznem velikoceličnem limfomu B. Primerjava ^{18}F -FDG PET/CT in biopsije kostnega mozga

Doma A, Zevnik K, Studen A, Kloboves Prevodnik V, Gašljević G, Jezeršek Novaković B

Izhodišča. Za odkrivanje infiltracije kostnega mozga pri difuznem velikoceličnem limfomu B običajno uporabljamo invazivno biopsija kostnega mozga, ki pa ima svoje omejitve. Pozitronska emisijska tomografija s hkratno računalniško tomografijo (^{18}F -FDG PET/CT) ponuja neinvazivno alternativo. Namen raziskave je bil analizirati uspešnost ^{18}F -FDG PET/CT pri odkrivanju infiltracije kostnega mozga pri difuznem velikoceličnem limfomu B, skladnost z rezultati biopsije kostnega mozga in vpliv na preživetje bolnikov.

Bolniki in metode. V retrospektivni raziskavi smo analizirali rezultate zamejitvenih preiskav ^{18}F -FDG PET/CT in biopsije kostnega mozga pri 145 bolnikih z difuznim velikoceličnim limfomu B v stadiju II–IV z uporabo statistične analize diagnostičnih testov in analize preživetja.

Rezultati. Infiltracijo kostnega mozga smo ugotovili pri 38 bolnikih (26,2 %) s PET/CT in pri 18 bolnikih (12,4 %) z biopsijo kostnega mozga. Skladne rezultate smo ugotovili pri 79,3 % bolnikov, pri 20,7 % pa so bili rezultati neskladni. S kombiniranjem podatkov PET/CT in biopsija kostnega mozga smo ugotovili, da je imelo infiltracijo kostnega mozga 29,7 % bolnikov. Občutljivost, specifičnost, pozitivna napovedna vrednost, negativna napovedna vrednost in natančnost PET/CT za odkrivanje izhodiščne infiltracije kostnega mozga so bile 88,4 %, 100 %, 100 %, 95,3 % in 96,5 %, medtem ko je biopsija kostnega mozga pokazala nižjo občutljivost (41,9 %) in negativno napovedno vrednost (46,8 %). Srednja vrednost celokupnega preživetja ni bila dosežena v nobeni podskupini glede na spol, celokupno petletno preživetje pa je znašalo 82 % (skupno), 84 % (ženske) in 80 % (moški) ($P = 0.461$). Različne skupine mednarodnega napovednega indeksa (*angl. International Prognostic Index, IPI*) so pokazale različne petletne stopnje celokupnega preživetja: 94 % v skupini z nizkim tveganjem, 91 % z nizko-srednjim tveganjem, 84 % z visoko-srednjim tveganjem in 65 % v skupini z visokim tveganjem ($P = 0.0027$). Infiltracije kostnega mozga kostnega mozga ni pomembno vplivala na celokupno petletno preživetje ($P = 0,979$).

Zaključki. Preiskava ^{18}F -FDG PET/CT je pokazala višjo diagnostično natančnost kot biopsija kostnega mozga. Medtem ko druge raziskave poročajo o slabšem petletnem preživetju pri celokupni skupini in skupini z infiltracijo kostnega mozga, so naše ugotovitve pokazale ugodne podatke o preživetju.

Radiol Oncol 2024; 58(1): 23-32.
doi: 10.2478/raon-2024-0014

Pogled skozi slikovno perspektivo. Pomen slikanja nekroze pri diagnozi glioma in napovedovanju poteka bolezni. Izkušnje posamičnega centra

Ma H, Zeng S, Xie D, Zeng W, Huang Y, Mazu L, Zhu N, Yang Z, Chu J, Zhao J

Izhodišče. Namen raziskave je bil proučiti diagnostično vrednost slikovne nekroze pri določanju gradus tumorja, napovedati genotip in potek bolezni gliomov ter dodatno oceniti tumorsko nekrozo z dinamičnim kontrastnim slikanjem magnetnoresonančne perfuzije (*angl. dynamic contrast-enhanced MR perfusion imaging, DCE-MRI*).

Bolniki in metode. Retrospektivno smo analizirali 150 bolnikov (104 moških, povprečna starost 46 let), pri katerih je bil patohistološko dokazan difuzni gliom pri odraslih. Diagnoza je temeljila na klasifikaciji Svetovne zdravstvene organizacije za centralni živčni sistem iz leta 2021. Zbrali smo podatke o patomorfološki nekrozi in genskih mutacijah. Pri vseh bolnikih smo naredili konvencionalne preiskave in preiskave z DCE-MRI ter jih spremljali do 31. maja 2021. Slikovno nekrozo sta opredelila dva izkušena nevrologa. Metrične karte, pridobljene z DCE-MRI, smo naknadno obdelali in določili povprečne vrednosti vsake metrike v tumorskem parenhimu ter peritumoralnem in kontralateralnem območju.

Rezultati. Pri opredelitvi slikovne nekroze smo dosegli visoko stopnjo soglasja med opazovalci ($Kappa = 0,668$, $p < 0,001$) in visoka stopnja soglasja med slikovno in patomorfološko nekrozo ($Kappa = 0,767$, $p < 0,001$). V primerjavi z gliomi nizke stopnje so imeli gliomi visoke stopnje več slikovne nekroze (85,37 %, $p < 0,001$). Slikovna nekroza se je z naraščanjem gradusa gliomov znatno povečevala. Značilno pogosteje smo jo ugotovili pri gliomih z nemutiranimi geni, ki kodirajo izocitratno dehidrogenazo (IDH divjega tipa), pri nekodiranem 1p19q in pri gliomih s homozigotno delekcijo CDKN2A/B. Z multivariatno Coxovo regresijsko analizo smo ugotovili, da je bila slikovna nekroza neodvisen in neugoden napovedni dejavnik poteka bolezni (razmerje tveganja = 2,113; $p = 0,046$). Poleg tega je ekstravaskularna ekstracelularna volumska frakcija v tumorskem parenhimu, ki smo jo določili z DCE-MRI, pokazala največjo diagnostično učinkovitost pri prepoznavanju slikovne in patomorfološke nekroze z visoko specifičnostjo (91,9 % in 83,3 %).

Zaključki. Slikovna nekroza lahko dodatno daje pri določanju gradusa, napovedovanju genotipa in napovedi poteka bolezni gliomov podatke o nekrozi, ki jo določamo patomorfološko. Ekstravaskularna ekstracelularna volumska frakcija v tumorskem parenhimu pa lahko z visoko specifičnostjo pomaga vnaprej napovedati tumorsko nekrozo.

Radiol Oncol 2024; 58(1): 33-42.

doi: 10.2478/raon-2024-0017

Pomen difuzijsko uteženega slikanja pri napovedovanju odgovora na zdravljenje in vrednotenju učinka brahiradioterapije z visoko hitrostjo doze pri bolnikih z metastazami kolorektalnega raka v jetrih

Karim S, Seidensticker R, Seidensticker M, Ricke J, Schinner R, Treitl K, Rübenthaler J, Ingenerf M, Schmid-Tannwald C

Izhodišča. Namen raziskave je bil oceniti pomen difuzijsko uteženega slikanja (*angl. diffusion-weighted imaging, DWI*) pri vrednotenju odgovora na zdravljenje pri bolnikih z jetrnimi metastazami kolorektalnega raka.

Bolniki in metode. V retrospektivno, opazovalno kohortno raziskavo smo vključili 19 bolnikov z 18 odzivnimi metastazami, ki so odgovorile na zdravljenje in smo jih spremljali vsaj eno leto ter z 11 neodzivnimi metastazami, ki niso odgovorile na zdravljenje in smo ugotovili ponovitev bolezni v enem letu. Bolnike smo zdravili z brahiradioterapijo z visoko hitrostjo doze (*angl. high-dose-rate brachytherapy, HDR-BT*) ter smo pred in po zdravljenju naredili preiskavo z MR. Z DWI smo določili srednjo vrednost koeficienta difuzije (*angl. apparent diffusion coefficient, ADCmean*) in najnižjo vrednost (*ADCmin*) ter intraindividualne njune spremembe ter ovrednotili odgovore na zdravljenje. Preiskavo smo izvedli pred brahiradioterapijo, nato po 3 mesecih, v času ponovitve bolezni (pri neodzivnih metastazah, srednja vrednost 284 \pm 122 dneva) in 12 mesecih po zdravljenju (pri odzivnih metastazah, srednja vrednost 387 \pm 64 dneva). Občutljivost, specifičnost, pozitivne in negativne napovedne vrednosti (PNV, NNV) za odkrivanje lokalne ponovitve bolezni smo izračunali pri drugi kontroli. Ocenjevali smo (1) samo slike DWI in (2) DWI s kontrastom Gd, T1 obtežene slike v hepatobiliarni fazi.

Rezultati. ADCmean se je pomembno povečal 3 mesece po HDR-BT v obeh skupinah, vendar so se vrednosti intraindividualnih sprememb ADCmean (175 % proti 127 %, $p = 0,03$) in ADCmin ($0,44 \pm 0,24$ do $0,82 \pm 0,58 \times 10^{-3} \text{ mm}^2/\text{s}$) značilno povečale le pri odzivnih metastazah ($p < 0,0001$ in $p < 0,001$). ADCmin je bil pomembno višji pri odzivnih metastazah v primerjavi z neodzivnimi ob prvi kontroli ($p = 0,04$). Občutljivost (1 v primerjavi z 0,72), specifičnost (0,94 v primerjavi z 0,72), PPV (0,91 v primerjavi z 0,61) in NPV (1 v primerjavi z 0,81) bi lahko izboljšali s kombinacijo DWI s kontrastno ojačanim T1 obteženim slikanjem v hepatobiliarni fazi.

Zaključki. Raziskava je pokazala, da bi lahko DWI z MR pripomoglo k boljšemu kvalitativnem in kvantitativnem vrednotenju odgovora na zdravljenje po HDR-BT pri jetrnih metastazah kolorektalnega raka.

Radiol Oncol 2024; 58(1): 43-50.
doi: 10.2478/raon-2024-0003

Kvantitativna ocena infiltracije kostnega mozga in opredelitev tumorskega bremena z uporabo dvojno spektralnega CT-ja pri bolnikih z multiplim mielomom

Xiong X, Hong R, Fan X, Hao Z, Zhang X, Zhang Y, Hu C

Izhodišča. Namen raziskave je bil oceniti, ali lahko z virtualno kalcijevo subtrakcijo, pridobljeno iz dvojnega spektralnega CT-ja ocenimo infiltracijo kostnega mozga pri bolnikih z multiplim mielomom. Pri tem za referenčni standard upoštevamo preiskavo MR in opišemo tumorsko breme.

Bolniki in metode. V raziskavo smo retrospektivno vključili 47 bolnikov z na novo diagnosticiranim multiplim mielomom. V enem tednu smo opravili dvojno spektralni CT in MR celega telesa. V korpusih vretenc L1–L5 smo kvantitativno analizirali slike s kalcijevo subtrakcijo in uporabili indekse z izničenjem kalcija (*angl. calcium-suppressed, CaSupp*) v razponu od 25 do 95 v intervalu 10. Ob tem smo naredili tudi mape difuzijskega koeficienta (*angl. apparent diffusion coefficient, ADC*). Optimalno kombinacijo smo izbrali s korelacijsko analizo med številkami CT in vrednostmi ADC. Nato smo s korelacijsko analizo in analizo krivulj ROC (*angl. receiver operating characteristic*) opredelili tumorsko breme, vključno s stopnjo infiltracije plazemskih celic, razmerjem visokih brezserumskih lahkih verig in citogenetskim statusom visokega tveganja.

Rezultati. Najpomembnejšo kvantitativno korelacijo med CT-jem s kalcijevo subtrakcijo in vrednostmi ADC je bilo mogoče ugotoviti pri indeksu CaSupp 85 za povprečje L1-L5 ($r = 0,612$; $p < 0,001$). To je omogočilo kvantitativno oceno stopnje infiltracije plazemskih celic ($r = 0,835$; $p < 0,001$). Prav tako smo lahko predvideli visoko razmerje visokih brezserumskih lahkih verig in citogenetski status visokega tveganja s površino pod krivuljo (*angl. area under the curve, AUC*), ki je bila 0,876 oziroma 0,760.

Zaključki. Meritve virtualne kalcijeve subtrakcije slik L1-L5 so pokazale najvišjo korelacijo z ADC pri indeksu CaSupp 85. Zato bi lahko ta indeks uporabili kot dodatni slikovni biološki označevalec za neinvazivno oceno tumorskega bremena, kadar ADC ni izvedljiv.

Enakovrednost različnih vrst električnih pulzov za elektrokemoterapijo s cisplatinom. Raziskava in vitro

Scuderi M, Dermol-Černe J, Ščančar J, Marković S, Rems L, Miklavčič D

Izhodišča. Elektrokemoterapija (EKT) je zdravljenje, ki vključuje injiciranje kemoterapevtika, sledi aplikacija osmih pravokotnih monopolarnih električnih pulzov s trajanjem 100 μ s in ponavljalno frekvenco 1 Hz ali 5000 Hz. Vendar vse več raziskovalcev zanima uporaba alternativnih vrst pulzov za EKT. Dokazano je, da uporaba visokofrekvenčnih kratkih bipolarnih pulzov ublaži bolečino in mišične kontrakcije. Uporaba milisekundnih pulzov pa je zanimiva pri kombiniranju EKT z gensko elektrotransfekcijo za vnos DNK. Ta kodira beljakovine za spodbujanje imunskega odziva, s čimer EKT spremenimo iz lokalnega v sistemsko zdravljenje. Zato smo v pričujoči raziskavi proučili, kako alternativne vrste pulzov vplivajo na vnos in citotoksičnost kemoterapevtika cisplatina.

Materiali in metode. Izvedli smo poskuse in vitro, pri katerih smo celice jajčnika kitajskega hrčka (angl. Chinese hamster ovary, CHO) izpostavili običajnim pulzom EKT, visokofrekvenčnim bipolarnim pulzom in milisekundnim pulzom v prisotnosti različnih koncentracij cisplatina. Vnos cisplatina smo določili z masno spektrometrijo z induktivno sklopljeno plazmo (angl. inductively coupled plasma mass spectrometry) citotoksičnost cisplatina pa s testom klonogenosti.

Rezultati. Ugotovili smo, da vse tri preizkušene vrste pulzov enakovredno povečajo vnos in citotoksičnost cisplatina, če je električno polje ustrezno prilagojeno za vsako vrsto pulzov. Potrebni je bilo $2-7 \times 10^7$ molekul cisplatina na celico, da smo dosegli uničenje večine celic.

Zaključki. Visokofrekvenčne bipolarne pulze in milisekundne pulze lahko potencialno uporabljamo pri EKT za zmanjšanje bolečine in krčenja mišic oziroma za povečanje učinka imunskega odziva v kombinaciji z gensko elektrotransfekcijo.

Radiol Oncol 2024; 58(1): 67-77.
doi: 10.2478/raon-2024-0007

RAD54B spodbuja migracijo in angiogenezo celic raka želodca prek poti Wnt/ β -katenin

Li J, Geng H, Li X, Zou S, Xu X

Izhodišča. Rak želodca je epidemično maligno obolenje, ki ga pogosto diagnosticiramo v pozni fazi. Dokazali so, da ima RAD54B ključno vlogo pri napredovanju različnih tumorjev, vendar njegova posebna vloga in mehanizem pri raku želodca ostajata neraziskana.

Materiali in metode. Raven RAD54B smo ugotovljali z metodo *western blot*. Izražanje RAD54B je bilo v celicah MKN45 in AGS zmanjšano ali povečano s transfekcijo plazmida shRAD54B oziroma plazmida za prekomerno izražanje. Vlogo RAD54B pri rasti, migraciji in invaziji pri raku želodca smo ocenjevali s testi Edu, tvorbe kolonij, *transwell* in s testi tvorbe cevč. Poleg tega smo molekularni mehanizem RAD54B pri raku želodca določili z metodo *western blot*. Dodatno smo izvedli poskus *in vivo* na ksenografiranih miših.

Rezultati. Na podlagi podatkovnih zbirk ATGC in GEPIA smo ugotovili, da je izražanje RAD54B pri raku želodca povečano, kar smo potrdili tudi v celičnih linijah raka želodca. Poleg tega je prekomerno izražanje RAD54B povečalo rast, migracijo, invazijo, tvorbo cevč in signalno os Wnt/ β -katenin v celicah AGS in MKN45. Po pričakovanjih je izničenje RAD54B v celicah AGS in MKN45 zmanjšalo omenjena spodbujanja. Še pomembneje je, da je test *in vivo* potrdil, da RAD54B pospešuje rast raka želodca in signalno pot Wnt/ β -katenin.

Zaključki. Rezultati poskusov izgube in pridobitve funkcije so pokazali, da RAD54B omogoča napredovanje celic raka želodca in angiogenezo prek osi Wnt/ β -katenin.

Radiol Oncol 2024; 58(1): 78-86.
doi: 10.2478/raon-2024-0008

Vloga endoskopskih ultrazvočno vodenih aspiracijskih biopsij s tanko iglo v diagnostiki neoplazem trebušne slinavke pri pediatrični populaciji. Izkušnje terciarnega centra in pregled literature

Kebe Radulović M, Breclj J, Gruden A, Strojjan Fležar M

Izhodišča. Endoskopska ultrazvočno vodena aspiracijska biopsija s tanko iglo (EUZ ABTI) je uveljavljena diagnostična metoda pri odraslih bolnikih, v pediatrični populaciji pa jo izvajamo redko. Klinični oddelek za gastroenterologijo Univerzitetnega Kliničnega Centra Ljubljana in Oddelek za citopatologijo Inštituta za patologijo Medicinske fakultete Univerze v Ljubljani sodelujeta pri EUZ ABTI od leta 2010. Namen raziskave je bil pregledati primere neoplazem trebušne slinavke, diagnosticiranih z EUZ ABTI pri otrocih.

Bolniki in metode. V digitalnem arhivu Inštituta za patologijo Medicinske fakultete Univerze v Ljubljani smo našli 6 pediatričnih bolnikov z EUZ ABTI, pri 3 je bila vzorčena trebušna slinavka, pri 2 od njih je bil citološko postavljen sum na neoplazmo. V celičnem vzorcu ultrazvočno solidne lezije so bile razvejane papilarne strukture obdane z zaokroženimi skupki drobnih celic z jedrnimi brazdami. V drugem primeru ultrazvočno cistične lezije je bila vidna pretežno nekroza, z le posameznimi ohranjenimi celicami. Pozitivno jedrno reakcijo na β -katenin smo dokazali v obeh primerih z imunocitokemičnimi barvanji.

Rezultati. V obeh primerih smo postavili citopatološko diagnozo solidne psevdopapilarne neoplazme trebušne slinavke, kar predstavlja tudi vse pediatrične primere neoplazem iz Pediatrične klinike v Ljubljani od 2010 do 2019. Med in po EUZ ABTI ni bilo zapletov. Sledila je resekcija tumorjev in histopatološka potrditev citopatološke diagnoze.

Zaključki. Naše izkušnje kažejo, da je EUZ ABTI varna, natančna in učinkovita diagnostična metoda pri diagnostiki neoplazem trebušne slinavke tudi pri pediatrični populaciji Slovenije, kar je skladno s pregledano literaturo.

Radiol Oncol 2024; 58(1): 87-98.
doi: 10.2478/raon-2024-0009

Dolžina telomerov in polimorfizmi *hTERT* kot biološki označevalci pri azbestnih boleznih

Mervič A, Goričar K, Franko A, Trebušak-Podkrajšek K, Dodič Fikfak M, Dolžan V, Kovač V

Izhodišča. Izpostavljenost azbestu so opredelili kot dejavnik tveganja za krajšo dolžino telomerov. V raziskavi pa smo želeli preučiti, ali lahko dolžina telomerov v levkocitih in genetski polimorfizmi gena *hTERT* služijo kot biološki označevalci tveganja za nastanek azbestnih boleznih in kot označevalci odgovora na zdravljenje ter napredovanja malignega mezotelioma.

Preiskovanci in metode. Izvedli smo dve retrospektivni raziskavi. V prvi raziskavi primerov s kontrolami smo pri bolnikih z malignim mezoteliomom, preiskovancih s pleuralnimi plaki in kontrolnih osebah brez azbestne bolezni, ki pa so bili poklicno izpostavljeni azbestu, določili dolžino telomerov in polimorfizme *hTERT*. V drugi raziskavi z longitudinalnim sledenjem smo dolžino telomerov določili tudi v vzorcih bolnikov z malignim mezoteliomom, odvzetih pred in po kemoterapiji. Dolžino telomerov smo določili z monokromatsko multipleksno kvantitativno polimerazno verižno reakcijo (PCR), prisotnost *hTERT* rs10069690, rs2736100 in rs2736098 pa s kompetitivno alelno specifično PCR. Statistično analizo smo izvedli z metodo logistične regresije in analizo preživetja.

Rezultati. Bolniki z malignim mezoteliomom so imeli krajšo dolžino telomerov kot preiskovanci s pleuralnimi plaki ($p < 0,001$). Po prilagoditvi na starost so bili genotipi rs2736098 CT ter rs10069690 TT in CT+TT statistično značilno povezani z večjim tveganjem za maligni mezoteliom ($p = 0,023$; $p = 0,026$ in $p = 0,017$), genotipa rs2736100 AA in CA+AA pa z manjšim tveganjem v primerjavi z vsemi ostalimi preiskovanci ($p = 0,017$; $p = 0,026$). Dolžina telomerov ni bila povezana z odgovorom na kemoterapijo ($p > 0,05$) ali časom do napredovanja bolezni ($p > 0,05$). Nosilci enega ali dveh polimorfni alelov rs10069690 T so dobro odgovorili na kemoterapijo ($p = 0,039$, oziroma $p = 0,048$), povezava je ostala statistično značilna tudi po prilagoditvi na starost ($p = 0,019$; $p = 0,017$). Nosilci dveh polimorfni alelov rs2736100 A pa so imeli daljši čas do napredovanja bolezni ($p = 0,038$).

Zaključki. Krajša dolžina telomerov v levkocitih in polimorfizmi *hTERT* lahko služijo kot biološki označevalci tveganja za pojav malignega mezotelioma. Z odgovorom na kemoterapijo oziroma napredovanjem malignega mezotelioma sta bila povezana le polimorfizma rs10069690 in rs2736100, ne pa tudi dolžina telomerov.

Napovedna vrednost izražanja receptorja programirane celične smrti 1 in njegovega liganda na limfomskih celicah in tumorsko-imunskih celicah pri difuznem velikoceličnem B-celičnem limfomu, brez drugih oznak

Čas Slak T, Miceska S, Gašljević G, Boltežar L, Kloboves Prevodnik V

Izhodišča. Difuzni velikocelični B-celični limfom, brez drugih oznak (DVBCL, BDO) je najpogostejša oblika ne-Hodgkinovega limfoma. Največji izziv pri načrtovanju zdravljenja predstavljajo bolniki s ponavljajočo boleznijo in tisti, ki niso odzivni na zdravljenje. Receptor programirane celične smrti (PD-1) in njegov ligand (PD-L1) igrata ključno vlogo pri negativni regulaciji imunskih odzivov pri bolnikih z DVBCL, BDO. V raziskavi smo analizirali izražanje PD-1 in PD-L1 na limfomskih celicah (LC) in tumorsko imunskih celicah (TIC) ter tudi njihovo povezavo s preživetjem.

Bolniki in metode. V raziskavo smo vključili vzorce 283 pacientov z DVBCL. Izražanje PD-1 in PD-L1 na LC in TIC smo določili na tkivnih mikromrežah z dvojnimi imunohistokemičnim barvanjem na PD-1/PAX5 ter PD-L1/PAX5. Z D-IHK smo natančneje prepoznali LC in s tem pridobili natančnejši rezultat. Za vse primere smo pridobili klinični podatke in podatke o histoloških diagnozah. Klinične značilnosti in podatke o izražanju PD-1 in PD-L1 na LC in TIC smo korelirali s preživetjem brez ponovitve bolezni in celokupnim preživetjem.

Rezultati. Izražanje PD-1 na TIC smo ugotovili v 38,4 % tkivnih vzorcih bolnikov z DVBCL in v 8,8 % vzorcih na LC. Podobno smo ugotovili izražanje PD-L1 na TIC v 46,8 % tkivnih vzorcev in na LC v 6,5 % vzorcih. PD-L1 na LC sta se pogosteje izražala pri podtipu non-GCB (angl. non-germinal center B cell like) ($p = 0.047$). Pacienti z izražanjem PD-L1 na LC so imeli statistično značilno krajše preživetje brez ponovitve bolezni ($p = 0.015$), ki je ostalo značilno tudi v multivariatni analizi ($p = 0.034$).

Zaključki. PD-L1 na LC se je pogosteje izražal pri non-GCB podtipu DVCLB. Prav tako je izražanje PD-L1 na LC napovedovalo krajši interval do ponovitve bolezni. Dvojno imunohistokemično barvanje na PD-L1/PAX5 se je pokazalo kot zanesljiva metoda za določanje izražanja PD-L1 na LC pri pacientih z DVBCL in bi jo lahko uporabljali za izbor pacientov, ki bi odgovorili na imunoterapijo z zaviralci kontrolnih točk.

Radiol Oncol 2024; 58(1): 110-123.
doi: 10.2478/raon-2024-0013

Vpliv prehranjenosti in telesne sestave na pooperativni potek in izhod bolniki pri lokaliziranega retroperitonealnega sarkoma

Ramanović M, Novak M, Perhavec A, Jordan T, Popuri K, Rotovnik Kozjek N

Izhodišča. Retroperitonealni sarkomi so redki tumorji mezenhimskega izvora. Velike tumorske mase so pogosto prisotne že ob času diagnoze. Raziskali smo vpliv telesne sestave na izhod zdravljenja operiranih bolnikov s primarnim retroperitonealnim sarkomom.

Bolniki in metode. V retrospektivno raziskavo smo vključili bolnike s primarnim lokaliziranim retroperitonealnim sarkomom, ki smo jih zdravili na Onkološkem inštitutu Ljubljana med leti 1999 in 2020. Iz predoperativnih posnetkov CT smo v višini 3. ledvenega vretenca določili količino mišičja, visceralnega in podkožnega maščobnega tkiva ter atenuacijo mišičja. Za oceno znižane mišične mase (miopenije) smo uporabili diagnostična merila Evropske delovne skupine za sarkopenijo pri starostnikih (angl. European Working Group on Sarcopenia in Older People, EWGSOP2). Z uporabo statistične metode največjega logaritemskega ranga smo določili optimalne razmejivne vrednosti parametrov telesne sestave. Maščobno infiltracijo mišičja (miosteatoza) smo opredelili na podlagi razmejivnih vrednosti za atenuacijo mišičja.

Rezultati. V raziskavo smo vključili 58 bolnikov. Srednji čas sledenja je bil 116 mesecev, v katerem je bilo 5-letno celokupno preživetje 66,8 %. Kumulativna verjetnost za lokalno ponovitev bolezni je bila 77,6 %. Bolniki z miopenijo so imeli bistveno nižjo stopnjo 5-letnega celokupnega preživetja ($p = 0,009$). V univariatni analizi sta bila indeks skeletne mišične mase in indeks podkožnega maščobnega tkiva neodvisna napovedna dejavnika preživetja brez lokalnega recidiva ($p = 0,052$ in $p = 0,039$). V multivariatni analizi je visoko razmerje med visceralnim in podkožnim maščevjem neodvisno napovedovalo višjo stopnjo pooperativnih zapletov ($p = 0,008$). Miosteatoza je bila povezana z večjo stopnjo pooperativne obolevnosti.

Zaključki. Miopenija je negativno vplivala na preživetje, vendar ne na pooperativni izid pri bolnikih s primarnim retroperitonealnim sarkomom. Visceralno maščobno tkivo, razmerje med visceralnim in podkožnim maščevjem ($> 0,26$) in miosteatoza so bili povezani z višjo splošno pooperativno obolevnost. Razmerje med visceralnim in podkožnim maščevjem je bilo boljši napovedni dejavnik kot visceralno maščobno tkivo.

Radiol Oncol 2024; 58(1): 124-132.

doi: 10.2478/raon-2024-0001

Retrospektivna raziskava o izboljšanju natančnosti radioterapije pri bolnicah z rakom dojke in metastazami v bezgavkah z uporabo Styrofoam-a

Li J, Yang L, Yao X, Xu L, Zhao L, Bai F

Izhodišča. Namen raziskave je bil retrospektivno analizirati natančnost radioterapije z računalniško tomografijo s stoščastim žarkom (CBCT), fiksacijo s Styrofoam-om in prsnim nosilcem v tarčnem področju prsne stene in nadključničnega drenažnega področja (nadključnično tarčno področje) pri bolnicah z rakom dojke ter primerjati učinkovitost nastavitve in zadovoljstvo z udobjem.

Bolnice in metode. Vključili smo skupaj 65 bolnic s postoperativnimi bezgavčnimi metastazami raka dojke, od tega 36 s fiksacijo s Styrofoam-om in 29 s prsnim nosilcem. Vključevali smo jih od marca 2021 do avgusta 2022 in retrospektivno analizirali. Vse bolnice so tedensko opravile CBCT preiskave: primerjali in zabeležili smo napake v nastavitvi tarčnih volumnov prsne stene in nadključnega področja. Robove planirnega tarčnega volumna (PTV) obeh skupin smo izračunali z uporabo korelacije $MPTV = 2,5\Sigma + 0,7\sigma$. Zabeležili in analizirali smo čase nastavitve in ocenili zadovoljstvo z udobjem za obe skupini. Korelacije med napakami v vsaki smeri smo analizirali s pomočjo Pearsonove korelacijske analize.

Rezultati. Med skupinama s fiksacijo s Styrofoam-om in s prsnim nosilcem je bila v tarčnem področju prsne stene pomembna razlika v levo-desni smeri (os X) ($1,59 \pm 1,47$ mm v primerjavi z $2,05 \pm 1,64$ mm, $P = 0,012$). Statistične razlike v nadključničnem tarčnem področju smo ugotovili v ventrodorzalni smeri (os Z) in kotu mize ($1,36 \pm 1,27$ mm v primerjavi z $1,75 \pm 1,55$ mm, $P = 0,046$; $0,47 \pm 0,47^\circ$ v primerjavi z $0,66 \pm 0,59^\circ$, $P = 0,006$). V smeri X, Y in Z so bile ustrezne meje PTV v tarčnem področju prsne stene za obe skupini 5,01 mm, 5,99 mm in 5,47 mm v skupini s fiksacijo s Styrofoam-om, medtem ko so v skupini s fiksacijo s prsnim nosilcem znašale 6,10 mm, 6,34 mm in 6,10 mm. Prav tako so bile meje PTV za nadključnično tarčno področje v treh smereh v skupini s fiksacijo s Styrofoam-om 3,69 mm, 3,86 mm in 4,28 mm, medtem ko so bile v skupini s prsnim nosilcem 3,99 mm, 3,72 mm in 5,45 mm. Čas nastavitve v obeh skupinah je znašal $3,4 \pm 1,1$ min in $5,5 \pm 3,1$ min ($P = 0,007$). Ocena subjektivnega zadovoljstva z udobjem obeh skupin je znašala $27,50 \pm 1,24$ in $25,44 \pm 1,23$ ($P < 0,001$).

Zaključki. Uporaba fiksacije s Styrofoam-om v radioterapiji raka dojke v področju nadključničnih bezgavk ima več prednosti v primerjavi s fiksacijo s prsnim nosilcem, vključno z večjo natančnostjo nastavitve, manjšim zunanjim ekspanzijskim robom, izboljšano učinkovitostjo dela in udobjem pacientov, kar bi lahko lahko bilo priporočilo za klinično delo.

Radiol Oncol 2024; 58(1): 133-144.
doi: 10.2478/raon-2024-0006

Vpliv citotoksičnih zdravil na imunofenotip blastnih celic B-celične akutne limfoblastne levkemije otrok

Prelog T, Buček S, Brožič A, Peterlin J, Kavčič M, Omerzel M, Markelc B, Jesenko T, Kloboves Prevodnik V

Izhodišča. Pretočna citometrija je ključna v diagnostiki akutne limfoblastne levkemije (ALL) in pri izbiri zdravljenja z imunoterapijo. Preučevali smo učinke prednizolona, vinkristina, daunorubicina, asparagina in metotreksata na imunofenotip blastnih celic, kar bi lahko vplivalo na razvrščanje bolnikov v skupine z različnim tveganjem in na obravnavo bolnikov pred pričetkom imunoterapije.

Bolniki in metode. V raziskavo smo vključili bolnike stare ≤ 17 let, z novo odkrito B-celično ALL. Blastne celice smo izolirali in jih v pogojih in vitro izpostavili naraščajočim koncentracijam testiranih zdravil ter s pretočno citometrijo določili izražanje antigenov CD10, CD19, CD20, CD27, CD34, CD45, CD58, CD66c in CD137.

Rezultati. Dokazali smo, da lahko zdravila povzročijo spremembe v izražanju opazovanih antigenov. Vpliv zdravil je lahko odvisen ali neodvisen od njihovega odmerka. Od odmerka odvisen učinek smo dokazali pri daunorubicinu, ki je povzročil zmanjšanje izražanja CD10, CD19, CD34, CD45, CD58 in povečanje izražanja CD137 ter pri vinkristinu, ki je povzročil zmanjšanje izražanja CD19 in CD58 ter povečanje izražanja CD45. Od odmerka neodvisen vpliv sta imela daunorubicin, ki je povzročil zmanjšanje izražanja CD27 ter prednizolon, ki je povzročil zmanjšanje izražanja CD10, CD19, CD27, CD34 in CD58. Spremembo v izražanju CD20 smo zaznali le v povezavi z odmerkom daunorubicina.

Zaključki. Rezultati raziskave kažejo, da daunorubicin, prednizolon in vinkristin lahko povzročijo zmanjšanje izražanja CD19 in CD58, kar kaže, da bi se bilo bolje izogibati omenjenim zdravilom v času premoščitvene terapije pred imunoterapijo, usmerjeno proti CD19. Dokazali smo tudi spremembe v imunofenotipu blastnih celic, ki bi lahko vplivale na razvrščanje bolnikov v skupine tveganja za ponovitev bolezni.

Radiol Oncol 2024; 58(1): 145-152.

doi: 10.2478/raon-2024-0002

Večinstitucijska študija »sendvič zdravljenja« velikih možganskih metastaz (VMM) s premerom več kot 3 cm v motoričnem predelu možganov

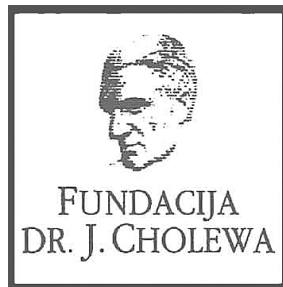
Wang Z, Chen H, Chen Q, Zhu Y, Li M, Zhou J

Izhodišča. Cilj raziskave je bil preučiti učinkovitost in varnost strategije »sendvič zdravljenja« velikih možganskih metastaz (LBM) s premerom več kot 3 cm (minimalna prostornina $\geq 15 \text{ cm}^3$), ki se nahajajo v motoričnem predelu možganov.

Bolniki in metode. Retrospektivno smo analizirali bolnike iz štirih centrov z gama nožem, ki so od januarja 2016 do marca 2023 prejeli »sendvič zdravljenje«. Strategija je vključevala enotedensko zdravljenje z 2 fazama stereotaktične radiokirurgije (SRS) in enkratno uporabo Bevacizumaba v intervalu med obema SRS. Analizirali smo volumen tumorja in spremembe obtumorskega edema pred in po »sendvič zdravljenju«. Ocena ročnega mišičnega testa preizkušanja (MMT) in ocena Barthel Index (BI) sta bili uporabljeni za oceno sprememb gibanja pacientov in rehabilitacijo telesne moči. Izračunana je bila stopnja celokupnega preživetja (OS) bolnikov in lokalne kontrole tumorja (TLC). Za analizo dejavnikov tveganja, povezanih z TLC, smo uporabili Coxov regresijski model.

Rezultati. »Sendvič zdravljenje« je prejelo 61 bolnikov z 72 lezijami. Predpisane srednja doza je bila 13,0 Gy in 12,5 Gy pri prvi in drugi SRS. Povprečni volumen tumorja ob času »sendvič zdravljenja« in 3 mesece pozneje je bil $20,1 \text{ cm}^3$ in $12,3 \text{ cm}^3$ ($P < 0,01$). Povprečni volumen obtumorskega edema ob prvi in drugi fazi SRS je bil $12,6 \text{ cm}^3$ in $5,2 \text{ cm}^3$ ($P < 0,01$). Srednja ocena MMT bolnikov se je izboljšala od začetnih 6 na končnih 8 ob koncu »sendvič zdravljenja« ($P < 0,01$), ocena BI pa se je izboljšala s 45 ob času »sendvič zdravljenja« na 95 po 3 mesecih ($P < 0,01$). Srednje OS bolnikov je bila 14,0 mesecev, in stopnja OS pri 3, 6, 12 mesecih pa 92,0 %, 86,0 % in 66,0 %. Stopnja TLC pri 3, 6, 12 mesecih je bila 98,4 %, 93,4 % in 85,3 %. Bolniki z rakom pljuč so imeli nižje tveganje za ponovitev tumorja. Kumulativna incidenca krvavitve in radiacijske nekroze pri bolnikih po »sendvič zdravljenju« je bila 4,92 % (3/61) in 13,11 % (8/61).

Zaključki. Za LBM, ki se nahajajo v motoričnem predelu možganov, je strategija »sendvič zdravljenja« varna in učinkovita. Ta strategija lahko hitro izboljša gibanje bolnikov in izboljša rehabilitacijo njihove telesne moči.



FUNDACIJA "DOCENT DR. J. CHOLEWA"
JE NEPROFITNO, NEINSTITUCIONALNO IN NESTRANKARSKO
ZDRUŽENJE POSAMEZNIKOV, USTANOV IN ORGANIZACIJ, KI ŽELIJO
MATERIALNO SPODBUJATI IN POGLABLJATI RAZISKOVALNO
DEJAVNOST V ONKOLOGIJI.

DUNAJSKA 106
1000 LJUBLJANA
IBAN: SI56 0203 3001 7879 431

ZA BOLNICE S HR+ HER2- RAKOM DOJKE Z VELIKIM TVEGANJEM
ZA PONOVIŠE BOLEZNI PRI ZGODNJEM RAKU ALI ZA BOLNICE Z MRD

ONA POTREBUJE VSE upanje tega sveta IN ŠE VEČ


Verzenios
abemaciclib

DAJTE JI
VEČ KOT UPANJE

SKRAJŠAN POVZETEK GLAVNIH ZNAČILNOSTI ZDRAVILA

IME ZDRAVILA Verzenios 50 mg/100 mg/150 mg filmsko obložene tablete **KAKOVOSTNA IN KOLIČINSKA SESTAVA** Ena filmsko obložena tableta vsebuje 50 mg/100 mg/150 mg abemacicliba. Ena filmsko obložena tableta vsebuje 14 mg/28 mg/42 mg laktoze (v obliki monohidrata). **Terapevtske indikacije** Zgodnji rak dojke Zdravilo Verzenios je v kombinaciji z endokrinim zdravljenjem indicirano za adjuvantno zdravljenje odraslih bolnikov z na hormonske receptorje (HR) pozitivnim, na receptorje humanega epidermalnega ravnega faktorja 2 (HER2) negativnim zgodnjim rakom dojke s pozitivnimi bezgavkami, pri katerih obstaja veliko tveganje za ponovitev. Pri ženskah v pred- ali perimenopavzi je treba endokrinno zdravljenje z zaviralcem aromataze kombinirati z agonistom gonadolibarina LHRH – luteinizirajočim hormone–releasing hormone). **Napredujevali ali metastatski rak dojke** Zdravilo Verzenios je indicirano za zdravljenje žensk z lokalno napredujevalim ali metastatskim, na hormonske receptorje (HR) pozitivnim in na receptorje humanega epidermalnega ravnega faktorja 2 (HER2) negativnim rakom dojke v kombinaciji z zaviralcem aromataze ali s fulvestrantom kot začetnim endokrinim zdravljenjem ali pri ženskah, ki so prejele predhodno endokrinno zdravljenje. Pri ženskah v pred- ali perimenopavzi je treba endokrinno zdravljenje kombinirati z agonistom LHRH. **Odmerjanje in način uporabe** Zdravljenje z zdravilom Verzenios mora uvesti in nadzorovati zdravnik, ki ima izkušnje z uporabo zdravil za zdravljenje rakavih bolezni. Priporočeni odmerek abemacicliba je 150 mg dvakrat na dan, kadar se uporablja v kombinaciji z endokrinim zdravljenjem. **Zgodnji rak dojke** Zdravilo Verzenios je treba jemati neprekinjeno dve leti, ali do ponovitve bolezni ali pojavnosti nesprejemljive toksičnosti. **Napredujevali ali metastatski rak dojke** Zdravilo Verzenios je treba jemati, dokler ima bolnica od zdravljenja klinično korist ali do pojavnosti nesprejemljive toksičnosti. Če bolnica bruha ali izpusti odmerek zdravila Verzenios, ji je treba naročiti, da naj naslednji odmerek vzame ob predvidenem času; dodatnega odmerka ne sme vzeti. Obvladovanje nekaterih neželenih učinkov lahko zahteva prekinitve in/ali zmanjšanje odmerka. Zdravljenje z abemaciclibom prekinite v primeru povišanja vrednosti AST in/ali ALT >3 x ZMN SKUPAJ s celokupnim bilirubinom > 2,0 x ZMN v odsotnosti holestaze ter pri bolnicah z intersticijsko pljučno boleznijo (ILD)/pneumonitis stopnje 3 ali 4. Sočasni uporabi močnih zaviralcev CYP3A4 se je treba izogibati. Če se uporabi močnih zaviralcev CYP3A4 ni mogoče izogniti, je treba odmerek abemacicliba znižati na 100 mg dvakrat na dan. Pri bolnicah, pri katerih je bil odmerek znižan na 100 mg abemacicliba dvakrat na dan in pri katerih se sočasno dajanje močnega zaviralca CYP3A4 ni mogoče izogniti, je treba odmerek abemacicliba dodatno znižati na 50 mg dvakrat na dan. Pri bolnicah, pri katerih je bil odmerek znižan na 50 mg abemacicliba dvakrat na dan in pri katerih se sočasno dajanje močnega zaviralca CYP3A4 ni mogoče izogniti, je mogoče z odmerkom abemacicliba nadaljevati ob natančnem spremljanju znakov toksičnosti. Alternativno je mogoče odmerek abemacicliba znižati na 50 mg enkrat na dan ali prekiniti dajanje abemacicliba. Če je uporaba zaviralca CYP3A4 prekinjena, je treba odmerek abemacicliba povečati na odmerek, kakršen je bil pred uvedbo zaviralca CYP3A4 (po 3–5 razpolovnih časih zaviralca CYP3A4). Prilaganje odmerka glede na starost in pri bolnicah z blago ali zmerno ledvično okvaro ter z blago (Child Pugh A) ali zmerno (Child Pugh B) jetrno okvaro ni potrebno. Pri dajanju abemacicliba bolnicam s hudo ledvično okvaro sta potrebna previdnost in skrbno spremljanje glede znakov toksičnosti. **Način uporabe** Zdravilo Verzenios je namenjeno za peroralno uporabo. Odmerek se lahko vzame s hrano ali brez nje. Zdravila se ne sme jemati z grenivko ali grenivkinim sokom. Bolnice naj odmerek vzamejo vsak dan ob približno istem času. Tableto je treba pogoltniti celo (bolnice tablet pred zaužitjem ne smejo gristi, drobiti ali deliti). **Kontraindikacije** Preobčutljivost na učinkovino ali katero koli pomožno snov. **Posebna opozorila in previdnostni ukrepi** Pri bolnicah, ki so prejele abemaciclib, so poročali o nevtropeniji, o večji pogostosti okužb kot pri bolnicah, zdravljenih s placebom in endokrinim zdravljenjem, o povečanih vrednostih ALT in AST. Pri bolnicah, pri katerih se pojavi nevtropenija stopnje 3 ali 4, je priporočljivo prilagoditi odmerek. Do primerov nevtropenične sepsa s smrtnim izidom je prišlo pri < 1 % bolnic z metastatskim rakom dojke. Bolnicam je treba naročiti, naj o vsaki epizodi povišane telesne temperature poročajo zdravstvenemu delavcu. Bolnice je treba spremljati za znake in simptome globoke venske tromboze (VTE) in pljučne embolije ter jih zdraviti, kot je medicinsko utemeljeno. Glede na stopnjo VTE bo morda treba spremeniti odmerek abemacicliba. Pri bolnicah, pri katerih se pojavi resni arterijski tromboembolični dogodek (ATE), je treba oceniti koristi in tveganja nadaljnega zdravljenja z abemaciclibom. Glede na povečanje vrednosti ALT ali AST je mogoče potrebna prilagoditev odmerka. Driska je najpogostejši neželeni učinek. Bolnice je treba ob prvem znaku tekočega blata začeti zdraviti z antidiaroički, kot je loperamid, povečati vnos peroralnih tekočin in obvestiti zdravnika. Sočasni uporabi induktorjev CYP3A4 se je treba izogibati zaradi tveganja za zmanjšano učinkovitost abemacicliba. Bolnice z redkimi dednimi motnjami, kot so intoleranca za galaktozo, popolno pomanjkanje laktaze ali malabsorpcija glukoze/galaktoze, tega zdravila ne smejo jemati. Bolnice je treba spremljati glede pljučnih simptomov, ki kažejo na ILD/pneumonitis, in jih ustrezno zdraviti. Glede na stopnjo ILD/pneumonitisa je morda potrebno prilaganje odmerka abemacicliba. **Medsebojno delovanje z drugimi zdravili in druge oblike interakcij** Abemaciclib se primarno presnavlja s CYP3A4. Sočasna uporaba abemacicliba in zaviralcev CYP3A4 lahko poveča plazemsko koncentracijo abemacicliba. Uporabi močnih zaviralcev CYP3A4 sočasno z abemaciclibom se je treba izogibati. Če je močne zaviralce CYP3A4 treba dajati sočasno, je treba odmerek abemacicliba zmanjšati, nato pa bolnico skrbno spremljati glede toksičnosti. Pri bolnicah, zdravljenih z zmerimi ali šibkimi zaviralci CYP3A4, ni potrebno prilaganje odmerka, vendar jih je treba skrbno spremljati za znake toksičnosti. Sočasni uporabi močnih induktorjev CYP3A4 (vključno, vendar ne omejeno na: karbamazepin, fenitoin, rifampicin in šentjanževko) se je treba izogibati zaradi tveganja za zmanjšano učinkovitost abemacicliba. Abemaciclib in njegovi glavni aktivni presnovki zavirajo prenašalce v ledvicah, in sicer kationski organski prenašalec 2 (OCT2) ter prenašalec MATE1. *In vivo* lahko pride do medsebojnega delovanja abemacicliba in klinično pomembnih substratov teh prenašalcev, kot je dofetilid ali kreatinin. Trenutno ni znano, ali lahko abemaciclib zmanjša učinkovitost sistemskih hormonskih kontraceptivov, zato se ženskam, ki uporabljajo sistemske hormonske kontraceptive, svetuje, da hkrati uporabljajo tudi mehansko metodo. **Neželeni učinki** Najpogostejši neželeni učinki so driska, okužbe, nevtropenija, levkopenija, anemija, utrujenost, navzea, bruhanje in zmanjšanje apetita. **Zelo pogosti:** okužbe, nevtropenija, levkopenija, anemija, trombotopenija, limfopenija, zmanjšanje apetita, glavobol, disgevizija, omotica, driska, bruhanje, navzea, stomatitis, alopecija, pruritus, izpuščaj, pike/sjaja, utrujenost, povečana vrednost alanin-aminotransferaze, povečana vrednost aspartat-aminotransferaze. **Pogosti:** povečano solzenje, venska tromboembolija, ILD/pneumonitis, dispneja, spremembe na nohtih, suha koža, mišična šibkost. **Občasni:** febrilna nevtropenija **Rok uporabnosti** 3 leta. **Posebna navodila za shranjevanje** Za shranjevanje zdravila niso potrebna posebna navodila. **Imetnik dovoljenja za promet z zdravilom:** Eli Lilly Nederland B.V., Papendorpseweg 83, 3528BJ, Utrecht, Nizozemska. Datum prve odobritve dovoljenja za promet: 27. september 2018 Datum zadnjega podaljšanja: 23. junij 2023 **Datum zadnje revizije besedila:** 9.11.2023 **Režim izdaje:** Rp/Spec - Predpisovanje in izdaja zdravila je le na recept zdravnika specialista ustreznega področja medicine ali od njega pooblaščenega zdravnika.

Reference: 1. Povzetek glavnih značilnosti zdravila Verzenios, zadnja odobrena verzija.

Pomembno: Predpisovanje in izdaja zdravila je le na recept zdravnika specialista ustreznega področja medicine ali od njega pooblaščenega zdravnika. Pred predpisovanjem zdravila Verzenios si preberite zadnji veljavni Povzetek glavnih značilnosti zdravil. Podrobne informacije o zdravilu so objavljene na spletni strani Evropske agencije za zdravila <http://www.ema.europa.eu>

Eli Lilly farmacevtska družba, d.o.o., Dunajska cesta 167, 1000 Ljubljana, telefon 01 / 580 00 10, faks 01 / 569 17 05

PP-AL-SI-0268, 5.2.2024, Samo za strokovno javnost.



TANTUM VERDE®

benzidaminijev klorid

Za lajšanje bolečine in oteklin v ustni in žrelu, ki so posledica radiomukozitisa

Bistvene informacije iz Povzetka glavnih značilnosti zdravila

Tantum Verde 1,5 mg/ml oralno pršilo, raztopina
Tantum Verde 3 mg/ml oralno pršilo, raztopina

Sestava 1,5 mg/ml: 1 ml raztopine vsebuje 1,5 mg benzidaminijevega klorida, kar ustreza 1,34 mg benzidamina. V enem razpršku je 0,17 ml raztopine. En razpršek vsebuje 0,255 mg benzidaminijevega klorida, kar ustreza 0,2278 mg benzidamina. **Sestava 3 mg/ml:** 1 ml raztopine vsebuje 3 mg benzidaminijevega klorida, kar ustreza 2,68 mg benzidamina. V enem razpršku je 0,17 ml raztopine. En razpršek vsebuje 0,51 mg benzidaminijevega klorida, kar ustreza 0,4556 mg benzidamina. **Terapevtske indikacije:** Samozdravljenje; Lajšanje bolečine in oteklin pri vnetju v ustni votlini in žrelu, ki so lahko posledica okužb in stanj po operaciji. Po nasvetu in navodilu zdravnika; Lajšanje bolečine in oteklin v ustni votlini in žrelu, ki so posledica radiomukozitisa. **Odmerjanje in način uporabe:** **Uporaba:** 2- do 6-krat na dan (vsake 1,5 do 3 ure). **Odmerjanje 1,5 mg/ml:** Odrasli: 4 do 8 razprškov 2- do 6-krat na dan. **Pediatrična populacija:** Mladostniki, stari od 12 do 18 let: 4-8 razprškov 2- do 6-krat na dan. Otroci od 6 do 12 let: 4 razprški 2- do 6-krat na dan. Otroci, mlajši od 6 let: 1 razpršek na 4 kg telesne mase; do največ 4 razprške 2- do 6-krat na dan. **Odmerjanje 3 mg/ml:** Odrasli: 2 do 4 razprški 2- do 6-krat na dan. **Pediatrična populacija:** Mladostniki, stari od 12 do 18 let: 2 do 4 razprški 2- do 6-krat na dan. Otroci od 6 do 12 let: 2 razprška 2- do 6-krat na dan. Otroci, mlajši od 6 let: 1 razpršek na 8 kg telesne mase; do največ 2 razprška 2- do 6-krat na dan. **Starejši bolniki, bolniki z jetrno okvaro in bolniki z ledvično okvaro:** niso potrebni posebni previdnostni ukrepi. Trajanje zdravljenja ne sme biti daljše od 7 dni. **Način uporabe:** Za orofaringealno uporabo. Zdravilo se razprši v usta in žrelo. **Kontraindikacije:** Preobčutljivost na učinkovino ali katero koli pomožno snov. **Posebna opozorila in previdnostni ukrepi:** Pri nekaterih bolnikih lahko resne bolezni povzročijo ustne/žrelne ulceracije. Če se simptomi v treh dneh ne izboljšajo, se mora bolnik posvetovati z zdravnikom ali zobozdravnikom, kot je primerno. Uporaba benzidamina ni priporočljiva za bolnike s preobčutljivostjo na salicilno kislino ali druga nesteroidna protivnetna zdravila. Pri bolnikih, ki imajo ali so imeli bronhialno astmo, lahko pride do bronhospazma. Pri takih bolnikih je potrebna previdnost. To zdravilo vsebuje 13,6 mg alkohola (etanola) v enem razpršku (0,17 ml), kar ustreza manj kot 0,34 ml piva oziroma 0,14 ml vina. Majhna količina alkohola v zdravilu ne bo imela nobenih opaznih učinkov. To zdravilo vsebuje metilparahidroksibenzoat (E218). Lahko povzroči alergijske reakcije (lahko zapoznele). To zdravilo vsebuje manj kot 1 mmol (23 mg) natrija v enem razpršku (0,17 ml), kar v bistvu pomeni 'brez natrija'. Zdravilo vsebuje aromo poprove mete z benzilalkoholom, cinamilalkoholom, citralom, citronelolom, geraniolom, izoevgenolom, linalolom, evgenolom in D-limonen, ki lahko povzročijo alergijske reakcije. Zdravilo z jakostjo 3 mg/ml vsebuje makrogolglicerol hidroksistearat 40. Lahko povzroči želodčne težave in drisko. **Medsebojno delovanje z drugimi zdravili in druge oblike interakcij:** Študij medsebojnega delovanja niso izvedli. **Nosečnost in dojenje:** O uporabi benzidamina pri nosečnicah in doječih ženskah ni zadostnih podatkov. Uporaba zdravila med nosečnostjo in dojenjem ni priporočljiva. **Vpliv na sposobnost vožnje in upravljanja strojev:** Zdravilo v priporočenem odmerku nima vpliva na sposobnost vožnje in upravljanja strojev. **Neželeni učinki:** Neznana pogostnost (ni mogoče oceniti iz razpoložljivih podatkov): anafilaktične reakcije, preobčutljivostne reakcije, odrevenelost, laringospazem, suha usta, navzea in bruhanje, oralna hipestezija, angioedem, fotosenzitivnost, pekoč občutek v ustih. Neposredno po uporabi se lahko pojavi občutek odrevenelosti v ustih in v žrelu. Ta učinek se pojavi zaradi načina delovanja zdravila in po kratkem času izgine. **Način in režim izdaje zdravila:** BRP-Izdaja zdravila je brez recepta v lekarnah in specializiranih prodajalnah. **Imetnik dovoljenja za promet:** Aziende Chimiche Riunite Angelini Francesco – A.C.R.A.F. S.p.A., Viale Amelia 70, 00181 Rim, Italija **Datum zadnje revizije besedila:** 05. 04. 2022

Pred svetovanjem ali izdajo preberite celoten Povzetek glavnih značilnosti zdravila.

Samo za strokovno javnost.

Datum priprave informacije: april 2022

Odgovoren za trženje: Bonifar d.o.o.



PREMIKAMO MEJE ZDRAVLJENJA Z UČINKOVITOSTJO, KI PRESEGA PRIČAKOVANJA

- Terapija izbora v smernici za LHER2+ raka dojč^{1,5}
- Prvo in edino zdravljenje proti HER2, ki je učinkovito tudi pri bolnikih z nizkim izražanjem HER2^{*,1,3-6}

SKRAJŠAN POVZETEK GLAVNIH ZNAČILNOSTI ZDRAVILA

▼ Za to zdravilo se izvaja dodatno spremljanje varnosti. Tako bodo hitreje na voljo nove informacije o njegovi varnosti. Zdravstvene delavce naprošamo, da poročajo o katerem koli domnevnem neželenem učinku zdravila. ENHERTU 100 mg prašek za koncentrat za raztopino za infundiranje

SESTAVA: Ena viala praška za koncentrat za raztopino za infundiranje vsebuje 100 mg trastuzumab derukstekana. Po rekonstituciji ena viala s 5 ml raztopine vsebuje 20 mg/ml trastuzumab derukstekana. Trastuzumab derukstekan je konjugat protitelesa in zdravila, ki vsebuje humanizirano monoklonsko protiteleso IgG1 proti HER2 z istim zaporedjem aminokislotin, kot ga ima trastuzumab. Proizvajajo ga sesalske celice (ovarij kitajskega hrčka) in je prek razcepljivega veznika na terapevtski deli kovalentno vezan na DXd, ki je derivat eksotekana in zaviralec topozomeraze I. Na vsako molekulo protitelesa je vezanih približno 8 molekul derukstekana. **Pomembne snovi:** L-histidin, L-histidinijev klorid monohidrat, saharoza, polisorbitat 80. **TERAPEVTSKE INDIKACIJE: Rak dojč:** HER2-pozitiven rak dojč: Zdravilo Enherthu kot monoterapija je indicirano za zdravljenje odraslih bolnikov z neresektabilnim ali metastatskim HER2-pozitivnim rakom dojč, ki so pred tem že prejeli eno ali več shem zdravljenja na podlagi anti-HER2. **Rak dojč z nizkim statusom HER2:** Zdravilo Enherthu kot monoterapija je indicirano za zdravljenje odraslih bolnikov z neresektabilnim ali metastatskim HER2-pozitivnim rakom dojč, ki so pred tem že prejeli kemoterapijo v prisotnosti metastaz ali pa se je pri njih bolezen ponovila med adjuvantno kemoterapijo ali znotraj 6 mesecev po njenem zaključku. **Nedrobnocelični rak pljuč (NSCLC - non-small cell lung cancer):** Zdravilo Enherthu kot monoterapija je indicirano za zdravljenje odraslih bolnikov z napredovalim NSCLC, ki imajo tumorje z aktivirajočo mutacijo HER2 (ERBB2) in potrebujejo sistemsko terapijo po kemoterapiji na podlagi platine z imunoterapijo ali brez nje. **Rak želodca:** Zdravilo Enherthu v obliki monoterapije je indicirano za zdravljenje odraslih bolnikov z napredovalim NSCLC, ki imajo tumorje z aktivirajočo mutacijo HER2 (ERBB2) in potrebujejo sistemsko terapijo po kemoterapiji na podlagi platine z imunoterapijo ali brez nje. **Rak želodca:** Zdravilo Enherthu v obliki monoterapije je indicirano za zdravljenje odraslih bolnikov z napredovalim NSCLC, ki imajo tumorje z aktivirajočo mutacijo HER2 (ERBB2) in potrebujejo sistemsko terapijo po kemoterapiji na podlagi platine z imunoterapijo ali brez nje. **ODMERJANJE IN NAČIN UPORABE:** Zdravilo Enherthu mora predpisati zdravnik in njegovo dajanje nadzorovati zdravstveni delavec, ki sta izkušena v uporabi zdravlil proti raku. Za preprečitev napak, povezanih z zdravili, je pomembno, da preverite nalepke na vialah in se pripravite, da je zdravilo, ki se pripravljata in daje, res zdravilo Enherthu (trastuzumab derukstekan), in ne trastuzumab ali trastuzumab emtanzin. Zdravilo Enherthu se ne sme zamenjati s trastuzumabom ali trastuzumab emtanzinom. Bolniki, ki se zdravijo s trastuzumab derukstekanom zaradi HER2-pozitivnega raka dojč, raka želodca ali gastroezofagealnega prehoda, morajo imeti dokumentiran HER2-pozitiven status tumorja, ki je opredeljen kot ocena 3+ na podlagi imunohistokemije (IHC) ali razmerje $\geq 2,0$ na podlagi *in situ* hibridizacije (ISH) ali fluorescenčne *in situ* hibridizacije (FISH), ocenjeno z *in vitro* diagnostičnim (IVD) medicinskim pripomočkom z oznako CE. Bolniki, ki se zdravijo s trastuzumab derukstekanom zaradi raka dojč z nizkim statusom HER2, morajo imeti dokumentiran nizki status HER2 tumorja, ki je opredeljen kot ocena IHC 1+ ali IHC 2+/ISH-, ocenjeno z IVD z oznako CE. Bolniki, ki se zdravijo s trastuzumab derukstekanom zaradi napredovalnega NSCLC, morajo imeti aktivirajočo mutacijo HER2 (ERBB2), odkrito z *in vitro* diagnostičnim (IVD) medicinskim pripomočkom, označenim s CE. Če IVD z oznako CE ni na voljo, je treba status HER2 in status mutacije HER2 oceniti z drugim potrjenim testom. **Odmerjanje: Rak dojč in NSCLC:** Priporočeni odmerki zdravila Enherthu je 5,4 mg/kg, ki se daje z intravensko infuzijo enkrat vsake 3 tedne (21-dnevni cikel) do napredovanja bolezni ali nesprejemljive toksičnosti. **Rak želodca:** Priporočeni odmerki zdravila Enherthu je 6,4 mg/kg, ki se daje z intravensko infuzijo enkrat vsake 3 tedne (21-dnevni cikel) do napredovanja bolezni ali nesprejemljive toksičnosti. **Načrt zmanjševanja odmerka:** Priporočeni začetni odmerki: Priporočeni začetni odmerki je 5,4 mg/kg pri raku dojč in NSCLC oz. 6,4 mg/kg pri raku želodca; prvo zmanjšanje odmerka (4,4 mg/kg oz. 5,4 mg/kg), drugo zmanjšanje odmerka (3,2 mg/kg oz. 4,4 mg/kg), pri potrebi po nadaljnjem zmanjšanju odmerka ukinite zdravljenje. **Prosimo, gledajte celoten povzetek glavnih značilnosti zdravila Enherthu za prilaganje odmerka zaradi neželenih učinkov: intersticijska pljučna bolezen (IPB)/pnevmonitis (asimptomatska IPB/asimptomatski pnevmonitis (stopnja 1), simptomatska IPB/simptomatski pnevmonitis (stopnja 2 ali višja)), nevropenija (stopnja 3 (manj kot $1,0-0,5 \times 10^9/l$), stopnja 4 (manj kot $0,5 \times 10^9/l$)), febrilna nevropenija (absolutno število nevtrofilcev manj kot $1,0 \times 10^9/l$ in telesna temperatura, višja od $38,3^\circ C$, ali telesna temperatura $38^\circ C$ ali višja, ki vztraja več kot eno uro), zmanjšanje iztisnega deleža levega prekata (LVEF) (LVEF več kot 45 % in absolutno zmanjšanje glede na izhodiščno vrednost za 10 % do 20 %; LVEF manj kot 40 % ali absolutno zmanjšanje vrednost za več kot 20 %; simptomatično kongestivno srčno popuščanje). **Zakasnjen ali izpuščen odemek:** Če se načrtovani odmeki zakasni ali izpusti, ga je treba dati takoj, ko je mogoče, brez čakanja na naslednji načrtovani cikel. Časovni načrt dajanja je treba prilagoditi, da se ohrani 3-tedenski razmik med odmerki. Infuzijo je treba dati s hitrostjo in odmerkom, ki ga je bolnik prenašal pri zadnji infuziji. **Posebne populacije: Starejši:** Pri bolnikih, starih 65 let ali starejših, prilaganje odmerka zdravila Enherthu ni potrebno. Podatki pri bolnikih, starih ≥ 75 let, so omejeni. **Okvara ledvic:** Prilaganje odmerka pri bolnikih z blago (očistek kreatinina [CLcr] ≥ 60 in < 90 ml/min) ali zmerno (CLcr ≥ 30 in < 60 ml/min) okvaro ledvic ni potrebno. Morebitne potrebe po prilaganju odmerka pri bolnikih s hudo okvaro ledvic ali končno ledvično odpovedjo ni mogoče opredeliti, ker je bila huda okvara ledvic v kliničnih študijah izključitveni kriterij. Pri bolnikih z zmerno okvaro ledvic so opazili višjo pogostost IPB stopnje 1 in 2/pnevmonitisa, ki sta vodila do zvečanja števila prekinitev zdravljenja. Pri bolnikih z zmerno okvaro ledvic v izhodišču, ki so prejeli zdravilo Enherthu 6,4 mg/kg, so ugotovili večjo pogostost resnih neželenih učinkov kot pri tistih z normalnim delovanjem ledvic. Bolnike z zmerno ali hudo okvaro ledvic je treba natančno spremljati glede neželenih učinkov, vključno z IPB/pnevmonitisom. **Okvara jeter:** Pri bolnikih, ki imajo celokupni bilirubin $\leq 1,5$ -kratnik zgornje meje normalnih vrednosti (ZMN), ne glede na vrednost aspartat transaminaze (AST), odmerka ni treba prilagajati. Morebitne potrebe po prilaganju odmerka pri bolnikih, ki imajo celokupni bilirubin $> 1,5$ -kratnik ZMN, ne glede na vrednost AST, ni mogoče opredeliti zaradi pomanjkanja podatkov. Zato je treba te bolnike natančno spremljati. **Način uporabe:** Zdravilo Enherthu je za intravensko uporabo. Zdravstveni delavec ga mora rekonstituirati in razredčiti. Treba ga je dati z intravenskim infundiranjem. Zdravilo Enherthu se ne sme dati kot hitro intravensko injekcijo ali bolus. **KONTRAINDIKACIJE:** Preobčutljivost na učinkovino ali katero koli pomožno snov. **POSEBNA OPOZORILO IN PREVIDNOSTNI UKREPI:** Intersticijska pljučna bolezen/pnevmonitis: Pri zdravilu Enherthu so poročali o primerih intersticijske pljučne bolezni (IPB) in/ali pnevmonitisa. Nekateri primeri so bili smrtni. Bolnikom je treba naročiti, naj takoj poročajo o kašlju, dispneji, zvišani telesni temperaturi in/ali katerih koli novih dihalnih simptomih ali poslabšanju obstoječih. Bolnike je treba spremljati glede znakov in simptomov IPB/pnevmonitisa. Dokaz je za IPB/pnevmonitis je treba takoj preučiti. Bolnik s sumom na IPB/pnevmonitis je treba oceniti z radiografskimi posnetki, najbolje z računalniško tomografijo (CT). Treba je razmisлити o posvetu s pulmologom. **Nevropenija:** V kliničnih študijah z zdravilom Enherthu so poročali o primerih nevropenije, vključno s primeri febrilne nevropenije s smrtnim izidom. Pred uvedbo zdravila Enherthu in pred vsakim odmerkom ter vsakič, ko je klinično indicirano, je treba preveriti celotno krvno sliko. Morda bo treba začasno prekiniti dajanje zdravila Enherthu ali zmanjšati odmek, odvisno od tega, kako huda je nevropenija. **Zmanjšanje iztisnega deleža levega prekata:** Pri zdravljenih anti-HER2 so poročali o zmanjšanem iztisnem deležu levega prekata (LVEF). Pred uvedbo zdravljenja z zdravilom Enherthu in v rednih intervalih med njim (v skladu s kliničnimi indikacijami) je treba izvesti standardne preiskave delovanja srca (ehokardiografija ali slikanje MUGA) za oceno LVEF. Zmanjšanje LVEF je treba obdelovati s prekinitvami zdravljenja. Zdravljenje z zdravilom Enherthu je treba trajno ukiniti, če se potrdi LVEF manj kot 40 % ali absolutno zmanjšanje vrednosti za več kot 20 %. Zdravilo Enherthu je treba trajno ukiniti pri bolnikih s simptomatskim kongestivnim srčnim popuščanjem. **Embrijo-fetalna toksičnost:** Zdravilo Enherthu lahko ima škodljiv vpliv na plod, če se da nosečnici. Pri ženskah v rodni dobi je treba pred uvedbo zdravljenja z zdravilom Enherthu preveriti status nosečnosti. Bolnice je treba seznaniti z možnimi tveganji za plod. Ženskam v rodni dobi je treba svetovati, da uporabljajo učinkovito kontracepcijo med zdravljenjem in še vsaj 7 mesecev po zadnjem odmerku zdravila Enherthu. Moškim bolnikom s partnerkami v rodni dobi je treba svetovati, da uporabljajo učinkovito kontracepcijo med zdravljenjem z zdravilom Enherthu in še vsaj 4 mesece po zadnjem odmerku zdravila Enherthu. **Bolniki z zmerno ali hudo okvaro jeter:** Zdravilo Enherthu je treba pri bolnikih z zmerno in hudo okvaro jeter dajati previdno. **MEDESEBNO DELOVANJE Z DRUGIMI ZDRAVILI IN DRUGE OBILNE INTERAKCIJE:** Pri sočasnem dajanju trastuzumab derukstekana z zdravili, ki so zaviralci CYP3A ali OATP1B ali prenašalcev P-gp, odmerka ni treba prilagajati. **PLODNOST, NOSEČNOST IN DOJENJE:** Nosečnost: Dajanje zdravila Enherthu nosečnicam se ne priporoča. Bolnice je treba seznaniti z možnimi tveganji za plod, preden zanosijo. Ženske, ki zanosijo, se morajo takoj obrniti na zdravnika. Če ženska zanosi med zdravljenjem z zdravilom Enherthu ali v obdobju 7 mesecev po zadnjem odmerku zdravila Enherthu, se priporoča natančno spremljanje. **Dojenje:** Ni znano, ali se trastuzumab derukstekan izloča v materino mleko. Humani IgG se izloča v materino mleko in potencial za absorpcijo in resne neželene učinke na dojenčka ni znan. Zato ženske ne smejo dojiti med zdravljenjem z zdravilom Enherthu in še 7 mesecev po zadnjem odmerku. Odlučiti se je treba med prenehanjem dojenja in prenehanjem zdravljenja z zdravilom Enherthu, pri čemer je treba pretehtati prednosti dojenja za otroka in prednosti zdravljenja za mater. **PloDNost:** Namenskimi študij plodnosti s trastuzumab derukstekanom niso izvedli. Ni znano, ali so trastuzumab derukstekan ali njegovi presnovki prisotni v semenski tekočini. Pred začetkom zdravljenja je treba moškim bolnikom svetovati, da se posvetujejo o možnosti shranjevanja semena. Moški bolniki v celotnem obdobju zdravljenja in še najmanj 4 mesece po zadnjem odmerku zdravila Enherthu ne smejo zamrzniti ali darovati semena. **NEŽELENI UČINKI:** Zdravilo Enherthu 5,4 mg/kg: Združeno varnostno populacijo so ocenili pri bolnikih, ki so v kliničnih študijah dobili vsaj en odmek 5,4 mg/kg zdravila Enherthu (N = 1449) zaradi različnih vrst tumorjev. Mediani čas trajanja zdravljenja v tej združeni populaciji je bil 9,8 meseca (razpon: 0,7-45,1 meseca). **Zelo pogosti:** okužba zgornjih dihal, anemija, nevropenija, trombotična, levkopenija, limfopenija, hipokaliemija, zmanjšani apetit, glavobol, omotica, intersticijska pljučna bolezen, dispneja, kašelj, epistaksa, navzea, bruhanje, zaprtje, driska, bolečina v trebuhu, stomatitis, dispesija, zvišane transaminaze, alopecija, mišično-skeletna bolečina, utrujenost, piroksija, zmanjšani iztisni delež, zmanjšanje telesne mase. **Pogosti:** pljučnica, dehidracija, disartrija, suhe oči, zamegljen vid, abdominalna distenzija, gastritis, flatulenca, izpuščaj, pruritus, hiperpigmentacija kože, periferi edem, zvišana alkalna fosfataza v krvi, zvišan bilirubin v krvi, zvišan kreatinin v krvi, reakcije, povezane z infuzijo. **Zdravilo Enherthu 6,4 mg/kg:** Združeno varnostno populacijo so ocenili za bolnike, ki so v kliničnih študijah dobili vsaj en odmek 6,4 mg/kg zdravila Enherthu (N = 669) zaradi različnih vrst tumorjev. Mediani čas trajanja zdravljenja v tej združeni populaciji je bil 5,7 meseca (razpon: 0,7-41,0 meseca). **Zelo pogosti:** pljučnica, okužba zgornjih dihal, anemija, nevropenija, trombotična, levkopenija, limfopenija, hipokaliemija, zmanjšani apetit, glavobol, dispneja, intersticijska pljučna bolezen, dispneja, kašelj, navzea, bruhanje, driska, zaprtje, bolečina v trebuhu, stomatitis, zvišane transaminaze, alopecija, mišično-skeletna bolečina, utrujenost, piroksija, periferi edem, zmanjšani iztisni delež, zmanjšanje telesne mase. **Pogosti:** febrilna nevropenija, dehidracija, omotica, suhe oči, zamegljen vid, epistaksa, dispesija, abdominalna distenzija, gastritis, flatulenca, izpuščaj, pruritus, hiperpigmentacija kože, zvišana alkalna fosfataza v krvi, zvišan bilirubin v krvi, zvišan kreatinin v krvi, reakcije, povezane z infuzijo. **IMETNIK DOVOLJENJA ZA PROMET Z ZDRAVILOM:** Daiichi Sankyo Europe GmbH, Zielstattstrasse 48, 81379 München, Nemčija **DATUM ZADNJE REVIZIJE BESEDILA:** 12. 10. 2023 (SI-3585) **REŽIM PREDPISOVANJA IN IZDAJE:** H Prosim, da pred predpisovanjem preberete celoten povzetek glavnih značilnosti zdravila. Dodatne informacije so na voljo pri podjetju AstraZeneca UK Limited, Podružnica v Sloveniji, Verovškova 55, 1000 Ljubljana, telefon: 01/51 35 600.**

Literatura: 1. Povzetek glavnih značilnosti zdravila ENHERTU, 12.10.2023. 2. Cortes J et al; Trastuzumab Deruxetecan versus Trastuzumab Emtansine for Breast Cancer; NEJM 2022;386(12):1143-1154. 3. Gennari A et al; Ann Oncol 2021;32(12): 1475-1495 4. Curigliano G et al. ESMO Metastatic Breast Cancer Living Guidelines, v1.1 May 2023, <https://www.esmo.org/living-guidelines/esmo-metastatic-breast-cancer-living-guideline>, dostopano 5.2.2024 5. NCCN guidelines Breast Cancer, v1.2024, https://www.nccn.org/professionals/physician_gls/pdf/breast.pdf, dostopano 5.2.2024. 6. Hurvitz SA. DESTINY-changing results for advanced breast cancer. N Engl J Med. 2022;387(1):75-76.

* rak dojč z nizkim izražanjem HER2 je definiran kot HK1+ ali HK2+/ISH-

KLJUČ ZA VEČ PRILOŽNOSTI PRI ZDRAVLJENJU VAŠIH BOLNIKOV

KEYTRUDA®

(pembrolizumab, MSD)

KEYTRUDA® je odobrena za zdravljenje več kot 25 indikacij rakavih obolenj¹

Referenca: 1. Keytruda EU SmPC

SKRAJŠAN POVZETEK GLAVNIH ZNAČILNOSTI ZDRAVILA - Pred predpisovanjem, prosimo, preberite celoten Povzetek glavnih značilnosti zdravila. **Ime zdravila:** KEYTRUDA 25 mg/ml koncentrat za raztopino za infundiranje vsebuje pembrolizumab. **Terapevtske indikacije:** Zdravilo KEYTRUDA je kot samostojno zdravljenje indicirano za zdravljenje: odraslih in mladostnikov, starih 12 let ali več, z napredovalim (neoperabilnim ali metastatskim) melanomom; za adjuvantno zdravljenje odraslih in mladostnikov, starih 12 let ali več, z melanomom v stadiju IIB, IIC ali III, in sicer po popolni kirurški odstranitvi; za adjuvantno zdravljenje odraslih z nedrobnoceličnim pljučnim rakom, ki imajo visoko tveganje za ponovitev bolezni po popolni kirurški odstranitvi in kemoterapiji na osnovi platine; metastatskega nedrobnoceličnega pljučnega raka (NSCLC) v prvi liniji zdravljenja pri odraslih, ki imajo tumorje z $\geq 50\%$ izraženostjo PD-L1 (TPS) in brez pozitivnih tumorskih mutacij EGFR ali ALK; lokalno napredovalega ali metastatskega NSCLC pri odraslih, ki imajo tumorje z $\geq 1\%$ izraženostjo PD-L1 (TPS) in so bili predhodno zdravljeni z vsaj eno shemo kemoterapije, bolniki s pozitivnimi tumorskimi mutacijami EGFR ali ALK so pred prejemom zdravila KEYTRUDA morali prejeti tudi tarčno zdravljenje; odraslih in pediatričnih bolnikov, starih 3 leta ali več, s ponovljenim ali neodzivnim klasičnim Hodgkinovim limfomom (CHL), pri katerih avtologna presaditev matičnih celic (ASCT) ni bila uspešna, ali po najmanj dveh predhodnih zdravljenjih kadar ASCT ne pride v poštev kot možnost zdravljenja; lokalno napredovalega ali metastatskega urotelijskega raka pri odraslih, ki imajo tumorje z izraženostjo PD-L1 ≥ 10 , ocenjeno s kombinirano pozitivno oceno (CPS); ponovljenega ali metastatskega ploščatoceličnega raka glave in vratu (HNSCC) pri odraslih, ki imajo tumorje z $\geq 50\%$ izraženostjo PD-L1 (TPS), in pri katerih je bolezen napredovala med zdravljenjem ali po zdravljenju s kemoterapijo, ki je vključevala platino; za adjuvantno zdravljenje odraslih z rakom ledvičnih celic s povišanim tveganjem za ponovitev bolezni po nefrektomiji, ali po nefrektomiji in kirurški odstranitvi metastatskih lezij, za zdravljenje odraslih z MSI-H (microsatellite instability-high) ali dMMR (mismatch repair deficient) kolorektalnega raka v naslednjih terapevtskih okoliščinah: prva linija zdravljenja metastatskega kolorektalnega raka; zdravljenje neoperabilnega ali metastatskega kolorektalnega raka po predhodnem kombiniranem zdravljenju, ki temeljijo na fluoropirimidinu; in za zdravljenje MSI-H ali dMMR tumorjev pri odraslih z: napredovalim ali ponovljenim rakom endometrija, pri katerih je bolezen napredovala med ali po predhodnem zdravljenju, ki je vključevalo platino, v katerih koli terapevtskih okoliščinah, in ki niso kandidati za kurativno operacijo ali obsevanje; neoperabilnim ali metastatskim rakom želodca, tankega črevesa ali biliarnega trakta, pri katerih je bolezen napredovala med ali po vsaj enem predhodnem zdravljenju. Zdravilo KEYTRUDA je kot samostojno zdravljenje ali v kombinaciji s kemoterapijo in 5-fluorouracilom (5-FU) indicirano za prvo linijo zdravljenja metastatskega ploščatoceličnega raka glave in vratu pri odraslih, ki imajo tumorje z izraženostjo PD-L1 s CPS ≥ 1 . Zdravilo KEYTRUDA je v kombinaciji s pemtreksedom in kemoterapijo na osnovi platine indicirano za prvo linijo zdravljenja metastatskega ploščatoceličnega NSCLC pri odraslih, pri katerih tumorji nimajo pozitivnih mutacij EGFR ali ALK; v kombinaciji s karboplatinom in bodisi paklitakselom bodisi nab-paklitakselom je indicirano za prvo linijo zdravljenja metastatskega ploščatoceličnega NSCLC pri odraslih; v kombinaciji z akstinibom ali v kombinaciji z lenvatinibom je indicirano za prvo linijo zdravljenja napredovalega raka ledvičnih celic (RCC) pri odraslih; v kombinaciji s kemoterapijo in platino in fluoropirimidinom je indicirano za prvo linijo zdravljenja lokalno napredovalega neoperabilnega ali metastatskega raka požiralnika pri odraslih, ki imajo tumorje z izraženostjo PD-L1 s CPS ≥ 10 ; v kombinaciji s kemoterapijo za neoadjuvantno zdravljenje, in v nadaljevanju kot samostojno adjuvantno zdravljenje po kirurškem posegu, je indicirano za zdravljenje odraslih z lokalno napredovalim trojno negativnim rakom dojke ali trojno negativnim rakom dojke v zgodnjem stadiju z visokim tveganjem za ponovitev bolezni; v kombinaciji s kemoterapijo je indicirano za zdravljenje lokalno ponovljenega neoperabilnega ali metastatskega trojno negativnega raka dojke pri odraslih, ki imajo tumorje z izraženostjo PD-L1 s CPS ≥ 10 in predhodno niso prejeli kemoterapije za metastatsko bolezen; v kombinaciji z lenvatinibom je indicirano za zdravljenje napredovalega ali ponovljenega raka endometrija (EC) pri odraslih z napredovalo boleznijo med ali po predhodnem zdravljenju s kemoterapijo, ki je vključevala platino, v katerih koli terapevtskih okoliščinah, in ki niso kandidati za kurativno operacijo ali obsevanje; v kombinaciji s kemoterapijo, z bevacizumabom ali brez njega, je indicirano za zdravljenje persistentnega, ponovljenega ali metastatskega raka materničnega vratu pri odraslih bolnicah, ki imajo tumorje z izraženostjo PD-L1 s CPS ≥ 1 ; v kombinaciji s trastuzumabom, fluoropirimidinom in kemoterapijo, ki vključuje platino, je indicirano za prvo linijo zdravljenja lokalno napredovalega neoperabilnega ali metastatskega HER2-pozitivnega adenokarcinoma želodca ali gastroezofagealnega prehoda pri odraslih, ki imajo tumorje z izraženostjo PD-L1 s CPS ≥ 1 ; v kombinaciji s fluoropirimidinom in kemoterapijo, ki vključuje platino, je indicirano za prvo linijo zdravljenja lokalno napredovalega neoperabilnega ali metastatskega HER2-negativnega adenokarcinoma želodca ali gastroezofagealnega prehoda pri odraslih, ki imajo tumorje z izraženostjo PD-L1 s CPS ≥ 1 ; v kombinaciji z gemcitabinom in cisplatinom je indicirano za prvo linijo zdravljenja lokalno napredovalega neoperabilnega ali metastatskega raka biliarnega trakta pri odraslih. **Odmerjanje in način uporabe:** Testiranje PD-L1: Če je navedeno v indikaciji, je treba izbrati bolnika za zdravljenje z zdravilom KEYTRUDA na podlagi izraženosti PD-L1 tumorja potrditi z validirano preiskavo. Testiranje MSI/MMR: Če je navedeno v indikaciji, je treba izbrati bolnika za zdravljenje z zdravilom KEYTRUDA na podlagi MSI-H/dMMR statusa tumorja potrditi z validirano preiskavo. **Odmerjanje:** Priporočeni odmerek zdravila KEYTRUDA pri odraslih je bodisi 200 mg na 3 tedne ali 400 mg na 6 tednov, apliciran z intravensko infuzijo v 30 minutah. Priporočeni odmerek zdravila KEYTRUDA za samostojno zdravljenje pri pediatričnih bolnikih s CHL, starih 3 leta ali več, ali bolnikih z melanomom, starih 12 let ali več, je 2 mg/kg telesne mase (do največ 200 mg) na 3 tedne, apliciran z intravensko infuzijo v 30 minutah. Za uporabo v kombinaciji glejte povzetke glavnih značilnosti zdravil sočasno uporabljenih zdravil. Če se uporablja kot del kombiniranega zdravljenja skupaj z intravensko kemoterapijo, je treba zdravilo KEYTRUDA aplicirati prvo. Bolnike je treba zdraviti do napredovanja bolezni ali nesprejemljivih toksičnih učinkov (in do maksimalnega trajanja zdravljenja, če je le to določeno za indikacijo). Pri adjuvantnem zdravljenju melanoma, NSCLC ali RCC je treba zdravilo uporabljati do ponovitve bolezni, pojava nesprejemljivih toksičnih učinkov oziroma mora zdravljenje trajati do enega leta. Za neoadjuvantno in adjuvantno zdravljenje TNBC morajo bolniki neoadjuvantno prejeti zdravilo KEYTRUDA v kombinaciji s kemoterapijo, in sicer 8 odmerkov po 200 mg na 3 tedne ali 4 odmerke po 400 mg na 6 tednov, ali do napredovanja bolezni, ki izključuje definitivni kirurški poseg, ali do pojava nesprejemljivih toksičnih učinkov, čemur sledi adjuvantno zdravljenje z zdravilom KEYTRUDA kot samostojnim zdravljenjem, in sicer 9 odmerkov po 200 mg na 3 tedne ali 5 odmerkov po 400 mg na 6 tednov ali do ponovitve bolezni ali pojava nesprejemljivih toksičnih učinkov. Bolniki, pri katerih pride do napredovanja bolezni, ki izključuje definitivni kirurški poseg, ali do nesprejemljivih toksičnih učinkov povezanih z zdravilom KEYTRUDA kot neoadjuvantnim zdravljenjem v kombinaciji s kemoterapijo, ne smejo prejeti zdravila

KEYTRUDA kot samostojnega zdravljenja za adjuvantno zdravljenje. Če je akstinib uporabljen v kombinaciji s pembrolizumabom, se lahko razmisli o povečanju odmerka akstiniba nad začetnih 5 mg v presledkih šest tednov ali več. V primeru uporabe v kombinaciji z lenvatinibom je treba zdravljenje z enim ali obema zdraviloma prekiniti, kot je primerno. Uporabo lenvatiniba je treba zadržati, odmerek zmanjšati ali prenehati z uporabo, v skladu z navodili v povzetku glavnih značilnosti zdravila za lenvatinib, in sicer za kombinacijo s pembrolizumabom. Pri bolnikih starih ≥ 65 let, bolnikih z blago do zmerno okvaro ledvic, bolnikih z blago ali zmerno okvaro jeter prilagoditev odmerka ni potrebna. Odložitev odmerka ali ukinitve zdravljenja: Zmanjšanje odmerka zdravila KEYTRUDA ni priporočljivo. Za obvladovanje neželenih učinkov je treba uporabo zdravila KEYTRUDA zadržati ali ukiniti, prosimo, glejte celoten Povzetek glavnih značilnosti zdravila. **Kontraindikacije:** Preobčutljivost na učinkovino ali katero koli pomožno snov. **Povzetek posebnih opozoril, previdnostnih ukrepov, interakcij in neželenih učinkov:** Imunsko pogojeni neželeni učinki (pnevmonitis, kolitis, hepatitis, nefritis, endokrinopatije, neželeni učinki na kožo in drugi): Pri bolnikih, ki so prejeli pembrolizumab, so se pojavili imunsko pogojeni neželeni učinki, vključno s hudimi in smrtnimi primeri. Večina imunsko pogojenih neželenih učinkov, ki so se pojavili med zdravljenjem s pembrolizumabom, je bila reverzibilnih in so jih obvladali s prekinitvami uporabe pembrolizumaba, uporabo kortikosteroidov in/ali podporno oskrbo. Pojavilo se lahko tudi po zadnjem odmerku pembrolizumaba in hkrati prizadanejo več organskih sistemov. V primeru suma na imunsko pogojene neželene učinke je treba poskrbeti za ustrezno oceno za potrditev etiologije oziroma izključitev drugih vzrokov. Glede na izrazitost neželenega učinka je treba zadržati uporabo pembrolizumaba in uporabiti kortikosteroide – za natančna navodila, prosimo, glejte Povzetek glavnih značilnosti zdravila Keytruda. Zdravljenje s pembrolizumabom lahko poveča tveganje za zavrnitev pri prejemnikih presadkov čvrstih organov. Pri bolnikih, ki so prejeli pembrolizumab, so poročali o hudih z infuzijo povezanih reakcijah, vključno s preobčutljivostjo in anafilaksijo. Pembrolizumab se iz obzora odstrani s katabolizmom, zato presnovnih medsebojnih delovanj zdravil ni pričakovati. Uporabi sistemskih kortikosteroidov ali imunosupresivov pred uvedbo pembrolizumaba se je treba izogibati, ker lahko vplivajo na farmakodinamično aktivnost in učinkovitost pembrolizumaba. Vendar pa je kortikosteroide ali druge imunosupresive mogoče uporabiti za zdravljenje imunsko pogojenih neželenih učinkov. Kortikosteroide je mogoče uporabiti tudi kot premedikacijo, če je pembrolizumab uporabljen v kombinaciji s kemoterapijo, kot antiemetično profilakso in/ali za ublažitev neželenih učinkov, povezanih s kemoterapijo. Zenske v rodni dobi morajo med zdravljenjem s pembrolizumabom in vsaj še 4 mesece po zadnjem odmerku pembrolizumaba uporabljati učinkovito kontracepcijo, med nesčnostjo in dojenjem se ga ne sme uporabljati. Varnost pembrolizumaba pri samostojnem zdravljenju so v kliničnih študijah ocenili pri 7.631 bolnikih, ki so imeli različne vrste raka, s štiri odmerki (2 mg/kg telesne mase na 3 tedne, 200 mg na 3 tedne in 10 mg/kg telesne mase na 2 ali 3 tedne). V tej populaciji bolnikov je mediana čas opazovanja znašal 8,5 meseca (v razponu od 1 dneva do 39 mesecev), najpogostejši neželeni učinki zdravljenja s pembrolizumabom pa so bili utrujenost (31 %), diareja (22 %) in navzea (20 %). Večina poročanih neželenih učinkov pri samostojnem zdravljenju je bila po izrazitosti 1. ali 2. stopnje. Najhujši neželeni učinki so bili imunsko pogojeni neželeni učinki in hude z infuzijo povezane reakcije. Pojavnost imunsko pogojenih neželenih učinkov pri uporabi pembrolizumaba samega za adjuvantno zdravljenje je znašala 37 % za vse stopnje in 9 % od 3. do 5. stopnje, pri metastatski bolezni pa 25 % za vse stopnje in 6 % od 3. do 5. stopnje. Pri adjuvantnem zdravljenju niso zaznali nobenih novih imunsko pogojenih neželenih učinkov. Varnost pembrolizumaba pri kombiniranem zdravljenju s kemoterapijo so ocenili pri 4.787 bolnikih z različnimi vrstami raka, ki so v kliničnih študijah prejeli pembrolizumab v odmerkih 200 mg, 2 mg/kg telesne mase ali 10 mg/kg telesne mase na vsake 3 tedne. V tej populaciji bolnikov so bili najpogostejši neželeni učinki naslednji: anemija (53 %), navzea (51 %), utrujenost (35 %), diareja (34 %), zaprtost (32 %), bruhanje (29 %), zmanjšanje apetita (28 %), netropenija (28 %), zmanjšano število nevtrofilcev (26 %) in alopecija (25 %). Pojavnost neželenih učinkov 3. do 5. stopnje je pri bolnikih z NSCLC pri kombiniranem zdravljenju s pembrolizumabom znašala 67 % in pri zdravljenju samo s kemoterapijo 66 %, pri bolnikih s HNSCC pri kombiniranem zdravljenju s pembrolizumabom 85 % in pri zdravljenju s kemoterapijo v kombinaciji s cetuximabom 84 %, pri bolnikih z rakom požiralnika pri kombiniranem zdravljenju s pembrolizumabom 86 % in pri zdravljenju samo s kemoterapijo 83 %, pri bolnikih s TNBC pri kombiniranem zdravljenju s pembrolizumabom 80 % in pri zdravljenju samo s kemoterapijo 77 %, pri bolnicah z rakom materničnega vratu pri kombiniranem zdravljenju s pembrolizumabom 82 % in pri zdravljenju s kemoterapijo z ali brez bevacizumaba 75 %, pri bolnikih z rakom želodca pri kombiniranem zdravljenju s pembrolizumabom (kemoterapija z ali brez trastuzumaba) 75 % in pri kemoterapiji v kombinaciji z ali brez trastuzumaba 79 %, in pri bolnikih z rakom biliarnega trakta pri kombiniranem zdravljenju s pembrolizumabom 85 % in pri samostojni kemoterapiji 84 %. Varnost pembrolizumaba v kombinaciji z akstinibom ali lenvatinibom pri napredovalem RCC in v kombinaciji z lenvatinibom pri napredovalem EC so ocenili pri skupno 1.456 bolnikih z napredovalim RCC ali napredovalim EC, ki so v kliničnih študijah prejeli 200 mg pembrolizumaba na 3 tedne skupaj s 5 mg akstiniba dvakrat na dan ali z 20 mg lenvatiniba enkrat na dan, kot je bilo ustrezno. V teh populacijah bolnikov so bili najpogostejši neželeni učinki diareja (58 %), hipertenzija (54 %), hipotiroidizem (46 %), utrujenost (41 %), zmanjšana apetit (40 %), navzea (40 %), artralgijska (30 %), bruhanje (28 %), zmanjšanje telesne mase (28 %), disonija (28 %), bolečine v trebuhu (28 %), proteinurija (27 %), sindrom palmarno-plantarne eritrodizestezije (26 %), izpuščaj (26 %), stomatitis (25 %), zaprtost (25 %), mišično-skeletna bolečina (23 %), glavobol (23 %) in kašelj (21 %). Neželenih učinkov od 3. do 5. stopnje je bilo pri bolnikih z RCC med uporabo pembrolizumaba v kombinaciji z akstinibom ali lenvatinibom 80 % in med uporabo sunitiniba samega 71 %, pri bolnicah z EC je bilo neželenih učinkov od 3. do 5. stopnje med uporabo pembrolizumaba v kombinaciji z lenvatinibom 89 % in med uporabo kemoterapije same 73 %. Za celoten seznam neželenih učinkov, prosimo, glejte celoten Povzetek glavnih značilnosti zdravila. **Način in režim izdaje zdravila:** H - Predpisovanje in izdaja zdravila je le na recept, zdravilo se uporablja samo v bolnišnicah. **Imetnik dovoljenja za promet z zdravilom:** Merck Sharp & Dohme B.V., Waarderweg 39, 2031 BN Haarlem, Nizozemska.



Merck Sharp & Dohme inovativna zdravila d.o.o.

Ameriška ulica 2, 1000 Ljubljana

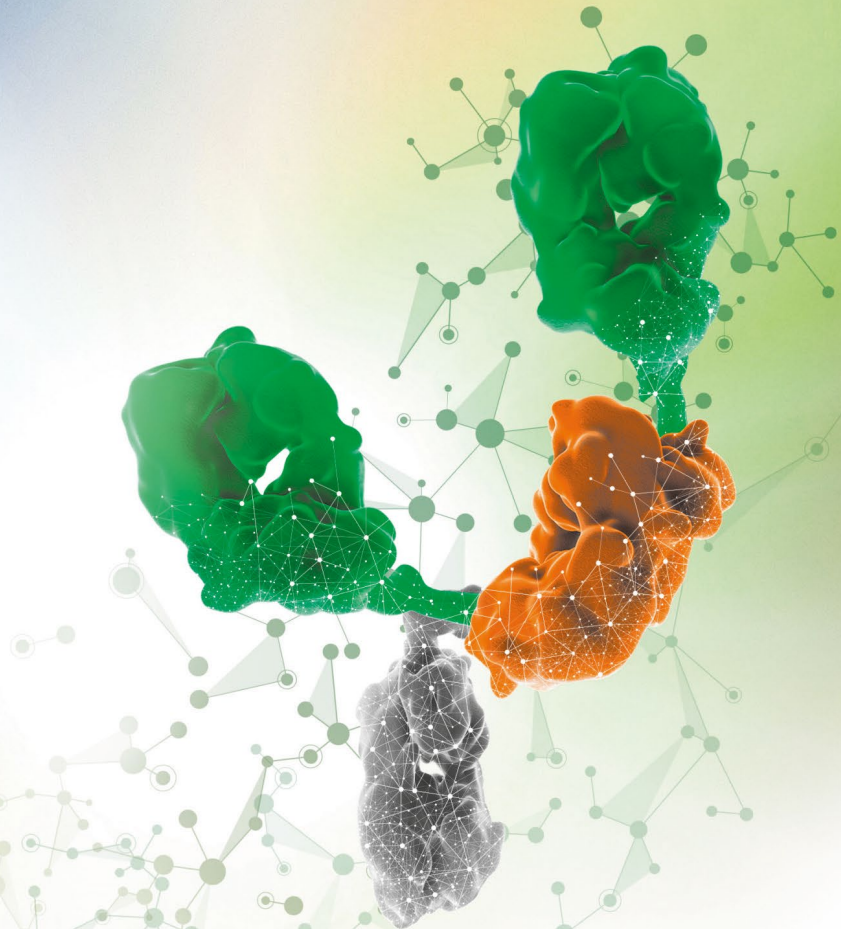
tel: +386 1 520 42 01, fax: +386 1 520 43 50

Vse pravice pridržane. Pripravljen v Sloveniji, 01/2024; SI-KEY-00624

Samo za strokovno javnost.

H - Predpisovanje in izdaja zdravila je le na recept, zdravilo pa se uporablja samo v bolnišnicah. Pred predpisovanjem, prosimo, preberite celoten Povzetek glavnih značilnosti zdravila Keytruda, ki je na voljo pri naših strokovnih sodelavcih ali na lokalnem sedežu družbe.

Zdravilo Columvi▼ je kot monoterapija indicirano za zdravljenje odraslih bolnikov s ponovljenim ali neodzivnim difuznim velikoceličnim limfomom B, ki so prejeli vsaj dve predhodni liniji sistemskega zdravljenja.¹



COLUMVI[®]
glofitamab

Reference: 1 Povzetek glavnih značilnosti zdravila Columvi, dostopano decembra 2023 na https://www.ema.europa.eu/si/documents/product-information/columvi-epar-product-information_sl.pdf

▼ Za to zdravilo se izvaja dodatno spremljanje varnosti. Tako bodo hitreje na voljo nove informacije o njegovi varnosti. Zdravstvene delavce naprošamo, da poročajo o katerem koli domnevnem neželenem učinku zdravila. Kako poročati o neželenih učinkih, si poglejte skrajšani povzetek glavnih značilnosti zdravila pod 'Poročanje o domnevnih neželenih učinkih'.

Ime zdravila: Columvi 2,5 mg in 10 mg koncentrat za raztopino za infundiranje. **Kakovostna in količinska sestava:** Ena viala z 2,5 ml/10 ml koncentrata vsebuje 2,5 mg/10 mg glofitamaba v koncentraciji 1 mg/ml. Glofitamab je humanizirano bispecifično monoklonsko protiteleso, usmerjeno proti CD20/proti CD3. **Terapevtske indikacije:** Zdravilo Columvi je kot monoterapija indicirano za zdravljenje odraslih bolnikov s ponovljenim ali neodzivnim difuznim velikoceličnim limfomom B (DVCLB), ki so prejeli vsaj dve predhodni liniji sistemskega zdravljenja. **Odmerjanje in način uporabe:** Zdravilo Columvi se sme uporabljati le pod nadzorom zdravnika, izkušeneega na področju diagnosticiranja in zdravljenja onkoloških bolnikov, ki lahko zagotavlja ustrezno zdravstveno obravnavo za obvladovanje hudih reakcij, povezanih s sindromom sproščanja citokinov (cytokine release syndrome CRS). **Odmerjanje:** Zdravilo Columvi je treba dajati v intravenski infuziji po shemi za postopno povečevanje odmerka do doseženega priporočene odmerka 30 mg (lopisano v SmPC v preglednici 2), po končanem predhodnem zdravljenju z obinutuzumabom. Vsak cikel traja 21 dni. Vse bolnike je treba seznaniti s tveganjem za pojav CRS, jih seznaniti z njegovimi znaki in simptomi ter jim naročiti, naj se v primeru pojava teh znakov in simptomov nemudoma posvetujejo z lečečim zdravnikom. **Trajanje zdravljenja:** Zdravljenje z zdravilom Columvi je priporočljivo izvajati največ 12 ciklov ali do napredovanja bolezni ali do pojava nesprejemljivih toksičnih učinkov. **Prilagoditev odmerka:** Zmanjšanja odmerka zdravila Columvi niso priporočena. **Način uporabe:** Zdravilo Columvi je namenjeno le za intravensko uporabo. Zdravilo Columvi mora pred intravensko uporabo razredčiti zdravstveni delavec ob upoštevanju aseptičnega postopka. Zdravilo je treba dati v intravenski infuziji po namenski infuzijski liniji. Za navodila o redčenju zdravila Columvi pred uporabo glejte SmPC. **Kontraindikacije:** Preobčutljivost na učinkovino, obinutuzumab ali katero koli pomožno snov. **Posebna opozorila in previdnostni ukrepi:** **CD20-negativna bolezen:** Na voljo je malo podatkov o bolnikih s CD20-negativnim DVCLB, ki so se zdravili z zdravilom Columvi. **Sindrom sproščanja citokinov:** Pri bolnikih, ki so prejeli zdravilo Columvi, so poročali o pojavu CRS, vključno z življenju ogrožajočimi reakcijami. Večina primerov CRS se je pojavila po prvem odmerku zdravila Columvi. Pred infundiranjem zdravila Columvi v 1. in 2. ciklu mora biti na voljo vsaj 1 odmerek tocilizumaba za uporabo v primeru pojava CRS. Bolnike je treba spremljati ob vsakem infundiranju zdravila Columvi in še vsaj 10 ur po koncu prvega infundiranja. Pri bolnikih je treba izključiti druge morebitne vzroke zvišane telesne temperature, hipoksije in hipotenzije, na primer okužbe ali sepsa. CRS je treba obravnavati glede na bolnikovo klinično sliko in v skladu s priporočili za vodenje CRS. **Kartica za bolnika:** Bolniku je treba izročiti kartico za bolnika in mu naročiti, naj jo ima vedno pri sebi. **Medsebojno delovanje s substrati CYP450:** Začetno sproščanje citokinov na začetku zdravljenja z zdravilom Columvi lahko zavira encime CYP450 in vodi v njihova koncentracij sočasno uporabljenih zdravil. Bolnike, ki se zdravijo s substrati CYP450 z ozkim terapevtskim indeksom, je treba po uvedbi zdravljenja z zdravilom Columvi spremljati, saj lahko njihova koncentracij sočasno uporabljenih zdravil vodijo v toksičnost, izgubo učinkovitosti ali neželene dogodke. **Resne okužbe:** Pri bolnikih, ki so prejeli zdravilo Columvi, so se pojavile resne okužbe. Zdravila Columvi ne smejo prejeti bolniki z aktivno okužbo. Zdravilo Columvi je treba uporabljati previdno pri bolnikih z anamnezno kroničnih ali ponavljajočih se okužb, bolnikih s pridruženimi boleznimi. Pri bolnikih, ki prejema zdravilo Columvi, je priporočljivo spremljati in ocenjevati kritična anatomska mesta glede pojava zagona tumorja in jih zdraviti, kot je klinično indicirano. Za zdravljenje zagona tumorja pridejo v poštev kortikosteroidi in analgetiki. **Sindrom razpada tumorja:** Pri bolnikih, ki so prejeli zdravilo Columvi, so poročali o sindromu razpada tumorja. Bolniki z velikim tumorskim bremenom, hitro rastočimi tumorji, motenim delovanjem ledvic ali dehidracijo imajo večje tveganje za pojav sindroma razpada tumorja. Bolnike s tveganjem je treba natančno spremljati z ustreznimi preiskavami elektrolitskega stanja, hidracije in delovanja ledvic. Pred predhodnim zdravljenjem z obinutuzumabom in pred infundiranjem zdravila Columvi prosidite o uporabi ustreznih preventivnih ukrepov. Med ukrepov v primeru sindroma razpada tumorja spadajo agresivna hidracija, korekcija elektrolitskih motenj, antihiperurikemični in podporno zdravljenje. **Čepljenje:** Čepljenje z živimi cepivi med zdravljenjem z zdravilom Columvi ni priporočljivo. **Medsebojno delovanje z drugimi zdravili in druge oblike interakcij:** Začetno sproščanje citokinov ob uvedbi zdravljenja z zdravilom Columvi lahko zavira delovanje encimov CYP450. Tveganje za medsebojno delovanje zdravil je največje znotraj enega tedna po vsakem od prvih 2 odmerkov zdravila Columvi pri bolnikih, ki sočasno prejema substrati CYP450 z ozkim terapevtskim indeksom. Bolnike, ki se zdravijo s substrati CYP450 z ozkim terapevtskim indeksom, je treba po uvedbi zdravljenja z zdravilom Columvi spremljati. **Neželeni učinki:** Najpogostejši neželeni učinki (≥ 20 %) so bili sindrom sproščanja citokinov, nevtropenija, anemija, trombocitopenija in izpuščaj. Najpogostejši resni neželeni učinki so bili sindrom sproščanja citokinov, sepsa, COVID-19, zagon tumorja, pljučnica COVID-19, febrilna nevtropenija, nevtropenija in pleuralni izliv. **Poročanje o domnevnih neželenih učinkih:** Poročanje o domnevnih neželenih učinkih zdravila po izdaji dovoljenja za promet je pomembno. Omogoča namreč stalno spremljanje razmerja med koristimi in tveganji zdravila. Od zdravstvenih delavcev se zahteva, da poročajo o katerem koli domnevnem neželenem učinku zdravila na: Javna agencija Republike Slovenije za zdravila in medicinske pripomočke, Sektor za farmakovigilanco, Nacionalni center za farmakovigilanco, Slovenčeva ulica 22, SI-1000 Ljubljana. Tel: +386 (0)8 2000 500, Faks: +386 (0)8 2000 510, e-pošta: h-farmakovigilanca@jazmp.si, spletna stran: www.jazmp.si. Za zagotavljanje sledljivosti zdravila je pomembno, da pri izpolnjevanju obrazca o domnevnih neželenih učinkih zdravila navedete številko serije biološkega zdravila. **Režim izdaje zdravila:** H Imetnik dovoljenja za promet: Roche Registration GmbH, Emil-Barell-Strasse 1, 79639 Grenzach-Wyhlen, Nemčija **Verzija:** 1.0/23



Samo za strokovno javnost
DODATNE INFORMACIJE SO NA VOLJO PRI: Roche farmacevtska družba d.o.o., Stegne 136, 1000 Ljubljana

Datum priprave informacije: december 2023
M-SI-00001083(v1.0)

ONIVYDE: IZDELAN POSEBEJ ZA BOJ PROTI RAKU TREBUŠNE SLINAVKE

ONIVYDE pegylated liposomal je odobren za zdravljenje metastatskega adenokarcinoma trebušne slinavke v kombinaciji s 5-fluorouracilom (5-FU) in levkovorinom (LV) pri odraslih bolnikih, pri katerih je bolezen po zdravljenju na osnovi gemcitabina napredovala.¹ Zdravilo ni bilo preizkušano pri otrocih, mlajših od 18 let, in je indicirano le za odrasle.

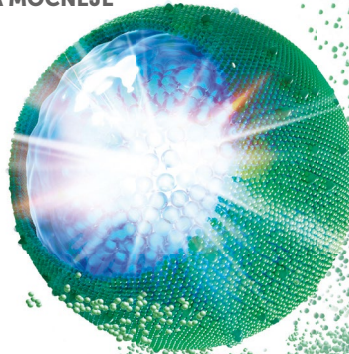
ONIVYDE VSEBUJE PEGILIRANE LIPOSOME Z IRINOTEKANOM IN JE IZDELAN POSEBEJ ZA UČINKOVITO ZDRAVLJENJE TE AGRESIVNE BOLEZNI. RAST TUMORJA ZAVIRA MOČNEJE KOT OBIČAJNI IRINOTEKAN.²⁻⁵

KLINIČNI PODATKI ŠTUDIJE 3. FAZE IN ŠTUDIJA Z KLINIČNE PRAKSE POTRjujeJO KLINIČNO VREDNOST ZDRAVILA ONIVYDE V KOMBINACIJI S 5-FU/LV:

- pomembno podaljšanje preživetja (OS, PFS) in večji ORR;⁶⁻⁸
- ohranjena kakovost življenja;⁶⁻⁹
- dobro poznan profil varnosti.^{1, 6, 7}

ONIVYDE + 5-FU/LV PRIPOROČAJO VSE GLAVNE MEDNARODNE SMERNICE.¹⁵⁻¹⁹

POMEMBNO JE ZGODNJE NAČRTOVANJE UVEDBE ZDRAVILA ONIVYDE + 5-FU/LV V TERAPIJO, DA BI DOSEGLI OPTIMALNI IZID ZDRAVLJENJA.^{6, 7, 20}



SKRAJŠAN POVZETEK GLAVNIH ZNAČILNOSTI ZDRAVILA Onivyde pegylated liposomal 4,3 mg/ml SESTAVA*: Onivyde pegylated liposomal 4,3 mg/ml koncentrat za disperzijo za infundiranje: ena viala z 10 ml koncentrata vsebuje 43 mg brezvodnega irinotekana (v obliki irinotekana oksalsulfata) in pegilirani liposomijski formulaciji. **TERAPEVTSKE INDIKACIJE*:** Zdravljenje metastatskega adenokarcinoma trebušne slinavke v kombinaciji s 5-fluorouracilom (5-FU) in levkovorinom (LV) pri odraslih bolnikih, pri katerih je bolezen po zdravljenju na osnovi gemcitabina napredovala. **ODMERJANJE IN NAČIN UPORABE*:** Onivyde pegylated liposomal smejo bolnikom predpisati in dajati samo zdravstveni delavci, ki imajo izkušnje pri uporabi zdravil za zdravljenje raka. Zdravilo Onivyde pegylated liposomal ni enakovredno drugim neliposomskim formulacijam irinotekana, zato jih ne smemo zamenjevati. Priporočeni odmerek in režim odmerjanja zdravila Onivyde pegylated liposomal je 70 mg/m² intravensko 90 minut, čemur sledi 400 mg/m² intravensko 30 minut in nato 5-FU 2400 mg/m² intravensko 46 ur, vsaka 2 tedna. Zdravilo Onivyde pegylated liposomal se ne daje kot samostojno zdravilo. Pri bolnikih z znano homozigotnostjo za alel UGT1A1*28 je treba razmisliti o manjšem začetnem odmerku zdravila Onivyde pegylated liposomal 50 mg/m². Če zdravilo bolniki dobro prenašajo, lahko v naslednjih ciklih razmislimo o odmerku zdravila Onivyde pegylated liposomal 70 mg/m². Prilaganje odmerka se priporoča za obvladovanje toksičnosti 3. ali 4. stopnje, povezane z zdravilom Onivyde pegylated liposomal. **KONTRAINDIKACIJE*:** Anamneza hude preobčutljivosti na irinotekan ali katero koli pomožno snov. **POZORILA*:** Zdravilo Onivyde pegylated liposomal ni enakovredno drugim neliposomskim formulacijam irinotekana, zato jih ne smemo zamenjevati. **Milosupresija/nevropatija.** Med zdravljenjem z zdravilom Onivyde pegylated liposomal se priporoča nadziranje celotne krvne slike. Bolniki se morajo zavedati tveganja za nevropatijo in pomena povišane telesne temperature. Febrilno nevropatijo je treba nujno zdraviti v bolnišnici s širokspektralnimi intravenskimi antibiotiki. Pri bolnikih, ki doživijo hude hematološke neželenne učinke, se priporoča zmanjšanje odmerka ali prekinitev zdravljenja. Bolnikov s hudo odpovedjo kostnega mozga ne smemo zdraviti z zdravilom Onivyde pegylated liposomal. Anamneza prehodnega obsevanja trebuha poveča tveganje za hudo nevropatijo in febrilno nevropatijo po zdravljenju z zdravilom Onivyde pegylated liposomal. Pri bolnikih, ki hkrati prejemajo zdravilo Onivyde pegylated liposomal in so obsevani, je potrebna previdnost. Bolniki s pomembno hipokalcemijo, hipokalcemijo, hipokalcemijo, kot so bolniki z Gilbertovim sindromom, imajo med zdravljenjem z zdravilom Onivyde pegylated liposomal lahko večje tveganje za mielosupresijo. Bolniki azijskega porekla imajo večje tveganje za hudo in febrilno nevropatijo. Posamezniki s homozigotnostjo 77 za alel UGT1A1*28 imajo povečano tveganje za nevropatijo. **Imunosupresivni učinki in cepiva:** Dajanje živih ali atenuiranih cepiv bolnikom z oslabilim imunskim sistemom lahko povzroči resne ali smrtne okužbe. **Interakcije z močnimi induktorji encima CYP3A4, močnimi zaviralci encima CYP3A4 in močnimi zaviralci encima UGT1A1:** Zdravilo Onivyde pegylated liposomal ne smemo dajati skupaj z močnimi induktorji encima CYP3A4, močnimi zaviralci encima CYP3A4, ali z močnimi zaviralci encima UGT1A1, razen če ni drugih terapevtskih možnosti. Zdravljenje z močnimi zaviralci encima CYP3A4 moramo prekiniti vsaj 1 teden pred začetkom zdravljenja z zdravilom Onivyde pegylated liposomal. **Driska:** Driska se lahko pojavi zgodaj (v < 24 urah) po začetku zdravljenja z zdravilom Onivyde pegylated liposomal ali pozno (> 24 ur). Pri bolnikih, ki doživijo zgodnji pojav driske (v < 24 urah) po začetku zdravljenja z zdravilom Onivyde pegylated liposomal, je treba razmisliti o terapevtskem in profilaktičnem zdravljenju z atropinom, razen če je kontraindicirano. Bolnike je treba opozoriti na tveganje za zapoznelo drisko (> 24 ur), ki je izčrpavajoča in v redkih primerih tudi življenjsko nevarna. Loperamid je treba uvesti ob prvem pojavu neoblikovane ali mehkega blata ali takoj, ko odvajanje blata postane pogostejše kot običajno. Loperamid je treba dajati, dokler bolnik ni brez driske vsaj 12 ur. Če driska traja tudi, ko bolnik prejema loperamid več kot 24 ur, je treba razmisliti o dodatni peroralni antibiotični podpori. Loperamid zaradi tveganja za paralični ileus ne smemo uporabljati več kot 48 ur zaporedoma. Zdravljenje z zdravilom Onivyde pegylated liposomal je treba odložiti, dokler se driska ne umiri do < 1. stopnje (2-3 odvajanja/dan več kot pred zdravljenjem). Zdravilo Onivyde pegylated liposomal ne smemo dajati bolnikom z zaporo črevesja ali kronično vnetno črevesno boleznijo, dokler se ta ne pozdravi. **Holinergetske reakcije:** Zgodnje drisko lahko spremljajo rinitis, povečano slinjenje, zardevanje, diaforeza, bradikardija, mioza in hiperperistaltika. Uporabiti je treba atropin. **Akutne infuzijske in povezane reakcije:** V primeru hudi preobčutljivostnih reakcij je treba zdravljenje z zdravilom Onivyde pegylated liposomal prekiniti. **Predhodna Wintoplova operacija:** Večje tveganje za resne okužbe. Bolnike je treba spremljati glede znakov okužbe. **Zilne boleznijo:** Zdravilo Onivyde pegylated liposomal je bilo povezano s trombotičnimi dogodki, kot so pljučna embolija, venska tromboza in arterijska tromboembolija. Treba je pridobiti podrobno zdravstveno anamnezo, da bi prepoznali bolnike z več dejavniki tveganja poleg osnovne neoplazme. Bolnike je treba obvestiti o znakih in simptomih tromboembolije in jim svetovati, da se v primeru katerega od teh znakov ali simptomov takoj obrnejo na svojega zdravnika ali medicinsko sestro. **Pljučna toksičnost:** Pri bolnikih, ki so prejeli neliposomski irinotekan, so se pojavili dogodki, podobni

intersticijski pljučni boleznijo (IPB), ki so vodili do smrtnih primerov. Pri bolnikih z dejavniki tveganja (obstoječe pljučno boleznijo, uporabo pnevmotoksičnih zdravil, kolonije stimulirajočimi dejavniki ali predhodnim zdravljenjem z obsevanjem) je treba pred zdravljenjem z zdravilom Onivyde pegylated liposomal in po njem skrbno nadzirati respiratorne simptome. Dokler ni opravljena diagnostična ocena, je treba ob pojavu nove ali napredovale dispneje, kašlja in povišane telesne temperature zdravljenje z zdravilom Onivyde pegylated liposomal takoj prekiniti. Pri bolnikih s potrjeno diagnozo IPB moramo zdravljenje z zdravilom Onivyde pegylated liposomal dokončno prekiniti. **Jetrna okvara:** Bolniki s hiperbilirubinemijo so imeli povišane koncentracije skupnega SN-38, zato je tveganje za nevropatijo povečano. Pri bolnikih z vrednostjo skupnega bilirubina 1,0-2,0 mg/dl je treba redno nadzirati celotno krvno sliko. Previdnost je potrebna pri bolnikih z jetrno okvaro (bilirubin > 2-kratna zgornja meja normalnih vrednosti [ULN]; aminotransferaze > 5-kratna ULN). Previdnost je potrebna, če zdravilo Onivyde pegylated liposomal dajemo v kombinaciji z drugimi hepatotoksičnimi zdravili. **Ledvična okvara:** Uporaba zdravila Onivyde pegylated liposomal pri bolnikih s pomembno ledvično okvaro ni bila ocenjena. **Bolniki s precejšno telesno maso (indeks telesne mase < 18,5 kg/m²):** Potrebna je previdnost. **Pomožne snovi:** To zdravilo vsebuje 33,1 mg natrija na vialo, kar je enako 1,65 % največjega dnevnega vnosa natrija za odrasle osebe, ki ga priporoča SZO in znaša 2 g. En mililiter zdravila Onivyde pegylated liposomal vsebuje 0,144 mmol (3,31 mg) natrija. **INTERAKCIJE*:** **Previdnostni ukrepi:** Sočasno dajanje z induktorji encima CYP3A4 (npr. antikonvulzivi, rifampicin, rifabutin in šentjanževka) lahko zmanjša sistemsko izpostavljenost zdravilu Onivyde pegylated liposomal. Sočasno dajanje z zaviralci encima CYP3A4 (npr. gresinimikom, klaritromicinom, indinavirjem, itrakonazolom, lopinavirjem, nefazodonom, nefinavirjem, ritonavirjem, sakvinavirjem, telaprevirjem, vorikonazolom) ali encima UGT1A1 (npr. atazanavirja, gemfibrozila, indinavirja, regorafenib) lahko poveča sistemsko izpostavljenost zdravilu Onivyde pegylated liposomal. Sočasna uporaba z zdravili z delovanjem na novotvorbe (flucitozinom) lahko poslabša neželenne učinke zdravila Onivyde pegylated liposomal. **PLODNOST* - NOSEČNOST*:** Uporaba ni priporočljiva. **DOJENJE*:** Zdravilo je kontraindicirano. **KONTRACEPCIJA*:** Zenske v rodni dobi morajo med zdravljenjem in še 7 mesecev po zdravljenju z zdravilom Onivyde pegylated liposomal uporabljati učinkovito kontracepcijo. Moški morajo med zdravljenjem z zdravilom Onivyde pegylated liposomal in 4 mesece po zdravljenju uporabljati kondome. **VPLIV NA SPOSOBNOST VOZNIJE IN UPRAVLJANJA STROJEV*:** Bolniki morajo biti med zdravljenjem pri vožnji in upravljanju strojev previdni. **NEZELENI UČINKI*:** Zelo pogosti: nevropatija, leukopenija, anemija, trombocitopenija, hipokalemija, hipomagnezija, dehidracija, zmanjšana apetit, omotica, driska, bruhanje, navzea, bolečine v trebuhu, stomatitis, alopecija, preiskaja, periferni edem, vnetje sluznic, utrujenost, astenija, zmanjšana telesna masa. **Pogosti:** septični sok, sepsa, pljučnica; febrilna nevropatija, gastroenteritis, oralna kandidoza, limfopenija, hipoglikemija, hiponatremija, hipofosfatemija, nespečnost, holinergetskega sindrom, dispepsija, hipotenzija, pljučna embolija, embolija, globoka venska tromboza, dispneja, disonija, kolitis, hemoroidi, hipobilirubinemia, pruritus, akutna ledvična odpoved, z infuzijo povezana reakcija, edem, zvišana raven bilirubina, zvišana raven alaninaminotransferaze, zvišana raven aspartat-aminotransferaze, zvišano mednarodno umerjeno razmerje. **Občasni:** biliarna sepsa, preobčutljivost, tromboza, hipoksija, ezofagitis, proktitis, urtikarija, izpuščaji, makulopapulozni izpuščaji, obarvanje nohtov. **Neznana pogostost:** anafilaktična/anafilaktoidna reakcija, angioedem, eritem. **PREVELIKO ODMERJANJE*:** Za preveliko odmerjanje zdravila ni znane antidote. Treba je uvesti maksimalno podporno nego, s katero preprečimo dehidracijo zaradi driske in zdravimo zaplete zaradi okužb. **FARMAKODINAMIČNE LASTNOSTI*:** Irinotekan (zaviralec topozimeraze I), inkapsuliran v vezikel z lipidnim dvojestvom oziroma liposom. Irinotekan je derivat kamptotecina. Kamptotecini delujejo kot specifični zaviralci encima DNA-topozimeraze I. Irinotekan in njegov aktivni presnovek SN-38 se reverzibilno vežeta na kompleks topozimeraze I in DNA ter sprožita poškodbe v enoveržni DNA, kar zavstavi replikacijske vilice pri podvajanju DNA in povzroča citotoksičnost. Irinotekan se presnavlja s karboksilesterazo do SN-38. SN-38 je približno 1.000-krat močnejši kot irinotekan kot zaviralec topozimeraze I, očiščene iz tumorskih celičnih linij človeka in glodavcev. **PKIRANJE*:** Pakiranje vsebuje eno vialo z 10 ml koncentrata. **NAČIN PREDPISOVANJA IN IZDAJE ZDRAVILA:** H - Predpisovanje in izdaja zdravila je le na recept, zdravilo pa se uporablja samo v bolnišnici. **DATUM ZADNJE REVIZIJE BESEDILA:** avgust 2022. **Imetnik dovoljenja za promet:** Les Laboratoires Servier, 50, rue Carnot, 92284 Suresnes cedex, Francija. *Pred predpisovanjem preberite celoten povzetek glavnih značilnosti zdravila. **Celoten povzetek glavnih značilnosti zdravila in podrobnejše informacije so na voljo pri:** Servier Pharma d.o.o., Podmilščakova ulica 24, 1000 Ljubljana, www.servier.si.

Zdravilo je na slovenskem trgu na voljo v tuji ovojnici. Za uporabnika so informacije v slovenskem jeziku dostopne na uradni spletni strani www.cbz.si. Navodila za uporabo v slovenskem jeziku so na voljo tudi na <https://servier-pro.si/>.

Kratice in literatura:

5-FU/LV: 5-fluorouracil, levkovorin; OS: celokupno preživetje; PFS: preživetje brez napredovanja bolezni; ORR: objektivna stopnja odziva

1. Povzetek glavnih značilnosti zdravila ONIVYDE pegylated liposomal, avgust 2022. 2. Lamb YN, Scott LJ. Drugs. 2017;77:785-792. 3. Drummond DC et al. Cancer Res. 2006;66:3271-3277.
4. Kalra AV et al. Cancer Res. 2014;74:7003-7013. 5. Carnevale J, Ko AH. Future Oncol. 2016;12:453-464. 6. Wang-Gillam A et al. Lancet. 2016;387:545-557. 7. Wang-Gillam A et al. Eur J Cancer. 2019;108:78-87. 8. Chen LT et al. Eur J Cancer. 2018;105:71-78. 9. Hubner R et al. Eur J Cancer. 2019;106:24-33. 10. Kieler M et al. Ther Adv Med Oncol. 2019;11:1-13. 11. Yoo C et al. Ther Adv Med Oncol. 2019;11:1-9. 12. Pellino A et al. J Clin Oncol 2020;38(4_Suppl):P66. 13. Imajima T et al. Ann Oncol 2022;33(Suppl 4):P113. 14. Cui J et al. J Natl Cancer Cent. 2022;2:205-215.
15. Nacionalna zdravstvena komisija Ljudske republike Kitajske. Chin J Cancer Res. 2022;34(3):238-255. 16. NCCN Guidelines Version 2, 2022. Pancreatic Adenocarcinoma. Objavljeno 6. decembra, 2022. 17. Ducreux M et al. Ann Oncol. 2015;25(suppl 5):v56-v68. 18. eUpdate Cancer of the Pancreas Treatment Recommendations. Objavljeno 15. marca, 2019. ESMO Guidelines Committee.
19. Okusaka T et al. Pancreas. 2020;49(3):326-335. 20. Kieler M et al. J Clin Med. 2020;9:1-15.

SERVIER
moved by you

onivyde[®]
pegylated liposomal irinotecan

Instructions for authors

The editorial policy

Radiology and Oncology is a multidisciplinary journal devoted to the publishing original and high-quality scientific papers and review articles, pertinent to oncologic imaging, interventional radiology, nuclear medicine, radiotherapy, clinical and experimental oncology, radiobiology, medical physics, and radiation protection. Papers on more general aspects of interest to the radiologists and oncologists are also published (no case reports).

The Editorial Board requires that the paper has not been published or submitted for publication elsewhere; the authors are responsible for all statements in their papers. Accepted cannot be published elsewhere without the written permission of the editors.

Submission of the manuscript

The manuscript written in English should be submitted to the journal via online submission system Editorial Manager available for this journal at: www.radioloncol.com.

In case of problems, please contact Sašo Trupej at saso.trupej@computing.si or the Editor of this journal at gsera@onko-i.si

All articles are subjected to the editorial review and when the articles are appropriated they are reviewed by independent referees. In the cover letter, which must accompany the article, the authors are requested to suggest 3-4 researchers, competent to review their manuscript. However, please note that this will be treated only as a suggestion; the final selection of reviewers is exclusively the Editor's decision. The authors' names are revealed to the referees, but not vice versa.

Manuscripts which do not comply with the technical requirements stated herein will be returned to the authors for the correction before peer-review. The editorial board reserves the right to ask authors to make appropriate changes of the contents as well as grammatical and stylistic corrections when necessary. Page charges will be charged for manuscripts exceeding the recommended length, as well as additional editorial work and requests for printed reprints.

Articles are published printed and on-line as the open access:

(<https://content.sciendo.com/raon>).

All articles are subject to 1500 EUR + VAT publication fee. Exceptionally, waiver of payment may be negotiated with editorial office, at the time of article submission.

Manuscripts submitted under multiple authorship are reviewed on the assumption that all listed authors concur in the submission and are responsible for its content; they must have agreed to its publication and have given the corresponding author the authority to act on their behalf in all matters pertaining to publication. The corresponding author is responsible for informing the co-authors of the manuscript status throughout the submission, review, and production process.

Preparation of manuscripts

Radiology and Oncology will consider manuscripts prepared according to the Uniform Requirements for Manuscripts Submitted to Biomedical Journals by International Committee of Medical Journal Editors (www.icmje.org). The manuscript should be written in grammatically and stylistically correct language. Abbreviations should be avoided. If their use is necessary, they should be explained at the first time mentioned. The technical data should conform to the SI system. The manuscript, excluding the references, tables, figures and figure legends, must not exceed 5000 words, and the number of figures and tables is limited to 8. Organize the text so that it includes: Introduction, Materials and methods, Results and Discussion. Exceptionally, the results and discussion can be combined in a single section. Start each section on a new page, and number each page consecutively with Arabic numerals. For ease of review, manuscripts should be submitted as a single column, double-spaced text. The template for preparation of the manuscript is available in the editorial manager.

The Title page should include a concise and informative title, followed by the full name(s) of the author(s); the institutional affiliation of each author; the name and address of the corresponding author (including telephone, fax and E-mail), and an abbreviated title (not exceeding 60 characters). This should be followed by the abstract page, summarizing in less than 250 words the reasons for the study, experimental approach, the major findings (with specific data if possible), and the principal conclusions, and providing 3-6 key words for indexing purposes. Structured abstracts are required. Slovene authors are requested to provide title and the abstract in Slovene language in a separate file. The text of the research article should then proceed as follows:

Introduction should summarize the rationale for the study or observation, citing only the essential references and stating the aim of the study.

Materials and methods should provide enough information to enable experiments to be repeated. New methods should be described in details.

Results should be presented clearly and concisely without repeating the data in the figures and tables. Emphasis should be on clear and precise presentation of results and their significance in relation to the aim of the investigation.

Discussion should explain the results rather than simply repeating them and interpret their significance and draw conclusions. It should discuss the results of the study in the light of previously published work.

Charts, Illustrations, Images and Tables

Charts, Illustrations, Images and Tables must be numbered and referred to in the text, with the appropriate location indicated. Charts, Illustrations and Images, provided electronically, should be of appropriate quality for good reproduction. Illustrations and charts must be vector image, created in CMYK color space, preferred font "Century Gothic", and saved as .AI, .EPS or .PDF format. Color charts, illustrations and Images are encouraged, and are published without additional charge. Image size must be 2.000 pixels on the longer side and saved as .JPG (maximum quality) format. In Images, mask the identities of the patients. Tables should be typed double-spaced, with a descriptive title and, if appropriate, units of numerical measurements included in the column heading. The files with the figures and tables can be uploaded as separate files.

References

References must be numbered in the order in which they appear in the text and their corresponding numbers quoted in the text. Authors are responsible for the accuracy of their references. References to the Abstracts and Letters to the Editor must be identified as such. Citation of papers in preparation or submitted for publication, unpublished observations, and personal communications should not be included in the reference list. If essential, such material may be incorporated in the appropriate place in the text. References follow the style of Index Medicus, DOI number (if exists) should be included.

instructions

All authors should be listed when their number does not exceed six; when there are seven or more authors, the first six listed are followed by "et al.". The following are some examples of references from articles, books and book chapters:

Dent RAG, Cole P. In vitro maturation of monocytes in squamous carcinoma of the lung. *Br J Cancer* 1981; **43**: 486-95. doi: 10.1038/bjc.1981.71

Chapman S, Nakielny R. *A guide to radiological procedures*. London: Bailliere Tindall; 1986.

Evans R, Alexander P. Mechanisms of extracellular killing of nucleated mammalian cells by macrophages. In: Nelson DS, editor. *Immunobiology of macrophage*. New York: Academic Press; 1976. p. 45-74.

Authorization for the use of human subjects or experimental animals

When reporting experiments on human subjects, authors should state whether the procedures followed the Helsinki Declaration. Patients have the right to privacy; therefore, the identifying information (patient's names, hospital unit numbers) should not be published unless it is essential. In such cases the patient's informed consent for publication is needed, and should appear as an appropriate statement in the article. Institutional approval and Clinical Trial registration number is required. Retrospective clinical studies must be approved by the accredited Institutional Review Board/Committee for Medical Ethics or other equivalent body. These statements should appear in the Materials and methods section.

The research using animal subjects should be conducted according to the EU Directive 2010/63/EU and following the Guidelines for the welfare and use of animals in cancer research (*Br J Cancer* 2010; 102: 1555 – 77). Authors must state the committee approving the experiments, and must confirm that all experiments were performed in accordance with relevant regulations.

These statements should appear in the Materials and methods section (or for contributions without this section, within the main text or in the captions of relevant figures or tables).

Transfer of copyright agreement

For the publication of accepted articles, authors are required to send the License to Publish to the publisher on the address of the editorial office. A properly completed License to Publish, signed by the Corresponding Author on behalf of all the authors, must be provided for each submitted manuscript.

The articles are open-access, distributed under the terms of the Creative Commons Attribution License (CC BY). The use, distribution or reproduction in other forums is permitted, provided the original author(s) and the copyright owner(s) are credited and that the original publication in this journal is cited, in accordance with accepted academic practice. No use, distribution or reproduction is permitted which does not comply with these terms.

Conflict of interest

When the manuscript is submitted for publication, the authors are expected to disclose any relationship that might pose real, apparent or potential conflict of interest with respect to the results reported in that manuscript. Potential conflicts of interest include not only financial relationships but also other, non-financial relationships. In the Acknowledgement section the source of funding support should be mentioned. The Editors will make effort to ensure that conflicts of interest will not compromise the evaluation process of the submitted manuscripts; potential editors and reviewers will exempt themselves from review process when such conflict of interest exists. The statement of disclosure must be in the Cover letter accompanying the manuscript or submitted on the form available on www.icmje.org/coi_disclosure.pdf

The use and explanation of AI and AI-assisted technologies in scientific writing

When authors use artificial intelligence (AI) and AI-assisted technologies in the writing process, they should consider that:

- These technologies should only be used to improve readability and language and to assist in the investigation of data. They should not replace researchers' primary tasks of explaining, the interpretation of data and drawing valid scientific conclusions.
- Apply the technology under human supervision and control, and carefully review and edit the result, because AI can produce authoritative-sounding results that may be incorrect, incomplete, or biased.
- Do not list AI or AI-assisted technologies as authors or co-authors, and do not cite AI as an author. Authorship carries with it responsibilities and tasks that only humans can perform.
- Disclose in your manuscript the use of AI and AI-enabled technologies in the writing process by following the instructions below. An appropriate statement should appear in the published paper. Please note that authors are ultimately responsible and accountable for the content of the paper.

Disclosure notes

Authors must disclose the use of AI and AI-assisted technologies in the writing process by adding a statement at the end of their manuscript in the main manuscript file before the bibliography, at the time of manuscript submission. The statement should be included in a new section titled 'Statement on the Use of AI and AI-Assisted Technologies in the Writing Process'.

Statement: during the preparation of this paper, the author(s) used [NAME TOOL / SERVICE] to create [REASON]. After using this tool/service, the author(s) have reviewed and edited the content as required and take full responsibility for the content of the publication.

This statement does not apply to the use of basic tools to check grammar, spelling, references, etc. If there is nothing to disclose, it is not necessary to add a statement.

Page proofs

Page proofs will be sent by E-mail to the corresponding author. It is their responsibility to check the proofs carefully and return a list of essential corrections to the editorial office within three days of receipt. Only grammatical corrections are acceptable at that time.

Open access

Papers are published electronically as open access on <https://content.sciendo.com/raon>, also papers accepted for publication as E-ahead of print.

